NANOPARTICLES IN CANCER THERAPY: NOVEL CONCEPTS, MECHANISMS AND APPLICATIONS

EDITED BY: Qingxin Mu and Bing Yan

PUBLISHED IN: Frontiers in Pharmacology and Frontiers in Oncology

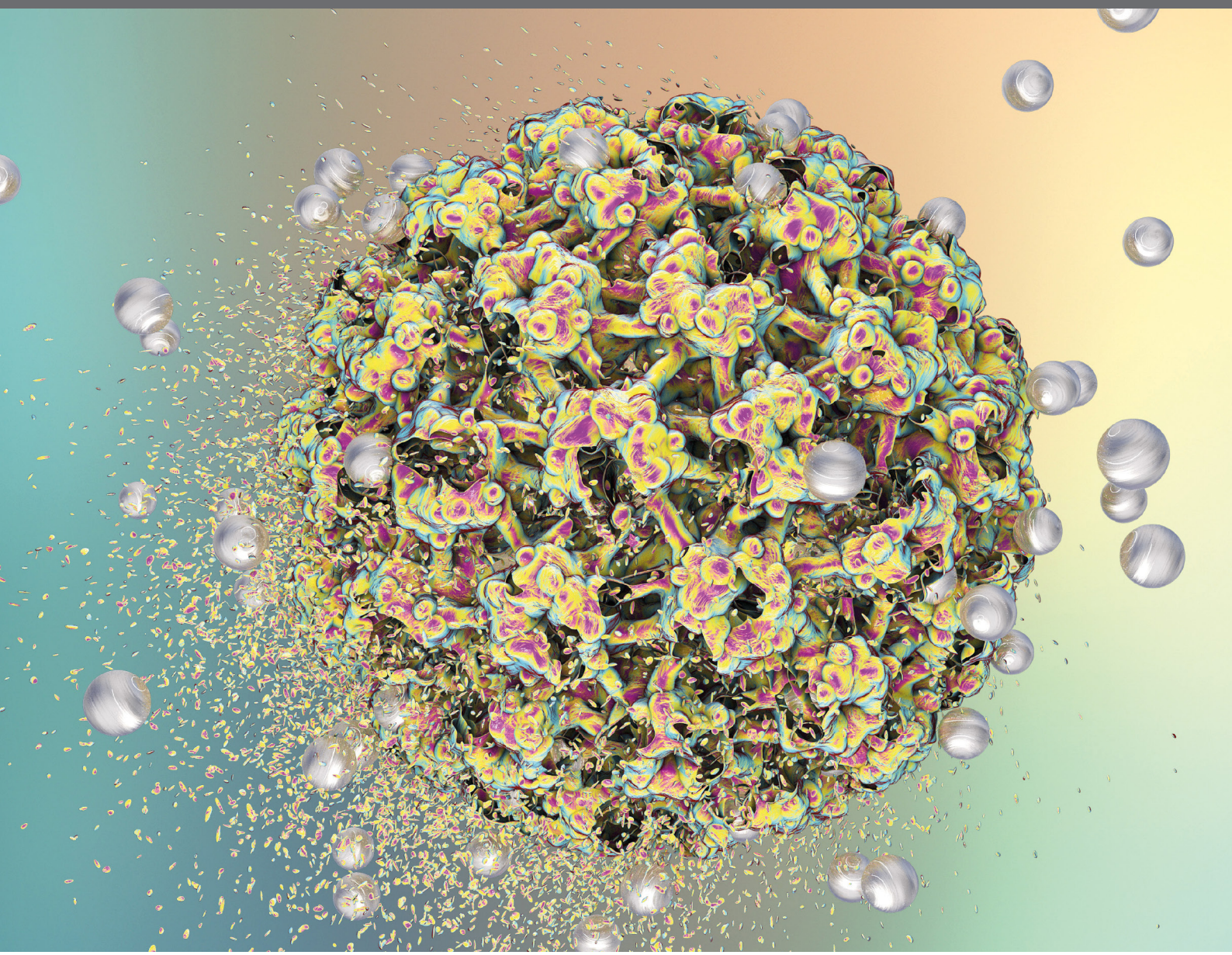

frontiers Research Topics

frontiers

ISSN 1664-8714
ISBN 978-2-88945-810-3
DOI 10.3389/978-2-88945-810-3

About Frontiers

Frontiers is more than just an open-access publisher of scholarly articles: it is a pioneering approach to the world of academia, radically improving the way scholarly research is managed. The grand vision of Frontiers is a world where all people have an equal opportunity to seek, share and generate knowledge. Frontiers provides immediate and permanent online open access to all its publications, but this alone is not enough to realize our grand goals.

Frontiers Journal Series

The Frontiers Journal Series is a multi-tier and interdisciplinary set of open-access, online journals, promising a paradigm shift from the current review, selection and dissemination processes in academic publishing. All Frontiers journals are driven by researchers for researchers; therefore, they constitute a service to the scholarly community. At the same time, the Frontiers Journal Series operates on a revolutionary invention, the tiered publishing system, initially addressing specific communities of scholars, and gradually climbing up to broader public understanding, thus serving the interests of the lay society, too.

Dedication to Quality

Each Frontiers article is a landmark of the highest quality, thanks to genuinely collaborative interactions between authors and review editors, who include some of the world's best academicians. Research must be certified by peers before entering a stream of knowledge that may eventually reach the public - and shape society; therefore, Frontiers only applies the most rigorous and unbiased reviews.
Frontiers revolutionizes research publishing by freely delivering the most outstanding research, evaluated with no bias from both the academic and social point of view. By applying the most advanced information technologies, Frontiers is catapulting scholarly publishing into a new generation.

What are Frontiers Research Topics?

Frontiers Research Topics are very popular trademarks of the Frontiers Journals Series: they are collections of at least ten articles, all centered on a particular subject. With their unique mix of varied contributions from Original Research to Review Articles, Frontiers Research Topics unify the most influential researchers, the latest key findings and historical advances in a hot research area! Find out more on how to host your own Frontiers Research Topic or contribute to one as an author by contacting the Frontiers Editorial Office: researchtopics@frontiersin.org

NANOPARTICLES IN CANCER THERAPY: NOVEL CONCEPTS, MECHANISMS AND APPLICATIONS

Topic Editors:
Qingxin Mu, University of Washington, United States
Bing Yan, Guangzhou University, Shandong University, China

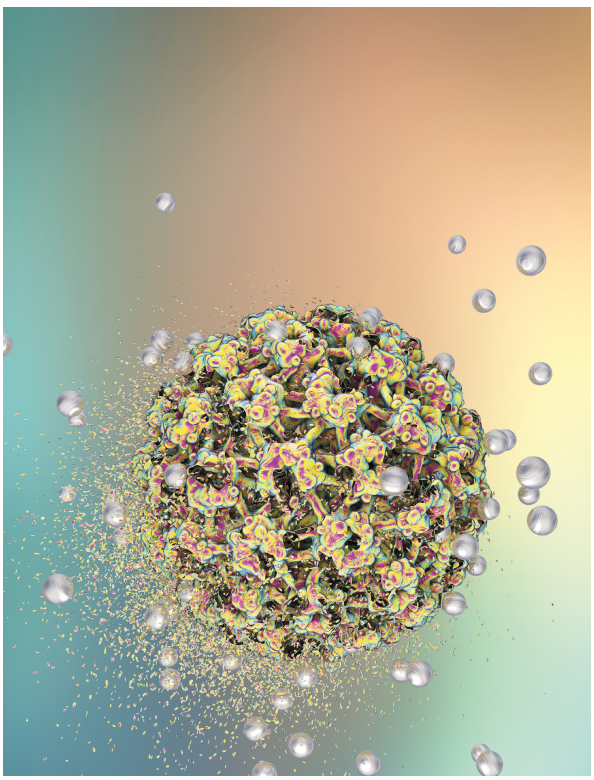

Image: Kateryna Kon/Shutterstock.com

Since the invention of nanomedicine decades ago, considerable progresses have been made, especially with cancer as a target. Nanoparticles have been proven to be powerful imaging tools or potent agents for cancer diagnosis, treatment and prevention. Active research spread from fundamental research to clinical investigations. This topic intends to cover several important aspects in this field including nanocarrier development, gene delivery, intrinsically active nanoparticles, tumor microenvironment, immunology, and toxicity.

Citation: Mu, Q., Yan, B., eds. (2019). Nanoparticles in Cancer Therapy: Novel Concepts, Mechanisms and Applications. Lausanne: Frontiers Media.
doi: 10.3389/978-2-88945-810-3

Table of Contents

SECTION III

NANOPARTICLES TARGETING SPECIFIC MALFUNCTIONS

SECTION IV

TOXICITY OF NANOPARTICLES

frontiers in Pharmacology

EDITORIAL
published: 22 January 2019
doi: 10.3389/fphar.2018.01552

Editorial: Nanoparticles in Cancer Therapy-Novel Concepts, Mechanisms, and Applications

Qingxin Mu[1]* *and Bing Yan*[2,3]*

[1] Department of Pharmaceutics, University of Washington, Seattle, WA, United States, [2] Key Laboratory for Water Quality and Conservation of the Pearl River Delta, Ministry of Education, Institute of Environmental Research at Greater Bay, Guangzhou University, Guangzhou, China, [3] School of Environmental Science and Engineering, Shandong University, Jinan, China

Keywords: nanoparticles, nanomedicine, nanotechnology, drug delivery, cancer therapy

Editorial on the Research Topic

Nanoparticles in Cancer Therapy-Novel Concepts, Mechanisms, and Applications

Since the invention of nanomedicine decades ago (Drexler et al., 1991; Weber, 1999; Kalb, 2000; Voss, 2000), considerable progresses have been made, especially with cancer as a target (Jain and Stylianopoulos, 2010; Shi et al., 2017). Active research spread from fundamental research to clinical investigations. The topic "Nanoparticles in Cancer Therapy-Novel Concepts, Mechanisms and Applications" intends to cover several important aspects in this field including nanocarrier development, gene delivery, intrinsically active nanoparticles (NPs), tumor microenvironment, immunology, and toxicity.

The mostly applied biocompatible nanocarriers in clinical trials are protein, lipid, and polymer-based materials. In this aspect, three reviews are included. Gou et al. comprehensively summarized protein-based nanoformulations for cancer theranostics. They discussed nanocarriers composed of albumin, ferritin, gelatin, and transferrin, which are the major materials investigated. Imaging modalities in addition to these nanocarriers are also discussed including near-IR fluorescence, magnetic resonance imaging, positron emission tomography, computed tomography, and photoacoustic imaging. The authors also analyzed challenges these formulations face such as reproducibility, colloidal stability in biological environments, drug-loading efficiency, and reticuloendothelial system accumulation. Rezvantalab et al. systematically reviewed the PLGA-based NPs in cancer treatment. The review article gives an overview of properties and preparation methods of PLGA NPs. Emphasis is also given to the passive and active tumor targeting, and combination therapy. The authors argued that researchers need to critically reflect on the clinical feasibility and give consideration to not only the optimization of size, drug loading and drug release, but also biocompatibility, pharmaceutical upscaling and batch-to-batch reproducibility. The authors also encourage more pharmacokinetic and pharmacodynamic understanding of NPs, and applicability of external stimuli for combination therapy. Raut et al. provides an in-depth review of recombinant high-density lipoprotein (rHDL)-based drug delivery systems in cancer therapy. The rHDL NPs are inherently capable of overcoming several biological barriers to cancer therapy. The small size, intrinsic targeting ability, endosomal escape, and safety in animals and humans make this platform highly attractive for chemotherapy drugs which suffer from off-target toxicity issues. In their review, detailed discussion was given in the following aspects: interactions of rHDL NPs with blood and immune cells, hemorheology, and blood vessel fluid dynamics, extravasation, cellular membrane transport, and endosomal escape, and drug resistance.

Polymeric micelles are a popular type of nanocarriers for drug delivery due to their biocompatibility, multifunctionality, and controllable release. In this topic, Qi et al. synthesized triblock copolymers PEG-DiHyd-PLA containing hydrazone bond. These copolymers can self-assemble into micelles with uniformed size below 100 nm and narrow size distribution. The

Edited and reviewed by:
Giuseppe Giaccone, Georgetown University, United States

***Correspondence:**
Qingxin Mu
qmu@uw.edu
Bing Yan
dr.bingyan@yahoo.com

Specialty section:
This article was submitted to Cancer Molecular Targets and Therapeutics, a section of the journal Frontiers in Pharmacology

Received: *09 December 2018*
Accepted: *20 December 2018*
Published: *22 January 2019*

Citation:
Mu Q and Yan B (2019) Editorial: Nanoparticles in Cancer Therapy-Novel Concepts, Mechanisms, and Applications. Front. Pharmacol. 9:1552. doi: 10.3389/fphar.2018.01552

size underwent obvious changes in mildly acidic environments while kept unchanged in neutral condition. Model drug doxorubicin was successfully loaded into the micelles and presented a rapid and complete drug release in acidic condition (pH 5.0). The drug loaded NPs possessed high anti-tumor activity to kill the cancer cells but minimum toxicity to normal cells. Li et al. synthesized an ibuprofen-based amphiphilic diblock copolymer (POEG-b-PVBIBU) via reversible addition fragmentation transfer polymerization of the drug-based vinyl monomer. The diblock copolymer was able to self-assemble into prodrug nanomicelles and load anti-cancer drugs with high capacity such as doxorubicin, paclitaxel and docetaxel. The drug containing polymeric micelles were more effective in inhibiting the tumor growth than free DOX *in vivo*.

Li et al. achieved RNA interference for cancer therapy using TDAPEI, a synthetic derivative of low-molecular-weight polyethylenimine (PEI) as a carrier of plasmid DNA encoding VEGF shRNA. The polymers were cross-linked with imine bonds by the conjugation of branched PEI (1.8 kDa) and 2,5-thiophenedicarboxaldehyde (TDA). The nanocomplex showed effective *in vivo* anti-tumor efficacy and gene silencing comparable to PEI (25 kDa) as carrier but greater biocompatibility.

NPs can also be intrinsically active for cancer therapy. Corsi et al. reviewed the biological effects of cerium oxide NPs. Despite cerium oxide NPs (CNPs) were found to exert strong anticancer activities which is a characteristic generally attributed to CNPs redox activity, other studies however reported non-redox mechanisms. The authors recently demonstrated that the radio-sensitizing effect of CNPs on human keratinocytes is independent from the redox switch. Mechanisms involving particle dissolution with release of toxic Ce^{4+} atoms, or differential inhibition of the catalase vs. superoxide dismutase-mimetic activity with accumulation of H_2O_2 have been proposed, explaining such intriguing findings only partially.

Another example of intrinsically active NPs are through interacting with human immune systems. Jia et al. discussed the interactions of NPs with dendritic cells and its applications in cancer therapy. Targeting dendritic cells (DCs) by nanotechnology stands as a promising strategy for cancer immunotherapy. The physicochemical properties of NPs influence their interactions with DCs, thus altering the immune outcome of DCs by changing their functions in the processes of maturation, homing, antigen processing, and antigen presentation. In their review, Jia et al. summarized the recent progress in targeting DCs using NPs as a drug delivery carrier in cancer immunotherapy, the recognition of NPs by DCs, and the ways the physicochemical properties of NPs affect DCs' functions. The molecular pathways in DCs that are affected by NPs were also discussed.

The tumor microenvironment plays a vital role in regulating nano-chemotherapeutics distribution and their biological effects. Fernandes et al. summarized the barriers in tumor microenvironment, their consequential effects on chemotherapeutics, considerations to improve nano-chemotherapeutics delivery and combinatorial strategies to overcome acquired resistance induced by tumor microenvironment. Nanotechnology based approach as well as combinatorial approaches based on ligand-mediated, redox-responsive, and enzyme-mediated strategies have been discussed in their review.

Nanotechnology has also shown several advantages over widely used traditional methods in uro-oncology. For example, different types of NPs improve the solubility of poorly soluble drugs, and multifunctional NPs have good specificity toward prostate, renal, and bladder cancer. Moreover, nanotechnology can also combine with other novel technologies to further enhance efficacy. As our understanding of nanotechnologies grows, additional opportunities to improve the diagnosis and treatment of urological cancer are expected to arise. In their review, He et al. focused on nanotechnologies with potential applications in urological cancer therapy and highlighted clinical areas that would benefit from nanomedicine therapy.

As concerns about the toxicity of nanomaterials are growing, a safety evaluation become a routine assessment nowadays as a prerequisite for nanomedicine. Chen et al. showed that carboxyl and amine-modified InP/ZnS quantum dots were able to enter the cells with high uptake efficiency. High doses of NPs caused the cell viability to decrease, and carboxyl or amine-modified quantum dots appeared to be more toxic than hydroxyl modified ones. In addition, all these NPs were able to induce intracellular reactive oxygen species generation and apoptosis. These results suggested that proper caution should be taken for the safe application of nanomedicine.

Although this topic included some key advances, we recognize that this field is growing very rapidly and our collection has not covered all aspects. In recent years, nanotechnology has shown many advantages over conventional approaches for cancer diagnosis, treatment and prevention, and clinical trials are being implemented every year (Tran et al., 2017). However, challenges are still overwhelming especially in human trials, formulation, and regulatory issues. With new advancements in materials chemistry, nanoscience, biology and medicine, one can envision that devastating cancer will be curable some day and in that achievement, the nanoscale approaches will have played an important role.

AUTHOR CONTRIBUTIONS

All authors listed have made a substantial, direct and intellectual contribution to the work, and approved it for publication.

FUNDING

This work was supported by the National Key R&D Program of China (2016YFA0203103), the National Natural Science Foundation of China (91543204 and 91643204), and the Strategic Priority Research Program of the Chinese Academy of Sciences (XDB14030401).

ACKNOWLEDGMENTS

We wish to thank all the authors contributing to this Frontiers Research Topic and all the reviewers who have helped to make it solid.

REFERENCES

Drexler, K. E., Peterson, C., and Pergamit, G. (1991). *Unbounding the Future*. New York, NY: William Morrow.

Jain, R. K., and Stylianopoulos, T. (2010). Delivering nanomedicine to solid tumors. *Nat. Rev. Clin. Oncol.* 7, 653–664. doi: 10.1038/nrclinonc.2010.139

Kalb, C. (2000). The war on disease goes miniature. Nanomedicine: drugs and cancer tests, cell by cell. *Newsweek* 134, 89.

Shi, J., Kantoff, P. W., Wooster, R., and Farokhzad, O. C. (2017). Cancer nanomedicine: progress, challenges and opportunities. *Nat. Rev. Cancer* 17, 20–37. doi: 10.1038/nrc.2016.108

Tran, S., DeGiovanni, P. J., Piel, B., and Rai, P. (2017). Cancer nanomedicine: a review of recent success in drug delivery. *Clin. Trans. Med.* 6:44. doi: 10.1186/s40169-017-0175-0

Voss, D. (2000). Nanomedicine nears the clinic. *Technol. Rev.* 103:60. Available online at: https://www.technologyreview.com/s/400632/nanomedicine-nears-the-clinic/

Weber, D. O. (1999). Nanomedicine. *Health Forum J.* 42, 36–37.

Conflict of Interest Statement: The authors declare that the research was conducted in the absence of any commercial or financial relationships that could be construed as a potential conflict of interest.

frontiers in Pharmacology

REVIEW
published: 27 April 2018
doi: 10.3389/fphar.2018.00421

Bio-Inspired Protein-Based Nanoformulations for Cancer Theranostics

Yi Gou[1], Dandan Miao[1], Min Zhou[1], Lijuan Wang[2], Hongyu Zhou[2] and Gaoxing Su[1]**

[1] Jiangsu Province Key Laboratory of Inflammation and Molecular Drug Targets, School of Pharmacy, Nantong University, Nantong, China, [2] Guangzhou Key Laboratory of Environmental Exposure and Health and Guangdong Key Laboratory of Environmental Pollution and Health, School of Environment, Jinan University, Guangzhou, China

Over the past decade, more interests have been aroused in engineering protein-based nanoformulations for cancer treatment. This excitement originates from the success of FDA approved Abraxane (Albumin-based paclitaxel nanoparticles) in 2005. The new generation of biocompatible endogenous protein-based nanoformulations is currently constructed through delivering cancer therapeutic and diagnostic agents simultaneously, as named potential theranostics. Protein nanoformulations are commonly incorporated with dyes, contrast agents, drug payloads or inorganic nanoclusters, serving as imaging-guided combinatorial cancer therapeutics. Employing the nature identity of proteins, the theranostics, escape the clearance by reticuloendothelial cells and have a long blood circulation time. The nanoscale sizet allows them to be penetrated deeply into tumor tissues. In addition, stimuli release and targeted molecules are incorporated to improve the delivery efficiency. The ongoing advancement of protein-based nanoformulations for cancer theranostics in recent 5 years is reviewed in this paper. Fine-designed nanoformulations based on albumin, ferritin, gelatin, and transferrin are highlighted from the literature. Finally, the current challenges are identified in translating protein-based nanoformulations from laboratory to clinical trials.

Keywords: protein nanoparticles, cancer therapeutics, theranostics, drug delivery, cancer diagnostics

OPEN ACCESS

Edited by:
Qingxin Mu,
University of Washington,
United States

Reviewed by:
Yanqi Ye,
University of North Carolina at Chapel Hill, United States
Shumei Zhai,
Shandong University, China

***Correspondence:**
Hongyu Zhou
hyzhou001@126.com
Gaoxing Su
sugaoxing@ntu.edu.cn

Specialty section:
This article was submitted to Cancer Molecular Targets and Therapeutics, a section of the journal Frontiers in Pharmacology

Received: *01 March 2018*
Accepted: *11 April 2018*
Published: *27 April 2018*

Citation:
Gou Y, Miao D, Zhou M, Wang L, Zhou H and Su G (2018) Bio-Inspired Protein-Based Nanoformulations for Cancer Theranostics. Front. Pharmacol. 9:421. doi: 10.3389/fphar.2018.00421

INTRODUCTION

Cancer, a leading cause of death globally, reaching approximately 8.2 million mortalities yearly, poses an enormous burden on society (Torre et al., 2015; Mehra et al., 2017). Cancer counts as a multifactorial and refractory disease caused by the local tissue micro-environmental and genetic factors intertwined (Hanahan and Weinberg, 2011). Common treatment strategies, including radiotherapy and/or chemotherapy with surgery, result in high treatment failure rate (Aoun et al., 2015; Kouchakzadeh and Abbas Shojaosadati, 2016). The reasons of treatment failure are generally diverse: (1) cancer is commonly detected at a later stage, thus accuracy and susceptibility of diagnosis and monitoring methods for early-stage cancer require further improvement (Ge and Liu, 2013; Torre et al., 2015); (2) in most cases, the conventional chemotherapy have been disappointing in efficacy due to multidrug resistance (MDR) and severe side effects (Gelperina et al., 2005; Pérez-Tomás, 2006; Szakács et al., 2006; Ge and Liu, 2013); (3) the cancer therapeutic biological agents (inclusive of antibodies, proteins and nucleic acids), the new class of anticancer drugs, are commonly unstable in *in vivo* circulation, with rapid degradation and inactivation before

reaching the target site (Panyam and Labhasetwar, 2003; Sinha and Trehan, 2003). Accordingly, early detection, effective diagnosis and effective treatment of cancer are needed to be optimized to increase the survival rate and decrease the cancer associated deaths.

"Theranostics," the portmanteau of therapeutics and diagnostics, has incorporated diagnostic and therapeutic functions into a single nanoplatform (Pene et al., 2009; Chen and Liu, 2016). It is noteworthy that the theranostics have been proposed as a new and revolutionary therapeutic concept in cancer therapy, enabling simultaneous diagnosis and treatment response monitoring using personalized medicine with high accuracy and specificity (Janib et al., 2010; Bardhan et al., 2011). Additionally, it is likely to incorporate numerous different therapeutic drugs into a single theranostics nanoplatform through judicious design to reach synergistic treatment of cancer (Moon et al., 2015; Chen and Liu, 2016). In this regard, theranostics have become a research orientation arousing great concern and been promising in the field of cancer treatment.

Considerable efforts have been recently made to develop new systems for cancer theranostics (Opoku-Damoah et al., 2016; Chen et al., 2017b; Guo et al., 2017; Mohammadi et al., 2017; Tekade and Sun, 2017; Yue et al., 2017). Thus, far, numerous types of theranostic platforms have been reported, consisting of protein nanocarriers (Ng et al., 2011; Chen and Liu, 2016; Truffi et al., 2016), liposome nanocarriers (Wang et al., 2014b; Dai and Yue, 2017), inorganic nanocarriers (Huang et al., 2011; Sharma et al., 2015), polymer nanocarriers (Kamaly et al., 2012; Charron et al., 2015; Sk and Kojima, 2015) and inorganic/organic hybrid nanocarriers (Barreto et al., 2011; Zhu et al., 2015; Li et al., 2017). Among these platforms, protein-based nanoplatforms have aroused the greatest concern by virtue of their biodegradability, biocompatibility, no or low toxicity and ease of modification (Maham et al., 2009; Elzoghby, 2013; Yewale et al., 2013; Chen and Liu, 2016; Kouchakzadeh and Abbas Shojaosadati, 2016). Some proteins, e.g., transferrin and lactoferrin, can be specifically bound to receptor(s) highly expressed in considerable cancer cells via receptor-ligand interaction, enabling the construction of active targeted theranostic nanoplatforms (Kanwar et al., 2016; Wang et al., 2016a, 2017a). Furthermore, in the presence of reactive groups such as –COOH, $–NH_2$, and –OH, protein-based theranostic platforms can be further decorated with functional molecules for different purposes. Numerous proteins as versatile platforms for delivering therapeutic agents have been elucidated in previous review articles (Yewale et al., 2013; Paliwal and Palakurthi, 2014; Kouchakzadeh and Abbas Shojaosadati, 2016).

This review article stresses the protein-based multifunctional theranostics progress in the past 5 years (**Table 1**) and summaries critical foundation for further studying theranostics. The therapeutic methods include photothermal therapy (PTT), photodynamic therapy (PDT) and chemotherapy. The diagnostic or imaging methods included magnetic resonance (MR) imaging, fluorescence imaging, computed tomography (CT) imaging, photoacoustic (PA) imaging, positron emission tomography (PET) imaging and so on. The combinatorial strategies between diagnostic and therapeutic methods are summarized in **Figure 1**. Properties of commonly used proteins, i.e., albumin, ferritin, gelatin, and transferrin, were introduced. The preparation methods and key outcomes of *in vitro* or *in vivo* studies of these protein-based nanoformulations for cancer theranostics were elaborated.

ALBUMIN-BASED NANOFORMULATIONS

Albumin and Its Properties

Albumins are obtained commercially in considerable amount from human serum (human serum albumin, HSA), bovine serum (bovine serum albumin, BSA), rat serum (RSA) and egg white (ovalbumin) (Karimi et al., 2016). Based on practicality, this review focus on HSA and BSA.

BSA shares ca. 76% sequence homology with HSA (Anand and Mukherjee, 2013), and is very soluble with a 69,323 Da molecular weight, consisting of 583 amino acid residues. BSA has an isoelectric point (pI) of 4.7 with a net charge of −18 mV (Anand and Mukherjee, 2013). BSA molecule is heart-shaped, consisting of three repeating domains (labeled I–III), with each of which falling into two sub-domains A and B (Majorek et al., 2012). BSA is extensively adopted for cancer theranostics by virtue of low cost, abundance, ease of purification and proper delivering properties.

HSA, the most abundant plasma protein (35–50 mg/mL human serum), is synthesized in the liver. HSA is a single-chain and non-glycosylated polypeptide with 66,500 Da in molecular weight, consisting of 585 amino acid residues, and heart-shaped with 80 × 80 × 30 Å in ca. dimensions (Sugio et al., 1999). From X-ray crystallographic analyses, the vital difference between BSA and HSA is that the former contains two tryptophan amino acid residues (Trp-135 and Trp-212), whereas the latter has merely one, Trp-214. HSA is very soluble, being extremely robust toward temperature (available at 60°C for 10 h), pH (stable in pH 4–9) and organic solvents. Besides, HSA protein has preferentially been uptaken to tumor interstitium via the pathway of SPARC glycoprotein and gp60 glycoprotein transcytosis. These properties as well as its deficient toxicity, immunogenicity, and biodegradability make it an ideal candidate for cancer theranostics.

HSA for Cancer Theranostics

HSA has broadly served as a natural carrier to isolate organic molecules or inorganic oxide, inclusive of IR780, superparamagnetic iron oxide, IR825, and chlorin e6 (Ce6), for synthesizing effective theranostic agents.

Individual HSA-Dye Complexes

HSA is well-known with multiple hydrophobic binding pockets, and able to be bound non-covalently with many organic dyes, forming HSA-dye complexes with a high fluorescence quantum yield. In recent years, near-infrared (NIR) dyes, e.g., IR780, indocyanine green (ICG) and IR825, are broadly employed for cancer theranostics because of their relatively deep penetration and low interference. IR825 can be bound to the hydrophobic domain of HSA (the molar ratio of 1:1) via hydrophobic interactions, which fabricates a HSA-IR825 complex (**Figure 2A**) (Chen et al., 2014c). The HSA-IR825 complex have a high

TABLE 1 | Overview of the protein-based nanoformulations for cancer theranostics.

Protein	Formulation	Application	Key outcomes of *in vitro*/*in vivo* study	References
HSA	HSA-ICG NPs	Fluorescence and PA dual-modal imaging-guided phototherapy	In 4T1 tumor-bearing mice, the normal, tumor and its margin tissue can be clearly identified via fluorescence and PA imaging. After i.v. injection of the NPs followed by imaging-guided precision PDT/PTT, the 4T1 tumor was completely eradicated, no treatments-induced toxicity and tumor recurrence were observed.	Sheng et al., 2014
HSA	HSA-IR825 complex	Imaging-guided PTT	The 4T1 tumor could be clearly identified from 1 to 12 h post injection. After i.v. injection of the complex followed by 808 nm laser irradiation, the 4T1 tumor was significant eradicated and no appreciable toxic side was observed.	Chen et al., 2014c
HSA	HSA-Gd-IR825 nanocomplex	Fluorescence and MR dual-modal imaging-guided PTT	The nanocomplex can be used for effective mapping of the sentinel lymph node nearby tumors, and the mapping signal is clearest at ∼30 min post injection. Photothermal ablation of the HSA-Gd-IR825 combined with surgical removal of primary tumors provides significant therapeutic advances in preventing 4T1 tumor metastasis and prolonging animal survival.	Chen et al., 2014a
HSA	HSA–ICG–PTX NPs	Imaging-guided PTT and chemotherapy	The 4T1 tumor could be clearly identified after 4 h post injection. After i.v. injection of the NPs followed by 808 nm laser irradiation, the 4T1 tumor was significant eradicated and no significant toxic side was observed.	Chen et al., 2015a
HSA	HSA-Ce6-PTX-RGD	MR and fluorescence-imaging-guided chemotherapy and PDT	Upon i.v. injection into U87MG tumor-bearing mice, the nano-drug could be effectively tracked by dual modal imaging and shown excellent tumor growth inhibition effect.	Chen et al., 2015b
HSA	Cy5/Qsy21 labeled-Pt(IV)-probe@HSA	Imaging-guided chemotherapy	Upon UV light irradiation, Pt(IV)-probe@HSA showed enhanced cell death and cell apoptosis at both cisplatin-resistant A2780cis and sensitive A2780 cell lines.	Li et al., 2015
HSA	Melanin/PTX-HSA NPs	PA-imaging-guided chemotherapy	*In vitro*, the NPs showed enhanced PA signal and cytotoxicity against MDA-MB-231 cancer cells. *In vivo*, the NPs efficiently accumulated inside the MDA-MB-231 tumor, resulting in inhibiting tumor growth effectively and visualizing tumors photoacoustically.	Sim et al., 2015
HSA	Porphyrin-MB-PTX-HSA NPs	PA and ultrasound-imaging-guided chemotherapy	The MDA-MB-231 tumor and neo-vessels in the tumor region could be clearly visualized after 3 min post injection. Exposure to the focused ultrasound triggered the collapse of the Porphyrin-MB-PTX-HSA NPs, resulting in the PTX-HSA-NPs suppressed MDA-MB-231 tumor growth 10-fold higher than without exposure to ultrasound.	Moon et al., 2015
HSA	HSA@CySCOOH	Fluorescence/PA/thermal multimodality imaging-guided PTT	The 41T tumor can be clearly differentiated from the surrounding normal tissue from 1 to 48 h injection. After injection of the HSA@CySCOOH followed by 808 nm laser irradiation, complete tumor eradication was achieved on 4T1 tumor-bearing mice, with no noticeable toxicity, weight loss, and tumor recurrence being observed.	Rong et al., 2015
HSA	HSA-Ce6 nanoassemblies	Fluorescence/PA/MR triple-modal imaging-guided PDT	The nanoassemblies could be used for PA, MRI and fluorescence triple-modal tumor imaging imaging in 4T1 tumor-bearing mice via i.v. injection. After i.v. injection of the nanoassemblies followed by low-energy NIR irradiation, the 4T1 tumor was completely suppressed without therapy-induced side effects and tumor recurrence.	Hu et al., 2016
HSA	HSA-FePc NPs	PA imaging-guided PTT	The NPs are excellent PA imaging agent, which can clearly show a clear 4T1 tumor microstructure with higher spatial and contrast resolution compared with FePc alone molecules. After i.v. injection, the NPs exhibited efficient cancer therapy, no obviously weight loss and low long-term toxicity were observed.	Jia et al., 2017
HSA	PFT-Hcy-HSA-Cy7-pTFT	Optical and ^{19}F MR imaging-guided chemotherapy	The ^{19}F signals of PFT-Hcy-HSA-Cy7-pTFT are clearly visible in tumor-bearing mouse. The inhibitory tumor (A549) growth effect of PFT-Hcy-HSA-Cy7-pTFT was found to be 0.8-fold more than that of the pTFT alone.	Lisitskiy et al., 2017
HSA	HSA-gemcitabine/IR780 complex	NIR imaging-guided chemotherapy	Compared to IR780 alone, the complex showed enhanced accumulation and long-term retention in BxPC-3 pancreatic tumor tissues, resulting in inhibiting tumor growth effectively with minimal side effects.	Han et al., 2017

(Continued)

TABLE 1 | Continued

Protein	Formulation	Application	Key outcomes of *in vitro*/*in vivo* study	References
HSA	HSA-coated superparamagnetic iron oxide NPs	MRI and thermoacoustic imaging-guided thermoacoustic therapy	Based on MRI and TA imaging, the NPs provide comprehensive and complementary information for 4T1 tumors. Meanwhile, the NPs mediated TA therapy exhibits excellent anti-tumor efficacy for deep tumor models.	Wen et al., 2017
BSA	BSA functionalized Nano-rGO	PA/ultrasonic dual-modality imaging-guided PTT	The theranostic agent not only showed rapid and significant PA signal enhancement in the MCF-7 tumor area, but also can effectively kill tumor cells *in vivo* with no noticeable organs toxic.	Sheng et al., 2013
BSA	squaraine@BSA	Dual-functional NIR probe for targeted optical imaging and selective PTT of cancer.	The optimal imaging and PTT window for KB xenografted tumor was within 6 h post-injection. After a tail veins injection of the theranostic agent followed by 680 nm laser irradiation, the KB xenografted tumor was significantly suppressed.	Gao et al., 2014
BSA	UCNP@BSA-RB&IR825	Imaging-guided combined photothermal and photodynamic therapy	The theranostic agent irradiated with dual lasers at 808 nm and 980 nm show stronger anti-cancer effect than that at individual wavelength both *in vitro* and *in vivo*.	Chen et al., 2014b
BSA	Fe_3O_4-BSA@DOX-PEG	Combined MRI diagnostics and chemotherapy	The theranostic agent showed superparamagnetic property and high T_2-relaxivity value, and displayed similar cytotoxicity against HEK293 and C6 cells as the DOX alone.	Semkina et al., 2015
BSA	Gemcitabine-loaded magnetic BSA nanospheres modified with cetuximab	Simultaneous targeting, MRI diagnostics, and double-targeted thermochemotherapy of pancreatic cancer cells	The theranostic agent not only can effectively distinguish different EGFR-expressing pancreatic cancer cells, but also can evaluate non-invasive methods for different targeting effects by MRI. Combined antibodies and magnetic targeting, the theranostic agent can efficiently inhibit or kill AsPC-1 cells.	Wang et al., 2015
BSA	Fe_5C_2-BSA-DOX NPs	Multi-stimuli-regulated photo-chemothermal cancer therapy	The NPs could be used for MRI and fluorescence tumor imaging in SK-OV-3 tumor-bearing mice via i.v. injection. Under the synergistic effect of magnetic targeting, PTT and the increased drug release, the NPs have no systemic toxicity and show good SK-OV-3 tumor elimination.	Yu et al., 2016
BSA	Gd:CuS@BSA NPs	PA/MR bimodal imaging-guided tumor-targeted PTT	The NPs have significant SK-OV-3 tumor-targeted PA/MR imaging performance, as well as effective SK-OV-3 tumor ablation.	Yang et al., 2016
BSA	PEG-BSA-imidazole modified with either Cy5.5 or BHQ-3	pH-activatable on/off tumor targeting probe for the theranostic	The theranostic agent displayed significant cytotoxicity for MCF-7 and A549 cells, and showed a strong fluorescence signal in the endosomal region of MCF-7 cells.	Lee et al., 2016
BSA	[FITC]-BSA-Gd/1,3-bis(2-chloroethyl)-1-nitrosourea NPs	MR and fluorescence imaging-guided chemotherapy	The NPs enable dual imaging for real-time tracking of chemotherapeutic agent *in vitro* and *in vivo*, and can also effectively inhibit MBR 261-2 tumor growth.	Wei et al., 2016
BSA	Folate(FA)-BSA-c-PheoA conjugate:GO complex incorporated free PheoA	Active-targeted and pH-responsive theranostic agent for fluorescence imaging-guided PTT and PDT	The theranostic agent showed the strongest fluorescence signal at the MCF7 tumor at 3 h post-injection. After i.v. injection of the theranostic agent followed by 671 nm laser irradiation, the B16F10 tumor was suppressed, and no acute toxicity was observed.	Battogtokh and Ko, 2016
BSA	Prussian blue-BSA-ICG NPs	MR and NIR fluorescence bimodal imaging guided laser mediated combinatorial phototherapy	After i.v. injection of the NPs, time dependent NIR fluorescence signal and MRI signal was increase at the SCC7 tumor site. Upon irradiation of 808 nm laser irradiation, the SCC7 tumor growth was efficiently suppressed without tumor recurrence.	Sahu et al., 2016
BSA	DOX-loaded UCN/ZnPc@FA-BSA-PCL	Simultaneous tumor cell imaging, PDT and chemotherapy	After 4 h of incubation, DOX and UCN fluorescent signals can be clearly detected in HeLa cells. Compared with single PDT or DOX chemotherapy groups, the theranostic agent showed significantly enhanced HeLa cell killing efficiency.	Dong et al., 2016
BSA	BSA-MnO_2-ICG NPs and BSA-MnO_2-PTX NPs	MR imaging-guided PTT and MR imaging-guided chemotherapy	Both NPs showed admirable renal and tumor imaging ability as well as significant 4T1 tumor inhibition via i.v. injection.	Pan et al., 2017
BSA	MoS_2-Gd-BSA	Dual-modality MR and PA imaging-guided PTT	The enhanced MR/PA signals were detected in the 4T1 tumor site post-injection of the theranostic agent. After i.v. injection of the theranostic agent followed by 808 nm laser irradiation, the 4T1 tumor was suppressed, and the negligible toxicity was observed.	Chen et al., 2017a
BSA	Mn_3O_4-BSA-EDTA	Multifunctional imaging-guided PTT	The theranostic agent exhibited applicability a T_1-T_2 dual-model MR imaging and strong NIR (700–1000 nm) imaging *in vitro* and *in vivo*. After i.v. injection of the theranostic agent followed by 785 nm laser irradiation, the HCT116 tumor was suppressed, and the low toxicity was observed.	Liu et al., 2017

(Continued)

TABLE 1 | Continued

Protein	Formulation	Application	Key outcomes of *in vitro*/*in vivo* study	References
BSA	Au-BSA-DOX-FA	pH-sensitive theranostics agent for CT imaging and targeting therapy	The highest CT value in MGC-803 tumor arose at 30 min post-injection. The theranostic agent showed selective antitumor activity effects on the MGC-803 tumor and no side effects on normal organs and tissues.	Huang et al., 2017
BSA	Gd_2O_3@BSA conjugating Chlorin e6	MR imaging-guided photo-induced therapy	The theranostic agent can be used for tumor localization and visualization the *in vivo* distribution of Chlorin e6. After i.v. injection of the theranostic agent followed by 660 nm laser irradiation, the 4T1 tumor was suppressed, and no influence on the normal tissues was observed.	Zhou et al., 2017
Ferritin	ZW800-labeled $ZnF_{16}Pc$-ferritin- RGD4C	Fluorescence imaging-guided PDT	The theranostic agent showed admirable liver and U87MG tumor imaging ability, significant U87MG tumor inhibition as well as minimal toxicity to normal tissues via i.v. injection.	Zhen et al., 2013b
Ferritin	ZW800-labeled DOX-ferritin- RGD4C	Fluorescence imaging-guided chemotherapy	After injection of the theranostic agent, the fluorescence signals in the tumor were the strongest and two-fold higher than those in the liver. The theranostic agent showed a longer circulation half-life, significant U87MG tumor inhibition as well low cardiotoxicityl via i.v. injection.	Zhen et al., 2013a
Ferritin	IR820 loaded ferritin nanocage	Fluorescence and PA imaging-guided PTT	In 4T1 tumor-bearing mice, the tumor and its margin normal tissue can be clearly identified via fluorescence (550 nm) imaging from 4 to 24 h post-injection. After i.v. injection of the theranostic agent followed by 808 nm laser irradiation, the 4T1 tumor was suppressed, and no significant body weight loss was observed.	Huang et al., 2014
Ferritin	Gd-HPDO3A-apoferritin-curcumin	MR imaging-guided targeting chemotherapy	The theranostic agent induced MR contrast is stronger in MCF-7 cells than in MDA-MB-231cells. The theranostic agent have a significant reduction of MCF-7 cell proliferation at a concentration of 97 μg/ml.	Geninatti Crich et al., 2015
Ferritin	Gd-HPDO3A-L-ferritin-curcumin	MR imaging-guided targeting chemotherapy	Although the theranostic agent showed relatively low MRI sensitivity, it can effectively destroy the viability and self-renewal of MDA-MB-231 and TUBO cells spheres *in vitro*, and to induce the regression of TUBO tumor in mice.	Conti et al., 2016
Ferritin	CuS-ferritin	PET and PA imaging-guided PTT	After i.v. injection, the theranostic agent showed admirable U87MG tumor imaging ability, significant U87MG tumor inhibition as well as low toxic side effects.	Wang et al., 2016b
Ferritin	L-ferritin decorated PLGA for the delivery of paclitaxel and Gd based MRI agent	MR imaging-guided targeting chemotherapy	The theranostic agent can generate sufficient MRI contrast and an increased cytotoxicity against the SCARA5 receptors over-expressed cancer cells.	Turino et al., 2017
Gelatin	Gelatin-iron oxide core/CaP-DOX NPs	pH-responsive theranostics agent for MR imaging-guided chemotherapy	The NPs showed efficient MR contrast and efficient cell uptake toward HeLa cells.	Li et al., 2013
Gelatin	Fe_3O_4@gelatin conjugating FITC and Pt(IV) prodrug	Enzyme-stimulated theranostics agent for chemotherapy, MR imaging and fluorescence sensor	The IC_{50} value of the theranostic agent is much lower than free Pt(IV) prodrug. Significant enhancement in MR signals was observed at the tumor site after *in situ* injection of the theranostic agent.	Cheng et al., 2014
Gelatin	Angio-DOX-dendrigraft poly-lysine-gelatin	Simultaneous cancer-targeted fluorescent imaging and chemotherapy	The theranostic agent showed good targeting efficiency, well penetration ability as well as significantly inhibited 4T1 tumor growth.	Hu et al., 2015
Gelatin	DOX-AuNPs@gelatin	Chemotherapy and intracellular imaging	DOX-based fluorescence allows real-time monitoring of drug uptake, release and distribution in MCF-7 cells. Free DOX is more toxic to MCF-7 cells than DOX-AuNPs@gelatin.	Suarasan et al., 2016
Gelatin	DOX- gelatin-EGCG AuNPs	Enzyme-responsive theranostics agent for real-time monitoring and chemotherapy	The theranostic agent could be effectively tracked by monitoring the recovery of the DOX fluorescence signal and shown significantly inhibit the growth of PC-3 cells.	Tsai et al., 2016
Gelatin	Paclitaxel-loaded gelatin oleic acid superparamagnetic NPs	MR imaging-guided chemotherapy	The NPs can be used as T_2-weighted MRI contrast agents in cancer cells. After the tail vein injection, the NPs have longer systemic circulation time and better anticancer activity than Taxol®.	Tran et al., 2017a,b

(Continued)

TABLE 1 | Continued

Protein	Formulation	Application	Key outcomes of *in vitro*/*in vivo* study	References
Transferrin	DOX-Graphene-SiO_2-coated quantum dots-Tf conjugates	Simultaneous cancer-targeted fluorescent imaging, monitoring and chemotherapy	DOX-based fluorescence allows real-time monitoring of drug release and distribution in HeLa cells. However, the conjugates showed lower toxicity effect than DOX alone on HeLa and HEK293 cell lines.	Chen et al., 2013
Transferrin	PEGylated fluorescent nanodiamond-Tf-DOX	Simultaneous cancer-targeted fluorescent imaging and chemotherapy	It can discriminate L-02 normal cells form HepG2 tumor cells in terms of fluorescence intensity and cytotoxicity.	Wang et al., 2014a
Transferrin	Docetaxel- and ultra bright gold clusters-loaded Tf-TPGS	Simultaneous cancer-targeted imaging and chemotherapy	The theranostic agent showed 71.73 times more potency than Taxotere® after 24 h treatment with MDA-MB-231-luc breast cancer cells. 24 h after the 4th injection on 24th day the fluorescence intensity was not significantly decreased in the tumor, liver and bladder. After i.v. injection of the theranostic agent, the MDA-MB-231-luc tumor was suppressed, and no significant body weight loss was observed.	Muthu et al., 2015
Transferrin	Paclitaxel-loaded Tf-Fe_3O_4/mesoporous silica (core/shell)-Cy7 NPs	Simultaneous cancer-targeted NIR fluorescence/MR imaging and chemotherapy	1 to 24 h after injection, the tumor can be clearly visualized. The NPs showed higher anti-cancer activity on HeLa cells than free PTX.	Jiao et al., 2015
Transferrin	Cy5.5-loaded N-NE3TA-Tf	Targeted iron chelation cancer therapy and NIR fluorescence imaging	The theranostic agent displayed significant inhibitory activity against HeLa, HT29 and PC3 cells, and the NIR fluorescence signals of the theranostic agent can be clearly detected in HeLa, HT29, and PC3 cells.	Kang et al., 2016
Transferrin	Docetaxel- and quantum dots-loaded TPGS-Tf	Brain-targeted imaging and chemotherapy	The theranostic agent can effectively cross the blood-brain barrier and show fluorescence in the brain of rats.	Sonali Singh et al., 2016
Transferrin	Tf-IR780 NPs	NIR imaging and PDT/PTT for Tfr-overexpressed tumors	The CT26 tumor and liver can be clearly visualized at 2 h post-injection, while only the CT26 tumor can be clearly visualized at 12 h post-injection. After injection of the NPs followed by 808 nm laser irradiation, the CT26 tumor was effectively suppressed, and no significant adverse effect was observed.	Wang et al., 2016a
Transferrin	Iron-dependent artesunate-loaded Tf-hollow mesoporous CuS NPs	PA imaging and chemo-phototherapy for Tfr-overexpressed tumors	The NPs can be effectively used for tumor imaging, and peritumoral injection is more conducive to tumor imaging than i.v. injection. After peritumoral injection of the NPs followed by 808 nm laser irradiation, the tumor was effectively suppressed.	Hou et al., 2017
Transferrin	Holo-Tf-ICG	Fluorescence and PA dual-modal imaging and PTT for glioma	The theranostic agent can provide high spatial resolution fluorescence and PA imaging for visualization of the distribution of ICG in subcutaneous- and orthotopic- brain tumors. After i.v. injection of the theranostic agent followed by 808 nm laser irradiation, the U87 tumor was effectively suppressed, and no significant adverse effect was observed.	Zhu et al., 2017
Transferrin	Iron oxide NPs conjugating Tf, TAT peptide and Cy7	Simultaneous cancer cell nuclear targeting, NIR/MR imaging and synchronous PTT	The theranostic agent can be used for the A549 tumor imaging, and the best imaging effect is at about 8 h postinjection. After i.v. injection of the theranostic agent, the A549 tumor was effectively eliminated, and no significant adverse effect was observed.	Peng et al., 2017
Transferrin	Protoporphyrin IX-loaded UCNP@Tf NPs	NIR light induced PDT of cancer cells and luminescence bioimaging	Under 980 nm laser irradiation, the NPs can not only kill MDA-MB-231 cells by PDT, but also show clear bright green in MDA-MB-231 cells.	Wang et al., 2017a
Silk	NIR-797-labeled anti-EGFR-iRGD-PTX-silk fibroin NPs	Fluorescence imaging-guided chemotherapy	In HeLa tumor-bearing mice, the NPs can be used for the tumor and liver fluorescence imaging, and the maximum fluorescence intensity in tumor and liver tissues arose at 24 h post-injection. After tail vein injection of the NPs, the HeLa tumor was eliminated, and no significant adverse effect was observed.	Bian et al., 2016
Silk	Nanodiamonds-silk fibroin-DOX	Fluorescence tracking and chemotherapy	–	Khalid et al., 2016
Silk	DOX-loaded sericin/dextran composite hydrogel	Drug monitoring and chemotherapy	After subcutaneous injection, the photoluminescence of hydrogel is long-term stable in C57BL/6 mice without being quenched. After injection the hydrogel into the vicinity of the B16-F10 tumor, the tumor was effectively suppressed, and no significant differences in body weight were observed.	Liu et al., 2016

(Continued)

TABLE 1 | Continued

Protein	Formulation	Application	Key outcomes of *in vitro*/*in vivo* study	References
Zein	Cy5-labeled hydroxycamptothecin @AuNPs-Zein-folate-conjugated polydopamine	Active targeting in drug delivery and cell imaging	The increase of fluorescence signals from the KB tumors was accompanied by the sharp decline in normal tissues at 3 h post injection, and the fluorescence signals at the tumor remains basically constant within 24 h. After i.v. injection of the theranostic agent, the KB tumor was effectively eliminated, and no acute toxicity was observed.	Wang et al., 2017b
Lipoprotein	Boron/Gd agent lipoprotein adducts	MRI/Boron Neutron Capture Therapy	After i.v. injection of the adducts, high MRI signal intensity was observed in the liver and in the tumor region. 30-40 days after neutron irradiation, the tumor growth of mice was negligible.	Alberti et al., 2015
Lactoferrin	Zinc-doped Fe_3O_4-saturated bovine lactoferrin	Real-time cancer imaging and simultaneous cancer-targeted therapy	Orally fed the theranostic agent gave a bright dark (T_2) contrast at the Caco2 tumor site. Oral administration of the theranostic agent exhibited significant antitumor efficacy and a nontoxic and biocompatible nature in the human breast cancer and xenograft colon tumors.	Kamalapuram et al., 2016
Lactoferrin	Fe_3O_4 -saturated bovine lactoferrin	Real-time imaging and monitoring the effect of drugs in real time	Oral administration of the theranostic agent exhibited significant antitumor efficacy in the human breast cancer tumor.	Kanwar et al., 2016

fluorescence quantum yield at 600 nm excitation and an even high absorbance whereas low fluorescence quantum yield under 808 nm excitation, showing a great performance in NIR imaging and PTT at separated wavelengths. A gadolinium was further fabricated on HSA-IR825 for dual-modal imaging-guided PTT of tumor in a follow-up study (**Figure 2B**) (Chen et al., 2014a). In this work, HSA was conjugated with the Gd(III) compound of diethylenetriamine pentaacetic acid, and further complexed with IR825, to form HAS-Gd-IR825 complex. The HAS-Gd-IR825 complex has great fluorescence and NIR absorbance, impressive T_1 relaxivity of 4.82 mM^{-1} s^{-1}. More recently, a gemcitabine functionalized HSA-IR780 agent was reported for chemotherapy and imaging-guided PTT of tumor (Han et al., 2017). HSA was first conjugated with gemcitabine via cathepsin B cleavable peptide GFLG, and then mixed with IR780 dye at the molar ratio of 1:1. IR780 could bound to HSA via hydrophobic interactions.

For above systems, the NIR dyes were bound to the HSA via non-covalent interactions, possibly causing dye leakage during *in vivo* circulation (Rong et al., 2015). To address this problem, heptamethine CySCOOH dye (a NIR cyanine dye) was covalently conjugated to the lysine residues of HSA (Rong et al., 2015) via a modified EDC/NHS reaction for effective photoacoustic (PA), NIR fluorescence, thermal multimodality imaging and PTT. Such conjugation, compared with free CySCOOH dye under the identical conditions, resulted in higher PTT efficacy, tumor accumulation and longer circulation. Moreover, the maleimide group can be rapidly and selectively bound to the Cys34 residue of HSA via a Michael addition reaction. Recently, the Michael addition reaction was employed to couple fluorescent dye Cy7 to Cys34 position of HAS (Lisitskiy et al., 2017). And meantime, the chemotherapeutic agent pTFT (5-trifluoromethyl-2′-deoxyuridine 5′-monophosphate) was coupled to lysine residues of HSA via a redox and pH dual-sensitive linker. The conjugates could not only serve as an optical and ^{19}F MR imaging, but also be applied for delivery of chemotherapeutics.

HSA-Based Complexes

HSA has an effective diameter of 7.2 nm. Yet nanocarriers with sizes of 100-200 nm are well known to tend to accumulate in tumor tissues more efficiently via the enhanced permeability and retention (EPR) effect (Peer et al., 2007). Besides, theranostic agents usually require more functional ingredients to expand the application. Accordingly, great efforts have been devoted to design HSA-based complexes with appropriate sizes and more characteristics, to establish multifunctional HSA-based theranostics. For example, melanin and paclitaxel (PTX)-loaded HSA nanoparticles (HMP-NPs) with size of ca. 192 nm were fabricated with a desolvation-crosslinking method (Mo et al., 2007; Sim et al., 2015). The HMP-NPs showed effective PA signal intensity in the tumor site and the capability to tumor chemotherapy with long circulation time, as confirmed by *in vivo* experiments. In addition, the desolvation-crosslinking method was adopted to form HSA-based NPs (Pt(IV)-probe@HSA) for theranostic application (Li et al., 2015). In this work, the HSA NPs surface were conjugated with Pt(IV) antitumor prodrug, NIR fluorophore Cy5, and quencher Qsy21. The Pt(IV)-probe@HSA can not only selectively trigger the localized activation of Pt(IV) prodrug, but also enable real-time tumor cell imaging with high resolution.

For the above systems, glutaraldehyde is employed to stabilize the HSA NPs, whereas possible aldehyde residue may cause some side effects for *in vivo* applications (Fürst and Banerjee, 2005). To address this problem, some facile methods involving no toxic chemicals or exogenous cross-linkers have been broadly adopted in the preparation (Sheng et al., 2014; Hu et al., 2016). As an example, HSA-ICG NPs was developed with an average hydrodynamic diameter of nearly 75 nm based on the intermolecular disulfide bond cross-linking within HSA, for imaging-guided PDT and PTT treatments (Sheng et al., 2014). In this work, they first broke up the intramolecular disulfide bonds of HSA with the endogenous reducing agent glutathione, and then fabricated the HSA NPs with a desolvation method. A

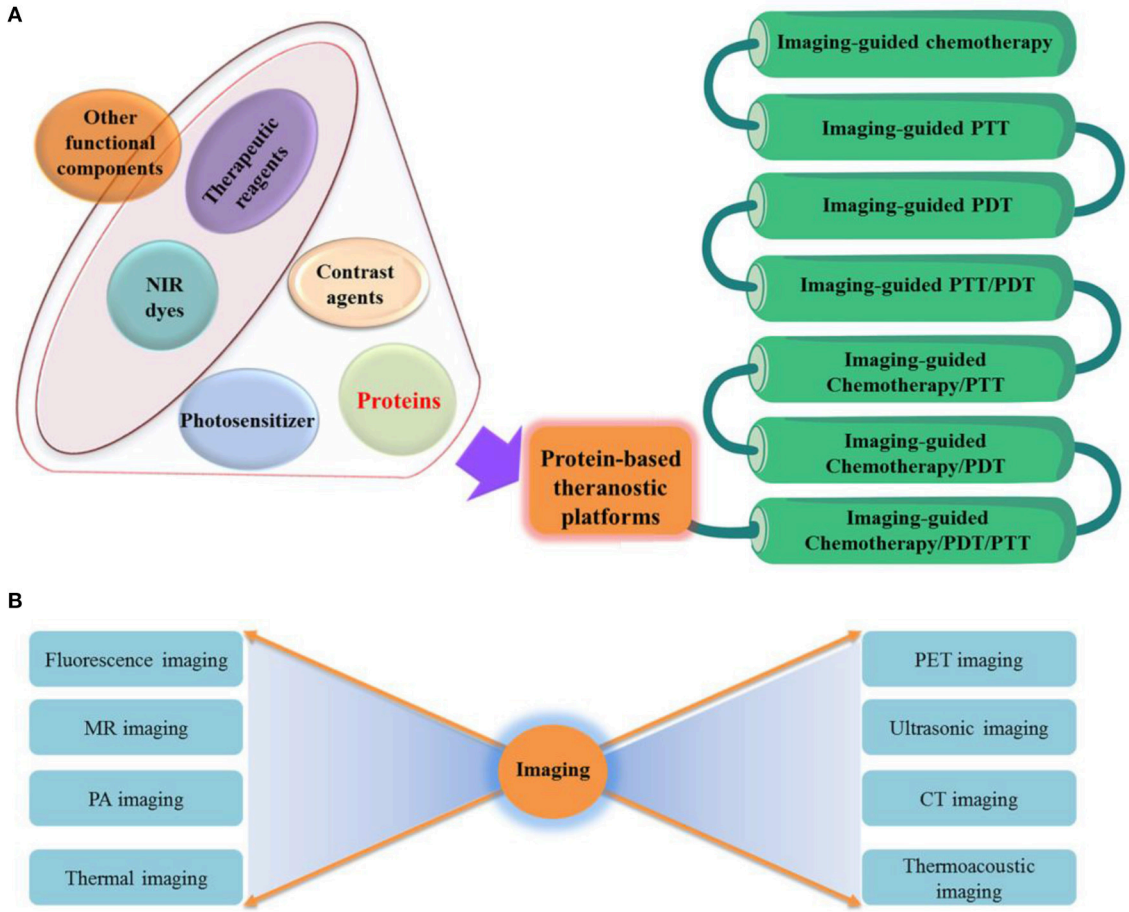

FIGURE 1 | (A) Engineering of protein-based nanoformulations as cancer theranostic platforms. **(B)** A series of imaging technologies are incorporated in the theranostic platforms.

similar strategy was also adopted in their recent work to fabricate HSA nanoassemblies (NAs) with photosensitizer chlorin e6 (HSA-Ce6 NAs) for multi-modal imaging-guided PDT (Hu et al., 2016). The proposed HSA-Ce6 NAs had a diameter of ca. 100 nm, excellent tumor selectivity, promising triple-modal (fluorescence, PA and MR) imaging, and effective PDT properties.

Another method proposed by Liu's group not introducing exogenous cross-linkers is to fabricate HSA-based multifunctional theranostic NPs with drug-induced protein assembly strategy (Chen et al., 2015a). In this work, a multifunctional "Abraxane-like" theranostics agent was formulated through simply incorporating three clinical approved agents, ICG, PTX and HSA together (**Figure 2C**). In this formulation, the NIR fluorescence imaging, thermal imaging, PTT and chemotherapy were efficiently combined. Accordingly, a synergistic therapeutic effect is demonstrated in treating metastatic and subcutaneous breast tumors. As a result, the strategy is enriched to design tumor-targeted theranostics agent for multimodal imaging-guided therapy of tumors (Chen et al., 2015b). HSA is pre-modified in their design, with either a tumor-targeting acyclic Arg-Gly-Asp (RGD) peptide (HSA-RGD) or a photosensitizing agent Ce6 (HSA-Ce6). The anticancer drug PTX is then employed to induce the self-assembly of HSA-RGD and HSA-Ce6 to fall into two different NPs. After incorporation of manganese(II), both of NPs could be tracked by MR imaging and fluorescence imaging, which can be adopted for combinatorial cancer PDT and chemotherapy. Similarly, photosensitizer agent iron (II) phthalocyanine (FePc)-induced HSA self-assembly, is employed in a recent study to fabricate multifunctional HSA-FePc NPs for PA imaging-guided PTT (Jia et al., 2017). The as-prepared HSA-FePc NPs exhibited high stability, high PA imaging quality, efficient PTT treatment, and low long-term toxicity *in vivo*.

HSA-Coated Complexes

PTX-loaded HSA NPs were conjugated to the surface of porphyrin microbubbles for cancer theranostics (Moon et al., 2015). In this system, porphyrin microbubbles were fabricated using porphyrin-phospholipid conjugates to simultaneously intensify ultrasound and PA signal. The developed multifunctional theranostics agent is high sensitive in PA and ultrasound imaging, and effective in delivery

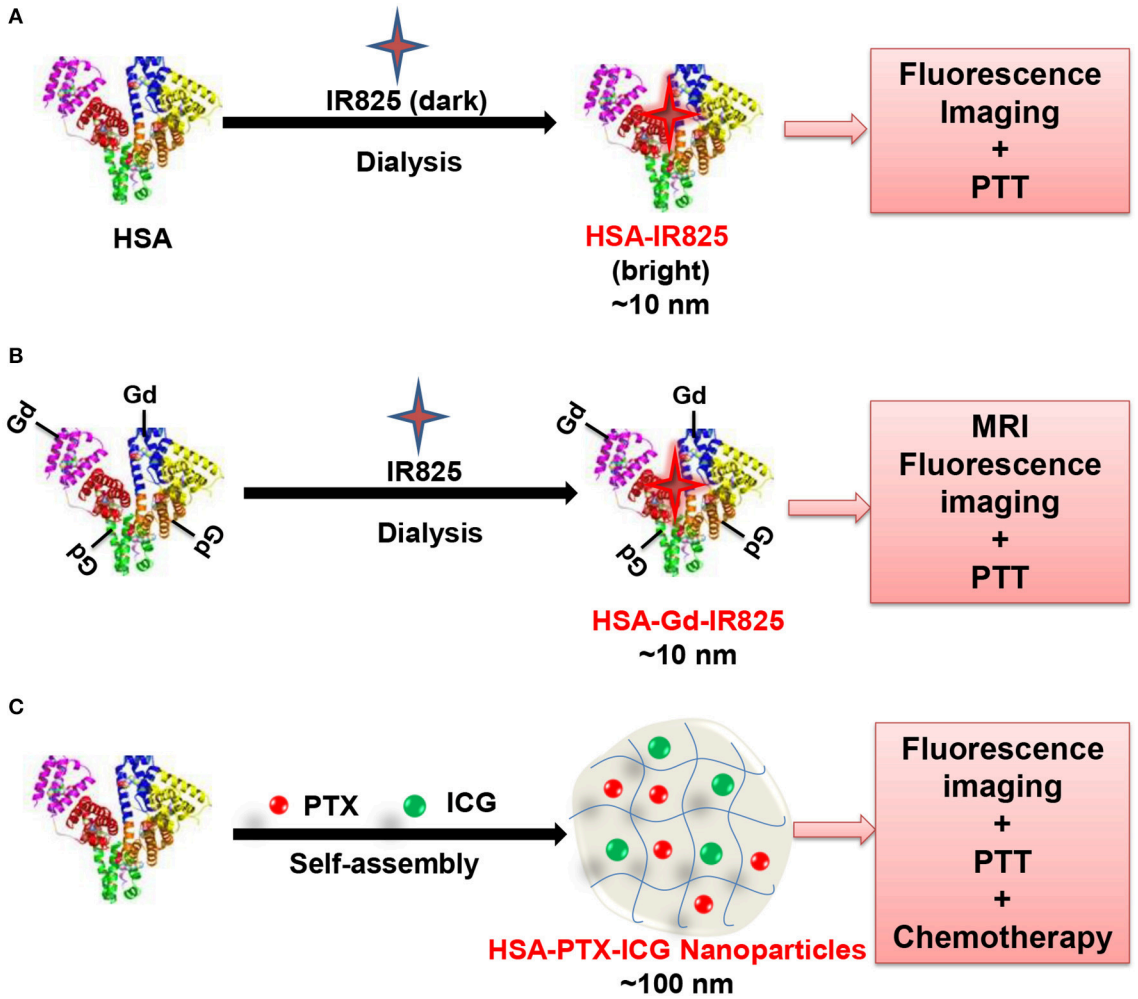

FIGURE 2 | Schematic illustration of the fabrication of HAS-IR825 complex **(A)** (Chen et al., 2014c), HAS-Gd-IR825 complex **(B)** (Chen et al., 2014a), and HSA-ICG-PTX nanoparticles **(C)** (Chen et al., 2015a).

of anticancer drug PTX to a tumor site. HSA-coated superparamagnetic iron oxide NPs were presented more recently, which can absorb pulsed microwave energy and transform efficiency into shockwave with the thermoelastic effect besides using as MR contrast agents (Wen et al., 2017).

BSA for Cancer Theranostics

Individual BSA–Dye Complexes

BSA consists of multiple hydrophobic binding sites, and can naturally serve as a carrier of numerous small NIR dyes agents. Squaraine (SQ) was selectively bound to hydrophobic domain of BSA via hydrogen bonding and hydrophobic interactions with 80-fold enhanced fluorescence intensity (Gao et al., 2014). Based on this, a supramolecular adducts of SQ and BSA (SQ@BSA) was constructed and served as PTT agent and effective bioimaging probe simultaneously. In addition, folic acid (FA) functionalized SQ@BSA (SQ@BSA-FA) has additional functions, e.g., monitoring the time-dependent bio-distribution of adducts and targeting tumor sites. ICG, an FDA-approved NIR dye, can be adsorbed on BSA for NIR fluorescence imaging, PTT and PDT as excited by single-wavelength (Chen and Liu, 2016). Besides, BSA-based theranostics system covalently modified with NIR dyes has been reported (Lee et al., 2016). For example, a zinc-coordinated pH-sensitive theranostics agent is reported, consisting of two types of polyethylene glycol-BSA-imidazole covalently modified with either BHQ-3 quencher (NIR dark quencher) or Cy5.5 dye (donor NIR dye). At pH 5.0 (e.g., endo/lysosomes in cancer cells), the theranostics agent was disassembled rapidly, and emitted strong NIR fluorescence (Lee et al., 2016).

BSA-Based Complexes

Besides bound to NIR dyes, BSA can be further engineered with other functional agents via complexation, such as gadolinium (Wei et al., 2016; Yang et al., 2016; Chen et al., 2017a; Zhou et al., 2017), manganese (Liu et al., 2017; Pan et al., 2017) and graphene's derivatives (Sheng et al., 2013). For

example, hollow BSA was employed to fabricate a size-tunable Gd_2O_3@BSA conjugating Ce6 theranostics agent for MR imaging-guided PDT and PTT (**Figure 3**) (Zhou et al., 2017). Notably, the BSA nanoreactor can not only effectively regulate the longitudinal relaxivity of Gd_2O_3, but conjugate readily with photosensitizers. A facile strategy is presented, adopting BSA as a biotemplate at physiological temperature, to construct a biocompatible Gd-integrated CuS multifunctional theranostics agent (Gd:CuS@BSA) (Yang et al., 2016). The fabricated Gd:CuS@BSA theranostics agent possessed ultrasmall sizes (about 9 nm), acceptable longitudinal r_1 relaxivity of 16.032 $mM^{-1}{\cdot}s^{-1}$, impressive temperature rise and intense PA signals under NIR irradiation. Recently, a multifunctional MoS_2-Gd-BSA theranostics agent was fabricated through incorporating the good photothermal effect of MoS_2 nanoflakes with the high longitudinal proton relaxivity of BSA-Gd complex via the amine reaction between carboxyl groups of MoS_2 nanoflakes and amino groups of BSA-Gd (Chen et al., 2017a). The MoS_2-Gd-BSA theranostics agent exhibits a strong NIR absorbance and high r_1 relaxivity, which are helpful for PA and T_1-weighted MR dual-modal imaging-guided PTT of cancer. Besides, a chemotherapeutic drug carmustine-encapsulated FITC-BSA NPs were prepared by desolvation/denaturation method and conjugated with a MR gadolinium(III) salt to form nanomedicine with dual imaging modalities (Wei et al., 2016).

At the identical stage, contrast agent Mn-based BSA complexes have been also reported for cancer theranostics (Liu et al., 2017; Pan et al., 2017). For example, a multifunctional BSA-MnO_2 theranostics agent was fabricated via a mimicking drug-substrate interaction strategy, adopting BSA as both reductant

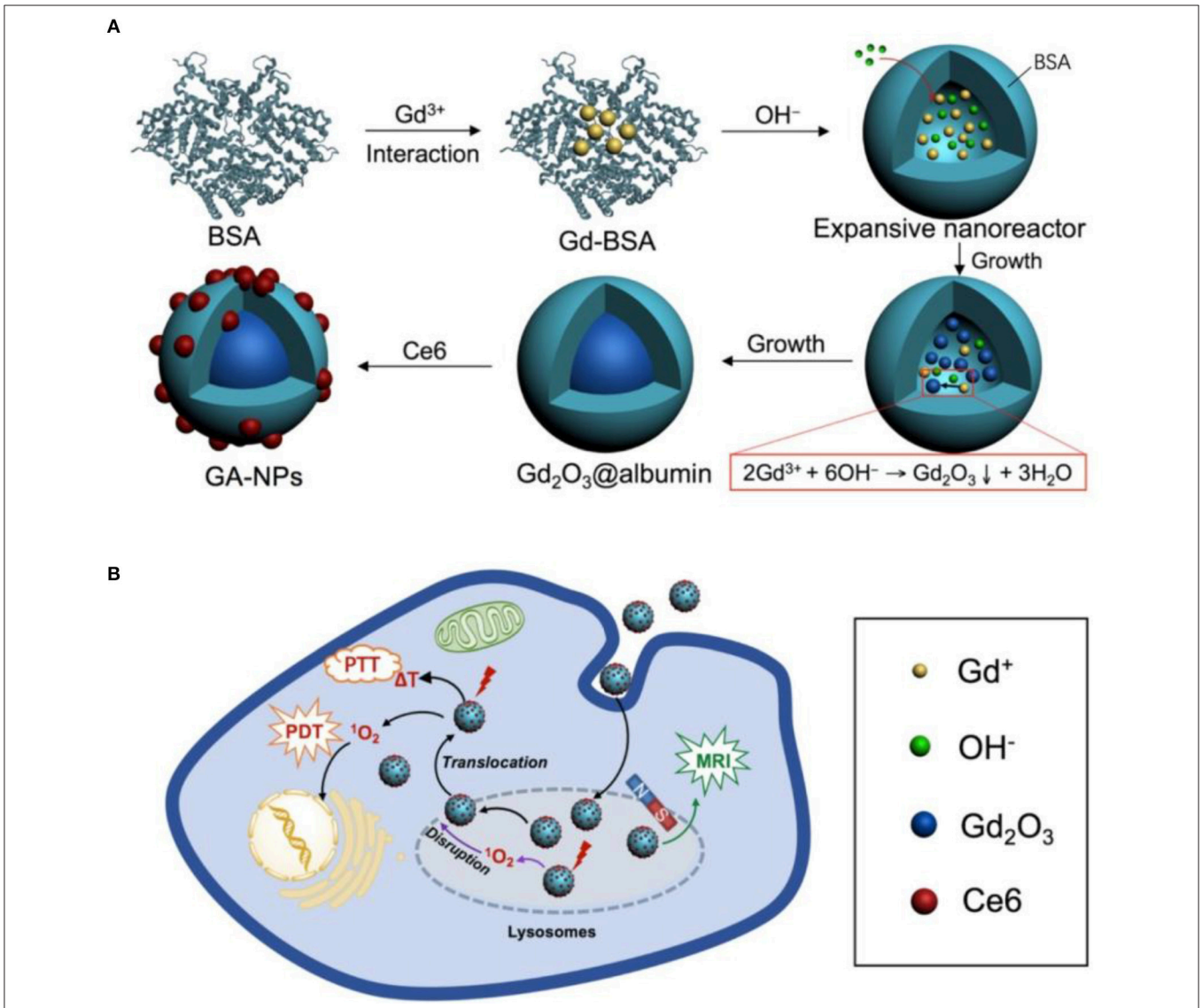

FIGURE 3 | Schematic illustration the synthesis of core-shell Gd_2O_3@BSA conjugating Ce6 **(A)** for MRI-guided cancer photothermal therapy (PTT) and photodynamic therapy (PDT) **(B)**. Reproduced with permission (Zhou et al., 2017).

agent and template (Pan et al., 2017). It is noteworthy that ICG and PTX can be loaded on BSA-MnO_2 with a facile and energy-saving mixing. The ICG/PTX-loaded BSA-MnO_2 theranostics agent could be adopted for MR imaging guided PTT and chemotherapy *in vitro* and *in vivo*.

Furthermore, a BSA-assisted synthesis route was developed to produce reduced graphene oxide (nano-rGO) theranostic agent (Sheng et al., 2013). The BSA functionalized nano-rGO displayed a high stability and low cytotoxicity, enabling PA imaging and PTT treatment without further surface modification. On that basis, a folate receptor active-targeted, pH-responsive BSA-pheophorbide-a (PheoA) photosensitizer incorporated GO nanocarrier (PheoA + GO:FA-BSA-c-PheoA NC) is developed as an theranostic agent (Battogtokh and Ko, 2016). The theranostic agent carries a good pH-responsive photosensitizer and generates a synergistic PTT and PDT effect against tumor by NIR irradiation.

BSA-Coated Complexes

BSA serves not only as a delivery platform to load various functional molecules, e.g., dyes and chemotherapy drugs, but also as a coating agent of other nanocarriers to increase the physiological stability, water-solubility and blood circulation time of theranostics systems. For example, BSA is employed to coat $NaGdY_4$-based upconversion NPs (UCNPs), resulting in UCNP@BSA NPs possessing well stability and water-solubility in physiological environments (Chen et al., 2014b). And meantime, two different dyes, consisting of an IR825 dye and a Rose Bengal (RB) photosensitizer, can be effectively loaded onto the BSA shell layer of the UCNP@BSA system. It is noteworthy that the characteristic absorbance peak of RB complies well with the green emission peak of UCNPs (980 nm excitation), which effectively kills cancer cells by PDT. Therefore, the dual-dye loaded theranostics agent can be adopted for MR diagnostic, upconversion optical imaging, PDT as well as PTT both *in vitro* and *in vivo*. BSA-coated magnetite Fe_3O_4 core-shell structures with anticancer drug (gemcitabine) were developed, where BSA serving as the outer shell was further functionalized by the active targeted agent Anti-EGFR mab C225 (Wang et al., 2015). The theranostics agent can efficiently regulate double-targeted thermochemotherapy against pancreatic tumor, monitor different cellular targeting by MR imaging, and distinguish various EGFR-expressing pancreatic tumor cells. On that basis, a BSA-coated magnetite Fe_5C_2 theranostics agent was developed with a high loading of antitumor drug doxorubicin (DOX) (Yu et al., 2016). Notably, the DOX can be released in acidic condition and irradiated by NIR. In this regard, the theranostics agent serves as a smart nanoplatform for MR imaging, effective chemotherapy and PTT. A pH-responsive protein–polymer bioconjugate-coated theranostics agent consisting of a superparamagnetic magnetite Fe_3O_4 core, BSA–poly(ethylene glycol) (PEG) shell and anticancer drug DOX were presented for combined MR imaging diagnostics and chemotherapy (Semkina et al., 2015). A BSA–poly(ε-caprolactone) bioconjugate-coated upconversion theranostics agent is constructed with the similar preparation method for simultaneous cancer cell imaging, PDT, and chemotherapy (Dong et al., 2016). BSA stabilized Prussian blue (PB) NPs were fabricated, and ICG molecules were further attached non-covalently by a biocompatible and simple method (Sahu et al., 2016). Here, PB serves as a MR contrast enhancer. Accordingly, the multifunctional theranostics system could provide dual mode MR signal and NIR fluorescence imaging as well as combined therapy with PDT and PTT. A pH-responsive Au–BSA core/shell theranostics agent consisting of Au core, BSA shell that conjugated with DOX and FA was developed recently, which manifested tumor computed tomography (CT) imaging application and targeted cancer therapy (Huang et al., 2017).

Albumin-based NPs could be synthesized by using albumin as a scaffold, template, or stabilizer, and conjugating to polymers, drugs, and contrast agents. Covalent and non-covalent conjugation or assembly were employed. Due to the success of Abraxane, researchers preferred the non-convalent self-assembly. However, NPs prepared using the non-convalent strategy will vary batch to batch, which need to be overcome in the future studies (An and Zhang, 2017).

FERRITIN-BASED NANOFORMULATIONS

Ferritin and Its Properties

Ferritin counts as an abundant protein in circulation, existing in intracellular and extracellular compartments. Ferritin is a 450 kDa hollow nanocage with internal and external dimensions of 8 and 12 nm, respectively (Banyard et al., 1978). It accumulates and stores approximately 4,500 iron atoms in a non-toxic whereas bioavailable form (Alkhateeb and Connor, 2013). In mammals, each ferritin protein consists of 24 subunits self-assembled into a spherical symmetrical protein shell (Alkhateeb and Connor, 2013). The ferritins from eukaryotes are produced by self-assembly of two subunit types, i.e., L-ferritin chain (19 kDa) and H-ferritin chain (21 kDa). The H-chain is centered by an iron oxidase center, required to oxidize Fe(II) to Fe(III), whereas the L-chain without ferroxidase activity nucleates iron (Bellini et al., 2014). Ferritin counts as a multifunctional protein with iron storage and metabolism. Ferritin is critical for angiogenesis, proliferation and immunosuppression, as demonstrated by growing number of evidence (Alkhateeb and Connor, 2013).

Ferritin is a ubiquitous protein robust extremely: it can be reversibly disassembled in the extremely acidic pH (pH 2–3) or basic pH (pH 10–12) and can be heated at 80°C exerting no deleterious effects (Truffi et al., 2016). These properties as well as its biocompatibility and biodegradability make it a suitable candidate for cancer theranostics (Bhushan et al., 2014).

Ferritin for Cancer Theranostics

The ferritin not only provides a reaction vessel to fabricate numerous non-native metallic NPs inside its core, but also serves as a nanocarrier for various applications (Bhushan et al., 2014). For example, Zn hexadecafluorophthalocyanine ($ZnF_{16}Pc$), a potent hydrophobic photosensitizer, is well encapsulated into the Cys-Asp-Cys-Arg-Gly-Asp-Cys-Phe-Cys (RGD4C)-modified ferritins (P-RFRTs) with a loading rate as high as ∼60 wt % for effective PDT (Zhen et al., 2013b). The P-RFRTs were further conjugated with ZW800 (a NIR dye molecule) in this work to better track P-RFRTs particles. With the identical

approach, the DOX-loaded RGD4C-modified ferritin was also reported (Zhen et al., 2013a). A self-assembly encapsulation strategy based on step-wise change of pH was developed in another report to fabricate ferritin NPs with NIR dye IR820 for fluorescence/PA multimodal imaging-guided PTT (Huang et al., 2014). The IR820-loaded ferritin nanocages can effectively treat and diagnose cancer adopting two different excitation wavelengths, i.e., 550 nm for high quantum-yield fluorescence imaging, and 808 nm for PA imaging and effective PTT. Additionally, CuS was fabricated inside the cavity of ferritin nanocages with a biomimetic and straightforward synthesis strategy (Wang et al., 2016b). The CuS-ferritin has strong NIR absorbance, high photothermal conversion efficiency, good biocompatibility and distinct PA contrast,. Notably, the ^{64}CuS-ferritin theranostic system, as incorporated with radionuclide ^{64}Cu, also served as an excellent PET imaging agent.

The higher level of L-ferritin in tumor versus normal tissue has been observed in some malignancies tissues like breast cancer, colon cancer, pancreatic cancer and testicular seminoma (Alkhateeb and Connor, 2013). High amount of L-ferritin is usually associated and bound with intensified expression of the L-ferritin receptor that mediates ferritin endocytosis. The higher the expression of L-ferritin receptors, the more intensified uptake of L-ferritin in breast cancer MCF-7 cells (Geninatti Crich et al., 2015). Based on this, a ferritin-based nanotheranostic system has been further developed to simultaneously deliver a MR contrast agent GdHPDO3A and a natural anticancer molecule curcumin (Geninatti Crich et al., 2015). The theranostics system selectively delivered therapeutic and imaging agents to breast cancer cells. In a follow-up study, L-ferritin was found to target breast cancer stem cells (Conti et al., 2016). In this regard, ferritin was further exploited to deliver curcumin and the GdHPDO3A MR contrast agent simultaneously for breast cancer stem cells (Conti et al., 2016). In a very recent report (Turino et al., 2017), multifunctional theranostics system was developed through coating poly (lactic-co-glycolic acid) NPs (PLGA NPs) with L-ferritin to increase their targeting capability to breast cancer MCF-7 cells. The L-ferritin functionalized PLGA NPs loaded with an amphiphilic Gd based MR contrast agent and PTX for MR imaging guided chemotherapy. In addition to this, ferritin coating makes PLGA NPs more stable, thus avoiding the non-specific and fast release of therapy/diagnosis agents before reaching the targeted sites.

Hollow structure make the ferritin become an ideal carrier, however, after loading therapeutic agents, the slight change in conformation and activity might take place. The toxicity of ferritin-based NPs should be studied carefully as other NPs. Also, the surface-modified ferritins may be recognized as foreign substances. Therefore, when surface targeting ligands were needed, the grafting density are important factors to be considered.

GELATIN-BASED NANOFORMULATIONS

Gelatin and Its Properties

Gelatin is a polyampholyte protein having both anion and cation along with hydrophobic groups (Elzoghby, 2013). Gelatins have repeating sequences of proline, alanine, and glycine amino acid triplets, which are essential for gelatin (Sahoo et al., 2015). They are obtained from alkaline-, acid- or enzymatic- hydrolysis of collagen. These chemically treated gelatins have varying isoelectric points, i.e., 4.5–6.0 for alkaline treatment and 7–9 for acid treatment (Patel et al., 2008; Ninan et al., 2011). In addition, anticancer agent release profiles from gelatin protein can be controlled through changing the molecular weight, gelatin source and the crosslinking degree (Foox and Zilberman, 2015). Gelatin is natural, biocompatible, biodegradable, water permeable, non-toxic, and soluble in water (Nezhadi et al., 2009). As a delivery carrier of therapeutic/diagnostic agents, gelatin has been revealed multifunctional properties, enabling the development and design of versatile theranostics.

Gelatin for Cancer Theranostics

Gelatin has native hydrophobic and hydrophilic segments in each single polypeptide chain, enabling itself a conducive coating agent for various metal NPs (Li et al., 2013; Cheng et al., 2014; Tran et al., 2017b). For example, a theranostic system was developed through coating iron oxide NPs with self-assembled gelatin (abbreviated as AGIO) (Li et al., 2013). In the meantime, calcium phosphate (CaP) and anticancer DOX could be loaded on gelatin by electrolytic co-deposition technique. The fabricated AGIO@CaP-DOX NPs had efficient MR contrast, superior cytocompatibility and potent cellular internalization toward HeLa cells. A gelatin coated multifunctional nanosystem, with oleylamine-coated Fe_3O_4 NPs core, amphiphilic gelatin shell, and fluorescent labeling molecules FITC and antitumor platinum(IV) prodrug, was elaborated for fluorescence and MR imaging guided chemotherapy (Cheng et al., 2014). Most recently, oleic acid and gelatin were adopted to modify a silica-coated iron oxide magnetic NPs, which was demonstrated to encrease biocompatibility and solubility of iron oxide magnetic NPs and facilitate treatment-response monitoring of the tumors (Tran et al., 2017b). Particularly, the oleic acid and gelatin coated NPs enables the hydrophobic anticancer drug PTX to be loaded into the lipophilic oleic acid-gelatin shell. The synthesized theranostic system have high r_2 value, low cellular toxicity, high drug delivery efficacy and well anticancer efficacy *in vitro*. The pharmacokinetics, bio-distribution, tumor diagnostic and antitumor efficacy of the theranostic system *in vivo* were studied in a follow-up study to further confirm its potential in clinical applications (Tran et al., 2017a).

Beside iron oxide NPs, gold NPs are commonly coated with gelatin to increase their stability and biocompatibility. For example, a gelatin-coated gold NP-based nanostructure was developed for fluorescence imaging-guided chemotherapy (Tsai et al., 2016). The gelatin was firstly covalent conjugated with DOX, and then coated onto the epigallocatechin gallate (EGCG)-functionalized Au NPs. Here, DOX serves both as an anticancer drug and a fluorescent indicator. The attained DOX-gelatin/EGCG Au NPs exert an apparent inhibitory effect on the proliferation of human prostate cancer cells (PC-3) and can trace the intracellular enzyme-induced release of DOX through measuring the recovery of the DOX fluorescence signal. The covalent conjugation of DOX to nanocarriers may

cause problems, e.g., insufficient *in vivo* release and decreased drug activity (Suarasan et al., 2016). A new temperature- and pH-responsive theranostic system was developed on the basis of DOX non-covalently bound to biosynthesized gelatin-coated Au NPs (DOX-AuNPs@gelatin) (Suarasan et al., 2016). The fabricated DOX-AuNPs@gelatin would be an ideal agent for cancer theranostics based on its good biocompatibility, high DOX loading capacity via non-covalent complexation and effective DOX release under the tumor environment.

Recently, angiopep-2 modified gelatin-based core-shell NPs (Angio-DOX-DGL-Gel-NP) have been designed to increase the tumor targeting efficiency, tumor retention and tumor penetration (Hu et al., 2015). In this system, the shell consisted of dendrigraft poly-lysine linked with angiopep-2 and DOX, whereas the core was made up of gelatin NPs degraded by matrix metalloproteinase-2. Fluorescence imaging-guided chemotherapy showed enhanced antitumor effects *in vitro* and *in vivo*,

Gelatins are used as carriers in versatile drug delivery systems, form nanoparticles to microparticles (Foox and Zilberman, 2015). Small drug molecules or large bioactive molecules were easily entrapped into gelatins and released in a controlled manner. However, the cancer theranostic platforms based on gelatin didn't attract much attention. In our opinion, the gelatin-based NPs are promise cancer theranostics, especially in oral administration and brain delivery.

TRANSFERRIN-BASED NANOFORMULATIONS

Transferrin and Its Properties

Transferrin is a monomeric glycoprotein with 679 amino acids and a large molecular weight of approximately 79 kDa (Parkkinen et al., 2002; Gomme et al., 2005). The molecule is protected by 3 carbohydrate side chains, one of which is O-linked (Ser-32) and the other are N-linked (Asn-413 and Asn-611) (Gomme et al., 2005). The polypeptide chain falls into two structurally similar lobes, known as the C-lobe (343 amino acids) and N-lobe (336 amino acids), which are connected by a short linear spacer sequence (Brandsma et al., 2011). Each lobe consists of one reversibly binding site for ferric iron with nearly 10^{22} M^{-1} affinity at pH 7.4 (Aisen et al., 1978). The major biological function of transferrin is to distribute and control circulating Fe, which is required for numerous biological processes, including cellular metabolism and proliferation, DNA synthesis, electron transfer, and oxygen transport (Dufès et al., 2013; Tortorella and Karagiannis, 2014). Particularly, transferrin specifically binds transferrin receptors (TfRs) on cell surface, forming a transferrin-TfR complex, and gets internalized by receptor-mediated endocytosis (Szoke and Panteghini, 2012; Dufès et al., 2013). Meantime, overexpression of TfRs has been observed in various cancer cells, including breast carcinoma, glioblastoma, melanoma, ovarian carcinoma and colon carcinoma (Calzolari et al., 2007; Tros de Ilarduya and Düzgüneş, 2013).

Transferrin for Cancer Theranostics

As a promising tumor targeting ligand, transferrin is frequently adopted to facilitate targeting delivery of theranostics. For example, transferrin–functionalized graphene quantum dots were developed to track and image tumor cells expressing the TfRs (Chen et al., 2013). In the meantime, the anticancer drug, DOX, was adsorbed on graphene surface in the system via hydrophobic interactions and π-π stacking, which could be used for fluorescence imaging-guided chemotherapy. Another transferrin-conjugated PEGylated fluorescent nanodiamond with Dox payload was developed, and its targeting ability and chemotherapeutic potential were investigated in the human hepatoma (HepG2) cell lines with overexpression of TfRs and normal cell lines (L-02) with low-expression of TfR, respectively (Wang et al., 2014a). A transferrin conjugated theranostic micelles of D-alpha-tocopheryl PEG 1000 succinate (TPGS) were synthesized, containing both ultra-bright gold clusters as a model imaging agent and docetaxel as anticancer drug for synchronous cancer imaging and therapy (Muthu et al., 2015). The transferrin conjugated micelles, compared with the non-transferrin functionalized theranostic micelles, showed higher cellular uptake, higher cytotoxicity in MDA-MB-231-luc breast cancer cells. In a follow-up study, a transferrin decorated TPGS coated theranostic liposomes was further developed for targeted co-delivery of quantum dots and docetaxel for imaging-guided chemotherapy of brain cancer (Sonali Singh et al., 2016). Indeed, the transferrin decorated theranostic liposomes, compared with the non-transferrin targeted preparations, showed an improved and prolonged brain targeting of quantum dots and docetaxel. In addition, rattle-type theranostic NPs of mesoporous silica-coated Fe_3O_4 were develop by conjugating transferrin for targeted co-delivery of NIR dye (Cy7) and hydrophobic anticancer drug PTX for NIR/MR bimodal imaging guided chemotherapy (Jiao et al., 2015).

Recently, transferrin and nuclear-targeted TAT peptide (YGRKKRRQRRR) conjugated magnetic NPs were proposed for PTT application (Peng et al., 2017). Magnetic NPs is pre-conjugated with transferrin and TAT peptide, and then bound to NIR dye Cy7. The theranostic system can efficiently target cancer cell nucleus and facilitate the NIR and MR imaging-guided PTT. A core-shell theranostic system UCNP core ($NaYF_4$:Gd^{3+}, Yb^{3+}, Er^{3+}) was developed, taking advantage of efficient NIR-to-visible up-conversion capability and increased tumor targeting ability and biocompatibility (Wang et al., 2017a). In the meantime, a clinically approved PTT agent, protoporphyrin IX, was loaded into the transferrin shell, being able to be drawn upon by cancer cells for efficient PDT with NIR irradiation and luminescence bio-imaging. A new strategy (diffusion molecular retention tumor targeting effect) was developed to fabricate tumor-targeted theranostic system for PA imaging-guided chemotherapy/photothermal with synergistic effect (Hou et al., 2017). In this study, hollow mesoporous CuS NPs (HMCuS NPs) were conjugated with transferrin and iron-dependent artesunate (AS), an effective anticancer drug. In this regard, the attained AS/Transferrin-HMCuS NPs facilitated local drug accumulation and retention, targeted to breast cancer MCF-7 cells specially

via TfR-mediated endocytosis, combined chemotherapy-phototherapy synergistically, and eventually improved the anticancer effect.

Transferrin is not only a conducive targeting ligand, but also able to load imaging and/or therapeutic agents. For example, a simple, effective and safe self-assembly strategy was developed to fabricate transferrin NPs with NIR dye IR780 (Transferrin-IR780 NPs) for targeted imaging and phototherapy of cancer (Wang et al., 2016a). The fabricated Transferrin-IR780 NPs had advantages on potent photo-stability, narrow size distribution as well as prominent photothermal conversion efficiency, and exhibited pronounced targeting and theranostics potential. A conjugate of transferrin, NIR dye Cy5.5 and cytotoxic chelating agent (NNE3TA:2,2′-(7-(2-((carboxymethyl)(4-nitrobenzyl)amino)ethyl)-1,4,7-triazonane-1,4-diyl)diacetic acid) (NNE3TA-Transferrin-Cy5.5) was developed to treat and detect cancers (Kang et al., 2016). Targeted iron chelation cancer therapy and NIR imaging were demonstrated effectively *in vitro* with NNE3TA-Transferrin-Cy5.5. Most recently, a drug-induced transferrin self-assembly strategy is developed to fabricate tumor-targeted NPs for fluorescence and PA dual-modal imaging-guided PTT of glioma (**Figure 4**) (Zhu et al., 2017). In this system, transferrin could effectively load ICG via hydrophobic interaction and hydrogen bonding. Specifically, the preparation method is safe, simple and mild without the use of any toxic reagents. The obtained Transferrin-ICG NAs showed effective active tumor-targeting, good biocompability, prominent dual-modal imaging as well as PTT efficacy, and could be adopted for theranostics of both subcutaneous and orthotopic brain tumors.

Notably, transferrin was employed not only as an delivery vehicle but also as a targeting agent in these works. It has been reported than transferrin-functionalized silica NPs lost targeting abilities completely in serum-rich media, due to shielding effects of the adsorbed proteins (Salvati et al., 2013). The bioavailability of the large transferrin determines the targeting functionality in complex biological media. It is a challenge to maintain the targeting efficiency of transferrin-based NPs *in vivo*.

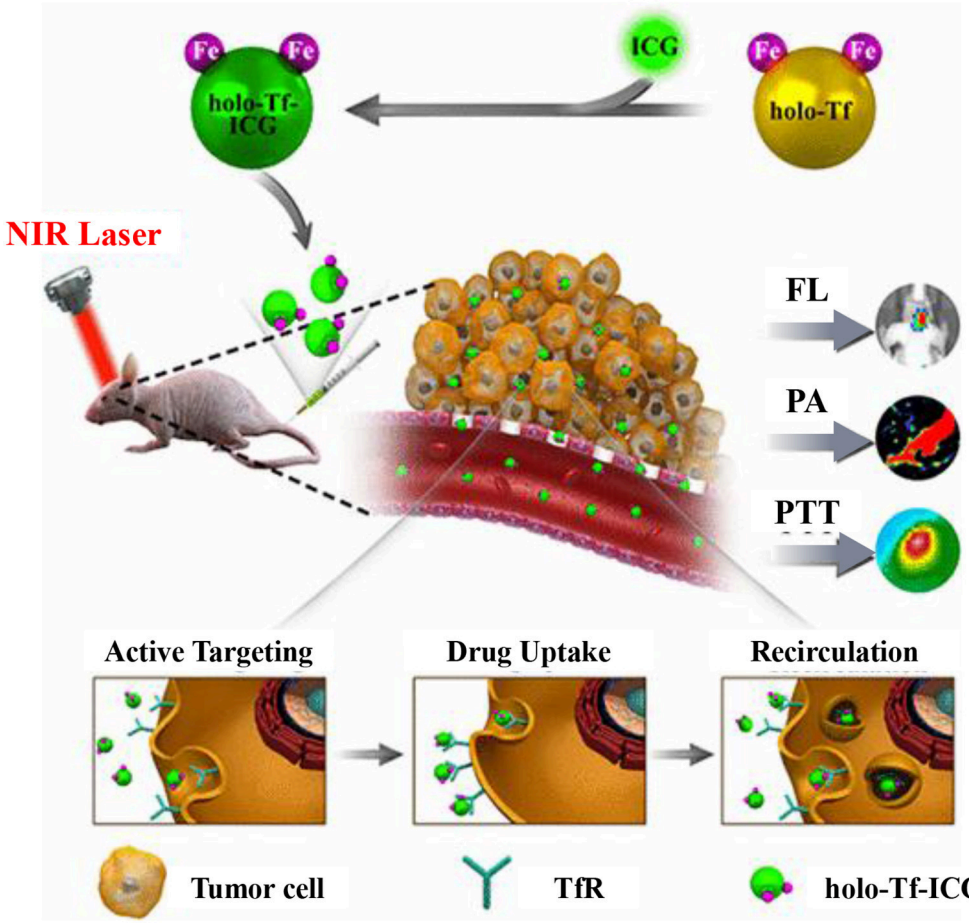

FIGURE 4 | Schematic illustration of holo-Transferrin-ICG complex for dual-modal imaging-guided cancer photothermal treatment *in vivo*. Reproduced with permission (Zhu et al., 2017). Copyright (2017) American Chemical Society.

OTHERS

With the exception of the foregoing proteins, several other proteins, e.g., silk fibroin (Bian et al., 2016; Khalid et al., 2016; Liu et al., 2016), zein (Wang et al., 2017b), lipoprotein (Mathew et al., 2013; Alberti et al., 2015) and lactoferrin (Kamalapuram et al., 2016; Kanwar et al., 2016), have also been successfully employed for cancer theranostics, as detailed in **Table 1**. For instance, multimodular zinc-doped Fe_3O_4-saturated bovine lactoferrin NPs (Zn-Fe-bLf NPs) were fabricated for a targeted theranostics application through oral administration (Kamalapuram et al., 2016).

Although natural proteins were used in most studies, the disadvantages of these protein-based platforms were obvious, such as poor permeability, ease of degradation, and potential immune responses. Moreover, after functionalization or conjugation of other molecules, the protein properties and functions might be altered. In recent years, encapsulation of proteins by *in situ* polymerization was developed as an alternative strategies for protein modification (Ye et al., 2016b). The protein nanogels were obtained by incorporation of cross-linkers to protein surface and polymerization. Such protein nanogels can maintain the protein properties and functions in complex chemical or biological environment, and avoid the immunogenicity of proteins. The out layer polymers were cleavable and degradable, while the inner proteins could be released by internal and external stimuli. Numerous therapeutic proteins have been developed using this method for cancer therapy (Ye et al., 2016a, 2017).

CONCLUSION AND PROSPECTS

Natural proteins as biocompatible nanocarriers are broadly adopted in delivering therapeutic and diagnostic agents simultaneously. These nanoformulations are fabricated progressively complex and "smart" to employ multi functions in one platform. To increase the accuracy of diagnostic and the efficiency of cancer therapy, "all-in-one" nanoplatforms are designed with more than two imaging strategies and more than two therapeutic methods. Surface modification with targeted molecules and controlled drug release are employed to spatially control the localization of administered NPs. The improved efficiencies in tumor imaging and ablation are verified both *in vitro* and *in vivo*. Despite these huge advances, the translation of natural protein nanoplatforms from laboratory to clinical trials remains an enormous challenge. More efforts should be made to improve the NP reproducibility, colloidal stability in biological environments, and drug-loading efficiency. Furthermore, live and spleen accumulation is a big barrier in clinical translation of all types of NPs. Accordingly, more understanding of bio-nano interactions is required, while more data of pharmacokinetics should be collected and analyzed. Long-term toxicity of nanoformulation is not well evaluated. In addition to mouse model, more animal models, e.g., beagle dogs, monkeys and gorillas, should serve for assessing the long-term toxicity and therapeutic effect. Engineering complex particles with multiple functions are currently achieved by chemists. Accurate diagnose of early stage of tumor and precision drug delivery to tumor site should be more considerable in the future developing of protein-based cancer theranostics.

AUTHOR CONTRIBUTIONS

YG, HZ, and GS: designed this work of review; DM, MZ, and LW: performed the literature search of the databases; YG: wrote the manuscript; HZ and GS: revised the manuscript. All authors approved the paper for publication.

ACKNOWLEDGMENTS

This work was supported by the National Natural Science Foundation of China (91743107, 21405084), Natural Science Foundation of Nantong City in China (MS12015053).

REFERENCES

Aisen, P., Leibman, A., and Zweier, J. (1978). Stoichiometric and site characteristics of the binding of iron to human transferrin. *J. Biol. Chem.* 253, 1930–1937.

Alberti, D., Protti, N., Toppino, A., Deagostino, A., Lanzardo, S., Bortolussi, S., et al. (2015). A theranostic approach based on the use of a dual boron/Gd agent to improve the efficacy of Boron Neutron Capture Therapy in the lung cancer treatment. *Nanomedicine* 11, 741–750. doi: 10.1016/j.nano.2014.12.004

Alkhateeb, A. A., and Connor, J. R. (2013). The significance of ferritin in cancer: anti-oxidation, inflammation and tumorigenesis. *Biochim. Biophys. Acta* 1836, 245–254. doi: 10.1016/j.bbcan.2013.07.002

An, F. F., and Zhang, X. H. (2017). Strategies for preparing albumin-based nanoparticles for multifunctional bioimaging and drug delivery. *Theranostics* 7, 3667–3689. doi: 10.7150/thno.19365

Anand, U., and Mukherjee, S. (2013). Binding, unfolding and refolding dynamics of serum albumins. *Biochim. Biophys. Acta* 1830, 5394–5404. doi: 10.1016/j.bbagen.2013.05.017

Aoun, F., Kourie, H. R., Artigas, C., and Roumeguère, T. (2015). Next revolution in molecular theranostics: personalized medicine for urologic cancers. *Future Oncol.* 11, 2205–2219. doi: 10.2217/fon.15.104

Banyard, S. H., Stammers, D. K., and Harrison, P. M. (1978). Electron density map of apoferritin at 2.8-A resolution. *Nature* 271, 282–284. doi: 10.1038/271282a0

Bardhan, R., Lal, S., Joshi, A., and Halas, N. J. (2011). Theranostic nanoshells: from probe design to imaging and treatment of cancer. *Acc. Chem. Res.* 44, 936–946. doi: 10.1021/ar200023x

Barreto, J. A., O'Malley, W., Kubeil, M., Graham, B., Stephan, H., and Spiccia, L. (2011). Nanomaterials: applications in cancer imaging and therapy. *Adv. Mater. Weinheim.* 23, H18–H40. doi: 10.1002/adma.201100140

Battogtokh, G., and Ko, Y. T. (2016). Graphene oxide-incorporated pH-responsive folate-albumin-photosensitizer nanocomplex as image-guided dual therapeutics. *J. Control. Release* 234, 10–20. doi: 10.1016/j.jconrel.2016.05.007

Bellini, M., Mazzucchelli, S., Galbiati, E., Sommaruga, S., Fiandra, L., Truffi, M., et al. (2014). Protein nanocages for self-triggered nuclear delivery of DNA-targeted chemotherapeutics in Cancer Cells. *J. Control. Release* 196, 184–196. doi: 10.1016/j.jconrel.2014.10.002

Bhushan, B., Kumar, S. U., Matai, I., Sachdev, A., Dubey, P., and Gopinath, P. (2014). Ferritin nanocages: a novel platform for biomedical applications. *J. Biomed. Nanotechnol.* 10, 2950–2976. doi: 10.1166/jbn.2014.1980

Bian, X., Wu, P., Sha, H., Qian, H., Wang, Q., Cheng, L., et al. (2016). Anti-EGFR-iRGD recombinant protein conjugated silk fibroin nanoparticles for enhanced

tumor targeting and antitumor efficiency. *Onco. Targets Ther.* 9, 3153–3162. doi: 10.2147/OTT.S100678

Brandsma, M. E., Jevnikar, A. M., and Ma, S. (2011). Recombinant human transferrin: beyond iron binding and transport. *Biotechnol. Adv.* 29, 230–238. doi: 10.1016/j.biotechadv.2010.11.007

Calzolari, A., Oliviero, I., Deaglio, S., Mariani, G., Biffoni, M., Sposi, N. M., et al. (2007). Transferrin receptor 2 is frequently expressed in human cancer cell lines. *Blood Cells Mol. Dis.* 39, 82–91. doi: 10.1016/j.bcmd.2007.02.003

Charron, D. M., Chen, J., and Zheng, G. (2015). Theranostic lipid nanoparticles for cancer medicine. *Cancer Treat. Res.* 166, 103–127. doi: 10.1007/978-3-319-16555-4_5

Chen, L., Zhou, X., Nie, W., Feng, W., Zhang, Q., Wang, W., et al. (2017a). Marriage of albumin-gadolinium complexes and MoS2 nanoflakes as cancer theranostics for dual-modality magnetic resonance/photoacoustic imaging and photothermal therapy. *ACS Appl. Mater. Interfaces* 9, 17786–17798. doi: 10.1021/acsami.7b04488

Chen, M. L., He, Y. J., Chen, X. W., and Wang, J. H. (2013). Quantum-dot-conjugated graphene as a probe for simultaneous cancer-targeted fluorescent imaging, tracking, and monitoring drug delivery. *Bioconjug. Chem.* 24, 387–397. doi: 10.1021/bc3004809

Chen, Q., Liang, C., Wang, C., and Liu, Z. (2015a). An imagable and photothermal "Abraxane-like" nanodrug for combination cancer therapy to treat subcutaneous and metastatic breast tumors. *Adv. Mater. Weinheim.* 27, 903–910. doi: 10.1002/adma.201404308

Chen, Q., Liang, C., Wang, X., He, J., Li, Y., and Liu, Z. (2014a). An albumin-based theranostic nano-agent for dual-modal imaging guided photothermal therapy to inhibit lymphatic metastasis of cancer post surgery. *Biomaterials* 35, 9355–9362. doi: 10.1016/j.biomaterials.2014.07.062

Chen, Q., and Liu, Z. (2016). Albumin carriers for cancer theranostics: a conventional platform with new promise. *Adv. Mater. Weinheim.* 28, 10557–10566. doi: 10.1002/adma.201600038

Chen, Q., Wang, C., Cheng, L., He, W., Cheng, Z., and Liu, Z. (2014b). Protein modified upconversion nanoparticles for imaging-guided combined photothermal and photodynamic therapy. *Biomaterials* 35, 2915–2923. doi: 10.1016/j.biomaterials.2013.12.046

Chen, Q., Wang, C., Zhan, Z., He, W., Cheng, Z., Li, Y., et al. (2014c). Near-infrared dye bound albumin with separated imaging and therapy wavelength channels for imaging-guided photothermal therapy. *Biomaterials* 35, 8206–8214. doi: 10.1016/j.biomaterials.2014.06.013

Chen, Q., Wang, X., Wang, C., Feng, L., Li, Y., and Liu, Z. (2015b). Drug-induced self-assembly of modified albumins as nano-theranostics for tumor-targeted combination therapy. *ACS Nano* 9, 5223–5233. doi: 10.1021/acsnano.5b00640

Chen, Y., Wu, Y., Sun, B., Liu, S., and Liu, H. (2017b). Two-dimensional nanomaterials for cancer nanotheranostics. *Small* 13:1603446. doi: 10.1002/smll.201603446

Cheng, Z., Dai, Y., Kang, X., Li, C., Huang, S., Lian, H., et al. (2014). Gelatin-encapsulated iron oxide nanoparticles for platinum (IV) prodrug delivery, enzyme-stimulated release and MRI. *Biomaterials* 35, 6359–6368. doi: 10.1016/j.biomaterials.2014.04.029

Conti, L., Lanzardo, S., Ruiu, R., Cadenazzi, M., Cavallo, F., Aime, S., et al. (2016). L-Ferritin targets breast cancer stem cells and delivers therapeutic and imaging agents. *Oncotarget* 7, 66713–66727. doi: 10.18632/oncotarget.10920

Dai, Z., and Yue, X. (2017). Liposomal nanotechnology for cancer theranostics. *Curr. Med. Chem.* doi: 10.2174/0929867324666170306105350. [Epub ahead of print].

Dong, C., Liu, Z., Wang, S., Zheng, B., Guo, W., Yang, W., et al. (2016). A protein-polymer bioconjugate-coated upconversion nanosystem for simultaneous tumor cell imaging, photodynamic therapy, and chemotherapy. *ACS Appl. Mater. Interfaces* 8, 32688–32698. doi: 10.1021/acsami.6b11803

Dufès, C., Al Robaian, M., and Somani, S. (2013). Transferrin and the transferrin receptor for the targeted delivery of therapeutic agents to the brain and cancer cells. *Ther. Deliv.* 4, 629–640. doi: 10.4155/tde.13.21

Elzoghby, A. O. (2013). Gelatin-based nanoparticles as drug and gene delivery systems: reviewing three decades of research. *J. Control. Release* 172, 1075–1091. doi: 10.1016/j.jconrel.2013.09.019

Foox, M., and Zilberman, M. (2015). Drug delivery from gelatin-based systems. *Expert Opin. Drug Deliv.* 12, 1547–1563. doi: 10.1517/17425247.2015.1037272

Fürst, W., and Banerjee, A. (2005). Release of glutaraldehyde from an albumin-glutaraldehyde tissue adhesive causes significant *in vitro* and *in vivo* toxicity. *Ann. Thorac. Surg.* 79, 1522–1528. doi: 10.1016/j.athoracsur.2004.11.054

Gao, F. P., Lin, Y. X., Li, L. L., Liu, Y., Mayerhöffer, U., Spenst, P., et al. (2014). Supramolecular adducts of squaraine and protein for noninvasive tumor imaging and photothermal therapy *in vivo*. *Biomaterials* 35, 1004–1014. doi: 10.1016/j.biomaterials.2013.10.039

Ge, Z., and Liu, S. (2013). Functional block copolymer assemblies responsive to tumor and intracellular microenvironments for site-specific drug delivery and enhanced imaging performance. *Chem. Soc. Rev.* 42, 7289–7325. doi: 10.1039/c3cs60048c

Gelperina, S., Kisich, K., Iseman, M. D., and Heifets, L. (2005). The potential advantages of nanoparticle drug delivery systems in chemotherapy of tuberculosis. *Am. J. Respir. Crit. Care Med.* 172, 1487–1490. doi: 10.1164/rccm.200504-613PP

Geninatti Crich, S., Cadenazzi, M., Lanzardo, S., Conti, L., Ruiu, R., Alberti, D., et al. (2015). Targeting ferritin receptors for the selective delivery of imaging and therapeutic agents to breast cancer cells. *Nanoscale* 7, 6527–6533. doi: 10.1039/C5NR00352K

Gomme, P. T., McCann, K. B., and Bertolini, J. (2005). Transferrin: structure, function and potential therapeutic actions. *Drug Discov. Today* 10, 267–273. doi: 10.1016/S1359-6446(04)03333-1

Guo, J., Rahme, K., He, Y., Li, L. L., Holmes, J. D., and O'Driscoll, C. M. (2017). Gold nanoparticles enlighten the future of cancer theranostics. *Int. J. Nanomed.* 12, 6131–6152. doi: 10.2147/IJN.S140772

Han, H., Wang, J., Chen, T., Yin, L., Jin, Q., and Ji, J. (2017). Enzyme-sensitive gemcitabine conjugated albumin nanoparticles as a versatile theranostic nanoplatform for pancreatic cancer treatment. *J. Colloid Interface Sci.* 507, 217–224. doi: 10.1016/j.jcis.2017.07.047

Hanahan, D., and Weinberg, R. A. (2011). Hallmarks of cancer: the next generation. *Cell* 144, 646–674. doi: 10.1016/j.cell.2011.02.013

Hou, L., Shan, X., Hao, L., Feng, Q., and Zhang, Z. (2017). Copper sulfide nanoparticle-based localized drug delivery system as an effective cancer synergistic treatment and theranostic platform. *Acta Biomater.* 54, 307–320. doi: 10.1016/j.actbio.2017.03.005

Hu, D., Sheng, Z., Gao, G., Siu, F., Liu, C., Wan, Q., et al. (2016). Activatablet albumin-photosensitizer nanoassemblies for triple-modal imaging and thermal-modulated photodynamic therapy of cancer. *Biomaterials* 93, 10–19. doi: 10.1016/j.biomaterials.2016.03.037

Hu, G., Chun, X., Wang, Y., He, Q., and Gao, H. (2015). Peptide mediated active targeting and intelligent particle size reduction-mediated enhanced penetrating of fabricated nanoparticles for triple-negative breast cancer treatment. *Oncotarget* 6, 41258–41274. doi: 10.18632/oncotarget.5692

Huang, H. C., Barua, S., Sharma, G., Dey, S. K., and Rege, K. (2011). Inorganic nanoparticles for cancer imaging and therapy. *J. Control. Release* 155, 344–357. doi: 10.1016/j.jconrel.2011.06.004

Huang, H., Yang, D. P., Liu, M., Wang, X., Zhang, Z., Zhou, G., et al. (2017). pH-sensitive Au-BSA-DOX-FA nanocomposites for combined CT imaging and targeted drug delivery. *Int. J. Nanomed.* 12, 2829–2843. doi: 10.2147/IJN.S128270

Huang, P., Rong, P., Jin, A., Yan, X., Zhang, M. G., Lin, J., et al. (2014). Dye-loaded ferritin nanocages for multimodal imaging and photothermal therapy. *Adv. Mater. Weinheim.* 26, 6401–6408. doi: 10.1002/adma.201400914

Janib, S. M., Moses, A. S., and MacKay, J. A. (2010). Imaging and drug delivery using theranostic nanoparticles. *Adv. Drug Deliv. Rev.* 62, 1052–1063. doi: 10.1016/j.addr.2010.08.004

Jia, Q., Ge, J., Liu, W., Zheng, X., Wang, M., Zhang, H., et al. (2017). Biocompatible Iron Phthalocyanine-Albumin Assemblies as Photoacoustic and Thermal Theranostics in Living Mice. *ACS Appl. Mater. Interf.* 9, 21124–21132. doi: 10.1021/acsami.7b04360

Jiao, Y., Sun, Y., Tang, X., Ren, Q., and Yang, W. (2015). Tumor-targeting multifunctional rattle-type theranostic nanoparticles for MRI/NIRF bimodal imaging and delivery of hydrophobic drugs. *Small* 11, 1962–1974. doi: 10.1002/smll.201402297

Kamalapuram, S. K., Kanwar, R. K., Roy, K., Chaudhary, R., Sehgal, R., and Kanwar, J. R. (2016). Theranostic multimodular potential of zinc-doped ferrite-saturated metal-binding protein-loaded novel nanocapsules in cancers. *Int. J. Nanomed.* 11, 1349–1366. doi: 10.2147/IJN.S95253

Kamaly, N., Xiao, Z., Valencia, P. M., Radovic-Moreno, A. F., and Farokhzad, O. C. (2012). Targeted polymeric therapeutic nanoparticles: design, development and clinical translation. *Chem. Soc. Rev.* 41, 2971–3010. doi: 10.1039/c2cs15344k

Kang, C. S., Ren, S., Sun, X., and Chong, H. S. (2016). Theranostic Polyaminocarboxylate-Cyanine-Transferrin Conjugate for Anticancer Therapy and Near-Infrared Optical Imaging. *Chem. Med. Chem.* 11, 2188–2193. doi: 10.1002/cmdc.201600072

Kanwar, J. R., Kamalapuram, S. K., Krishnakumar, S., and Kanwar, R. K. (2016). Multimodal iron oxide (Fe3O4)-saturated lactoferrin nanocapsules as nanotheranostics for real-time imaging and breast cancer therapy of claudin-low, triple-negative (ER(-)/PR(-)/HER2(-)). *Nanomedicine (Lond).* 11, 249–268. doi: 10.2217/nnm.15.199

Karimi, M., Bahrami, S., Ravari, S. B., Zangabad, P. S., Mirshekari, H., Bozorgomid, M., et al. (2016). Albumin nanostructures as advanced drug delivery systems. *Expert Opin. Drug Deliv.* 13, 1609–1623. doi: 10.1080/17425247.2016.1193149

Khalid, A., Mitropoulos, A. N., Marelli, B., Tomljenovic-Hanic, S., and Omenetto, F. G. (2016). Doxorubicin loaded nanodiamond-silk spheres for fluorescence tracking and controlled drug release. *Biomed. Opt. Express* 7, 132–147. doi: 10.1364/BOE.7.000132

Kouchakzadeh, H., and Abbas Shojaosadati, S. (2016). The prominent role of protein-based delivery systems on the development of cancer treatment. *Curr. Pharm. Des.* 22, 3455–3465. doi: 10.2174/1381612822666160204120643

Lee, C., Lee, S., Thao, L. Q., Hwang, H. S., Kim, J. O., Lee, E. S., et al. (2016). An albumin nanocomplex-based endosomal pH-activatable on/off probe system. *Colloids Surf. B Biointerf.* 144, 327–334. doi: 10.1016/j.colsurfb.2016.04.022

Li, F., Liang, Z., and Ling, D. (2017). Smart organic-inorganic nanogels for activatable theranostics. *Curr. Med. Chem.* doi: 10.2174/0929867324666170920164614. [Epub ahead of print].

Li, W. M., Chen, S. Y., and Liu, D. M. (2013). *In situ* doxorubicin-CaP shell formation on amphiphilic gelatin-iron oxide core as a multifunctional drug delivery system with improved cytocompatibility, pH-responsive drug release and MR imaging. *Acta Biomater.* 9, 5360–5368. doi: 10.1016/j.actbio.2012.09.023

Li, X., Mu, J., Liu, F., Tan, E. W., Khezri, B., Webster, R. D., et al. (2015). Human transport protein carrier for controlled photoactivation of antitumor prodrug and real-time intracellular tumor imaging. *Bioconjug. Chem.* 26, 955–961. doi: 10.1021/acs.bioconjchem.5b00170

Lisitskiy, V. A., Khan, H., Popova, T. V., Chubarov, A. S., Zakharova, O. D., Akulov, A. E., et al. (2017). Multifunctional human serum albumin-therapeutic nucleotide conjugate with redox and pH-sensitive drug release mechanism for cancer theranostics. *Bioorg. Med. Chem. Lett.* 27, 3925–3930. doi: 10.1016/j.bmcl.2017.05.084

Liu, J., Qi, C., Tao, K., Zhang, J., Zhang, J., Xu, L., et al. (2016). Sericin/dextran injectable hydrogel as an optically trackable drug delivery system for malignant melanoma treatment. *ACS Appl. Mater. Interfaces* 8, 6411–6422. doi: 10.1021/acsami.6b00959

Liu, Y., Zhang, G., Guo, Q., Ma, L., Jia, Q., Liu, L., et al. (2017). Artificially controlled degradable inorganic nanomaterial for cancer theranostics. *Biomaterials* 112, 204–217. doi: 10.1016/j.biomaterials.2016.10.028

Maham, A., Tang, Z., Wu, H., Wang, J., and Lin, Y. (2009). Protein-based nanomedicine platforms for drug delivery. *Small* 5, 1706–1721. doi: 10.1002/smll.200801602

Majorek, K. A., Porebski, P. J., Dayal, A., Zimmerman, M. D., Jablonska, K., Stewart, A. J., et al. (2012). Structural and immunologic characterization of bovine, horse, and rabbit serum albumins. *Mol. Immunol.* 52, 174–182. doi: 10.1016/j.molimm.2012.05.011

Mathew, S., Murakami, T., Nakatsuji, H., Okamoto, H., Morone, N., Heuser, J. E., et al. (2013). Exclusive photothermal heat generation by a gadolinium bis(naphthalocyanine) complex and inclusion into modified high-density lipoprotein nanocarriers for therapeutic applications. *ACS Nano* 7, 8908–8916. doi: 10.1021/nn403384k

Mehra, N. K., Jain, A. K., and Nahar, M. (2017). Carbon nanomaterials in oncology: an expanding horizon. *Drug Discov. Today*. doi: 10.1016/j.drudis.2017.09.013. [Epub ahead of print].

Mo, Y., Barnett, M. E., Takemoto, D., Davidson, H., and Kompella, U. B. (2007). Human serum albumin nanoparticles for efficient delivery of Cu, Zn superoxide dismutase gene. *Mol. Vis.* 13, 746–757.

Mohammadi, M., Ramezani, M., Abnous, K., and Alibolandi, M. (2017). Biocompatible polymersomes-based cancer theranostics: Towards multifunctional nanomedicine. *Int. J. Pharm.* 519, 287–303. doi: 10.1016/j.ijpharm.2017.01.037

Moon, H., Kang, J., Sim, C., Kim, J., Lee, H., Chang, J. H., et al. (2015). Multifunctional theranostic contrast agent for photoacoustics- and ultrasound-based tumor diagnosis and ultrasound-stimulated local tumor therapy. *J. Control. Release* 218, 63–71. doi: 10.1016/j.jconrel.2015.09.060

Muthu, M. S., Kutty, R. V., Luo, Z., Xie, J., and Feng, S. S. (2015). Theranostic vitamin E TPGS micelles of transferrin conjugation for targeted co-delivery of docetaxel and ultra bright gold nanoclusters. *Biomaterials* 39, 234–248. doi: 10.1016/j.biomaterials.2014.11.008

Nezhadi, S. H., Choong, P. F., Lotfipour, F., and Dass, C. R. (2009). Gelatin-based delivery systems for cancer gene therapy. *J. Drug Target.* 17, 731–738. doi: 10.3109/10611860903096540

Ng, K. K., Lovell, J. F., and Zheng, G. (2011). Lipoprotein-inspired nanoparticles for cancer theranostics. *Acc. Chem. Res.* 44, 1105–1113. doi: 10.1021/ar200017e

Ninan, G., Jose, J., and Abubacker, Z. (2011). Preparation and characterization of gelatin extracted from the skins of rohu (labeo rohita) and common carp (cyprinus carpio). *J. Food Process. Pres.* 35, 143–162. doi: 10.1111/j.1745-4549.2009.00467.x

Opoku-Damoah, Y., Wang, R., Zhou, J., and Ding, Y. (2016). Versatile nanosystem-based cancer theranostics: design inspiration and predetermined routing. *Theranostics* 6, 986–1003. doi: 10.7150/thno.14860

Paliwal, R., and Palakurthi, S. (2014). Zein in controlled drug delivery and tissue engineering. *J. Control. Release* 189, 108–122. doi: 10.1016/j.jconrel.2014.06.036

Pan, J., Wang, Y., Pan, H., Zhang, C., Zhang, X., Fu, Y.-Y., et al. (2017). Mimicking drug–substrate interaction: a smart bioinspired technology for the fabrication of theranostic nanoprobes. *Adv. Funct. Mater.* 27:1603440. doi: 10.1002/adfm.201603440

Panyam, J., and Labhasetwar, V. (2003). Biodegradable nanoparticles for drug and gene delivery to cells and tissue. *Adv. Drug Deliv. Rev.* 55, 329–347. doi: 10.1016/S0169-409X(02)00228-4

Parkkinen, J., von Bonsdorff, L., Ebeling, F., and Sahlstedt, L. (2002). Function and therapeutic development of apotransferrin. *Vox Sang* 83 (Suppl. 1), 321–326. doi: 10.1111/j.1423-0410.2002.tb05327.x

Patel, Z. S., Yamamoto, M., Ueda, H., Tabata, Y., and Mikos, A. G. (2008). Biodegradable gelatin microparticles as delivery systems for the controlled release of bone morphogenetic protein-2. *Acta Biomater.* 4, 1126–1138. doi: 10.1016/j.actbio.2008.04.002

Peer, D., Karp, J. M., Hong, S., Farokhzad, O. C., Margalit, R., and Langer, R. (2007). Nanocarriers as an emerging platform for cancer therapy. *Nat. Nanotechnol.* 2, 751–760. doi: 10.1038/nnano.2007.387

Pene, F., Courtine, E., Cariou, A., and Mira, J. P. (2009). Toward theragnostics. *Crit. Care Med.* 37, S50–S58. doi: 10.1097/CCM.0b013e3181921349

Peng, H., Tang, J., Zheng, R., Guo, G., Dong, A., Wang, Y., et al. (2017). Nuclear-targeted multifunctional magnetic nanoparticles for photothermal therapy. *Adv. Healthc. Mater.* 6:1601289. doi: 10.1002/adhm.201601289

Pérez-Tomás, R. (2006). Multidrug resistance: retrospect and prospects in anti-cancer drug treatment. *Curr. Med. Chem.* 13, 1859–1876. doi: 10.2174/092986706777585077

Rong, P., Huang, P., Liu, Z., Lin, J., Jin, A., Ma, Y., et al. (2015). Protein-based photothermal theranostics for imaging-guided cancer therapy. *Nanoscale* 7, 16330–16336. doi: 10.1039/C5NR04428F

Sahoo, N., Sahoo, R. K., Biswas, N., Guha, A., and Kuotsu, K. (2015). Recent advancement of gelatin nanoparticles in drug and vaccine delivery. *Int. J. Biol. Macromol.* 81, 317–331. doi: 10.1016/j.ijbiomac.2015.08.006

Sahu, A., Lee, J. H., Lee, H. G., Jeong, Y. Y., and Tae, G. (2016). Prussian blue/serum albumin/indocyanine green as a multifunctional nanotheranostic agent for bimodal imaging guided laser mediated combinatorial phototherapy. *J. Control. Release* 236, 90–99. doi: 10.1016/j.jconrel.2016.06.031

Salvati, A., Pitek, A. S., Monopoli, M. P., Prapainop, K., Bombelli, F. B., Hristov, D. R., et al. (2013). Transferrin-functionalized nanoparticles lose their targeting capabilities when a biomolecule corona adsorbs on the surface. *Nat. Nanotechnol.* 8, 137–143. doi: 10.1038/nnano.2012.237

Semkina, A., Abakumov, M., Grinenko, N., Abakumov, A., Skorikov, A., Mironova, E., et al. (2015). Core-shell-corona doxorubicin-loaded superparamagnetic Fe3O4 nanoparticles for cancer theranostics. *Colloids Surf. B Biointerfaces* 136, 1073–1080. doi: 10.1016/j.colsurfb.2015.11.009

Sharma, H., Mishra, P. K., Talegaonkar, S., and Vaidya, B. (2015). Metal nanoparticles: a theranostic nanotool against cancer. *Drug Discov. Today* 20, 1143–1151. doi: 10.1016/j.drudis.2015.05.009

Sheng, Z., Hu, D., Zheng, M., Zhao, P., Liu, H., Gao, D., et al. (2014). Smart human serum albumin-indocyanine green nanoparticles generated by programmed assembly for dual-modal imaging-guided cancer synergistic phototherapy. *ACS Nano* 8, 12310–12322. doi: 10.1021/nn5062386

Sheng, Z., Song, L., Zheng, J., Hu, D., He, M., Zheng, M., et al. (2013). Protein-assisted fabrication of nano-reduced graphene oxide for combined *in vivo* photoacoustic imaging and photothermal therapy. *Biomaterials* 34, 5236–5243. doi: 10.1016/j.biomaterials.2013.03.090

Sim, C., Kim, H., Moon, H., Lee, H., Chang, J. H., and Kim, H. (2015). Photoacoustic-based nanomedicine for cancer diagnosis and therapy. *J. Control. Release* 203, 118–125. doi: 10.1016/j.jconrel.2015.02.020

Sinha, V. R., and Trehan, A. (2003). Biodegradable microspheres for protein delivery. *J. Control. Release* 90, 261–280. doi: 10.1016/S0168-3659(03)00194-9

Sk, U. H., and Kojima, C. (2015). Dendrimers for theranostic applications. *Biomol. Concepts* 6, 205–217. doi: 10.1515/bmc-2015-0012

Sonali Singh, R. P., Singh, N., Sharma, G., Vijayakumar, M. R., Koch, B., and Muthu, M. S. (2016). Transferrin liposomes of docetaxel for brain-targeted cancer applications: formulation and brain theranostics. *Drug Deliv.* 23, 1261–1271. doi: 10.3109/10717544.2016.1162878

Suarasan, S., Focsan, M., Potara, M., Soritau, O., Florea, A., Maniu, D., et al. (2016). Doxorubicin-incorporated nanotherapeutic delivery system based on gelatin-coated gold nanoparticles: formulation, drug release, and multimodal imaging of cellular internalization. *ACS Appl. Mater. Interfaces* 8, 22900–22913. doi: 10.1021/acsami.6b07583

Sugio, S., Kashima, A., Mochizuki, S., Noda, M., and Kobayashi, K. (1999). Crystal structure of human serum albumin at 2.5 A resolution. *Protein Eng.* 12, 439–446. doi: 10.1093/protein/12.6.439

Szakács, G., Paterson, J. K., Ludwig, J. A., Booth-Genthe, C., and Gottesman, M. M. (2006). Targeting multidrug resistance in cancer. *Nat. Rev. Drug Discov.* 5, 219–234. doi: 10.1038/nrd1984

Szoke, D., and Panteghini, M. (2012). Diagnostic value of transferrin. *Clin. Chim. Acta* 413, 1184–1189. doi: 10.1016/j.cca.2012.04.021

Tekade, R. K., and Sun, X. (2017). The Warburg effect and glucose-derived cancer theranostics. *Drug Discov. Today* 22, 1637-1653. doi: 10.1016/j.drudis.2017.08.003

Torre, L. A., Bray, F., Siegel, R. L., Ferlay, J., Lortet-Tieulent, J., and Jemal, A. (2015). Global cancer statistics, 2012. *CA Cancer J. Clin.* 65, 87–108. doi: 10.3322/caac.21262

Tortorella, S., and Karagiannis, T. C. (2014). Transferrin receptor-mediated endocytosis: a useful target for cancer therapy. *J. Membr. Biol.* 247, 291–307. doi: 10.1007/s00232-014-9637-0

Tran, T. T., Tran, P. H., Amin, H. H., and Lee, B. J. (2017a). Biodistribution and *in vivo* performance of fattigation-platform theranostic nanoparticles. *Mater. Sci. Eng. C Mater. Biol. Appl.* 79, 671–678. doi: 10.1016/j.msec.2017.05.029

Tran, T. T., Tran, P. H., Yoon, T. J., and Lee, B. J. (2017b). Fattigation-platform theranostic nanoparticles for cancer therapy. *Mater. Sci. Eng. C Mater. Biol. Appl.* 75, 1161–1167. doi: 10.1016/j.msec.2017.03.012

Tros de Ilarduya, C., and Düzgüneş, N. (2013). Delivery of therapeutic nucleic acids via transferrin and transferrin receptors: lipoplexes and other carriers. *Expert Opin. Drug Deliv.* 10, 1583–1591. doi: 10.1517/17425247.2013.837447

Truffi, M., Fiandra, L., Sorrentino, L., Monieri, M., Corsi, F., and Mazzucchelli, S. (2016). Ferritin nanocages: a biological platform for drug delivery, imaging and theranostics in cancer. *Pharmacol. Res.* 107, 57–65. doi: 10.1016/j.phrs.2016.03.002

Tsai, L. C., Hsieh, H. Y., Lu, K. Y., Wang, S. Y., and Mi, F. L. (2016). EGCG/gelatin-doxorubicin gold nanoparticles enhance therapeutic efficacy of doxorubicin for prostate cancer treatment. *Nanomedicine* 11, 9–30. doi: 10.2217/nnm.15.183

Turino, L. N., Ruggiero, M. R., Stefanìa, R., Cutrin, J. C., Aime, S., and Geninatti Crich, S. (2017). Ferritin decorated PLGA/paclitaxel loaded nanoparticles endowed with an enhanced toxicity toward MCF-7 breast tumor cells. *Bioconjug. Chem.* 28, 1283–1290. doi: 10.1021/acs.bioconjchem.7b00096

Wang, D., Li, Y., Tian, Z., Cao, R., and Yang, B. (2014a). Transferrin-conjugated nanodiamond as an intracellular transporter of chemotherapeutic drug and targeting therapy for cancer cells. *Ther. Deliv.* 5, 511–524. doi: 10.4155/tde.14.17

Wang, D., Zhu, L., Pu, Y., Wang, J. X., Chen, J. F., and Dai, L. (2017a). Transferrin-coated magnetic upconversion nanoparticles for efficient photodynamic therapy with near-infrared irradiation and luminescence bioimaging. *Nanoscale* 9, 11214–11221. doi: 10.1039/C7NR03019C

Wang, F., Chen, L., Zhang, R., Chen, Z., and Zhu, L. (2014b). RGD peptide conjugated liposomal drug delivery system for enhance therapeutic efficacy in treating bone metastasis from prostate cancer. *J. Control. Release* 196, 222–233. doi: 10.1016/j.jconrel.2014.10.012

Wang, H., Zhu, W., Huang, Y., Li, Z., Jiang, Y., and Xie, Q. (2017b). Facile encapsulation of hydroxycamptothecin nanocrystals into zein-based nanocomplexes for active targeting in drug delivery and cell imaging. *Acta Biomater.* 61, 88–100. doi: 10.1016/j.actbio.2017.04.017

Wang, K., Zhang, Y., Wang, J., Yuan, A., Sun, M., Wu, J., et al. (2016a). Self-assembled IR780-loaded transferrin nanoparticles as an imaging, targeting and PDT/PTT agent for cancer therapy. *Sci. Rep.* 6:27421. doi: 10.1038/srep27421

Wang, L., An, Y., Yuan, C., Zhang, H., Liang, C., Ding, F., et al. (2015). GEM-loaded magnetic albumin nanospheres modified with cetuximab for simultaneous targeting, magnetic resonance imaging, and double-targeted thermochemotherapy of pancreatic cancer cells. *Int. J. Nanomed.* 10, 2507–2519. doi: 10.2147/IJN.S77642

Wang, Z., Huang, P., Jacobson, O., Wang, Z., Liu, Y., Lin, L., et al. (2016b). Biomineralization-inspired synthesis of copper sulfide-ferritin nanocages as cancer theranostics. *ACS Nano* 10, 3453–3460. doi: 10.1021/acsnano.5b07521

Wei, K. C., Lin, F. W., Huang, C. Y., Ma, C. C., Chen, J. Y., Feng, L. Y., et al. (2016). 1,3-Bis(2-chloroethyl)-1-nitrosourea-loaded bovine serum albumin nanoparticles with dual magnetic resonance-fluorescence imaging for tracking of chemotherapeutic agents. *Int. J. Nanomed.* 11, 4065–4075. doi: 10.2147/IJN.S113589

Wen, L., Yang, S., Zhong, J., Zhou, Q., and Xing, D. (2017). Thermoacoustic imaging and therapy guidance based on ultra-short pulsed microwave pumped thermoelastic effect induced with superparamagnetic iron oxide nanoparticles. *Theranostics* 7, 1976–1989. doi: 10.7150/thno.17846

Yang, W., Guo, W., Le, W., Lv, G., Zhang, F., Shi, L., et al. (2016). Albumin-bioinspired Gd:CuS nanotheranostic agent for *in vivo* photoacoustic/magnetic resonance imaging-guided tumor-targeted photothermal therapy. *ACS Nano* 10, 10245–10257. doi: 10.1021/acsnano.6b05760

Ye, Y. Q., Yu, J. C., and Gu, Z. (2016b). Versatile protein nanogels prepared by *in situ* polymerization. *Macromol. Chem. Phys.* 217, 333–343. doi: 10.1002/macp.201500296

Ye, Y., Wang, C., Zheng, X., Hu, Q., Zhang, Y., Liu, Q., et al. (2017). A melanin-mediated cancer immunotherapy patch. *Sci. Immunol.* 2:eaan5692. doi: 10.1126/sciimmunol.aan5692

Ye, Y., Wang, J., Hu, Q., Hochu, G. M., Xin, H., Wang, C., et al. (2016a). Synergistic transcutaneous immunotherapy enhances antitumor immune responses through delivery of checkpoint inhibitors. *ACS Nano* 10, 8956–8963. doi: 10.1021/acsnano.6b04989

Yewale, C., Baradia, D., Vhora, I., and Misra, A. (2013). Proteins: emerging carrier for delivery of cancer therapeutics. *Expert Opin. Drug Deliv.* 10, 1429–1448. doi: 10.1517/17425247.2013.805200

Yu, J., Ju, Y., Zhao, L., Chu, X., Yang, W., Tian, Y., et al. (2016). Multistimuli-regulated photochemothermal cancer therapy remotely controlled via Fe5C2 nanoparticles. *ACS Nano* 10, 159–169. doi: 10.1021/acsnano.5b04706

Yue, X., Zhang, Q., and Dai, Z. (2017). Near-infrared light-activatable polymeric nanoformulations for combined therapy and imaging of cancer. *Adv. Drug Deliv. Rev.* 115, 155–170. doi: 10.1016/j.addr.2017.04.007

Zhen, Z., Tang, W., Chen, H., Lin, X., Todd, T., Wang, G., et al. (2013a). RGD-modified apoferritin nanoparticles for efficient drug delivery to tumors. *ACS Nano* 7, 4830–4837. doi: 10.1021/nn305791q

Zhen, Z., Tang, W., Guo, C., Chen, H., Lin, X., Liu, G., et al. (2013b). Ferritin nanocages to encapsulate and deliver photosensitizers for efficient photodynamic therapy against cancer. *ACS Nano* 7, 6988–6996. doi: 10.1021/nn402199g

Zhou, L., Yang, T., Wang, J., Wang, Q., Lv, X., Ke, H., et al. (2017). Size-Tunable Gd2O3@albumin nanoparticles conjugating chlorin e6 for magnetic resonance imaging-guided photo-induced therapy. *Theranostics* 7, 764–774. doi: 10.7150/thno.15757

Zhu, H., Zhang, S., Ling, Y., Meng, G., Yang, Y., and Zhang, W. (2015). pH-responsive hybrid quantum dots for targeting hypoxic tumor siRNA delivery. *J. Control. Release* 220, 529–544. doi: 10.1016/j.jconrel.2015.11.017

Zhu, M., Sheng, Z., Jia, Y., Hu, D., Liu, X., Xia, X., et al. (2017). Indocyanine Green-holo-Transferrin Nanoassemblies for Tumor-Targeted Dual-Modal Imaging and Photothermal Therapy of Glioma. *ACS Appl. Mater. Interf.* 9, 39249–39258. doi: 10.1021/acsami.7b14076

Conflict of Interest Statement: The authors declare that the research was conducted in the absence of any commercial or financial relationships that could be construed as a potential conflict of interest.

frontiers in Pharmacology

REVIEW
published: 02 November 2018
doi: 10.3389/fphar.2018.01260

PLGA-Based Nanoparticles in Cancer Treatment

Sima Rezvantalab[1,2†], Natascha Ingrid Drude[2,3†], Mostafa Keshavarz Moraveji[1], Nihan Güvener[2], Emily Kate Koons[4], Yang Shi[2], Twan Lammers[2] and Fabian Kiessling[2*]*

[1] Department of Chemical Engineering, Amirkabir University of Technology (Tehran Polytechnic), Tehran, Iran, [2] Institute for Experimental Molecular Imaging, University Clinic and Helmholtz Institute for Biomedical Engineering, RWTH Aachen University, Aachen, Germany, [3] Department of Nuclear Medicine, Uniklinik RWTH Aachen University, Aachen, Germany, [4] Department of Pharmacology and Toxicology, College of Pharmacy & UA Cancer Center, University of Arizona, Tucson, AZ, United States

OPEN ACCESS

Edited by:
Bing Yan, Shandong University, China

Reviewed by:
Paolo Armando Gagliardi, Universität Bern, Switzerland
Ajaikumar B. Kunnumakkara, Indian Institute of Technology Guwahati, India

***Correspondence:**
Mostafa Keshavarz Moraveji
moraveji@aut.ac.ir
Fabian Kiessling
fkiessling@ukaachen.de

† These authors have contributed equally to this work

Specialty section:
This article was submitted to Cancer Molecular Targets and Therapeutics, a section of the journal Frontiers in Pharmacology

Received: *09 July 2018*
Accepted: *15 October 2018*
Published: *02 November 2018*

Citation:
Rezvantalab S, Drude NI, Moraveji MK, Güvener N, Koons EK, Shi Y, Lammers T and Kiessling F (2018) PLGA-Based Nanoparticles in Cancer Treatment. Front. Pharmacol. 9:1260. doi: 10.3389/fphar.2018.01260

Nanomedicines can be used for a variety of cancer therapies including tumor-targeted drug delivery, hyperthermia, and photodynamic therapy. Poly (lactic-co-glycolic acid) (PLGA)-based materials are frequently used in such setups. This review article gives an overview of the properties of previously reported PLGA nanoparticles (NPs), their behavior in biological systems, and their use for cancer therapy. Strategies are emphasized to target PLGA NPs to the tumor site passively and actively. Furthermore, combination therapies are introduced that enhance the accumulation of NPs and, thereby, their therapeutic efficacy. In this context, the huge number of reports on PLGA NPs used as drug delivery systems in cancer treatment highlight the potential of PLGA NPs as drug carriers for cancer therapeutics and encourage further translational research.

Keywords: PLGA, nanoparticles, drug delivery, cancer treatment, combination therapy

INTRODUCTION

The field of nanomedicine, which refers to the application of nanotechnology in medicine, offers valuable tools for the diagnosis and treatment of diseases. In this regard, a wide range of submicron materials has been designed and engineered, especially for defeating cancer. Its applications expedite the development of contrast agents, therapeutics, drug delivery vehicles and theranostics. Nanoparticles (NPs) for drug delivery applications have been composed of biodegradable and biocompatible polymers based on natural and/or synthetic materials. Synthetic polymers can be produced with high purities in a precise and well-controlled production process, as compared to natural products (Lai et al., 2014).

One extensively investigated polymer is poly (lactic-co-glycolic acid) (PLGA), synthetic thermoplastic aliphatic biocompatible polyester. There are specific formulations based on PLGA and its related homopolymers; poly (lactic acid) (PLA) and poly (glycolic acid) (PGA), which have been approved by the US Food and Drug Administration (FDA) for medical applications (Pandey et al., 2015). PLGA NPs have also proved their potential as drug delivery systems for many therapeutic agents (e.g., chemotherapy, antibiotics, antiseptic, anti-inflammatory and antioxidant drugs, proteins), and can be favorable for tumor- and/or DNA-targeting (Danhier et al., 2012; Berthet et al., 2017).

Scientists are trying to find new and different methods of NPs preparation and modification to gain tight control over PLGA degradation, drug release, and other characteristics. In this regard, researchers are evaluating various targeting strategies including, e.g., active targeting moieties to improve the retention of NPs at the target site. However, the correlation between PLGA NPs' physicochemical properties, targeting strategies and treatment modalities on cancer therapy resemble a complex puzzle like a Rubik's cube. As illustrated in **Figure 1** it is not possible to move (and change) one brick without moving a whole plane. On the upper face of the cube, we illustrate polymers' properties, and NPs' features that correlate with, e.g., NPs size, which is determined by the molecular weight of the polymer (Mw), charge, coiling, and the type of surface modification. Moreover, any change in lactic acid (LA)/glycolic acid (GA) ratio varies the crystallinity and hydrophobicity of the formulation.

While a Rubik's cube can be solved by defined algorithms, analog algorithms do not yet exist for the design of drug delivery systems due to its high complexity. Optimizing and altering chemical parameters will as well influence the other parts of the puzzle. Polymers' properties and NPs features can affect the choice of the targeting strategy, and *vice versa*. For example, an external stimuli-based targeting strategy facilitates the tumor retention of NPs but it can exacerbate the size and might stimulate uptake by the mononuclear phagocytic system (MPS) (Kunjachan et al., 2014; Al-Jamal et al., 2016). Those changes in biodistribution and pharmacokinetics are the "hidden" faces of the cube, which can only be manipulated to a certain (rather low) extent via co-medication or interventions, e.g., sonoporation (Dasgupta et al., 2016; Dimcevski et al., 2016; Koczera et al., 2017) or *in vivo* modulation of oxidative stress via administration of buthionine sulfoximine (BSO), an inhibitor of the antioxidant glutathione (GSH). GSH neutralizes reactive oxygen species (ROS) and its depletion cannot only prevent premature degradation of a redox-sensitive nanoformulation but can also serve as a hypoxic cell sensitizer in combination with radiation and some chemotherapeutic drugs (Drude et al., 2018; Miran et al., 2018).

However, even a regular Rubik's cube does not represent the full complexity: in drug targeting with nanomedicines some blocks are connetced and this connection might even increase or decrease until a very late stage of a given study to reach the optimal treatment outcome.

In this review article, we will address the displayed aspects of this cube for PLGA-based NPs and we will discuss how they can be tailored by synthesis methods as well as strategies for drug delivery with PLGA to improve cancer treatment.

PLGA PROPERTIES

Poly (lactic-co-glycolic acid) is one of the best characterized biodegradable copolymers that decomposes to non-toxic products (H_2O and CO_2) that are eliminated from the body. Its polymeric NP degrades *in vivo* through hydrolysis of the ester bonds to its monomeric anions (lactate and glycolate). While D-Lactate is not further metabolized before excretion, L-lactate is converted into CO_2, which is excreted through the lungs and it is converted to pyruvate, which enters the Krebs cycle. Glycolate on the other hand is either directly excreted through the renal system or it can be oxidized to glyoxylate, which is afterward further converted into glycine, serine, and pyruvate. The latter can again enter the Krebs cycle and is metabolized into CO_2 and H_2O. (Danhier et al., 2012; Silva et al., 2015). Typically, PLGA is produced by a catalyzed ring-opening copolymerization of LA and GA (Dechy-Cabaret et al., 2004). PGA is a crystalline hydrophilic polymer with low water solubility and fast degradation rate under physiological conditions. On the contrary, PLA is a stiff and hydrophobic polymer with low mechanical strength. As a copolymer of both, PLGA inherits the intrinsic properties of its constitutional monomers where the polymeric content, based on LA/GA ratio and Mw, strongly affect its degradation rate. For example, with an increase in the LA/GA ratio, the overall PLGA hydrophobicity increases, which leads to lower degradation and thus slower drug release rate (Engineer et al., 2011). Furthermore, the final Mw of the polymer also influences the degradation and drug release kinetics of the resulting formulations; i.e., with a decrease in the Mw, degradation as well as drug release rates both increase (Xu et al., 2017). Next, degradation, release kinetics, and the Mw also correlate with the size of the resulting NPs formulate. These are crucial factors for the therapeutic performance of PLGA NPs. Despite the higher drug loading potential of larger sized formulations, achieving a lower nano-size range is essentially important for the ability of the NPs to overcome biological barriers and to reach the disease site. In this context, a study pointed to the impact of the Mw of four 1:1 (LA:GA) PLGA copolymers with different Mw of 14.5, 45, 85, and 213 kDa on polymeric degradation and release rate (Mittal et al., 2007). With increasing Mw, the PLGA NPs degradation as well as its drug release decreased with a payload release under physiological conditions on day 18 of 95, 66, 50, and 23%, respectively. In addition it has been observed that the is higher the Mw of PLGA (6, 14.5, 63.6 kDa), the bigger is the size of NPs loaded with paclitaxel (PTX) (122 ± 3, 133 ± 2, 160 ± 2 nm) and also of NPs without PTX (117 ± 2, 132 ± 2, 159 ± 3 nm) (Fonseca et al., 2002; Song et al., 2008). LA/GA ratio is an effective parameter in tailoring degradation time and drug release rate. The higher the GA content, the faster the resulting degradation rate (Xu et al., 2017). *Vice versa* the drug release is prolonged with an increase in LA content (LA/GA: 50/50, 75/25 showed faster release kinetics then 100/0) (Horisawa et al., 2002). Hence, these polymeric characteristics, as well as their size, are important to tailor hydrophobicity, drug loading efficacy, and the pharmacokinetic profile of PLGA formulations.

Another important factor that affects the outcome of cancer treatment is the shape of PLGA NPs. Up to date, rod- (Bowerman et al., 2017), needle- (Kolhar et al., 2011), and cylindrical- (Chu et al., 2013) NPs have been synthesized and compared with the most frequently used spherical-shaped PLGA NPs regarding cellular uptake, internalization, biodistribution, and blood half-life. For instance, the needle-shaped PLGA NPs seem to more efficiently cross endothelial cell membranes, and deliver siRNA into the cellular cytoplasm (*in vitro*) as

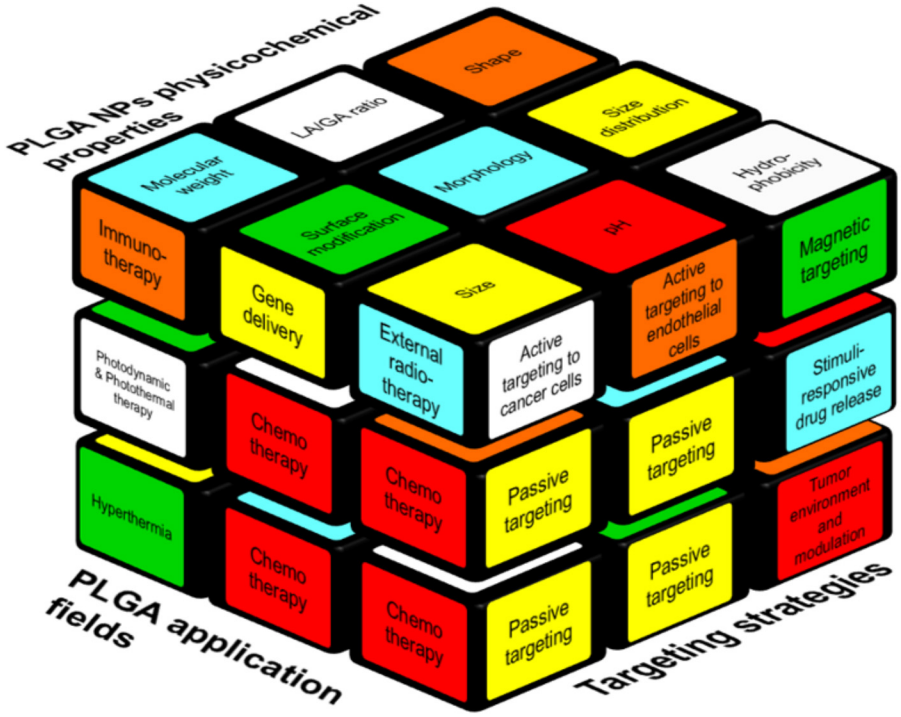

FIGURE 1 | Interplay between various factors relevant to the design of PLGA-based NP formulations. The factors that are contributing to a successful cancer treatment by PLGA NPs are represented as a Rubik's cube. Passive targeting is the cornerstone of the all targeting strategies (right side) beside other strategies like specific cancer cell- or endothelial cell targeting. Moreover, internal (e.g., pH) and external (e.g., heat, magnetic field) stimuli can be used for targeted delivery. Polymer and NPs properties such as size, molecular weight, hydrophobicity (upper side) play a role to formulate suitable carriers to deliver the drugs to the cancer site. On the left side, applications of PLGA NPs are reported, of which the use as a chemotherapeutic cargo is most common.

compared to their spherically shaped analogs. The mechanism of uptake is not yet fully understood but was narrowed down to three possible pathways: endocytosis, direct delivery and/or membrane portion with possible membrane disruption. The internalization was 150% higher with a threefold increased silencing efficacy compared to the spherical counterparts (Kolhar et al., 2011). However, the needle-shaped PLGA NP can also induce considerably cytotoxicity. After endocytosis the needle-shaped particles are in the lysosomes where they can damage the lysosomal membrane and by this activate apoptosis signaling pathways and finally induce cell apoptosis (Zhang et al., 2017).

Furthermore, cylindrical docetaxel (DTX)-loaded PLGA NPs accumulated less in liver, spleen, and lung in comparison with the free drug and DTX-loaded spherical NPs (Chu et al., 2013). Likewise, the shape of PLGA copolymer structure can influence the efficiency of drug encapsulation. Tao et al. (2013) demonstrated that star-shaped PLGA copolymer show higher DTX encapsulation efficiency (97%) compared to linear block copolymers (83%).

Next to the intrinsic properties of PLGA NPs, their surface modification plays an important role with respect to targeting strategy, biocompatibility, and blood half-life. The latter can particularly be increased when PLGA is combined with other polymers such as polyethylene glycol (PEG), polyvinyl alcohol (PVA), and d-α-tocopheryl PEG 1000 succinate (TPGS). Surface modification with, e.g., PEG (PEGylation) increases the hydrophilicity of the formulation yielding a stealth particle with enhanced blood circulation time and improved pharmacokinetics by preventing opsonization, and uptake by the mononuclear phagocyte system (Vllasaliu et al., 2014; Turecek et al., 2016). However, due to the same reasons, the cellular uptake by target cells (which might be mandatory depending on the treatment) might as well be decreased and the targeting capabilities of those particles are strongly dependent on the exact chemical composition of the surface. For instance, Khalil et al. synthesized curcumin (CUR)-loaded PLGA NPs with and without PEGylation via single emulsion solvent-evaporation technique and compared both formulations with the free drug, showing that PEGylation could improve the pharmacokinetic properties of the drug and the PLGA particle. The CUR biological half-life after per os administration was also increased for PEGylated PLGA NP formulations compared to non-PEGylated ones and the bioavailability of the loaded CUR could be increased by 55.4 times. However, despite improved pharmacokinetics, the stealth PEG-PLGA NP showed a slightly faster release of the drug as the PLGA NPs (Khalil et al., 2013). Another study by Bertrand et al. (2017) investigated, the impact of the PEG density on blood circulation times for various NPs sizes (55, 90, and 120 nm) with varying PEG density on the PLGA surface. Interestingly, results have shown that above a certain threshold

of repeating units and Mw of the PEG chain (20 PEG chains (5 kDa) per 100 nm^2) the circulation times of the $PEG_{5\ kDa}$-PLGA NPs were dependent on the PEG density rather than the size of the PLGA NP. This effect might be attributed to the shielding properties of the densed PEG surface and the resulting hydration of the PLGA NP. However, a further increase of the PEG density did not show an additional benefit, thus indicating that surface modification can solely alter the biodistribution to a certain extent. On the contrary, PEGylation can promote PLGA NPs degradation and consequently accelerates the loaded drug release. This phenomenon is attributed to the hydrophilic nature of PEG chains that absorb water and stimulate the decomposition of PLGA chains (Rafiei and Haddadi, 2017). Thus, PLGA properties can be further tuned by the introduction of "third party" components as shown for surface modification with stealth polymers. With respect to active targeting approaches, the attachment efficacy of targeting ligands to the NPs and their targeting specificity may vary. Besides the requirement of multiple production steps, their therapeutic effect is often less fruitful than expected. For instance, a previous study performed with prostate-specific membrane antigen (PSMA)-targeted PLA/PLGA-NPs containing DTX showed that the effect of active targeting was not as high as expected (Hrkach et al., 2012). This could be explained by, e.g., PEGylation. Backfilling of the targeted NP with hydrophilic polymers can cover and hide the targeting ligand, and by thus hindering it's binding. Furthermore, incorporation of a targeting moiety might cause size enlargement in NPs and thus, may reduce its ability to cross biological barriers (such as the vascular wall and the extravascular stroma) and/or simultaneously increase the uptake by MPS (Lammers et al., 2012).

PLGA-BASED NPs PREPARATION METHODS

The production techniques of NPs play an important role in their final features such as the shape, size, size distribution, and stability. A wide range of techniques have been used for PLGA-based NPs synthesis such as (single- or double-) emulsification, nanoprecipitation, dialysis, and spray drying. Herein, we highlight the most frequently used approaches (**Figure 2**) in the production of PLGA-based drug delivery nano-sized systems. For detailed information on rather sophisticated techniques, the reader can refer to previous publications (Sharma et al., 2016; Ding and Zhu, 2018).

Emulsification-Evaporation Method

Emulsification is the most commonly used method for PLGA NPs production, where the drug dissolved in a volatile organic solvent is added to an aqueous phase containing surfactants under continuous stir. Subsequently, evaporation is applied to achieve the oil/water (O/W) emulsion form (**Figure 2A**). This procedure can be further followed by adding the resulting (O/W) emulsion to another aqueous solution to form a water/oil/water (W/O/W) (Kamaly et al., 2016; Masood, 2016). Alternative types of advanced emulsion techniques used for PLGA-based microparticle production based on $W/O_1/O_2$ or solid/oil/water (S/O/W) (Ramazani et al., 2016). For hydrophilic drugs the encapsulation efficiency is lower than in single emulsion compared to double- or multiple-emulsion techniques (Mendoza-Muñoz et al., 2016). The polymer concentration and evaporating step determine the NPs size. The higher the concentration of polymer in the discontinuous phase, the larger the size of the resulting particles. This method aims at the incorporation of a wide range of drugs, as well as, contrast agents (i.e., iron oxides) or the co-encapsulation of both substances in one formulation (Acharya and Sahoo, 2011; Lai et al., 2014; Mirakabad et al., 2014; Pérez et al., 2014; Shubhra et al., 2014). Despite the relatively poor loading of temozolomide in PLGA NPs, the single emulsion method performed best with respect to encapsulation efficiency compared with other preparation methods (Ananta et al., 2016). The pitfall of this commonly used method is the presence of surfactant residues on the NPs surface even after several washing steps (Pérez et al., 2014).

Salting Out Method

In the salting-out method, a solution consists of polymer, drug, and a water-miscible organic solvent, which is added to an aqueous phase where salt and stabilizer are dissolved and stirred to form an emulsion (**Figure 2B**). The sudden introduction of water content causes the organic solvent to diffuse into the water and leads to NP formation (Mirakabad et al., 2014). The method is favorable for high concentrations of the polymer and also applicable to heat-sensitive drugs/agents since heat is not required during the process (Mir et al., 2017). However, it is not suitable for lipophilic drugs and its purification procedure is time-consuming since it requires several washing steps to remove stabilizers (Dinarvand et al., 2011).

Sengul et al. reported a method combining the salting out and emulsification approach to encapsulate meloxicam in PLGA NPs with varying Mw (PLGA (50:50 ratio), 5–15 and 40–75 kDa). In this context, the PLGA polymer with higher Mw produced the most stable NPs (Sengel-Turk et al., 2012).

Nanoprecipitation Method

If a solution that consists of polymer, drug, and water-miscible organic solvent is added drop wise to an aqueous solution, the resulting precipitation process results in NPs (**Figure 2C**). This method is a straightforward single-step process with high reproducibility and was initially applied for hydrophobic drugs. Its advantages are scalability and low energy requirement where the NPs properties depend on polymer content and Mw, the nature of the solvents, and the ratios accompanied by mixing rate (Miladi et al., 2016). PLGA NPs (with various surface modifications such as PEGylation) and targeted PLGA NPs were prepared with this method and used to deliver anticancer drugs to the tumor site (Danhier et al., 2009; Valencia et al., 2012; Almoustafa et al., 2017). Further adjustments like pH variation and incorporation of salt additives and/or oil solutions have been applied to improve encapsulation efficiency (Rivas et al., 2017). For example, replacing water with cottonseed oil and Tween-80 as non-solvent made it possible to load hydrophilic drugs in PLGA

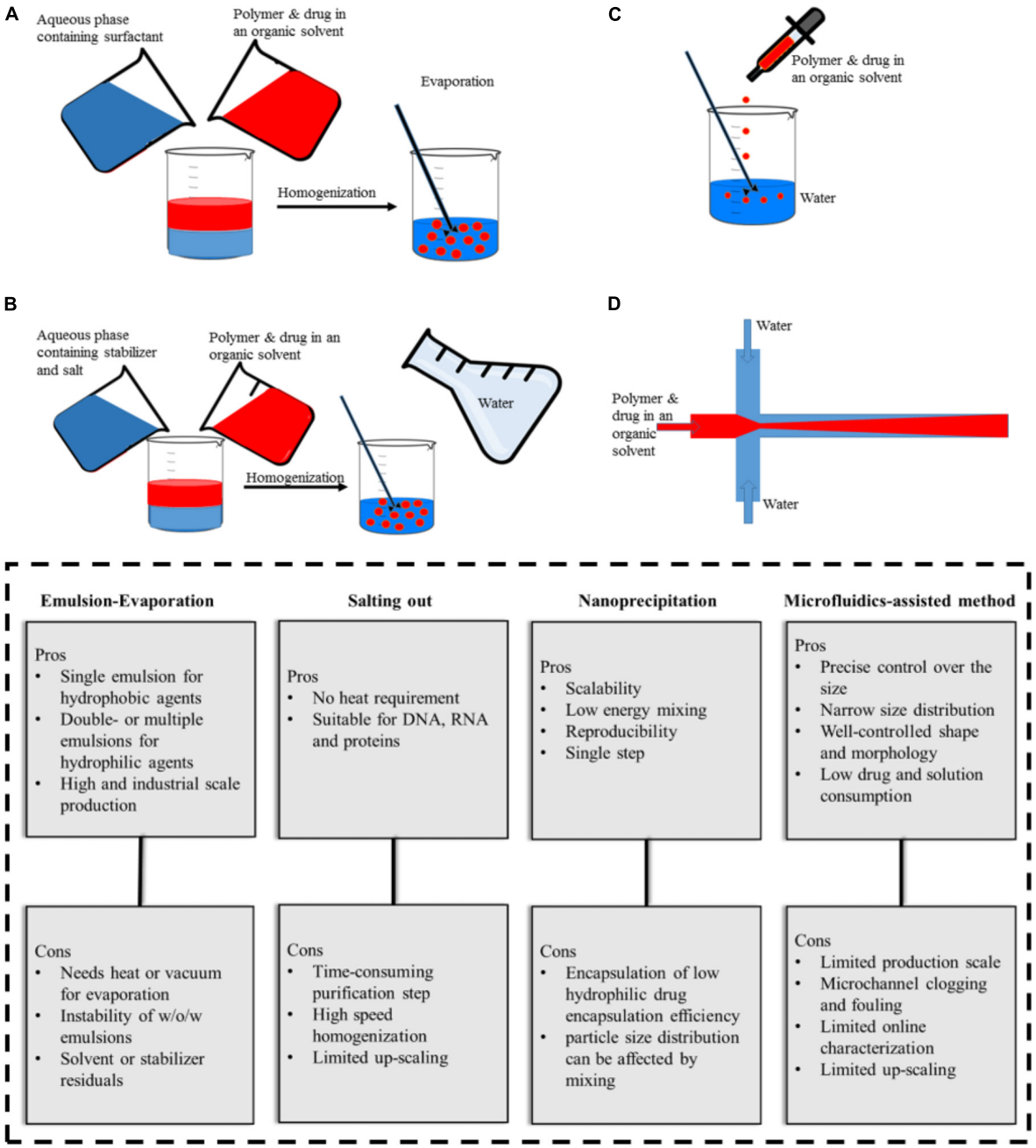

FIGURE 2 | Illustration of PLGA NPs production methods and their advantages and disadvantages. **(A)** emulsification-evaporation, **(B)** salting-out, **(C)** nanoprecipitation, **(D)** microfluidic-assisted method.

NPs (Dalpiaz et al., 2009, 2016). In addition an increase in pH from 5.8 to 9.3 and exchanging procaine hydrochloride with procaine dehydrate resulted in an increase in drug entrapment from 11.0 to 58.2% (Govender et al., 1999). Niu et al. (2009) increased the encapsulation efficiency (>95%) of DNA into PLGA NPs with a modified nanoprecipitation method in which protein and polymer solution in DMSO nanoprecipitated in an aqueous solution of plaxomer. The authors also claimed that this method could outperform the conventional emulsion-evaporation techniques (encapsulation efficiency ∼65%). Moreover, Alshamsan (2014) showed that nanoprecipitation is more efficient than emulsion-based methods in encapsulating cucurbitacin I in PLGA.

Microfluidics-Assisted Method

In microfluidic systems, small volumes (micro- or nano-liter) of liquids are processed in microchannels to achieve better results in comparison with the conventional bulk system. Depending

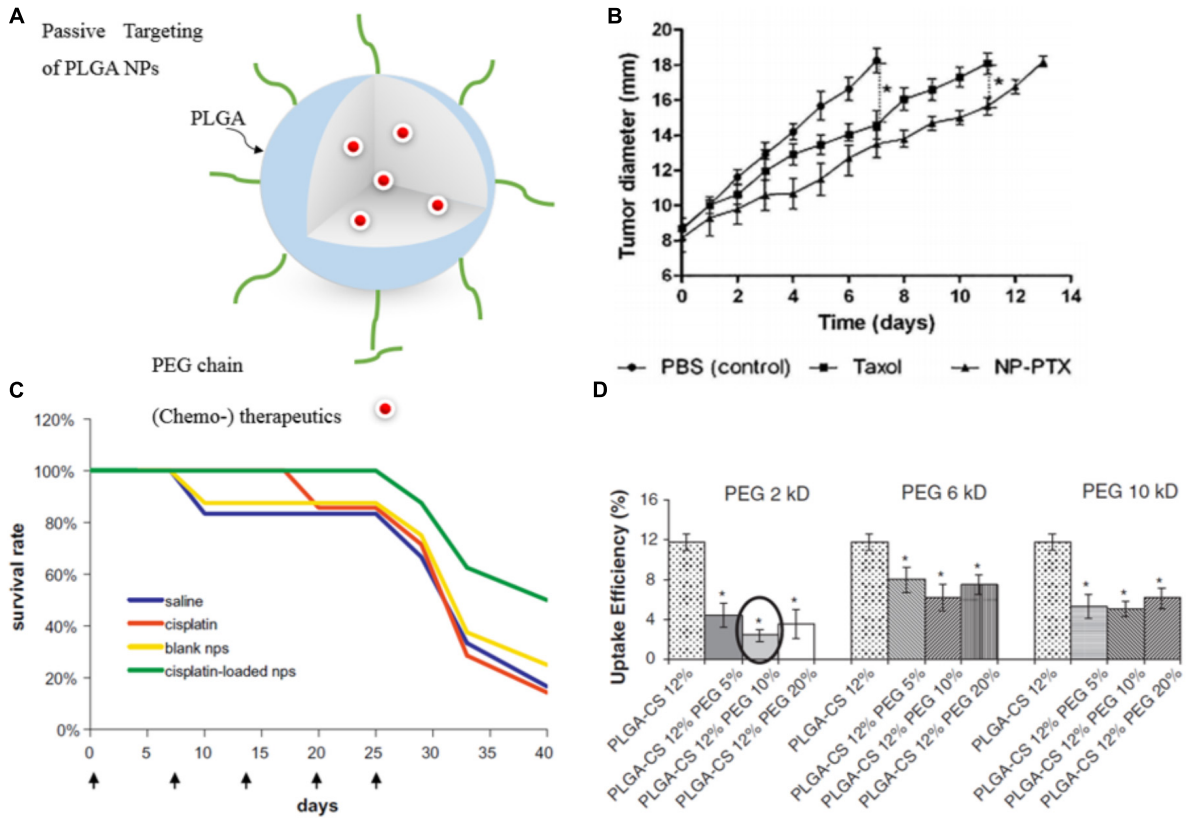

FIGURE 3 | Examples of passively targeted drug-loaded PLGA NPs. **(A)** Illustration of a drug-loaded stealth PLGA NP. **(B)** Antitumor effect of passive targeted PTX-loaded NPs and PTX (Taxol®) on mice with orthotopic hepatocellular carcinomas. Untreated control animals received PBS injection. The control treatments groups received PTX-loaded NPs or PTX only. Highest response was shown for the nanomedicine formulation (*$p < 0.05$). Reprinted from Danhier et al. (2009) with permission from Elsevier. **(C)** The survival rate of colorectal adenocarcinoma HT 29 tumor-bearing mice injected intravenously with cisplatin-loaded PEGylated-PLGA NPs is higher than for the free drug, naive control and vehicle control. Figure reprinted from Mattheolabakis et al. (2009) with permission from Elsevier. **(D)** Phagocytic uptake efficiency of PTX-loaded PLGA NPs in dependence of the surface modification with different amount of PEG with varying Mw. Results showed that NPs with 10% of 2 kDa PEG Mw, along with 12% CS were most efficient in terms of evading phagocytic uptake and consequently are expected to have the most prolonged blood circulation time (*$p < 0.05$). Reprinted from Parveen and Sahoo (2011) with permission from Elsevier.

on the type of reagents flow, microfluidic systems can be classified into two general types, (1) continuous-phase flow, and (2) segmented/droplet-phase flow microfluidic systems. The continuous phase flow microfluidics can be used to produce PLGA particles in the nanoscale while particles produced by segmented flow are typically in the micron size range. To produce PLGA nano-scale particles by continuous phase flow, an organic mixture of polymer and drug is assisted by a flow of aqueous phase solution on both sites along the microchannel, and the precipitation takes place in the organic phase (**Figure 2D**). PLGA NPs produced by microfluidic systems have several advantages; narrow size distribution, well-controlled NP synthesis by controlled reaction time and temperature, improved heat and mass transfer, expedited synthesis, and an overall high reproducibility rate from batch-to-batch (Valencia et al., 2011; Li and Jiang, 2018). Moreover, microfluidically produced NPs have a compact morphology, which can hinder initial burst release (Hasani-Sadrabadi et al., 2015). There are reports on microfluidic systems for the synthesis of various PLGA NPs (e.g., PEGylated, lipid coated and targeted NPs) (Valencia et al., 2013b) for anticancer drug loading ranging from simple two dimensional (Dashtimoghadam et al., 2016; Bramosanti et al., 2017), to more complex 3D (Kranz et al., 2000), and also origami designs (Sun et al., 2013).

DRUG TARGETING

Typically, cancer therapies involve the systemic administration of drugs into the body or its oral uptake, both of which can damage healthy tissues by significant off-target accumulation and thus, generate serious side effects. Off-target accumulation limits the dosage that can be administered. To overcome this limitation, various targeting strategies are being investigated.

Passive Targeting

Tumor accumulation of nanoformulations is first and foremost based on the enhanced permeability and retention (EPR) effect. A leaky, permeable tumor vasculature in combination with the lack of functional lymphatic drainage is a pathophysiological

phenomenon, which leads to an enhanced accumulation of nanosized molecules in tumor tissue (Maeda et al., 2001). PLGA NPs characteristics such as high stability and tunable prolonged blood circulation time are ideal to use this so-called passive targeting approach (Danhier et al., 2012; Wicki et al., 2015).

This passive targeting strategy has been applied for PLGA-based NPs encapsulating chemotherapeutics (**Figure 3A**) such as doxorubicin (DOX) (Park et al., 2009), PTX (**Figure 3B**) (Danhier et al., 2009), cisplatin (**Figure 3C**) (Mattheolabakis et al., 2009; Moreno et al., 2010), and CUR (Mohanty and Sahoo, 2010) to enhance antitumor activity, prolong circulation time and improve stability of the drug by protecting it from the blood components. For instance, CUR-loaded PEGylated PLGA nanocapsules with castor oil core exhibited increased blood circulation time to overcome CUR's short half-life in the biological environment (Klippstein et al., 2015). Similarly, the elimination half-life of PEGylated PLGA-NPs loaded with DTX was shown to be 3.7-fold higher than observed for the free drug (Rafiei and Haddadi, 2017). For the passively targeted NPs, phagocytic uptake inversely reflects the blood circulation time since NPs with stealth properties can evade phagocytic uptake and thus circulate longer in the blood. Parveen and Sahoo evaluated PTX loaded PLGA NPs with various surface modifications [a blend of constant Chitosan (12%) and different PEG percentages (5, 10, and 20%) and Mws (2, 6, and 10 kDa)]. Results revealed that NPs with 10% of PEG (Mw = 2 kDa), along with 12% Chitosan were the most efficient NPs in terms of evading phagocytic uptake (**Figure 3D**) and consequently showed the highest blood circulation time (Parveen and Sahoo, 2011). Moreover, encapsulation of anticancer drugs within the biocompatible polymers and their passive delivery to the tumor site significantly reduced drug side effects. In line with this, also cisplatin encapsulated NPs induced no significant change in body weight and blood urea nitrogen (BUN) plasma levels in tumor-bearing mice (while the free drug resulted in an increase of both parameters) pointing to reduced side effects for the PLGA NPs compared to the free drug. Thus, the encapsulation of antitumor drugs into PLGA NPs not only improves antitumor efficacy but also can significantly reduce the side effects (Moreno et al., 2010).

However, passive targeting has several limitations (Lammers et al., 2012): the heterogeneous vascularization, and permeability, and the highly increased interstitial fluid pressure in many tumors are obstacles that limit the success of passive targeting. These, however, cannot be overcome just via NP adjustment. The EPR effect varies among patients, tumors, tumor types and even changes over time (Shi et al., 2017). This inter- and intra-tumoral variance of the EPR effect encouraged many researchers to question the existence and usefulness of this effect (Danhier, 2016). However, understanding the vascular tumor pathophysiology in more detail can help to address this limitation. For example, imaging protocols, which are able to visualize and quantify the extent of the EPR-mediated tumor targeting in individual patients, or histopathological biomarkers, can be used to predict nanomedicine accumulation and thus to select a responsive patient cohort (Lammers et al., 2012; Danhier and Préat, 2015). To facilitate the translation of NPs into the clinic, and to allow for individualized and improved anticancer nanomedicine therapies, several pharmacological and physical means can be employed to enhance the tumor accumulation and the efficacy of EPR-based nanomedicines. In the class of pharmacological strategies, the most prominent are treatments with drugs, which modulate vascular endothelial growth factor (VEGF) signaling, that act agonistic or antagonistic to angiotensin, enhance the local concentrations of nitric oxide, or, in case of tumor necrosis factor-α (TNF-α), enhance vascular leakiness. Other pharmacological strategies base on vessel promotion, with, e.g., recombinant human erythropoietin (Epo) or cilengitide, both inducing an increase in vessel density and in the relative blood volume and by this enhance drug delivery to the tumor site (Bridges and Harris, 2015; Doleschel et al., 2015; Wong et al., 2015; Nel et al., 2017). Alternatively, physical interventions can be applied including hyperthermia, radiotherapy and sonoporation. Hyperthermia typically leads to an increase in tumor perfusion and to an enhanced vascular permeability, thus promoting drug (and oxygen) supply to tumors (Kong et al., 2001). Radiotherapy can, next to an increase in vascular leakiness (Park et al., 2001), lead to a decrease in cell density within tumors and consequently also to a reduction in interstitial fluid pressure (Znati et al., 1996). In that line, microbubbles (which are routinely used as contrast agents for ultrasound imaging) can also be employed to temporarily increase vessel permeability and perfusion by sonoporation and thus increase drug delivery to the region of interest (Theek et al., 2014).

Active Targeting

To increase the specificity of NPs for the target site and to promote cellular uptake, specific ligands can be attached to the surface of NPs (**Figure 4A**) that bind to receptors or antigens on tumor cells, the tumor microenvironment or the tumor vasculature (Perez-Herrero and Fernandez-Medarde, 2015).

Biotin, folic acid, aptamers, antibodies, and peptides are ligands that were used frequently in case of PLGA NPs (**Table 1**). For instance, DTX-loaded PLGA NPs surface modified with poly(dopamine) (a hydrophilic neutral polymer) and TPGS, functionalized with the DNA aptamer AS1411 improved tumor growth inhibition (**Figure 4B**) compared to all control groups, namely saline, Taxotere®, DTX-loaded NPs and most importantly passive targeted DTX-loaded poly(dopamine)-NPs. However, active targeting may also induce adverse effects: upon surface modification, circulation time is often decreased due to increased opsonization and recognition by the MPS (Theek et al., 2014). In addition, it has been stated that receptor expression on the tumor cells can change over time and next to pathway switching between different receptors, alternative receptors can be upregulated on the tumor cells (Zhu et al., 2018). These facts encouraged researchers to develop NPs that are targeting receptors that are overexpressed at different tumor cell differentiation states. For instance, hyaluronic acid functionalized NPs bind to the CD44 receptor, which is overexpressed in both breast cancer stem cells and regular cancer cells. These hyaluronic acid-cystamine-PLGA (HA-SS-PLGA) NPs that were loaded with DOX and an inhibitor of the hedgehog signaling pathway

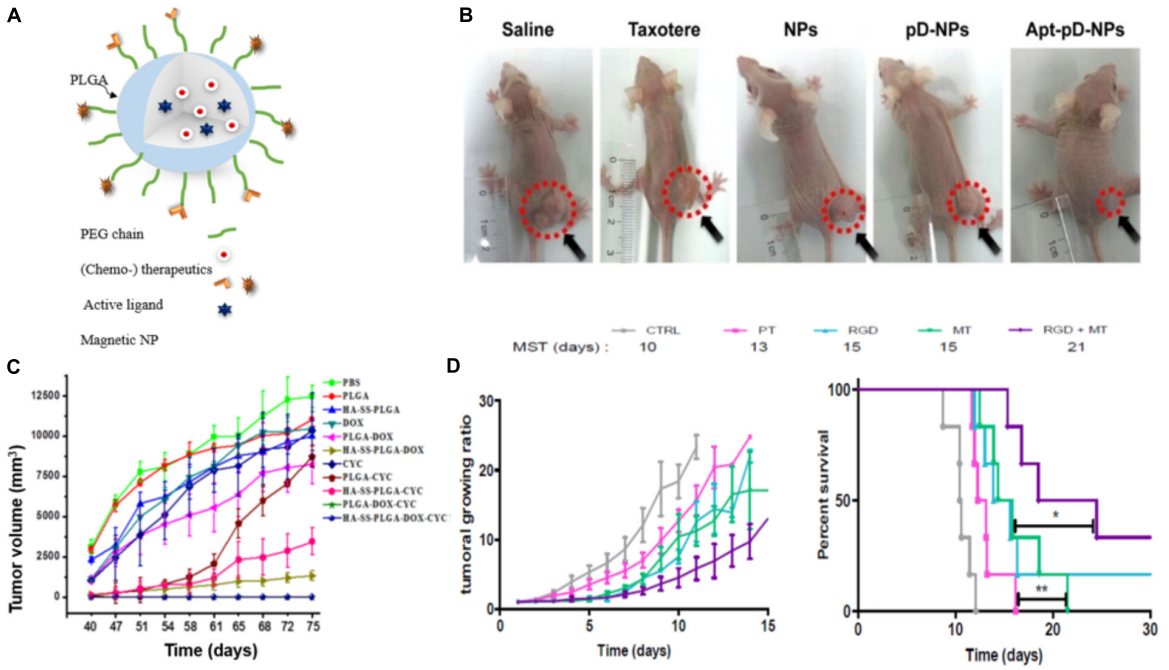

FIGURE 4 | Examples of actively targeted drug-loaded PLGA NPs. **(A)** Scheme of a magnetically and molecularly targeted stealth PLGA NP. **(B)** Tumor growth inhibition was most effective for HeLa xenografted mice treated with DTX-loaded Aptamer-poly(dopamine)-NPs (Apt-pD-NPs) compared to all control groups (NPs: DTX-loaded PLGA NPs; pD-NPs: poly(dopamine) coated-NPs; Apt-pD-NPs: AS1411 aptamer conjugated pD-NPs). Image republished with permission of Dove Medical Press Ltd., from Xu et al. (2016). **(C)** Tumor volume curves after withdrawing of the different drugs at day 40. Breast cancer tumor-bearing mice were treated with PBS, PLGA NPs, hyaluronic acid-cystamine-PLGA (HA-SS-PLGA), free DOX, DOX-loaded PLGA NPs, DOX-loaded HA-SS-PLGA, free cyclopamine (CYC), CYC-loaded PLGA NPs, CYC-loaded HA-SS-PLGA, DOX- and CYC-loaded PLGA, DOX-and CYC-loaded HA-SS-PLGA NPs. Drug-loaded PLGA-HA particles (HA-SS-PLGA-DOX, HA-SS-PLGA-CYC and HA-SS-PLGA-DOX-CYC) and dual-drug-loaded particles (PLGA-DOX-CYC and HA-SS- PLGA-DOX-CYC) significantly delayed tumor recurrence, while tumors rapidly regrew in case of treatments without CYC. Reproduced from Hu et al. (2015) with permission of The Royal Society of Chemistry. **(D)** Tumor growth curves (left) and survival rate (right) of colon carcinoma bearing mice treated with either SPIONs/PTX co-loaded PLGA NPs (PT), RGD grafted on PT NPs (RGD), PT NPs with 4 h magnetic targeting (MT), and RGD grafted on PT NPs with 4 h magnetic targeting (RGD + MT). Tumor growth curves show no significant difference between the groups solely treated with active or magnetic targeting, while the combination of both (CityRGD + MT) increased the survival rate significantly (*$p < 0.05$ and **$p < 0.01$). Tumor growth curves (left) and survival rate (right) reprinted from Schleich et al. (2014) with permission from Elsevier.

of cancer stem cell (cyclopamine) showed superior antitumor activity *in vitro* and *in vivo* (**Figure 4C**) due to internalization into both types of cells. Without combination treatment tumor cells proliferated after withdrawal of the drug in case of treatment with PLGA-NPs loaded with only one of each drugs (Hu et al., 2015).

Magnetic Targeting

Another (active) targeting strategy for drug delivery is magnetic guidance of NPs to the tumor site. In this approach, NPs are loaded with magnetic NPs, which are accumulated at the tumor site by applying an external magnetic field (Polyak and Friedman, 2009). For instance, Schleich et al. co-loaded SPIONs and the chemotherapeutic drug PTX into PLGA NPs and actively targeted them with RGD to αvβ3 integrins. NPs combining active and magnetic targeting promoted an up to eightfold increase in tumor accumulation compared to passive targeted NPs (no RGD or SPIONs), resulting in a prolonged survival rate of colon carcinoma (CT 26) xenografted mice and an inhibition in tumor growth (**Figure 4D**). While magnetic targeting improved the accumulation of the NPs in the tumor, penetration and internalization could not be promoted. This was mediated via the EPR effect and cellular uptake could be enhanced via conjugation of RGD mediating NPs' binding to αvβ3 integrins on the tumor cells (Schleich et al., 2013, 2014).

In a similar approach, Al-Jamal et al. (2016) showed tumor growth inhibition in CT26 colon cancer tumor-bearing mice after magnetically targeted drug delivery of long circulating PEGylated-PLGA nanocapsules (NCs) co-loaded with DTX and varying amounts of SPIONs (0–7% w/w). They also reported that with increasing SPION load, the >200 nm sized NCs showed an increased uptake by liver and spleen, lower blood circulation time, and decreased tumor accumulation. Within the investigated period tumor uptake was significantly higher for tumors that were exposed to a magnetic field compared to tumors that were not exposed while the overall biodistribution of the NCs was not significantly altered by the magnetic field. All investigated NCs showed less systemic toxicity compared to the free drug. Moreover, they computed the magnetic, viscoelastic, convective and diffusive forces and extrapolated the observed efficiency from the rodent experiment to the human body (Al-Jamal et al., 2016).

TABLE 1 | Examples of targeted PLGA NPs formulations: targeting ligands, anticancer drugs, polymer molecular weights and NPs sizes along with key results.

Targeting ligand	Drug	Polymeric NPs (Mw in kDa) (NPs size in nm)	Results	Reference
Folic acid	Disulfiram	NPs size: 28–250 PLGA-PEG PLGA Mw: 38 PEG Mw: 10 NPs size: 165, 204	*In vitro*: higher cellular internalization and higher cytotoxic effect compared to free drug and passive targeted NPs *In vivo*: higher tumor growth inhibition in mice treated with encapsulated NPs compared to passive targeted analogs and free drug	Fasehee et al., 2016
	Boron-CUR complex (RbCur) + Gd complexes	PLGA-PEG PLGA Mw: 30–60 PEG Mw: 2 NPs size: 149 ± 3	*In vitro*: complete inhibition of proliferation in combination with neutron irradiation	Alberti et al., 2017
	DOX and MSA-capped	PLGA-PEG PLGA Mw: 10 PEG Mw: 3.5 NPs size ∼150–170	*In vitro*: enhanced delivery of anticancer drug to MCF-7 and 4T1 cancer cells *In vivo*: no sign of cardiotoxicity as compared to free DOX	Alibolandi et al. (2016)
S,S-2-(3-[5-amino-1-carboxypentyl]-ureido)-pentanedioic acid	Irinotecan + cisplatin	PLGA-PEG PLGA Mw: 45 PEG Mw: 5 NPs size: 55	*In vitro*: analysis with PSMA-expressing LNCaP cells presented eightfold increase in internalization of targeted NPs compared to non-targeted NPs	Valencia et al., 2013a
cRGD (arginine-glycine-aspartic-glutamic-valine acid)	Mitoxantrone (DHAQ)	$mPEG_2$-PLGA-PLL overall Mw: 11 NPs size: 180	*In vitro*: enhanced cytotoxicity toward breast cancer cell *In vivo*: higher antitumor efficiency compared to free drug and non-targeted NPs	Liu et al., 2012
RGD	DOX	PLGA-PEG PLGA Mw: 45 PEG Mw: 5 NPs size: 48–72	*In vitro*: Compared to non-targeted NPs, NPs with up to 50% PLGA-PEG-RGD showed marginal uptake by macrophages, but still efficient uptake by targeted Human Umbilical Vein Endothelial Cells (HUVEC)	Valencia et al., 2011
Cyclic pentapeptide cRGDfK	Gemcitabine	PLGA NPs size ∼80–90	*In vitro:* Higher cytotoxicity toward ovarian cancer cells (SKOV-3 cell), IC50 of the targeted NPs was 16.4 fold and 3.8 fold lower than for free drug and non-targeted NPs	Kulhari et al., 2016
A10 aptamer	DTX	PLGA-PEG PLGA Mw: 0.67 PEG Mw: 3.4 NPs size: 150–250	*in vitro*: Increased uptake by LNCaP cells *in vivo*: Increase in the aptamer density led to accumulation in liver and spleen due to the aptamer covering effect on PEG layer	Gu et al., 2008
Aptamers A15 and aptamers CL4	Salinomycin	PLGA-PEG PLGA Mw: 17 PEG Mw: 3 NPs size: ∼100–170	*In vivo*: Enhanced antitumor activity compared to non-targeted drug-loaded NPs Ability to target cancer stem cell (CSC) and non-(CSC) in hepatocellular carcinoma	Jiang et al., 2015
Transferrin (Tf)	–	PLGA PLGA Mw: 26.5 NPs size: 40–117	*In vitro:* Twofold elevation in tumor accumulation Enhanced uptake of Tf-NPs compared to non-targeted NPs (bovine serum albumin coated)	Chang et al., 2012
	DOX + PTX	Magnetic silica PLGA NPs (MNP-MSN-PLGA-Tf NPs) NPs size: ∼150	*In vitro*: 2.2-fold reduction of the IC_{50} after Tf-conjugation and 2.9-fold reduction after additional magnetic targeting *In vivo*: 47.5-fold tumor size reduction for the dual-drug-loaded NPs on day 20, compared with control treatment	Cui et al., 2013
EGFR-targeting peptide (YHWYGYTPQNVI) and scrambled peptide (non-targeted) (HWPYAHPTHPSW)	Tylocrebrine	PLGA-PEG PLGA Mw: 40 PEG Mw: 3.4 NPs size: 300–400	*In vitro*: twofold to threefold higher uptake of targeted NPs compared with non-targeted ones (scrambled) *In vivo*: threefold higher tumor accumulation of targeted NPs compared to free drug and non-targeted NPs	Kirtane et al., 2015
Vascular Endothelial Growth Factor (VEGFR-C)	PTX	PLGA PLGA Mw: 27 NPs size: 710	*In vitro*: targeted NPs were more associated to HUVECs by binding to VEGFR compared to non-targeted NPs Lower IC_{50} values Stronger antitumor activity	Shi et al., 2015

Cui et al. (2016) evaluated a combination of chemotherapeutics (PTX and CUR) along with magnetic NPs encapsulated in PEGylated PLGA and active targeting with a transferrin receptor binding peptide. In line with the results reported previously, the authors reported that the combination of active and magnetic targeting increased the NPs accumulation and cellular uptake. In detail, a more than 10-fold higher tumor accumulation and improved crossing of the blood–brain barrier by fivefold was achieved in an orthotopic glioma model compared with non-targeted NPs. The application of the magnetic field in combination with transferrin receptor targeting also resulted in an increase in the overall survival rate of the animals and a higher therapeutic efficacy as compared to control groups treated with either magnetic or active targeting alone. However, indications for magnetic targeting are limited by of the difficulty to focus the magnetic field to deep body locations. One loophole for that limitation can be the application of magnetic particle imaging (MPI). Iron oxide NPs are responsive to a given magnetic field and the magnetic moments will line up in the direction of the induced magnetic field. In this context MPI might not only be used as a non-invasive imaging modality, but also promote magnetic targeting and guide the, e.g., SPIONs to the target tissue. Additionally, MPI can be combined with magnetic hyperthermia as the SPIONs can be excited to generate heat yielding an image-guided theranostic tool (Bauer et al., 2016) (see section "Magnetic Hyperthermia"). Nevertheless maintaining the high magnetic gradient strength needed for clinical translation remains challenging and costly (Tay et al., 2018).

COMBINATION TREATMENTS WITH PLGA NPs

Clinically Approved PLGA NPs—Lost in Translation?

Chemotherapeutic PLGA formulations with varying properties (i.e., shape, carrier, size, etc.) are currently available and FDA-approved for several types of cancer treatments. The most prominent among them are based on PLGA microspheres, namely Lupron Depot® (Abbvie Endocrine Inc.) and Trelstar® (Allergan Sales Inc.). Other PLGA formulations in the market are PLGA-based gels (e.g., Eligard®, Tomar Therap) and implants (e.g., Zoladex®, Tersera Theraps LLC.). In a set of PLGA NPs with varying LA/GA ratios tested, the only NP formulation, which was further used in clinical trials did not contain GA and the NP was synthesized from PLA-PEG. This first targeted PLA NP (BIND-014, BIND Therapeutics) encapsulating DTX was applied for targeting the PSMA and the neovasculature that over-expresses PSMA receptor (Von Hoff et al., 2016). The early clinical trials of BIND-014 reported an enhanced anti-tumor activity compared with conventional DTX. Reasonably, many further potential clinical applications of this drug delivery system family for various cancer types, e.g., urothelial carcinoma, metastatic prostate cancer and squamous cell carcinoma of the head and neck were mentioned in related clinical trials (NCT02479178, 2016). However, the study failed in phase II due to low response rates and the company was sold with substantially all of BIND's assets to Pfizer in 2016.

With respect to drug development, researchers often need to take a step back to the fundamental research to continue improving anticancer drug delivery such as enhancing hydrophilicity, reducing uptake by the MPS, increase tumor to background ratios and tumor-targeted specificity to achieve a higher response rate (Chidambaram et al., 2011).

In daily clinical practice patients often receive a combination treatment like, e.g., AC- or TAC-chemotherapy (A = Adriamycin (DOX); C = cyclophosphamide; T = Taxotere (DTX)) for breast cancer or BEAM-chemotherapy (BICNU®, Etoposide, Ara-C cytarabine and melphalan) for the treatment of lymphomas.

The synergism of those standard combination treatments might be increased by the use of nanoformulations and researchers are evaluating their potential *in vitro* and in pre-clinical *in vivo* studies. The NPs offer a platform to co-encapsulate various pairs of drugs with varying hydrophobicity and pharmacokinetic profiles ensuring simultaneous long term distribution to the target site. Such NP co-formulations can extend the drugs' circulation time (Tian et al., 2017), sustain drug release (Khuroo et al., 2018) and also inhibit development of drug resistance (Misra and Sahoo, 2011) as well as increase drug accumulation in tumors (Afrooz et al., 2017). Among the many combinations co-loaded in one particle are PTX-Cisplatin (Tian et al., 2017), PTX-Erlotinib (Khuroo et al., 2018), DOX-CUR (Misra and Sahoo, 2011), PTX-Verapamil (Afrooz et al., 2017), and PTX-epigallocatechin gallate (EGCG). The latter was used for the sequential release of first EGCG and second PTX from PLGA-based core-shell NPs to improve therapeutic efficiency. In this context, the multiple signaling inhibitor EGCG was released first and increased the sensitivity of resistant breast cancer cells toward PTX as indicated by the suppression of the permeability glycoprotein (Pgp) (Narayanan et al., 2014, 2015).

Next to the synergistic effect of different chemotherapeutic drugs, an additional beneficial therapeutic outcome can be achieved via combination treatment with radiotherapy. Ionizing irradiation can increase vascular leakiness and furthermore lead to a decrease in cell density within tumors, and thus reduce the interstitial fluid pressure (Znati et al., 1996; Peschke et al., 1999). These effects contribute to an increased accumulation of both low-molecular-weight drugs and nanomedicine formulations in tumors (Higgins et al., 2015). Consequently, the efficacy of nanomedicine-based chemotherapy can increase (Wasan et al., 2017). *Vice versa* radiosensitizers can be used to improve the effect of radiotherapy (Jin et al., 2007; Wang et al., 2010; Kwatra et al., 2013; Bergs et al., 2015). The most prominent radiosensitizing drugs are PTX, DOX, and DTX. In this context, Werner et al. encapsulated DTX in PLGA NPs with a lecithin-PEG folate surface modification to optimize radiotherapy. Results revealed that radiation 12 h post NPs administration had a maximum effect on tumor growth inhibition (Werner et al., 2011). In a comparable study, prostate cancer cell penetrating peptide (R11) conjugated PLGA NPs were used for targeted radiosensitization of prostate cancer cells leading to higher antitumor activity under the exposure (Menon et al., 2015).

Magnetic Hyperthermia

In hyperthermia the body temperature is increased to damage and kill tumor cells. Hyperthermia can be applied to the whole-body or regionally. The techniques used to induce local hyperthermia are radiofrequency, (high intensity focused) ultrasound, microwave, and laser irradiation as well as alternating magnetic fields. Regarding the latter, PLGA is considered as a suitable carrier to load and deliver magnetic NPs and (chemo-) therapeutics (**Figure 5A**). It has also been indicated that PLGA encapsulation can improve SPIONs stability without changing or affecting the photothermal ability of the nanocomposites (Sivakumar et al., 2017). For local hyperthermia SPIONs or fluid containing magnetic NPs have been injected into the tumors and an alternating magnetic field applied to raise the temperature to 42–46°C. The efficiency of magnetic hyperthermia depends on the size and magnetization of the particles and also on the maximum temperature that can be reached by the particle (Curie temperature) (Thorat et al., 2016).

Hyperthermia is generally applied in combination with chemotherapy or radiotherapy (Rao et al., 2010; Cabuy, 2011; Kaur et al., 2011). Eynali et al. (2017) encapsulated 5-FU into 30–100 nm PLGA NPs with and without an iron oxide core and showed a reduction in the proliferation rate of the colon cancer cell line HT-29 for the combination treatment of hyperthermia and chemotherapy *in vitro*.

In a similar setup Aravind et al. designed and evaluated a multimodal theranostic PLGA nanocomposite containing a magnetic fluid of Fe_3O_4 for hyperthermia induction and MRI imaging, the chemotherapeutic drug PTX, and the fluorescent dye Nile red (NR). Additionally the surface was conjugated with an aptamer targeting the nucleoline receptor yielding a particle with an overall size of 218 nm (Aravind et al., 2013). The *in vitro* analysis showed that the aptamer ligand on the NPs surface increased the tumor cell (MCF7) uptake while lowering the uptake in normal, mouse fibroblast cell line (L929) and thus lowered the *in vitro* cytotoxicity at 5 days after treatment (**Figure 5B**).

In agreement with these findings Vivek et al. evaluated a multifunctional pH-sensitive nanocarrier (PLGA-PVP (polyvinylpyrrolidone) NPs) co-loaded with tamoxifen (TAM) for chemotherapy and Fe_3O_4 for hyperthermia with and without Herceptin on the surface for targeting the human epidermal growth factor receptor 2 (HER 2). They observed a 90% higher reduction in tumor sizes for actively compared to passively targeted NPs (60% reduction) in mice 14 days post-injection (**Figure 5C**). In addition, immunohistochemistry did not reveal any visible morphological change of healthy tissue after treatment

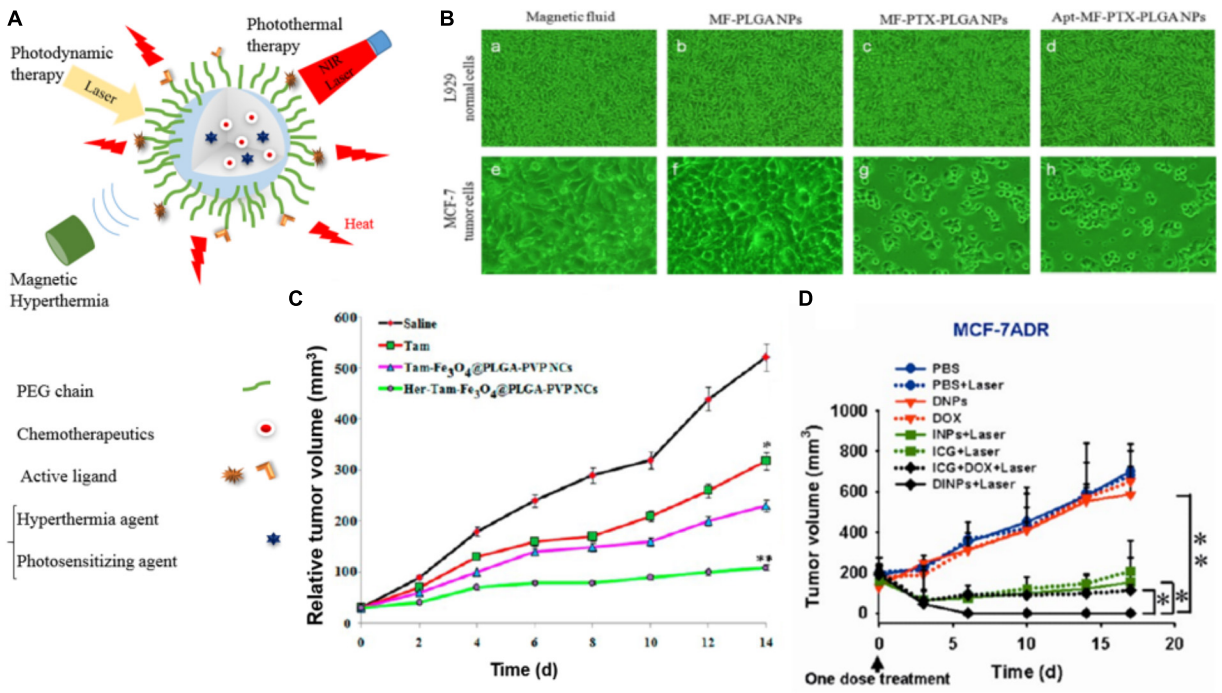

FIGURE 5 | Examples of the performance of PLGA-based NPs used for magnetic hyperthermia, photodynamic therapy, and photothermal therapy drug-loaded PLGA NPs. **(A)** Illustration of drug-loaded NPs used for magnetic hyperthermia, photodynamic therapy, and photothermal therapy. **(B)** Microscopic images of fibroblasts (L929) and MCF-7 cells 5 days after treatment with MF, MF-PLGA, MF-PTX-PLGA, and Apt-MF-PTX-PLGA NPs indicate that actively targeted NPs have the highest cytotoxicity toward cancer cells *in vitro*. Images reprinted from Aravind et al. (2013) with permission from Elsevier. **(C)** Tumor volume changes in breast cancer xenografts in mice treated with PLGA NPs co-loaded with tamoxifen (TAM) and Fe_3O_4 for hyperthermia with and without trastuzumab. Reprinted with permission from Vivek et al. (2016). Copyright (2016) American Chemical Society. **(D)** Tumor growth curves of different groups of mice inoculated with drug resistant breast cancer cells (MCF-7/ADR) after treatments with DOX and ICG co-loaded PLGA@lecithin@PEG NPs (DINPs) prove the added value of PDT (*$p < 0.05$ and **$p < 0.01$). Figure reprinted with permission from Zheng et al. (2013). Copyright (2013) American Chemical Society.

with the PLGA-PVP (polyvinylpyrrolidone) NPs (Vivek et al., 2016). However, the superiority of actively targeted versus passively targeted nanocomposites could as well be an effect of the additional therapeutic interaction of the Herceptin, which upon binding to HER2 prevents the cells from proliferating.

In general, promising therapeutic efficacy could exclusively be achieved via combination treatments; neither the sole delivery of chemotherapy nor the local magnetic hyperthermia could outperform the proposed and presented combination treatments. This can be due to synergistic effects and/or due to an increased drug accumulation following the hyperthermia-related enhancement of the EPR effect. However, despite those promising pre-clinical results (and as already discussed for magnetic targeting) the challenges for successful clinical translation remain unchanged. Importantly, even with MPI-guided induction of hyperthermia, the main challenge is to meet the clinical SPION dose limits and still achieve a therapeutically relevant heating in the region of interest (Tay et al., 2018).

Photodynamic and Photothermal Therapy

In photodynamic treatments a photosensitizing agent (PS) is applied to generate highly ROS via photoexcitation (Chatterjee et al., 2008; Paszko et al., 2011; Calixto et al., 2016). However, most of the PS agents are hydrophobic, show a rapid decomposition under laser irradiation, do not accumulate well in the tumor and cannot be efficiently excited in the near infrared range (which is prerequisite for reaching deeper tissues). Nanocarriers like PLGA-NPs can be used to overcome some of these drawbacks (Paszko et al., 2011; Lim et al., 2013). In line with this, the most commonly used PS agents that have been loaded into nanocarriers like PLGA NPs are poly(anilin) (Nguyen et al., 2017), indocyanine green (ICG) (Zheng et al., 2013; Lee and Chang, 2017), and zinc(II)-meso-tetraphenylporphyrin (ZnTPP) (Boix-Garriga et al., 2015).

Among them, ICG is not only a suitable PS agent, but is also categorized as a photothermal agent and in addition allows for optical imaging. In this context, Zheng et al. designed a lipid-polymer hybrid NP (PLGA-lecithin-PEG) that was co-loaded with DOX and ICG for combinational chemo- and photodynamic treatment. The NPs were synthesized by a single-step sonication method with an average diameter of 90 nm and were evaluated *in vitro* as well as *in vivo* in chemotherapy resistant (MCF-7/ADR) and sensitive (MCF-7) breast cancer cells. After laser irradiation, the combined treatment of DOX and ICG-loaded PLGA-lecithin-PEG synergistically promoted cell death and tumor growth inhibition in both tumor models (**Figure 5D**) (Zheng et al., 2013; Lee and Chang, 2017).

In photothermal therapy (PTT) a therapeutic agent absorbs photon energy and dissipates it in form of heat. This heat results in the disruption of cellular membranes and induces apoptosis and/or necrosis. PTT can be applied with various organic nanomaterials (e.g., carbon and gold nanomaterials, etc.) and polymeric NPs with NIR-absorbing agents like ICG (Cheng et al., 2014). In that line PLGA and its copolymers (e.g., PLGA-PEG, PLGA-lipid) have been used for co-loading and combination therapy with, e.g., DTX and gold (Au) (Hao et al., 2015), DTX and poly(dopamine) (Peng et al., 2018) or DTX and polypyrrole (PPy) (Yuan et al., 2016). The latter PTT agent, PPy, is considered an ideal heat inductive material, which was used by Yuan et al. to build a DOX encapsulated PLGA-PPy NP. An additional surface modification with 2-Deoxy-glucose terminated PEG resulted in a sugar promoted 17-fold increased uptake of the NPs by MCF-7 cells without altering the photothermal properties of the compound. In a comparable NP design Peng et al. synthesized PLGA-NPs with a poly(dopamine) (PDA) coating modified with TPGS, yielding PLGA NPs@PDA-TPGS. Those NPs were loaded with DOX, and the combination treatment was evaluated *in vitro* and *in vivo* in BALB/c MCF-7 (drug resistant) breast cancer xenografted mice. The NIR irradiation triggered DTX release, and a synergistic antitumor efficacy indicated that the DOX-loaded PLGA NPs@PDA-TPGS could overcome drug resistance.

Next to the therapeutic effect of the generated heat and/or triggered drug release, PTT can like (magnetic) hyperthermia increase vascular permeability and blood flow and thus enhance EPR effect and increase drug delivery (Chen et al., 2006; Yuan et al., 2016).

Even though the combination treatment of chemotherapy and PTT/PDT holds great potential, also with respect to the synergistic effect on therapeutic outcome, the sites for PDT are limited by the penetration depth of the applied laser light (max. 1–2 cm), as well as by the short migration distance of the produced oxygen radicals (Moan and Berg, 1991). For optimal efficacy, photodynamic therapy, therefore, has to be directed to specific (sub-) cellular targets (mitochondria, lysosomes, or the cell membrane), which can be challenging in a clinical setting.

Gene Therapy

Next to standard chemotherapeutic treatments and immunotherapies, gene delivery and gene silencing are emerging approaches in the anticancer field. Here, a double-stranded DNA (dsDNA) or a single-stranded DNA (ssDNA) is used for replacing (or completing) a gene while short interfering RNA (siRNA) is typically used for silencing a gene (Ibraheem et al., 2014). When cancer is initiated by cellular mutation, siRNAs can inhibit genes responsible for multidrug-resistance and in combination with, e.g., targeted chemotherapeutics, the self-defense mechanism can be inhibited (Xiao et al., 2017). The major obstacle in gene therapy is the delivery of the large, negatively charged and very fragile nucleic acids into the cell cytoplasm, respectively, the cell nucleus. PLGA has been used as a carrier to protect and deliver nucleic acids (Wang et al., 2016). Tang et al. used calcium phosphate–pDNA complexes embedded in PLGA NPs, which were able to inhibit the proliferation of breast cancer cells (4T1) and induce apoptosis. The transfection of the cells with the plasmid DNA encoding for the MsurvivinT34A gene resulted in tumor angiogenesis inhibition and a decrease in microvessel density. Furthermore, in combination with Doxil (DOX encapsulating liposomes) a significant suppression of tumor growth could be observed (Tang et al., 2014).

Recently, the PLGA nanomedicine platform has also been used for genome editing via the CRISPR (Clustered Regularly

Interspaced Short Palindromic Repeats) technology. Delivery of the CRISPR-associated protein-9 nuclease (Cas9) complexed with a synthetic guide RNA (gRNA) into a cell enables genome cutting at a desired location, allowing existing genes to be silenced, removed or added. In chronic myeloid leukemia (CML) reciprocal translocation of chromosome 9 and 22t results in a breakpoint cluster region-abelson (BCR-ABL) fusion oncogene, which translates a relating BCR-ABL fusion protein. In a study by Liu and colleagues, this BCR-ABL fusion protein was knocked out via the delivery of a CRISPR/Cas9 plasmid (pCas9/gBCR-ABL), which was encapsulated in a PEG-PLGA-based cationic lipid-assisted polymeric NP. Successful knockout of the gene of interest was confirmed *in vitro* as well as *in vivo* in a CML mouse model. Mice that were i.v. injected with the nanocarrier showed a reduced number of myelogenous leukemia cells (K562) in blood and bone marrow and a significant prolonged survival rate after the treatment compared to naive and vehicle controls (Liu et al., 2018).

Challenges remain regarding the simultaneous entrapment and encapsulation of gene- and chemotherapy agents in polymeric NPs (Lee et al., 2016; Wang et al., 2017). In this context, pioneering work was done by Yang et al. who synthesized a DOX encapsulated PLGA-NP with a surface modification by a positively charged poly(ethyleneimine) for adsorption of condensed shRNA onto the NP, yielding a theranostic nanobubble that could also be visualized by ultrasound imaging. The shRNA downregulated the P-glycoprotein associated with the adenosine triphosphate-dependent drug efflux pump. This P-glycoprotein knockdown accelerated cellular uptake of the NPs, and due to the suppressed drug efflux increased the nuclear accumulation of DOX in drug resistant tumors (MCF-7/ADR) (Yang et al., 2015). In another approach, Zhang et al. used PEG-PLGA-poly (L-lysine) NPs to co-delivery DOX with siRNA. The presented NPs were surface modified with epidermal growth factor (EGF) for targeted delivery and treatment of lung cancer. The siRNA knocks down the anti-apoptosis protein B-cell lymphoma 2 and thus induced apoptosis in the targeted tissue. Biodistribution and therapy studies were performed using xenografts of the human non-small cell lung carcinoma cell line (H1299) in mice. The combination treatment suppressed lung cancer growth, and reduced expression of the anti-apoptosis protein, which was confirmed by *ex vivo* analysis of the tumor tissue (Yang et al., 2015; Yin et al., 2015; Zhang et al., 2016).

Cancer Immunotherapy

Cancer immunotherapy can be performed via cancer vaccines, cytokine therapy, checkpoint-blockade therapy, adoptive T-cell transfer, and chimeric antigen receptor T (CAR-T) cell therapy

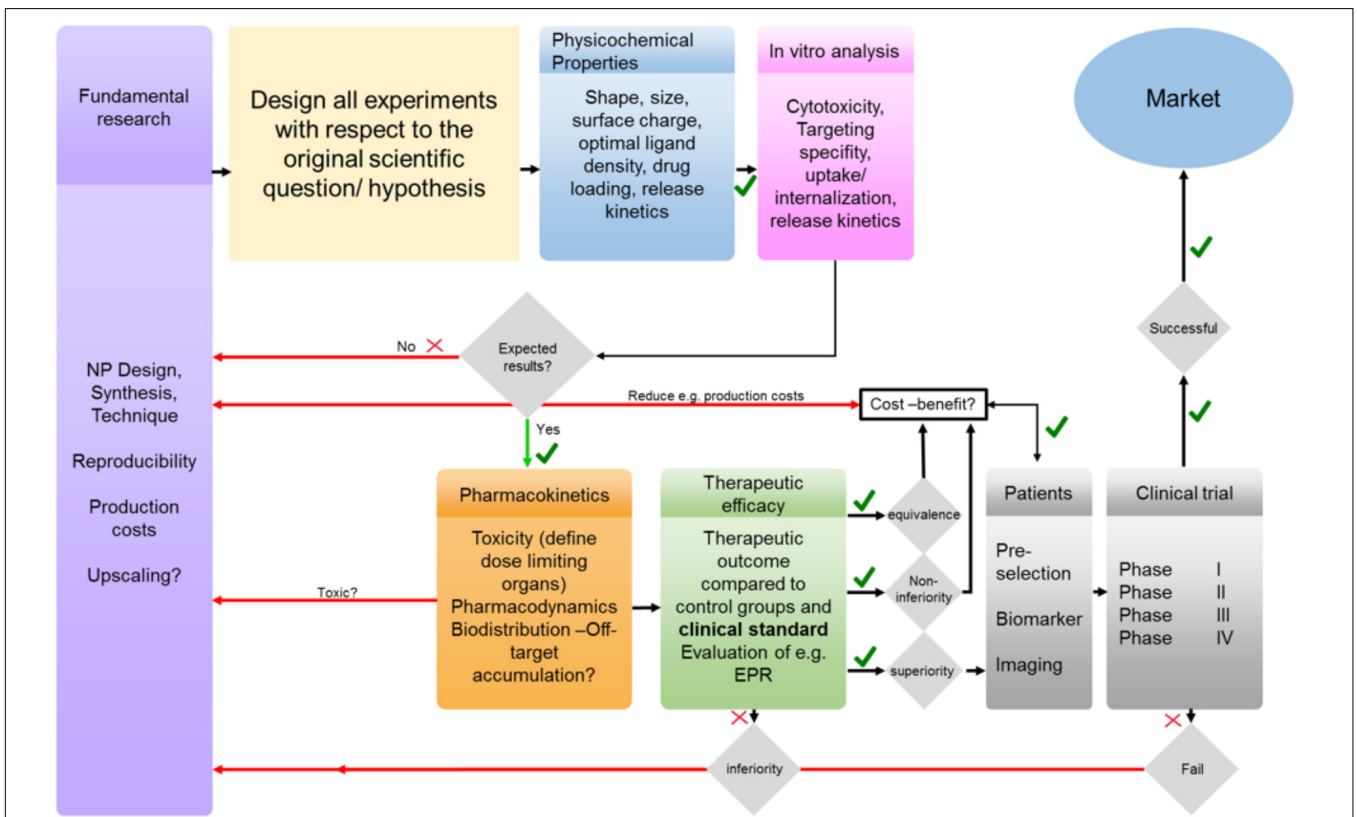

FIGURE 6 | From bench to bedside: simplified illustration of several barriers and challenges that need to be tackled to achieve clinical translation. In fundamental research NP design and production should be performed with respect to a clinical relevant scientific question and all experiments should be designed accordingly and not *vice versa*. The effect of NPs physicochemical properties on their *in vivo* performance needs to be evaluated and optimized if necessary. Any failures in *in vitro*, *in vivo* and/or clinical trials need to be addressed and reconsidered in fundamental research.

(Yoon et al., 2018). Here, PLGA-based NPs can not only protect the sensitive cargos (e.g., antigens, adjuvants, etc.) from degradation but can also promote passive accumulation by the EPR effect and can facilitate additional active targeting strategies via surface modification. However, the stimulation of the immune system, which enables the recognition and attack of malignant cells, does not solely rely on tumor accumulation, but might as well be achieved or enhanced by targeting of immune cells, e.g., in liver, spleen, and lymph nodes. Thus, high affinity of many NPs to cells of the mononuclear phagocyte system as well as macrophage uptake might even be used to promote the desired immune-response (Jiang et al., 2017a,b).

In that regard, NPs can be used to deliver, e.g., immunogenic cell death (ICD) promoters, vaccines or immune checkpoint inhibitors through intravenous injection. Zhao et al. (2016) showed that mPEG-PLGA based NPs loaded with the chemotherapeutic ICD promoter oxaliplatin lead to a high response in an *in vivo* mouse model of pancreatic cancer. As a non-immunogenic control the same PLGA-NPs were loaded with the chemotherapeutic gemcitabine leading to a less effective therapeutic response (Zhao et al., 2016).

In another study, PLGA NPs coated with an agonistic αCD40-monoclonal antibody (mAb) were applied for vaccine delivery to dendritic cells (DCs) as the main antigen presenting cells. The PLGA NPs were loaded with the adjuvants Pam3Csk4 (a synthetic triacylated lipopeptide to stimulate toll-like receptor 2) and Poly (I:C) (Polyinosinic:polycytidylic; an immune-stimulator to toll-like receptor 3) to induce potent $CD8^+$ T cell response. *In vivo* experiments in murine melanoma-OVA mouse model indicated that active targeting of DCs and vaccine delivery resulted in efficient priming of $CD8^+$ T cells, tumor control, and prolonged survival of the tumor-bearing mice (Rosalia et al., 2015).

Furthermore, the use of cells as vaccines for generation of effective and adaptive immune responses is well established in cancer immunotherapy. Ahmed et al. coupled γ-irradiated non-vital prostate cancer cells with PLGA NPs. The particle-cell hybrid was then additionally functionalized with the adjuvant CpG ODN, which selectively activates the toll-like receptor 9. This activation resulted in efficient cancer vaccination in a prostate cancer model. Interestingly, comparable results could not be achieved with a similar particle-melanoma cell hybrid. Due to this, the authors concluded that a careful selection of the tumor entity in such hybrid NPs might be a prerequisite to elicit DCs (Ahmed et al., 2017).

Moreover, a combination of cancer immunotherapy with other modalities like PTT can provide a more effective treatment (Chen et al., 2016). In this context, multifunctional PLGA-PEG NPs co-loaded with ICG (photothermal and PS agent) and imiquimod (R837), an immune-adjuvant TLR-7 agonist, triggered vaccine-like immune responses. Additional combination of this NIR heater-loaded PLGA-based nanovaccine with an anti-cytotoxic T-lymphocyte antigen-4 checkpoint-blockade therapy synergistically inhibited the growth of metastasis and prevented recurrence of cancer.

CONCLUSION

In this review article, we summarize the physicochemical properties of polymers and NPs based on PLGA, and discuss their preparation methods, and applications for various drug delivery approaches. While several different PLGA-based therapeutics are already routinely used in the clinic, despite promising pre-clinical results, PLGA-NPs are neither listed nor approved and the only formulation (BIND-014) that made it into clinical trials was based on PLA-PEG and failed in phase II due to non-responders.

As a consequence, researchers need to critically reflect the clinical feasibility of their approaches and develop NPs that better match the biomedical need (**Figure 6**). This not only relates to the optimization of size, drug loading and drug release, but also to biocompatibility, pharmaceutical upscaling and batch-to-batch reproducibility. In this context, it is advantageous if the experimental setup is from beginning on tailored to a concrete clinical problem. Especially in the case of PLGA NP synthesis batch-to-batch consistency (due to the heterogenous mixing conditions required for self-assembly), which directly relates to drug loading efficacy, and the challenge to obtain particle sizes below 100 nm in an up-scalable process are remaining issues regarding PLGA-NP production. The lack in reproducibility and the need for additional purification steps impede manufacturing according to good manufacturing practices (GMP) that is mandatory for successful clinical translation. Furthermore, awareness of pharmacokinetics and pharmacodynamics of the NPs is mandatory to avoid off-target accumulation and potential side effects. The (often too large) sizes of NPs as well as their surface charge can result in severe off-target accumulation and can even prevent targeted NPs from binding to the target tissue/cell. Surface modifications, yielding, e.g., in a stealth NP, might avoid the recognition by the immune system but will simultaneously increase the size, may prevent penetration of the nanomedicine, hide targeting motifs, and reduce cellular uptake (which is mandatory for the therapeutic effect of many drugs). Any even minor chemical modification of a nanomedicine formulation can alter the physicochemical properties and thus the *in vitro* and *in vivo* performance as well as therapeutic efficacy. Furthermore, when combining nanomedicines with approaches like PDT/PTT or magnetic guidance, one needs to consider that these concepts of drug delivery will only be operant if the external stimulus (e.g., magnet) can be applied to the target region of the human body (which is often not the case for tumors located deeply below the skin).

Next to the influence of the NPs design and the challenges regarding the application of (external) stimuli-induced delivery and cancer treatment, it has been increasingly recognized that the high inter- and intra-individual heterogeneity of the EPR effect is an important reason for the moderate clinical translation of many nanomedicine formulations including PLGA-NPs. Thus, nanomedicine research will strongly take advantage from concepts that consider and address

pathophysiological features that impact the EPR effect and affect the accumulation, penetration, distribution, retention and efficacy of NPs formulations.

In conclusion, for an efficient clinical translation a more rational design of PLGA-NPs, along with clinically relevant preclinical therapy settings, in which nanomedicines are tested are mandatory to close the currently huge gap between material research, preclinical experimentation and clinical reality.

AUTHOR CONTRIBUTIONS

FK contributed toward conceptualization and planning of the manuscript. SR and ND wrote the paper and designed the figures. SR, ND, NG, and TL contributed toward data collection. FK, MM, TL, EK, YS, and FK contributed toward revising the paper and agree to be accountable for all aspects of the work. All authors agreed on the finally submitted version of the manuscript.

REFERENCES

Acharya, S., and Sahoo, S. K. (2011). PLGA nanoparticles containing various anticancer agents and tumour delivery by EPR effect. *Adv. Drug Deliv. Rev.* 63, 170–183. doi: 10.1016/j.addr.2010.10.008

Afrooz, H., Ahmadi, F., Fallahzadeh, F., Mousavi-Fard, S. H., and Alipour, S. (2017). Design and characterization of paclitaxel-verapamil co-encapsulated PLGA nanoparticles: Potential system for overcoming P-glycoprotein mediated MDR. *J. Drug Deliv. Sci. Technol.* 41, 174–181. doi: 10.1016/j.jddst.2017.06.020

Ahmed, K. K., Geary, S. M., and Salem, A. K. (2017). Surface engineering tumor cells with adjuvant-loaded particles for use as cancer vaccines. *J. Control. Release* 248, 1–9. doi: 10.1016/j.jconrel.2016.12.036

Alberti, D., Protti, N., Franck, M., Stefania, R., Bortolussi, S., Altieri, S., et al. (2017). Theranostic nanoparticles loaded with imaging probes and rubrocurcumin for combined cancer therapy by folate receptor targeting. *ChemMedChem* 12, 502–509. doi: 10.1002/cmdc.201700039

Alibolandi, M., Abnous, K., Sadeghi, F., Hosseinkhani, H., Ramezani, M., and Hadizadeh, F. (2016). Folate receptor-targeted multimodal polymersomes for delivery of quantum dots and doxorubicin to breast adenocarcinoma: in vitro and in vivo evaluation. *Int. J. Pharm.* 500, 162–178. doi: 10.1016/j.ijpharm.2016.01.040

Al-Jamal, K. T., Bai, J., Wang, J. T., Protti, A., Southern, P., Bogart, L., et al. (2016). Magnetic drug targeting: preclinical in vivo studies. Mathematical modeling, and extrapolation to humans. *Nano Lett.* 16, 5652–5660. doi: 10.1021/acs.nanolett.6b02261

Almoustafa, H. A., Alshawsh, M. A., and Chik, Z. (2017). Technical aspects of preparing PEG-PLGA nanoparticles as carrier for chemotherapeutic agents by nanoprecipitation method. *Int. J. Pharm.* 533, 275–284. doi: 10.1016/j.ijpharm.2017.09.054

Alshamsan, A. (2014). Nanoprecipitation is more efficient than emulsion solvent evaporation method to encapsulate cucurbitacin I in PLGA nanoparticles. *Saudi Pharm. J.* 22, 219–222. doi: 10.1016/j.jsps.2013.12.002

Ananta, J. S., Paulmurugan, R., and Massoud, T. F. (2016). Temozolomide-loaded PLGA nanoparticles to treat glioblastoma cells: a biophysical and cell culture evaluation. *Neurol. Res.* 38, 51–59. doi: 10.1080/01616412.2015.1133025

Aravind, A., Nair, R., Raveendran, S., Veeranarayanan, S., Nagaoka, Y., Fukuda, T., et al. (2013). Aptamer conjugated paclitaxel and magnetic fluid loaded fluorescently tagged PLGA nanoparticles for targeted cancer therapy. *J. Magn. Magn. Mater.* 344, 116–123. doi: 10.1016/j.jmmm.2013.05.036

Bauer, L. M., Situ, S. F., Griswold, M. A., and Samia, A. C. (2016). High-performance iron oxide nanoparticles for magnetic particle imaging - guided hyperthermia (hMPI). *Nanoscale* 8, 12162–12169. doi: 10.1039/c6nr01877g

Bergs, J. W., Wacker, M. G., Hehlgans, S., Piiper, A., Multhoff, G., Rodel, C., et al. (2015). The role of recent nanotechnology in enhancing the efficacy of radiation therapy. *Biochim. Biophys. Acta* 1856, 130–143. doi: 10.1016/j.bbcan.2015.06.008

Berthet, M., Gauthier, Y., Lacroix, C., Verrier, B., and Monge, C. (2017). Nanoparticle-based dressing: the future of wound treatment? *Trends Biotechnol.* 35, 770–784. doi: 10.1016/j.tibtech.2017.05.005

Bertrand, N., Grenier, P., Mahmoudi, M., Lima, E. M., Appel, E. A., Dormont, F., et al. (2017). Mechanistic understanding of in vivo protein corona formation on polymeric nanoparticles and impact on pharmacokinetics. *Nat. Commun.* 8:777. doi: 10.1038/s41467-017-00600-w

Boix-Garriga, E., Acedo, P., Casado, A., Villanueva, A., Stockert, J. C., Canete, M., et al. (2015). Poly(D, L-lactide-co-glycolide) nanoparticles as delivery agents for photodynamic therapy: enhancing singlet oxygen release and phototoxicity by surface PEG coating. *Nanotechnology* 26:365104. doi: 10.1088/0957-4484/26/36/365104

Bowerman, C. J., Byrne, J. D., Chu, K. S., Schorzman, A. N., Keeler, A. W., Sherwood, C. A., et al. (2017). Docetaxel-loaded PLGA nanoparticles improve efficacy in taxane-resistant triple-negative breast cancer. *Nano Lett.* 17, 242–248. doi: 10.1021/acs.nanolett.6b03971

Bramosanti, M., Chronopoulou, L., Grillo, F., Valletta, A., and Palocci, C. (2017). Microfluidic-assisted nanoprecipitation of antiviral-loaded polymeric nanoparticles. *Colloids Surf. A Physicochem. Eng. Asp.* 532, 369–376. doi: 10.1016/j.colsurfa.2017.04.062

Bridges, E., and Harris, A. L. (2015). Vascular-promoting therapy reduced tumor growth and progression by improving chemotherapy efficacy. *Cancer Cell* 27, 7–9. doi: 10.1016/j.ccell.2014.12.009

Cabuy, E. (2011). Hyperthermia in cancer treatment. *Reliab. Cancer Ther. Energy Based Ther.* 1, 1–48.

Calixto, G. M. F., Bernegossi, J., de Freitas, L. M., Fontana, C. R., and Chorilli, M. (2016). Nanotechnology-based drug delivery systems for photodynamic therapy of cancer: a review. *Molecules* 21:342. doi: 10.3390/molecules21030342

Chang, J., Paillard, A., Passirani, C., Morille, M., Benoit, J. P., Betbeder, D., et al. (2012). Transferrin adsorption onto PLGA nanoparticles governs their interaction with biological systems from blood circulation to brain cancer cells. *Pharm. Res.* 29, 1495–1505. doi: 10.1007/s11095-011-0624-1

Chatterjee, D. K., Fong, L. S., and Zhang, Y. (2008). Nanoparticles in photodynamic therapy: an emerging paradigm. *Adv. Drug Deliv. Rev.* 60, 1627–1637. doi: 10.1016/j.addr.2008.08.003

Chen, B., Pogue, B. W., Luna, J. M., Hardman, R. L., Hoopes, P. J., and Hasan, T. (2006). Tumor vascular permeabilization by vascular-targeting photosensitization: effects, mechanism, and therapeutic implications. *Clin. Cancer Res.* 12, 917–923. doi: 10.1158/1078-0432.CCR-05-1673

Chen, Q., Xu, L., Liang, C., Wang, C., Peng, R., and Liu, Z. (2016). Photothermal therapy with immune-adjuvant nanoparticles together with checkpoint blockade for effective cancer immunotherapy. *Nat. Commun.* 7:13193. doi: 10.1038/ncomms13193

Cheng, L., Wang, C., Feng, L., Yang, K., and Liu, Z. (2014). Functional nanomaterials for phototherapies of cancer. *Chem. Rev.* 114, 10869–10939. doi: 10.1021/cr400532z

Chidambaram, M., Manavalan, R., and Kathiresan, K. (2011). Nanotherapeutics to overcome conventional cancer chemotherapy limitations. *J. Pharm. Pharm. Sci.* 14, 67–77. doi: 10.18433/J30C7D

Chu, K. S., Hasan, W., Rawal, S., Walsh, M. D., Enlow, E. M., Luft, J. C., et al. (2013). Plasma, tumor and tissue pharmacokinetics of Docetaxel delivered via nanoparticles of different sizes and shapes in mice bearing SKOV-3 human ovarian carcinoma xenograft. *Nanomedicine* 9, 686–693. doi: 10.1016/j.nano.2012.11.008

Cui, Y., Xu, Q., Chow, P. K., Wang, D., and Wang, C. H. (2013). Transferrin-conjugated magnetic silica PLGA nanoparticles loaded with doxorubicin and paclitaxel for brain glioma treatment. *Biomaterials* 34, 8511–8520. doi: 10.1016/j.biomaterials.2013.07.075

Cui, Y., Zhang, M., Zeng, F., Jin, H., Xu, Q., and Huang, Y. (2016). Dual-targeting magnetic PLGA nanoparticles for codelivery of paclitaxel and curcumin for brain tumor therapy. *ACS Appl. Mater. Interfaces* 8, 32159–32169. doi: 10.1021/acsami.6b10175

Dalpiaz, A., Sacchetti, F., Baldisserotto, A., Pavan, B., Maretti, E., Iannuccelli, V., et al. (2016). Application of the "in-oil nanoprecipitation" method in the

encapsulation of hydrophilic drugs in PLGA nanoparticles. *J. Drug Deliv. Sci. Technol.* 32, 283–290. doi: 10.1016/j.jddst.2015.07.020

Dalpiaz, A., Vighi, E., Pavan, B., and Leo, E. (2009). Fabrication via a nonaqueous nanoprecipitation method, characterization and in vitro biological behavior of N(6)-cyclopentyladenosine-loaded nanoparticles. *J. Pharm. Sci.* 98, 4272–4284. doi: 10.1002/jps.21710

Danhier, F. (2016). To exploit the tumor microenvironment: since the EPR effect fails in the clinic, what is the future of nanomedicine? *J. Control. Release* 244, 108–121. doi: 10.1016/j.jconrel.2016.11.015

Danhier, F., Ansorena, E., Silva, J. M., Coco, R., Le Breton, A., and Préat, V. (2012). PLGA-based nanoparticles: an overview of biomedical applications. *J. Control. Release* 161, 505–522. doi: 10.1016/j.jconrel.2012.01.043

Danhier, F., Lecouturier, N., Vroman, B., Jérôme, C., Marchand-Brynaert, J., Feron, O., et al. (2009). Paclitaxel-loaded PEGylated PLGA-based nanoparticles: in vitro and in vivo evaluation. *J. Control. Release* 133, 11–17. doi: 10.1016/j.jconrel.2008.09.086

Danhier, F., and Préat, V. (2015). Strategies to improve the EPR effect for the delivery of anti-cancer nanomedicines. *Cancer Cell Microenvironment* 2:e808.

Dasgupta, A., Liu, M., Ojha, T., Storm, G., Kiessling, F., and Lammers, T. (2016). Ultrasound-mediated drug delivery to the brain: principles, progress and prospects. *Drug Discov. Today Technol.* 20, 41–48. doi: 10.1016/j.ddtec.2016.07.007

Dashtimoghadam, E., Fahimipour, F., Davaji, B., Hasani-Sadrabadi, M., and Tayebi, L. (2016). Microfluidic-directed synthesis of polymeric nanoparticles for bone cancer therapy. *Dent. Mater.* 32, e59–e60. doi: 10.1016/j.dental.2016.08.123

Dechy-Cabaret, O., Martin-Vaca, B., and Bourissou, D. (2004). Controlled ring-opening polymerization of lactide and glycolide. *Chem. Rev.* 104, 6147–6176. doi: 10.1021/cr040002s

Dimcevski, G., Kotopoulis, S., Bjanes, T., Hoem, D., Schjott, J., Gjertsen, B. T., et al. (2016). A human clinical trial using ultrasound and microbubbles to enhance gemcitabine treatment of inoperable pancreatic cancer. *J. Control. Release* 243, 172–181. doi: 10.1016/j.jconrel.2016.10.007

Dinarvand, R., Sepehri, N., Manoochehri, S., Rouhani, H., and Atyabi, F. (2011). Polylactide-co-glycolide nanoparticles for controlled delivery of anticancer agents. *Int. J. Nanomedicine* 6, 877–895. doi: 10.2147/IJN.S18905

Ding, D., and Zhu, Q. (2018). Recent advances of PLGA micro/nanoparticles for the delivery of biomacromolecular therapeutics. *Mater. Sci. Eng. C Mater. Biol. Appl.* 92, 1041–1060. doi: 10.1016/j.msec.2017.12.036

Doleschel, D., Rix, A., Arns, S., Palmowski, K., Gremse, F., Merkle, R., et al. (2015). Erythropoietin improves the accumulation and therapeutic effects of carboplatin by enhancing tumor vascularization and perfusion. *Theranostics* 5, 905–918. doi: 10.7150/thno.11304

Drude, N., Winz, O. H., Mottaghy, F. M., Roller, M., Konigs, H., Moller, M., et al. (2018). Impact of glutathione modulation on stability and pharmacokinetic profile of redox-sensitive nanogels. *Small* 14:e1704093. doi: 10.1002/smll.201704093

Engineer, C., Parikh, J., and Raval, A. (2011). Review on hydrolytic degradation behavior of biodegradable polymers from controlled drug delivery system. *Trends Biomater. Artif. Organs* 25, 79–85.

Eynali, S., Khoei, S., Khoee, S., and Esmaelbeygi, E. (2017). Evaluation of the cytotoxic effects of hyperthermia and 5-fluorouracil-loaded magnetic nanoparticles on human colon cancer cell line HT-29. *Int. J. Hyperthermia* 33, 327–335. doi: 10.1080/02656736.2016.1243260

Fasehee, H., Dinarvand, R., Ghavamzadeh, A., Esfandyari-Manesh, M., Moradian, H., Faghihi, S., et al. (2016). Delivery of disulfiram into breast cancer cells using folate-receptor-targeted PLGA-PEG nanoparticles: in vitro and in vivo investigations. *J. Nanobiotechnology* 14:32. doi: 10.1186/s12951-016-0183-z

Fonseca, C., Simoes, S., and Gaspar, R. (2002). Paclitaxel-loaded PLGA nanoparticles: preparation, physicochemical characterization and in vitro anti-tumoral activity. *J. Control. Release* 83, 273–286. doi: 10.1016/S0168-3659(02)00212-2

Govender, T., Stolnik, S., Garnett, M. C., Illum, L., and Davis, S. S. (1999). PLGA nanoparticles prepared by nanoprecipitation: drug loading and release studies of a water soluble drug. *J. Control. Release* 57, 171–185. doi: 10.1016/S0168-3659(98)00116-3

Gu, F., Zhang, L., Teply, B. A., Mann, N., Wang, A., Radovic-Moreno, A. F., et al. (2008). Precise engineering of targeted nanoparticles by using self-assembled biointegrated block copolymers. *Proc. Natl. Acad. Sci. U.S.A.* 105, 2586–2591. doi: 10.1073/pnas.0711714105

Hao, Y., Zhang, B., Zheng, C., Ji, R., Ren, X., Guo, F., et al. (2015). The tumor-targeting core–shell structured DTX-loaded PLGA@Au nanoparticles for chemo-photothermal therapy and X-ray imaging. *J. Control. Release* 220, 545–555. doi: 10.1016/j.jconrel.2015.11.016

Hasani-Sadrabadi, M. M., Dashtimoghadam, E., Bahlakeh, G., Majedi, F. S., Keshvari, H., Van Dersarl, J. J., et al. (2015). On-chip synthesis of fine-tuned bone-seeking hybrid nanoparticles. *Nanomedicine* 10, 3431–3449. doi: 10.2217/nnm.15.162

Higgins, G. S., O'cathail, S. M., Muschel, R. J., and Mckenna, W. G. (2015). Drug radiotherapy combinations: review of previous failures and reasons for future optimism. *Cancer Treat. Rev.* 41, 105–113. doi: 10.1016/j.ctrv.2014.12.012

Horisawa, E., Hirota, T., Kawazoe, S., Yamada, J., Yamamoto, H., Takeuchi, H., et al. (2002). Prolonged anti-inflammatory action of DL-lactide/glycolide copolymer nanospheres containing betamethasone sodium phosphate for an intra-articular delivery system in antigen-induced arthritic rabbit. *Pharm. Res.* 19, 403–410. doi: 10.1023/A:1015123024113

Hrkach, J., Von Hoff, D., Mukkaram Ali, M., Andrianova, E., Auer, J., Campbell, T., et al. (2012). Preclinical development and clinical translation of a PSMA-targeted docetaxel nanoparticle with a differentiated pharmacological profile. *Sci. Transl. Med.* 4:128ra139. doi: 10.1126/scitranslmed.3003651

Hu, K., Zhou, H., Liu, Y., Liu, Z., Liu, J., Tang, J., et al. (2015). Hyaluronic acid functional amphipathic and redox-responsive polymer particles for the co-delivery of doxorubicin and cyclopamine to eradicate breast cancer cells and cancer stem cells. *Nanoscale* 7, 8607–8618. doi: 10.1039/c5nr01084e

Ibraheem, D., Elaissari, A., and Fessi, H. (2014). Gene therapy and DNA delivery systems. *Int. J. Pharm.* 459, 70–83. doi: 10.1016/j.ijpharm.2013.11.041

Jiang, J. X., Chen, H. W., Yu, C., Zhang, Y. Y., Chen, M. Y., Tian, S., et al. (2015). The promotion of salinomycin delivery to hepatocellular carcinoma cells through EGFR and CD133 aptamers conjugation by PLGA nanoparticles. *Nanomedicine* 10, 1863–1879. doi: 10.2217/nnm.15.43

Jiang, W., Von Roemeling, C. A., Chen, Y. X., Qie, Y. Q., Liu, X. J., Chen, J. Z., et al. (2017a). Designing nanomedicine for immuno-oncology. *Nat. Biomed. Eng.* 1:0029.

Jiang, W., Yuan, H., Chan, C. K., Von Roemeling, C. A., Yan, Z., Weissman, I. L., et al. (2017b). Lessons from immuno-oncology: a new era for cancer nanomedicine? *Nat. Rev. Drug Discov.* 16, 369–370. doi: 10.1038/nrd.2017.34

Jin, C., Bai, L., Wu, H., Tian, F., and Guo, G. (2007). Radiosensitization of paclitaxel, etanidazole and paclitaxel + etanidazole nanoparticles on hypoxic human tumor cells in vitro. *Biomaterials* 28, 3724–3730. doi: 10.1016/j.biomaterials.2007.04.032

Kamaly, N., Yameen, B., Wu, J., and Farokhzad, O. C. (2016). Degradable controlled-release polymers and polymeric nanoparticles: mechanisms of controlling drug release. *Chem. Rev.* 116, 2602–2663. doi: 10.1021/acs.chemrev.5b00346

Kaur, P., Hurwitz, M. D., Krishnan, S., and Asea, A. (2011). Combined hyperthermia and radiotherapy for the treatment of cancer. *Cancers* 3, 3799–3823. doi: 10.3390/cancers3043799

Khalil, N. M., Do Nascimento, T. C. F., Casa, D. M., Dalmolin, L. F., De Mattos, A. C., Hoss, I., et al. (2013). Pharmacokinetics of curcumin-loaded PLGA and PLGA–PEG blend nanoparticles after oral administration in rats. *Colloids Surf. B Biointerfaces* 101, 353–360. doi: 10.1016/j.colsurfb.2012.06.024

Khuroo, T., Verma, D., Khuroo, A., Ali, A., and Iqbal, Z. (2018). Simultaneous delivery of paclitaxel and erlotinib from dual drug loaded PLGA nanoparticles: formulation development, thorough optimization and in vitro release. *J. Mol. Liq.* 257, 52–68. doi: 10.1016/j.molliq.2018.02.091

Kirtane, A. R., Wong, H. L., Guru, B. R., Lis, L. G., Georg, G. I., Gurvich, V. J., et al. (2015). Reformulating tylocrebrine in epidermal growth factor receptor targeted polymeric nanoparticles improves its therapeutic index. *Mol. Pharm.* 12, 2912–2923. doi: 10.1021/acs.molpharmaceut.5b00173

Klippstein, R., Wang, J. T., El-Gogary, R. I., Bai, J., Mustafa, F., Rubio, N., et al. (2015). Passively targeted curcumin-loaded PEGylated PLGA nanocapsules for colon cancer therapy in vivo. *Small* 11, 4704–4722. doi: 10.1002/smll.201403799

Koczera, P., Appold, L., Shi, Y., Liu, M., Dasgupta, A., Pathak, V., et al. (2017). PBCA-based polymeric microbubbles for molecular imaging and drug delivery. *J. Control. Release* 259, 128–135. doi: 10.1016/j.jconrel.2017.03.006

Kolhar, P., Doshi, N., and Mitragotri, S. (2011). Polymer nanoneedle-mediated intracellular drug delivery. *Small* 7, 2094–2100. doi: 10.1002/smll.201100497

Kong, G., Braun, R. D., and Dewhirst, M. W. (2001). Characterization of the effect of hyperthermia on nanoparticle extravasation from tumor vasculature. *Cancer Res.* 61, 3027–3032.

Kranz, H., Ubrich, N., Maincent, P., and Bodmeier, R. (2000). Physicomechanical properties of biodegradable poly(D,L-lactide) and poly(D,L-lactide-co-glycolide) films in the dry and wet states. *J. Pharm. Sci.* 89, 1558–1566. doi: 10.1002/1520-6017(200012)89:12<1558::AID-JPS6>3.0.CO;2-8

Kulhari, H., Pooja, D., Kota, R., Reddy, T. S., Tabor, R. F., Shukla, R., et al. (2016). Cyclic RGDfK peptide functionalized polymeric nanocarriers for targeting gemcitabine to ovarian cancer cells. *Mol. Pharm.* 13, 1491–1500. doi: 10.1021/acs.molpharmaceut.5b00935

Kunjachan, S., Pola, R., Gremse, F., Theek, B., Ehling, J., Moeckel, D., et al. (2014). Passive versus active tumor targeting using RGD- and NGR-modified polymeric nanomedicines. *Nano Lett.* 14, 972–981. doi: 10.1021/nl404391r

Kwatra, D., Venugopal, A., and Anant, S. (2013). Nanoparticles in radiation therapy: a summary of various approaches to enhance radiosensitization in cancer. *Transl. Cancer Res.* 2, 330–342.

Lai, P., Daear, W., Lobenberg, R., and Prenner, E. J. (2014). Overview of the preparation of organic polymeric nanoparticles for drug delivery based on gelatine, chitosan, poly(d,l-lactide-co-glycolic acid) and polyalkylcyanoacrylate. *Colloids Surf. B Biointerfaces* 118, 154–163. doi: 10.1016/j.colsurfb.2014.03.017

Lammers, T., Kiessling, F., Hennink, W. E., and Storm, G. (2012). Drug targeting to tumors: principles, pitfalls and (pre-) clinical progress. *J. Control. Release* 161, 175–187. doi: 10.1016/j.jconrel.2011.09.063

Lee, S. J., Kim, M. J., Kwon, I. C., and Roberts, T. M. (2016). Delivery strategies and potential targets for siRNA in major cancer types. *Adv. Drug Deliv. Rev* 104, 2–15. doi: 10.1016/j.addr.2016.05.010

Lee, Y. H., and Chang, D. S. (2017). Fabrication, characterization, and biological evaluation of anti-HER2 indocyanine green-doxorubicin-encapsulated PEG-b-PLGA copolymeric nanoparticles for targeted photochemotherapy of breast cancer cells. *Sci. Rep.* 7:46688. doi: 10.1038/srep46688

Li, X., and Jiang, X. (2018). Microfluidics for producing poly (lactic-co-glycolic acid)-based pharmaceutical nanoparticles. *Adv. Drug Deliv. Rev.* 128, 101–114. doi: 10.1016/j.addr.2017.12.015

Liu, P., Qin, L., Wang, Q., Sun, Y., Zhu, M., Shen, M., et al. (2012). cRGD-functionalized mPEG-PLGA-PLL nanoparticles for imaging and therapy of breast cancer. *Biomaterials* 33, 6739–6747. doi: 10.1016/j.biomaterials.2012.06.008

Lim, C.-K., Heo, J., Shin, S., Jeong, K., Seo, Y. H., Jang, W.-D., et al. (2013). Nanophotosensitizers toward advanced photodynamic therapy of Cancer. *Cancer Lett.* 334, 176–187. doi: 10.1016/j.canlet.2012.09.012

Liu, Y., Zhao, G., Xu, C. F., Luo, Y. L., Lu, Z. D., and Wang, J. (2018). Systemic delivery of CRISPR/Cas9 with PEG-PLGA nanoparticles for chronic myeloid leukemia targeted therapy. *Biomater. Sci.* 6, 1592–1603. doi: 10.1039/C8BM00263K

Maeda, H., Sawa, T., and Konno, T. (2001). Mechanism of tumor-targeted delivery of macromolecular drugs, including the EPR effect in solid tumor and clinical overview of the prototype polymeric drug SMANCS. *J. Control. Release* 74, 47–61. doi: 10.1016/S0168-3659(01)00309-1

Masood, F. (2016). Polymeric nanoparticles for targeted drug delivery system for cancer therapy. *Mater. Sci. Eng. C Mater. Biol. Appl.* 60, 569–578. doi: 10.1016/j.msec.2015.11.067

Mattheolabakis, G., Taoufik, E., Haralambous, S., Roberts, M. L., and Avgoustakis, K. (2009). In vivo investigation of tolerance and antitumor activity of cisplatin-loaded PLGA-mPEG nanoparticles. *Eur. J. Pharm. Biopharm.* 71, 190–195. doi: 10.1016/j.ejpb.2008.09.011

Mendoza-Muñoz, N., Alcalá-Alcalá, S., and Quintanar-Guerrero, D. (2016). "preparation of polymer nanoparticles by the emulsification-solvent evaporation method: from vanderhoff's pioneer approach to recent adaptations," in *Polymer Nanoparticles for Nanomedicines*, eds C. Vauthier and G. Ponchel (Cham: Springer), 87–121.

Menon, J. U., Tumati, V., Hsieh, J. T., Nguyen, K. T., and Saha, D. (2015). Polymeric nanoparticles for targeted radiosensitization of prostate cancer cells. *J. Biomed. Mater. Res. A* 103, 1632–1639. doi: 10.1002/jbm.a.35300

Miladi, K., Sfar, S., Fessi, H., and Elaissari, A. (2016). "Nanoprecipitation process: from particle preparation to in vivo applications," in *Polymer Nanoparticles for Nanomedicines*, eds C. Vauthier, and G. Ponchel (Cham: Springer), 17–53. doi: 10.1007/978-3-319-41421-8_2

Mir, M., Ahmed, N., and Rehman, A. U. (2017). Recent applications of PLGA based nanostructures in drug delivery. *Colloids Surf. B Biointerfaces* 159, 217–231. doi: 10.1016/j.colsurfb.2017.07.038

Mirakabad, F. S. T., Nejati-Koshki, K., Akbarzadeh, A., Yamchi, M. R., Milani, M., Zarghami, N., et al. (2014). PLGA-based nanoparticles as cancer drug delivery systems. *Asian Pac. J. Cancer Prev.* 15, 517–535. doi: 10.7314/APJCP.2014.15.2.517

Miran, T., Vogg, A. T. J., Drude, N., Mottaghy, F. M., and Morgenroth, A. (2018). Modulation of glutathione promotes apoptosis in triple-negative breast cancer cells. *FASEB J.* 32, 2803–2813. doi: 10.1096/fj.201701157R

Misra, R., and Sahoo, S. K. (2011). Coformulation of doxorubicin and curcumin in poly(D,L-lactide-co-glycolide) nanoparticles suppresses the development of multidrug resistance in K562 cells. *Mol. Pharm.* 8, 852–866. doi: 10.1021/mp100455h

Mittal, G., Sahana, D. K., Bhardwaj, V., and Ravi Kumar, M. N. (2007). Estradiol loaded PLGA nanoparticles for oral administration: effect of polymer molecular weight and copolymer composition on release behavior in vitro and in vivo. *J. Control. Release* 119, 77–85. doi: 10.1016/j.jconrel.2007.01.016

Moan, J., and Berg, K. (1991). The photodegradation of porphyrins in cells can be used to estimate the lifetime of singlet oxygen. *Photochem. Photobiol.* 53, 549–553. doi: 10.1111/j.1751-1097.1991.tb03669.x

Mohanty, C., and Sahoo, S. K. (2010). The in vitro stability and in vivo pharmacokinetics of curcumin prepared as an aqueous nanoparticulate formulation. *Biomaterials* 31, 6597–6611. doi: 10.1016/j.biomaterials.2010.04.062

Moreno, D., Zalba, S., Navarro, I., Tros, De Ilarduya, C., and Garrido, M. J. (2010). Pharmacodynamics of cisplatin-loaded PLGA nanoparticles administered to tumor-bearing mice. *Eur. J. Pharm. Biopharm.* 74, 265–274. doi: 10.1016/j.ejpb.2009.10.005

Narayanan, S., Mony, U., Vijaykumar, D. K., Koyakutty, M., Paul-Prasanth, B., and Menon, D. (2015). Sequential release of epigallocatechin gallate and paclitaxel from PLGA-casein core/shell nanoparticles sensitizes drug-resistant breast cancer cells. *Nanomedicine* 11, 1399–1406. doi: 10.1016/j.nano.2015.03.015

Narayanan, S., Pavithran, M., Viswanath, A., Narayanan, D., Mohan, C. C., Manzoor, K., et al. (2014). Sequentially releasing dual-drug-loaded PLGA–casein core/shell nanomedicine: design, synthesis, biocompatibility and pharmacokinetics. *Acta Biomater.* 10, 2112–2124. doi: 10.1016/j.actbio.2013.12.041

NCT02479178, I (2016). *ClinicalTrials.gov, Identifier: NCT02479178* [Online]. Available at: https://clinicaltrials.gov/ct2/show/NCT02479178.

Nel, A., Ruoslahti, E., and Meng, H. (2017). New insights into "permeability" as in the enhanced permeability and retention effect of cancer nanotherapeutics. *ACS Nano* 11, 9567–9569. doi: 10.1021/acsnano.7b07214

Nguyen, H. T., Dai Phung, C., Thapa, R. K., Pham, T. T., Tran, T. H., Jeong, J.-H., et al. (2017). Multifunctional nanoparticles as somatostatin receptor-targeting delivery system of polyaniline and methotrexate for combined chemo–photothermal therapy. *Acta Biomater.* 68, 154–167. doi: 10.1016/j.actbio.2017.12.033

Niu, X., Zou, W., Liu, C., Zhang, N., and Fu, C. (2009). Modified nanoprecipitation method to fabricate DNA-loaded PLGA nanoparticles. *Drug Dev. StateInd. Pharm.* 35, 1375–1383. doi: 10.3109/03639040902939221

Pandey, A., Jain, D. S., and Chakraborty, S. (2015). Poly Lactic-Co-Glycolic Acid (PLGA) copolymer and its pharmaceutical application. *Handb. Polym. Pharm. Technol.* 2, 151–172. doi: 10.1002/9781119041412.ch6

Park, J., Fong, P. M., Lu, J., Russell, K. S., Booth, C. J., Saltzman, W. M., et al. (2009). PEGylated PLGA nanoparticles for the improved delivery of doxorubicin. *Nanomedicine* 5, 410–418. doi: 10.1016/j.nano.2009.02.002

Park, J.-S., Qiao, L., Su, Z.-Z., Hinman, D., Willoughby, K., Mckinstry, R., et al. (2001). Ionizing radiation modulates vascular endothelial growth factor (VEGF) expression through multiple mitogen activated protein kinase dependent pathways. *Oncogene* 20, 3266–3280. doi: 10.1038/sj.onc.1204258

Parveen, S., and Sahoo, S. K. (2011). Long circulating chitosan/PEG blended PLGA nanoparticle for tumor drug delivery. *Eur. J. Pharmacol.* 670, 372–383. doi: 10.1016/j.ejphar.2011.09.023

Paszko, E., Ehrhardt, C., Senge, M. O., Kelleher, D. P., and Reynolds, J. V. (2011). Nanodrug applications in photodynamic therapy. *Photodiagnosis Photodyn. Ther.* 8, 14–29. doi: 10.1016/j.pdpdt.2010.12.001

Peng, Y., Nie, J., Cheng, W., Liu, G., Zhu, D., Zhang, L., et al. (2018). A multifunctional nanoplatform for cancer chemo-photothermal synergistic therapy and overcoming multidrug resistance. *Biomater. Sci.* 6, 1084–1098. doi: 10.1039/c7bm01206c

Pérez, A., Mijangos, C., and Hernández, R. (2014). Preparation of Hybrid Fe3O4/Poly (lactic-co-glycolic acid)(PLGA) particles by emulsion and evaporation method. optimization of the experimental parameters. *Macromol. Symp.* 333, 62–69. doi: 10.1002/masy.201200123

Perez-Herrero, E., and Fernandez-Medarde, A. (2015). Advanced targeted therapies in cancer: drug nanocarriers, the future of chemotherapy. *Eur. J. Pharm. Biopharm.* 93, 52–79. doi: 10.1016/j.ejpb.2015.03.018

Peschke, P., Klein, V., Wolber, G., Friedrich, E., and Hahn, E. (1999). Morphometric analysis of bromodeoxyuridine distribution and cell density in the rat Dunning prostate tumor R3327-AT1 following treatment with radiation andtor hyperthermia. *Histol. Histopathol.* 14, 461–469. doi: 10.14670/HH-14.461

Polyak, B., and Friedman, G. (2009). Magnetic targeting for site-specific drug delivery: applications and clinical potential. *Expert Opin. Drug Deliv.* 6, 53–70. doi: 10.1517/17425240802662795

Rafiei, P., and Haddadi, A. (2017). Docetaxel-loaded PLGA and PLGA-PEG nanoparticles for intravenous application: pharmacokinetics and biodistribution profile. *Int. J. Nanomedicine* 12, 935–947. doi: 10.2147/IJN.S121881

Ramazani, F., Chen, W., Van Nostrum, C. F., Storm, G., Kiessling, F., Lammers, T., et al. (2016). Strategies for encapsulation of small hydrophilic and amphiphilic drugs in PLGA microspheres: state-of-the-art and challenges. *Int. J. Pharm.* 499, 358–367. doi: 10.1016/j.ijpharm.2016.01.020

Rao, W., Deng, Z. S., and Liu, J. (2010). A review of hyperthermia combined with radiotherapy/chemotherapy on malignant tumors. *Crit. Rev. Biomed. Eng.* 38, 101–116. doi: 10.1615/CritRevBiomedEng.v38.i1.80

Rivas, C. J. M., Tarhini, M., Badri, W., Miladi, K., Greige-Gerges, H., Nazari, Q. A., et al. (2017). Nanoprecipitation process: from encapsulation to drug delivery. *Int. J. Pharm.* 532, 66–81. doi: 10.1016/j.ijpharm.2017.08.064

Rosalia, R. A., Cruz, L. J., Van Duikeren, S., Tromp, A. T., Silva, A. L., Jiskoot, W., et al. (2015). CD40-targeted dendritic cell delivery of PLGA-nanoparticle vaccines induce potent anti-tumor responses. *Biomaterials* 40, 88–97. doi: 10.1016/j.biomaterials.2014.10.053

Schleich, N., Po, C., Jacobs, D., Ucakar, B., Gallez, B., Danhier, F., et al. (2014). Comparison of active, passive and magnetic targeting to tumors of multifunctional paclitaxel/SPIO-loaded nanoparticles for tumor imaging and therapy. *J. Control. Release* 194, 82–91. doi: 10.1016/j.jconrel.2014.07.059

Schleich, N., Sibret, P., Danhier, P., Ucakar, B., Laurent, S., Muller, R. N., et al. (2013). Dual anticancer drug/superparamagnetic iron oxide-loaded PLGA-based nanoparticles for cancer therapy and magnetic resonance imaging. *Int. J. Pharm.* 447, 94–101. doi: 10.1016/j.ijpharm.2013.02.042

Sengel-Turk, C. T., Hascicek, C., Dogan, A. L., Esendagli, G., Guc, D., and Gonul, N. (2012). Preparation and in vitro evaluation of meloxicam-loaded PLGA nanoparticles on HT-29 human colon adenocarcinoma cells. *Drug Dev. Ind. Pharm.* 38, 1107–1116. doi: 10.3109/03639045.2011.641562

Sharma, S., Parmar, A., Kori, S., and Sandhir, R. (2016). PLGA-based nanoparticles: a new paradigm in biomedical applications. *Trac Trends Anal. Chem.* 80, 30–40. doi: 10.1016/j.trac.2015.06.014

Shi, J., Kantoff, P. W., Wooster, R., and Farokhzad, O. C. (2017). Cancer nanomedicine: progress, challenges and opportunities. *Nat. Rev. Cancer* 17, 20–37. doi: 10.1038/nrc.2016.108

Shi, Y., Zhou, M., Zhang, J., and Lu, W. (2015). Preparation and cellular targeting study of VEGF-conjugated PLGA nanoparticles. *J. Microencapsul.* 32, 699–704. doi: 10.3109/02652048.2015.1035683

Shubhra, Q. T., Kardos, A. F., Feczko, T., Mackova, H., Horak, D., Toth, J., et al. (2014). Co-encapsulation of human serum albumin and superparamagnetic iron oxide in PLGA nanoparticles: part I. Effect of process variables on the mean size. *J. Microencapsul.* 31, 147–155. doi: 10.3109/02652048.2013.814729

Silva, A. T. C. R., Cardoso, B. C. O., Silva, M. E. S. R., Freitas, R. F. S., and Sousa, R. G. (2015). Synthesis, characterization, and study of PLGA copolymer in vitro degradation. *J. Biomater. Nanobiotechnol.* 6, 8–19. doi: 10.4236/jbnb.2015.61002

Sivakumar, B., Aswathy, R. G., Romero-Aburto, R., Mitcham, T., Mitchel, K. A., Nagaoka, Y., et al. (2017). Highly versatile SPION encapsulated PLGA nanoparticles as photothermal ablators of cancer cells and as multimodal imaging agents. *Biomater. Sci.* 5, 432–443. doi: 10.1039/c6bm00621c

Song, X., Zhao, Y., Wu, W., Bi, Y., Cai, Z., Chen, Q., et al. (2008). PLGA nanoparticles simultaneously loaded with vincristine sulfate and verapamil hydrochloride: systematic study of particle size and drug entrapment efficiency. *Int. J. Pharm.* 350, 320–329. doi: 10.1016/j.ijpharm.2007.08.034

Sun, J., Xianyu, Y., Li, M., Liu, W., Zhang, L., Liu, D., et al. (2013). A microfluidic origami chip for synthesis of functionalized polymeric nanoparticles. *Nanoscale* 5, 5262–5265. doi: 10.1039/c3nr01289a

Tang, J., He, J., Yang, C., Mao, Y., Hu, T., Zhang, L., et al. (2014). Antitumor effects of MsurvivinT34A–CaPi complex-embedded PLGA nanoparticles in combination with Doxil in mice. *J. Nanopart. Res.* 16:2682. doi: 10.1007/s11051-014-2682-x

Tao, W., Zeng, X., Liu, T., Wang, Z., Xiong, Q., Ouyang, C., et al. (2013). Docetaxel-loaded nanoparticles based on star-shaped mannitol-core PLGA-TPGS diblock copolymer for breast cancer therapy. *Acta Biomater.* 9, 8910–8920. doi: 10.1016/j.actbio.2013.06.034

Tay, Z. W., Chandrasekharan, P., Chiu-Lam, A., Hensley, D. W., Dhavalikar, R., Zhou, X. Y., et al. (2018). Magnetic particle imaging-guided heating in vivo using gradient fields for arbitrary localization of magnetic hyperthermia therapy. *ACS Nano* 12, 3699–3713. doi: 10.1021/acsnano.8b00893

Theek, B., Gremse, F., Kunjachan, S., Fokong, S., Pola, R., Pechar, M., et al. (2014). Characterizing EPR-mediated passive drug targeting using contrast-enhanced functional ultrasound imaging. *J. Control. Release* 182, 83–89. doi: 10.1016/j.jconrel.2014.03.007

Thorat, N., Bohara, R., Yadav, H., Otari, S., Pawar, S., and Tofail, S. (2016). *Multifunctional Magnetic Nanostructures for Cancer Hyperthermia Therapy*. Amsterdam: Elsevier Inc. doi: 10.1016/B978-0-323-47347-7.00021-5

Tian, J., Min, Y., Rodgers, Z., Au, K. M., Hagan, C. T., Zhang, M., et al. (2017). Co-delivery of paclitaxel and cisplatin with biocompatible PLGA–PEG nanoparticles enhances chemoradiotherapy in non-small cell lung cancer models. *J. Mater. Chem. B* 5, 6049–6057. doi: 10.1039/C7TB01370A

Turecek, P. L., Bossard, M. J., Schoetens, F., and Ivens, I. A. (2016). PEGylation of biopharmaceuticals: a review of chemistry and nonclinical safety information of approved drugs. *J. Pharm. Sci.* 105, 460–475. doi: 10.1016/j.xphs.2015.11.015

Valencia, P. M., Farokhzad, O. C., Karnik, R., and Langer, R. (2012). Microfluidic technologies for accelerating the clinical translation of nanoparticles. *Nat. Nanotechnol.* 7, 623–629. doi: 10.1038/nnano.2012.168

Valencia, P. M., Hanewich-Hollatz, M. H., Gao, W., Karim, F., Langer, R., Karnik, R., et al. (2011). Effects of ligands with different water solubilities on self-assembly and properties of targeted nanoparticles. *Biomaterials* 32, 6226–6233. doi: 10.1016/j.biomaterials.2011.04.078

Valencia, P. M., Pridgen, E. M., Perea, B., Gadde, S., Sweeney, C., Kantoff, P. W., et al. (2013a). Synergistic cytotoxicity of irinotecan and cisplatin in dual-drug targeted polymeric nanoparticles. *Nanomedicine* 8, 687–698. doi: 10.2217/nnm.12.134

Valencia, P. M., Pridgen, E. M., Rhee, M., Langer, R., Farokhzad, O. C., and Karnik, R. (2013b). Microfluidic platform for combinatorial synthesis and optimization of targeted nanoparticles for cancer therapy. *ACS Nano* 7, 10671–10680. doi: 10.1021/nn403370e

Vivek, R., Thangam, R., Kumar, S. R., Rejeeth, C., Sivasubramanian, S., Vincent, S., et al. (2016). HER2 Targeted Breast Cancer Therapy with Switchable "Off/On" Multifunctional "Smart" Magnetic Polymer Core–Shell Nanocomposites. *ACS Appl. Mater. Interfaces* 8, 2262–2279. doi: 10.1021/acsami.5b11103

Vllasaliu, D., Fowler, R., and Stolnik, S. (2014). PEGylated nanomedicines: recent progress and remaining concerns. *Expert Opin. Drug Deliv.* 11, 139–154. doi: 10.1517/17425247.2014.866651

Von Hoff, D. D., Mita, M. M., Ramanathan, R. K., Weiss, G. J., Mita, A. C., Lorusso, P. M., et al. (2016). Phase I study of PSMA-targeted docetaxel-containing

nanoparticle BIND-in014 in patients with advanced solid tumors. *Clin. Cancer Res.* 22, 3157–3163. doi: 10.1158/1078-0432.CCR-15-2548

Wang, A. Z., Yuet, K., Zhang, L., Gu, F. X., Huynh-Le, M., Radovic-Moreno, A. F., et al. (2010). ChemoRad nanoparticles: a novel multifunctional nanoparticle platform for targeted delivery of concurrent chemoradiation. *Nanomedicine* 5, 361–368. doi: 10.2217/nnm.10.6

Wang, K., Kievit, F. M., and Zhang, M. (2016). Nanoparticles for cancer gene therapy: Recent advances, challenges, and strategies. *Pharmacol. Res.* 114, 56–66. doi: 10.1016/j.phrs.2016.10.016

Wang, M., Wang, J., Li, B., Meng, L., and Tian, Z. (2017). Recent advances in mechanism-based chemotherapy drug-siRNA pairs in co-delivery systems for cancer: a review. *Colloids Surf. B Biointerfaces* 157, 297–308. doi: 10.1016/j.colsurfb.2017.06.002

Wasan, H. S., Gibbs, P., Sharma, N. K., Taieb, J., Heinemann, V., Ricke, J., et al. (2017). First-line selective internal radiotherapy plus chemotherapy versus chemotherapy alone in patients with liver metastases from colorectal cancer (FOXFIRE, SIRFLOX, and FOXFIRE-Global): a combined analysis of three multicentre, randomised, phase 3 trials. *Lancet Oncol.* 18, 1159–1171. doi: 10.1016/S1470-2045(17)30457-6

Werner, M. E., Copp, J. A., Karve, S., Cummings, N. D., Sukumar, R., Li, C. X., et al. (2011). Folate-targeted polymeric nanoparticle formulation of docetaxel is an effective molecularly targeted radiosensitizer with efficacy dependent on the timing of radiotherapy. *ACS Nano* 5, 8990–8998. doi: 10.1021/nn203165z

Wicki, A., Witzigmann, D., Balasubramanian, V., and Huwyler, J. (2015). Nanomedicine in cancer therapy: challenges, opportunities, and clinical applications. *J. Control. Release* 200, 138–157. doi: 10.1016/j.jconrel.2014.12.030

Wong, P.-P., Demircioglu, F., Ghazaly, E., Alrawashdeh, W., Stratford, M. R., Scudamore, C. L., et al. (2015). Dual-action combination therapy enhances angiogenesis while reducing tumor growth and spread. *Cancer Cell* 27, 123–137. doi: 10.1016/j.ccell.2014.10.015

Xiao, B., Ma, L., and Merlin, D. (2017). Nanoparticle-mediated co-delivery of chemotherapeutic agent and siRNA for combination cancer therapy. *Expert Opin. Drug Deliv.* 14, 65–73. doi: 10.1080/17425247.2016.1205583

Xu, G., Yu, X., Zhang, J., Sheng, Y., Liu, G., Tao, W., et al. (2016). Robust aptamer–polydopamine-functionalized M-PLGA–TPGS nanoparticles for targeted delivery of docetaxel and enhanced cervical cancer therapy. *Int. J. Nanomedicine* 11, 2953–2965. doi: 10.2147/IJN.S103513

Xu, Y., Kim, C. S., Saylor, D. M., and Koo, D. (2017). Polymer degradation and drug delivery in PLGA-based drug–polymer applications: a review of experiments and theories. *J. Biomed. Mater. Res. B Appl. Biomater.* 105, 1692–1716. doi: 10.1002/jbm.b.33648

Yang, H., Deng, L. W., Li, T. T., Shen, X., Yan, J., Zuo, L. M., et al. (2015). Multifunctional PLGA nanobubbles as theranostic agents: combining doxorubicin and P-gp siRNA Co-delivery into human breast cancer cells and ultrasound cellular imaging. *J. Biomed. Nanotechnol.* 11, 2124–2136. doi: 10.1166/jbn.2015.2168

Yin, F., Yang, C. B., Wang, Q. Q., Zeng, S. W., Hu, R., Lin, G. M., et al. (2015). A light-driven therapy of pancreatic adenocarcinoma using gold nanorods-based nanocarriers for co-delivery of doxorubicin and siRNA. *Theranostics* 5, 818–833. doi: 10.7150/thno.11335

Yoon, H. Y., Selvan, S. T., Yang, Y., Kim, M. J., Yi, D. K., Kwon, I. C., et al. (2018). Engineering nanoparticle strategies for effective cancer immunotherapy. *Biomaterials* 178, 597–607. doi: 10.1016/j.biomaterials.2018.03.036

Yuan, J., Liu, J. L., Song, Q., Wang, D., Xie, W. S., Yan, H., et al. (2016). Photoinduced mild hyperthermia and synergistic chemotherapy by one-pot-synthesized docetaxel-loaded poly(lactic-co-glycolic acid)/Polypyrrole Nanocomposites. *ACS Appl. Mater. Interfaces* 8, 24445–24454. doi: 10.1021/acsami.6b07669

Zhang, B., Sai Lung, P., Zhao, S., Chu, Z., Chrzanowski, W., and Li, Q. (2017). Shape dependent cytotoxicity of PLGA-PEG nanoparticles on human cells. *Sci. Rep.* 7:7315. doi: 10.1038/s41598-017-07588-9

Zhang, X. Y., Wang, Q., Qin, L. B., Fu, H., Fang, Y. W., Han, B. S., et al. (2016). EGF-modified mPEG-PLGA-PLL nanoparticle for delivering doxorubicin combined with Bcl-2 siRNA as a potential treatment strategy for lung cancer. *Drug Deliv.* 23, 2936–2945. doi: 10.3109/10717544.2015.1126769

Zhao, X., Yang, K., Zhao, R., Ji, T., Wang, X., Yang, X., et al. (2016). Inducing enhanced immunogenic cell death with nanocarrier-based drug delivery systems for pancreatic cancer therapy. *Biomaterials* 102, 187–197. doi: 10.1016/j.biomaterials.2016.06.032

Zheng, M., Yue, C., Ma, Y., Gong, P., Zhao, P., Zheng, C., et al. (2013). Single-step assembly of DOX/ICG loaded lipid–polymer nanoparticles for highly effective chemo-photothermal combination therapy. *ACS Nano* 7, 2056–2067. doi: 10.1021/nn400334y

Zhu, Y. Q., Feijen, J., and Zhong, Z. Y. (2018). Dual-targeted nanomedicines for enhanced tumor treatment. *Nano Today* 18, 65–85. doi: 10.1016/j.nantod.2017.12.007

Znati, C. A., Rosenstein, M., Boucher, Y., Epperly, M. W., Bloomer, W. D., and Jain, R. K. (1996). Effect of radiation on interstitial fluid pressure and oxygenation in a human tumor xenograft. *Cancer Res.* 56, 964–968.

Conflict of Interest Statement: The authors declare that the research was conducted in the absence of any commercial or financial relationships that could be construed as a potential conflict of interest.

frontiers in Pharmacology

REVIEW
published: 15 October 2018
doi: 10.3389/fphar.2018.01154

Reconstituted HDL: Drug Delivery Platform for Overcoming Biological Barriers to Cancer Therapy

Sangram Raut, Linda Mooberry, Nirupama Sabnis, Ashwini Garud, Akpedje Serena Dossou and Andras Lacko**

Lipoprotein Drug Delivery Research Laboratory, Department of Physiology and Anatomy, University of North Texas Health Science Center, Fort Worth, TX, United States

Drug delivery to malignant tumors is limited by several factors, including off-target toxicities and suboptimal benefits to cancer patient. Major research efforts have been directed toward developing novel technologies involving nanoparticles (NPs) to overcome these challenges. Major obstacles, however, including, opsonization, transport across cancer cell membranes, multidrug-resistant proteins, and endosomal sequestration of the therapeutic agent continue to limit the efficiency of cancer chemotherapy. Lipoprotein-based drug delivery technology, "nature's drug delivery system," while exhibits highly desirable characteristics, it still needs substantial investment from private/government stakeholders to promote its eventual advance to the bedside. Consequently, this review focuses specifically on the synthetic (reconstituted) high-density lipoprotein rHDL NPs, evaluating their potential to overcome specific biological barriers and the challenges of translation toward clinical utilization and commercialization. This highly robust drug transport system provides site-specific, tumor-selective delivery of anti-cancer agents while reducing harmful off-target effects. Utilizing rHDL NPs for anti-cancer therapeutics and tumor imaging revolutionizes the future strategy for the management of a broad range of cancers and other diseases.

Keywords: rHDL, tumor targeting, SR-B1 receptor, cancer therapy and imaging, cholesterol, HDL, biological barriers

OPEN ACCESS

Edited by:
Qingxin Mu,
University of Washington,
United States

Reviewed by:
Colby Shad Thaxton,
Northwestern University,
United States
Ajaikumar B. Kunnumakkara,
Indian Institute of Technology Guwahati, India
Yuhen Zhang,
University of Washington,
United States

****Correspondence:***
Sangram Raut
sangram.raut@unthsc.edu
Andras Lacko
Andras.lacko@unthsc.edu

Specialty section:
This article was submitted to Cancer Molecular Targets and Therapeutics, a section of the journal Frontiers in Pharmacology

Received: *31 May 2018*
Accepted: *24 September 2018*
Published: *15 October 2018*

Citation:
Raut S, Mooberry L, Sabnis N, Garud A, Dossou AS and Lacko A (2018) Reconstituted HDL: Drug Delivery Platform for Overcoming Biological Barriers to Cancer Therapy. Front. Pharmacol. 9:1154. doi: 10.3389/fphar.2018.01154

INTRODUCTION

Our laboratory has been engaged in reconstituted high-density lipoproteins (rHDL) drug delivery research for more than a decade, focusing on formulating and evaluating rHDL drug delivery vehicles for a multitude of anti-cancer agents. Lipoprotein drug transporters have traditionally been used to deliver hydrophobic and amphiphilic drugs. Recently, our laboratory and others have succeeded in the encapsulation of hydrophilic drugs, including doxorubicin (Yuan et al., 2013). Our hypothesis of utilizing the rHDL drug delivery platform for cancer therapy is based on our understanding of the process of 'reverse cholesterol transport' and apolipoprotein/receptor interactions. Endogenous plasma high-density lipoproteins (HDL) delivers cholesterol from peripheral tissues to the liver for metabolism and excretion via a specific receptor, Scavenger Receptor Type B1 (SR-B1) expressed primarily on hepatocytes and steroidogenic tissues (Connelly and Williams, 2004). Several recent articles have shown that SR-B1 is overexpressed by the majority of malignant tumors, promoting their proliferation, and metastasis (Twiddy et al., 2012; Zheng et al., 2013; Yuan et al., 2016; Panchoo and Lacko, 2017). Thus, several laboratories are directing

their efforts toward developing rHDL-based formulations to deliver anti-cancer agents to malignant tumors, facilitated by the SR-B1 receptor. While developing/designing a nanoparticulate system for cancer therapy, several biological barriers remain as recently discussed by Blanco et al. (2015). This communication deals with specific biological/physiological challenges based on the innate ability of the rHDL drug delivery platform to overcome them and considering optimization strategies to improve the drug delivery performance of rHDL.

The basic structure of rHDL NPs resembles those of their natural counterparts, circulating HDL particles. Details of the structure and composition of lipoproteins have been described earlier (Damiano et al., 2013; Pownall et al., 2016; Thaxton et al., 2016). Briefly, lipoproteins are composed of triglycerides (TG) and cholesterol esters (CE) as core components, phospholipids, and unesterified cholesterol in their outer monolayer, and amphipathic apolipoproteins on their surface that facilitate solubility and stability in the bloodstream (**Figure 1**). Although there are several classes of lipoproteins (VLDL, IDL, LDL, and HDL) in the blood of mammals, the present paper focuses only on high-density lipoproteins because of their preferred use in drug delivery research (Ng et al., 2011; Kuai et al., 2016). Other lipoproteins (VLDL, IDL) and their synthetic analogs have not been studied extensively as drug delivery vehicles although they are known to bind and transport several drugs in blood circulation (Yamamoto et al., 2017). Synthetic LDL nanoparticles (NPs) have been used for drug delivery and diagnostic imaging (Corbin et al., 2006; Corbin and Zheng, 2007).

Apolipoprotein A-1 (Apo A-1) is a major protein component of HDL which also serves as a ligand for the SR-B1 receptor. Several methods have been used to assemble rHDL NPs. including cholate dialysis, sonication, thermal cycling, and microfluidics (Kuai et al., 2016). Synthetic HDL NPs have been prepared using self-assembling peptides (Zhang et al., 2010), polymers (Sanchez-Gaytan et al., 2015), and inorganic template ingredients (McMahon et al., 2017). These platforms have been used for drug delivery, siRNA delivery, and modulating cellular cholesterol levels. The rHDL NPs, Apo A-1 protein, and its mimetic peptides are also known to have anti-inflammatory and anti-apoptotic properties. This feature of potential HDL therapeutics has been reviewed by Barter et al. (2004) and Navab et al. (2007). In this review, we are focusing on the challenges (immune system, hemodynamics, cell membrane transport, and drug resistance) faced by drug delivery systems and how these barriers may be effectively overcome by the rHDL platform for cancer therapy.

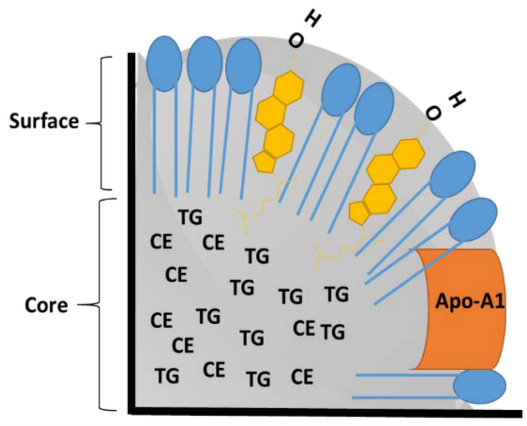

FIGURE 1 | Schematic of cross section of high-density lipoproteins (HDL) nanoparticle (NP). Phospholipids are shown in blue, free cholesterol is shown in yellow, TG: Triglycerides, CE: Cholesterol Esters, and Apo A-1: Apolipoprotein A-1.

INTERACTION OF rHDL WITH BLOOD AND IMMUNE CELLS

The innate immune system (IIS) is the first line of defense against external pathogens or foreign substances, including NPs. The IIS consists of epithelial barriers, phagocytes, dendritic cells, and plasma proteins (complement). The complement system, one of fundamental components of innate immunity is highly organized and designed to remove/clear 'foreign' substances (Medzhitov and Janeway, 2002). The complement system has several protein components that are activated once the pathogen/foreign substances are encountered and subsequently undergoes a cascade of reactions to clear the pathogen/foreign substance(s). There are three branches of the complement system viz classical, lectin and alternative pathway responding to different types of pathogens/foreign sunstances. The classical pathway involves binding of C1q protein to antigen-antibody complex marking it to be cleared. The lectin pathway involves the binding of the carbohydrate component of the lectin to carbohydrates on the surface of pathogens thus initiating the cascade reaction for its removal. An alternative pathway may be activated spontaneously by adsorption of the complement proteins to the surface of pathogens, externally injected materials, including potentially all NP formulations (Moghimi et al., 2011; Szeto and Lavik, 2016). The complement system is activated very rapidly following injury or introduction of external materials into the circulation, therefore, it is critical to evaluate the immune response to NPs immediately following their administration. It is also important to select early time points when evaluating immune responses to novel NP systems as their blood residence times vary markedly, presumably due to the complement response. Other circulating and resident immune cells facilitate clearance and opsonization of pathogens in conjunction with the complement system. Immune cells use a diverse set of receptors (e.g., toll-like receptors, TLRs and C-type lectin receptors, CLRs) to recognize 'self' and 'non-self' antigens on the pathogen or on the nanomaterial surface. Granulocytes (mostly neutrophils) and antigen presenting cells (APC; monocytes, macrophages, and dendritic cells) phagocytose and degrade pathogens/nanomaterials.

Because the rHDL complex is assembled from essentially the same constituents as endogenous HDL, rHDL also mimics its endogenous counterpart as reflected by its function of delivering drugs to cancer cells via the SR-B1 receptor

(Cruz et al., 2013). Exposure of Apo A-1 and lipids to the external environment makes them accessible to innate immune cells and complement proteins. However, because the phospholipids (e.g., phosphatidylcholine) and Apo A-1 (used to construct rHDL NPs) would be recognized as 'self' (endogenous blood components) they are not expected to elicit an immune response (Hogquist et al., 2005). To the best of our knowledge, there are no reports of adverse immune responses to rHDL in small animals or humans. Moreover, recent clinical trials (TANGO) conducted by Cerenis Therapeutics testing an engineered HDL mimetic NP formulation (CER-001) in human subjects, did not reveal any adverse reactions, compared to control (Tardif et al., 2014). Several other clinical trials have also demonstrated the safety of rHDL formulations (Nanjee et al., 1999; van Oostrom et al., 2007). The overall maximum tolerated dose (MTD) has been determined to be between 10 and 30 g of synthetic HDL (Kuai et al., 2016). Thus, it is feasible to inject a 500–1500 mg drug dose (assuming 5% loading in rHDL) to patients without anticipating adverse effects from the rHDL NPs (Kuai et al., 2016).

Apart from complement activation, several other plasma proteins can adsorb onto the NP surface and modify its surface properties (**Figure 2**). Adsorption or binding of different serum proteins determines the fate of injected NPs. Opsonins such as complement proteins and immunoglobulin adsorption will facilitate nanomaterial removal from the plasma while adsorption of dysopsonins such as bovine serum albumin, apolipoproteins will enhance the circulation time via avoiding the mononuclear phagocyte system. Barrán-Berdón et al. (2013) performed time-evolution studies for investigating the adsorption of different types of proteins to the surface of NPs Their findings indicate that apolipoproteins (Apo A-1, Apo C-II, Apo D, and Apo E), complement component proteins (C1q, C1r, C1s, C3OS, C4-B OS, C5OS, C6OS, C7OS, C8 Alpha Beta and gamma, C9OS, BOS, HOS, and I OS), fibrinogen (alpha, beta, and gamma), and several additional serum proteins, including IgG, serum albumin, serotransferrin, and vitronectin may be associated with the externally introduced NPs (Barrán-Berdón et al., 2013). Lundqvist et al. (2008) showed that polystyrene NPs (PSNP) adsorb to different plasma proteins using mass spectrometry analysis. In general, large 100 nm PSNPs were found to complex with immunoglobulins while smaller 50 nm particles were found to be complexed with apolipoproteins, suggesting that particle size may determine the kind of protein corona acquired by the particles and their role in enhancing the removal from or extended stay in the circulation. The same authors reported that the HDL in plasma binds to copolymer NPs (Hellstrand et al., 2009). These observations have important implications as bound apolipoproteins or entire endogenous HDL complexes may carry NPs to the SR-B1 receptors, expressed by liver cells and macrophages. Several other articles report on the relationship between NP surface properties (size, charge, and functional groups) and protein adsorption (Tenzer et al., 2011; Barrán-Berdón et al., 2013). Unlike rHDL, Endogenous plasma HDL size is known to vary (Lagrost et al., 1996). In-depth studies are needed for drug-loaded synthetic or rHDL NPs to study the serum protein adsorption (if any) and possible re-distribution of the drug payload to other lipoproteins in the plasma. The distribution of payload will also depend upon its hydrophobic characteristics. Findings of McConathy et al. (2011) suggest only a limited re-distribution of a fluorescent lipid analog, compared to the distribution of cholesteryl esters (McConathy et al., 2011).

Among several safety metrics, hemolysis is often investigated to indicate toxicity following administration of a nanoformulation. Hemolysis may involve direct erythrocyte damage and/or an immune-mediated hemolytic process. Generally, positively charged NPs tend to damage erythrocytes in a dose-dependent manner, as found with C60 fullerenes (Bosi et al., 2004), PAMAM (Domański et al., 2004), carbosilane (Bermejo et al., 2007), polypropylene imine (Agashe et al., 2006), and polylysine (Shah et al., 2000) dendrimers. In the case of drug loaded rHDL NPs, several reports indicate no hemolysis when NPs were incubated with red blood cells, perhaps due to the absence of SR-B1 receptor expression by erythrocytes (Oda et al., 2006; Yuan et al., 2013; Lu et al., 2015). Thus, rHDL drug formulations seem to be safe based on their interactions with blood cells and immune components.

Interaction of rHDL with macrophages in atherosclerotic plaques is well documented. HDL interacts with ABCA1 and ABCG1 (ATP binding cassette family) receptors to acquire cholesterol from macrophage foam cells in atherosclerotic plaques, considered to be contributing to its anti-atherosclerotic effect, and attributed to the inverse relationship between HDL-C levels and the risk of coronary heart disease (Yvan-Charvet et al., 2010). Synthetic HDL has been used to image atherosclerotic deposits by delivering radio-imaging agents to macrophages in plaques (Frias et al., 2007; Cormode et al., 2010). Similar to its endogenous counterpart, rHDL can also interact with macrophages and can facilitate cholesterol efflux. However, this interaction may be altered by modifying the Apo A-1 amino acid sequence (without changing its ability to bind to SR-B1) thus providing an important tool to develop novel therapeutic strategies (von Eckardstein et al., 1993). The interaction of rHDL with tumor macrophages may also be exploited to develop an effective immunotherapy strategy (Norata et al., 2012). This interaction may further be exploited to control the expansion of myeloid-derived suppressor cells (MDSC) in infectious diseases, cancer, inflammation and consequently reversing the suppression of the immune response (Plebanek et al., 2018). On the other hand, HDL carrying sphingosine-1 phosphate has been shown to suppress components of the immune system, a potentially valuable tool for treating auto-immune disorders (Blaho et al., 2015). Thus, based on the payload, rHDL can be targeted to activate or suppress specific functions of the immune system.

HEMORHEOLOGY AND BLOOD VESSEL FLUID DYNAMICS FOR rHDL

Movement of NPs in the bloodstream, adhesion to endothelial cells, and extravasation into the leaky tumor vasculature are highly dependent on the NP geometry. Decuzzi et al have discussed how the different shape/size may impact circulation, margination, adhesion to vessel walls and cellular uptake of the NPs (Decuzzi et al., 2009). Decuzzi et al. (2009) and others have

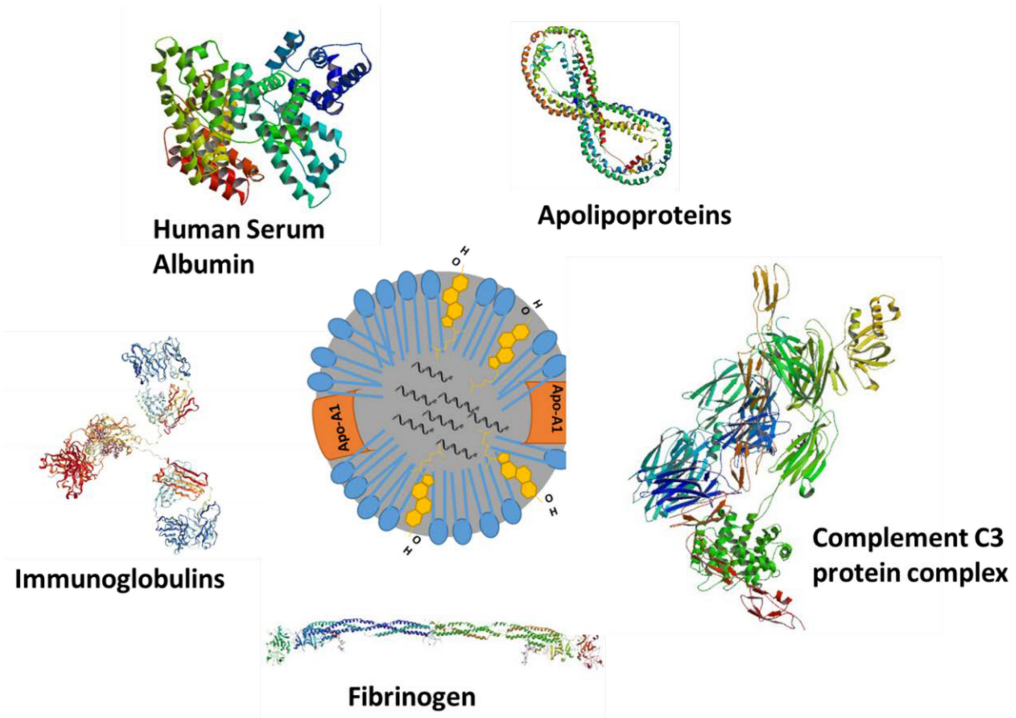

FIGURE 2 | Various types of protein that can adsorb on NPs injected in blood circulation.

also shown that non-spherical particles are more likely to move closer to the vessel wall due to tumbling and rolling dynamics than spherical ones which tend to stay toward the center of the vessel lumen; parallel to vessel walls (Decuzzi et al., 2005; Shah et al., 2011; Tan et al., 2013; **Figure 3**). Two types of rHDL NPs have been reported in the literature; discoidal; and spherical (Kingwell et al., 2014). However, there are no studies evaluating their vessel dynamics in theoretical models or in animals including the bio-distribution, and intended pharmacodynamics and anti-tumor effects. Moreover, these different shapes of HDL NPs may have different affinities toward SR-B1 receptors, and the ABCA1 and ABCG1 transporters.

Nanoparticle size will also play role in blood circulation residence time. It is known that larger NPs (>200 nm) tend to accumulate in the liver and spleen while smaller ones (<10 nm) tend to get cleared by the kidney (Alexis et al., 2008; He et al., 2010). Thus, size considerations along with adsorption properties will likely, collectively affect the mean blood residence time of NP formulations, including drug loaded rHDL NPs. Moreover, NP surface charge will also contribute to fluid dynamics in the blood circulation. Generally, highly positively charged NPs are easily removed from the blood circulation compared to highly negatively charged NPs (Arvizo et al., 2011). In the case of rHDL NPs, their surface charge may be easily manipulated by using different phospholipid surface components, thus controlling the time in the circulation. The rHDL NPs seem to have an only minimal impact on their overall size when encountering blood components. Skajja et al investigated the stability of iron oxide loaded rHDL NPs *in-vitro* as well as in animals. After incubating the rHDL NPs in plasma for 24 h, the change in size was less than 4% demonstrating the absence of protein adsorption. Moreover, Skajaa et al. (2011) reported that after 24 h incubation NPs remained individually dispersed without aggregation, further at testing to the robust nature of rHDL NPs (Skajaa et al., 2011). The extended circulation times (>24 h) of rHDL formulations have been discussed by elsewhere (Kuai et al., 2016) acknowledging that in clinical studies SRC-rHDL, CSL-111, CSL-112, Pro Apo A-1 liposomes, ETC-216, CER-001, and ETC-642 all displayed extended circulation times with no major safety/toxicity issues. (Kuai et al., 2016).

EXTRAVASATION AND rHDL

Numerous research articles have discussed the potential of NPs for targeted drug delivery to cancer cells and tumors. An ideal nanocarrier is expected to have a small size, the extended residence time in the circulation, biocompatibility, and absence of immunogenicity. Although the drug-containing NP formulations exhibited much better delivery efficiency compared to the free drug formulations, they were not as efficacious in limiting off-target effects (Desai, 2012). This discrepancy in clinical translation of nanomedicines has been discussed by several authors (Kamaly et al., 2012; Xue et al., 2014; Min et al., 2015). A crucial element could be a variation of the NP uptake by the reticuloendothelial system in humans compared to that in immune-deficient small animal models. In addition,

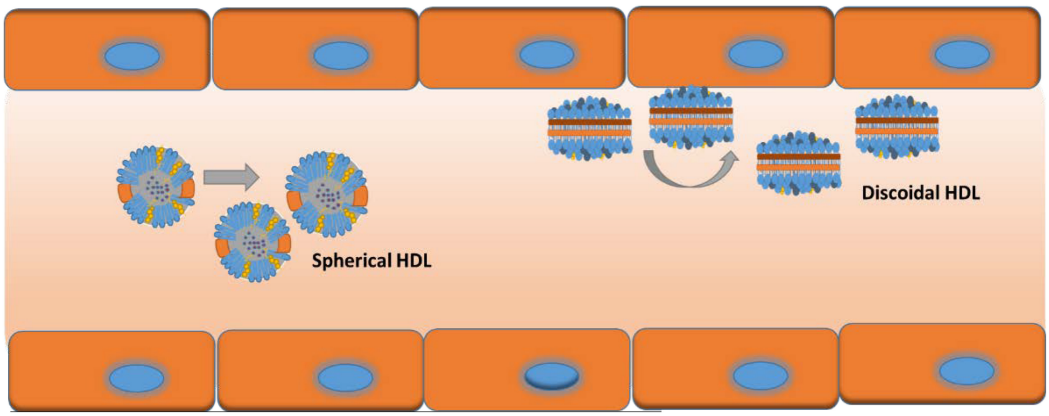

FIGURE 3 | Possible vessel dynamics of spherical (toward center of vessel) vs discoidal (toward vessel wall) HDL NPs in a blood vessel.

the physiology, in spontaneously emerging tumors, compared to xenografts may vary significantly. Furthermore, huge dose discrepancies between those administered to humans compared to those used to treat small animals may result in different degrees of drug retention. Heterogeneity in tumor vasculature and the size of the NPs involved may further impact the drug distribution. More importantly, despite an overall increase in the amount of drug delivered to the tumor via NPs, a significant portion of the tumor cells may still have only limited exposure to the drug.

The drug delivery via NPs usually occurs via extravasation of NPs through the leaky tumor vasculature (passive targeting) or targeted delivery via ligand modified surface of the drug carrier (active targeting) (Torchilin, 2010; Ngoune et al., 2016). Although enhanced permeability and retention (EPR) plays an important role in the passive accumulation of nanoformulations at the tumor site, it is dependent on tumor type and the organ in which the malignancy resides (Yokoi et al., 2014b). Studies by Chen et al have demonstrated multi-functional rHDL NP platform for tumor targeting and imaging via both non-specific accumulation and specific binding to angiogenically activated blood vessels (Chen et al., 2010). In this study, the authors decorated rHDL with amphiphilic gadolinium chelates and fluorescent near infra-red (NIR) imaging dye. Angiogenic endothelial cells were targeted via rHDL that was functionalized with αvβ3-integrin-specific RGD peptides (rHDL-RGD). Non-specific RAD peptides were conjugated to rHDL NPs as a control (rHDL-RAD). The *in vitro* studies indicated a clear distinction between non-specific and specific uptake of the two types of NPs. All 3 NPs (rHDL-RGD, rHDL-RAD, and rHDL) were phagocytosed by macrophages, while the endothelial cells were involved in the uptake of only αvβ3-integrin-specific rHDL-RGD NPs. Furthermore, *in-vivo* studies using NIR and MR imaging demonstrated that rHDL-RGD was associated with tumor endothelial cells, whereas HDL and rHDL-RAD NPs were mainly found in the interstitial space. Thus, it is possible to re-route the rHDL NPs via active targeting.

In another study, Zhang et al. (2010) have demonstrated that sub −30 nm HDL mimicking NPs, functionalized with an EGFR targeting ligand, preferentially accumulated in the tumor interstitial spaces, suggesting that the small size, neutral surface charge, specific targeting ligand and long circulation half-life were instrumental in successful extravasation of the NPs into the tumor mass (Zhang et al., 2010). Thus, rHDL possessed therapeutic potential and versatility in mediating Chol-siRNA-VEGF direct cytosolic delivery for target-specific anti-angiogenic therapy in breast cancer. Another factor involved in the successful extravasation of nano-formulations is the collagen content in the capillary walls in the tumor vasculature (Yokoi et al., 2014a) A similar study may reveal whether the capillary collagen content has any effect on extravasation of rHDL NPs.

The potential utility of HDL mimicking NPs as programmable, and biocompatible drug delivery vehicles suitable for the targeted delivery of tumor imaging and anti-cancer agents has now been established. The HDL NPs owing to their small size, close to neutral charge and long circulation time are able to move out of the circulation and accumulate in malignant tissues. Aforementioned studies also demonstrate the ability to reroute rHDL from its natural target to tumor blood vessels and its potential for multimodal imaging of tumor-associated processes. An analysis of NP payload uptake and drug delivery on the microscopic level in small animal studies will be essential to understanding the efficiency of therapeutic effects. Based on clinical studies, rHDL has already been proven safe for human administration (Krause and Remaley, 2013).

CELLULAR MEMBRANE TRANSPORT AND ENDOSOMAL ESCAPE OF rHDL

Unlike small molecules which readily diffuse into cells and tissues, drugs, encapsulated in NPs must have facilitated delivery across cell membranes. Cellular internalization and endosomal/lysosomal entrapment are of great concern in NP design. Whether trapped in compartments or subjected to the low pH and enzymatic environment of the lysosome, endosomal escape is necessary for the efficient delivery of the NP drug cargo to the tumor site. Size, charge and surface

decoration of NPs determine which endocytic pathway they may enter and their subsequent intracellular fate (Blanco et al., 2015). Concerns about the endosomal escape of therapeutic agents became paramount with the advent of RNA interference for clinical applications. However, nucleic acids, charged molecules with high molecular weight (5–1000s kD), are easily degraded by endogenous nucleases and are thus unable to reach their pharmaceutical target without assistance. To achieve an effective cellular response, nucleic acid therapeutics has to involve an endosomal escape process.

Several pathways exist for movement of the NP or its cargo into the cell interior. Endocytosis is a process of forming vesicles and moving them toward intracellular targets usually involving clathrin-coated pits where the specific receptors reside (e.g., uptake of low density lipoprotein (LDL) and the LDL receptor described by Brown and Goldstein (Doherty and McMahon, 2009; Goldstein and Brown, 2009; Kaksonen and Roux, 2018). Several clathrin-independent pathways such as endophilin-mediated, flotillin-mediated and macropinocytosis have also been reported (Doherty and McMahon, 2009; Amaddii et al., 2012; Sorkina et al., 2013; Ferreira and Boucrot, 2017). Cargo contained in endosomes can be recycled back to the plasma membrane or other organelles, delivered to the lysosome for degradation, or undergo a process called transcytosis (Elkin et al., 2016). Once vesicles pinch off from the plasma membrane, loaded with cargo, they mature into early endosomes and are sorted to determine their final destination (Salzman and Maxfield, 1988; Huotari and Helenius, 2011). As endosomes continue to mature from the early to the late stage and into the lysosome, they become progressively more acidic due to the ATP-dependent pumping of hydrogen ions into the lumen (Mellman et al., 1986). The early endosomal interior has a pH in the range of ≈6.5 compared to ≈5.5 for late endosomes. These pH changes are needed for the dissociation of receptors from their ligands in order to be processed via recycling of the receptor or ligand degradation. Degradation of the cargo occurs when the late endosome fuses with the lysosome, creating an endolysosome with a pH of ≈4.5 exposing the cargo to a full spectrum of hydrolases (Huotari and Helenius, 2011). The endolysosomal environment is considered detrimental to targeted NP cargo delivery, particularly to intracellular nucleic acid transport (Blanco et al., 2015).

Strategies for Endosomal Escape

Strategies for the endosomal escape is a wide-ranging topic that merits a review of its own. However, these strategies could represent key steps in the design, and manufacturing of NP formulations. Rather than designing and preparing complex formulations, direct cytosolic delivery of the therapeutic payload could be achieved with a drug delivery NP platform such as the reconstituted/recombinant high-density lipoproteins (rHDL). The receptor for HDL, Scavenger Receptor Class B, Type 1 (SR-B1) facilitates the endogenous delivery mechanism directly into the cytosol, a process known as selective lipid uptake (Zhang et al., 2009)

SR-B1 and Selective Uptake

There are five isoforms of SR-B1 from splice variants encoded by the SCARB1 gene. The first isoform was named as SR-B1 and shown to be the HDL receptor (Acton et al., 1996; Calvo et al., 1997). The receptor protein consists of 509 amino acids and has an apparent molecular weight of 82–85 kDa. Isoform 3 has a length of 552 amino acids and has been set as the canonical sequence (Gutierrez-Pajares et al., 2016). The highest expression of SR-B1 in normal tissues can be found in the liver and steroidogenic organs (Landschulz et al., 1996; Calvo et al., 1997; Arenas et al., 2004; Shahzad et al., 2011). In murine adrenocortical cells and an SR-B1 transfected Chinese hamster ovary cell line, SR-B1 appears to co-localize with caveolae (Babitt et al., 1997). In hepatocytes, SR-B1 interacts with an adaptor protein, PDZK1, which mediates its localization and function (Kocher and Krieger, 2009). When rat SR-B1 was over-expressed in an adrenal cell model, the receptor was reported to dimerize, restructure plasma membrane architecture, and to increase cholesteryl ester uptake (Reaven et al., 2006). Malignant tissues have been found to over-express the SR-BI receptor (Lacko et al., 2002, Shahzad et al., 2011) and patients with high expression levels have a tendency for worse prognoses (Shahzad et al., 2011; Schörghofer et al., 2015; Yuan et al., 2016; Feng et al., 2018). It is not known if over-expressed SR-B1 is in a dimeric or oligomeric state in cancer cells, but it is known that cancer patients have lowered blood cholesterol levels, particularly HDL cholesterol (Rose et al., 1974; Fiorenza et al., 2000; Shah et al., 2008; Muntoni et al., 2009).

HDL and Small Molecules

In case of HDL, the 'selective lipid uptake mechanism' involves HDL docking with its receptor (Murao et al., 1997) followed by internalization of only the core contents (cholesteryl esters), not the whole particle (**Figure 4**). The exact mechanism of how SR-B1 achieves selective lipid uptake is yet to be fully elucidated. It was postulated that SR-B1 forms a hydrophobic channel or pore when docked with HDL to allow passage of cholesteryl esters across the cell membrane (Rodrigueza et al., 1999). It has been reported that HDL undergoes retroendocytosis, in which the lipoprotein is taken up just inside the plasma membrane, delivers its cargo, and exits the cell without entering the endocytic pathway (Pagler et al., 2006; Sun et al., 2006; Rohrer et al., 2009). It is possible that the formation of an SR-B1 pore allows all hydrophobic materials (other than cholesteryl esters) to traverse the cell membrane, particularly when the receptor is over-expressed in cancer (Mooberry et al., 2010).

One of the early reports in the literature observed that 82% of paclitaxel from the core of rHDL was taken up by the cell in a selective SR-B1-like mechanism (Mooberry et al., 2010). The drug uptake could be partially blocked by Apo A-I, discoidal Apo A-I/PC complexes or isolated human HDL (Mooberry et al., 2010). Further validation of selective delivery was shown with a model compound dilauryl fluorescein taken up in SR-B1-transfected cells that could be limited by adding either Apo-AI or excess rHDL (McConathy et al., 2011). Yang et al have also shown that gold templated HDL mimetic NPSs were found in the cytoplasm after administration to mice (Yang et al., 2013).

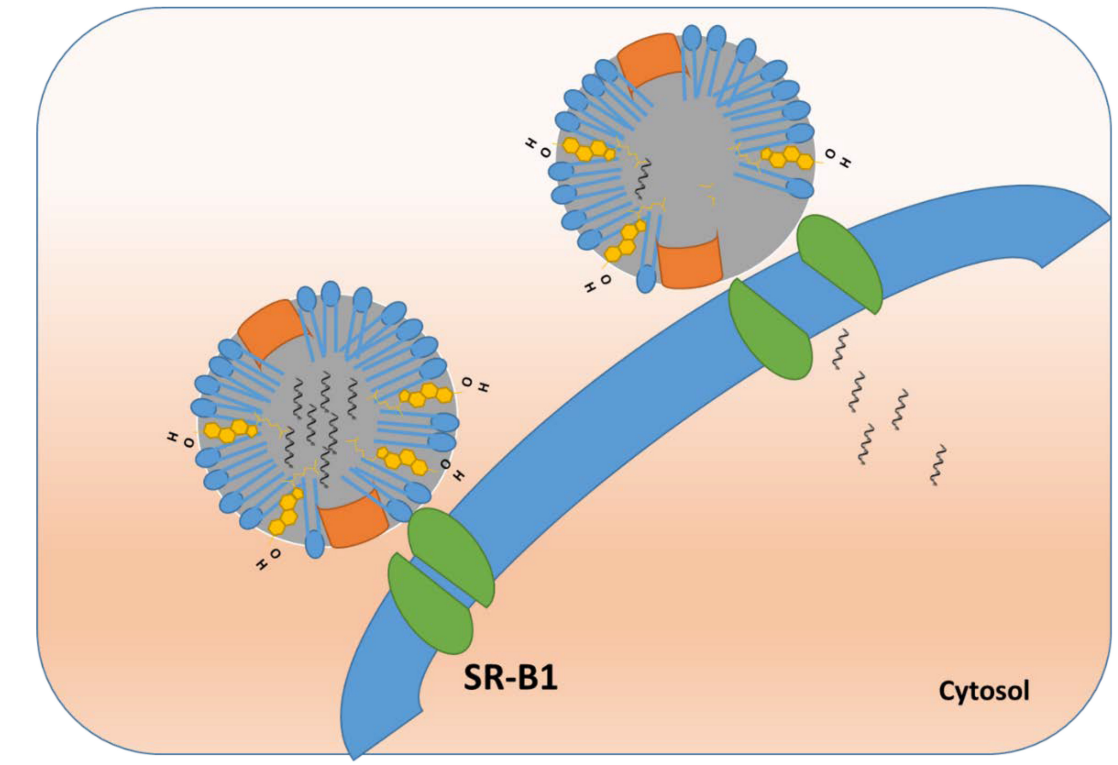

FIGURE 4 | Endosomal escape and direct cytosolic delivery of cargo using rHDL NPs.

Selective cytosolic delivery was also shown with an Apo A-I mimetic peptide/phospholipid nanocarrier created to carry the hydrophobic fluorophore, DiR-BOA (1, 1′-dioctadecyl-3, 3, 3′, 3′-tetramethylindotricarbocyanine iodide bis-oleate) in its core (Zhang et al., 2009; Case et al., 2012). Uptake of DiR-BOA did not co-localize with the lysosomal marker, LysoTracker. Z stacks obtained by confocal microscopy showed a cytosolic location for the fluorophore (Zhang et al., 2009). Additional reports with other drugs, such as valrubicin and fenretinide, have shown that SR-B1-mediated drug uptake from rHDL can be inhibited via the Block Lipid Transporter 1 (BLT1) or antibody blocking of SR-B1 (Sabnis et al., 2012, 2013; Johnson et al., 2017).

In an elegantly designed study, Lin et al used a multi-fluorophore-labeled NP, termed HDL-mimicking peptide phospholipid scaffold (HPPS) to probe uptake via the SR-B1-mediated pathway (Lin et al., 2014). The core of the HPPS NPs was fluorescently labeled with either DiR-BOA or Fluo-BOA (dioleyl fluorescein) (Zhang et al., 2010). Rhodamine-B-labeled phospholipids were incorporated into the phospholipid monolayer of the HPPS NPs. An 18-amino acid Apo A-I mimetic peptide was conjugated to a FITC label and complexed with HPPS NPs. The selective uptake was monitored in SR-B1-transfected cells. Lin et al. (2014) reported that a synthetic cholesteryl ester analog selectively entered the cells, leaving the phospholipids and peptide on the exterior of the cell. (Lin et al., 2014). Cytosolic delivery of the hydrophobic core content of the HPPS NP could not be inhibited by temperature changes or energy depletion. Utilizing endocytosis inhibitors to target either clathrin or actin revealed that the SR-B1-mediated uptake was an endocytic process. In contrast, the cytosolic delivery could be affected by disruption of lipid rafts or caveolae or the SR-B1 inhibitor, BLT1. However, it is known that disruption of lipid rafts/caveolae has minimal effect on the uptake of CE from HDL (Rhainds et al., 2004; Wustner et al., 2004). Mooberry et al. (2010) have shown that only 18% of the paclitaxel-loaded rHDL entered the cell via whole particle uptake, suggesting that these particles were endocytosed (Mooberry et al., 2010). The quantitative aspects of the multiple mechanisms involved in the uptake of the drug payload from rHDL NPs are yet to be elucidated.

HDL and Nucleic Acids

It important to cite the pioneering work done by several researchers in siRNA delivery and SR-B1 involvement. Bijsterbosch et al studied the biodistribution and organ accumulation of phosphorothioate antisense oligo whereby most of it (>90%) was found to be in the liver at 90 min indicating that scavenger receptors were involved (Bijsterbosch et al., 1997, 2000). Regarding the selective delivery of nucleic acids, the molecular weight differences are striking; the molecular weight of an average siRNA is approximately 20-fold that of the average drug molecule. However, it appears that direct cytosolic delivery of nucleic acids also occurs through SR-B1. It has been reported that endogenous HDL in the circulation

carried endogenous microRNA and delivered it to target cells through SR-B1 (Vickers et al., 2011). Uptake of a fluorescently labeled siRNA via rHDL in SR-B1-expressing tumors and the liver in an ovarian cancer mouse model illustrates the ability of rHDL to deliver nucleic acids through SR-B1 (Shahzad et al., 2011). Using a fluorescently labeled cholesterol-conjugated siRNA (FAM-Chol-siRNA) packaged in rHDL, Ding et al observed delivery, specifically to the cytosol in the hepatocellular carcinoma cell line, HepG2 (Ding et al., 2012). Further studies validated the SR-B1-mediated direct cytosolic delivery of the FAM-Chol-siRNA by blocking uptake with endogenous HDL in the MCF7 breast cancer cell line. Secondly, the intracellular location of the FAM-Chol-siRNA was compared to the location of a LysoTracker signal and found to not colocalize (Ding et al., 2014). Other studies used fluorescently labeled transferrin as an endocytosis marker and found no co-localization with siRNA, delivered via an HDL-mimicking NP (Yang et al., 2011).

Direct cytosolic delivery of siRNA could be the explanation as to why HDL-type NPs exhibit favorable *in vivo* efficacy in tumor models (Shahzad et al., 2011; Ding et al., 2012, 2014). Concerns about off-target toxicity toward other SR-B1-expressing organs (particularly the liver) can be allayed by a study in which 72 h after administration, the fluorescent signal was still strong in the tumor, but cleared from the liver (Ding et al., 2014). Furthermore, liver function tests revealed no difference between control groups and rHDL/siRNA therapy groups (Shahzad et al., 2011). Additional preclinical and translational research will be necessary to demonstrate the advantages of an HDL-like NP platform. (McMahon and Thaxton, 2014). An excellent review by McMahon et al. (2016) further discusses HDL and its ability to transport and deliver different RNAi species for therapeutic applications (McMahon et al., 2016).

DRUG RESISTANCE AND rHDL

Resistance to therapy (chemo-resistance) leads to relapse and metastasis and thus substantially diminishes the prospects for remission or cure for cancer patients (Zheng, 2017). Consequently, resistance to anti-cancer drugs has continued to be a major impediment to effectively treating many cancers (Robey et al., 2018). The process is known as "multidrug resistance", is a particularly difficult barrier to overcome, especially during the treatment of metastatic disease (Robey et al., 2018). Consequently, a reversal (Angelini et al., 2008) or prevention (Cole, 2014) of drug resistance, displayed by aggressively growing malignant tumors. Although numerous approaches (Harker et al., 1986; Hyafil et al., 1993; Choi et al., 2010), including administration of drugs (Koo et al., 2008) have been explored, the clinical efficacy of these treatments met only with limited success. Drug resistance thus remains to be a major obstacle in oncology (Robey et al., 2018).

Because the well-described mechanisms of drug resistance (Lin et al., 2014; Robey et al., 2018) often involve pumping units located in the membranes of malignant cells, the idea that *cytoplasmic delivery* of cytotoxic anti-cancer agents could overcome these obstacles has been considered by several investigators (Lin et al., 2014; Yang et al., 2014; Yin et al., 2015). These references include one of the earliest reports, providing data on cytoplasmic delivery of drug payloads via rHDL NPs (Lin et al., 2014). Our laboratory was the first to report that paclitaxel delivery to prostate cancer cells takes place primarily via facilitation of the SR-B1 receptor (Mooberry et al., 2010). This delivery route (not requiring the entry of the whole NP into the cell) is known to result in the transport of the lipoprotein payload directly to the cytosol (Ding et al., 2014). Drug resistance to chemotherapy may be avoided by utilizing the SR-B1-HDL interaction. The Thaxton lab has been using the gold templated HDL mimetic NPs to alter the cholesterol flux in cancer (leukemia and lymphoma) cells and to induce apoptosis, thereby completely avoiding the need for the use of cytotoxic drugs (Plebanek et al., 2015; Rink et al., 2017). Because each of these cell types has differing needs for cholesterol, it may be explored to determine whether other drug-resistant solid tumors may be successfully treated using gold core HDL mimetic NPs.

While this mechanism is attractive and our laboratory has now collected additional evidence for the selective delivery of the rHDL drug payload and for the endosomal escape, so far, there is no direct validation available for the hypothesis that rHDL transported therapeutic agents would be able to mediate or limit drug resistance. All indications point to the success of this approach that is likely to have 'game-changing' significance in the therapeutics of aggressive tumors and the management of other diseases as well.

CONCLUSION

In summary, rHDL NPs are inherently capable of overcoming several biological barriers to cancer therapy. Their small size, intrinsic targeting ability, endosomal escape, demonstrated safety in animal and human studies makes this platform highly attractive for new as well as traditional chemotherapy drugs which suffer from off-target toxicity issues. Liver toxicity could be a potential concern, however, we have not come across any report showing liver toxicity of rHDL delivered drugs in murine models. Our laboratory did not find any change in liver enzymes with STAT3 targeted siRNA for ovarian cancer therapy (Shahzad et al., 2011). Clearly, more research work is needed in this area to establish the effect of various drugs via this delivery system that they may have on hepatocytes and the liver itself. Although several aspects such as drug resistance need to be investigated further, we submit that rHDL based chemotherapy approach will likely shift the risk/benefit ratio associated with current chemotherapy.

AUTHOR CONTRIBUTIONS

SR conceived the idea, wrote and coordinated all the sections in the manuscript. LM, NS, AG, AD, and AL have contributed to writing different sections and revising this manuscript.

FUNDING

The author's research was supported by Cancer Prevention and Research Institute of Texas (DP150091), Rutledge Cancer Foundation, Wheels for Wellness of Fort Worth, Texas, to Andras Lacko. This work in part was supported by Texas Alzheimer's Research Care and Consortium (2018-48-51-JI) and Leukemia Texas Foundation grants to SR.

REFERENCES

Acton, S., Rigotti, A., Landschulz, K. T., Xu, S., Hobbs, H. H., and Krieger, M. (1996). Identification of scavenger receptor SR-BI as a high density lipoprotein receptor. *Science* 271, 518–520. doi: 10.1126/science.271.5248.518

Agashe, H. B., Dutta, T., Garg, M., and Jain, N. (2006). Investigations on the toxicological profile of functionalized fifth-generation poly (propylene imine) dendrimer. *J. Pharm. Pharmacol.* 58, 1491–1498. doi: 10.1211/jpp.58.11.0010

Alexis, F., Pridgen, E., Molnar, L. K., and Farokhzad, O. C. (2008). Factors affecting the clearance and biodistribution of polymeric nanoparticles. *Mol. Pharm.* 5, 505–515. doi: 10.1021/mp800051m

Amaddii, M., Meister, M., Banning, A., Tomasovic, A., Mooz, J., Rajalingam, K., et al. (2012). Flotillin-1/reggie-2 protein plays dual role in activation of receptor-tyrosine kinase/mitogen-activated protein kinase signaling. *J. Biol. Chem.* 287, 7265–7278. doi: 10.1074/jbc.M111.287599

Angelini, A., Iezzi, M., Di Febbo, C., Di Ilio, C., Cuccurullo, F., and Porreca, E. (2008). Reversal of P-glycoprotein-mediated multidrug resistance in human sarcoma MES-SA/Dx-5 cells by nonsteroidal anti-inflammatory drugs. *Oncol. Rep.* 20, 731–735.

Arenas, M. I., Lobo, M. V., Caso, E., Huerta, L., Paniagua, R., and Martin-Hidalgo, M. A. (2004). Normal and pathological human testes express hormone-sensitive lipase and the lipid receptors CLA-1/SR-BI and CD36. *Hum. Pathol.* 35, 34–42. doi: 10.1016/j.humpath.2003.08.015

Arvizo, R. R., Miranda, O. R., Moyano, D. F., Walden, C. A., Giri, K., Bhattacharya, R., et al. (2011). Modulating pharmacokinetics, tumor uptake and biodistribution by engineered nanoparticles. *PLoS One* 6:e24374. doi: 10.1371/journal.pone.0024374

Babitt, J., Trigatti, B., Rigotti, A., Smart, E. J., Anderson, R. G., Xu, S., et al. (1997). Murine SR-BI, a high density lipoprotein receptor that mediates selective lipid uptake, is N-glycosylated and fatty acylated and colocalizes with plasma membrane caveolae. *J. Biol. Chem.* 272, 13242–13249. doi: 10.1074/jbc.272.20.13242

Barrán-Berdón, A. L., Pozzi, D., Caracciolo, G., Capriotti, A. L., Caruso, G., Cavaliere, C., et al. (2013). Time evolution of nanoparticle–protein corona in human plasma: relevance for targeted drug delivery. *Langmuir* 29, 6485–6494. doi: 10.1021/la401192x

Barter, P. J., Nicholls, S., Rye, K., Anantharamaiah, G., Navab, M., and Fogelman, A. M. (2004). Antiinflammatory properties of HDL. *Circ. Res.* 95, 764–772. doi: 10.1161/01.RES.0000146094.59640.13

Bermejo, J. F., Ortega, P., Chonco, L., Eritja, R., Samaniego, R., Müllner, M., et al. (2007). Water-soluble carbosilane dendrimers: synthesis biocompatibility and complexation with oligonucleotides. *Eval. Med. Appl.* 13, 483–495.

Bijsterbosch, M. K., Manoharan, M., Rump, E. T., De Vrueh, R. L., van Veghel, R., Tivel, K. L., et al. (1997). In vivo fate of phosphorothioate antisense oligodeoxynucleotides: predominant uptake by scavenger receptors on endothelial liver cells. *Nucleic Acids Res.* 25, 3290–3296. doi: 10.1093/nar/25.16.3290

Bijsterbosch, M. K., Rump, E. T., Vrueh, R. L. D., Dorland, R., van Veghel, R., Tivel, K. L., et al. (2000). Modulation of plasma protein binding and in vivo liver cell uptake of phosphorothioate oligodeoxynucleotides by cholesterol conjugation. *Nucleic Acids Res.* 28, 2717–2725. doi: 10.1093/nar/28.14.2717

Blaho, V. A., Galvani, S., Engelbrecht, E., Liu, C., Swendeman, S. L., Kono, M., et al. (2015). HDL-bound sphingosine-1-phosphate restrains lymphopoiesis and neuroinflammation. *Nature* 523, 342–346. doi: 10.1038/nature14462

Blanco, E., Shen, H., and Ferrari, M. (2015). Principles of nanoparticle design for overcoming biological barriers to drug delivery. *Nat. Biotechnol.* 33, 941–951. doi: 10.1038/nbt.3330

Bosi, S., Feruglio, L., Da Ros, T., Spalluto, G., Gregoretti, B., Terdoslavich, M., et al. (2004). Hemolytic effects of water-soluble fullerene derivatives. *J. Med. Chem.* 47, 6711–6715. doi: 10.1021/jm0497489

Calvo, D., Gomez-Coronado, D., Lasuncion, M. A., and Vega, M. A. (1997). CLA-1 is an 85-kD plasma membrane glycoprotein that acts as a high-affinity receptor for both native (HDL, LDL, and VLDL) and modified (OxLDL and AcLDL) lipoproteins. *Arterioscler. Thromb. Vasc. Biol.* 17, 2341–2349. doi: 10.1161/01.ATV.17.11.2341

Case, D., Darden, T., Cheatham, T. III, Simmerling, C., Wang, J., Duke, R., et al. (2012). *AMBER 12*. San Francisco, CA: University of California.

Chen, W., Jarzyna, P. A., van Tilborg, G. A., Nguyen, V. A., Cormode, D. P., Klink, A., et al. (2010). RGD peptide functionalized and reconstituted high-density lipoprotein nanoparticles as a versatile and multimodal tumor targeting molecular imaging probe. *FASEB J.* 24, 1689–1699. doi: 10.1096/fj.09-139865

Choi, J. S., Kang, N. S., Min, Y. K., and Kim, S. H. (2010). Euphorbiasteroid reverses P-glycoprotein-mediated multi-drug resistance in human sarcoma cell line MES-SA/Dx. *Phytother. Res.* 24, 1042–1046.

Cole, S. P. (2014). Targeting multidrug resistance protein 1 (MRP1, ABCC1): past, present, and future. *Annu. Rev. Pharmacol. Toxicol.* 54, 95–117. doi: 10.1146/annurev-pharmtox-011613-135959

Connelly, M. A., and Williams, D. L. (2004). SR-BI and HDL cholesteryl ester metabolism. *Endocr. Res.* 30, 697–703. doi: 10.1081/ERC-200043979

Corbin, I. R., Li, H., Chen, J., Lund-Katz, S., Zhou, R., Glickson, J. D., et al. (2006). Low-density lipoprotein nanoparticles as magnetic resonance imaging contrast agents. *Neoplasia* 8, 488–498. doi: 10.1593/neo.05835

Corbin, I. R., and Zheng, G. (2007). Mimicking nature's nanocarrier: synthetic low-density lipoprotein-like nanoparticles for cancer-drug delivery. *Nanomedicine* 2, 375–380. doi: 10.2217/17435889.2.3.375

Cormode, D. P., Jarzyna, P. A., Mulder, W. J., and Fayad, Z. A. (2010). Modified natural nanoparticles as contrast agents for medical imaging. *Adv. Drug Deliv. Rev.* 62, 329–338. doi: 10.1016/j.addr.2009.11.005

Cruz, P. M., Mo, H., McConathy, W., Sabnis, N. A., and Lacko, A. G. (2013). The role of cholesterol metabolism and cholesterol transport in carcinogenesis: a review of scientific findings, relevant to future cancer therapeutics. *Front. Pharmacol.* 4:119. doi: 10.3389/fphar.2013.00119

Damiano, M. G., Mutharasan, R. K., Tripathy, S., McMahon, K. M., and Thaxton, C. S. (2013). Templated high density lipoprotein nanoparticles as potential therapies and for molecular delivery. *Adv. Drug Deliv. Rev.* 65, 649–662. doi: 10.1016/j.addr.2012.07.013

Decuzzi, P., Lee, S., Bhushan, B., and Ferrari, M. (2005). A theoretical model for the margination of particles within blood vessels. *Ann. Biomed. Eng.* 33, 179–190. doi: 10.1007/s10439-005-8976-5

Decuzzi, P., Pasqualini, R., Arap, W., and Ferrari, M. (2009). Intravascular delivery of particulate systems: does geometry really matter? *Pharm. Res.* 26, 235–243. doi: 10.1007/s11095-008-9697-x

Desai, N. (2012). Challenges in development of nanoparticle-based therapeutics. *AAPS J.* 14, 282–295. doi: 10.1208/s12248-012-9339-4

Ding, Y., Wang, W., Feng, M., Wang, Y., Zhou, J., Ding, X., et al. (2012). A biomimetic nanovector-mediated targeted cholesterol-conjugated siRNA delivery for tumor gene therapy. *Biomaterials* 33, 8893–8905. doi: 10.1016/j.biomaterials.2012.08.057

Ding, Y., Wang, Y., Zhou, J., Gu, X., Wang, W., Liu, C., et al. (2014). Direct cytosolic siRNA delivery by reconstituted high density lipoprotein for target-specific therapy of tumor angiogenesis. *Biomaterials* 35, 7214–7227. doi: 10.1016/j.biomaterials.2014.05.009

Doherty, G. J., and McMahon, H. T. (2009). Mechanisms of endocytosis. *Annu. Rev. Biochem.* 78, 857–902. doi: 10.1146/annurev.biochem.78.081307.110540

Domański, D., Klajnert, B., and Bryszewska, M. (2004). Influence of PAMAM dendrimers on human red blood cells. *Bioelectrochemistry* 63, 189–191. doi: 10.1016/j.bioelechem.2003.09.023

Elkin, S. R., Lakoduk, A. M., and Schmid, S. L. (2016). Endocytic pathways and endosomal trafficking: a primer. *Wien. Med. Wochenschr.* 166, 196–204. doi: 10.1007/s10354-016-0432-7

Feng, H., Wang, M., Wu, C., Yu, J., Wang, D., Ma, J., et al. (2018). High scavenger receptor class B type I expression is related to tumor aggressiveness and poor prognosis in lung adenocarcinoma: A STROBE compliant article. *Medicine* 97:e0203. doi: 10.1097/MD.0000000000010203

Ferreira, A. P., and Boucrot, E. (2017). Mechanisms of carrier formation during clathrin-independent endocytosis. *Trends Cell Biol.* 28, 188–200. doi: 10.1016/j.tcb.2017.11.004

Fiorenza, A., Branchi, A., and Sommariva, D. (2000). Serum lipoprotein profile in patients with cancer. A comparison with non-cancer subjects. *Int. J. Clin. Lab. Res.* 30, 141–145. doi: 10.1007/s005990070013

Frias, J. C., Lipinski, M. J., Lipinski, S. E., and Albelda, M. T. (2007). Modified lipoproteins as contrast agents for imaging of atherosclerosis. *Contrast Media Mol. Imag.* 2, 16–23. doi: 10.1002/cmmi.124

Goldstein, J. L., and Brown, M. S. (2009). The LDL receptor. *Arterioscler. Thromb. Vasc. Biol.* 29, 431–438. doi: 10.1161/ATVBAHA.108.179564

Gutierrez-Pajares, J. L., Hassen, C. B., Chevalier, S., and Frank, P. G. (2016). SR-BI: linking cholesterol and lipoprotein metabolism with breast and prostate cancer. *Front. Pharmacol.* 7:338. doi: 10.3389/fphar.2016.00338

Harker, W. G., Bauer, D., Etiz, B. B., Newman, R. A., and Sikic, B. I. (1986). Verapamil-mediated sensitization of doxorubicin-selected pleiotropic resistance in human sarcoma cells: selectivity for drugs which produce DNA scission. *Cancer Res.* 46, 2369–2373.

He, C., Hu, Y., Yin, L., Tang, C., and Yin, C. (2010). Effects of particle size and surface charge on cellular uptake and biodistribution of polymeric nanoparticles. *Biomaterials* 31, 3657–3666. doi: 10.1016/j.biomaterials.2010.01.065

Hellstrand, E., Lynch, I., Andersson, A., Drakenberg, T., Dahlbäck, B., Dawson, K. A., et al. (2009). Complete high-density lipoproteins in nanoparticle corona. *FEBS J.* 276, 3372–3381. doi: 10.1111/j.1742-4658.2009.07062.x

Hogquist, K. A., Baldwin, T. A., and Jameson, S. C. (2005). Central tolerance: learning self-control in the thymus. *Nat. Rev. Immunol.* 5, 772–782. doi: 10.1038/nri1707

Huotari, J., and Helenius, A. (2011). Endosome maturation. *EMBO J.* 30, 3481–3500. doi: 10.1038/emboj.2011.286

Hyafil, F., Vergely, C., Du Vignaud, P., and Grand-Perret, T. (1993). In vitro and in vivo reversal of multidrug resistance by GF120918, an acridonecarboxamide derivative. *Cancer Res.* 53, 4595–4602.

Johnson, R., Sabnis, N., Sun, X., Ahluwalia, R., and Lacko, A. G. (2017). SR-B1-targeted nanodelivery of anti-cancer agents: a promising new approach to treat triple-negative breast cancer. *Breast Cancer* 9, 383–392.

Kaksonen, M., and Roux, A. (2018). Mechanisms of clathrin-mediated endocytosis. *Nat. Rev. Mol. Cell Biol.* 19, 313–326. doi: 10.1038/nrm.2017.132

Kamaly, N., Xiao, Z., Valencia, P. M., Radovic-Moreno, A. F., and Farokhzad, O. C. (2012). Targeted polymeric therapeutic nanoparticles: design, development and clinical translation. *Chem. Soc. Rev.* 41, 2971–3010. doi: 10.1039/c2cs15344k

Kingwell, B. A., Chapman, M. J., Kontush, A., and Miller, N. E. (2014). HDL-targeted therapies: progress, failures and future. *Nat. Rev. Drug Discov.* 13, 445–464. doi: 10.1038/nrd4279

Kocher, O., and Krieger, M. (2009). Role of the adaptor protein PDZK1 in controlling the HDL receptor SR-BI. *Curr. Opin. Lipidol.* 20, 236–241. doi: 10.1097/MOL.0b013e32832aee82

Koo, J., Choi, W., Rhee, Y., Lee, H., Lee, E., Ahn, K. S., et al. (2008). Quinoline derivative KB3-1 potentiates paclitaxel induced cytotoxicity and cycle arrest via multidrug resistance reversal in MES-SA/DX5 cancer cells. *Life Sci.* 83, 700–708. doi: 10.1016/j.lfs.2008.09.009

Krause, B. R., and Remaley, A. T. (2013). Reconstituted HDL for the acute treatment of acute coronary syndrome. *Curr. Opin. Lipidol.* 24, 480–486. doi: 10.1097/MOL.0000000000000020

Kuai, R., Li, D., Chen, Y. E., Moon, J. J., and Schwendeman, A. (2016). High-density lipoproteins: nature's multifunctional nanoparticles. *ACS Nano* 10, 3015–3041. doi: 10.1021/acsnano.5b07522

Lacko, A. G., Nair, M., Paranjape, S., Johnson, S., and McConathy, W. J. (2002). High density lipoprotein complexes as delivery vehicles for anticancer drugs. *Anticancer Res.* 22, 2045–2050.

Lagrost, L., Athias, A., Herbeth, B., Guyard-Dangremont, V., Artur, Y., Paille, F., et al. (1996). Opposite effects of cholesteryl ester transfer protein and phospholipid transfer protein on the size distribution of plasma high density lipoproteins. Physiological relevance in alcoholic patients. *J. Biol. Chem.* 271, 19058–19065. doi: 10.1074/jbc.271.32.19058

Landschulz, K. T., Pathak, R. K., Rigotti, A., Krieger, M., and Hobbs, H. H. (1996). Regulation of scavenger receptor, class B, type I, a high density lipoprotein receptor, in liver and steroidogenic tissues of the rat. *J. Clin. Invest.* 98, 984–995. doi: 10.1172/JCI118883

Lin, Q., Chen, J., Ng, K. K., Cao, W., Zhang, Z., and Zheng, G. (2014). Imaging the cytosolic drug delivery mechanism of HDL-like nanoparticles. *Pharm. Res.* 31, 1438–1449. doi: 10.1007/s11095-013-1046-z

Lu, H., Zhang, H., Zhang, D., Lu, H., and Ma, D. (2015). A biocompatible reconstituted high-density lipoprotein nano-system as a probe for lung cancer detection. *Med. Sci. Monit.* 21, 2726–2733. doi: 10.12659/MSM.895255

Lundqvist, M., Stigler, J., Elia, G., Lynch, I., Cedervall, T., and Dawson, K. A. (2008). Nanoparticle size and surface properties determine the protein corona with possible implications for biological impacts. *Proc. Natl. Acad. Sci. U.S.A.* 105, 14265–14270. doi: 10.1073/pnas.0805135105

McConathy, W. J., Paranjape, S., Mooberry, L., Buttreddy, S., Nair, M., and Lacko, A. G. (2011). Validation of the reconstituted high-density lipoprotein (rHDL) drug delivery platform using dilauryl fluorescein (DLF). *Drug Deliv. Transl. Res.* 1, 113–120. doi: 10.1007/s13346-010-0012-0

McMahon, K. M., Plebanek, M. P., and Thaxton, C. S. (2016). Properties of native high-density lipoproteins inspire synthesis of actively targeted in vivo siRNA delivery vehicles. *Adv. Funct. Mater.* 26, 7824–7835. doi: 10.1002/adfm.201602600

McMahon, K. M., Scielzo, C., Angeloni, N. L., Deiss-Yehiely, E., Scarfo, L., Ranghetti, P., et al. (2017). Synthetic high-density lipoproteins as targeted monotherapy for chronic lymphocytic leukemia. *Oncotarget* 8, 11219–11227. doi: 10.18632/oncotarget.14494

McMahon, K. M., and Thaxton, C. S. (2014). High-density lipoproteins for the systemic delivery of short interfering RNA. *Expert Opin. Drug Deliv.* 11, 231–247. doi: 10.1517/17425247.2014.866089

Medzhitov, R., and Janeway, C. A. (2002). Decoding the patterns of self and nonself by the innate immune system. *Science* 296, 298–300. doi: 10.1126/science.1068883

Mellman, I., Fuchs, R., and Helenius, A. (1986). Acidification of the endocytic and exocytic pathways. *Annu. Rev. Biochem.* 55, 663–700. doi: 10.1146/annurev.bi.55.070186.003311

Min, Y., Caster, J. M., Eblan, M. J., and Wang, A. Z. (2015). Clinical translation of nanomedicine. *Chem. Rev.* 115, 11147–11190. doi: 10.1021/acs.chemrev.5b00116

Moghimi, S. M., Andersen, A. J., Ahmadvand, D., Wibroe, P. P., Andresen, T. L., and Hunter, A. C. (2011). Material properties in complement activation. *Adv. Drug Deliv. Rev.* 63, 1000–1007. doi: 10.1016/j.addr.2011.06.002

Mooberry, L. K., Nair, M., Paranjape, S., McConathy, W. J., and Lacko, A. G. (2010). Receptor mediated uptake of paclitaxel from a synthetic high density lipoprotein nanocarrier. *J. Drug Target* 18, 53–58. doi: 10.3109/10611860903156419

Muntoni, S., Atzori, L., Mereu, R., Satta, G., Macis, M. D., Congia, M., et al. (2009). Serum lipoproteins and cancer. *Nutr. Metab. Cardiovasc. Dis.* 19, 218–225. doi: 10.1016/j.numecd.2008.06.002

Murao, K., Terpstra, V., Green, S. R., Kondratenko, N., Steinberg, D., and Quehenberger, O. (1997). Characterization of CLA-1, a human homologue of rodent scavenger receptor BI, as a receptor for high density lipoprotein and apoptotic thymocytes. *J. Biol. Chem.* 272, 17551–17557. doi: 10.1074/jbc.272.28.17551

Nanjee, M. N., Doran, J. E., Lerch, P. G., and Miller, N. E. (1999). Acute effects of intravenous infusion of ApoA1/phosphatidylcholine discs on plasma lipoproteins in humans. *Arterioscler. Thromb. Vasc. Biol.* 19, 979–989. doi: 10.1161/01.ATV.19.4.979

Navab, M., Yu, R., Gharavi, N., Huang, W., Ezra, N., Lotfizadeh, A., et al. (2007). High-density lipoprotein: antioxidant and anti-inflammatory properties. *Curr. Atheroscler. Rep.* 9, 244–248. doi: 10.1007/s11883-007-0026-3

Ng, K. K., Lovell, J. F., and Zheng, G. (2011). Lipoprotein-inspired nanoparticles for cancer theranostics. *Acc. Chem. Res.* 44, 1105–1113. doi: 10.1021/ar200017e

Ngoune, R., Peters, A., von Elverfeldt, D., Winkler, K., and Pütz, G. (2016). Accumulating nanoparticles by EPR: a route of no return. *J. Control. Release* 238, 58–70. doi: 10.1016/j.jconrel.2016.07.028

Norata, G. D., Pirillo, A., Ammirati, E., and Catapano, A. L. (2012). Emerging role of high density lipoproteins as a player in the immune system. *Atherosclerosis* 220, 11–21. doi: 10.1016/j.atherosclerosis.2011.06.045

Oda, M. N., Hargreaves, P. L., Beckstead, J. A., Redmond, K. A., van Antwerpen, R., and Ryan, R. O. (2006). Reconstituted high density lipoprotein enriched with the polyene antibiotic amphotericin B. *J. Lipid Res.* 47, 260–267. doi: 10.1194/jlr.D500033-JLR200

Pagler, T. A., Rhode, S., Neuhofer, A., Laggner, H., Strobl, W., Hinterndorfer, C., et al. (2006). SR-BI-mediated high density lipoprotein (HDL) endocytosis leads to HDL resecretion facilitating cholesterol efflux. *J. Biol. Chem.* 281, 11193–11204. doi: 10.1074/jbc.M510261200

Panchoo, M., and Lacko, A. (2017). Scavenger receptor class B type 1 regulates neuroblastoma cell proliferation, migration and invasion. *Biochem. Biophys. Res. Commun.* 495, 614–620. doi: 10.1016/j.bbrc.2017.10.154

Plebanek, M. P., Bhaumik, D., and Thaxton, C. S. (2018). HDL and the golden key to cancer immunity? *Oncoscience* 5, 164–166.

Plebanek, M. P., Mutharasan, R. K., Volpert, O., Matov, A., Gatlin, J. C., and Thaxton, C. S. (2015). Nanoparticle targeting and cholesterol flux through scavenger receptor type B-1 inhibits cellular exosome uptake. *Sci. Rep.* 5:15724. doi: 10.1038/srep15724

Pownall, H. J., Rosales, C., Gillard, B. K., and Ferrari, M. (2016). Native and reconstituted plasma lipoproteins in nanomedicine: physicochemical determinants of nanoparticle structure, stability, and metabolism. *Methodist Debakey Cardiovasc. J.* 12, 146–150. doi: 10.14797/mdcj-12-3-146

Reaven, E., Nomoto, A., Cortez, Y., and Azhar, S. (2006). Consequences of over-expression of rat Scavenger Receptor, SR-BI, in an adrenal cell model. *Nutr. Metab.* 3:43.

Rhainds, D., Bourgeois, P., Bourret, G., Huard, K., Falstrault, L., and Brissette, L. (2004). Localization and regulation of SR-BI in membrane rafts of HepG2 cells. *J. Cell. Sci.* 117, 3095–3105. doi: 10.1242/jcs.01182

Rink, J. S., Yang, S., Cen, O., Taxter, T., McMahon, K. M., Misener, S., et al. (2017). Rational targeting of cellular cholesterol in diffuse large B-cell lymphoma (DLBCL) enabled by functional lipoprotein nanoparticles: a therapeutic strategy dependent on cell of origin. *Mol. Pharm.* 14, 4042–4051. doi: 10.1021/acs.molpharmaceut.7b00710

Robey, R. W., Pluchino, K. M., Hall, M. D., Fojo, A. T., Bates, S. E., and Gottesman, M. M. (2018). Revisiting the role of ABC transporters in multidrug-resistant cancer. *Nat. Rev. Cancer.* 18, 452–464. doi: 10.1038/s41568-018-0005-8

Rodrigueza, W. V., Thuahnai, S. T., Temel, R. E., Lund-Katz, S., Phillips, M. C., and Williams, D. L. (1999). Mechanism of scavenger receptor class B type I-mediated selective uptake of cholesteryl esters from high density lipoprotein to adrenal cells. *J. Biol. Chem.* 274, 20344–20350. doi: 10.1074/jbc.274.29.20344

Rohrer, L., Ohnsorg, P. M., Lehner, M., Landolt, F., Rinninger, F., and von Eckardstein, A. (2009). High-density lipoprotein transport through aortic endothelial cells involves scavenger receptor BI and ATP-binding cassette transporter G1. *Circ. Res.* 104, 1142–1150. doi: 10.1161/CIRCRESAHA.108.190587

Rose, G., Blackburn, H., Keys, A., Taylor, H., Kannel, W., Paul, O., et al. (1974). Colon cancer and blood-cholesterol. *Lancet* 303, 181–183. doi: 10.1016/S0140-6736(74)92492-1

Sabnis, N., Nair, M., Israel, M., McConathy, W. J., and Lacko, A. G. (2012). Enhanced solubility and functionality of valrubicin (AD-32) against cancer cells upon encapsulation into biocompatible nanoparticles. *Int. J. Nanomed.* 7, 975–983. doi: 10.2147/IJN.S28029

Sabnis, N., Pratap, S., Bowman, P., Akopova, I., and Lacko, A. G. (2013). Pre-clinical evaluation of rHDL encapsulated retinoids for the treatment of neuroblastoma. *Front. Pediatr.* 1:6. doi: 10.3389/fped.2013.00006

Salzman, N. H., and Maxfield, F. R. (1988). Intracellular fusion of sequentially formed endocytic compartments. *J. Cell Biol.* 106, 1083–1091. doi: 10.1083/jcb.106.4.1083

Sanchez-Gaytan, B. L., Fay, F., Lobatto, M. E., Tang, J., Ouimet, M., Kim, Y., et al. (2015). HDL-mimetic PLGA nanoparticle to target atherosclerosis plaque macrophages. *Bioconjug. Chem.* 26, 443–451. doi: 10.1021/bc500517k

Schörghofer, D., Kinslechner, K., Preitschopf, A., Schütz, B., Röhrl, C., Hengstschläger, M., et al. (2015). The HDL receptor SR-BI is associated with human prostate cancer progression and plays a possible role in establishing androgen independence. *Reprod. Biol. Endocrinol.* 13:88. doi: 10.1186/s12958-015-0087-z

Shah, D. S., Sakthivel, T., Toth, I., Florence, A. T., and Wilderspin, A. F. (2000). DNA transfection and transfected cell viability using amphipathic asymmetric dendrimers. *Int. J. Pharm.* 208, 41–48. doi: 10.1016/S0378-5173(00)00534-2

Shah, F. D., Shukla, S. N., Shah, P. M., Patel, H. R., and Patel, P. S. (2008). Significance of alterations in plasma lipid profile levels in breast cancer. *Integr. Cancer Ther.* 7, 33–41. doi: 10.1177/1534735407313883

Shah, S., Liu, Y., Hu, W., and Gao, J. (2011). Modeling particle shape-dependent dynamics in nanomedicine. *J. Nanosci. Nanotechnol.* 11, 919–928. doi: 10.1166/jnn.2011.3536

Shahzad, M. M., Mangala, L. S., Han, H. D., Lu, C., Bottsford-Miller, J., Nishimura, M., et al. (2011). Targeted delivery of small interfering RNA using reconstituted high-density lipoprotein nanoparticles. *Neoplasia* 13, 309–319. doi: 10.1593/neo.101372

Skajaa, T., Cormode, D. P., Jarzyna, P. A., Delshad, A., Blachford, C., Barazza, A., et al. (2011). The biological properties of iron oxide core high-density lipoprotein in experimental atherosclerosis. *Biomaterials* 32, 206–213. doi: 10.1016/j.biomaterials.2010.08.078

Sorkina, T., Caltagarone, J., and Sorkin, A. (2013). Flotillins regulate membrane mobility of the dopamine transporter but are not required for its protein kinase C dependent endocytosis. *Traffic* 14, 709–724. doi: 10.1111/tra.12059

Sun, B., Eckhardt, E. R., Shetty, S., van der Westhuyzen, D. R., and Webb, N. R. (2006). Quantitative analysis of SR-BI-dependent HDL retroendocytosis in hepatocytes and fibroblasts. *J. Lipid Res.* 47, 1700–1713. doi: 10.1194/jlr.M500450-JLR200

Szeto, G. L., and Lavik, E. B. (2016). Materials design at the interface of nanoparticles and innate immunity. *J. Mater. Chem. B* 4, 1610–1618. doi: 10.1039/C5TB01825K

Tan, J., Shah, S., Thomas, A., Ou-Yang, H. D., and Liu, Y. (2013). The influence of size, shape and vessel geometry on nanoparticle distribution. *Microfluid. Nanofluidics* 14, 77–87. doi: 10.1007/s10404-012-1024-5

Tardif, J., Ballantyne, C. M., Barter, P., Dasseux, J., Fayad, Z. A., Guertin, M., et al. (2014). Effects of the high-density lipoprotein mimetic agent CER-001 on coronary atherosclerosis in patients with acute coronary syndromes: a randomized trial. *Eur. Heart J.* 35, 3277–3286. doi: 10.1093/eurheartj/ehu171

Tenzer, S., Docter, D., Rosfa, S., Wlodarski, A., Kuharev, J., Rekik, A., et al. (2011). Nanoparticle size is a critical physicochemical determinant of the human blood plasma corona: a comprehensive quantitative proteomic analysis. *ACS Nano* 5, 7155–7167. doi: 10.1021/nn201950e

Thaxton, C. S., Rink, J. S., Naha, P. C., and Cormode, D. P. (2016). Lipoproteins and lipoprotein mimetics for imaging and drug delivery. *Adv. Drug Deliv. Rev.* 106, 116–131. doi: 10.1016/j.addr.2016.04.020

Torchilin, V. P. (2010). "Passive and active drug targeting: drug delivery to tumors as an example," in *Drug Delivery Anonymous*, Vol. 197, eds M. Schäfer-Korting (Berlin: Springer), 3–53.

Twiddy, A. L., Cox, M. E., and Wasan, K. M. (2012). Knockdown of scavenger receptor class B type I reduces prostate specific antigen secretion and viability of prostate cancer cells. *Prostate* 72, 955–965. doi: 10.1002/pros.21499

van Oostrom, O., Nieuwdorp, M., Westerweel, P. E., Hoefer, I. E., Basser, R., Stroes, E. S., et al. (2007). Reconstituted HDL increases circulating endothelial progenitor cells in patients with type 2 diabetes. *Arterioscler. Thromb. Vasc. Biol.* 27, 1864–1865. doi: 10.1161/ATVBAHA.107.143875

Vickers, K. C., Palmisano, B. T., Shoucri, B. M., Shamburek, R. D., and Remaley, A. T. (2011). MicroRNAs are transported in plasma and delivered to recipient cells by high-density lipoproteins. *Nat. Cell Biol.* 13, 423–433. doi: 10.1038/ncb2210

von Eckardstein, A., Castro, G., Wybranska, I., Theret, N., Duchateau, P., Duverger, N., et al. (1993). Interaction of reconstituted high density lipoprotein discs containing human apolipoprotein A-I (ApoA-I) variants with murine adipocytes and macrophages. Evidence for reduced cholesterol efflux promotion by apoA-I(Pro165– > Arg). *J. Biol. Chem.* 268, 2616–2622.

Wustner, D., Mondal, M., Huang, A., and Maxfield, F. R. (2004). Different transport routes for high density lipoprotein and its associated free sterol in polarized hepatic cells. *J. Lipid Res.* 45, 427–437. doi: 10.1194/jlr.M300440-JLR200

Xue, H. Y., Liu, S., and Wong, H. L. (2014). Nanotoxicity: a key obstacle to clinical translation of siRNA-based nanomedicine. *Nanomedicine* 9, 295–312. doi: 10.2217/nnm.13.204

Yamamoto, H., Takada, T., Yamanashi, Y., Ogura, M., Masuo, Y., Harada-Shiba, M., et al. (2017). VLDL/LDL acts as a drug carrier and regulates the transport and metabolism of drugs in the body. *Sci. Rep.* 7:633. doi: 10.1038/s41598-017-00685-9

Yang, M., Jin, H., Chen, J., Ding, L., Ng, K. K., Lin, Q., et al. (2011). Efficient cytosolic delivery of siRNA using HDL-mimicking nanoparticles. *Small* 7, 568–573. doi: 10.1002/smll.201001589

Yang, S., Damiano, M. G., Zhang, H., Tripathy, S., Luthi, A. J., Rink, J. S., et al. (2013). Biomimetic, synthetic HDL nanostructures for lymphoma. *Proc. Natl. Acad. Sci. U.S.A.* 110, 2511–2516. doi: 10.1073/pnas.1213657110

Yang, X., Yi, C., Luo, N., and Gong, C. (2014). Nanomedicine to overcome cancer multidrug resistance. *Curr. Drug Metab.* 15, 632–649. doi: 10.2174/1389200215666140926154443

Yin, Q., Shen, J., Yu, H., Huang, Y., Zhang, Z., and Li, Y. (2015). Bioreducible micelles with endosomal buffering and multidrug resistance-reversing function enhance anti-tumor efficacy of doxorubicin. *J. Biomed. Nanotechnol.* 11, 1764–1775. doi: 10.1166/jbn.2015.2004

Yokoi, K., Kojic, M., Milosevic, M., Tanei, T., Ferrari, M., and Ziemys, A. (2014a). Capillary-wall collagen as a biophysical marker of nanotherapeutic permeability into the tumor microenvironment. *Cancer Res.* 74, 4239–4246. doi: 10.1158/0008-5472.CAN-13-3494

Yokoi, K., Tanei, T., Godin, B., van de Ven, A. L., Hanibuchi, M., Matsunoki, A., et al. (2014b). Serum biomarkers for personalization of nanotherapeutics-based therapy in different tumor and organ microenvironments. *Cancer Lett.* 345, 48–55. doi: 10.1016/j.canlet.2013.11.015

Yuan, B., Wu, C., Wang, X., Wang, D., Liu, H., Guo, L., et al. (2016). High scavenger receptor class B type I expression is related to tumor aggressiveness and poor prognosis in breast cancer. *Tumor Biol.* 37, 3581–3588. doi: 10.1007/s13277-015-4141-4

Yuan, Y., Wang, W., Wang, B., Zhu, H., Zhang, B., and Feng, M. (2013). Delivery of hydrophilic drug doxorubicin hydrochloride-targeted liver using apoAI as carrier. *J. Drug Target* 21, 367–374. doi: 10.3109/1061186X.2012.757769

Yvan-Charvet, L., Wang, N., and Tall, A. R. (2010). Role of HDL, ABCA1, and ABCG1 transporters in cholesterol efflux and immune responses. *Arterioscler. Thromb. Vasc. Biol.* 30, 139–143. doi: 10.1161/ATVBAHA.108.179283

Zhang, Z., Cao, W., Jin, H., Lovell, J. F., Yang, M., Ding, L., et al. (2009). Biomimetic nanocarrier for direct cytosolic drug delivery. *Angew. Chem. Int. Ed Engl.* 48, 9171–9175. doi: 10.1002/anie.200903112

Zhang, Z., Chen, J., Ding, L., Jin, H., Lovell, J. F., Corbin, I. R., et al. (2010). HDL-mimicking peptide–lipid nanoparticles with improved tumor targeting. *Small* 6, 430–437. doi: 10.1002/smll.200901515

Zheng, H. (2017). The molecular mechanisms of chemoresistance in cancers. *Oncotarget* 8, 59950–59964. doi: 10.18632/oncotarget.19048

Zheng, Y., Liu, Y., Jin, H., Pan, S., Qian, Y., Huang, C., et al. (2013). Scavenger receptor B1 is a potential biomarker of human nasopharyngeal carcinoma and its growth is inhibited by HDL-mimetic nanoparticles. *Theranostics* 3, 477–486. doi: 10.7150/thno.6617

Conflict of Interest Statement: The authors declare that the research was conducted in the absence of any commercial or financial relationships that could be construed as a potential conflict of interest.

frontiers in Pharmacology

ORIGINAL RESEARCH
published: 23 January 2018
doi: 10.3389/fphar.2018.00012

Hydrazone-Containing Triblock Copolymeric Micelles for pH-Controlled Drug Delivery

Peilan Qi, Xiaohe Wu, Lei Liu, Huimin Yu and Shiyong Song**

Institute of Pharmacy, Pharmaceutical College of Henan University, Kaifeng, China

In this study, the structure–activity relationship of amphiphilic block copolymer micelles as nanosized drug delivery system was revealed. Firstly, a biodegradable triblock polymers PEG-DiHyd-PLA containing hydrazone bond was synthesized through the ring-opening polymerization. In this method, PEG-DiHyd-Phenol was used as the initiator and L-lactide as the monomer. Then, the polymeric micelles were formed and used as nano-drug carriers with pH sensitivity. The structure and composition of the polymer were characterized by infrared (IR), nuclear magnetic resonance (^{1}H-NMR), and gel permeation chromatography (GPC), we characterized the self-assembling process of the triblock polymers and the pH sensitivity of the micelles by the means of transmission electron microscopy (TEM), dynamic light scattering method (DLS). Doxorubicin (DOX) acts as the model drug, and we researched the capacities of drug loading and release *in vitro* of the micelles. MTT experiments showed that the blank micelles of PEG-DiHyd-PLA were not cytotoxic to tumor cells (HepG-2, MCF-7) and normal cell (L-02 cells), but the DOX loaded ones displayed more toxicity than the ones without hydrazone, which was consistent to the further confocal laser scanning microscopy and flow cytometry study.

Keywords: triblock copolymer, pH-sensitive, cytotoxicity, micelles, tumor targeting

OPEN ACCESS

Edited by:
Qingxin Mu,
University of Washington,
United States

Reviewed by:
Liwen Li,
University of Pittsburgh Cancer Institute, United States
Lei Xing,
China Pharmaceutical University, China

****Correspondence:***
Lei Liu
liulei@henu.edu.cn
Shiyong Song
pharmsong@outlook.com

Specialty section:
This article was submitted to Cancer Molecular Targets and Therapeutics, a section of the journal Frontiers in Pharmacology

Received: *30 October 2017*
Accepted: *05 January 2018*
Published: *23 January 2018*

Citation:
Qi P, Wu X, Liu L, Yu H and Song S (2018) Hydrazone-Containing Triblock Copolymeric Micelles for pH-Controlled Drug Delivery. Front. Pharmacol. 9:12. doi: 10.3389/fphar.2018.00012

INTRODUCTION

In the past two decades, a large number of nanoparticulate drug delivery systems have been extensively explored as in cancer treatment. Some formulations in the form of liposome, polymer–drug conjugates, and micelle particulate have found their applications in clinics and even more are advanced to the stage of clinical trials. Recently, more sophisticated nano-system have been developed to increase the therapeutic efficacy of cancer by controlling of the drug release temporally or spatially. Stimuli-response functionality is becoming increasingly important due to applications in biotechnology and the crafting of smart materials. Stimulus (Xing et al., 2011), such as pH (Hrubý et al., 2005; Huang et al., 2015; Mei et al., 2016), temperature (Seo et al., 2015), reductant (Deng et al., 2015), and so on (Cheng et al., 2015), were applied to modulate the release profile of the therapeutic agents. Polymeric micelles that possess stimuli-responsive properties have been demonstrated their great potentials in maximizing the therapeutic efficacy by prolonging circulation life of drug, and minimizing side effects (Makino et al., 2015).

It was reported that it is more acidic around tumor than in blood and normal tissue (Webb et al., 2011). The inherent characteristic of tumor tissue makes pH-sensitive drug delivery systems more suitable for cancer chemotherapy. Furthermore, after endocytosis of the pH-sensitive micelles, an accelerated release of the payload occurs in endosomes and lysosomes, which have the low-pH of pH 5.5–6.0 and pH 4.5–5.0, respectively (Zheng et al., 2013).

A pH sensitive drug delivery system can be formed chemically or physically. Polymer-drug conjugate is one of the pH-responsive drug delivery systems that bearing with acid sensitive linkages between therapeutic molecule and polymer. Ulbrich (Hrubý et al., 2005; Ulbrich and Šubr, 2010) and Kataoka (Bae et al., 2003) conjugated block copolymers with doxorubicin (DOX) with an acid labile hydrazone containing linkage. The conjugates can form micelles and a boost release of DOX were found in an acidic environment upon the cleavage of hydrazone bonds. Hu et al. (2010) prepared biodegradable polymeric micelles with DOX conjugated block copolymer via hydrazone and carbamate linkage for DOX and the hydrazone ones have higher pH-sensitivity than the others. While, the frequently used hydrazone bond can only be formed between the DOX and hydrazine motif containing polymer. Anticancer drugs, such as paclitaxel, camptothecin and gemcitabine, are not appropriate for the linkage of hydrazone.

Physical entrapment of hydrophobic anticancer drugs in the core of a pH-responsive polymeric micelles is another way of forming a pH responsive system. In this case, pH sensitive parts are fixed on the body of carrier, on the side chain or backbone of the copolymer which forms the micelle, where sufficient structural changes are initiated in the low pH environment, triggering a boost release of drug simultaneously. Ding et al. (2009) connected poly(ethylene glycol) with stearic acid via a Schiff base bond linkage to form a pH-sensitive amphiphilic molecule mPEG-b-C18. The cleavage of the Schiff base bond under acidic condition resulted in disassociation of micelle and accelerated drug release. It is obvious that this kind of pH sensitive linkage is applicable for DOX but not limited to. The chemistry of pH-sensitive bond determines the performance of the drug delivery systems. There should be a perfect sensitivity that be able to hydrolyze quickly in acidic environments and stay unchanged in others. Acid labile linkages such as hydrazone (Bae et al., 2003; Hrubý et al., 2005; Hu et al., 2010; Ulbrich and Šubr, 2010), acetal (Gillies et al., 2004; Lu et al., 2010), orthoester (Tang et al., 2011; Cheng et al., 2012), citraconic amide (Cao et al., 2014), and Schiff base bonds (Ding et al., 2009) were reported. Among them, hydrazones were studied extensively for the easy preparations, moderate stability and favorable sensitivity.

In addition, the nature of micelle-forming amphiphilic copolymer should be also considered with respect to the biocompatibility, biodegradability, and capacity of drug loading. Usually biodegradable polymers such as polyester, poly (amino acid), and poly (anhydride) are core-forming materials and polyethylene glycols (PEG) (McPherson et al., 1998; Vonarbourg et al., 2006) form hydrophilic shell of micelles. The polyesters are preferred for their good biocompatibility and degradability (Witschi and Doelker, 1998). Poly (lactic acid) is widely used in drug delivery systems for its moderate degradation rate (Sinha et al., 2004).

In our previous studies, hydrazone containing di-block copolymers were used to form pH-sensitive carriers (Qi et al., 2017). Furthermore, with the discovery of more and more biocompatible polymer materials and atom transfer radical polymerization (ATRP) is becoming more and more mature (Cavallaro et al., 2014; Park et al., 2014; Ran et al., 2014; Visnevskij et al., 2014), triblock polymer has become favorable. Triblock polymers also can be used as drug carriers that aremore stable and controllable (Han et al., 2016). In this work, it was started with rational designing of PEG-based marcro-initiators with hydrazone bond imbedded, then hydrophobic polyester segment was incorporated by ring-opening polymerization. Micelles from the amphiphilic block polymer are both biodegradable and pH sensitive, for the controlled release of DOX.

MATERIALS AND METHODS

Materials

Polyethylene glycol (PEG; Mn = 6,000) was purchased from Sigma-Aldrich (St. Louis, MO, USA) and dried in a vacuum oven at 70°C before use. L-Lactide (99.5%, Jinan Daigang Biomaterials Co. Ltd., Jinan, China), stannous octanoate [$Sn(Oct)_2$, 95%, Sigma-Aldrich, St. Louis, MO, USA], 4-carboxybenzaldehyde (98%, Shanghai Darui, Shanghai, China), N,N′-dicyclohexylcarbodiimide (DCC, 98% Shanghai Darui, Shanghai, China), 4-dimethylaminopyridine (DMAP, 98% Shanghai Darui, Shanghai, China), methyl 4-hydroxybenzoate (98%, Shanghai Darui, Shanghai, China), and hydrazine hydrate aqueous solution (80%,Tianjin Kemiou, Tianjin, China) were used as received. Doxorubicin hydrochloride (Dalan Meilun Biotech., Dalian, China) was stirred with TEA (3 equiv.) in DMSO overnight before the solvent was evaporated using a rotary evaporator to get doxorubicin, i.e., DOX. All organic solvents were analytical reagents and used as received, except that toluene was dried by the sodium method to get anhydrous toluene.

Preparation of Tri-block Copolymer PEG-DiHyd-PLA

Synthesis of Dialdehyde Polyethylene Glycol (CHO-PEG-CHO)

CHO-PEG-CHO was prepared according to the reported procedure with some modifications (Ding et al., 2009). Firstly, PEG (8 g) in dichloromethane (DCM) (100 mL) reacted with 4-carboxybenzaldehyde in the presence of DCC (3 g) and DMAP (0.5 g) for 72 h in the oil bath of 40°C. Secondly, the solution was filtered and remove the white precipitate impurities of generated. After that, the filtrate was poured into a large amount of ether for precipitation and the solid was recrystallized three times with isopropyl alcohol. Finally, the product is dried in a vacuum drying chamber at 40°C to obtain a white powder solid. CHO-PEG-CHO white powder was obtained with a yield of 92.4%. Nuclear magnetic resonance (^{1}H-NMR) (400 MHz, $CDCl_3$): δ10.12 (Ar-CHO), δ8.21, δ7.97 (aromatic protons), δ3.65 (–OCH_2CH_2O–), δ4.52(–COOCCHO–).

Synthesis of (PEG-DiHyd-Phenol) Containing a Hydrazone Bond Initiator

Fristly, 4-hydroxybenzoylhydrazine was synthesized according to the previous method (Zheng et al., 2007). Then, 4-Hydroxybenzoichydrazine (0.3 g) reacted with CHO-PEG-CHO (4 g) in 30 ml methanol and 10 ml N,N-methyl formamide (DMF) at 68°C for 18 h. PEG-DiHyd-Phenol was also obtained

by precipitation in ethylether, and yellow powder was obtained. ^{1}H-NMR (400 MHz, $CDCl_3$): δ8.41 (Ar-CH=N), δ10.58 (Ar-OH), δ3.60 (–OCH_2CH_2O–).

Synthesis of Triblock Copolymer PEG-DiHyd-PLA by Ring-Opening Polymerization

PEG-DiHyd-Phenol and L-lactide reacted in anhydrous toluene in the presence of stannous octanoate (100 μL). PEG-DiHyd-PLA with different molecular weights were synthesized by varying the ratio between PEG-DiHyd-Phenol and L-lactide. The reactions were conducted at 110°C under the protection of nitrogen gas for 24 h. The copolymer was precipitated three times with cold ethyl ether. It was dried at 45°C in vacuum. PEG-DiHyd-PLA were obtained with a yield of 72%. ^{1}H-NMR (400 MHz, $CDCl_3$): δ3.64 (–OCH_2CH_2O–); δ8.42 (Ar–CH=N); δ5.21 [protons on poly(L-lactic acid) part]; and δ8.09, δ7.92, δ7.84, and δ6.98 (aromatic protons). Meanwhile, PLA-PEG-PLA copolymers without hydrazone linkage were also prepared as pH non-responsive counterpart using PEG as the initiator.

Characterization

An AVATAR360 (Nicolet, USA) and an AVANCE 400 spectrometer (Brucker, Switzerland) were used to determine the chemical structure of the polymers. A Damn Eos (Wyatt, USA) gel permeation chromatograph (GPC) instrument equipped with Phenogel 10E6A column and an OPTILAB rEX refractive-index detector was used to determine the molecular weight and polydispersity. Tetrahydrofuran (THF) was used as the eluent at a flow rate of 1.0 mL/min at 30°C and polystyrene standards for the calibration. A Zetasizer Nano-ZS90 (Malvern Instruments, UK) and Transmission electron microscopy (JEM-100CX II TEM) were employed to determine the size and the morphology of the micelles.

Formation of the pH-Sensitive Micelles

PLA-PEG-PLA or PEG-DiHyd-PLA (30 mg) dissolved in THF 2 mL was added into 40 mL pure water by dropwise. The mixture was stirred for 36 h at room temperature. The sizes evolution in different solutions of the micelles were measured to determine the pH sensitivity. Ten milliliters freshly prepared micelle dispersions was adjusted to pH 5.0 or pH 4.0. The sizes were measured on DLS after 24 h incubation at 37°C with shaking. CMC was determined using pyrene as a fluorescence probe (Xu et al., 2016).

Drug Loading and Release

DOX was loaded into the micelles by solvent evaporation method. Typically, copolymers (25 mg) and DOX (2 mg) were dissolved in 1 mL acetone. The solution was added dropwise into 30 mL pure water stirring. Then, the micellar solution was dialyzed against water for 36 h. After filtered through a 0.22 μm syringe filter to remove undissolved DOX, DOX-loaded micelle dispersion was freeze-dried. The drug loading content (DLC was determined by the measurement of fluorescence of DOX (excitation wavelength at 481 nm and emission wavelength at 558 nm). DLC was calculated by the formula below:

$$\text{DLC (wt \%)} = (\text{weight of loaded drug/weight of drug loaded micelles}) \times 100\%$$

The *in vitro* release experiments of DOX were conducted at 37°C. Dialysis bag (molecular weight cut-off: 8,000–14,000) filled with 3 mL micellar solution was sealed and immersed in 40 mL buffers solution. Three buffer solutions were used: acetate buffer (0.01 M, pH = 4), acetate buffer (0.01 M, pH = 5), and PBS (0.01 M, pH = 7.4). At desired time intervals, 4 mL of solution outside was taken out for fluorescence measurement. Meanwhile, 4 mL fresh medium was replenished. Cumulative released DOX was calculated according to following formula:

$$E_r = \frac{V_e \sum_{1}^{n-1} C_i + V_0 C_n}{m_{drug}}$$

In this equation, E_r means cumulative release of DOX (%); V_e means volume to be taken very time (mL); V_0, the volume of medium (mL); C_i, concentration when certain volume to be taken (μg/mL); m_{drug}, total mass of DOX contained in the release system (μg); n, sampling times.

In Vitro Toxicity Evaluation

MTT assay was applied to evaluate the cytotoxicity of the blank micelles, DOX-loaded micelles, using HepG-2, MCF-7, and normal L-02 cells (from the Shanghai cell bank of the Chinese Academy of Sciences, Shanghai, China). Cells were seeded and incubated for 24 h (37°C, 5% CO_2) on a 96-well plate. The cell density is 5×10^3 cells per well in 100 μL of 1640 medium (containing 10% FBS). 24 h later, the medium in each well was removed and 100 μL DOX-loaded micelles or free DOX solution were added into the wells. Each concentration has four replicates. Each sample was performed in quintuplicate. After incubation for 48 h, and the viability of cells was measured using the methylthiazoletetrazolium method. Cell viability (%) was calculated by the following equation (Ahmad et al., 2014):

$$\text{Cell Viability (\%)} = (A_{\text{sample}}/A_{\text{control}}) \times 100$$

where A_{sample} and A_{control} is absorbance of the sample well and control well, respectively. Data are presented as average SD ± ($n = 3$).

Confocal Laser Scanning Microscopy

HepG-2 cells were seeded on the cover slips in culture dish with a density of 8×10^4 cell using RPMI-1640 medium supplemented with 10% FBS. 24 h later, free DOX, DOX-loaded PEG-DiHyd-PLA, and PLA-PEG-PLA micelles were added into the wells at the same DOX concentration of 10 μg/mL. After being incubated at 37°C for 3 and 12 h, the cells were washed with PBS and fixed with PBS containing 4% formaldehyde for 15 min at room temperature. The cell nuclei were stained with 4′,6-diamidino-2-phenylindole (DAPI) for 15 min. The fluorescence signals of DOX and DAPI staining were investigated and imaged by the confocal laser scanning microscopy system (CLSM).

Flow Cytometry Measurements

DOX-loaded micelles and free DOX uptake HepG-2 cells was assessed using the flow cytometry cell analyzer. HepG-2 cells were seeded in culture dish (5×10^5 cells) in 1640 media and incubated for 24 h at 37°C. Then, HepG-2 Cells were treated with 1.5 mL of fresh cell culture medium and containing free DOX and DOX-loaded nanoparticles (equivalent concentration of DOX was 10 μg/mL) were added. After 48 h of incubation, the drug containing media was collected, and cells were trypsinized (without EDTA), centrifuged, washed with Binding Buffer (1X) for two times. Then collect the cells, and stained with Annexin V-FITC and propidium iodide (PI) for 20 min following the operating instructions (In the dark environment). Finally, the sample was tested by flow cytometry within 1 h.

Statistical Analysis

Origin 8.5 and GraphPad Prism 5.0 Software were used for the statistical analysis Differences were considered statistically significant at $P < 0.05$, via one-way ANOVA and Student's *t*-test.

RESULTS AND DISCUSSION

Synthesis of pH Sensitive Tri-block Copolymers

The triblock polymer with hydrazone on the backbone was prepared by a direct polymerization method (**Figure 1**). A hydrazone containing macro-initiator was synthesized first which followed by a ring opening polymerization. The synthesis is illustrated in **Figure 2**. CHO-PEG-CHO was firstly obtained by conjugation of PEG with 4-carboxybenzaldehyde. And 4-hydroxybenzoichydrazide was synthesized from methyl 4-hydroxybenzoate. The reaction between CHO-PEG-CHO and 4-hydroxybenzoichydrazide gave a molecule which embedded with hydrazone bond and terminal hydroxyl group. It could initiate ring-opening polymerization of lactide, to produce the copolymer PEG-DiHyd-PLA. The ^{1}H-NMR spectra of CHO-PEG-CHO (**Figure 3A**) show signals characteristic of δ10.12 (Ar-CHO), δ8.21, δ7.97 (aromatic protons), δ3.65 (–OCH_2CH_2O–), and δ4.52 (–COOCCHO–). Through the above analysis, we can confirm the success of the synthesis of CHO-PEG-CHO. ^{1}H-NMR showed that the macroinitiator PEG-DiHyd-Phenol was successfully synthesized, as indicated by the signal at δ8.41, which was assigned to hydrazone protons (Ar-CH=N) (**Figure 3B**). In the spectra of PEG-DiHyd-PLA (**Figure 3C**), characteristic signals of PEG (δ3.64), and poly (L-lactic acid) part (δ5.21, δ8.09, δ7.92, δ7.84, and δ6.98) appeared. The characteristic signals of hydrazone bond (δ8.42) were found to confirm the successful synthesis of PEG-DiHyd-PLA. PLA-PEG-PLA without pH-sensitive linkage was also synthesized.

Molecular weights of synthesized polymers are listed in **Table 1**. PEG-DiHyd-PLA-15K, PEG-DiHyd-PLA-18K, and PEG-DiHyd-PLA-20K are three copolymers with different molecule weights by designation, corresponding to the feed ratios 1:127, 1:169, and 1:197 between initiator and monomer, respectively. They have the same hydrophilic block PEG (Mn = 5,267 g/mol) and different hydrophobic blocks in different molecular weights. The molecular weights were

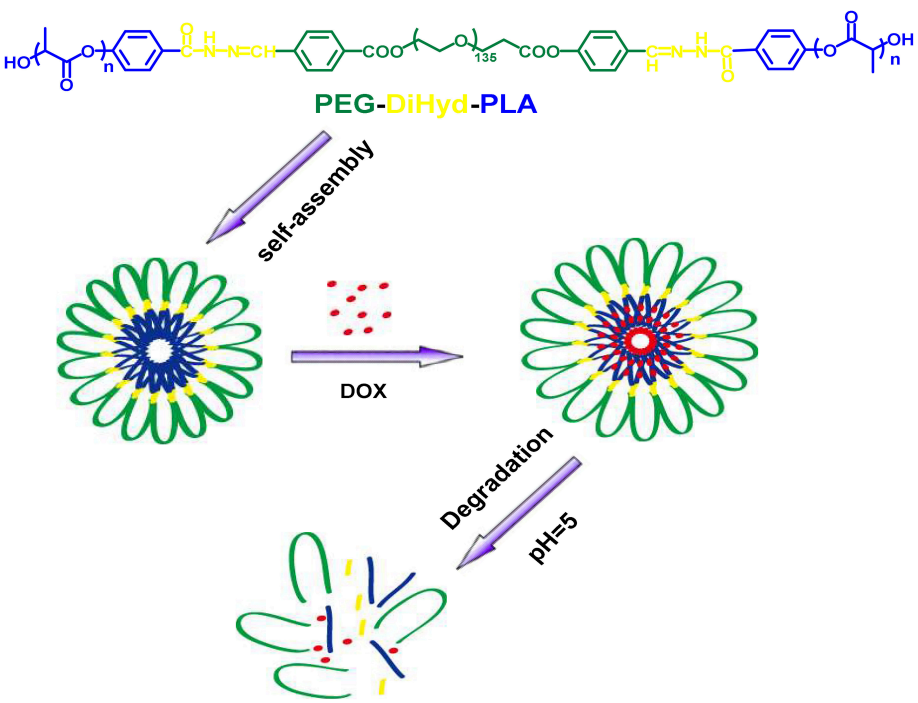

FIGURE 1 | Schematic illustration of the formation of ABA triblock polymer micelle and its degradation in acidic condition.

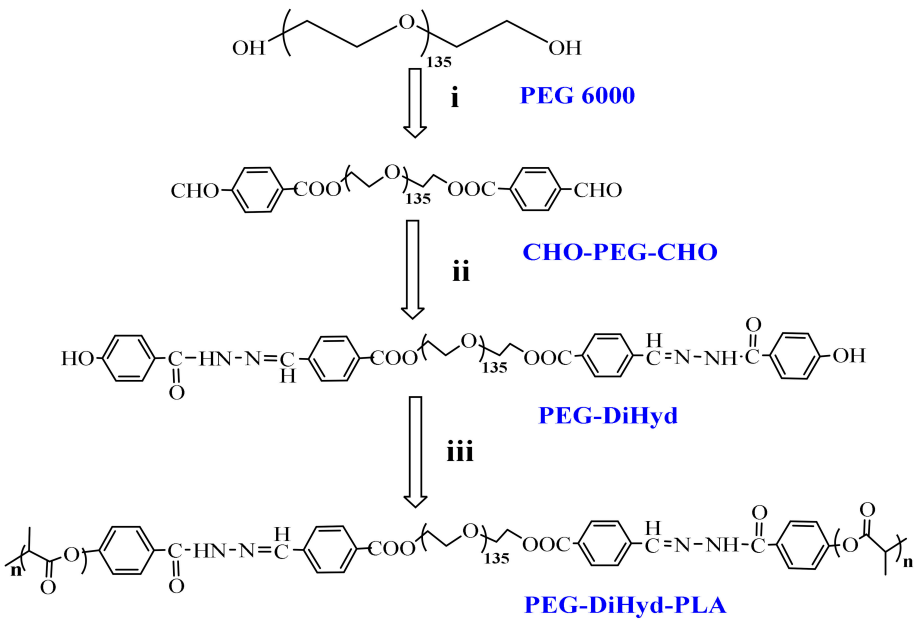

FIGURE 2 | Synthesis route of copolymers PEG-DiHyd-PLA. **(i)** 4-Formylbenzoic acid, DCC, DMAP,R.T.; **(ii)** (4-Hydroxybenzoyl) hydrazine, Methanol, DMF, 68°C; **(iii)** Lactide, $Sn(oct)_2$, Toluene,110°C, N_2.

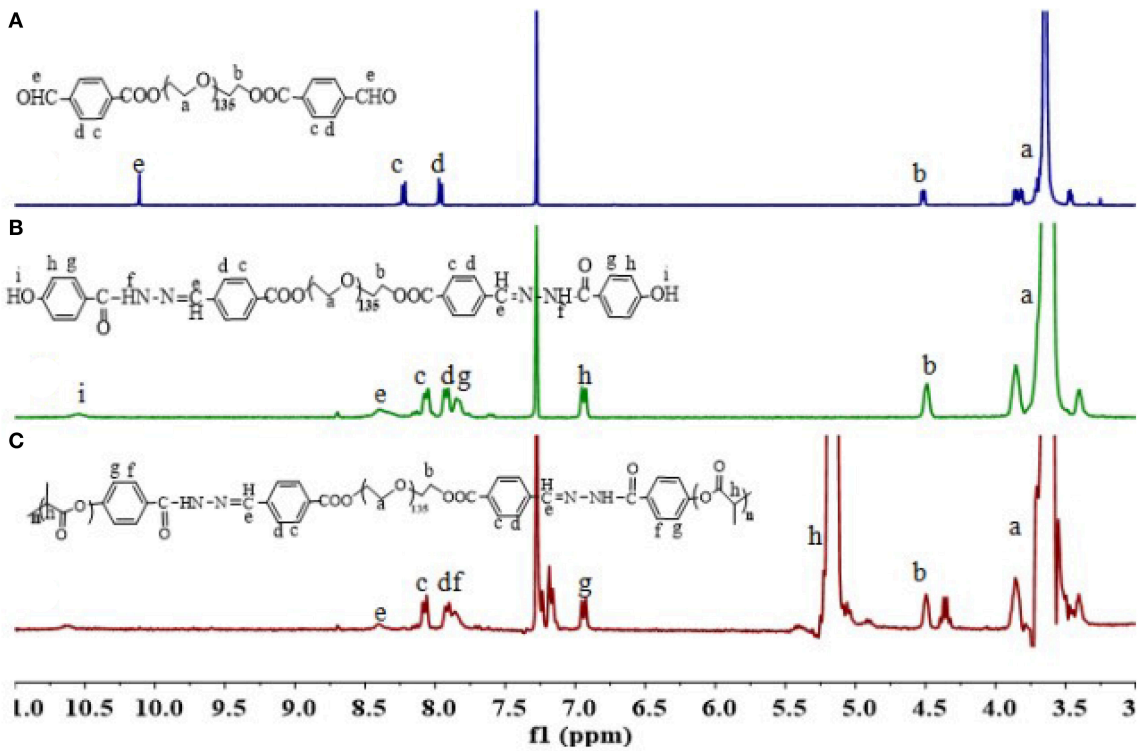

FIGURE 3 | ^{1}H-NMR spectra of polymers CHO-PEG-CHO **(A)**, PEG-DiHyd **(B)**, and PEG-DiHyd-PLA **(C)**.

calculated using the integral ratio between resonances at δ5.16 (one of methylidyne protons on PLA) and δ3.64 (methoxy proton of PEG) in ^{1}H-NMR spectra. The calculated values based on ^{1}H-NMR spectra were consistent with the designed ones. Gel permeation chromatography (GPC) measurements confirmed a unimodal distribution of Mn (16.3, 18.1, and 19.7

kg/mol, respectively) and narrow distribution [polydispersity index (PDI): 1.31, 1.71, and 1.44]. Therefore, well-defined biodegradable triblock polymers PEG-DiHyd-PLA was successfully synthesized.

Micelles were formed by adding the amphiphilic polymers PEG-DiHyd-PLA into aqueous solution. The micelles have diameters ranged from 70 to 130 nm and increase with their molecular weight. The average particle size of the drug loaded micelles was larger than that of the blank micelles, which may be due to the larger volume of micelles after the hydrophobic core of the drug loaded with the micelles (Guo et al., 2012; Bao et al., 2014). The loading capacity of DOX loaded polymer PEG-DiHyd-PLA-18K micelles was about 4.3%, and the PLA-PEG-PLA was 2.7%. As shown in **Table 1**, the CMC of the polymeric micelles were 1.6, 0.87, and 0.53 mg/L for PEG-DiHyd-PLA-15K, PEG-DiHyd-PLA-18K, and PEG-DiHyd-PLA-20K, respectively, determined by fluorescence measurements using pyrene as a probe. CMC-values of the polymers decreased from PEG-DiHyd-PLA-15K to PEG-DiHyd-PLA-20K, which originated from the increased hydrophobic interaction of micelle core. Such a low value of CMC indicates an excellent stability under diluted conditions *in vivo*, which is so important for the micellar drug delivery system.

The polymer PEG-DiHyd-PLA-18K micelles observed by TEM have a spherical core-shell like structure and are uniformly distributed (**Figure 4a**), the particle size of the polymer PEG-DiHyd-PLA-18K micelles measured by DLS is relatively small, both of which are about 70 nm, and the particle size distribution is narrow and PDI is lower than 0.2 (**Figure 4b**). It shows that the size of micelles is relatively uniform, and the particle

TABLE 1 | Synthesis of triblock polymers PEG-DiHyd-PLA.

Polymer	(Mi/Mm)[a]	Yield (%)	Mn[b] (kg/mol)	Mn[c] (kg/mol)	PDI[d]	CMC[e] (mg/L)
PEG-DiHyd-PLA-15k	1:127	72	15.9	16.3	1.31	1.6
PEG-DiHyd-PLA-18k	1:169	82	19.3	18.1	1.71	0.87
PEG-DiHyd-PLA-20k	1:197	69	21.8	19.7	1.44	0.53

[a]*Feed ratios in mole between initiator and monomer.*
[b]*Calculated from ^{1}H-NMR spectra.*
[c]*GPC results.*
[d]*is molecular weight distribution index.*
[e]*Critical micelle concentration determined using pyrene as a fluorescent probe.*

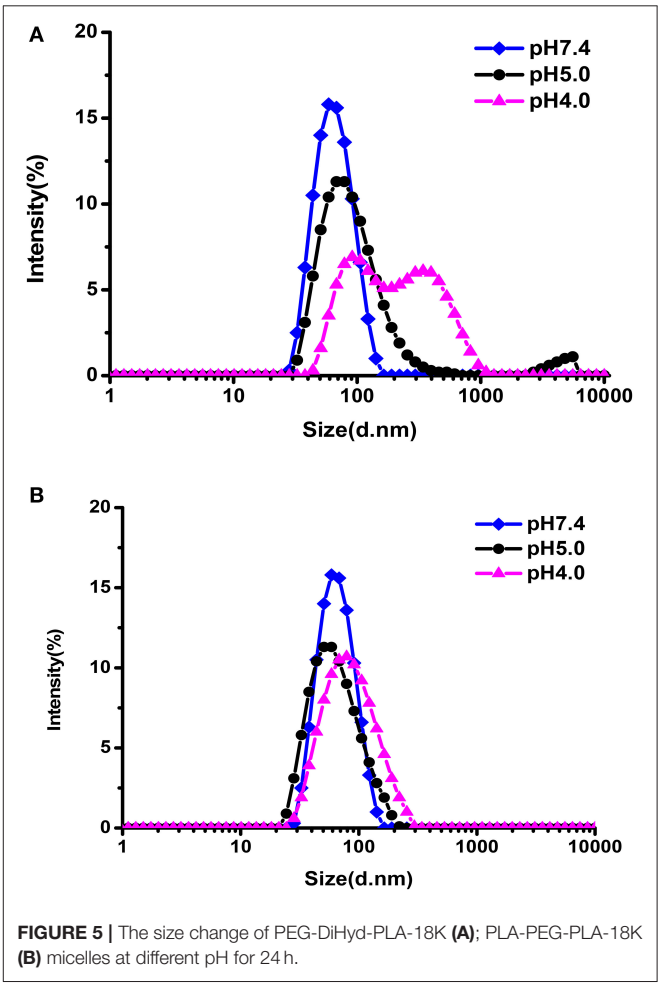

FIGURE 5 | The size change of PEG-DiHyd-PLA-18K **(A)**; PLA-PEG-PLA-18K **(B)** micelles at different pH for 24 h.

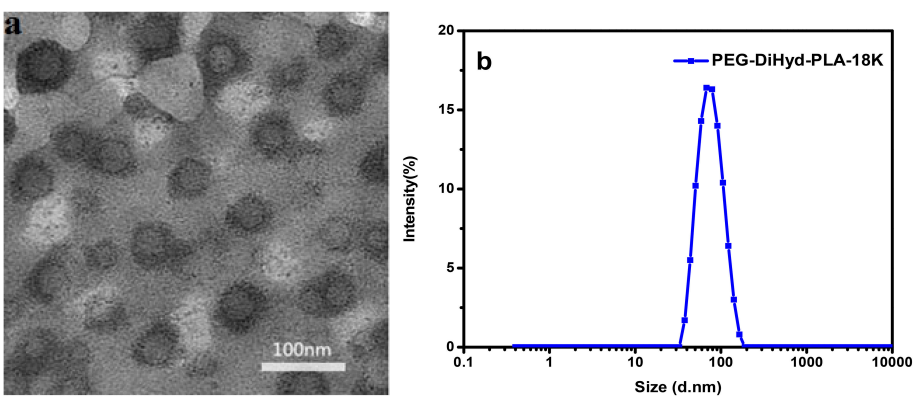

FIGURE 4 | Images of micelles formed by PEG-DiHz-PLA-18K **(a)**. The particle size of PEG-DiHyd-PLA-18K micelles **(b)**.

size of micelle is basically consistent with the result of TEM determination. It was reported that nanoparticulate drug carriers can accumulate in tumor tissue via the enhanced permeability and retention (EPR) effect (Baish et al., 2011; Maeda and Matsumura, 2011) when their sizes are <200 nm. Thus, PEG-DiHyd-PLA micelles would effectively reach lesion sites, and achieve the goal of pH-controlled drug delivery.

pH-Triggered Size Change of the Blank Micelles

The pH-responsive evolution of micelle was monitored by DLS measurements. As illustrated in **Figure 5A**, the size distribution of hydrazone-containing PEG-DiHyd-PLA-18K micelles underwent obvious changes under acidic conditions (pH 4.0, pH 5.0) while stable under physiological condition (pH 7.4). Multiple peaks appeared in the DLS curve and the solution became turbid due to precipitation, which was resulted from the decomposition of the pH-sensitive micelles in acidic environments. In contrast, PLA-PEG-PLA-18K micelles without hydrazone bonds kept almost unchanged under all pH conditions (**Figure 5B**) in 24 h. It is supported that the pH sensitive micelles will keep stable in blood circulation and protect their payload from being released before access targeting tumor tissue. After they encounter tumor tissue via EPR effector internalized by tumor cell where there is acidic condition, the loaded drug will be released instantly.

In Vitro Controlled Release of DOX

The *in vitro* drug release behaviors under various conditions were investigated (**Figure 6A**). DOX released from DOX loaded PEG-DiHyd-PLA-18K micelles at physiological pH was about ca. 38% in 24 h. The release rate was significantly promoted at pH 5.0 and 4.0, with accumulated release above 75% in 24 h, and there is no obvious difference between them. It is the pH-sensitive hydrazone bond results the pH-controlled drug release profile of polymeric PEG-DiHyd-PLA-18K micelles. Comparably, **Figure 6B**, the release of DOX from pH insensitive polymeric micelles showed a similar rate of release. Under different pH conditions, there was no pH-dependent release profile, with cumulative release of about 40% in 24 h. This results are consistent with the size changes in different conditions for the two types of micelles. The pH-responsive release of the hydrazone containing micelles might underwent a cleavage-disassociation-release process.

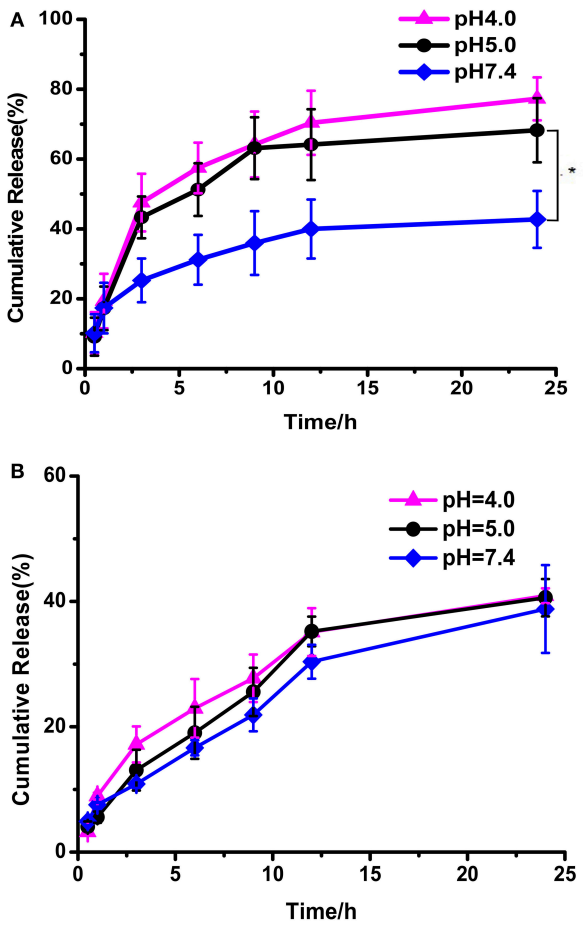

FIGURE 6 | *In vitro* release of DOX from PEG-DiHZ-PLA-18K **(A)**; PLA-PEG-PLA-18K **(B)** micelles. Error bars indicate the standard error of the mean (SEM) for $n = 3$ independent experiments (*$p < 0.05$).

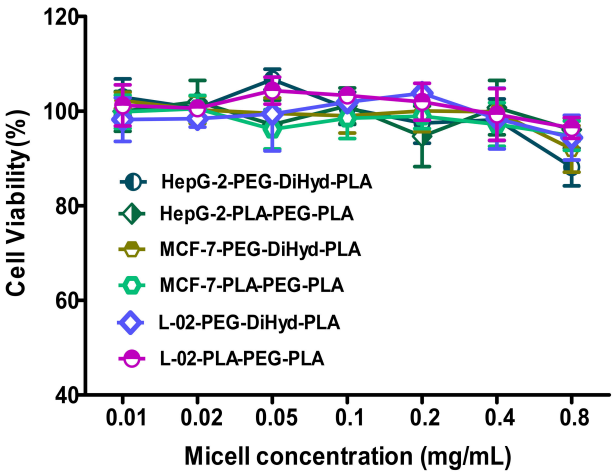

FIGURE 7 | The cytotoxicity of blank PLA-PEG-PLA-18K, PEG-DiHyd-PLA-18K micelles incubated with HepG-2, MCF-7, and L-02 cells for 48 h. Error bars indicate the standard error of the mean (SEM) for ($n = 3$) independent experiments.

TABLE 2 | Half-inhibitory concentration (IC_{50}) of loaded-DOX micelles and free DOX on HepG-2, MCF-7, and L-02 cells.

IC_{50}(μg/mL)	HepG-2 48 h	MCF-7 48 h	L-02 48 h
PLA-PEG-PLA-DOX	4.601	4.053	6.464
PEG-DiHyd-PLA-DOX	3.098	2.303	7.178
Free DOX	2.182	1.615	1.486

MTT Assay of DOX-Loaded Micelles

The cytotoxicity of the blank micelles were tested in MCF-7, HepG-2, and normal hepatocyte L-02 cells by a MTT assay. Cells viabilities of cells was above 90% for both blank PLA-PEG-PLA-18K and PEG-DiHyd-PLA-18K micelles following 48 h incubation (**Figure 7**), which meant that the blank micelles are remarkably no-toxic and biocompatible up to a concentration of 0.8 mg/mL.

In vitro antitumor capability of PEG-DiHyd-PLA-18K based drug delivery systems are tested. Formulations including free DOX, DOX loaded PLA-PEG-PLA-18K, and PEG-DiHyd-PLA-18K micelles were evaluated against MCF-7, HepG-2, and L-02 cell lines. The IC_{50}-values for various DOX for mutations and free DOX are summarized in **Table 2**, As shown in **Figure 8**, for

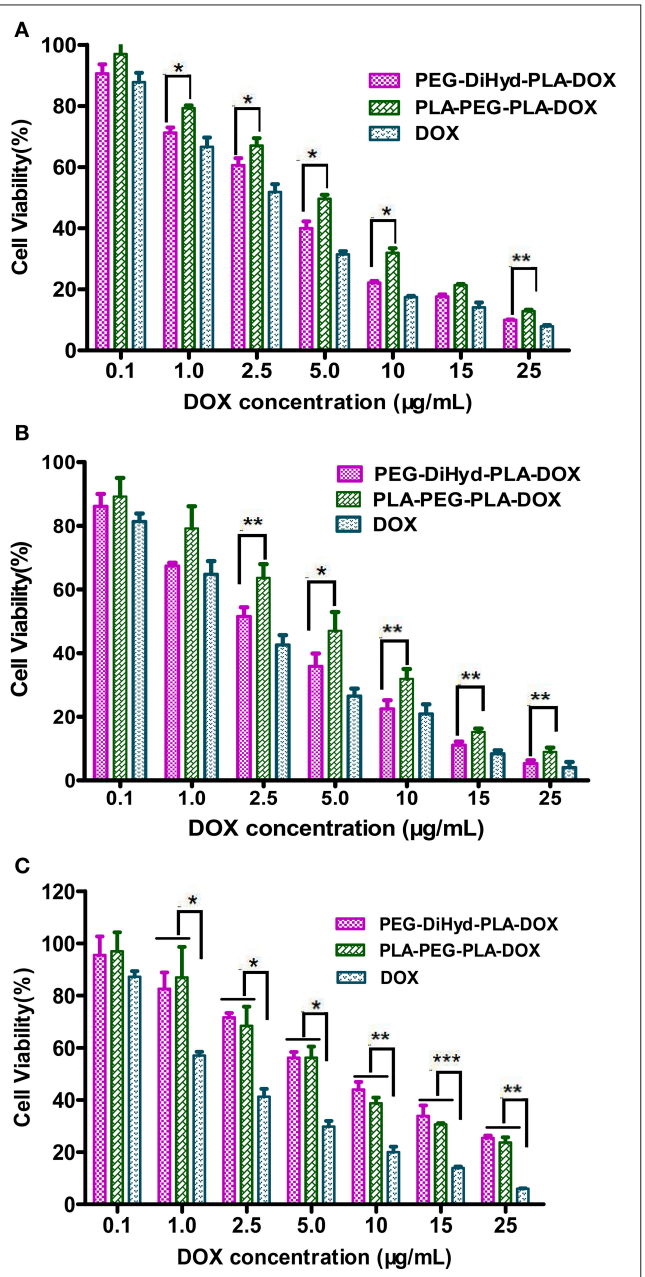

FIGURE 8 | The cytotoxicity of DOX loaded PLA-PEG-PLA-18K, PEG-DiHyd-PLA-18K micelles and Free DOX incubated with HepG-2 cells **(A)**, MCF-7 cells **(B)**, and L-02 **(C)** at different DOX concentrations 48 h. Data were presented as mean ± standard deviation ($n = 3$) (*$p < 0.05$, **$p < 0.01$, ***$p < 0.001$).

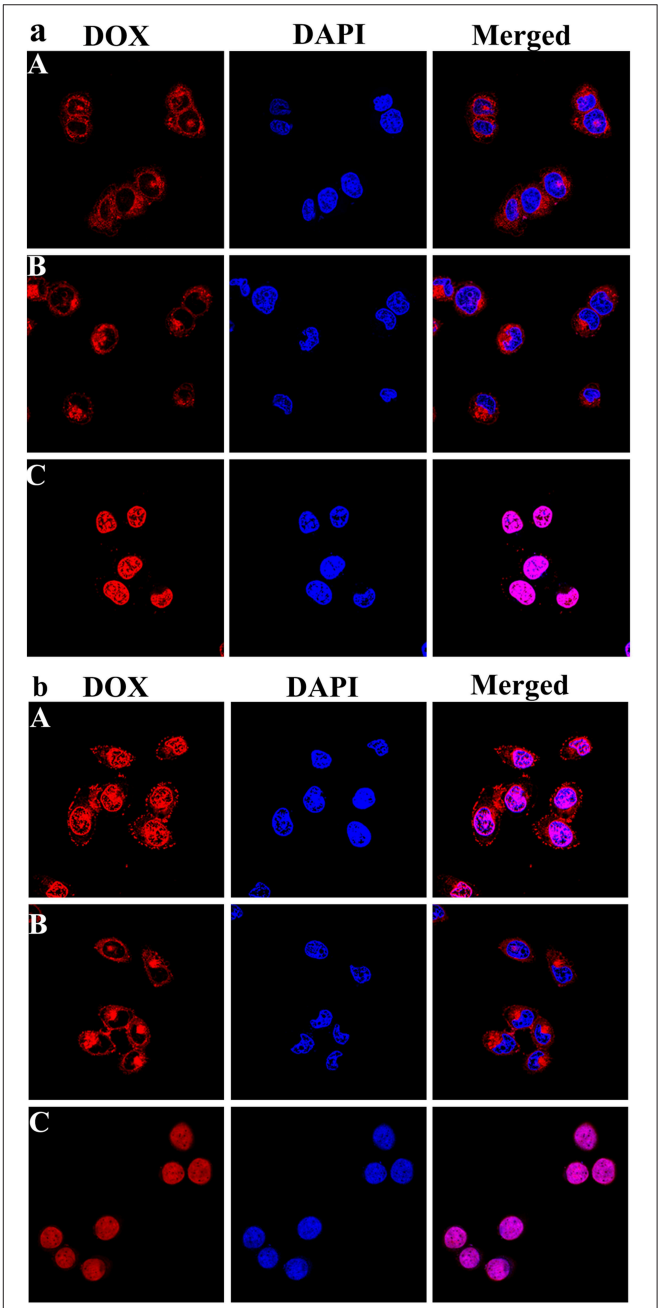

FIGURE 9 | Representative CLSM images of HepG-2 cells incubated with DOX-loaded mPEG-DiHyd-PLA-18K Micelle solution **(A)**, DOX loaded PLA-PEG-PLA-18K micelle solution **(B)**, and free DOX **(C)** solution for 3 h **(a)** and 12 h **(b)**. The cellular nuclei and cytoskeleton of cells were stained with DAPI (blue) and DOX (red), respectively. DOX concentration is 10 μg/mL for any DOX containing solutions.

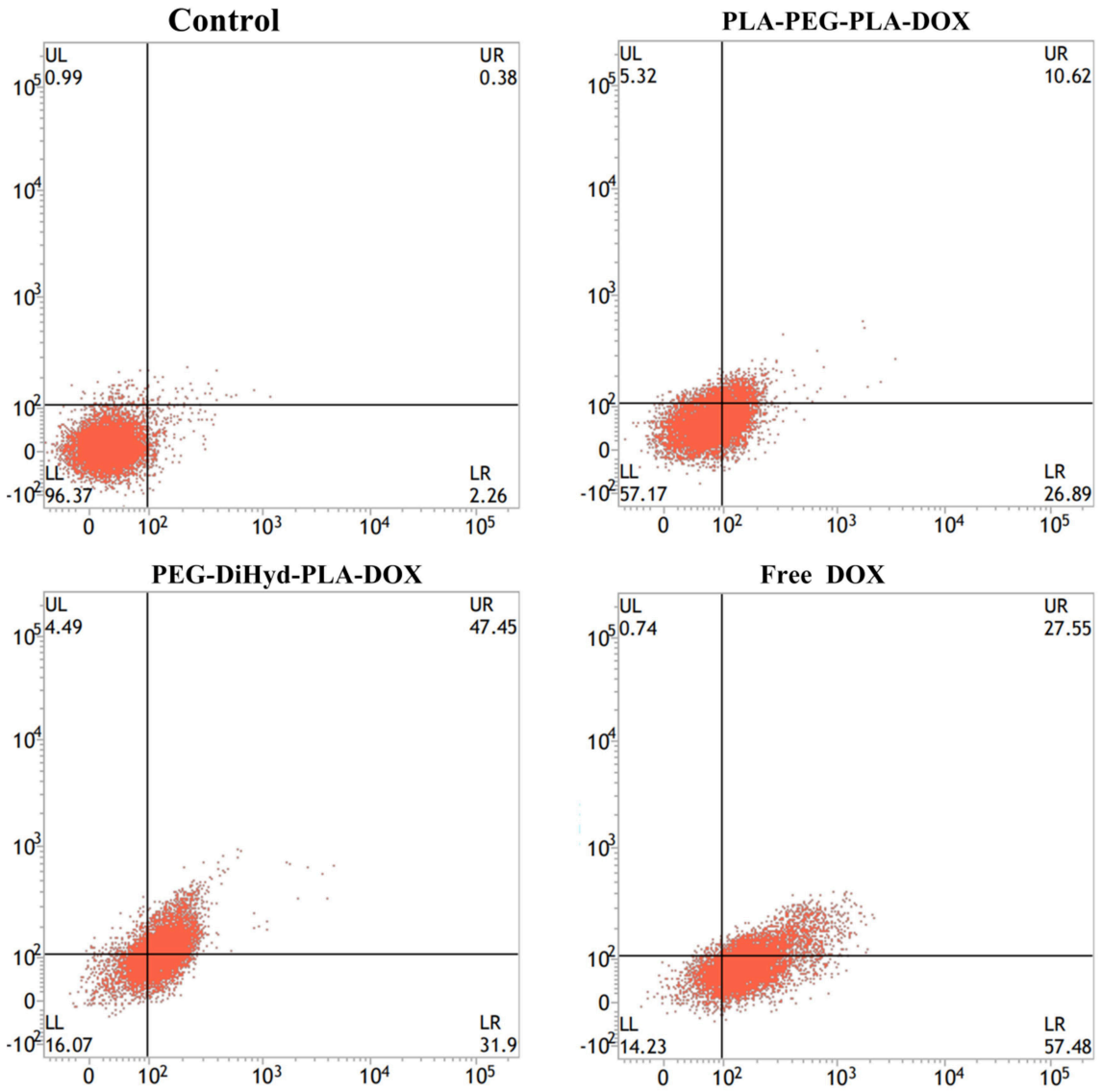

FIGURE 10 | Apoptotic cell populations determined by flow cytometric analysis with Annexin V-FITC and PI staining after incubating HepG-2 cells for 48 h, DOX equivalent concentration was 10 μg/mL. The **lower-left** and **upper-left** quadrants in each panel indicate the populations of normal cells and necrotic cells, respectively. While the **lower-right** and **upper-right** quadrants in each panel indicate the populations of early and late apoptotic cells, respectively.

all of the cells, the formulations showed a dose dependent cell proliferation inhibition behaviors after a 48 h incubation, free DOX showed higher *in vitro* toxicity to each cell, compared to the other two micelle formulations. DOX is a small molecule, so it can be quickly transported into cells and reach nuclei by passive diffusion (Cui et al., 2013). This is why the inhibition effect of free DOX was the strongest. While, for HepG-2 and MCF-7 cells (**Figures 8A,B**), pH sensitive DOX loaded PEG-DiHyd-PLA-18K micelles was more toxic than DOX loaded PLA-PEG-PLA-18K. Superior cell-killing capability of DOX loaded PEG-DiHyd-PLA-18K micelles may be due to the fact that entry of pH-sensitive micelles through endocytosis and drug release into the cytoplasm triggered by endosome pH are quick and efficient processes (Tang et al., 2011). As shown in **Figure 8C**, compared with free DOX, the DOX-loaded micelles exhibited significantly reduced cytotoxicity on L-02 cells, which is probably due to their slower uptake of DOX-loaded micelles by L-02 cells. While, there was no significant difference in the cytotoxicity between the two DOX-loaded micelles, which could be attributed to the limited of acid environment in L-02 cells compared with tumor cells (Qin et al., 2017).

Cellular Uptake of the Drug-Loaded Micelles

The intracellular localization and distribution of DOX-loaded micelles were investigated in HepG-2 cells using CLSM after

incubation for 3 and 12 h (**Figure 9**). As shown in **Figure 9a**, for the DOX loaded micelles, most of the red fluorescence appears in the cytoplasm, and there is no obvious difference between the two drug loaded micelles. But with extended incubation time to 12 h, it was also observed that the pH sensitive DOX-loaded PEG-DiHyd-PLA-18K micelles showed relatively strong red fluorescence in the nucleus, while the red fluorescence of the DOX-loaded PLA-PEG-PLA-18K micelles was mainly in the cytoplasm and the nuclei were less (**Figure 9b**). That was due to the accelerated DOX release from hydrazone-containing micelles in the acidic tumor microenvironment. The accumulation of DOX-loaded micelles was lower than that of free DOX with the same incubation time, the possible reason is that free DOX transported into cells via a passive diffusion mechanism (Li et al., 2014). Compared to DOX-loaded PLA-PEG-PLA-18K micelles, the quick and efficient uptake of DOX from pH sensitive micelles greatly inhibited the growth of the tumor cell.

Apoptosis of the Drug-Loaded Micelles

Apoptosis has been reported to be one of the primary mechanisms of action of DOX (Wang et al., 2017). Incubated with HepG-2 cells at a equivalent concentration of 10 μg/mL DOX for 48 h (Yang et al., 2016), the effect of free DOX, DOX loaded PLA-PEG-PLA-18K, and PEG-DiHyd-PLA-18K micelles on apoptosis was shown in **Figure 10**, the total apoptosis ratio of DOX-loaded PLA-PEG-PLA-18K micelles was about 38% (a sum of the early apoptosis ratio of 26.89% and the late apoptosis ratio of 10.62%). With the HepG-2 cells treated with pH sensitive DOX loaded PEG-DiHyd-PLA-18K micelles, there is a 78% apoptosis ratio which is higher than 38%, which is likely due to the e accelerated release of the drug molecules from micelles with acid-labile hydrazone linkage by sensing the acidic environment of the endosomal compartments. The higher apoptosis rate of free DOX with the same incubation time, most likely because free DOX could diffuse passively through cell membranes quicker, whereas drug loaded micelles were internalized into cells via slower endocytosis (Hu et al., 2010). Apoptosis experiment again confirms the superiority advantages of pH sensitive micelles in tumor targeting therapy.

CONCLUSIONS

In this work, a type of pH-sensitive polymeric micelles was prepared as carrier of DOX. A triblock copolymer has one hydrophilic PEG segment and two hydrophobic PLA segments. pH-sensitive hydrazone bond was used to connect them together, denoted as PEG-DiHyd-PLA. The copolymercan self-assemble into micelles with uniformed size below 100 nm and narrow size distribution. The size of the hydrazone-containing micelles underwent obviously changes in mildy acidic environments while kept unchanged in the neutral. Almost no change was found for polymeric micelles without hydrazone (PLA-PEG-PLA). DOX was successfully loaded into the micelles and presented a more rapid and complete drug release in acidic condition (pH 5.0). The results of *in vitro* cell assay revealed that the blank micelles were non-toxic and good biocompatibility. DOX-loaded PEG-DiHyd-PLA micelles possessed higher anti-tumor activity to kill the MCF-7 and HepG-2 cells in comparison with DOX loaded PLA-PEG-PLA micelles and less cytotoxicity to normal L-02 cells at similar DOX concentrations. Confocal and apoptotic experiments also proved that superiority advantages of pH sensitive micelles for tumor therapy.

AUTHOR CONTRIBUTIONS

PQ, performed the synthesis and characterizations; XW, performed the cell experiments; LL, designed the synthesis and wrote the paper; HY, performed the formulations; SS, designed the whole experiment.

ACKNOWLEDGMENTS

Thanks to the supported of the National Natural Science Foundation of China (NSFC 51375142) and a key project funded by the Education Department of Henan Province (13A360054).

REFERENCES

Ahmad, Z., Tang, Z. H., Shah, A., Lv, S. X., Zhang, D. W., Zhang, Y., et al. (2014). Cisplatin loaded methoxy poly (ethylene glycol)-block-poly (L-glutamic acid-co-L-phenylalanine) nanoparticles against human breast cancer cell. *Macromol. Biosci.* 14, 1337–1345. doi: 10.1002/mabi.201400109

Bae, Y., Fukushima, S., Harada, A., and Kataoka, K. (2003). Design of environment-sensitive supramolecular assemblies for intracellular drug delivery: polymeric micelles that are responsive to intracellular pH change. *Angew. Chem. Int. Edn.* 42, 4640–4643. doi: 10.1002/anie.200250653

Baish, J. W., Stylianopoulos, T., Lanning, R. M., Kamoun, W. S., Fukumura, D., Munn, L. L., et al. (2011). Scaling rules for diffusive drug delivery in tumor and normal tissues. *Proc. Natl. Acad. Sci. U.S.A.* 108, 1799–1803. doi: 10.1073/pnas.1018154108

Bao, Y., Guo, Y., Zhuang, X., Cheng, B., Tan, S., and Zhang, Z. (2014). D-tocopherol polyethylene glycol succinate-based redox-sensitive paclitaxel prodrug for overcoming multidrug resistance in cancer cells. *Mol. Pharm.* 11, 3196–3209. doi: 10.1021/mp500384d

Cao, J., Su, T., Zhang, L., Liu, R., Wang, G., He, B., et al. (2014). Polymeric micelles with citraconic amide as pH-sensitive bond in backbone for anticancer drug delivery. *Int. J. Pharm.* 471, 28–36. doi: 10.1016/j.ijpharm.2014.05.010

Cavallaro, G., Licciardi, M., Amato, G., Sardo, C., Giammona, G., Farra, R., et al. (2014). Synthesis and characterization of polyaspartamide copolymers obtained by ATRP for nucleic acid delivery. *Int. J. Pharm.* 466, 246–257. doi: 10.1016/j.ijpharm.2014.03.026

Cheng, J., Ji, R., Gao, S. J., Du, F. S., and Li, Z. C. (2012). Facile synthesis of acid-labile polymers with pendent ortho esters. *Biomacromolecules* 13, 173–179. doi: 10.1021/bm201410c

Cheng, R., Meng, F. H., Deng, C., and Zhong, Z. Y. (2015). Bioresponsive polymeric nanotherapeutics for targeted cancer chemotherapy. *Nano Today* 10, 656–670. doi: 10.1016/j.nantod.2015.09.005

Cui, C., Xue, Y. N., Wu, M., Zhang, Y., Yu, P., Liu, L., et al. (2013). Cellular uptake, intracellular trafficking, and antitumor efficacy of doxorubicin-loaded reduction-sensitive micelles. *Biomaterials* 34, 3858–3869. doi: 10.1016/j.biomaterials.2013.01.101

Deng, B., Ma, P., and Xie, Y. (2015). Reduction-sensitive polymeric nanocarriers in cancer therapy: a comprehensive review. *Nanoscale* 7, 12773–12795. doi: 10.1039/C5NR02878G

Ding, C., Gu, J., Qu, X., and Yang, Z. (2009). Preparation of multifunctional drug carrier for tumor-specific uptake and enhanced intracellular delivery through the conjugation of weak acid labile linker. *Bioconjug. Chem.* 20, 1163–1170. doi: 10.1021/bc800563g

Gillies, E. R., Goodwin, A. P., and Fréchet, J. M. (2004). Acetals as pH-sensitive linkages for drug delivery. *Bioconjug. Chem.* 15, 1254–1263. doi: 10.1021/bc049853x

Guo, Y., Wang, X., Shu, X., Shen, Z., and Sun, R. C. (2012). Self-assembly and paclitaxel loading capacity of cellulose-graft-poly(lactide) nanomicelles. *J. Agric. Food Chem.* 60, 3900–3908. doi: 10.1021/jf3001873

Han, Y. N., Liu, S. X., Mao, H. G., Tian, L., and Ning, W. Y. (2016). Studies on the synthesis, micellization and gelation of novel temperature and pH-sensitive ABA triblock copolymers. *Acta Chim. Sinica* 74, 744–751. doi: 10.6023/A16060302

Hrubý, M., Konák, C., and Ulbrich, K. (2005). Polymeric micellar pH-sensitive drug delivery system for doxorubicin. *J. Control. Release* 103, 137–148. doi: 10.1016/j.jconrel.2004.11.017

Hu, X., Liu, S., Huang, Y., Chen, X., and Jing, X. (2010). Biodegradable block copolymer-doxorubicin conjugates via different linkages: preparation, characterization, and *in vitro* evaluation. *Biomacromolecules* 11, 2094–2102. doi: 10.1021/bm100458n

Huang, F., Cheng, R., Meng, F., Deng, C., and Zhong, Z. (2015). Micelles based on acid degradable poly(acetal urethane): preparation, pH-sensitivity, and triggered intracellular drug release. *Biomacromolecules* 16, 2228–2236. doi: 10.1021/acs.biomac.5b00625

Li, N., Li, N., Yi, Q. Y., Luo, K., Guo, C. H., Pan, D., et al. (2014). Amphiphilic peptide dendritic copolymer-doxorubicin nanoscale conjugate self-assembled to enzyme-responsive anti-cancer agent. *Biomaterials* 35, 9529–9545. doi: 10.1016/j.biomaterials.2014.07.059

Lu, J. S., Li, N. J., Xu, Q. F., Ge, J. F., Lu, J. M., and Xia, X. W. (2010). Acetals moiety contained pH-sensitive amphiphilic copolymer self-assembly used for drug carrier. *Polymer* 51, 1709–1715. doi: 10.1016/j.polymer.2009.12.034

Maeda, H., and Matsumura, Y. (2011). EPR effect based drug design and clinical outlook for enhanced cancer chemotherapy. *Adv. Drug Delivery Rev.* 63, 129–130. doi: 10.1016/j.addr.2010.05.001

Makino, J., Cabral, H., Miura, Y., Matsumoto, Y., Wang, M., Kinoh, H., et al. (2015). cRGD-installed polymeric micelles loading platinum anticancer drugs enable cooperative treatment against lymph node metastasis. *J. Control. Release* 220, 783–791. doi: 10.1016/j.jconrel.2015.10.017

McPherson, T., Szleifer, I., Park, K., and Kidane, A. (1998). Prevention of protein adsorption by tethered poly(ethylene oxide) layers: experiments and single-chain mean-field analysis. *Langmuir* 14, 176–186. doi: 10.1021/la9706781

Mei, L., Liu, Y. Y., Zhang, H. J., Zhang, Z. R., and Gao, H. L. (2016). Antitumor and antimetastasis activities of heparin-based micelle served as both carrier and drug. *ACS Appl. Mater. Inter.* 8, 9577–9589. doi: 10.1021/acsami.5b12347

Park, K. C., Idota, N., and Tsukahara, T. (2014). Synthesis of NIPAAm-based polymer-grafted silica beads by surface-initiated ATRP using Me 4 cyclam ligands and the thermo-responsive behaviors for lanthanide(III) ions. *React. Funct. Polym.* 79, 36–46. doi: 10.1016/j.reactfunctpolym.2014.03.011

Qi, P. L., Bu, Y. Q., Xu, J., Qin, B. K., Luan, S. J., and Song, S. Y. (2017). pH-responsive release of paclitaxel from hydrazone-containing biodegradable micelles. *Colloid Polym. Sci.* 295, 1–12. doi: 10.1007/s00396-016-3968-6

Qin, B. K., Liu, L., Wu, X., Liang, F., Hou, T., Pan, Y., et al. (2017). mPEGylated solanesol micelles as redox-responsive nanocarriers with synergistic anticancer effect. *Acta Biomater.* 64, 211–222. doi: 10.1016/j.actbio.2017.09.040

Ran, J., Wu, L., Zhang, Z. H., and Xu, T. W. (2014). Atom transfer radical polymerization (ATRP): a versatile and forceful tool for functional membranes. *Prog. Polym. Sci.* 39, 124–144. doi: 10.1016/j.progpolymsci.2013.09.001

Seo, B. B., Choi, H., Koh, J. T., and Song, S. C. (2015). Sustained BMP-2 delivery and injectable bone regeneration using thermosensitive polymeric nanoparticle hydrogel bearing dual interactions with BMP-2. *J. Control. Release* 209, 67–76. doi: 10.1016/j.jconrel.2015.04.023

Sinha, V. R., Bansal, K. R., Kumria, R., and Trehan, A. (2004). Poly-epsilon-caprolactone microspheres and nanospheres: an overview. *Int. J. Pharm.* 278, 1–23. doi: 10.1016/j.ijpharm.2004.01.044

Tang, R., Ji, W., Panus, D., Palumbo, R. N., and Wang, C. (2011). Block copolymer micelles with acid-labile ortho ester side-chains: synthesis, characterization, and enhanced drug delivery to human glioma cells. *J. Control. Release* 151, 18–27. doi: 10.1016/j.jconrel.2010.12.005

Ulbrich, K., and Šubr, V. (2010). Structural and chemical aspects of HPMA copolymers as drug carriers. *Adv. Drug Deliv. Rev.* 62, 150–166. doi: 10.1016/j.addr.2009.10.007

Visnevskij, C., Ciuta, G., Ketleriute, S., Savickaite, M., and Makuska, R. (2014). ISARA ATRP of methacrylic acid neutralized by simple amines yielding linear polymers and anionic molecular brushes. *R. Eur. Polym. J.* 55, 66–75. doi: 10.1016/j.eurpolymj.2014.03.031

Vonarbourg, A., Passirani, C., Saulnier, P., and Benoit, J. P. (2006). Parameters influencing the stealthiness of colloidal drug delivery systems. *Biomaterials* 27, 4356–4373. doi: 10.1016/j.biomaterials.2006.03.039

Wang, Y. D., Chen, J. W., Liang, X., Han, H. B., Wang, H., and Li, Q. S. (2017). An ATP-responsive codelivery system of doxorubicin and MiR-34a to synergistically inhibit cell proliferation and migration. *Mol. Pharm.* 14, 2323–2332. doi: 10.1021/acs.molpharmaceut.7b00184

Webb, B. A., Chimenti, M., Jacobson, M. P., and Barber, D. L. (2011). Dysregulated pH: a perfect storm for cancer progression. *Nat. Rev. Cancer* 11, 671–677. doi: 10.1038/nrc3110

Witschi, C., and Doelker, E. (1998). Influence of the microencapsulation method and peptide loading on poly(lactic acid) and poly(lactic-co-glycolic acid) degradation during *in vitro* testing. *J. Control. Release* 51, 327–341. doi: 10.1016/S0168-3659(97)00188-0

Xing, L., Zheng, H. Q., and Che, S. A. (2011). A pH-responsive cleavage route based on a metal-organic coordination bond. *Chem. Eur. J.* 17, 7271–7275. doi: 10.1002/chem.201003005

Xu, J., Luan, S. J., Qin, B. K., Wang, Y. Y., Wang, K., and Qi, P. L. (2016). Backbone-hydrazone-containing biodegradable copolymeric micelles for anticancer drug delivery. *J. Nanopart. Res.* 18, 316–331. doi: 10.1007/s11051-016-3626-4

Yang, J., Wu, Y. P., Shen, Y., Zhou, C. G., Li, Y. F., and He, R. R. (2016). Enhanced therapeutic efficacy of doxorubicin for breast cancer using chitosan oligosaccharide-modified halloysite nanotubes. *ACS Appl. Mater. Inter.* 40, 26578–26590. doi: 10.1021/acsami.6b09074

Zheng, H. Q., Xing, L., Cao, Y. Y., and Che, S. A. (2013). Coordination bonding based pH-responsive drug delivery systems. *Chem. Rev.* 257, 1933–1944. doi: 10.1016/j.ccr.2013.03.007

Zheng, H. T., Hua, D. B., Bai, R. K., Hu, K. L., An, L. J., and Pan, C. Y. (2007). Control led/living free-radical copolymerization of 4-(azidocarbonyl) phenyl methacrylate with methyl acrylate under Co-60 gamma-ray irradiation. *J. Polym. Sci. Pol. Chem.* 45, 2609–2616. doi: 10.1002/pola.22018

Conflict of Interest Statement: The authors declare that the research was conducted in the absence of any commercial or financial relationships that could be construed as a potential conflict of interest.

frontiers in Pharmacology

ORIGINAL RESEARCH
published: 14 August 2018
doi: 10.3389/fphar.2018.00781

A Nanomicellar Prodrug Carrier Based on Ibuprofen-Conjugated Polymer for Co-delivery of Doxorubicin

Zuojun Li[1,2], Jingjing Sun[3], Yixian Huang[3], Yanhua Liu[4], Jieni Xu[3], Yichao Chen[3], Lei Liang[5], Jiang Li[3], Qiongfeng Liao[6], Song Li[3] and Kechao Zhou[2]**

[1] Department of Pharmacy, The Third Xiangya Hospital of Central South University, Changsha, China, [2] State Key Laboratory of Powder Metallurgy, Department of Pharmaceutical Sciences, School of Pharmacy, Central South University, Changsha, China, [3] Center for Pharmacogenetics, Department of Pharmaceutical Sciences, School of Pharmacy, University of Pittsburgh, Pittsburgh, PA, United States, [4] Department of Pharmaceutics, School of Pharmacy, Ningxia Medical University, Yinchuan, China, [5] Guangdong Second Provincial General Hospital, Guangzhou, China, [6] School of Pharmaceutical Sciences, Guangzhou University of Chinese Medicine, Guangzhou, China

Ibuprofen (IBU) is a non-steroidal anti-inflammatory drug (NSAID), which is widely used to reduce fever and treat inflammation and acute pain. Recently, its application in cancer treatment is also being explored. In this work, we synthesized a well-defined IBU-based amphiphilic diblock copolymer via reversible addition fragmentation transfer (RAFT) polymerization of IBU-based vinyl monomer. The amphiphilic copolymer POEG-*b*-PVBIBU (denoted as POVI) was composed of a hydrophilic poly(oligo(ethylene glycol)) block and a hydrophobic IBU-bearing prodrug block, which was able to self-assemble into prodrug nanomicelles. In addition, it could serve as a carrier to co-load other drugs including doxorubicin (DOX), paclitaxel (PTX), and docetaxel (DTX). By using DOX as a model anti-cancer drug, the delivery function of POVI carrier, including the drug release, *in vitro* cytotoxicity, cellular uptake, and *in vivo* antitumor activity, was evaluated. DOX-loaded POVI micelles exhibited sustained release of DOX. Besides, DOX/POVI micelles were effectively taken up by tumor cells with an efficiency comparable to that of free DOX. Moreover, *in vivo* studies showed that POVI carrier itself had modest antitumor activity. After loading DOX, the antitumor activity was significantly increased, which was significantly higher than that of free DOX. Our results suggest that POVI polymer represents a simple and effective dual-functional carrier for co-delivery of IBU and DOX to improve the anticancer activity.

Keywords: ibuprofen, nanomicellar, prodrug, carrier, doxorubicin, co-delivery

OPEN ACCESS

Edited by:
Qingxin Mu,
University of Washington,
United States

Reviewed by:
Zhi-xiang Yuan,
Sichuan University, China
Shiyong Song,
Henan University, China

***Correspondence:**
Song Li
sol4@pitt.edu
Kechao Zhou
zhoukechao@csu.edu.cn

Specialty section:
This article was submitted to Cancer Molecular Targets and Therapeutics, a section of the journal Frontiers in Pharmacology

Received: *30 April 2018*
Accepted: *27 June 2018*
Published: *14 August 2018*

Citation:
Li Z, Sun J, Huang Y, Liu Y, Xu J, Chen Y, Liang L, Li J, Liao Q, Li S and Zhou K (2018) A Nanomicellar Prodrug Carrier Based on Ibuprofen-Conjugated Polymer for Co-delivery of Doxorubicin. Front. Pharmacol. 9:781. doi: 10.3389/fphar.2018.00781

INTRODUCTION

The clinical applications of many antitumor drugs, such as doxorubicin (DOX), paclitaxel (PTX), and docetaxel (DTX), were limited by their low water solubility, poor bioavailability, and high toxic side effects (Lee et al., 2011; Senevirathne et al., 2016). To overcome these problems, various nanocarriers including micelles, dendrimers, and liposomes have been designed and developed for delivery of these hydrophobic antitumor drugs (Cho et al., 2008; Shen et al., 2010; Wei et al., 2013; Koudelka et al., 2015; Wang et al., 2015, 2017; Miao et al., 2017). Due to the small size, good stability, and unique core–shell structure, polymeric micelles have gained tremendous interest in the drug delivery field (Gaucher et al., 2005; Rösler et al., 2012). The hydrophobic core of micelles can encapsulate hydrophobic antitumor drugs via hydrophobic interactions, and the hydrophilic shell endows the micelles colloidal stability and protects the loaded drug from premature burst release.

It is well known that the constructing material, especially the hydrophobic domain of the polymeric micelles, plays a very important role in the delivery function of carriers (Zhang et al., 2014). Recently, increasing attention has been focused on the usage of bioactive compounds as hydrophobic moieties of polymeric carriers. These carriers themselves possess biological activity, which are termed as prodrug carriers (Craparo et al., 2013; Chen et al., 2016; Sun et al., 2017a). More importantly, some bioactive compounds with special structures in the prodrug carriers could interact with the co-loaded drug via π–π stacking effect, thereby improving the drug loading capacity (DLC; Sun et al., 2017b).

Non-steroidal anti-inflammatory drugs (NSAIDs), such as ibuprofen (IBU), indomethacin, and aspirin, are widely used to treat fever, arthritis, and rheumatic diseases. The anti-inflammatory effect of NSAIDs comes from the inhibition of the cyclooxygenase (COX) enzymes, including COX-1 and COX-2, which leads to the decrease of the production of prostaglandin, an important signaling molecule in the inflammation (Lim et al., 1999). Recently, accumulating evidences demonstrate that NSAIDs not only have anti-inflammatory effect, but also hold great potential in the prevention and treatment of several types of cancers (Ulrich et al., 2006). It has been suggested that the antitumor activity of NSAIDs can be partially explained by COX inhibition of prostaglandin synthesis (Ahnen, 1998). Other COX-independent mechanisms including inhibition of cell cycle progression (Gately and Kerbel, 2003) and induction of apoptosis (Davies et al., 2002) also contribute to the antitumor activity of NSAIDs. IBU is a commonly used NSAID that has been proven to inhibit proliferation of many tumor cells (Dial et al., 2006; Bonelli et al., 2011). Studies also demonstrate that IBU exhibited superior antitumor effect compared to other NSAIDs, mainly through the alteration of cell-cycle and induction of apoptosis (Andrews et al., 2002; Janssen et al., 2008). Moreover, compared to conventional anticancer drugs, IBU shows decreased side effect. Due to the potential of IBU in cancer treatment, IBU-conjugated prodrug polymers with various molecular structures have been developed to improve the water solubility and bioavailability of IBU. For example, Hasegawa and colleagues synthesized a series of amphiphilic diblock copolymers (PEG-PIBU) containing a hydrophilic poly(ethylene glycol) block and a hydrophobic IBU-bearing prodrug block (Hasegawa et al., 2013). By adjusting the length of hydrophobic IBU block, these polymers could self-assemble to form micelles with different morphologies. Wang et al. (2014) prepared another amphiphilic micellar carrier based on IBU-conjugated polymer for delivery of IBU. They found that in addition to the chemical conjugation, IBU could also be physically encapsulated into the micelles.

Although NSAIDs have potential antitumor activity, very high dosages of NSAIDs are needed to achieve a modest antitumor effect (Smalley and DuBois, 1997). Combination treatment of NSAIDs with other chemotherapeutic drugs is still necessary for cancer therapy (Endo et al., 2014; Lee et al., 2016). Recently, our group prepared a nanomicellar carrier that was self-assembled from PEG-Fmoc-IBU conjugate for co-delivery of IBU and PTX (Zhao et al., 2016). The IBU-based carrier showed synergistic antitumor effect with PTX, but there is only one IBU unit per carrier molecule, and thereby, large amounts of carriers were needed to deliver enough IBU dosage to tumor tissues, which might cause the unfavorable side effects.

Thus, in this work, we developed another IBU-containing polymeric carrier system with increased number of IBU units per polymer molecule via a simple synthesis method. We synthesized a POEG-b-PVBIbu diblock copolymer with a hydrophilic POEG block and a hydrophobic IBU block by reversible addition fragmentation transfer (RAFT) polymerization. The IBU-based prodrug polymer can form stable micelles with multiple IBU hydrophobic moieties in the core, which increases the solubility of IBU and allows more IBU being delivered into the tumor. Additionally, the micelle can serve as a carrier to encapsulate other hydrophobic chemotherapeutic drugs including DOX, DTX, and PTX. The size distribution and morphologies of drug-loaded micelles were evaluated. By using DOX as a model drug, the drug release, cellular uptake and antitumor activity were investigated *in vitro* and *in vivo*.

MATERIALS AND METHODS

Materials

Vinylbenzyl chloride, 2, 2-Azobis(isobutyronitrile) (AIBN), 1,4-dioxane, trypsin-EDTA solution, 3-(4,5-dimethylthiazol-2-yl)-2,5-diphenyl tetrazolium bromide (MTT), and Dulbecco's Modified Eagle's Medium (DMEM) were all purchased from Sigma-Aldrich (St. Louis, MO, United States). AIBN was purified by recrystallization in anhydrous ethanol. DOX·HCl and DTX were purchased from LC Laboratories (Woburn, MA, United States). PTX was purchased from AK Scientific Inc. (Union City, CA, United States). Fetal bovine serum (FBS) and penicillin-streptomycin solution were all purchased from Invitrogen (NY, United States). POEG macroCTA were prepared as previously reported (Sun et al., 2016a).

Synthesis of Ibu-Monomer

Vinylbenzyl chloride (1 eq.), IBU (1.5 eq.), and K_2CO_3 (2 eq.) were dissolved in DMF (5 eq.). The mixture was stirred at 50°C for 24 h, and then equal volume of water was added. The crude product was extracted by DCM for three times, and then purified by silica gel column chromatography.

Synthesis of POEG-b-PVBIbu Polymers

Ibu-monomer (180 mg, 0.559 mmol), POEG macroCTA (280 mg, 0.0372 mmol), AIBN (2 mg, 0.0124 mmol), and 2 mL dried 1, 4-dioxane were placed in a Schlenk tube. The mixture was degassed under N_2 by three freeze-pump-thaw cycles, and then immersed into an oil bath at 90°C. After 24 h, the polymerization was quenched by placing the Schlenk tube into liquid nitrogen. The polymer mixture was precipitated in petroleum ether for three times and dried in vacuum.

Characterization of the Synthesized Monomer and Polymers

^{1}H NMR spectrum was conducted on a Varian 400 FT-NMR spectrometer at 400.0 MHz with $CDCl_3$ as the solvent. Molecular weight (M_n and M_w) and polydispersity index (M_w/M_n) of the synthesized polymers were determined by gel permeation chromatography (GPC) equipped with a Waters 2414 refractive index detector, a Waters 515 HPLC pump, and a Waters 717 Plus Autosampler. THF was used as the eluent with a flowing rate of 1.0 mL/min at 35°C. A series of polystyrene standards with narrow molecular weight distribution were used for calibration.

Preparation of Drug-Free Micelle and Drug-Loaded Micelles

The blank POVI micelles and drug-loaded micelles were prepared by dialysis method. The polymer POVI and drug (DOX, PTX, or DTX) with certain mass ratio were dissolved in DMSO, which were then transferred to dialysis bags (MWCO 3.5 kDa), and dialyzed against PBS for 24 h. The size distributions and morphologies of blank and drug-loaded micelles were measured by dynamic light scattering (DLS) and transmission election microscopy with negative staining.

Doxorubicin concentration was detected by Fluorescence Microplate Reader with excitation wavelength of 490 nm and emission wavelength of 590 nm. PTX concentration was measured by reverse phase high-performance liquid chromatography (RP-HPLC) with a mobile phase of methanol/water (70:30 v/v) at the flow rate of 1.0 mL/min, and UV detection at 227 nm. DTX concentration was detected by RP-HPLC with a mobile phase of acetonitrile/water (50:50 v/v) at the flow rate of 1.0 mL/min, and UV detection at 230 nm.

Drug loading capacity and drug loading efficiency (DLE) were calculated according to the following formula:

DLC (%) = [weight of drug loaded/(weight of polymer + drug used)] × 100%

DLE (%) = (weight of loaded drug/weight of input drug) × 100%.

Critical Micelle Concentration (CMC) of POVI Micelle

Critical micelle concentration (CMC) of POVI micelle was measured using Nile red as a fluorescence probe

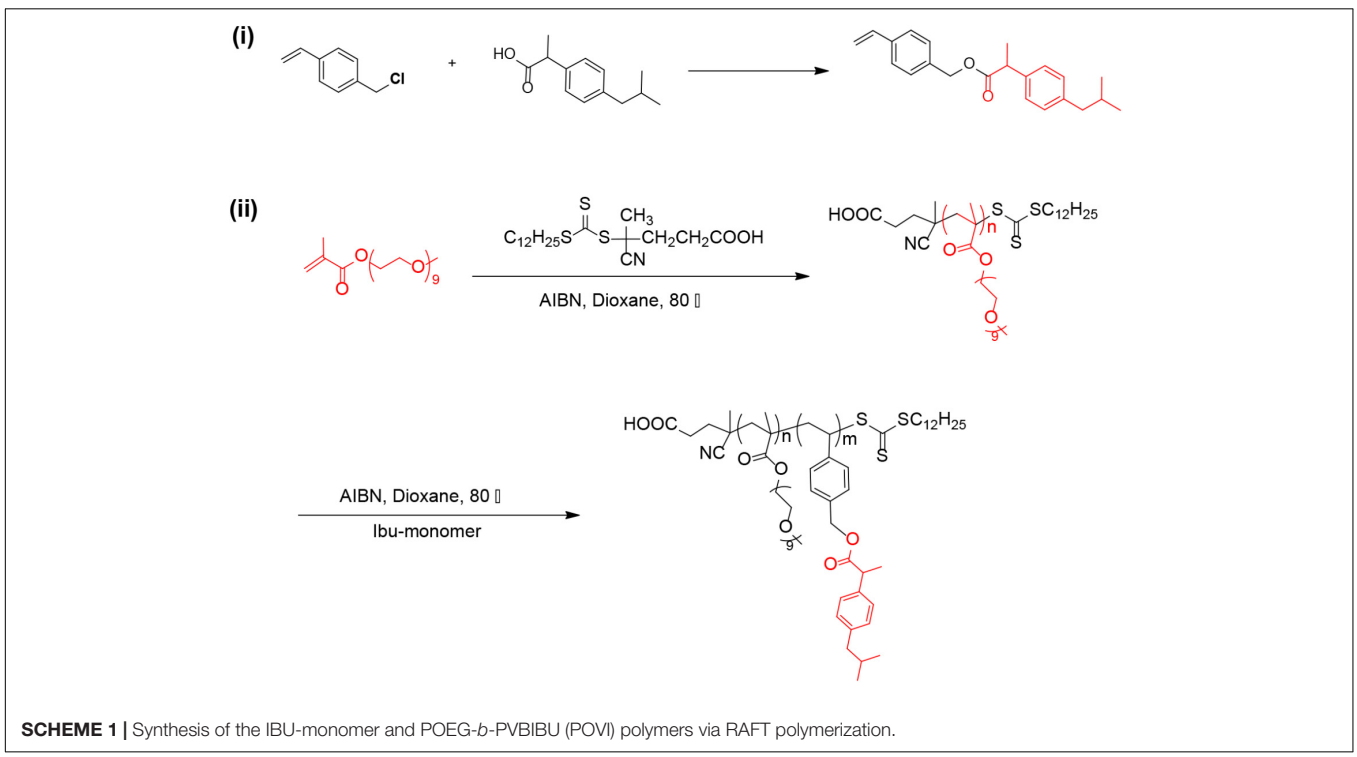

SCHEME 1 | Synthesis of the IBU-monomer and POEG-*b*-PVBIBU (POVI) polymers via RAFT polymerization.

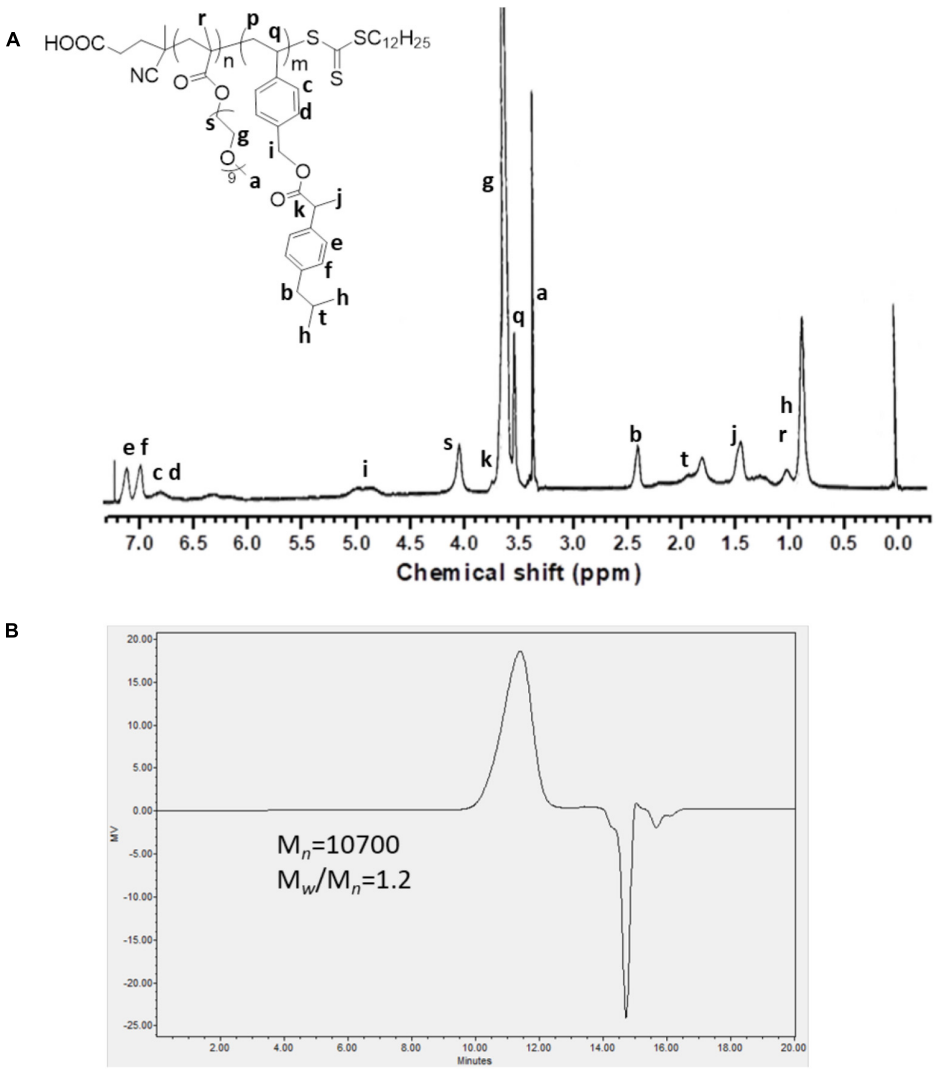

FIGURE 1 | (A) ^{1}H NMR spectrum of the POEG-*b*-PVBIBU (POVI) diblock copolymer in $CDCl_3$. **(B)** Gel permeation chromatography curve of the POVI diblock polymer.

TABLE 1 | Physicochemical characterization of POVI blank micelle and drug-loaded micelles.

Micelles	Size (nm)[b]	PDI[c]	Carrier: DOX mass ratio	DLE%[d]	DLC%[d]
POVI[a]	82.35	0.207	–	–	–
DOX/POVI	92.78	0.194	10: 1	69.98%	6.4%
PTX/POVI	106.7	0.281	20: 1	72.90%	3.5%
DTX/POVI	98.30	0.204	20: 1	41.74%	2.0%

[a]Concentration of blank micelle was 20 mg/mL. [b]Measured by DLS. [c]PDI, polydispersity index; [d]DLC%, drug loading capacity; DLE%, drug loading efficiency.

(Klaikherd et al., 2009; Sun et al., 2016b); 10 μL Nile red in chloroform was added into each tube, and the solvent was removed by air flow and vacuum pump. Polymer solution (120 μL) with concentrations ranging from 1×10^{-4} to 0.5 mg/mL was added to each tube, and incubated overnight. The fluorescence intensity of each sample was detected by a Synergy H1 Hybrid Multi-Mode Microplate Reader (Winooski, VT, United States) at a wavelength of 480/620 nm (excitation/emission).

In vitro Drug Release Study

Doxorubicin-loaded POVI micelles (0.5 mg DOX/mL) in PBS (pH = 7.4) was placed in a dialysis bag (MWCO = 12 kDa, Spectrum Laboratories), and incubated in a 200-mL beaker with PBS containing 0.5% (w/v) Tween 80, with gentle shaking (100 rpm/min) at 37°C. DOX solution in saline with the same concentration was used as a control. The concentration of DOX outside the dialysis bag was measured

by a fluorescence microplate reader at designated time points and the values were reported as the means of triplicate samples.

Cell Culture

Mouse metastatic breast cancer cell line 4T1.2, human breast cancer cell line MCF-7, and androgen-independent human prostate cancer cell line PC-3 were cultured at 37°C in DMEM containing 10% FBS and 1% penicillin-streptomycin in a humidified environment with 5% CO_2.

In vitro Cytotoxicity Study

4T1.2 (1500 cells/well), MCF-7 (4000 cells/well), or PC-3 (2500 cells/well) were seeded in 96-well plates and incubated for 24 h. Then the cells were treated with various concentrations of drug-free POVI micelles, DOX-loaded POVI micelles, or DOX. After incubation for 72 h, 20 μL of MTT in PBS (5 mg/mL) was added into each well and further incubated for 4 h. The medium was then removed, and DMSO was added to solubilize the MTT formazan. The absorbance of each well was measured with a microplate reader at a wavelength of 550 nm and a reference wavelength of 630 nm. Untreated cells were used as a control. Cell viability was calculated as $[(OD_{treat} - OD_{blank})/(OD_{control} - OD_{blank}) \times 100\%]$.

Intracellular Trafficking

4T1.2 cells (15,000/well) were seeded in glass bottom dishes (*in vitro* Scientific, United States), and incubated overnight. The cells were treated with free DOX and DOX/POVI micelles (DOX concentration: 15.5 μg/mL) for 2 and 4 h separately. Then cells were stained with Hoechst 3342 for 15 min, and washed with cool PBS for three times. The intracellular distributions of different DOX formulations were observed under a confocal laser scanning microscope (CLSM, FluoView 1000, Olympus, Japan).

Animals

Female BALB/c mice (6–8 weeks) were purchased from Charles River (Davis, CA, United States). All animals were housed under pathogen-free conditions according to Association for Assessment and Accreditation of Laboratory Animal Care (AAALAC) guidelines. All animal-related experiments were performed in full compliance with institutional guidelines and approved by the Animal Use and Care Administrative Advisory Committee at the University of Pittsburgh.

In vivo Therapeutic Study

A syngeneic murine breast cancer model (4T1.2) was used to evaluate the therapeutic efficacy of DOX-loaded POVI micelles. 4T1.2 cells (2×10^5 cells/mouse) were inoculated s.c. at the right flank of female BALB/c mice. When the tumor volume reached ~50 mm^3 (day 0), mice were randomly divided into four groups ($n = 3$) and received i.v. administration of saline (control), POVI micelles, free DOX, and DOX-loaded POVI micelles, respectively, on days 0, 3, 6, 9, 12, 15, and 18. The DOX dosage for free DOX and DOX-loaded POVI micelles was 5 mg DOX/kg. The dosage for POVI micelles was 73 mg POVI/kg, which was the same as that of POVI in DOX-loaded POVI micelles. Tumor volumes were measured with digital caliper and calculated as $V = (L \times W^2)/2$, where L is the longest and W is the shortest tumor diameters (mm). Each group was compared by relative tumor volume (RTV = V/V_0, V_0 was the tumor volume prior to first treatment). Mice were sacrificed when the tumor volume reached ~2000 mm^3. The size and weight of tumor stripped from the

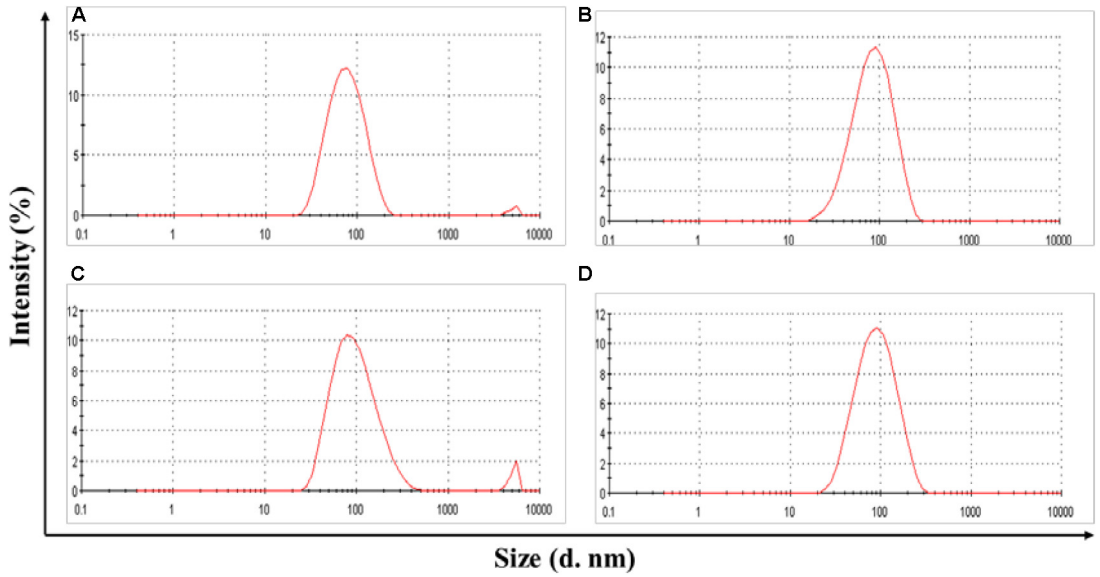

FIGURE 2 | Size distribution of POVI **(A)**, DOX/POVI **(B)** (mass ratio of micelle to DOX = 10:1), PTX/POVI **(C)**, and DTX/POVI micelles **(D)** (mass ratio of micelle to PTX/DTX = 20:1).

mice were measured. To evaluate the potential toxicity, the body weights were also monitored during the entire course of treatment.

Histochemical Staining

After *in vivo* therapeutic study, tumor tissues were excised and preserved in 4% formaldehyde in PBS, followed by embedment in paraffin. The paraffin-embedded tumor samples were cut into thin slices of 5 μm with an HM 325 Rotary Microtome. Then the slices were stained with hematoxylin and eosin (H&E) for histopathological examination under a Zeiss Axiostar plus Microscope (PA, United States).

Statistical Analysis

All results were reported as the mean ± SD unless otherwise indicated. Statistical analysis was performed with Student's *t*-test for two groups, and one-way ANOVA for multiple groups, followed by Newman–Keuls test if $P < 0.05$. In all statistical analysis, $P < 0.05$ was considered statistically significant.

RESULTS

Synthesis of POEG-b-PVBIbu Polymers

Reversible addition fragmentation transfer polymerization of functional monomer has become an attractive strategy to obtain well-defined functional polymers for drug/gene delivery (Sun et al., 2013a,b; Tucker et al., 2015). In this work, we synthesized a well-defined IBU-based prodrug polymer via RAFT polymerization of IBU-conjugated monomer, and investigated its function as a dual-functional carrier for co-delivery of other chemotherapeutic drugs.

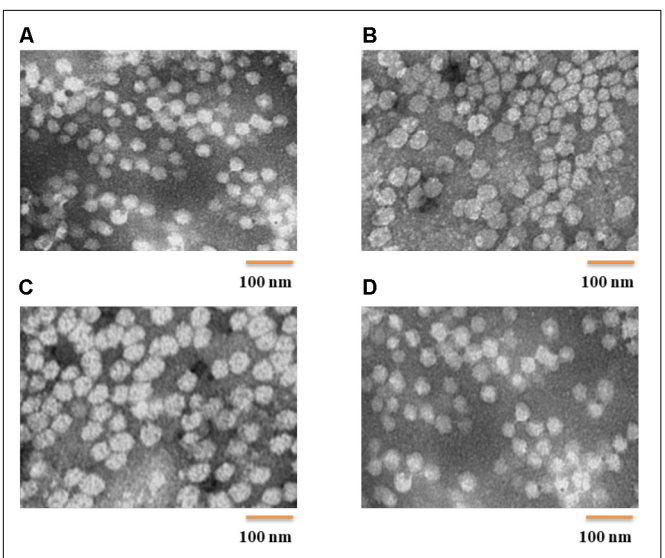

FIGURE 3 | TEM images (direct mag: 150,000X) of POVI **(A)**, DOX/POVI **(B)** PTX/POVI **(C)**, and DTX/POVI **(D)** micelles.

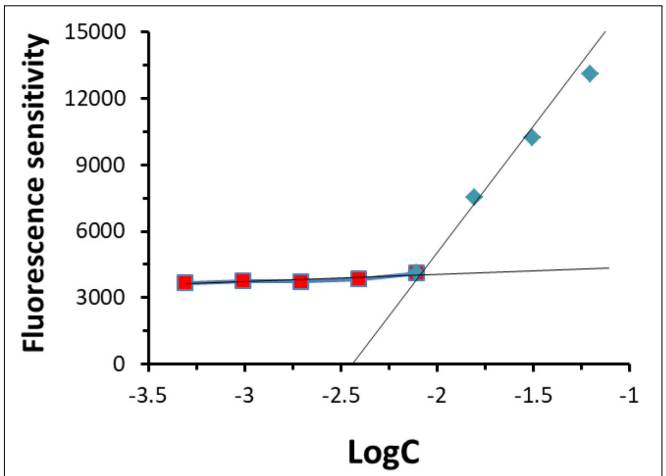

FIGURE 4 | Critical micelle concentration (CMC) of POVI micelle.

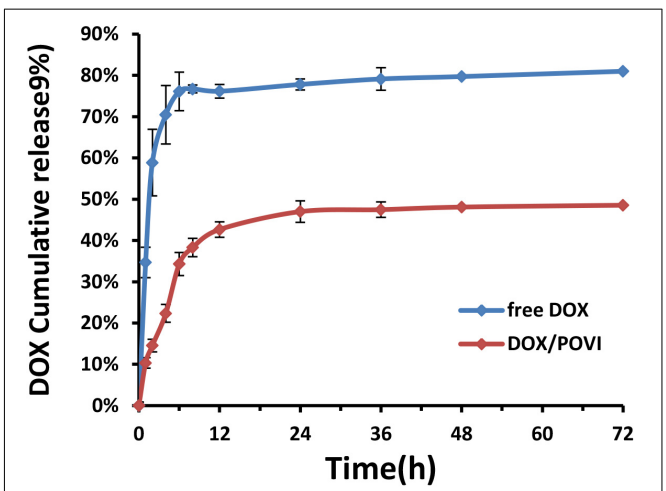

FIGURE 5 | DOX release from DOX-loaded POVI micelles via a dialysis method. PBS solution was used as release medium, and DOX concentrations were analyzed at 0, 1, 2, 4, 6, 8, 12, 24, 36, 48, and 72 h.

As shown in **Scheme 1**, we first designed and synthesized a vinylbenzyl derivative of IBU (IBU-monomer) where IBU was conjugated with vinylbenzyl chloride via a hydrolyzable ester linkage. Then, the macro-chain transfer agent POEG macroCTA was synthesized by RAFT polymerization as previously reported (Sun et al., 2016a), which further initiated the polymerization of IBU-monomer to give the POEG-*b*-PVBIbu block copolymers. The structures of the monomer and polymer were confirmed by ^{1}H NMR (**Figure 1**). As shown in **Figure 1A**, the average degree of polymerization (DP) of the Ibu-monomer was determined to be 12 by comparing the intensities of I_b and I_a. GPC showed unimodal peaks for the polymer with number-average molecular weight M_n of 10,700, and polydispersity of 1.20 (**Figure 1B**), which indicated the successful synthesis of the well-defined POEG-*b*-PVBIbu (POVI) block copolymers.

Preparation and Physicochemical Characterization of POVF Blank Micelles and Drug-Loaded Micelles

POVF blank micelles and drug-loaded micelles (including DOX/POVI, PTX/POVI, and DTX/POVI) were successfully prepared by dialysis method, and the physicochemical characterization is summarized in **Table 1**. DLS analysis showed that POVF polymers could form nano-sized micelles with a diameter of 82 nm. The sizes of micelles slightly increased to 92, 106, and 98 nm after loading of DOX, PTX, and DTX, respectively (**Figure 2**), which may be due to that the encapsulated hydrophobic drugs enlarged hydrophobic core of the micelles. The morphologies of the blank and drug-loaded micelles were evaluated by transmission electron microscopy (TEM). As shown in **Figure 3**, these micelles are spherical in morphology with uniform size. DLE and capacity were measured by a fluorescence microplate reader. As shown in the **Table 1**, POVI polymer was able to load DOX with a loading capacity of 6.4%. In addition, POVI polymers could also serve as a carrier to load other drugs such as PTX and DTX.

The CMC value of POVF micelles was evaluated with Nile red as a fluorescence probe. As shown in **Figure 4**, the CMC of POVI micelles was measured to be 9.8 mg/L. The low CMC suggests a good stability of our micelles following dilution in the blood after i.v. administration.

Release Kinetics of DOX

The release kinetics of DOX from DOX/POVI micelles was evaluated using a dialysis method, and free DOX solution was used as a control. As shown in **Figure 5**, free DOX solution showed a burst DOX release of almost 80% within the first 12 h, while DOX/POVI micelles showed a slow DOX release of about 43%. Even after 72 h, less than 50% of DOX was released from DOX/POVI micelles.

In vitro Cytotoxicity of DOX/POVI

In vitro cytotoxicity of DOX/POVI micelles was evaluated in 4T1.2, MCF7, and PC3 cell lines. As shown in **Figure 6**, POVI carrier did not show any remarkable cytotoxicity among all cell lines tested. DOX/POVI micelles and DOX solution exhibited potent cytotoxicity in a concentration-dependent manner. DOX/POVI micelles exhibited lower cytotoxicity than free DOX in the three cell lines, which is likely due to the slow release of DOX from DOX/POVI micelles.

Intracellular Trafficking

Intracellular trafficking and distribution of DOX/POVF micelles were studied by confocal laser scanning microcopy (CLSM). 4T1.2 cells were incubated with free DOX and DOX/POVF micelles for 2 and 4 h, respectively. At 2 h,

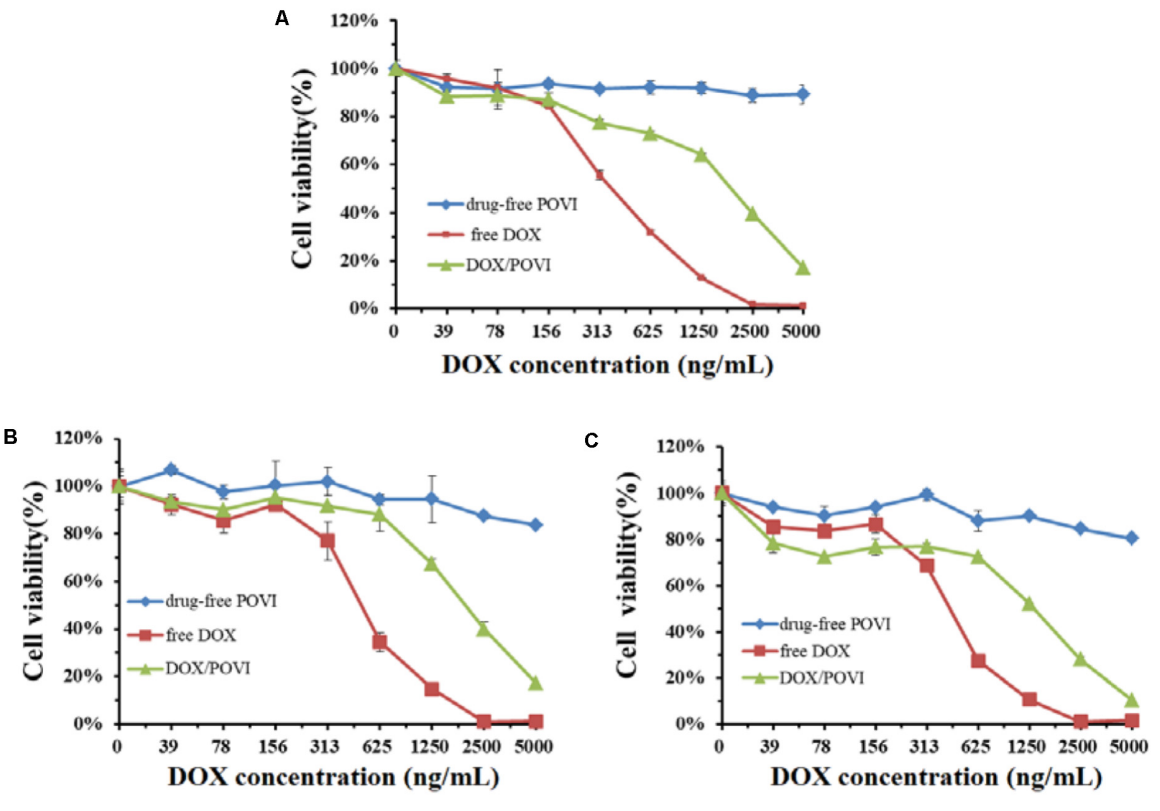

FIGURE 6 | *In vitro* cytotoxicity of DOX/POVI micelles. 4T1.2 **(A)**, MCF7 **(B)**, and PC3 **(C)** cells were treated with DOX-free POVI, DOX/POVI micelles, and free DOX for 72 h, and the cytotoxicity was determined by MTT assay, respectively.

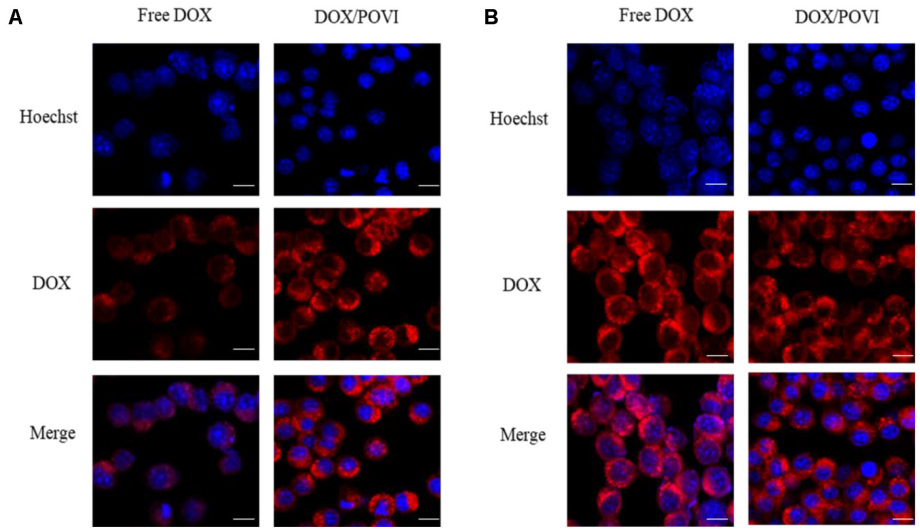

FIGURE 7 | Intracellular trafficking of DOX in 4T1.Cells were treated with free DOX, DOX/POVI micelle at 15.5 μg/mL for 2 h **(A)** and 4 h **(B)**. The nuclei were stained with Hoechst 33342. Scale bar: 20 μm.

cells treated with DOX/POVF micelles exhibited strong DOX fluorescence signals around the nucleus, similar to the cells treated with free DOX (**Figure 7A**). At 4 h, increased signals of red fluorescence appeared in nuclei, both for DOX/POVF micelle group and free DOX group (**Figure 7B**).

In vivo Therapeutic Efficacy Evaluation

The *in vivo* therapeutic efficacy of DOX/POVI micelles was evaluated in the 4T1.2 breast tumor-bearing BALB/c mice. The mice were treated with saline, POVI carrier, free DOX, and DOX/POVI micelles by i.v. injection, respectively. As shown in **Figure 8A**, DOX exhibited a modest tumor growth inhibition at a dose of 5 mg DOX/kg. DOX/POVI micelles were more effective than DOX in inhibiting tumor growth ($p < 0.05$) at the same dose. Interestingly, POVI carrier alone also showed tumor growth inhibition effect, although it was less effective than DOX.

No significant changes were found in the body weights of mice following various treatments (**Figure 8B**), indicating that all treatments were well tolerated. **Figure 8C** shows the photographs of tumors removed from the mice after various treatments. Compared to saline treatment group, DOX/POVI treatment led to an obvious decrease in tumor size. The tumor growth inhibition rate of DOX/POVI micelles is calculated to be significantly higher than those of free DOX and POVI blank micelles ($P < 0.05$; **Figure 8D**).

Figure 9 shows the images of H&E-stained slices of tumors collected after the completion of *in vivo* therapy study. Tumors treated with saline showed normal tumor morphology with large nuclei. In contrast, tumors in other treatment groups showed shrunk nuclei. Among them, DOX/POVF treatment resulted in the most significant tumor necrosis.

DISCUSSION

Ibuprofen is one type of NSAID that not only possesses anti-inflammatory effect, but also demonstrates great potential in inhibiting proliferation of various types of tumor cells (Dial et al., 2006; Bonelli et al., 2011). Currently, combination of IBU with chemotherapeutic drugs is being evaluated as a new regimen for clinical cancer treatment. However, free drugs are readily eliminated in the blood and they lack tumor targeting. Thus, co-delivery of IBU and a chemotherapeutic drug into tumors using a delivery vehicle is highly needed. Previously, we reported a nanomicellar carrier based on PEG-Fmoc-IBU conjugate for co-delivery of IBU and PTX (Zhao et al., 2016). Although PEG-Fmoc-IBU carrier was effective in loading and delivering PTX into tumors, the efficiency of delivery of IBU itself was relatively low because there was only one IBU unit per polymer molecule. In the present work, we developed a new IBU-conjugated polymeric carrier POVI with increased units of IBU per carrier molecule via a facile RAFT polymerization method. Compared to the previous system, the IBU loading capacity in the new POVI system was increased from 8.2 to 20.9%, indicating that more IBU could be delivered into the tumor tissues when injecting the same amount of carriers.

First, we designed and synthesized a novel IBU-conjugated vinylbenzyl monomer, which was further polymerized to yield the IBU-containing block copolymers. Compared with the post-conjugation method in which a drug was conjugated to the polymerized backbone, our method has an obvious advantage of simplicity. In addition, it avoids the low drug conjugation efficiency caused by the steric hindrance.

The synthesized POVI polymer could serve as a carrier that is effective in loading various types of chemotherapeutic drugs, including DOX, PTX, and DTX. We found that the monomer

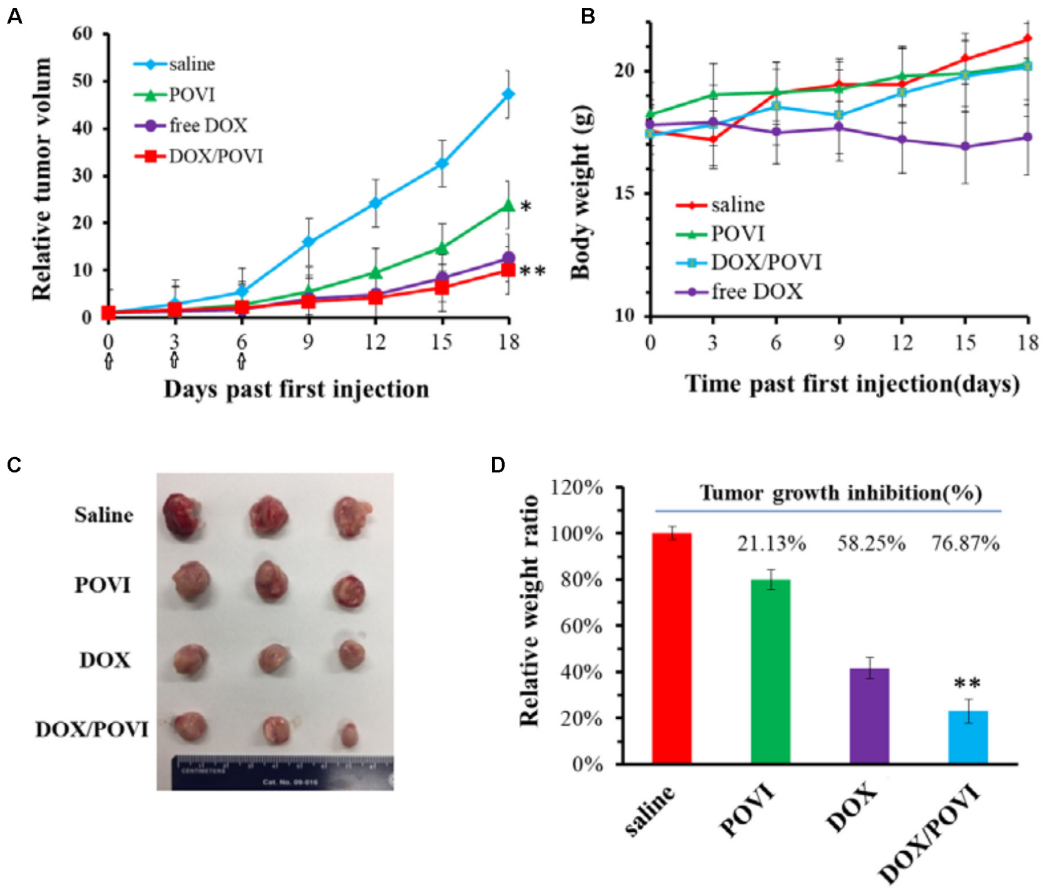

FIGURE 8 | *In vivo* therapeutic efficacy of DOX/POVI micelles. BALB/c mice in 4T1.2 murine breast cancer model were injected with saline, POVI, free DOX, and DOX/POVI (5 mg DOX/kg body weight) on days 0, 3, and 6, separately. $^{*}P < 0.05$; $^{**}P < 0.01$ (vs saline). **(A)** Relative tumor volume curves of mice receiving different treatments. **(B)** Changes of body weight in mice were monitored. **(C)** Image of tumors stripped from mice on the day 18. **(D)** Tumor weights of mice were measured on day 21 and tumor growth inhibition (%) was calculated. $^{**}P < 0.05$ (vs free DOX).

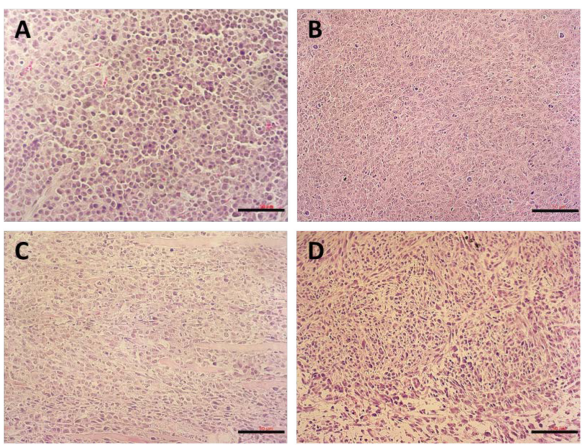

FIGURE 9 | H&E stained tumor tissues from mice received different treatments: **(A)** saline, **(B)** POVI, **(C)** free DOX, and **(D)** DOX/POVI at a dosage of 5 mg DOX/kg. Three injections were made into BALB/c mice bearing 4T1.2 tumor on days 0, 3, and 6, separately. Tumor tissues were harvested on day 18. Scale bar: 50 μm.

structure is critical for the loading capacity of the carrier. In the preliminary study, we also synthesized another IBU-based polymer using IBU-conjugated hydroxyethyl methacrylate monomer. However, the polymer obtained performed poorly in encapsulating other chemotherapeutic drugs (data not shown). When we introduced vinylbenzyl group into the polymers, the DLC was significantly improved, suggesting that, in addition to hydrophobic interaction, the π–π stacking effect between carrier and the chemotherapeutic drug may also contribute to the overall DLC. Moreover, the structures of chemotherapeutic drugs also affected the loading capacity. The POVI carrier was more effective in encapsulating DOX compared to other chemotherapeutic drugs, which might be due to the stronger carrier/DOX interaction.

The DOX-loaded micelles showed small size with a diameter of ∼90 nm (**Figure 2**), which was optimal for a long blood circulation time and passive targeting to solid tumor sites through the enhanced permeability and retention (EPR) effect (Mitra et al., 2001; Meng et al., 2011; Kobayashi et al., 2014). DOX-loaded micelles showed slow and sustained drug release (**Figure 5**), which could prevent the premature release of

encapsulated DOX before entering into tumors. The slow release of DOX from the micelles may be due to the strong interaction (e.g., hydrophobic interaction and π–π stacking effect) between DOX and POVI carrier (Sun et al., 2016a).

In vitro cytotoxicity showed that DOX formulated in the carrier was less effective in inhibiting the proliferation of tumor cells compared to free DOX. The *in vitro* cytotoxicity comes from the overall outcome of intracellular uptake and drug release. The DOX/POVI micelles showed similar cellular uptake compared to free DOX (**Figure 7**); the lower *in vitro* cytotoxicity of DOX/POVI micelles might be attributed to the slow release of DOX from the micelles.

POVI carrier was not effective in inhibiting the proliferation of cultured tumor cells *in vitro* (**Figure 6**) at the concentrations that were used for DOX delivery *in vitro*. This may be due to the slow release of IBU during a short period of culture and its relatively low potency. However, *in vivo* data showed that the POVI carrier itself showed moderate antitumor activity (**Figure 8**). In our previous study, PEG-IBU conjugate could also inhibit tumor growth compared with control group (Zhao et al., 2016). So the antitumor activity of POVI carrier *in vivo* may come from the released IBU mediated by various kinds of enzymes in the tumor tissues over a relatively long period of time. Moreover, DOX-loaded micelles showed a much more pronounced antitumor activity compared with free DOX, which is different from the *in vitro* cytotoxicity assay. The improved therapeutic efficacy of DOX/POVI micelles is likely attributed to the combination effect of the carrier with co-delivered DOX. The improved delivery of DOX by the POVI carrier may also play a role. More studies are warranted to further investigate the underlying mechanisms.

CONCLUSION

We have developed a new IBU-based prodrug di-block polymer POVI via facile RAFT polymerization. POVI polymer could load various hydrophobic drugs including DOX, PTX, and DTX with high loading capacity. DOX/POVI micelles showed similar cytotoxicity and cellular uptake compared to free DOX. More importantly, DOX/POVI micelles were more effective in inhibiting the tumor growth than free DOX *in vivo*. Our results suggest that POVI polymer can be employed as a safe and effective dual-functional carrier for co-delivery of other chemotherapeutic drugs.

AUTHOR CONTRIBUTIONS

SL, JS, and YH conceived and designed the study. JS and ZL contributed to chemical synthesis and micelle characterization. ZL, YL, JX, YC, LL, JL, and QL contributed to biological study. ZL, JS, YL, and JX analyzed the data. ZL, JS, and SL drafted the manuscript. All authors approved the final version of the manuscript.

FUNDING

This work was supported by NIH Grant Nos. RO1CA174305, RO1CA219399, and RO1CA223788.

REFERENCES

Ahnen, D. J. (1998). Colon cancer prevention by NSAIDs: what is the mechanism of action? *Eur. J. Surg.* 164, 111–114. doi: 10.1080/11024159850191544

Andrews, J., Djakiew, D., Krygier, S., and Andrews, P. (2002). Superior effectiveness of ibuprofen compared with other NSAIDs for reducing the survival of human prostate cancer cells. *Cancer Chemother. Pharmacol.* 50, 277–284. doi: 10.1007/s00280-002-0485-8

Bonelli, P., Tuccillo, F., Calemma, R., Pezzetti, F., Borrelli, A., Martinelli, R., et al. (2011). Changes in the gene expression profile of gastric cancer cells in response to ibuprofen: a gene pathway analysis. *Pharmacogenomics J.* 11, 412–428. doi: 10.1038/tpj.2010.55

Chen, Y., Xia, R., Huang, Y., Zhao, W., Li, J., Zhang, X., et al. (2016). An immunostimulatory dual-functional nanocarrier that improves cancer immunochemotherapy. *Nat. Commun.* 7:13443. doi: 10.1038/ncomms13443

Cho, K., Wang, X., Nie, S., and Shin, D. M. (2008). Therapeutic nanoparticles for drug delivery in cancer. *Clin. Cancer Res.* 14, 1310–1316. doi: 10.1158/1078-0432.CCR-07-1441

Craparo, E. F., Teresi, G., Licciardi, M., Bondí, M. L., and Cavallaro, G. (2013). Novel composed galactosylated nanodevices containing a ribavirin prodrug as hepatic cell-targeted carriers for HCV treatment. *J. Biomed. Nanotechnol.* 9, 1107–1122. doi: 10.1166/jbn.2013.1608

Davies, G., Martin, L.-A., Sacks, N., and Dowsett, M. (2002). Cyclooxygenase-2 (COX-2), aromatase and breast cancer: a possible role for COX-2 inhibitors in breast cancer chemoprevention. *Ann. Oncol.* 13, 669–678. doi: 10.1093/annonc/mdf125

Dial, E. J., Doyen, J. R., and Lichtenberger, L. M. (2006). Phosphatidylcholine-associated nonsteroidal anti-inflammatory drugs (NSAIDs) inhibit DNA synthesis and the growth of colon cancer cells in vitro. *Cancer Chemother. Pharmacol.* 57, 295–300. doi: 10.1007/s00280-005-0048-x

Endo, H., Yano, M., Okumura, Y., and Kido, H. (2014). Ibuprofen enhances the anticancer activity of cisplatin in lung cancer cells by inhibiting the heat shock protein 70. *Cell Death Dis.* 5:e1027. doi: 10.1038/cddis.2013.550

Gately, S., and Kerbel, R. (2003). Therapeutic potential of selective cyclooxygenase-2 inhibitors in the management of tumor angiogenesis. *Prog. Exp. Tumor. Res.* 37, 179–192. doi: 10.1159/000071373

Gaucher, G., Dufresne, M.-H., Sant, V. P., Kang, N., Maysinger, D., and Leroux, J.-C. (2005). Block copolymer micelles: preparation, characterization and application in drug delivery. *J. Control Release* 109, 169–188. doi: 10.1016/j.jconrel.2005.09.034

Hasegawa, U., Van Der Vlies, A. J., Wandrey, C., and Hubbell, J. A. (2013). Preparation of well-defined ibuprofen prodrug micelles by RAFT polymerization. *Biomacromolecules* 14, 3314–3320. doi: 10.1021/bm4009149

Janssen, A., Schiffmann, S., Birod, K., Maier, T. J., Wobst, I., Geisslinger, G., et al. (2008). p53 is important for the anti-proliferative effect of ibuprofen in colon carcinoma cells. *Biochem. Biophys. Res. Commun.* 365, 698–703. doi: 10.1016/j.bbrc.2007.11.051

Klaikherd, A., Nagamani, C., and Thayumanavan, S. (2009). Multi-stimuli sensitive amphiphilic block copolymer assemblies. *J. Am. Chem. Soc.* 131, 4830–4838. doi: 10.1021/ja809475a

Kobayashi, H., Watanabe, R., and Choyke, P. L. (2014). Improving conventional enhanced permeability and retention (EPR) effects; what is the appropriate target? *Theranostics* 4, 81–89. doi: 10.7150/thno.7193

Koudelka, S., Knotigova, P. T., Masek, J., Prochazka, L., Lukac, R., Miller, A. D., et al. (2015). Liposomal delivery systems for anti-cancer analogues of vitamin E. *J. Control Release* 207, 59–69. doi: 10.1016/j.jconrel.2015.04.003

Lee, A., Di Mascolo, D., Francardi, M., Piccardi, F., Bandiera, T., and Decuzzi, P. (2016). Spherical polymeric nanoconstructs for combined chemotherapeutic and anti-inflammatory therapies. *Nanomedicine* 12, 2139–2147. doi: 10.1016/j.nano.2016.05.012

Lee, H., Lee, Y. S., Lee, K. D., and Park, S. Y. (2011). Development of disulfide core-crosslinked pluronic nanoparticles as an effective anticancer-drug-delivery system. *Macromol. Biosci.* 11, 1264–1271. doi: 10.1002/mabi.201100083

Lim, J. T., Piazza, G. A., Han, E. K.-H., Delohery, T. M., Li, H., Finn, T. S., et al. (1999). Sulindac derivatives inhibit growth and induce apoptosis in human prostate cancer cell lines. *Biochem. Pharmacol.* 58, 1097–1107. doi: 10.1016/S0006-2952(99)00200-2

Meng, H., Xue, M., Xia, T., Ji, Z., Tarn, D. Y., Zink, J. I., et al. (2011). Use of size and a copolymer design feature to improve the biodistribution and the enhanced permeability and retention effect of doxorubicin-loaded mesoporous silica nanoparticles in a murine xenograft tumor model. *ACS Nano* 5, 4131–4144. doi: 10.1021/nn200809t

Miao, L., Guo, S., Lin, C. M., Liu, Q., and Huang, L. (2017). Nanoformulations for combination or cascade anticancer therapy. *Adv. Drug Deliv. Rev.* 115, 3–22. doi: 10.1016/j.addr.2017.06.003

Mitra, S., Gaur, U., Ghosh, P., and Maitra, A. (2001). Tumour targeted delivery of encapsulated dextran–doxorubicin conjugate using chitosan nanoparticles as carrier. *J. Control Release* 74, 317–323. doi: 10.1016/S0168-3659(01)00342-X

Rösler, A., Vandermeulen, G. W., and Klok, H.-A. (2012). Advanced drug delivery devices via self-assembly of amphiphilic block copolymers. *Adv. Drug Deliv. Rev.* 64, 270–279. doi: 10.1016/j.addr.2012.09.026

Senevirathne, S. A., Washington, K. E., Biewer, M. C., and Stefan, M. C. (2016). PEG based anti-cancer drug conjugated prodrug micelles for the delivery of anti-cancer agents. *J. Mater. Chem. B* 4, 360–370. doi: 10.1039/C5TB02053K

Shen, Y., Jin, E., Zhang, B., Murphy, C. J., Sui, M., Zhao, J., et al. (2010). Prodrugs forming high drug loading multifunctional nanocapsules for intracellular cancer drug delivery. *J. Am. Chem. Soc.* 132, 4259–4265. doi: 10.1021/ja909475m

Smalley, W. E., and DuBois, R. N. (1997). Colorectal cancer and nonsteroidal anti-inflammatory drugs. *Adv. Pharmacol.* 39, 1–20. doi: 10.1016/S1054-3589(08)60067-8

Sun, J., Chen, Y., Huang, Y., Zhao, W., Liu, Y., Venkataramanan, R., et al. (2017a). Programmable co-delivery of the immune checkpoint inhibitor NLG919 and chemotherapeutic doxorubicin via a redox-responsive immunostimulatory polymeric prodrug carrier. *Acta Pharmacol. Sin.* 38, 823–834. doi: 10.1038/aps.2017.44

Sun, J., Liu, Y., Chen, Y., Zhao, W., Zhai, Q., Rathod, S., et al. (2017b). Doxorubicin delivered by a redox-responsive dasatinib-containing polymeric prodrug carrier for combination therapy. *J. Control Release* 258, 43–55. doi: 10.1016/j.jconrel.2017.05.006

Sun, J., Chen, Y., Li, K., Huang, Y., Fu, X., Zhang, X., et al. (2016a). A prodrug micellar carrier assembled from polymers with pendant farnesyl thiosalicylic acid moieties for improved delivery of paclitaxel. *Acta Biomater.* 43, 282–291. doi: 10.1016/j.actbio.2016.07.014

Sun, J., Luo, T., Sheng, R., Li, H., Wang, Z., and Cao, A. (2016b). Intracellular plasmid DNA delivery by self-assembled nanoparticles of amphiphilic PHML-b-PLLA-b-PHML copolymers and the endocytosis pathway analysis. *J. Biomater. Appl.* 31, 606–621.

Sun, J., Luo, T., Sheng, R., Li, H., and Cao, A. (2013a). Preparation of cationic l-lysine conjugated poly (2-hydroxyethyl methacrylate) s and their potential application as low cytotoxic efficient gene delivery vectors. *J. Control Release* 172:e108. doi: 10.1016/j.jconrel.2013.08.263

Sun, J., Luo, T., Sheng, R., Li, H., Chen, S., Hu, F., et al. (2013b). Preparation of functional water-soluble low-cytotoxic poly(methacrylate)s with pendant cationic l-lysines for efficient gene delivery. *Macromol. Biosci.* 13, 35–47. doi: 10.1002/mabi.201200304

Tucker, B. S., Getchell, S. G., Hill, M. R., and Sumerlin, B. S. (2015). Facile synthesis of drug-conjugated PHPMA core-crosslinked star polymers. *Polym. Chem.* 6, 4258–4263. doi: 10.1039/C5PY00497G

Ulrich, C. M., Bigler, J., and Potter, J. D. (2006). Non-steroidal anti-inflammatory drugs for cancer prevention: promise, perils and pharmacogenetics. *Nat. Rev. Cancer* 6, 130–140. doi: 10.1038/nrc1801

Wang, Y., Luo, Q., Gao, L., Gao, C., Du, H., Zha, G., et al. (2014). A facile strategy to prepare redox-responsive amphiphilic PEGylated prodrug with high drug loading content and low critical micelle concentration. *Biomater. Sci.* 2, 1367–1376. doi: 10.1039/C4BM00065J

Wang, Z., Luo, T., Sheng, R., Li, H., Sun, J., and Cao, A. (2015). Amphiphilic diblock terpolymer PMAgala-b-P (MAA-co-MAChol) s with attached galactose and cholesterol grafts and their intracellular pH-responsive doxorubicin delivery. *Biomacromolecules* 17, 98–110. doi: 10.1021/acs.biomac.5b01227

Wang, Z., Sheng, R., Luo, T., Sun, J., and Cao, A. (2017). Synthesis and self-assembly of diblock glycopolypeptide analogues PMAgala-b-PBLG as multifunctional biomaterials for protein recognition, drug delivery and hepatoma cell targeting. *Polym. Chem.* 8, 472–484. doi: 10.1039/C6PY01526C

Wei, H., Zhuo, R.-X., and Zhang, X.-Z. (2013). Design and development of polymeric micelles with cleavable links for intracellular drug delivery. *Prog. Polym. Sci.* 38, 503–535. doi: 10.1016/j.progpolymsci.2012.07.002

Zhang, X., Huang, Y., Zhao, W., Chen, Y., Zhang, P., Li, J., et al. (2014). PEG-farnesyl thiosalicylic acid telodendrimer micelles as an improved formulation for targeted delivery of paclitaxel. *Mol. Pharm.* 11, 2807–2814. doi: 10.1021/mp500181x

Zhao, M., Huang, Y., Chen, Y., Xu, J., Li, S., and Guo, X. (2016). PEG-fmoc-ibuprofen conjugate as a dual functional nanomicellar carrier for paclitaxel. *Bioconjug. Chem.* 27, 2198–2205. doi: 10.1021/acs.bioconjchem.6b00415

Conflict of Interest Statement: The authors declare that the research was conducted in the absence of any commercial or financial relationships that could be construed as a potential conflict of interest.

frontiers in Oncology

ORIGINAL RESEARCH
published: 25 September 2018
doi: 10.3389/fonc.2018.00354

pH-Responsive Cross-Linked Low Molecular Weight Polyethylenimine as an Efficient Gene Vector for Delivery of Plasmid DNA Encoding Anti-VEGF-shRNA for Tumor Treatment

Xiaoming Li[1], Xiaoshuang Guo[1], Yuan Cheng[1], Xiaotian Zhao[1], Zhiwei Fang[1], Yanli Luo[2], Shujun Xia[3], Yun Feng[4], Jianjun Chen[5]* and Wei-En Yuan[1]**

[1] Engineering Research Center of Cell and Therapeutic Antibody, Ministry of Education, School of Pharmacy, Shanghai Jiao Tong University, Shanghai, China, [2] Department of Pathology, Shanghai Jiao Tong University Affiliated Sixth People's Hospital, Shanghai, China, [3] Department of Ultrasound, Rui Jin Hospital Shanghai Jiao Tong University School of Medicine, Shanghai, China, [4] Department of Respiration, Institute of Respiratory Diseases, School of Medicine, Ruijin Hospital, Shanghai Jiao Tong University, Shanghai, China, [5] Guangdong Provincial Key Laboratory of New Drug Screening, School of Pharmaceutical Sciences, Southern Medical University, Guangzhou, China

OPEN ACCESS

Edited by:
Qingxin Mu,
University of Washington,
United States

Reviewed by:
Ling Wu,
Wayne State University School of Medicine, United States
Mikhail Durymanov,
South Dakota State University,
United States

***Correspondence:**
Yanli Luo
luoyanli2000@163.com
Jianjun Chen
jchen21@smu.edu.cn
Wei-En Yuan
yuanweien@sjtu.edu.cn

Specialty section:
This article was submitted to Cancer Molecular Targets and Therapeutics, a section of the journal Frontiers in Oncology

Received: 21 May 2018
Accepted: 10 August 2018
Published: 25 September 2018

Citation:
Li X, Guo X, Cheng Y, Zhao X, Fang Z, Luo Y, Xia S, Feng Y, Chen J and Yuan W-E (2018) pH-Responsive Cross-Linked Low Molecular Weight Polyethylenimine as an Efficient Gene Vector for Delivery of Plasmid DNA Encoding Anti-VEGF-shRNA for Tumor Treatment. Front. Oncol. 8:354. doi: 10.3389/fonc.2018.00354

RNA interference (RNAi) is a biological process through which gene expression can be inhibited by RNA molecules with high selectivity and specificity, providing a promising tool for tumor treatment. Two types of molecules are often applied to inactivate target gene expression: synthetic double stranded small interfering RNA (siRNA) and plasmid DNA encoding short hairpin RNA (shRNA). Vectors with high transfection efficiency and low toxicity are essential for the delivery of siRNA and shRNA. In this study, TDAPEI, the synthetic derivative of low-molecular-weight polyethylenimine (PEI), was cross-linked with imine bonds by the conjugation of branched PEI (1.8 kDa) and 2,5-thiophenedicarboxaldehyde (TDA). This biodegradable cationic polymer was utilized as the vector for the delivery of plasmid DNA expressing anti-VEGF-shRNA. Compared to PEI (25 kDa), TDAPEI had a better performance since experimental results suggest its higher transfection efficiency as well as lower toxicity both in cell and animal studies. TDAPEI did not stimulate innate immune response, which is a significant factor that should be considered in vector design for gene delivery. All the results suggested that TDAPEI delivering anti-VEGF-shRNA may provide a promising method for tumor treatment.

Keywords: nanoparticles, polyethylenimine, gene vector, anti-VEGF, tumor treatment

INTRODUCTION

Angiogenesis is an essential prerequisite for the growth and spread of tumors since abundant blood supply is needed to get adequate oxygen and other essential nutrients for tumors to grow rapidly (1, 2). Tumors often induce angiogenesis by secreting various growth factors such as vascular endothelial growth factor (VEGF) (3, 4). In many studies, over expression of VEGF has proven

to be a critical factor contributing to tumor angiogenesis (5, 6). Hence, the inhibition of VEGF expression has been a therapeutic strategy for tumor treatment.

RNA interference (RNAi) is a biological process through which gene expression can be inhibited by RNA molecules with high selectivity and specificity, providing a promising tool for tumor treatment (7–9). RNAi techniques overcome the disadvantages of chemotherapy (10), a traditional way for tumor treatment, in which normal cells and tumor cells cannot be distinguished effectively and chemotherapy is often with severe side effects (11, 12). Many studies have confirmed that RNAi can specifically silence cancer-related genes to inhibit tumor growth (13–15), angiogenesis (16–18), chemoresistance (19, 20) and metastasis (13, 21, 22).

Two types of molecules are often applied to inactivate the expression of target genes: synthetic double stranded small interfering RNA (siRNA) and plasmid DNA encoding short hairpin RNA (shRNA). For siRNA mediated RNAi, siRNA is delivered into the cytoplasm and then RNA-induced silencing complex (RISC) formed (23). After that, RISC binds to target mRNA by intermolecular expression of base pairing, contributing to cleavage and degradation of target mRNA (24). As for plasmid DNA encoding shRNA, it is transported into the cell nucleus for transcription of pre-shRNA. The formed pre-shRNA will be transported to the cytoplasm by exportin 5, processed by Dicer to form mature shRNA and loaded into RISC to play the role of gene silencing (25).

Efficacy of RNAi tumor treatments is partially dependent on the choice of gene vectors. Viral vectors are commonly employed for laboratory delivery of shRNA due to their high transfection efficiency. However, problems of immunogenicity and toxicity have limited their applications (26–28). In contrast, cationic polymers, a kind of non-viral vector, have no immunogenicity and are easier to be chemically modified for targeted gene delivery. However, the low transfection efficiency remains a problem to be solved for this system. In recent years, polycation vectors have been well studied by many researchers (29–31). Polyethyleneimine (PEI) is a kind of cationic polymer regarded as an effective transfection agent with high buffering effect due to the existence of protonated amine groups in the structure, which can enhance the "proton sponge effect" and accomplish the tasks of gene condensation, cellular uptake, endosome escape and release of therapeutic genes. The transfection efficiency and toxicity of PEI are positively correlated with molecular weight, so high transfection efficiency is accompanied by high toxicity (32, 33). To get a safe and efficient cationic polymer, a biodegradable PEI derivative named TDAPEI was synthesized by conjugating branched PEI 1.8 kDa with 2,5-thiophenedicarboxaldehyde (TDA). The formed imine bond is liable to be degraded in low pH environment theoretically, which could significantly lower the biological toxicity of polymers.

In our study, the cationic polymer TDAPEI was synthesized and characterized by fourier transform infrared spectroscopy (FTIR) and proton nuclear magnetic resonance (^{1}H NMR). We then further investigated the characteristics of TDAPEI/pDNA complexes, including condensation ability, particle size, zeta potential and morphology. Transfection efficiency, intracellular uptake, cytotoxicity and innate immune response were tested *in vitro*. We evaluated the therapeutic effect and *in vivo* toxicity in tumor bearing mice.

MATERIALS AND METHODS

Materials

Branched PEI (1.8 and 25 kDa), N,N-Dimethylformamide (DMF), agarose and dimethyl sulfoxide were acquired from Sigma-Aldrich (St Louis, MO, USA). 2,5-thiophenedicarboxaldehyde (TDA) was purchased from Meryer (Shanghai) Chemical Technology Co., Ltd. Dialysis bags made by cellulose membrane (MWCO = 10 kDa) were acquired from Thermo Fisher Scientific. A milli-Q instrument (Millipore) was used to purify water. Plasmid DNA expressing mouse-VEGF-shRNA and GFP was constructed by PHY-310 vector (Bioroot Biology, Shanghai, China). The single strain oligonucleotides sequence was 5′- GATCCGATGTGAATG CAGACCAAAGAATTCAAGAGATTCTTTGGTCTGCAT TCACATTTTTTTG-3′. Plasmid extraction kits were purchased from Bioteke Corporation. CT26.WT and SMMC7721 cells were purchased from the Cell Bank of Chinese Academy of Sciences (Shanghai, China). The complete medium for cells was composed of 90% Roswell Park Memorial Institute (RPMI) 1640 Medium (Media Tech, Herndon, VA, USA), 9% fetal bovine serum (FBS; HyClone, Logan, UT, USA) and 1% penicillin-streptomycin solution (Gibco, Grand Island, N.Y.). Cell Counting Kit-8 (CCK-8) was purchased from Dojindo Molecular Technologies, Inc. BALB/c mice were obtained from Shanghai Slac Laboratory Animal Co., Ltd.

Synthesis and Characterization of TDAPEI

The synthesis of TDAPEI was performed according to the process previously reported in our published paper (34–40). In brief, 1 mmol PEI (1.8 kDa) was added to 30 mL anhydrous DMF and stirred vigorously to be dissolved. 2 mmol TDA was dissolved in 30 mL anhydrous DMF and then dropwisely added to the PEI solution with vigorous stirring at room temperature for 24 h. The solvent was removed by reduced pressure rotary evaporation. The sticky residue was re-dissolved in deionized water. Dialysis bags made by cellulose membrane (MWCO = 10 kDa) were used to remove small fragments for another 48 h. The yellowish spongy product, TDAPEI, was obtained after 48 h of lyophilization. The final product was stored at −20°C for later use. The structure of TDAPEI was confirmed by fourier transform infrared spectroscopy (FTIR) and proton nuclear magnetic resonance (^{1}H NMR). The molecular weight of TDAPEI was determined by high performance size exclusion chromatography (SEC). A series of polyethylene glycol (PEG) standards were used for the standard curve and PEI 25k Da for calibration. The M_w and polydispersity index (PDI) were calculated by the software Agilent GPC-Addon. To assess the degradability, TDAPEI was dissolved in FORMIC buffer solutions of different pH values (pH = 7.4, 6.0, 5.0) respectively and incubated at 37°C for 72 h. The samples were collected at certain time points and the average molecule weight was determined by SEC. The three pH values were selected to

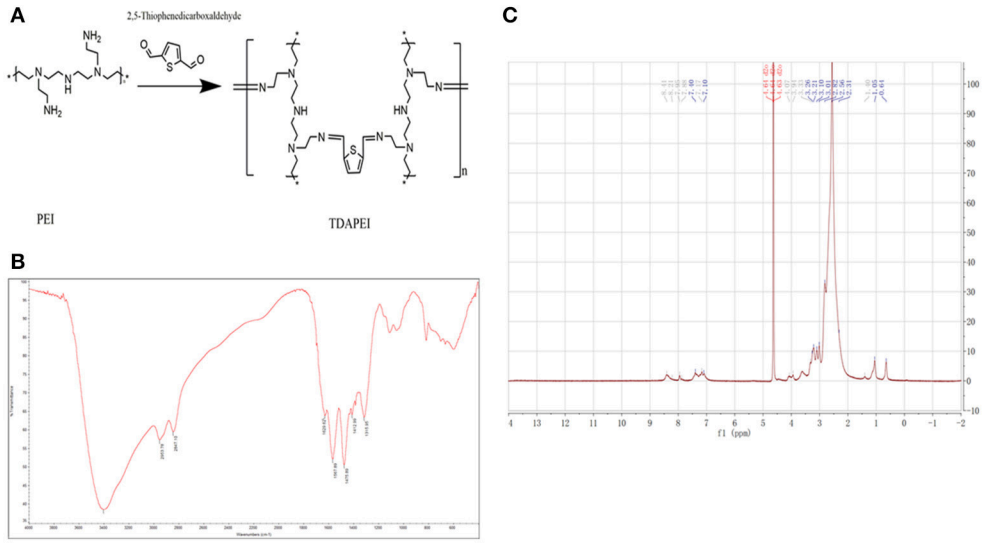

FIGURE 1 | Synthesis and characterization of TDAPEI. **(A)** Chemical structure and polymerization reaction of TDAPEI. **(B)** FTIR spectrum of TDAPEI. **(C)** ^{1}HNMR spectrum of TDAPEI.

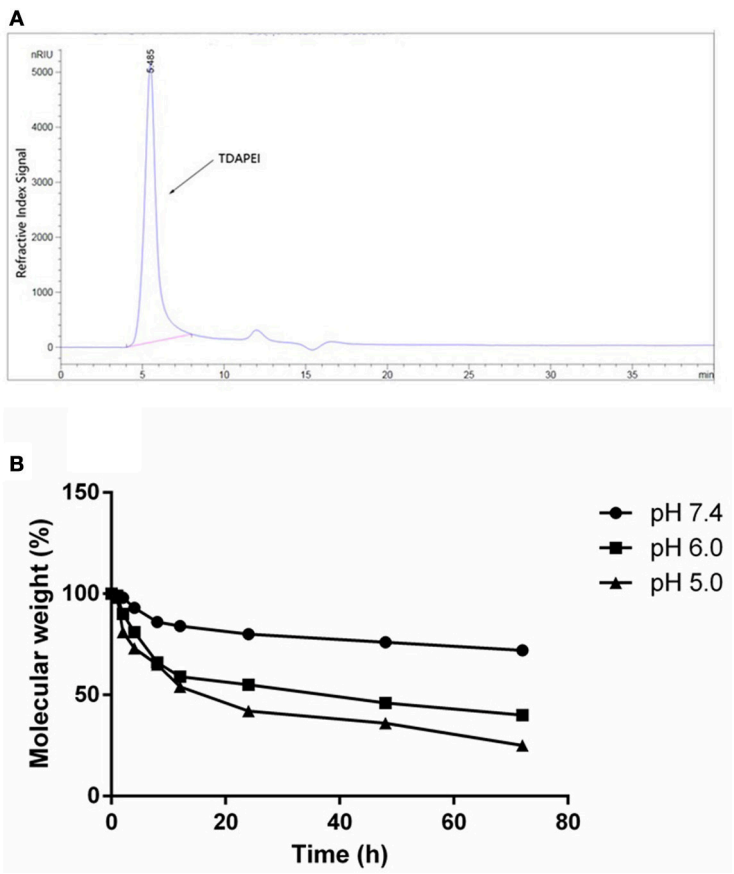

FIGURE 2 | (A) GPC spectrum of TDAPEI. **(B)** pH-responsive degradation of TDAPEI. TDAPEI was dissolved in FORMIC buffer solutions of different pH values (pH = 7.4, 6.0, 5.0) respectively and incubated at 37°C, followed by SEC tests. The molecular weights of the degraded polymers were determined as the weights measured by SEC test relative to the original molecular weight of TDAPEI (100%).

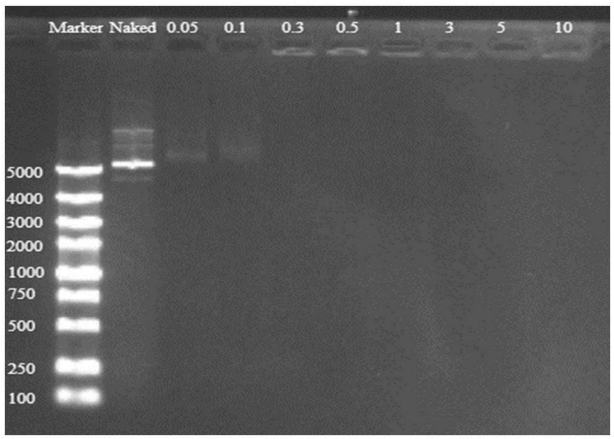

FIGURE 3 | TDAPEI/pDNA agarose gel electrophoresis. 100-5000bp marker was loaded in the first lane and naked DNA was in the second lane. The polyplexes were at 0.05, 0.1, 0.3, 0.5, 1, 3, 5, and 10 w/w ratios.

simulate the environment of blood plasma, endosomes and lysosomes, respectively.

Preparation of TDAPEI/pDNA Polyplexes

TDAPEI was dissolved in ultrapure water and diluted into 2 mg/mL. pDNA was diluted into 20 μg/mL as stock solutions. The TDAPEI/pDNA polyplexes were prepared in various weight/weight (w/w) ratios. The TDAPEI stock solution (2 mg/mL) was diluted into certain concentrations and added to pDNA stock solution (20 μg/mL). The mixture was thoroughly mixed by pipetting for 30 times and then incubated at room temperature for 30 min to obtain self-assembled polyplexes. PEI (25 kDa)/pDNA polyplexes at 2 w/w ratio were prepared with the same method, which is a classical positive control group in many gene delivery studies (34, 38, 41).

Agarose Gel Electrophoresis

Agarose gel electrophoresis was used to evaluate the stability of the TDAPEI/pDNA polyplexes. Polyplexes at various w/w ratios were respectively mixed with 6 × loading buffer containing GelRed (30 mM EDTA, 36% (v/v) Glycerol, 0.05% (w/v) Bromophenol Blue and 0.05%(w/v) Xylene Cyanol FF). Naked pDNA solution stained with GelRed was set as a negative control. Then these different mixtures were loaded into 1% (w/v) agarose gel. Electrophoresis was carried out with 1 × TAE running buffer at 110 V for 45 min. The stripes of DNA were visualized by UV transilluminator (Gel Imaging System, Tanon-3500).

Physicochemical Characterization of TDAPEI/pDNA Polyplexes

The particle size and polydispersity index (PDI) of the TDAPEI/pDNA polyplexes at various w/w ratios were determined by dynamic light scattering (90 Plus Particle Size Analyzer, Brookhaven Instruments Corporation, NY, USA) at room temperature. Zeta potential of polyplexes was measured at room temperature by Zetasizer Nano ZSP (Malvern Instruments, UK). All measurements were repeated for three times. Morphology of TDAPEI/pDNA polyplexes (w/w ratio = 10) was observed with a transmission electron microscope (JEOL JEM-2010 TEM) at an acceleration voltage of 200 kV.

In vitro Cell Transfection

Human hepatocarcinoma cells SMMC7721 and mouse colon adenocarcinoma cells CT 26.WT acquired from Cell Bank of the Chinese Academy of Sciences were used to determine *in vitro* cell transfection efficiency of TDAPEI/pDNA polyplexes. Cells were cultured in RPMI-1640 complete medium at 37°C in a 5% CO_2 moist atmosphere. Cells were digested by trypsin and diluted to 5–10 × 10^4/mL with RPMI-1640 complete medium. Then the cells were seeded in 48-well plates, with 500 μL dilute solution per well, and cultured for 24 h at 37°C in a 5% CO_2 moist atmosphere. The culture medium was removed and the cells were washed with PBS for three times. 250 μL RPMI-1640 medium and 50 μL polyplexes of various w/w ratios (the pDNA mass is 0.5 μg per well) were added into each well and the cells were incubated for 4 h. Meanwhile, naked pDNA was used as negative control and PEI (25 kDa)/pDNA polyplexes at 2 w/w ratio (optimal mass ratio) was prepared as positive control group, which is currently the gold standard for *in vitro* transfection. The culture medium was replaced by RPMI-1640 complete medium and incubated for another 44 h. Transfection efficiency is directly observed by fluorescence microscope (Olympus, Tokyo, Japan) and quantitatively measured by flow cytometry (BD FACSCalibur).

In vitro Expression of VEGF-A

The *in vitro* expression of VEGF-A was tested in CT26 cells. The cells were seeded in 48-well plates and incubated for 24 h at 37°C in a 5% CO2 moist atmosphere. Then, the cells were respectively treated with TDAPEI/pDNA polyplexes (w/w = 20), PEI (25 kDa)/pDNA polyplexes (w/w = 2), naked pDNA and PBS for 4 h. The culture medium was replaced by RPMI-1640 complete medium and incubated for another 44 h. The culture supernatant of cells was centrifuged and analyzed by Mouse VEGF-A ELISA kit (DKW12-2734-048) to determine the *in vitro* expression of VEGF-A.

In vitro Cytotoxicity

The *in vitro* cytotoxicity assay was conducted in SMMC7721 and CT26 cells by CCK-8 method. The two kinds of cells (1 × 10^4/well) were respectively seeded in 96-well plates and incubated for 24 h at 37°C in a 5% CO_2 moist atmosphere. The culture medium was removed and cells were washed by PBS for three times. 50 μL RPMI-1640 medium and 10 μL PBS (negative control), PEI (25 kDa)/pDNA polyplexes (positive control), and TDAPEI/pDNA complexes at various w/w ratios were respectively added into each well and the cells were incubated for 4 h. Then, 10 μL CCK-8 was added into each well. The plate was incubated in 37°C, 5% CO_2 incubator for 2 h. Auto Microplate Reader (Spectra Max M3 Multi- Mode) was used to read the absorption value under the wavelength of 450 and 630 nm. The percentage of cell viability was calculated as follow.

$$\text{Cell viability}(\%) = \frac{\text{Sample(OD450)-Sample(OD630)}}{\text{Normal cell(OD450)-Normal cell(OD630)}} \times 100\%$$

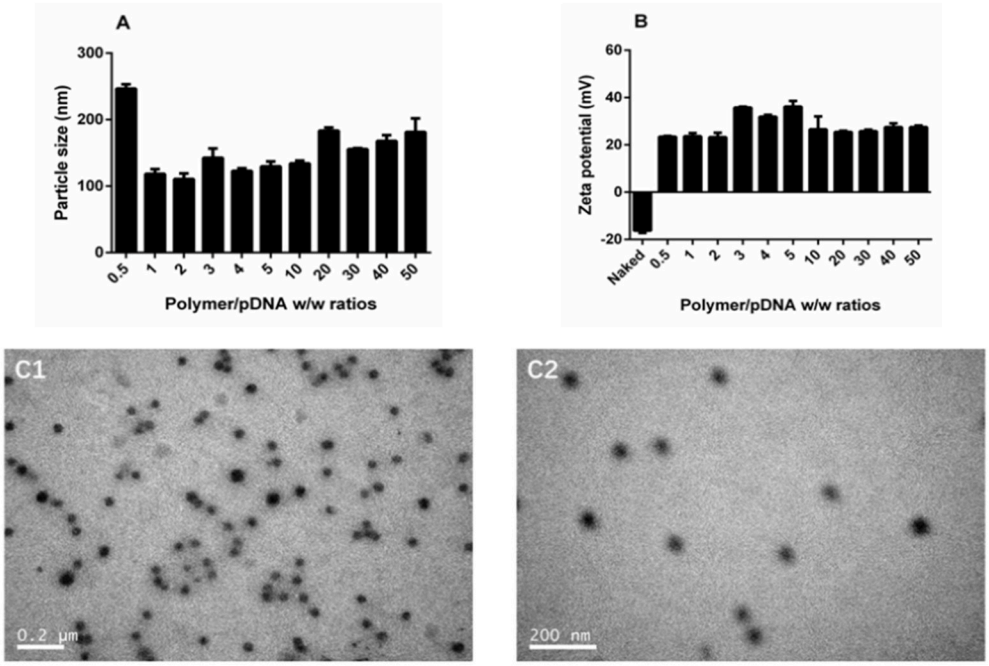

FIGURE 4 | Characterization of TDAPEI/pDNA complexes. Particle size **(A)** and Zeta potential **(B)** of TDAPEI/pDNA polyplexes at 0.5,1,2,3,4,5,10, 20, 30, 40, and 50 w/w ratios in water. **(C)** TEM images of polyplexes at w/w ratio of 10.

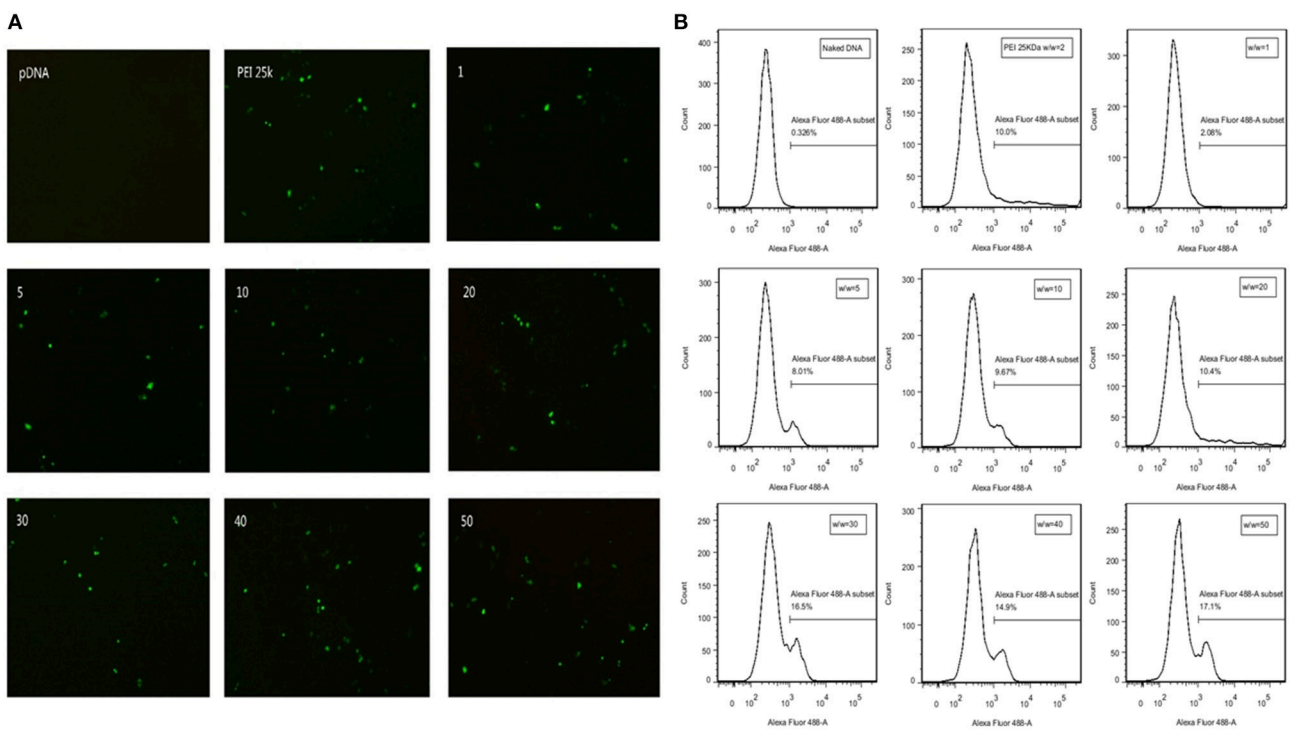

FIGURE 5 | (A) GFP expression in SMMC7721 cells transfected with naked pDNA, PEI 25k Da/pDNA (w/w ratio = 2), TDAPEI/pDNA complexes at w/w ratios of 1,5,10, 20, 30, 40, and 50. **(B)** Transfection efficiency in CT26 cells quantified by GFP-expressing cells using the flow cytometer.

Innate Immune Response Test

The innate immune response caused by TDAPEI/pDNA polyplexes was tested in murine macrophage RAW264.7 cells. The cells were cultured in Dulbecco's Modified Eagle Medium (DMEM) with 10% FBS and seeded on 6-well plates. When the cell density reached about 85%, the culture medium was replaced by fresh DMEM and cells were respectively treated with TDAPEI/pDNA polyplexes (w/w = 20), PEI (25 kDa)/pDNA polyplexes (w/w = 2) and naked pDNA for 4 h. Then, the polyplexes and pDNA were removed and the cells were incubated in DMEM with 10% FBS for another 24 h. The culture supernatant of cells was centrifuged and analyzed by Mouse IL-6 ELISA kit (DKW12-2060-096) and Mouse TNF-α ELISA kit (DKW12-2720-096).

In vivo Treatment in Tumor Model Mice

To assess the tumor treatment efficacy of TDAPEI/pDNA polyplexes, CT26 tumor model mice were established. The 5-week old female BALB/c mice, weighed 20 ± 2 g, were housed in Specific Pathogen Free (SPF) environment for 1 week before the animal study.

To establish *in vivo* tumor models, 0.1 ml CT26 cell suspension (5×10^6/ml) was subcutaneously injected to the mice at the right armpit. The mice were kept in SPF environment until the tumor volume reached about 200 mm^3. Then, the mice were divided into 4 groups randomly (6 mice in each group): blank group (saline), negative control group (naked pDNA), positive control group (PEI (25 kDa)/pDNA polyplexes) and experimental group (TDAPEI/pDNA polyplexes). The mice were treated by intra-tumor injection of 0.1 mL saline or therapeutic solutions containing 10 μg pDNA. The injection was given every 3 days. The shortest diameters (width, W) and longest diameters (length, L) of tumors were measured by vernier caliper to calculate the tumor volume. The formula is: $V = W^2 \times L/2$. At the 14th day after the first injection, the mice were sacrificed and the tumors were separated and analyzed.

Microvessel Quantification

To assess the anti-angiogenesis effect of the polyplexes, microvessel quantity was measured by CD31 immuno-histochemical staining. At the 14th day after the first injection, the separated tumors were fixed in 4% paraformaldehyde for 24 h and made into paraffin-embedded samples and then sectioned. The sections were stained with anti-CD31 antibody to mark microvessels. The sections were photographed by optical microscope and the images were analyzed by Image-Pro Plus software to get the number of positively stained microvessels.

In vivo Expression of VEGF-A

To identify the silence efficiency of polyplex in tumor tissue, we measured the concentration of expressed VEGF-A protein in tumor tissue homogenate at the 14th day after the first injection by using Mouse VEGF-A ELISA Kit (DKW12-2734-048).

In vivo Toxicity

Histological examination was adopted to demonstrate the toxicity of polyplexes to main organs. The organs were removed at the 14th day after the first injection and fixed in 4% paraformaldehyde. Hematoxylin and eosin (H&E) was used to stain organ sections and the slides were observed by optical microscope to observe the lesion.

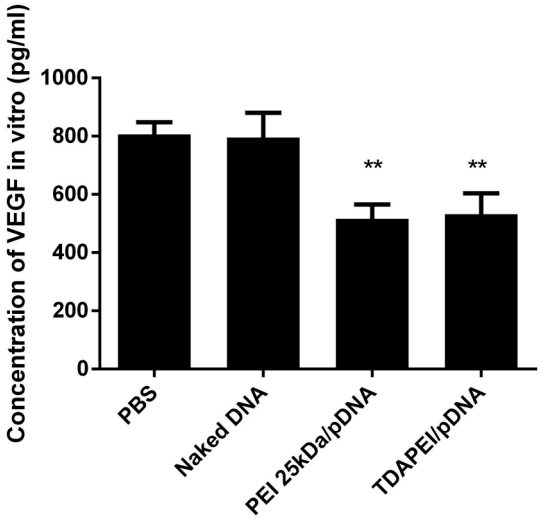

FIGURE 6 | *In vitro* expression of VEGF-A in CT26 cells treated with TDAPEI/pDNA polyplexes (w/w = 20), PEI (25 kDa)/pDNA polyplexes (w/w = 2), naked pDNA and PBS. Data were displayed as mean ± SD. ($n = 6$). $^{**}P < 0.01$.

Ethics Statement

All the experiments followed the Regulations for the Administration of Affairs Concerning Experimental Animals (China, 2014) and the National Institutes of Health Guide for Care and Use of Laboratory Animals (GB14925-2010). The Committee for Laboratory Animal Ethics of Shanghai Jiao Tong University approved the experiments.

Statistical Analysis

The data were presented as mean ± standard deviation of replicates. Analysis of variance (ANOVA) and independent samples *t*-test was performed and a value for $^{*}P < 0.05$, $^{**}P < 0.01$, and $^{***}P < 0.001$ was considered statistically significant.

RESULTS AND DISCUSSION

Synthesis and Characterization of TDAPEI

Results of FTIR and ^{1}H NMR of TDAPEI were shown in **Figure 1.** TDAPEI is formed by polymerization of branched PEI (1.8 kDa) and TDA through imine bonds (**Figure 1A**). Characteristic IR adsorption peak of imine bonds is at 1690-1590 cm^{-1} and a moderate adsorption peak at 1629.62 cm^{-1} was shown in the spectrum, which indicated that imine bonds were formed and the original aldehyde group (characteristic IR adsorption peak 1755-1665 cm^{-1}) disappeared (**Figure 1B**). The ^{1}H NMR spectrum of TDAPEI in D_2O was consistent with our expectation. Signal at δ = 7.96-8.41 ppm indicated the presence of methyne protons close to imino groups, while signal

at $\delta = 10$ ppm disappeared, which indicated that aldehyde group in TDA completely reacted with amino and formed imine bonds. The FTIR spectrum and ^{1}H NMR spectrum of TDAPEI were in consistent and confirmed the successful synthesis of TDAPEI.

The GPC spectrum of TDAPEI was shown in **Figure 2A.** M_w of polymer TDAPEI was calculated to be 23.2k Da, and the PDI was 1.65. As shown in **Figure 2B**, TDAPEI degraded at different rates in the three solutions with different pH values (pH=7.4, 6.0, 5.0). The degradation rate was relatively high in an acidic environment and the polymer remained stable in a neutral environment.

Agarose Gel Electrophoresis

Good binding and condensation ability is a prerequisite for a gene carrier to protect gene from degradation. To determine the ability of binding and condensing pDNA of TDAPEI and the stability of TDAPEI/pDNA polyplexes, agarose gel electrophoresis test was performed. TDAPEI/pDNA polyplexes at w/w ratios of 0.05, 0.1, 0.3, 0.5, 1, 3, 5, and 10 were chosen. As shown in **Figure 3**, with the increase of w/w ratio, the stripes of pDNA started to disappear at 0.3 w/w ratio, which indicated that the migration of pDNA in electric field was retarded in this case and pDNA was completely bound and wrapped by TDAPEI. A conclusion could be made that the polymer TDAPEI had a strong ability to condense pDNA into tight polyplexes to protect pDNA from nuclease.

Physicochemical Characterization of TDAPEI/pDNA Polyplexes

The DNA binding and condensing ability are closely related to the particle size and zeta potential of polyplexes, which also has significant impacts on cell endocytosis and gene transfection. The ideal particle size for cell endocytosis is about 20–200 nm. In our study, particle size of TDAPEI/pDNA complexes at various w/w ratios ranging from 0.5 to 50 were measured by 90 Plus Particle Size Analyzer. As is shown in **Figure 4A**, the particle size was 246.5 ± 6.7 nm at 0.5 w/w ratio. When the mass ratio increased to 10, the particle size of polyplexes decreased and reached a stable value around 130 nm, implying the tight pDNA condensation at this ratio. Theoretically, increased number of protons captured by the polymer enhanced the DNA binding and condensing ability of polymers. The DNA condensing ability was positively related to the surface charge density, so the particle size increased. On the other hand, higher concentration of TDAPEI caused a larger occupation in volume, which also contributed to the larger particle size. Particle sizes ranged from 110.5 to 183.4 nm and PDI were all lower than 0.3 (w/w ratio 1∼50), which indicated the polyplexes had a narrow dispersity and kept stable in this environment.

The zeta potential of polyplexes has an important effect on gene transfection efficiency and cytotoxicity. The surface of cell membrane is negatively charged, so it is difficult for naked DNA to cross cell membrane barrier. Particles with positive charge can cross cell membrane barrier but high cationic charge density may lead to the disruption of the cell membrane, which is responsible for the high cytotoxicity. As shown in **Figure 4B**, the zeta potential of polyplexes at different w/w ratios ranged from 23.2 to 36.1 mV and stabilized around 27 mV. The changing trend of zeta potential was in accordance with particle size and can be explained with similar reason. At low w/w ratios, more polymer brought higher positive charge density, resulting in the increase of zeta potential. Then the pH value rose, which in turn contributed to the decrease of positive charge. The result indicated that the disperse system was stable and implied the possibility for gene transfection.

The morphology of polyplexes at 10 w/w ratio observed by transmission electron microscopy is shown in **Figure 4C**. The polyplexes had uniform size and a spherical shape, which was in accordance with the results tested by Particle Size Analyzer.

In vitro Cell Transfection

GFP expression vector was constructed in our plasmid DNA. Cells successfully transfected by polyplexes could express GFP protein and thus emit fluorescence at wavelength of 488 nm. Transfection efficiency is directly observed by fluorescence microscope in SMMC7721 cells (**Figure 5A**) and quantitatively measured by flow cytometry in CT26 cells (**Figure 5B**). There is almost no fluorescence in the naked DNA group, which means naked DNA could not get into cells due to its instability and negative charge. Hence, positive charge of the polymer played an important role in entering the cells. At high w/w ratios, the transfection efficiency of TDAPEI/pDNA poplyplexes was comparable to or even higher than PEI (25 kDa)/pDNA polyplexes and no significant change in morphology of cells was observed in TDAPEI/pDNA poplyplexes treated groups. We believe the high transfection efficiency of these groups was owing to the better ability in releasing pDNA during the endosomal escape, as has been discussed in the previous study. Ur, et al. (42) High-molecular-weight PEI has a high density of positive charge, which is advantageous in crossing cell membrane barrier. However, after rupturing the endosomes through "proton sponge effect," it is more difficult for high-molecular-weight PEI to unbind pDNA than that with low molecular weight, such as PEI (1.8 kDa) used in our polymer design. Before entering the cells, TDAPEI was of high molecular weight, thus it provided comparable positive charge density to that of PEI (25 kDa). The advantage of our constructed polycation TDAPEI is that it could be degraded in low acidic medium. The imine linkages broken down and the polymer was metabolized into PEI (1.8 kDa) fragments. After that, the binding ability greatly weakened and it was easier for the polyplex to release pDNA, which led to higher transfection efficiency.

In vitro Expression of VEGF-A

The expression level of VEGF-A in CT26 cells was determined by ELISA. As shown in **Figure 6**, compared with PBS group and naked DNA group, the expression level of VEGF-A was significantly lower in TDAPEI/pDNA poplyplexes and PEI (25 kDa)/pDNA poplyplexes treated groups ($^{***}p < 0.001$, $^{**}p < 0.01$). TDAPEI/pDNA poplyplexes had equally excellent silence efficiency compared with PEI (25 kDa)/pDNA poplyplexes.

In vitro Cytotoxicity

In vitro cytotoxicity of TDAPEI/pDNA complexes in SMMC7721 and CT26 cells were evaluated by CCK-8 assay. As is shown

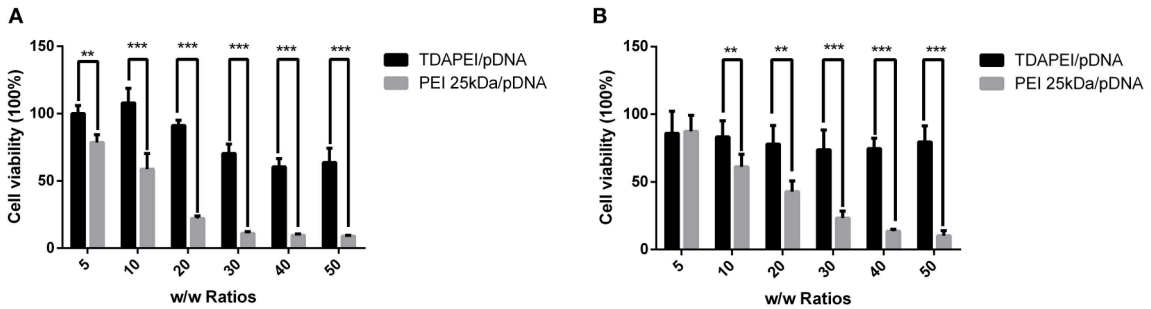

FIGURE 7 | Viability of SMMC **(A)** and CT26 cells **(B)** transfected by TDAPEI/pDNA complexes and PEI 25kDa/pDNA complexes at w/w ratios of 5, 10, 20, 30, 40, and 50. Data were displayed as mean ± SD. ($n = 6$). $^{**}P < 0.01$, $^{***}P < 0.001$.

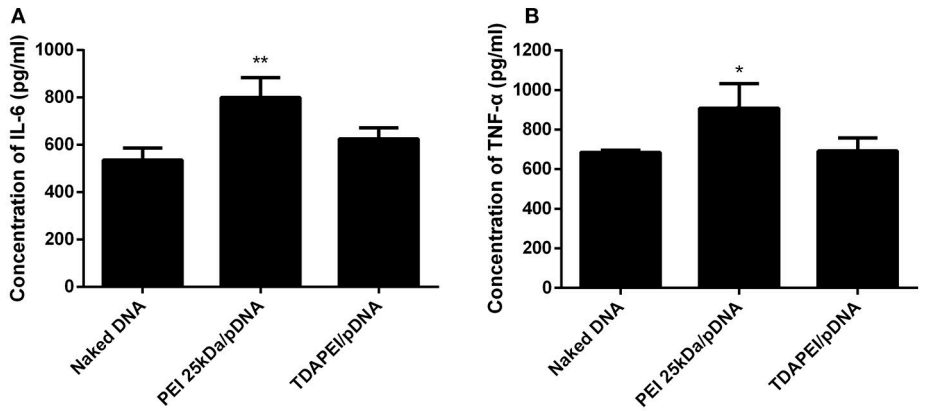

FIGURE 8 | The concentration of IL-6 **(A)** and TNF-α **(B)** secreted in the culture supernatant of murine macrophage RAW264.7 cells. Data were displayed as mean ± SD. ($n = 6$). $^{*}P < 0.05$, $^{**}P < 0.01$.

in **Figure 7**, the cell viability of TDAPEI/pDNA complexes in SMMC7721 cells was in the range from 107.98 to 60.47% at w/w ratios of 5, 10, 20, 30, 40, and 50, while that of PEI (25 kDa)/pDNA poplyplexes was from 78.62 to 8.98%. In CT26 cells, the cell viability of TDAPEI/pDNA and PEI (25 kDa)/pDNA polyplexes was from 85.93 to 73.85% and from 87.33 to 10.24%, respectively. In both cells, the cell viability of TDAPEI /pDNA is relatively stable while an apparent decline occurred in PEI (25 kDa)/pDNA poplyplexes group. There was a significant difference in cytotoxicity between TDAPEI/pDNA poplyplexes and PEI (25 kDa)/pDNA poplyplexes groups, especially at high w/w ratios ($^{***}p < 0.001$). The lower cytotoxicity of TDAPEI /pDNA could be explained by its biodegradable quality. Based on the results of *in vitro* cell transfection and cytotoxicity, we chose TDAPEI/pDNA poplyplexes at w/w ratio of 20 in the following animal study.

Innate Immune Response Test

Innate immune response can stimulate the secretion of IL-6 and TNF-α. The level of innate immune response activated by our treatment was evaluated by the concentration of IL-6 and TNF-α in murine macrophage RAW264.7 cells. As is shown in **Figure 8**, for TDAPEI/pDNA poplyplexes group, the concentrations of IL-6 and TNF-α secreted in the culture supernatant of cells were similar to that in naked DNA group, while the concentrations in PEI 25 kDa group were significantly higher than that in naked DNA group (IL-6: $^{**}P < 0.01$; TNF-α: $^{*}P < 0.05$). The result indicated that TDAPEI/pDNA polyplexes (w/w = 20) had a low innate immune response. However, considering the significant heterogeneity of RAW264.7 cells used in this study, further *in vivo* experiments are needed to confirm this preliminary conclusion. We will testify this in future *in vivo* studies.

In vivo Anti-tumor Treatment

Plasmid DNA expressing mouse-VEGF-shRNA was used as the antiangiogenic agent in our anti-tumor study. TDAPEI/pDNA poplyplexes at 20 w/w ratio, PEI (25 kDa)/pDNA poplyplexes, naked pDNA and saline were intratumorally injected in four groups of tumor-bearing BALB/c mice. **Figure 9A** showed the tumor growth curves during the 14-day treatment period. In saline and naked DNA groups, the tumor grew rapidly and no statistical significance in final tumor volume was observed between these two groups ($p > 0.05$), which indicated that naked pDNA had hardly any therapeutic effect on tumor. In TDAPEI/pDNA poplyplexes and PEI (25 kDa)/pDNA

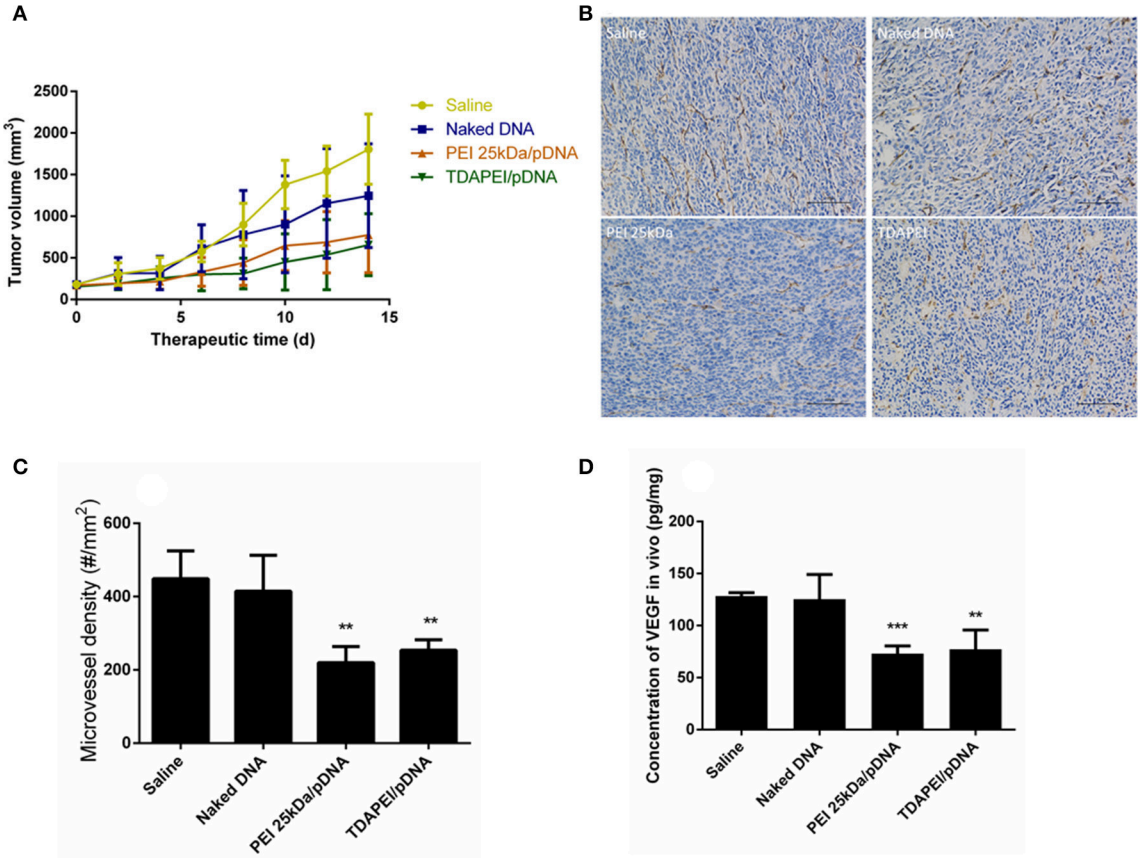

FIGURE 9 | (A) Tumor growth curves in CT26 tumor bearing mice treated by saline, naked DNA, PEI 25kDa and TDAPEI/pDNA. Data are displayed as mean ± SD, $n = 6$. $^{**}P < 0.01$. **(B)** Tumor section images of immunohistochemical staining for CD31 in saline, naked DNA, PEI 25kDa and TDAPEI groups. **(C)** Microvessel density in CT26 tumor bearing mice treated by saline, naked DNA, PEI 25kDa and TDAPEI/pDNA at Day 14. Data are displayed as mean ± SD, $n = 6$. $^{**}P < 0.01$. **(D)** *in vivo* concentration of expressed VEGF-A protein in tumor tissue homogenate at Day 14. Data are displayed as mean ± SD, n = 6. $^{**}P < 0.01$.

poplyplexes treated groups, the growth rates of tumors were similarly low. There existed significant differences for these two groups in final tumor volume compared to that in saline group (TDAPEI: $^{***}p < 0.001$; PEI 25 kDa: $^{**}p < 0.01$). Besides, when evaluating the anti-tumor effect of polyplexes *in vivo*, the cytotoxicity of gene vector of polyplexes should be considered as well, which may be a potentially additional contributor to the anti-VEGF therapy. In this case, the more toxic the gene vectors are, the more anti-tumor effects of polyplexes are observed. It is possible that the cytotoxicity of PEI (25 kDa) in this study may finally contribute to the tumor treatment. The final tumor volumes of the four groups were listed as follows: 1,805 ± 171.7 mm^3 in saline group; 1,247 ± 254.3 mm^3 in naked pDNA group; 775.7 ± 185.6 mm^3 in TDAPEI/pDNA poplyplexes group and 657.6 ± 151.9 mm^3 in PEI (25 kDa)/pDNA poplyplexes group.

To quantitatively evaluate the antiangiogenic effect, tumors were taken out at the last day of treatment period and CD31 immuno-histochemical staining was conducted to determine the number of endothelial cells. The figures of slices were analyzed by Image-Pro Plus. As shown in **Figures 9B,C,** the microvessel densities in groups of saline, naked pDNA, TDAPEI/pDNA poplyplexes and PEI (25 kDa)/pDNA poplyplexes were: 414.5 ± 40.20/mm^3, 448.5 ± 31.08/mm^3, 253.8 ± 11.63/mm^3, 219.5 ± 18.11/mm^3. The quantity of microvessels in PEI (25 kDa) and TDAPEI group was significantly lower than that in saline group ($^{**}p < 0.01$). There was no significant difference between PEI (25 kDa) and TDAPEI groups.

To assess the *in vivo* silence efficiency of the poplyplexes, the concentration of expressed VEGF-A protein in tumor tissue homogenate at the 14th day after the first injection was measured by ELISA. As shown in **Figure 9D**, the expression level of VEGF-A was significantly lower in TDAPEI and PEI (25 kDa groups ($^{**}p < 0.01$) and there was no significant difference between PEI (25 kDa) and TDAPEI groups.

The results indicated that both in TDAPEI and PEI (25 kDa) groups, tumor cells were successfully transfected and VEGF shRNA was transcribed (**Figures 6**, **9**). Then siRNA was produced by Dicer, which inhibited VEGF expression and played the important role of anti-angiogenesis (34). The

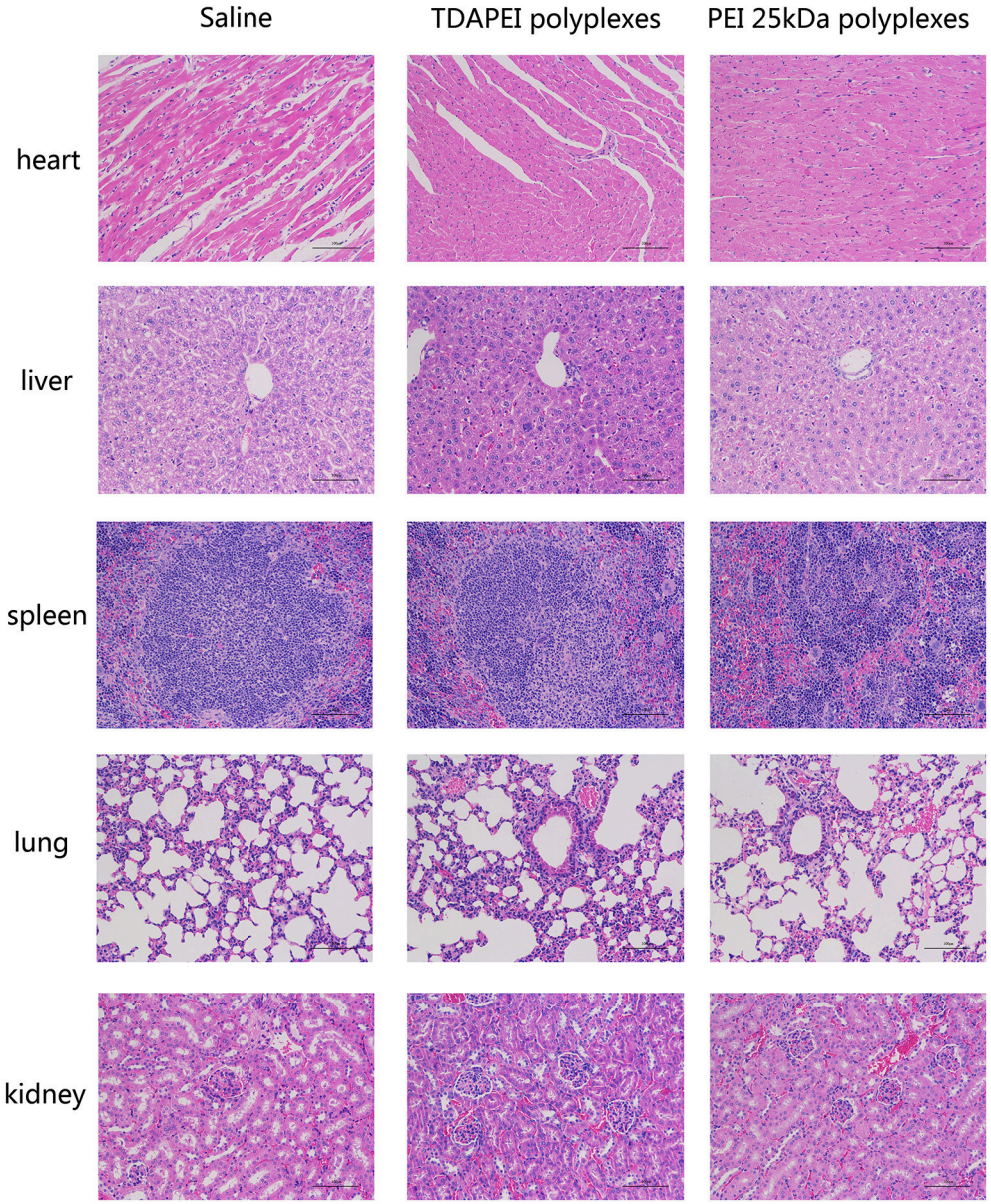

FIGURE 10 | In vivo toxicity to main organs in saline, TDAPEI and PEI 25kDa groups measured by frozen section at Day 14. The organ sections were stained with hematoxylin and eosin (H&E).

growth rate of the tumor decreased due to the lack of oxygen and nutrition (34). The *in vivo* transfection efficiency of TDAPEI group was similar to that in PEI (25 kDa) group.

Histological examination was adopted to demonstrate the toxicity of the polyplexes to organs *in vivo*. As is shown in **Figure 10**, almost no obvious lesion was observed in TDAPEI group compared to that in saline group, while in PEI (25 kDa) group, inflammation possibly occurred in the organs (34). A primary conclusion could be drawn that TDAPEI had negligible toxicity to the main organs.

CONCLUSION

In general, the biodegradable polycation TDAPEI showed great potential as a non-viral gene vector for tumor treatment. TDAPEI had strong ability to condense pDNA into tight polyplexes to protect pDNA from nuclease. Particle sizes ranged from 110.5 to 183.4 nm and the zeta potential stabilized at about 27 mV, which was suitable for endocytosis. Compared to PEI (25 kDa), TDAPEI had a better performance both in cell and animal studies since the experimental results suggest its high transfection efficiency as well as significantly low toxicity. We believe it is owing to our design strategy that TDAPEI is

biodegradable in low acidic medium and could be metabolized into low-molecular-weight PEI fragments, which was of low toxicity and could be eliminated by cells. All results in this article suggested that TDAPEI delivering plasmid DNA encoding anti-VEGF-shRNA may provide a promising method for tumor treatment.

AUTHOR CONTRIBUTIONS

W-EY conceived the initial idea, the conceptualization, and the study design, and participated in the data extraction and analysis. YL, JC, and W-EY revised the manuscript. XL, XG, YC, XZ, ZF, YL, and JC and participated in the study design, searched databases, extracted and assessed studies and helped draft the manuscript. XL wrote the manuscript. All authors have read and approved the final manuscript.

FUNDING

The study was supported by the Projects of National Science Foundation of China (No. 81570992, and 81602099), SUMHS seed foundation project (No. HMSF-16-21-010), Science and Technology Development Foundation of Pudong New District, Shanghai, China (No. PKJ2016-Y55 and PWZxq2017-03). The study was also partly sponsored by the Interdisciplinary Program of Shanghai Jiao Tong University (No. YG2015MS06, YG2017MS22, YG2015QN12, YG2017MS64, YG2017QN56, and YG2016QN22), scientific research project of high level talents (No. C1034335) in Southern Medical University of China, and Thousand Youth Talents Program (No. C1080094) from the Organization Department of the CPC Central Committee. We appreciate the help from faculties of Instrumental Analysis Centre (IAC) of Shanghai Jiao Tong University.

REFERENCES

1. Mcdougall SR, Anderson AR, Chaplain MA. Mathematical modelling of dynamic adaptive tumour-induced angiogenesis: clinical implications and therapeutic targeting strategies. *J Theor Biol.* (2006) 241:564–89. doi: 10.1016/j.jtbi.2005.12.022
2. Spill F, Guerrero P, Alarcon T, Maini PK, Byrne HM. Mesoscopic and continuum modelling of angiogenesis. *J Mathematical Biol.* (2015) 70:485–532. doi: 10.1007/s00285-014-0771-1
3. Saharinen P, Eklund L, Pulkki K, Bono P, Alitalo K. VEGF and angiopoietin signaling in tumor angiogenesis and metastasis. *Trends Mol Med.* (2011) 17:347–62. doi: 10.1016/j.molmed.2011.01.015
4. Pradeep CR, Sunila ES, Kuttan G. Expression of vascular endothelial growth factor (VEGF) and VEGF receptors in tumor angiogenesis and malignancies. *Integr Cancer Therap.* (2015) 4:315. doi: 10.1177/1534735405282557
5. Murillas R. VEGF/VPF overexpression in skin of transgenic mice induces angiogenesis, vascular hyperpermeability and accelerated tumor development. *Oncogene* (1998) 17:303–11. doi: 10.1038/sj.onc.1201928
6. Song ZJ, Gong P, Wu YE. Relationship between the expression of iNOS,VEGF,tumor angiogenesis and gastric cancer. *World J Gastroenterol.* (2002) 8:591. doi: 10.3748/wjg.v8.i4.591
7. Ligtenberg MA, Coaña YPD, Shmushkovich T, Yoshimoto Y, Truxova I, Yang Y, et al. Self-delivering RNA interference targeting PD-1 improves tumor specific T cell functionality for adoptive cell therapy of malignant melanoma. *Mol Ther.* (2018) 26:1482–93. doi: 10.1016/j.ymthe.2018.04.015
8. Lozadadelgado EL, Grafalsruiz N, Vivasmejía PE. RNA interference for glioblastoma therapy: innovation ladder from the bench to clinical trials. *Life Sci.* (2017) 188:26–36. doi: 10.1016/j.lfs.2017.08.027
9. Zins K, Sioud M, Aharinejad S, Lucas T, Abraham D. Modulating the tumor microenvironment with RNA interference as a cancer treatment strategy. *Methods Mol Biol.* (2015) 1218:143. doi: 10.1007/978-1-4939-1538-5_9
10. Jian LI. Targeting BCRP/ABCG2 by RNA interference enhances the chemotherapy sensitivity of human colon cancer side population cells. *J Huazhong Univ Sci Technol.* (2017) 37:231–6. doi: 10.1007/s11596-017-1720-1
11. Mailliez A, Baldini C, Van JT, Servent V, Mallet Y, Bonneterre J. Nasal septum perforation: a side effect of bevacizumab chemotherapy in breast cancer patients. *Br J Cancer* (2010) 103:772–5. doi: 10.1038/sj.bjc.6605828
12. Thomay AA, Nagorney DM, Cohen SJ, Sigurdson ER, Truty MJ, Burtness B, et al. Modern chemotherapy mitigates adverse prognostic effect of regional nodal metastases in stage iv colorectal cancer. *J Gastrointest Surg.* (2014) 18:69–74. doi: 10.1007/s11605-013-2329-8
13. Chen Y, Xie D, Yin LW, Man CC, Yao H, Chan CY, et al. RNAi targeting EZH2 inhibits tumor growth and liver metastasis of pancreatic cancer *in vivo*. *Cancer Lett.* (2010) 297:109. doi: 10.1016/j.canlet.2010.05.003
14. Singh A, Boldinadamsky S, Thimmulappa RK, Rath SK, Ashush H, Coulter J, et al. RNAi mediated silencing of Nrf2 gene expression in non-small cell lung cancer inhibits tumor growth and increases efficacy of chemotherapy. *Cancer Res.* (2008) 68:7975–84. doi: 10.1158/0008-5472
15. Yu T, Wu Y, Huang Y, Yan C, Liu Y, Wang Z, et al. RNAi targeting CXCR4 inhibits tumor growth through inducing cell cycle arrest and apoptosis. *Mol Ther J Am Soc Gene Ther.* (2012) 20:398. doi: 10.1038/mt.2011.257
16. Lin J, Pang H, Guo X, Ding Y, Geng J, Zhang J, et al. Lentivirus-mediated RNAi silencing of VEGF inhibits angiogenesis and growth of renal cell carcinoma in a nude mouse xenograft model. *DNA Cell Biol.* (2015) 34:717. doi: 10.1089/dna.2015.2918
17. Tripathy S, Vinokour E, Mcmahon KM, Volpert OV, Thaxton CS. High density lipoprotein nanoparticles deliver rnai to endothelial cells to inhibit angiogenesis. *Part Syst Charact.* (2015) 31:1141–50. doi: 10.1002/ppsc.201400036
18. Xi HQ, Zhang KC, Li JY, Cui JX, Gao YH, Wei B, et al. RNAi-mediated inhibition of Lgr5 leads to decreased angiogenesis in gastric cancer. *Oncotarget* (2017) 8:31581–31591. doi: 10.18632/oncotarget.15770
19. You H, Jie J, Shu H, Yu B, Milito AD, Lozupone F, et al. Small interfering RNA targeting the subunit ATP6L of proton pump V-ATPase overcomes chemoresistance of breast cancer cells. *Cancer Lett.* (2009). 280:110–9. doi: 10.1016/j.canlet.2009.02.023
20. Wang H, Zhang SY, Wang S, Lu J, Wu W, Weng L, et al. REV3L confers chemoresistance to cisplatin in human gliomas: the potential of its RNAi for synergistic therapy. *Neuro Oncol.* (2009) 11:790–802. doi: 10.1215/15228517-2009-015
21. Byrne FL, Yang L, Phillips PA, Hansford LM, Fletcher JI, Ormandy CJ, et al. RNAi-mediated stathmin suppression reduces lung metastasis in an orthotopic neuroblastoma mouse model. *Oncogene* (2014) 33:882. doi: 10.1038/onc.2013.11
22. Zhou H, Tang Y, Liang X, Yang X, Yang J, Zhu G, et al. RNAi targeting urokinase-type plasminogen activator receptor inhibits metastasis and progression of oral squamous cell carcinoma *in vivo*. *Int J Cancer* (2009) 125:453–62. doi: 10.1002/ijc.24360
23. Provost P, Dishart D, Doucet J, Frendewey D, Samuelsson B, Rådmark O. Ribonuclease activity and RNA binding of recombinant human Dicer. *EMBO J.* (2002) 21:5864–74. doi: 10.1093/emboj/cdf578
24. Preall, Jonathan B, Sontheimer, Erik J. RNAi: RISC Gets Loaded. *Cell* (2005) 123:543–545. doi: 10.1016/j.cell.2005.11.006

25. Cullen BR. RNAi the natural way. *Nature Genetics* (2005) 37:1163–5. doi: 10.1038/ng1105-1163
26. Börner K, Niopek D, Cotugno G, Kaldenbach M, Pankert T, Willemsen J, et al. Robust RNAi enhancement via human Argonaute-2 overexpression from plasmids, viral vectors and cell lines. *Nucleic Acids Res.* (2013) 41:e199. doi: 10.1093/nar/gkt836
27. Cruz PE, Mueller C, Cossette TL, Golant A, Tang Q, Beattie SG, et al. *In vivo* post-transcriptional gene silencing of alpha-1 antitrypsin by adeno-associated virus vectors expressing siRNA. *Lab Invest.* (2007) 87:893–902. doi: 10.1038/labinvest.3700629
28. Hiller T, Röhrs V, Dehne E-M, Wagner A, Fechner H, Lauster R, et al. Study of viral vectors in a three-dimensional liver model repopulated with the human hepatocellular carcinoma cell line HepG2. *J Visual Exp.* (2016) 54633. doi: 10.3791/54633
29. Ewe A, Höbel S, Heine C, Merz L, Kallendrusch S, Bechmann I, et al. Optimized polyethylenimine (PEI)-based nanoparticles for siRNA delivery, analyzed *in vitro* and in an ex vivo tumor tissue slice culture model. *Drug Delivery Transl Res.* (2017) 7:206–16. doi: 10.1007/s13346-016-0306-y
30. Guan X, Guo Z, Wang T, Lin L, Chen J, Tian H, et al. A pH-responsive detachable peg shielding strategy for gene delivery system in cancer therapy. *Biomacromolecules* (2017). 18:1342–9. doi: 10.1021/acs.biomac.7b00080
31. Yang H, Che O, Chen S, Sun L, Ji AM. Silence of VEGFR2 expression mediated by PEI/siRNA complexes. *Yaoxue Xuebao* (2010) 45:576. doi: doi: 10.16438/j.0513-4870.2010.05.010
32. Akinc A, Thomas M, Klibanov AM, Langer R. Exploring polyethylenimine-mediated DNA transfection and the proton sponge hypothesis. *J Gene Med.* (2005) 7:657–63. doi: 10.1002/jgm.696
33. Godbey WT, Barry MA, Saggau P, Wu KK, Mikos AG. Poly(ethylenimine)-mediated transfection: a new paradigm for gene delivery. *J Biomed Mater Res B Appl Biomater.* (2015) 51:321–8. doi: 10.1002/1097-4636(20000905)51:3<321::AID-JBM5>3.0.CO;2-R
34. Che J, Tao A, Chen S, Li X, Yi Z, Yuan W. Biologically responsive carrier-mediated anti-angiogenesis shRNA delivery for tumor treatment. *Sci Rep.* (2016) 6:35661. doi: 10.1038/srep35661
35. Liu G, Fang Z, Yuan M, Li W, Yang Y, Jiang M, et al. Biodegradable carriers for delivery of VEGF plasmid DNA for the treatment of critical limb Ischemia. *Front Pharmacol.* (2017) 8:528. doi: 10.3389/fphar.2017.00528
36. Song J, Chen Y, Jiang S, Yang K, Li X, Zhao X, et al. Efficient and non-toxic biological response carrier delivering TNF-α shRNA for gene silencing in a murine model of rheumatoid arthritis. *Front Immunol.* (2016) 7:305. doi: 10.3389/fimmu.2016.00305
37. Song J, Li X, Li Y, Che J, Li X, Zhao X, et al. Biodegradable and biocompatible cationic polymer delivering microRNA-221/222 promotes nerve regeneration after sciatic nerve crush. *Int J Nanomed.* (2017) 12:4195–4208. doi: 10.2147/IJN.S132190
38. Duan S, Yuan W, Wu F, Jin T. Inside cover: polyspermine imidazole-4,5-imine, a chemically dynamic and biologically responsive carrier system for intracellular delivery of siRNA. *Angewandte Chemie* (2012) 51:7938–41. doi: 10.1002/anie.201201793
39. Ge X, Feng J, Chen S, Zhang C, Ouyang Y, Liu Z, et al. Biscarbamate cross-linked low molecular weight Polyethylenimine polycation as an efficient intracellular delivery cargo for cancer therapy. *J Nanobiotechnol.* (2014) 12:1–8. doi: 10.1186/1477-3155-12-13
40. Ge X, Zhang Q, Cai Y, Duan S, Chen S, Lv N, et al. PEG-PCL-DEX polymersome-protamine vector as an efficient gene delivery system via PEG-guided self-assembly. *Nanomedicine* (2014) 9:1193–1207. doi: 10.2217/nnm.13.83
41. Duan S, Ge X, Lu N, Wu F, and Yuan W, Jin T. Synthetic polyspermine imidazole-4, 5-amide as an efficient and cytotoxicity-free gene delivery system. *Int J Nanomed.* (2012) 7:3813–22. doi: 10.2147/IJN.S33101
42. Ur RZ, Hoekstra D, Zuhorn IS. Mechanism of polyplex- and lipoplex-mediated delivery of nucleic acids: real-time visualization of transient membrane destabilization without endosomal lysis. *ACS Nano* (2013) 7:3767–77. doi: 10.1021/nn3049494

Conflict of Interest Statement: The authors declare that the research was conducted in the absence of any commercial or financial relationships that could be construed as a potential conflict of interest.

frontiers in Oncology

PERSPECTIVE
published: 14 August 2018
doi: 10.3389/fonc.2018.00309

Not Only Redox: The Multifaceted Activity of Cerium Oxide Nanoparticles in Cancer Prevention and Therapy

Francesca Corsi[1], *Fanny Caputo*[1,2], *Enrico Traversa*[3]* *and Lina Ghibelli*[2]*

[1] Department of Chemical Science and Technologies, University of Rome Tor Vergata, Rome, Italy, [2] Department of Biology, University of Rome Tor Vergata, Rome, Italy, [3] School of Materials and Energy, University of Electronic Science and Technology of China, Sichuan, China

Much information is accumulating on the effect of cerium oxide nanoparticles (CNPs) as cell-protective agents, reducing oxidative stress through their unique ability of scavenging noxious reactive oxygen species *via* an energy-free, auto-regenerative redox cycle, where superoxides and peroxides are sequentially reduced exploiting the double valence (Ce^{3+}/Ce^{4+}) on nanoparticle surface. *In vitro* and *in vivo* studies consistently report that CNPs are responsible for attenuating and preventing almost any oxidative damage and pathology. Particularly, CNPs were found to exert strong anticancer activities, helping correcting the aberrant homeostasis of cancer microenvironment, normalizing stroma-epithelial communication, contrasting angiogenesis, and strengthening the immune response, leading to reduction of tumor mass *in vivo*. Since these homeostatic alterations are of an oxidative nature, their relief is generally attributed to CNPs redox activity. Other studies however reported that CNPs exert selective cytotoxic activity against cancer cells and sensitize cancer cells to chemotherapy- and radiotherapy-induced apoptosis: such effects are hardly the result of antioxidant activity, suggesting that CNPs exert such important anticancer effects through additional, non-redox mechanisms. Indeed, using Sm-doped CNPs devoid of redox activity, we could recently demonstrate that the radio-sensitizing effect of CNPs on human keratinocytes is independent from the redox switch. Mechanisms involving particle dissolution with release of toxic Ce^{4+} atoms, or differential inhibition of the catalase vs. SOD-mimetic activity with accumulation of H_2O_2 have been proposed, explaining such intriguing findings only partially. Much effort is urgently required to address the unconventional mechanisms of the non-redox bioactivity of CNPs, which may provide unexpected medicinal tools against cancer.

Keywords: cerium oxide nanoparticles, redox-independent, cancer treatment, cancer prevention, antioxidant, radio-protection, radio-sensitization, tumor microenvironment

OPEN ACCESS

Edited by:
Qingxin Mu,
University of Washington,
United States

Reviewed by:
Ashutosh Kumar,
Ahmedabad University, India
Gianni Ciofani,
Politecnico di Torino, Italy

***Correspondence:**
Enrico Traversa
traversa@uestc.edu.cn
Lina Ghibelli
ghibelli@uniroma2.it

Specialty section:
This article was submitted to Cancer Molecular Targets and Therapeutics, a section of the journal Frontiers in Oncology

Received: *28 June 2018*
Accepted: *23 July 2018*
Published: *14 August 2018*

Citation:
Corsi F, Caputo F, Traversa E and Ghibelli L (2018) Not Only Redox: The Multifaceted Activity of Cerium Oxide Nanoparticles in Cancer Prevention and Therapy. Front. Oncol. 8:309. doi: 10.3389/fonc.2018.00309

INTRODUCTION

Materials acquire peculiar activities at the nanoscale (1–100 nm), due to their increased reactive surface/bulk ratio with respect to larger structures: for example, gold, essentially inert in the bulk, becomes highly reactive in the form of nanoparticles, displaying catalytic activity (1). Industrial exploitation of nanomaterials allows unprecedented applications in almost every field,

including important biomedical applications. In addition to the well-recognized use of tailored nanostructures for drug delivery (2), nanomedicine can indeed exploit intrinsically bioactive nanoparticles as effective medicinal tools where, rather than being an inert platform, the material itself acts as the therapeutic agent (3, 4). In particular, in clinical cancer research, bioactive materials are emerging as a possible tool to overcome the intrinsic limitations of conventional anticancer therapies.

Cerium oxide nanoparticles (CNPs) are receiving much attention for their unusual antioxidant properties, promising to act as potent antioxidant and anticancer drugs. Cerium is a rare earth element belonging to the lanthanide series, possessing a stable cerium (IV) oxidation state that coexists with cerium (III). In the nanoparticle form, cerium oxide atoms form a cubic crystalline fluorite lattice structure where Ce^{3+}, and the compensating oxygen vacancies, localize at the nanoparticle surface (5). The double valence generates a redox couple responsible for a robust catalytic activity, widely exploited in industrial applications, including catalysis (6), UV screens (7), gas sensors (8), solar, and fuel cells (9, 10).

The medicinal appeal of CNPs is mainly due to their unprecedented auto-regenerative antioxidant activity, which can scavenge noxious reactive oxygen/nitrogen species (ROS/RNS) generated by exogenous or endogenous sources (11) by combining (i), a superoxide dismutase (SOD) mimetic activity, responsible for reducing superoxide or peroxynitrite to peroxide and nitrate (respectively) undergoing oxidation from Ce^{3+} to Ce^{4+} (12, 13), with (ii), a catalase mimetic activity, where Ce^{4+} is reduced back to Ce^{3+} by oxidizing hydrogen peroxide to molecular oxygen and water (14). Thus, CNPs undergo a complete, energy-free redox cycle, eliminating the most toxic ROS while regenerating the original redox status (15).

Here, we will review literature data reporting the cancer preventive and therapeutic potentials of CNPs. Intriguingly, they do not deal exclusively with antioxidant actions: non-redox activity of CNPs are indeed emerging, with mechanisms that still need to be understood, and that may provide CNPs with the potential to act as unconventional anticancer agents via multiple, unrelated mechanisms.

CANCER PREVENTING ACTIVITY OF CNPS

Cancer origin is mainly attributed to accumulation of mutation events, due to environmental mutagens including pollution and radiation, and endogenous disequilibria such as chronic inflammation. A main mediator of both is oxidative stress, thereby antioxidants, such as e.g., dietary vitamins, are precious sources of cancer preventing agents.

ROS-promoted damage is a major cause of cell and genetic alterations, and the basis of almost any pathology, including cancer (16); accordingly, much effort has been posed to identify antioxidant agents able to protect against oxidative stress and the related pathologies. However, no satisfactory antioxidant has been identified so far: the canonical molecular antioxidant proved being short-lasting and indiscriminate, eliminating also ROS acting as signaling molecules in many cellular pathways, thereby endangering the correct redox homeostasis and cell functioning.

In this scenario, CNPs act as long-lasting regulators of redox metabolism rather than simple scavengers, efficiently eliminating ROS only when required, thus preserving basal cell activities, proposing them as bio-compatible antioxidant tools (17).

In particular, CNPs were shown to exert a potent antioxidant action, preventing oxidative stress, cell damage and death by apoptosis (3, 15, 18). CNPs also affect the cellular consequences of oxidative imbalance, modulating the activity of redox-responding proteins, for example, inactivating the transcription factor NFκB (19) and the downstream signaling cascade, which are implicated in cancer genesis and progression. Thus, by scavenging ROS, CNPs may modulate many cellular signal transduction processes regulating stress response, cellular metabolism, proliferation and cell cycle checkpoints (20), and control homeostatic pathways, including those involved in cancer and other oxidative-related pathologies (21–26).

Intriguingly, other CNPs-dependent effects are reported, hardly compatible with antioxidant action. For instance, (27) reported in gastrointestinal epithelial cells the upregulation of SOD2 gene expression while exerting a ROS scavenging action, which is a paradoxical effect since antioxidant enzymes are generally downregulated by the presence of antioxidant agents. Again, (28) showed that CNPs can hydrolyze phosphate ester bonds in abiotic systems, potentially interacting with ATP and phosphorylated proteins also inside cells. Other effects involve particle dissolution in acidic environment with release of bioactive Ce^{4+} ions (29), or to differential sensitivity of the SOD-*vs*- catalase-mimetic activity to low pH (30), mainly dealing with induced toxicity, which can be exploited against cancer cells, as we will discuss later.

Radiotherapy and all diagnostic procedures involving X-rays pose serious risks for exposed individuals, causing direct and ROS-mediated toxicity; therefore, radio-protective agents, including antioxidants, ameliorate radiation-induced acute and delayed damage (4, 31). Preventing radiotherapy-induced death of healthy (i.e., non-cancer) cells is an important task; however, to avoid a paradoxical pro-mutagenic effect, efficient radio-protectors should not merely inhibit apoptosis, but also reduce genetic radiation damage. Importantly, CNPs strongly reduce UV-induced apoptosis and at the same time, they decrease DNA damage, accelerate repair, and abate mutagenesis (18), thus promising to be efficient and safe UV-protectors.

The antioxidant properties of CNPs have attracted attention as possible effective countermeasure against ionizing radiations. CNPs ability to protect tissues from radiation-induced damage was reported in many systems, for instance gastrointestinal epithelium, where CNPs act as direct ROS scavengers (27) or breast epithelial cells, where CNPs rescue almost 99% of normal irradiated cells: interestingly, no protection was provided to tumor cells (32). The reason for this very important selectivity was not investigated; conceivably, it may be linked to the differential toxicity toward cancer vs. normal cells, discussed below.

CNPS AS ANTICANCER THERAPEUTIC AGENTS

Relief of Tumor Microenvironment Malignant Features

Tissues are composed not only of epithelial (i.e., tissue specific) cells, but also of "accessory" components such as blood vessel (endothelial cells), stroma fibroblasts, extracellular matrix, and a range of active biomolecules produced by all cell types, creating a complex signal network responsible for tissue functioning and homeostasis. Cancer genesis and progression is caused by homeostatic errors occurring within the tumor microenvironment (33), related or not with genetic mutations, dealing with all components of the cancer tissue (34), and implying many alterations, including increased oxidative status. ROS play a major role in promoting the aberrant cancer homeostasis, favoring vicious communications between cancer cells and stroma, endothelium, and matrix, thus favoring tumor neo-angiogenesis, matrix degradation, and improper immune infiltrations (35). Hence, antioxidant therapy is considered as a mean to prevent and revert the alteration of tumor microenvironment: CNPs have raised much attention in this regard.

As a matter of fact, CNPs administration at the tumor site helps correcting cancer microenvironment homeostasis in animal models (36), effect attributed to restoration of a proper redox asset. In fact, CNPs act more efficiently than canonical antioxidants: for example, SOD (or catalase, or the combination of the two), whose activity is mimicked by CNPs, is not as effective, protecting in the initial steps of carcinogenesis but promoting progression in advanced stages (37, 38). This suggests that either CNPs antioxidant action is "better" than the enzymatic one, or that they may exert additional, non-redox effects. For instance, (39) showed that CNPs inhibited the migration and proliferation of gastric cancer cells by transactivating the box helicase 15 (DHX15) and its downstream MAPK signal pathway without affecting ROS levels. Therefore, when the role of CNPs in tumor microenvironment are mechanistically investigated, non-redox effects begin to emerge.

Stroma changes occurring during tumorigenesis include the trans-differentiation of fibroblasts into myofibroblasts, modulated by cytokines such as tumor transforming factor beta 1 (TGFβ1) released by tumor cells, implying an oxidative cascade (34). CNPs efficiently inhibit myofibroblast formation and localization at the tumor front, preventing promotion of tumor growth, and invasion (40); the effects were attributed to CNPs redox switch. However, also in this case, CNPs were shown to contrast myofibroblast formation without altering ROS level (41).

Promotion of endothelial cell proliferation, generating new blood vessels for feeding and sustaining tumor growth and invasion (35), occurs through redox-sensitive angiogenic growth factors, including vascular endothelial growth factors (VEGF), fibroblast growth factor (FGF), and their receptors (42). CNPs were shown to efficiently contrast angiogenesis in ovarian carcinoma mouse model (43), attenuating VEGF-mediated proliferation of human umbilical vein endothelial cells, and inhibiting VEGF-induced matrix metalloproteinase 2 activity, clearly inhibiting VEGF mediated downstream signaling.

These effects on tumor microenvironment seem not only circumstantial, rather possibly leading to the real control of tumor growth: indeed, many studies report that administration of CNPs in tumor-bearing mice causes tumor reduction (27, 36), which is a logical consequence of restoration of a more correct microenvironment.

Direct and Selective Killing of Cancer Cells

In light of CNPs antioxidant activity, usually resulting in protective effects against oxidant-promoted apoptosis (15, 18, 44), it is difficult to consider CNPs as cytotoxic agents able to kill cancer cells, as often proposed. Nevertheless, in some instances CNPs do act as pro-oxidant and pro-apoptotic agents. For instance, (36) reported that CNPs induced apoptosis on melanoma, but not on stroma cells; this is related to selective ROS production, leading to mitochondria dysfunction (45). The finding that CNPs exerted similar pro-apoptotic effects on other cancer cells (46), led to hypothesize a differential effect on normal vs. cancer cells, which was attributed to the increased acidification of cancer microenvironment, which would turn CNPs into toxic agents. It is known that at pH $\leq$ 4 the catalase, but not the SOD-mimetic activity of CNPs is inhibited (30), with consequent accumulation of H_2O_2, more toxic than superoxides: in these conditions, CNPs would act as pro-oxidants. Moreover, CNPs release toxic Ce^{4+} ions due to nanoparticle acidic dissolution at pH $\leq$ 4. Attributing CNPs anticancer effect to strong pH decrease is however nonsense: the tumor microenvironment is indeed more acidic than normal tissues due to the Warburg effect (47, 48), but only of a few decimals, and cannot reach pH 4: this would lead to immediate cell and tissue collapse. However, pH 4 is reached within lysosomes, intracellular organelles that increase in volume and activity in cancer cells (49). This may favor CNPs lysosomal localization (50), implying that CNPs dissolution and/or H_2O_2 accumulation may occur to a greater extent in cancer than in normal cells. However, (51) did not find any correlation between CNPs lysosomal localization and intracellular ROS modulation in human ovarian and colon cancer cells.

A literature survey reveals so many exceptions to the pseudo-rule of CNP-selective killing of cancer cells, with examples of cancer cells protection against induced apoptosis [e.g., (15, 52, 53)], and of normal cells killing [e.g., (54)], to question the universality of the selective cytotoxicity. Rather, the pro- or anti-apoptotic effect of CNPs may depend on individual cell sensitivities, independently of being normal or cancerous, possibly consisting of different lysosomal trafficking, favoring or not Ce^{4+} release or H_2O_2 accumulation. The cancer cell selective killing may be then an epiphenomenon, suggesting that CNPs anticancer effects rather rely on microenvironment control.

Radio-Sensitization

Beside surgery, radiotherapy with ionizing radiation remains the standard care for many advanced carcinomas, either alone or

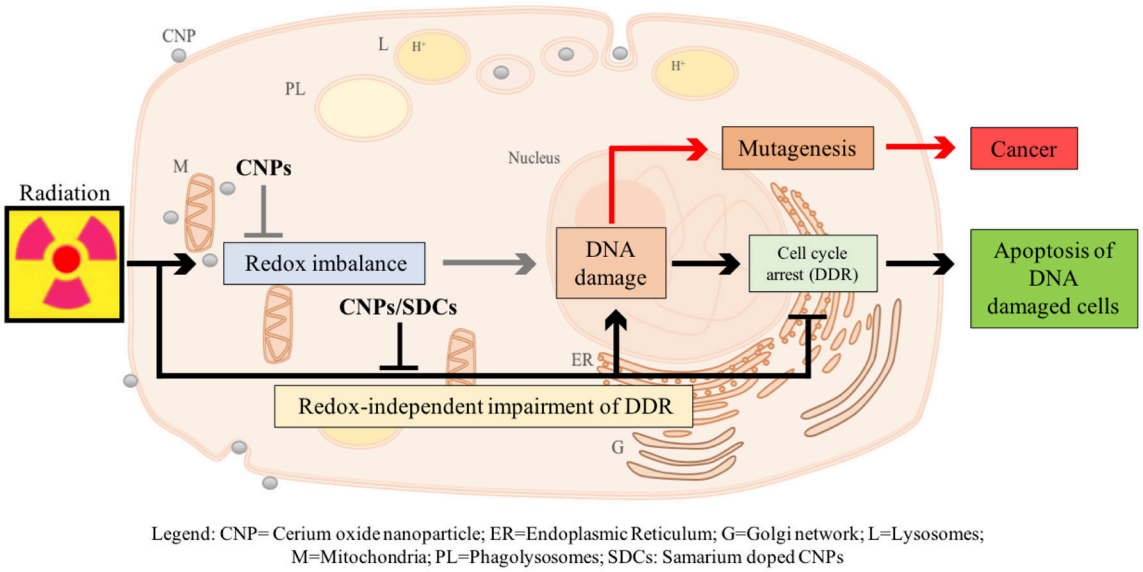

FIGURE 1 | Proposed model of action of CNPs as redox-independent radio-sensitizing agents in HaCat keratinocytes cells. CNPs administration may promote in a redox-independent fashion the strengthening of cell DNA damage response (DDR) after exposure to radiations, diminishing X-ray-induced DNA lesions on one side, and increasing the stringency of cell cycle checkpoints and forcing damaged cells to undergo apoptosis on the other, thus preventing radiation-induced mutagenesis.

in combination with other therapies; the rationale is promoting cell killing by apoptosis *via* direct radiation damage (i.e., promotion of double-strand DNA breaks) or through radiation-induced ROS (single-strand DNA breaks and protein and lipid peroxidation). Unfortunately, many tumor cells become radio-resistant as part of tumor progression, therefore it is necessary to use adjuvant treatments favoring radiation-induced cell death (55, 56). CNPs are potential radio-sensitizing agents acting through different strategies.

One strategy consists in enhancing radiation toxic effect at the tumor site: nanoparticles made of high atomic number materials, including CNPs, when irradiated with specific energy beams, emit ROS or heat, causing a "dose-enhancement effect" (4, 57, 58) leading to extra toxicity on cells present in the treated area. An additional effect was proposed for CNPs, where X-rays induce a pH-mediated dissolution in aqueous media, resulting in the release of the toxic Ce^{4+} ions (29).

Wason et al. (59) proposed a CNPs-dependent selective, acidic-mediated increase of radio-toxicity against cancer cells; however, it remains hard to hypothesize that pH levels ≤ 4 may be reached even in irradiated contexts.

CNPs-induced sensitization includes other cytotoxic treatments, *e.g.*, they enhance toxicity of doxorubicin, a DNA-damaging chemotherapeutic drug, on melanoma cells via ROS production (60).

We have recently described a radio-sensitization effect of CNPs, showing that they increase X-ray-induced apoptosis on HaCat keratinocytes, without affecting untreated cells (Caputo et al., submitted)[1]. However, this is not due to

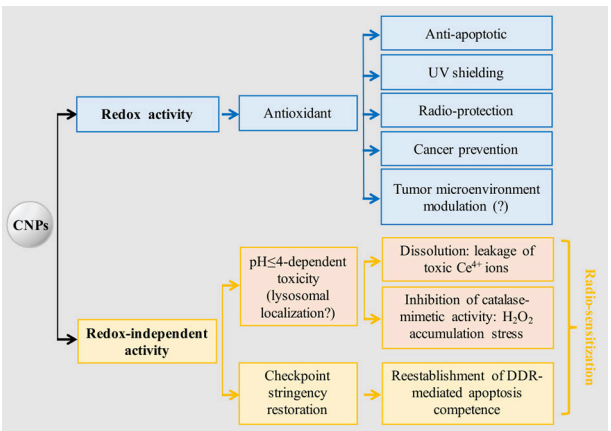

FIGURE 2 | CNPs main redox-dependent and independent biological effects. Tumor microenvironment modulation supposedly occurs via antioxidant effect, but no experimental evidence is available. It is hypothesized that acidic-induced toxicity occurs in lysosomes, being the only biological site where a suitable pH (≤ 4) is reached; however, no experimental evidence is available. Radio-sensitization may be achieved through toxic and non-toxic activation of the apoptotic program, the latter being selective for cancer cells possessing defective DNA integrity checkpoints. DDR, DNA damage response.

H_2O_2 accumulation: on the contrary, CNPs restore catalase activity destroyed by X-rays, preventing radiation-promoted ROS and DNA damage. Searching for a mechanism, we observed that CNPs, in spite of reducing DNA breaks, improved

[1]Caputo F, Giovannetti A, Corsi F, Maresca V, Briganti S, Licoccia S, et al. Cerium oxide nanoparticles re-establish cell integrity checkpoints and apoptosis competence in irradiated HaCat cells via novel redox-independent activity. *Front Pharmacol.* (2018).

the efficiency of the cell perception of/reaction to, DNA damage, increasing the apoptotic outcome *via* damage-unrelated mechanisms. In fact, CNPs restored DNA integrity checkpoints, generally lost in cancer cells, thereby almost abolishing X-ray-induced mutagenesis, by acting on the intimate pathways controlling survival of injured cancer cells. Intriguingly, this radio-sensitization is independent from CNPs redox switch because it was unaffected by Sm-doping, a strategy preventing the Ce^{3+}/Ce^{4+} switch and the correlated antioxidant action providing stable 3+ valence (15, 18) (**Figure 1**).

Overall, the abiotic dose-enhancement effect and the biological regulatory role of restoring cell integrity checkpoints seem very promising strategies to exploit CNPs as radio-sensitizing devices.

CONCLUSIONS

The survey we have presented here shows that combining CNPs with radiation or conventional chemotherapeutics may represent a novel anticancer strategy, helping re-modulating cancer microenvironment, killing tumor cells while sparing normal ones, thus improving the therapeutic outcome. So far, such appealing potentialities are limited to research aspects: is it conceivable that CNPs may turn into real therapeutic tools?

CNPs toxicity issues were abundantly investigated (3); overall, CNPs are considered biocompatible agents, rapidly cleared from organs (61) with very little toxicity (62, 63); in fact, CNPs play a substantial role as protectors against induced damage (64). However, the implications of nanoparticle-organism interactions in therapeutic perspectives are still a highly debated issue, generally considered a hazard, even though, pharmacologically, cell internalization of bioactive nanoparticles may provide an extra bonus, allowing persistence of the therapeutic effect for long time after the initial administration (65), avoiding the necessity of chronic treatments as required for molecular drugs, exerting only transient effects. Nevertheless, it is hard to foresee a rapid approval of CNPs clinical usage, apart perhaps for topic applications, apparently devoid of risk.

CNP abilities to act against different cancer features are diverse and occur through disparate mechanisms, making CNPs multifaceted, pleiotropic, and non-conventional anticancer tools. A very intriguing aspect is the multiple, un-related non-redox effects, spanning from leakage of toxic ions, to the paradoxical oxidative stress due to the differential inhibition of catalase-vs- SOD-mimetic activity, to the still ill-defined ability to restore cell-integrity checkpoints. In comparison, the antioxidant activity implying the self-regenerating redox state appears straightforward, explaining, in a univocal sense, antioxidant, anti-apoptotic, and environmental protective effects (**Figure 2**).

The fact that CNPs may affect cell survival in two opposite ways, reducing the extent of damage-induced apoptosis on one side, and promoting apoptosis restoring cell integrity checkpoints on the other, may at first appear paradoxical. However, it must be considered that apoptosis is not only the result of induced damage, but also a physiological response to supernumerary or dangerous cells, induced to die by purely signaling activities, e.g., *via* activation of the Fas/Fas ligand system (66), or p53 activation (67): apoptosis is thus a way to free the organism of possibly mutated cells. In this scenario, the two effects are not one the reverse of the other, but the result of two different, unrelated anticancer actions of CNPs. Cancer cells, as a rule, lose cell integrity check-points during tumor progression, thereby surviving and replicating in spite of DNA damage (68), increasing malignancy. Agents that restore the signaling responsible for checkpoints induction, can re-establish apoptosis competence without direct toxicity: therefore, CNPs are radio-sensitizers in the strictest sense. It will be important to uncover the mechanism of this intriguing effect and explore whether it can be at the basis also of the other examples of CNPs-dependent radio-sensitization reported.

Finally, it must be underscored that even if the effects mediated by CNPs (e.g., on cancer microenvironment) are apparently redox-mediated, this must be proven experimentally: cell signaling pathways are so much intersecting, that it is risky to attribute mechanisms *a priori*. The tool of inhibiting CNPs antioxidant activity by Sm doping is a straightforward way to simply address this point, and may help in unequivocally describing the mechanisms at the basis of the diverse anticancer activities of CNPs.

AUTHOR CONTRIBUTIONS

The elaboration of the concepts reported in this Perspective paper comes from the joint effort of FrC, FaC, ET, and LG. FrC and LG wrote the paper, which was discussed and approved by all authors.

ACKNOWLEDGMENTS

FrC and FaC are present and former students, respectively, of the Ph.D. school in Materials for Health, Environment and Energy, University of Rome Tor Vergata.

REFERENCES

1. Zhou X, Xu W, Liu G, Panda D, Chen P. Size-dependent catalytic activity and dynamics of gold nanoparticles at the single-molecule level. *JACS* (2010) 132:138–46. doi: 10.1021/ja904307n
2. Sharma B, Crist R, Adiseshaiah P. Nanotechnology as a delivery tool for precision cancer therapies. *AAPS J.* (2017) 19:1632–42. doi: 10.1208/s12248-017-0152-y
3. Celardo I, Pedersen J, Traversa E, Ghibelli L. Pharmacological potential of cerium oxide nanoparticles. *Nanoscale* (2011) 3:1411. doi: 10.1039/c0nr00875c
4. Caputo F, De Nicola M, Ghibelli L. Pharmacological potential of bioactive engineered nanomaterials. *Biochem Pharmacol.* (2014) 92:112–30. doi: 10.1016/j.bcp
5. Trovarelli A. Fornasiero, P. *Catalysis by Ceria and Related Materials*. London: Imperial College Press (2013).

6. Zheng X, Zhang X, Wang X, Wang S, Wu S. Preparation and characterization of CuO/CeO_2 catalysts and their applications in low-temperature CO oxidation. *Appl Catal A General* (2005) 295:142–9. doi: 10.1016/j.apcata.2005.07.048
7. Yamashita M, Kameyama K, Yabe S, Yoshida S, Fujishiro Y, Kawai T, et al. Synthesis and microstructure of calcia doped ceria as UV filters. *J Mater Sci.* (2002) 37:683–7. doi: 10.1023/A:1013819310041
8. Izu N, Shin W, Matsubara I, Murayama N. Development of resistive oxygen sensors based on cerium oxide thick film. *J Electroceram.* (2004) 13:703–6. doi: 10.1007/s10832-004-5179-7
9. Corma A, Atienzar P, García H, Chane-Ching J. Hierarchically mesostructured doped CeO_2 with potential for solar-cell use. *Nat Mater.* (2004) 3:394–7. doi: 10.1038/nmat1129
10. Murray E, Tsai T, Barnett S. A direct-methane fuel cell with a ceria-based anode. *Nature* (1999) 400:649–51. doi: 10.1038/23220
11. Schieber M, Chandel N. ROS function in redox signaling and oxidative stress. *Curr Biol.* (2014) 24:453–62. doi: 10.1016/j.cub.2014.03.034
12. Heckert E, Karakoti A, Seal S, Self W. The role of cerium redox state in the SOD mimetic activity of nanoceria. *Biomaterials* (2008) 29:2705–9. doi: 10.1016/j.biomaterials
13. Dowding J, Seal S, Self W. Cerium oxide nanoparticles accelerate the decay of peroxynitrite (ONOO–). *Drug Deliver Transl Res.* (2013) 3:375–9. doi: 10.1007/s13346-013-0136-0
14. Pirmohamed T, Dowding J, Singh S, Wasserman B, Heckert E, Karakoti A, et al. Nanoceria exhibit redox state-dependent catalase mimetic activity. *Chem Commun.* (2010) 46:2736. doi: 10.1039/b922024k
15. Celardo I, De Nicola M, Mandoli C, Pedersen J, Traversa E, Ghibelli L. Ce^{3+} Ions determine redox- dependent anti-apoptotic effect of cerium oxide nanoparticles. *ACS Nano* (2011) 5:4537–49. doi: 10.1021/nn200126a
16. Waris G, Ahsan H. Reactive oxygen species: role in the development of cancer and various chronic conditions. *J Carcinogen.* (2006) 5:14. doi: 10.1186/1477-3163-5-14
17. Brenneisen P, Reichert AS. Nanotherapy and reactive oxygen species (ROS) in cancer: a novel perspective. *Antioxidants* (2018) 7:31. doi: 10.3390/antiox7020031
18. Caputo F, De Nicola M, Sienkiewicz A, Giovanetti A, Bejarano I, Licoccia S, et al. Cerium oxide nanoparticles, combining antioxidant and UV shielding properties, prevent UV-induced cell damage and mutagenesis. *Nanoscale* (2015) 7:15643–56. doi: 10.1039/c5nr03767k
19. Niu J, Wang K, Kolattukudy P. Cerium Oxide nanoparticles inhibits oxidative stress and nuclear factor- B activation in H9c2 cardiomyocytes exposed to cigarette smoke extract. *J Pharmacol Exp Ther.* (2011) 338:53–61. doi: 10.1124/jpet.111.179978
20. Thai S, Wallace K, Jones C, Ren H, Grulke E, Castellon B, et al. Differential genomic effects of six different Tio_2nanomaterials on human liver HepG2 cells. *J Biochem Mol Toxicol.* (2015) 30:331–41. doi: 10.1002/jbt.21798
21. Walkey C, Das S, Seal S, Erlichman J, Heckman K, Ghibelli L, et al. Catalytic properties and biomedical applications of cerium oxide nanoparticles. *Environ Sci Nano* (2015) 2:33–53. doi: 10.1039/c4en00138a
22. D'Angelo B, Santucci S, Benedetti E, Di Loreto S, Phani R, Falone S, et al. cerium oxide nanoparticles trigger neuronal survival in a human alzheimer disease model by modulating BDNF pathway. *Curr Nanosci.* (2009) 5:167–76. doi: 10.2174/157341309788185523
23. Rzigalinski B, Carfagna C, Ehrich M. Cerium oxide nanoparticles in neuroprotection and considerations for efficacy and safety. *Wiley Interdisciplin Rev Nanomedi Nanobiotechnol.* (2016) 9:e1444. doi: 10.1002/wnan.1444
24. Niu J, Azfer A, Rogers L, Wang X, Kolattukudy P. Cardioprotective effects of cerium oxide nanoparticles in a transgenic murine model of cardiomyopathy. *Cardiovasc Res.* (2007) 73:549–59. doi: 10.1016/j.cardiores.2006.11.031
25. Pourkhalili N, Hosseini A, Nili-Ahmadabadi A, Hassani S, Pakzad M, Baeeri M, et al. Biochemical and cellular evidence of the benefit of a combination of cerium oxide nanoparticles and selenium to diabetic rats. *World J Diabetes* (2011) 2:204. doi: 10.4239/wjd.v2.i11.204
26. Hirst S, Karakoti A, Tyler R, Sriranganathan N, Seal S, Reilly C. Anti-inflammatory properties of cerium oxide nanoparticles. *Small* (2009) 5:2848–56. doi: 10.1002/smll.200901048
27. Colon J, Hsieh N, Ferguson A, Kupelian P, Seal S, Jenkins D, et al. Cerium oxide nanoparticles protect gastrointestinal epithelium from radiation-induced damage by reduction of reactive oxygen species and upregulation of superoxide dismutase 2. *Nanomedicine* (2010) 6:698–705. doi: 10.1016/j.nano.2010.01.010
28. Kuchma M, Komanski C, Colon J, Teblum A, Masunov A, Alvarado B, et al. Phosphate ester hydrolysis of biologically relevant molecules by cerium oxide nanoparticles. *Nanomedicine* (2010) 6:738–44. doi: 10.1016/j.nano.2010.05.004
29. Asghar M, Inkson B, Möbus, G. Giant radiolytic dissolution rates of aqueous ceria observed in situ by liquid-cell TEM. *ChemPhysChem* (2017) 18:1247–51. doi: 10.1002/cphc.201601398
30. Perez J, Asati A, Nath S, Kaittanis C. Synthesis of biocompatible dextran-coated nanoceria with ph-dependent antioxidant properties. *Small* (2008) 4:552–6. doi: 10.1002/smll.200700824
31. Patel VN, Gupta S, Shareef MM, Ahmed MM. Contemporary radiation countermeasures *Defen Sci J.* (2011) 61:138–45. doi: 10.14429/dsj.61.834
32. Tarnuzzer R, Colon J, Patil S, Seal S. Vacancy engineered ceria nanostructures for protection from radiation-induced cellular damage. *Nano Lett.* (2005) 5:2573–7. doi: 10.1021/nl052024f
33. Huang A, Cao S, Tang L. The tumor microenvironment and inflammatory breast cancer. *J Cancer* (2017) 8:1884–91. doi: 10.7150/jca.17595
34. De Wever O, Mareel M. Role of tissue stroma in cancer cell invasion. *J Pathol.* (2003) 200:429–47. doi: 10.1002/path.1398
35. Tertil M, Jozkowicz A, Dulak J. Oxidative stress in tumor angiogenesis - therapeutic targets. *Curr Pharm Design* (2010) 16:3877–94. doi: 10.2174/138161210794454969
36. Alili L, Sack M, von Montfort C, Giri S, Das S, Carroll K, et al. Downregulation of tumor growth and invasion by redox-active nanoparticles. *Antioxid Redox Signal.* (2013) 19:765–78. doi: 10.1089/ars.2012.4831
37. Dhar S, St. Clair D. Manganese superoxide dismutase regulation and cancer. *Free Radical Biol Med.* (2012) 52:2209–22. doi: 10.1016/j.freeradbiomed.2012.03.009
38. Kinnula V, Crapo J. Superoxide dismutases in malignant cells and human tumors. *Free Radical Biol Med.* (2004) 36:718–44. doi: 10.1016/j.freeradbiomed.2003.12.010
39. Xiao Y, Li J, Wang S, Yong X, Tang B, Jie M, et al. Cerium oxide nanoparticles inhibit the migration and proliferation of gastric cancer by increasing DHX15 expression. *Int J Nanomed.* (2016) 11:3023–34. doi: 10.2147/ijn.s103648
40. Alili L, Sack M, Karakoti A, Teuber S, Puschmann K, Hirst S, et al. Combined cytotoxic and anti-invasive properties of redox-active nanoparticles in tumor–stroma interactions. *Biomaterials* (2011) 32:2918–29. doi: 10.1016/j.biomaterials.2010.12.056
41. Sack-Zschauer M, Karaman-Aplak E, Wyrich C, Das S, Schubert T, Meyer H, et al. Efficacy of different compositions of cerium oxide nanoparticles in tumor-stroma interaction. *J Biomed Nanotechnol.* (2017) 13:1735–46. doi: 10.1166/jbn.2017.2452
42. Maulik N, Das D. Redox signaling in vascular angiogenesis. *Free Radical Biol Med.* (2002) 33:1047–60. doi: 10.1016/s0891-5849(02)01005-5
43. Giri S, Karakoti A, Graham R, Maguire J, Reilly C, Seal S, et al. Nanoceria: a rare-earth nanoparticle as a novel anti-angiogenic therapeutic agent in ovarian cancer. *PLoS ONE* (2013) 8:e54578. doi: 10.1371/journal.pone.0054578
44. Clark A, Zhu A, Sun K, Petty H. Cerium oxide and platinum nanoparticles protect cells from oxidant-mediated apoptosis. *J Nanopart Res.* (2011) 13:5547–55. doi: 10.1007/s11051-011-0544-3
45. Pezzini I, Marino A, Del Turco S, Nesti C, Doccini S, Cappello V, et al. Cerium oxide nanoparticles: the regenerative redox machine in bioenergetic imbalance. *Nanomedicine* (2017) 12:403–16. doi: 10.2217/nnm-2016-0342
46. Mittal S, Pandey A. Cerium oxide nanoparticles induced toxicity in human lung cells: role of ROS mediated DNA damage and apoptosis. *BioMed Res Int.* (2014) 2014:1–14. doi: 10.1155/2014/891934
47. Vander Heiden M, Cantley L, Thompson C. Understanding the warburg effect: the metabolic requirements of cell proliferation. *Science* (2009) 324:1029–33. doi: 10.1126/science.1160809
48. Mazzio EA, Boukli N, Rivera N, Soliman KF. Pericellular pH homeostasis is a primary function of the Warburg effect: inversion of metabolic systems

to control lactate steady state in tumor cells. *Cancer Sci.* (2012) 103:422–32. doi: 10.1111/j.1349-7006.2012.02206.x
49. Kirkegaard T, Jäättelä M. Lysosomal involvement in cell death and cancer. *Biochim Biophys Acta* (2009) 1793:746–54. doi: 10.1016/j.bbamcr
50. Lord M, Tsoi B, Gunawan C, Teoh W, Amal R, Whitelock J. Anti-angiogenic activity of heparin functionalised cerium oxide nanoparticles. *Biomaterials* (2013) 34:8808–18. doi: 10.1016/j.biomaterials.2013.07.083
51. Vassie J, Whitelock J, Lord M. Endocytosis of cerium oxide nanoparticles and modulation of reactive oxygen species in human ovarian and colon cancer cells. *Acta Biomater.* (2017) 50:127–41. doi: 10.1016/j.actbio.2016.12.010
52. Rubio L, Marcos R, Hernández A. Nanoceria acts as antioxidant in tumoral and transformed cells. *Chem Biol Interact.* (2018) 291:7–15. doi: 10.1016/j.cbi.2018.06.002
53. González-Flores D, De Nicola M, Bruni E, Caputo F, Rodríguez AB, Pariente JA, et al. Nanoceria protects from alterations in oxidative metabolism and calcium overloads induced by TNFα and cycloheximide in U937 cells: pharmacological potential of nanoparticles. *Mol Cell Biochem.* (2014) 397:245–53. doi: 10.1007/s11010-014-2192-2.
54. Park E, Choi J, Park Y, Park K. Oxidative stress induced by cerium oxide nanoparticles in cultured BEAS-2B cells. *Toxicology* (2008) 245:90–100. doi: 10.1016/j.tox.2007.12.022
55. Nakata E, Mason K, Hunter N, Husain A, Raju U, Liao Z, et al. Potentiation of tumor response to radiation or chemoradiation by selective cyclooxygenase-2 enzyme inhibitors. *Int J Radiat Oncol Biol Phys.* (2004) 58:369–75. doi: 10.1016/j.ijrobp.2003.09.061
56. Milas L. Cyclooxygenase-2 (COX-2) enzyme inhibitors as potential enhancers of tumor radioresponse. *Seminars Radiat Oncol.* (2001) 11:290–9. doi: 10.1053/srao.2001.26018
57. Misawa M, Takahashi J. Generation of reactive oxygen species induced by gold nanoparticles under x-ray and UV Irradiations. *Nanomedicine* (2011) 7:604–14. doi: 10.1016/j.nano.2011.01.014
58. Hainfeld J, Dilmanian F, Slatkin D, Smilowitz H. Radiotherapy enhancement with gold nanoparticles. *J Pharm Pharmacol.* (2008) 60:977–85. doi: 10.1211/jpp.60.8.0005
59. Wason M, Colon J, Das S, Seal S, Turkson J, Zhao J, et al. Sensitization of pancreatic cancer cells to radiation by cerium oxide nanoparticle-induced ROS production. *Nanomedicine* (2013) 9:558–69. doi: 10.1016/j.nano.2012.10.010
60. Sack M, Alili L, Karaman E, Das S, Gupta A, Seal S, et al. Combination of conventional chemotherapeutics with redox-active cerium oxide nanoparticles–a novel aspect in cancer therapy. *Mol Cancer Therapeut.* (2014) 13:1740–9. doi: 10.1158/1535-7163.mct-13-0950
61. Heckman KL, DeCoteau W, Estevez A, Reed KJ, Costanzo W, Sanford D, et al. Custom cerium oxide nanoparticles protect against a free radical mediated autoimmune degenerative disease in the brain. *JSACS Nano* (2013) 7:10582–96. doi: 10.1021/nn403743b
62. Gao Y, Gao F, Chen K, Ma J. Cerium oxide nanoparticles in cancer. *OncoTargets Ther.* (2014) 7:835–40. doi: 10.2147/ott.s62057
63. Wang Y, Yang F, Zhang H, Zi X, Pan X, Chen F, et al. Cuprous oxide nanoparticles inhibit the growth and metastasis of melanoma by targeting mitochondria. *Cell Death Dis.* (2013) 4:e783. doi: 10.1038/cddis.2013.314
64. Azari A, Shokrzadeh M, Zamani E, Amani N, Shaki F. Cerium oxide nanoparticles protects against acrylamide induced toxicity in HepG2 cells through modulation of oxidative stress. *Drug Chem Toxicol.* (2018) 6:1–6. doi: 10.1080/01480545.2018.1477793
65. Pagliari F, Mandoli C, Forte G, Magnani E, Pagliari S, Nardone G, et al. Cerium oxide nanoparticles protect cardiac progenitor cells from oxidative stress. *ACS Nano* (2012) 6:3767–75. doi: 10.1021/nn2048069
66. Nagata S. Fas ligand-induced apoptosis. *Annu Rev Genet.* (1999) 33:29–55.
67. Chipuk JE, Kuwana T, Bouchier-Hayes L, Droin NM, Newmeyer DD, Schuler M, et al. Direct activation of Bax by p53 mediates mitochondrial membrane permeabilization and apoptosis. *Science* (2004) 303:1010–4. doi: 10.1126/science.1092734
68. Caputo F, Vegliante R, Ghibelli L. Redox modulation of the DNA damage response. *Biochem Pharmacol.* (2012) 84:1292–306. doi: 10.1016/j.bcp.2012.07.022

Conflict of Interest Statement: The authors declare that the research was conducted in the absence of any commercial or financial relationships that could be construed as a potential conflict of interest.

frontiers in Oncology

REVIEW
published: 25 September 2018
doi: 10.3389/fonc.2018.00404

Interactions Between Nanoparticles and Dendritic Cells: From the Perspective of Cancer Immunotherapy

Jianbo Jia[1], Yi Zhang[2], Yan Xin[2], Cuijuan Jiang[3], Bing Yan[1,3] and Shumei Zhai[2]**

[1] *Key Laboratory for Water Quality and Conservation of the Pearl River Delta, Ministry of Education, Institute of Environmental Research at Greater Bay, Guangzhou University, Guangzhou, China,* [2] *School of Chemistry and Chemical Engineering, Shandong University, Jinan, China,* [3] *School of Environmental Science and Engineering, Shandong University, Jinan, China*

Dendritic cells (DCs) are the primary antigen-presenting cells and play key roles in the orchestration of the innate and adaptive immune system. Targeting DCs by nanotechnology stands as a promising strategy for cancer immunotherapy. The physicochemical properties of nanoparticles (NPs) influence their interactions with DCs, thus altering the immune outcome of DCs by changing their functions in the processes of maturation, homing, antigen processing and antigen presentation. In this review, we summarize the recent progress in targeting DCs using NPs as a drug delivery carrier in cancer immunotherapy, the recognition of NPs by DCs, and the ways the physicochemical properties of NPs affect DCs' functions. Finally, the molecular pathways in DCs that are affected by NPs are also discussed.

Keywords: nanoparticles, physicochemical properties, DC targeting, cancer immunotherapy, DC functions

OPEN ACCESS

Edited by:
Giuseppe Giaccone, Georgetown University, United States

Reviewed by:
Lina Ghibelli, Università degli Studi di Roma Tor Vergata, Italy
Chao Wang, University of North Carolina at Chapel Hill, United States

****Correspondence:***
Bing Yan
drbingyan@yahoo.com
Shumei Zhai
smzhai@sdu.edu.cn

Specialty section:
This article was submitted to Cancer Molecular Targets and Therapeutics, a section of the journal Frontiers in Oncology

Received: *28 June 2018*
Accepted: *04 September 2018*
Published: *25 September 2018*

Citation:
Jia J, Zhang Y, Xin Y, Jiang C, Yan B and Zhai S (2018) Interactions Between Nanoparticles and Dendritic Cells: From the Perspective of Cancer Immunotherapy. Front. Oncol. 8:404. doi: 10.3389/fonc.2018.00404

INTRODUCTION

The human body relies on two well-coordinated immune mechanisms for foreign invader defense, antigen non-specific innate immunity and highly evolved antigen specific adaptive immunity. The major functions of innate immunity are to rapidly eliminate pathogens and in a late stage, to transmit risk signals to adaptive immunity to activate the specific responses. While macrophages and natural killer (NK) cells primarily degrade and remove pathogens in non-specific ways, antigen processing cells (APCs) process and present pathogen signals to adaptive effector cells including T cells (1) and B cells (2, 3). Dendritic cells (DCs) are professional APCs. Originating from the bone marrow as progenitor cells with high phagocytic capabilities, DCs undergo maturation in the peripheral lymphatic organs. Maturation of DCs is triggered by pathogen uptake and is characterized by morphological changes, the expression of co-stimulatory molecules and the release of cytokines. During the maturation process, DCs migrate to lymphatic organs, where they activate both memory and naïve T cells, and thus are regarded as the most potent APCs. Because of their central role in inducing adaptive immunity, in recent decades, DCs have been extensively studied toward the aim of vaccine development and cancer immunotherapy (4, 5).

Cancer immunotherapy is regarded as an important progress for cancer treatment in the first decade of the 21st century. The success of some small-scale trials based on two major strategies, checkpoint blockage with antibodies and *ex vivo* T cells engineering, has boosted the development of cancer immunotherapy in recent years (6, 7). Because of the limits of these approaches (8), a third strategy, DC vaccination has been considered (9). Although less developed and with unknown efficacy, some clinical trials based on this approach have shown promise (10, 11).

In this strategy, DCs are manipulated by either *ex vivo* or *in vivo* approaches. Compared to an *in vivo* approach in which molecules are directly applied to patients to target DCs, in an *ex vivo* approach, DC precursors isolated from patients are stimulated in the laboratory for maturation by specific antigen and adjuvants, and then are applied back to the patient to activate adaptive immunity. Until now, the functional equality was unknown between *ex vivo* and *in vivo* matured DCs, but studies implicate that DCs undergo maturation differently *ex vivo* than *in vivo*.

Nanoparticles (NPs) in human blood and lymph are primarily captured by macrophages in the circulation and in tissues composed of the reticuloendothelial system, such as the liver and spleen. The latest studies revealed that precursor DCs patrolling the blood and immature DCs residing in peripheral tissues, such as the kidney and skin, also actively capture NPs, and subject their functions to alteration. These discoveries encouraged interests in using NPs to control DC functions in favor of cancer immunotherapy. The physicochemical attributes of NPs make them especially intriguing for both *ex vivo* and *in vivo* DC manipulation. As a novel DC targeting tool, NPs have at least the following advantages compared to traditional tools. (1) NPs such as gold nanorods (12) and carbon black NPs (13), are adjuvants *per se* and are able to prime DC maturation, thus enhancing humoral and cellular immune responses by synergizing the immunogenicity of antigens. (2) By optimizing the physicochemical properties, NPs can carry antigens or vaccines and directly deliver them to the mature DCs within the secondary lymph organs. In this way, stronger immune responses can be achieved without the accompanying immune tolerance induced by premature DCs (14–16). (3) NPs protect some antigens, such as peptides, from degradation by proteases (17, 18). (4) Using NPs as a platform, co-delivery of two or even more moieties can be realized to achieve stronger immune responses (17–25). Widely used combinations include tumor antigens together with adjuvants such as Toll-like receptor agonists (18, 23–30), or antigens with siRNAs, which silence immunosuppressive genes (31). This property is especially important for some antigens with weak immunogenicity (18). (5) Within DCs, a sustainable release of therapeutics can be achieved by NP carriers through chemical modification on their surface, thus activating DCs more efficiently (22, 32). Until now, different NPs, such as carbon nanotubes (CNTs) (23–25, 33), gold NPs (16, 34, 35), natural NPs [starch (36) and chitosan (37)] or synthetic polymer NPs (38–40) have been studied as vaccine carriers and/or adjuvants by distinct strategies. Even though the rapid advancement, the *status quo* is that this is still a newly emerging field and its maturation has been hindered by hurdles such as safety of NPs, and a costly and time-consuming process to harvest DCs from patients. An example of using NPs to stimulate the *ex vivo* maturation of immature DCs (iDCs) for immunotherapy was shown in **Figure 1**. NP applications for DC manipulation have been well reviewed in some recent excellent literature (41–43). In this article, we first summarize the latest progress of using NPs for cancer immunotherapy. With the aim of providing mechanistic insights on NPs-DCs interactions, we next focus on the latest knowledge in the recognition and uptake of NPs by DCs, and the ways NPs affect DC functions. We also discuss possible mechanisms underlying these effects.

DC-TARGETING STRATEGY USING NPs FOR CANCER IMMUNOTHERAPY

By using NPs as a multifunctional drug delivery carrier for *in vivo* DC-targeting, some promising cancer immunotherapeutic outcomes have been achieved. In some cases, animal survival rates improved because of the success of tumor growth inhibition. For example, multi-walled CNTs (MWCNTs) loaded with cancer testis antigen and Toll-like receptor agonist were quickly taken up by DCs after administered to animals. Inside DCs, the carried antigen was slowly released, driving DCs to continually activate $CD4^+$ and $CD8^+$ T cell immune responses. Consequently, tumor development was greatly delayed and mouse survival was prolonged (23). In another study, co-delivery of OVA and immune-adjuvants by MWCNTs to DCs dramatically inhibited the growth of OVA-expressing melanoma cells in mice (44).

In some other studies, cancer killing molecules and cytotoxic T cells were activated by a NPs mediated targeting strategy. For example, single-walled CNTs (SWCNTs) carrying a peptide tumor antigen to DCs induced specific IgG responses against this antigen in mice, while there were no such responses when mice were challenged with antigen alone (18). When uploaded by upconversion NPs, the injected ovalbumin enhanced the homing capability of DCs to draining lymph nodes in mice, and significantly induced cytotoxic T lymphocytes and the production of cancer killing molecules such as IFN-γ (17). After administration to mice, gold NPs with polyelectrolyte multilayer coatings increased DC activation and antigen presentation and induced a high level of antigen specific $CD8^+$ T cell immune response in blood (45). Although in these studies cancer inhibition or animal survival data were not reported, the stimulation of cancer killing cytokines and cytotoxic T cells is an indication of better cancer therapeutic efficacy. Some more examples of NPs that were studied for DC-targeted antigen delivery were summarized in **Table 1.**

RECOGNITION AND UPTAKE OF NPS BY DCs

In vitro studies using DC models derived from different species (54–56) revealed that, as in other cell types, the uptake of NPs by DCs is either energy dependent or independent (57). Depending on the physicochemical properties of NPs, all four endocytosis pathways are reportedly used by DCs for NPs uptake **(Table 2)** (52, 60, 63, 64). For example, small sized NPs take a clathrin- and scavenger receptors-dependent pathway (55), while those with diameters larger than 250 nm enter DCs primarily by clathrin independent ways (60–62).

Physicochemical properties of NPs dictate the recognition and uptake process. Recent studies consistently reveal that smaller NPs are easier for DCs to take up. For example, compared to those with a diameter larger than 1 μm, PLGA NPs of 300 nm have the higher uptake efficiency by DCs (64–66). Another example is that polypropylene sulfide NPs with a size of 20 nm accumulated in DCs in the lymph nodes more efficiently than

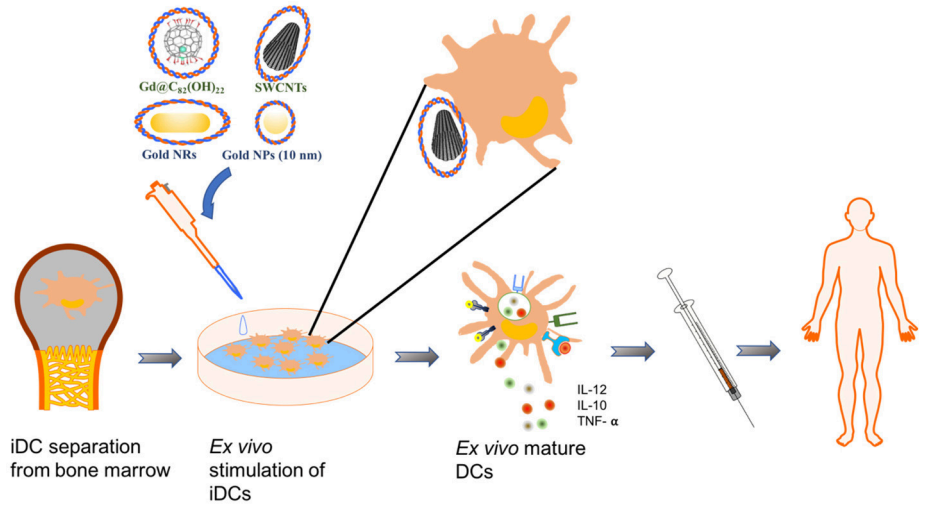

FIGURE 1 | Schematics of an example using NPs for DC-mediated immunotherapy. In this example, immature DCs (iDCs) are harvested from patients' bone marrow. NPs loaded with effect molecules are used to pulse and stimulate the maturation of iDCs *ex vivo*. The mature DCs were reapplied to patients for immunotherapy.

TABLE 1 | NPs used for DC-targeted antigen delivery.

Category	NP materials	Antigen/pathogen	References
Liposome	Lipid	NY-ESO-1	(46)
	Lipid	OVA	(47)
	Cationic lipid	OVA	(48)
Polymer	PLGA	OVA and monophosphoryl lipid A	(49)
	PLGA	Tetanus toxoid	(50)
	γ-PGA	OVA	(51)
	Poly(propylene sulfide)	OVA	(52)
Inorganic	MWCNTs	OVA, CpG	(44)
	Upconversion NPs	OVA	(17)
	GNPs	Peptide antigen and receptor agonist	(45)
Viruses particle	Adenoviral vectors	TRP2	(53)

NY-ESO-1,a human tumor antigen that is highly expressed in melanomas; PLGA, poly(lactic-co-glycolic acid); γPGA, poly-γ-glutamic acid; OVA, Ovalbumin; TRP2, tyrosinase-related proteins 2.

those of 45 and 100 nm, thus inducing more greater immunity (67). Shorter MWCNTs showed better cellular uptake compared to longer ones, and consequently induced more potent immune responses (25, 33). However, there are paradoxical opinions on the relationship between NPs size and their adjuvant activity, since NPs with different material components have their own optimum size for the induction of immune response (68).

Surface chemistry, such as charge and ligand organization pattern, affects NP internalization by DCs. An example is the positive charge on the gold NP surface led to a higher uptake efficiency by human monocyte-derived DCs (69). Early studies showed that the surface hydrophobicity of NPs was correlated with DCs mediated immune effects (70, 71). For example, hydrophobic segments in amphiphilic γ-PGA NPs' surface significantly increased their interactions with DCs and the consequent immune responses (72, 73). Another example is the zwitterionic ligand coated gold NPs (<3 nm in size) had a higher DCs uptake efficiency compared to those coated with PEGylated ligands (58). In one study, DCs took up NPs coated with PEG-3000 in a higher efficiency compared to those coated with shorter or longer PEG chain (74). Phosphatidylserine modification increased the internalization of SWCNTs by DCs compared to pristine ones or those coated with phosphocholine (75). The presence of aromatic structures on the NP surface resulted in the enhanced uptake of negatively charged GNPs and the activation of DCs (76). Not only chemistry type but also structural organization of surface chemical molecules affects the uptake process by DCs. For example, gold NPs coated with organized striations of alternating anionic and hydrophobic groups penetrated the plasma membrane and entered the cytosol, whereas those with randomly organized functional groups of the same composition were mostly trapped in endosomes of DCs (57).

The shape of the NPs also affects the recognition and uptake by DCs. Compared to spherical counterparts of the same size, gold nanorods and peptide nanofibers showed higher uptake efficiency by DCs in regards to the number of internalized NPs per cell (34, 77). Interestingly, only higher uptake of peptide nanofibers led to a stronger adjuvant efficiency, and gold nanorods actually did not. In another study, the uptake efficiency of rod-shaped PEG-based hydrogel NPs by mouse bone marrow-derived DCs was lower than that of disc-shaped NPs with similar volume and dimensions (78).

In *in vivo* models, physicochemical properties of NPs again govern their interaction with DCs. In one study, cationic NPs

TABLE 2 | Effect of NPs' properties on cellular uptake.

ID of ENPs	Physicochemical properties	Cell source	Cellular uptake	References
Gold nanoclusters (GNCs)	~2 nm in size, coated with mixture of zwitterionic and carbohydrate ligands	hDCs from blood	Clathrin-, F-actin-, and C-lectin dependent uptake	(54, 58)
Hybrid TiO_2/para-amino benzoic acid NPs	5–6 nm	hDCs from blood	Macropinocytosis	(59)
GNPs	~6 nm, coated with ordered or random arranged hydrophilic and hydrophobic groups	DC2.4 cells	Ordered structure: energy-independent; Random structure: energy-dependent	(57)
QDs with cadmium/selenide core and a zinc sulfide shell	18 nm, coated with carboxylic acid	Pig MDCs from blood	Clathrin- and scavenger receptor dependent endocytosis	(55)
Poly(propylene sulfide) NPs	45 nm, labeled with Alexa488	BMDCs	Clathrin-mediated endocytosis, and Macropinocytosis	(52)
PLGA NPs	135 nm, untargeted PEGylated surface	BMDCs	Clathrin-mediated endocytosis, caveolin-mediated endocytosis, and macropinocytosis	(56)
Gelatin NPs	245 nm, carrying model drug	BMDCs	Phagocytosis	(60)
PLGA NPs	360 nm, carrying model drug	BMDCs	Phagocytosis	(61)
PLGA NPs	500~600 nm, carrying model drug	hMDCs from blood	Phagocytosis	(62)

**h denotes human; BMDCs, bone marrow-derived DCs; PEG, Polyethylene glycol.*

more readily associated with both CD11b and CD103 DC subtypes in the lung than anionic ones, thus resulting in a higher expression level of *Ccl2* and *Cxc10*, two important chemokines that recruit DCs into the drainage lymph nodes (79). NPs uptake by DCs in administration sites and the accumulation in drainage lymph nodes was reported after administration by different routes (67, 80–84). In some studies, the uptake of NPs by DCs residing in lymph nodes was also detected (67, 80, 85, 86). Detailed studies showed that the locally injected NPs migrate to lymph nodes by two routes, i.e., through direct draining of NPs, or through DCs migration from injection site to lymph nodes, where NPs are re-taken up (86). Studies suggest that depending on the composition, NPs with a diameter less than 200 nm usually take the first route, while larger ones take the second route (27, 67, 85–88).

NPs AFFECT DC FUNCTIONS

In peripheral organs and in the blood, premature DCs internalize pathogens or foreign antigens and migrate to draining lymphoid tissue, where they undergo the maturation process characterized by morphological changes and increased expression of cytokines required for priming T cell and membrane molecules, such as CD40, CD80, CD86, DEC205, and MHC molecules (89). In the draining lymphoid tissues, mature DCs activate effector T cells (90). Mature DCs strongly stimulate naïve and memory T cells by presenting antigens. Depending on the way DCs are activated, T cells are stimulated by DCs to differentiate into distinct lineages of T helper (Th) cells, primarily including Th1, Th2, and Th17, which lead to cellular immunity, humoral immunity, and tissue inflammation, respectively. Recent studies revealed NPs affect all steps of DCs induced immunity.

NPs Affect DC Maturation

Long-term immune protection against tumors or pathogens requires the expansion of antigen-specific effector and memory T cells. Naïve T cell expansion can only be efficiently stimulated by mature DCs; therefore, the maturation of premature DCs is critical for the realization of efficient immunotherapy. Recent studies have shown that NPs favor the maturation process of DCs. For example, in *in vitro* culture, γ-PGA-Phe NPs induced a significant increase in the expression of maturation markers of DCs, and this capability is size-dependent (39, 86, 87). Gold nanorods were also reported to promote DC maturation and downstream immunity, and this effect depended on their surface chemistry (35, 91). Chitosan and other polymer NPs induced DC maturation in a similar way to LPS treatment (92, 93). According to recent research, ZnO NPs at a concentration of 30 μg/mL upregulated the expression of costimulatory molecules CD80 and CD86, and the secretion of IL-6 and TNF-α (94), but they did not show such effects at lower concentrations (10 μg/mL) (95). These effects are shape-independent, since spherical and sheet-shaped ZnO NPs with similar specific surface area showed similar effects (94). C60 fullerenes (96), carbon black (97, 98), $(Gd@C_{82}(OH)_{22})n$ (99, 100), and layered double hydroxide (LDH) NPs (101) were all reported to increase the expression of MHC and co-stimulatory molecules on DC surface. In another study, polyanhydrides NPs activated DCs with an efficiency that was dependent on their shape and surface hydrophilicity/hydrophobicity (102).

However, NPs are also reported to inhibit the maturation of DCs. For example, treatment with negatively charged QD655-COOH (18 nm) suppressed the expression of CD80/CD86 stimulated by LPS in porcine monocyte-derived DCs (55). In human DCs, gold NPs with a diameter of 10 nm inhibited the expression of CD86, CD83, and IL-12p70 induced by LPS

treatment (103). These findings warrant further investigations to avoid side effects of NPs when used for cancer immunotherapy.

NPs Affect Homing Capability of DCs

To activate T cells, DCs must migrate to lymphoid organs and localize closely to the residence T cells, a process known as DCs homing. A high homing efficiency is critical for a successful DCs-based immunotherapy. The homing of DCs can be improved by approaches including pre-injection of pro-inflammatory cytokines or DC homing receptors (104), and optimization of DCs' administration route and times (105). Even with this, the DC homing efficiency remains unsatisfactory (106). Recently, magnetic NPs have been used under an external magnetic field to promote the homing capability of DCs after *in vitro* activation (107). Some studies suggested that *in vitro* pulsed DCs by NPs accumulate in draining lymph nodes (17, 18), however, very little is known about NPs' effects on homing capability of DCs. One study suggested that NPs may improve DC homing by increasing the expression of chemokine receptor 7 (CCR7) on DCs surface and leading to the rearrangement of the cytoskeleton (16).

In addition to chemokines on the surface, it is well known that the maturation status of DCs determines their migration to draining lymph nodes (108). It is possible that NPs affects DCs' homing capability by influencing the maturation status of DCs. Future studies are necessary to further understanding of this aspect.

NPs Compromised Antigen Processing and Presentation Capability of DCs

After digestion by APC cells, antigen fragments will be displayed on the cell surface together with either class I or class II MHC molecules, and consequently are recognized by $CD4^+$ (helper) or $CD8^+$ (cytotoxic) T cells, respectively. This process is known as processing and presentation of APC (109–111). It is well reported that NPs change the antigen processing capability of DCs. *In vivo*, after pharyngeal aspiration, SWCNTs inhibited DCs' functions of antigen capture/processing and presentation but not their maturation process, thus causing decreased proliferation of splenic T cells (112). In *in vitro* culture, murine DCs treated with graphene oxide (GO) engulfed antigen normally but showed an impaired capability to process antigen and activate antigen-specific T lymphocytes (96). This effect was specific to GO and was not found for other carbon-based NPs, probably due to its planar and negative charged surface. Another example is that treatment with super-paramagnetic iron oxide NPs (PVA-SPIONs) compromised DCs' capability of processing model antigen DQ-OVA with or without concomitant LPS exposure but did not impair their maturation after antigen uptake. As a consequence, the expression of MHCII and the capacity to stimulate autologous $CD4^+$ T cells *in vitro* were compromised (113).

Harnessing the ability of DCs to induce antigen-specific $CD8^+$ T cell immunity (cross-presentation) is crucial for development of antitumor vaccines. As potential vaccine carriers, NPs could enhance antigen cross-presentation of DCs, thereby produce stronger antitumor immunity. For example, as shown in both *in vivo* and *in vitro* experiments, treatment with polymer NPs such as γ-PGA NPs (114, 115), PLGA NPs (116), polyethyleneimine NPs (117) and poly(propylene sulfide) NPs (52) promoted OVA-mediated cross-presentation in DCs by different mechanisms. Changing size and surface chemistry of NPs were effective ways to regulate their effects on antigen cross-presentation intensity of DCs (118, 119). Some metal oxide NPs such as aluminum hydroxide (120) and super-paramagnetic iron oxide NPs (SPIONs) (121) were also reported to improve the cross-presentation ability of DCs. These above studies suggested a potential strategy of using nanotechnology to develop DCs-based cancer immunotherapy.

NPs Affect DC Induced T Cell Differentiation

NPs have long been known to affect DCs' induction of T cell differentiation. For example, exposure to carbon black NPs or diesel exhaust of different sizes significantly enhanced the capacity of bone marrow-derived DCs to stimulate T-cell proliferation (97, 98). When cultured with $CD4^+$ T cells, human monocyte-derived DCs after treatment with poly(vinylalcohol)-coated SPIONs (PVA-SPIONs) showed an impaired capability to activate $CD4^+$ T cell and altered the cytokine release profiles (113). Mechanistically, NP exposure suppressed DCs' capacity to process and present antigen. In another study, porous silicon NPs modified by high C-H structures strongly enhanced DCs' activation of T cell differentiation (122).

Some NPs promoted DCs capability to stimulate both Th1 and Th2 differentiation (123). However, recent studies revealed that treatment with NPs may bias DC induced T cell differentiation directions. For example, SWCNTs (124), $(Gd@C_{82}(OH)_{22})_n$ (99, 100), magnetic iron oxide NPs (MIONs) (125), oxidative TiO_2 NPs (126), and PLGA NPs (127) were reported to increase Th1 cell proliferations, while 10 nm gold NPs (103) and CeO_2 NPs (126) potentiate DCs' capability to promote Th2 polarization. Moreover, this polarization effect is related to the surface chemistry. For example, gold nanorods coated with poly(diallydimethylammonium chloride) (PDDAC) and polyethyleneimine (PEI) showed a Th2 polarization activity, while those coated with cetyltrimethylammonium bromide did not (35). In another study, TiO_2 NPs induced DC maturation and polarized T cells toward Th1-based responses, while CeO_2 NPs treated DCs induced Th2-dominated T cell profile (128). Some NPs, such as polystyrene NPs (50 nm) (129), were found to inhibit Th2 polarization without affecting Th1 immunity. Not only NPs composition but also the NPs treatment conditions determines DCs induction effects on T cell differentiation. For example, SWCNTs at 0.5 μg/mL increased Th1 cell proliferation, while suppressing it at 10 μg/mL (124).

NPs were also reported to affect DCs' induction of T cells to differentiate into Th17 cells. For example, carbon black induced Th17-dependent inflammation in mice (130) and gold NPs of 50 nm (but not 10 nm) favored Th17 polarization (103). In comparison, PLGA NP induced nasal tolerance and inhibited T-cell differentiation into Th17 cells (131).

To sum up, the uptake of NPs affects DCs' functional steps from maturation to induction of T cell differentiation (**Figure 2**). The NPs' physicochemical properties and exposure scenarios govern the outcomes and intensity of these effects. The interactions between NPs and DCs may favor or impair the functions of DCs in immunotherapy. While some

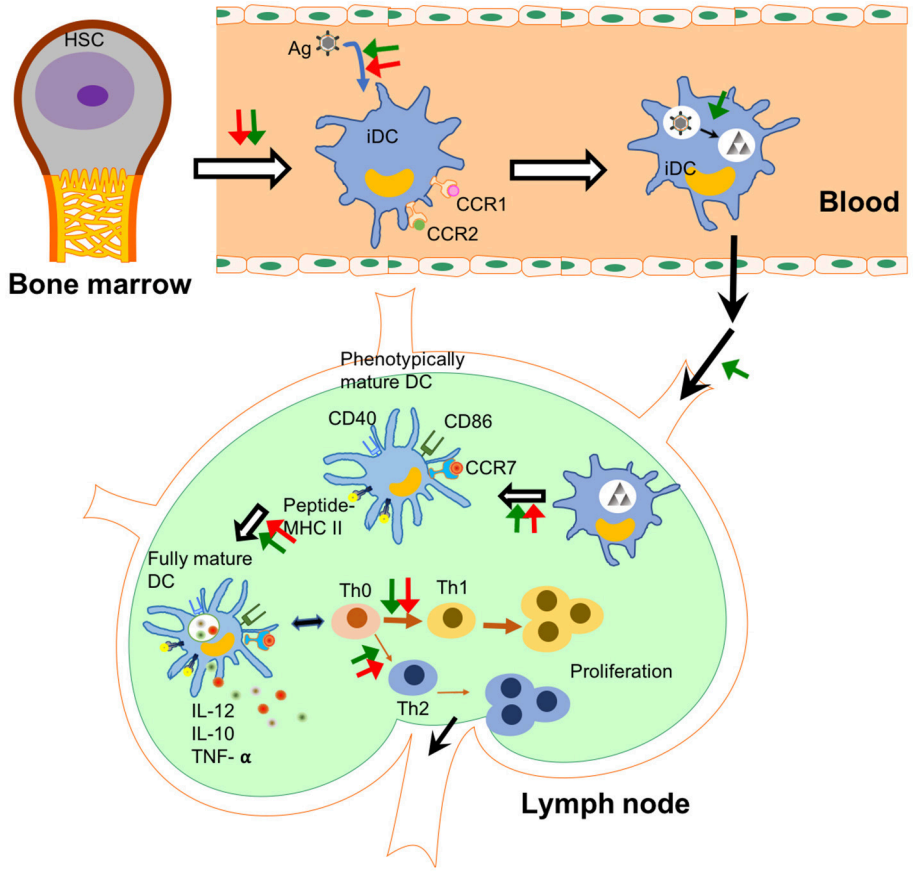

FIGURE 2 | NPs affect DCs' functions in different steps. The checkpoints of DC immunology are shown in this figure and the steps under the probable influence of NPs are summarized. NPs affect the differentiation from haematopoietic stem cells (HSCs) to immature dendritic cells (iDCs) in the bone marrow (132). They change the capability of DCs to uptake and process antigens in peripheral tissues. Some NPs enhance the homing capability of DCs into lymph node. In lymph node, NPs affect antigen presentation capability and maturation of DCs including the release of pro-inflammatory cytokines. Finally, NPs lead to polarization of T cell differentiation induced by DCs. Green arrows show an enhancement effect, while red arrows show an inhibition effect. Black arrows indicate the flow of immune cells.

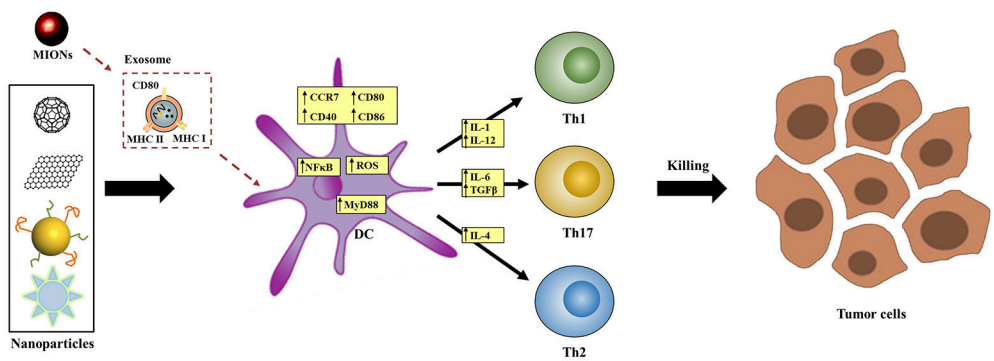

FIGURE 3 | Proposed molecular mechanisms by which NPs affect DCs' functions. NPs may interfere signal transduction (e.g., TLR-MyD88 signaling), exosome-mediated process, intracellular redox balance, or calcium oscillation inside DCs to affect DCs' functional process.

molecular mechanisms have been proposed, more are yet to be revealed.

POSSIBLE MECHANISMS: MOLECULAR PATHWAYS IN DCs AFFECTED BY NPs

Understanding the immunomodulatory mechanisms is a premise to optimize the functions of NPs for immunotherapy. Currently available literature supports that the effects of NPs on DCs may be triggered by binding with extracellular membrane receptors or acting on intracellular molecules. Both interactions depend heavily on the physicochemical properties, especially the surface chemistry of NPs.

One possible mechanism by which NPs affect DCs' fate is via the interference of the intracellular signaling pathways after recognition by cell surface receptor(s). Recent studies have proposed TLR (Toll-like receptor)-MyD88 signaling (133) as one of the most likely pathways that mediates NPs' effects. This mechanism was first identified by a micro-array analysis (134) and was later supported by observations in MyD88-knockout and TLR4-deficient DC models and mice (39). For example, after treatment with γ-PGA NPs, the maturation of DCs with MyD88- or TLR4-knockout but not wild-type was impaired. In addition, in wild-type mice, NPs augmented OVA-induced adaptive immune responses, including T cell activation and anti-OVA antibody production, but these effects were largely diminished in TLR4-deficient mice (39). In some studies, the activity of NF-κB and MAPK signaling pathways, both of which are downstream of TLR-MyD88 signaling, was found changed by NPs treatment in DCs (135). These results further support that TLR4-MyD88 is at least one of the signaling pathways that mediated the effects of NPs **(Figure 3)**.

Another reported mechanism is related to the generation of exosomes. *In vivo* investigations showed that magnetic iron oxide NPs (MIONs) stimulated the generation of exosomes in the alveolar region of mice after respiratory exposure (125, 136). These exosomes transferred to the reticuloendothelial and immune systems, where the maturation of DCs was induced. *Ex vivo* studies indicated that when incubated with MION-Exo, immature DCs underwent maturation, as shown by the stimulated expression of MHC class II I-A^d, MHC class I H-$2K^d$, CD80, and CD86, and differentiated into DC1 subtype as shown by the increased secretion of cytokine IL-12. In contrast, MIONs *per se* did not have the same effects, suggesting that MIONs-induced exosomes mediated the effects of MIONs in stimulating host immunity **(Figure 3)**.

Some other plausible mechanisms have also been proposed. Based on the link between redox equilibrium with phenotypic and functional maturation of DCs (137), oxidative stress may play a key role for DC activation after treatment with NPs including carbon blacks (CBs) (130, 138) and SWCNTs (124). In one study, 10 nm gold NPs were found to inhibit the change of Ca^{2+} oscillation during LPS-induced DC maturation (103). However, blocking Ca^{2+} oscillation cannot totally impair DCs' maturation, suggesting that calcium oscillations-dependent signaling is not the sole target of gold NPs in the regulation of DCs' maturation.

Till now, our knowledge about the ways NPs modulate intracellular molecular pathways in DCs is very limit. Since the interactions between NPs and intracellular molecules may be dominated by the physicochemical properties, especially the surface chemistry of NPs, future studies of the structure-activity relationship will help rational design of NPs-based tools to harness immunotherapeutic functions of DCs.

PERSPECTIVE

For successful DCs-based immunotherapy, three strategies have been considered. First, to deliver tumor specific antigens to DCs and to stimulate their maturation *ex vivo* followed by re-infusion back to patients. Second, *in vivo* targeting of DCs with DC-specific targeting molecules together with tumor antigens and activators to induce cytotoxic T cell activation. Finally, *in vivo* targeting of DCs augments tumor rejection inflammation in the tumor microenvironment (9). For all of these strategies, NPs are perfect antigen or adjuvant delivery carriers of high molecular quantity and variety. *In vivo* manipulation can better mimic the natural maturation process of DCs, thus can probably produce safer and more efficient immunotherapeutic outcomes. In the future, a deeper understanding of the mechanisms by which the physicochemical properties of NPs affect DCs' functions, such as maturation, homing, antigen process, and induction of T cell differentiation, will be required for safe and efficient DCs-based cancer immunotherapy.

AUTHOR CONTRIBUTIONS

JJ, YZ and SZ designed this work of review. YX and CJ performed the literature search of the databases. JJ, YZ, and SZ wrote the manuscript. YZ and BY revised the manuscript. All authors approved the paper for publication.

ACKNOWLEDGMENTS

This work was supported by the National Natural Science Foundation of China (21677090, 91543204 and 91643204), the National Key Research and Development Program of China (2016YFA0203103), the Strategic Priority Research Program of the Chinese Academy of Sciences (XDB14030401), China Postdoctoral Science Foundation (2016T90634), and the Science Starting Foundation of Guangzhou University (69-18ZX10332).

REFERENCES

1. Shortman K, Liu YJ. Mouse and human dendritic cell subtypes. *Nat Rev Immunol.* (2002) 2:151–61. doi: 10.1038/nri746
2. Batista FD, Harwood NE. The who, how and where of antigen presentation to B cells. *Nat Rev Immunol.* (2009) 9:15–27. doi: 10.1038/nri2454
3. Wykes M, MacPherson G. Dendritic cell-B-cell interaction: dendritic cells provide B cells with CD40-independent proliferation signals

and CD40-dependent survival signals. *Immunology* (2000) 100:1–3. doi: 10.1046/j.1365-2567.2000.00044.x
4. Cruz LJ, Tacken PJ, Rueda F, Carles Domingo J, Albericio F, Figdor CG. Targeting nanoparticles to dendritic cells for immunotherapy. *Methods Enzymol.* (2012) 509:143–63. doi: 10.1016/B978-0-12-391858-1.00008-3
5. Engleman EG. Dendritic cell-based cancer immunotherapy. *Semin Oncol.* (2003) 30(Suppl. 8):23–9. doi: 10.1016/S0093-7754(03)00229-X
6. Couzin-Frankel J. Cancer Immunotherapy. *Science* (2013) 342:1432–3. doi: 10.1126/science.342.6165.1432
7. Fan Q, Chen Z, Wang C, Liu Z. Toward biomaterials for enhancing immune checkpoint blockade therapy. *Adv Funct Mater* (2018) 28:1802540. doi: 10.1002/adfm.201802540
8. Jackson HJ, Rafiq S, Brentjens RJ. Driving CAR T-cells forward. *Nat Rev Clin Oncol.* (2016) 13:370–83. doi: 10.1038/nrclinonc.2016.36
9. Palucka K, Banchereau J. Cancer immunotherapy via dendritic cells. *Nat Rev Cancer* (2012) 12:265–77. doi: 10.1038/nrc3258
10. Zhang ZQ, Kim T, Bao MS, Facchinetti V, Jung SY, Ghaffari AA, et al. DDX1, DDX21, and DHX36 helicases form a complex with the adaptor molecule TRIF to sense dsRNA in dendritic cells. *Immunity* (2011) 34:866–78. doi: 10.1016/j.immuni.2011.03.027
11. Barrat FJ, Meeker T, Gregorio J, Chan JH, Uematsu S, Akira S, et al. Nucleic acids of mammalian origin can act as endogenous ligands for toll-like receptors and may promote systemic lupus erythematosus. *J Exp Med.* (2005) 202:1131–9. doi: 10.1084/jem.20050914
12. Matsusaki M, Larsson K, Akagi T, Lindstedt M, Akashi M, Borrebaeck CA. Nanosphere induced gene expression in human dendritic cells. *Nano Lett.* (2005) 5:2168–73. doi: 10.1021/nl050541s
13. de Haar C, Kool M, Hassing I, Bol M, Lambrecht BN, Pieters R. Lung dendritic cells are stimulated by ultrafine particles and play a key role in particle adjuvant activity. *J Allergy Clin Immunol.* (2008) 121:1246–54. doi: 10.1016/j.jaci.2008.01.010
14. Su H, Mou Y, An Y, Han W, Huang X, Xia G, et al. The migration of synthetic magnetic nanoparticle labeled dendritic cells into lymph nodes with optical imaging. *Int J Nanomed.* (2013) 8:3737–44. doi: 10.2147/IJN.S52135
15. Chua BY, Al Kobaisi M, Zeng W, Mainwaring D, Jackson DC. Chitosan microparticles and nanoparticles as biocompatible delivery vehicles for peptide and protein-based immunocontraceptive vaccines. *Mol Pharm.* (2011) 9:81–90. doi: 10.1021/mp200264m
16. Zhou Q, Zhang Y, Du J, Li Y, Zhou Y, Fu Q, et al. Different-sized gold nanoparticle activator/antigen increases dendritic cells accumulation in liver-draining lymph nodes and CD8+ T cell responses. *ACS Nano* (2016) 10:2678–92. doi: 10.1021/acsnano.5b07716
17. Xiang J, Xu L, Gong H, Zhu W, Wang C, Xu J, et al. Antigen-Loaded upconversion nanoparticles for dendritic cell stimulation, tracking, and vaccination in dendritic cell-based immunotherapy. *ACS Nano* (2015) 9:6401–11. doi: 10.1021/acsnano.5b02014
18. Villa CH, Dao T, Ahearn I, Fehrenbacher N, Casey E, Rey DA, et al. Single-walled carbon nanotubes deliver peptide antigen into dendritic cells and enhance IgG responses to tumor-associated antigens. *ACS Nano* (2011) 5:5300–11. doi: 10.1021/nn200182x
19. Sokolova V, Knuschke T, Kovtun A, Buer J, Epple M, Westendorf AM. The use of calcium phosphate nanoparticles encapsulating Toll-like receptor ligands and the antigen hemagglutinin to induce dendritic cell maturation and T cell activation. *Biomaterials* (2010) 31:5627–33. doi: 10.1016/j.biomaterials.2010.03.067
20. Carrillo-Conde B, Song E-H, Chavez-Santoscoy A, Phanse Y, Ramer-Tait AE, Pohl NL, et al. Mannose-functionalized "pathogen-like" polyanhydride nanoparticles target C-type lectin receptors on dendritic cells. *Mol Pharm.* (2011) 8:1877–86. doi: 10.1021/mp200213r
21. Petersen LK, Ramer-Tait AE, Broderick SR, Kong CS, Ulery BD, Rajan K, et al. Activation of innate immune responses in a pathogen-mimicking manner by amphiphilic polyanhydride nanoparticle adjuvants. *Biomaterials* (2011) 32:6815–22. doi: 10.1016/j.biomaterials.2011.05.063
22. Leleux J, Roy K. Micro and nanoparticle-based delivery systems for vaccine immunotherapy: an immunological and materials perspective. *Adv Healthc Mater* (2013) 2:72–94. doi: 10.1002/adhm.201200268
23. de Faria PCB, dos Santos LI, Coelho JP, Ribeiro HB, Pimenta MA, Ladeira LO, et al. Oxidized multiwalled carbon nanotubes as antigen delivery system to promote superior CD8(+) T cell response and protection against cancer. *Nano Lett.* (2014) 14:5458–70. doi: 10.1021/nl502911a
24. Sun Z, Wang W, Meng J, Chen S, Xu H, Yang XD. Multi-walled carbon nanotubes conjugated to tumor protein enhance the uptake of tumor antigens by human dendritic cells *in vitro*. *Cell Res.* (2010) 20:1170–3. doi: 10.1038/cr.2010.133
25. Hassan HA, Smyth L, Rubio N, Ratnasothy K, Wang JTW, Bansal SS, et al. Carbon nanotubes' surface chemistry determines their potency as vaccine nanocarriers *in vitro* and *in vivo*. *J Control Release* (2016) 225:205–16. doi: 10.1016/j.jconrel.2016.01.030
26. Ballester M, Jeanbart L, De Titta A, Nembrini C, Marsland BJ, Hubbell JA, et al. Nanoparticle conjugation enhances the immunomodulatory effects of intranasally delivered CpG in house dust mite-allergic mice. *Sci Rep.* (2015) 5:14274. doi: 10.1038/srep14274
27. Nembrini C, Stano A, Dane KY, Ballester M, van der Vlies AJ, Marsland BJ, et al. Nanoparticle conjugation of antigen enhances cytotoxic T-cell responses in pulmonary vaccination. *Proc Natl Acad Sci USA*. (2011) 108:E989–97. doi: 10.1073/pnas.1104264108
28. Molino NM, Anderson AK, Nelson EL, Wang S-W. Biomimetic protein nanoparticles facilitate enhanced dendritic cell activation and cross-presentation. *ACS Nano* (2013) 7:9743–52. doi: 10.1021/nn403085w
29. Chong CS, Cao M, Wong WW, Fischer KP, Addison WR, Kwon GS, et al. Enhancement of T helper type 1 immune responses against hepatitis B virus core antigen by PLGA nanoparticle vaccine delivery. *J Control Release* (2005) 102:85–99. doi: 10.1016/j.jconrel.2004.09.014
30. Ruiz-de-Angulo A, Zabaleta A, Gómez-Vallejo V, Llop J, Mareque-Rivas JC. Microdosed lipid-coated 67Ga-magnetite enhances antigen-specific immunity by image tracked delivery of antigen and CpG to lymph nodes. *ACS Nano* (2015) 10:1602–18. doi: 10.1021/acsnano.5b07253
31. Heo MB, Lim YT. Programmed nanoparticles for combined immunomodulation, antigen presentation and tracking of immunotherapeutic cells. *Biomaterials* (2014) 35:590–600. doi: 10.1016/j.biomaterials.2013.10.009
32. Vela Ramirez J, Roychoudhury R, Habte H, Cho M, Pohl N, Narasimhan B. Carbohydrate-functionalized nanovaccines preserve HIV-1 antigen stability and activate antigen presenting cells. *J Biomater Sci-Polym Ed*. (2014) 25:1387–406. doi: 10.1080/09205063.2014.940243
33. Parra J, Abad-Somovilla A, Mercader JV, Taton TA, Abad-Fuentes A. Carbon nanotube-protein carriers enhance size-dependent self-adjuvant antibody response to haptens. *J Control Release* (2013) 170:242–51. doi: 10.1016/j.jconrel.2013.05.019
34. Niikura K, Matsunaga T, Suzuki T, Kobayashi S, Yamaguchi H, Orba Y, et al. Gold nanoparticles as a vaccine platform: influence of size and shape on immunological responses *in vitro* and *in vivo*. *ACS Nano* (2013) 7:3926–38. doi: 10.1021/nn3057005
35. Xu L, Liu Y, Chen Z, Li W, Liu Y, Wang L, et al. Surface-engineered gold nanorods: promising DNA vaccine adjuvant for HIV-1 treatment. *Nano Lett.* (2012) 12:2003–12. doi: 10.1021/nl300027p
36. Heritage PL, Loomes LM, Jianxiong J, Brook MA, Underdown BJ, McDermott MR. Novel polymer-grafted starch microparticles for mucosal delivery of vaccines. *Immunology* (1996) 88:162–8. doi: 10.1046/j.1365-2567.1996.d01-639.x
37. Illum L. Chitosan and its use as a pharmaceutical excipient. *Pharm Res.* (1998) 15:1326–31.
38. Uto T, Wang X, Sato K, Haraguchi M, Akagi T, Akashi M, et al. Targeting of antigen to dendritic cells with poly(gamma-glutamic acid) nanoparticles induces antigen-specific humoral and cellular immunity. *J Immunol.* (2007) 178:2979–86. doi: 10.4049/jimmunol.178.5.2979
39. Uto T, Akagi T, Yoshinaga K, Toyama M, Akashi M, Baba M. The induction of innate and adaptive immunity by biodegradable poly (γ-glutamic acid) nanoparticles via a TLR4 and MyD88 signaling pathway. *Biomaterials* (2011) 32:5206–12. doi: 10.1016/j.biomaterials.2011.03.052
40. Mundargi RC, Babu VR, Rangaswamy V, Patel P, Aminabhavi TM. Nano/micro technologies for delivering macromolecular therapeutics using poly(D,L-lactide-co-glycolide) and its derivatives. *J Control Release* (2008) 125:193–209. doi: 10.1016/j.jconrel.2007.09.013
41. Klippstein R, Pozo D. Nanotechnology-based manipulation of dendritic cells for enhanced immunotherapy strategies.

Nanomed-Nanotechnol Biol Med (2010) 6:523–9. doi: 10.1016/j.nano.2010.01.001
42. Paulis LE, Mandal S, Kreutz M, Figdor CG. Dendritic cell-based nanovaccines for cancer immunotherapy. *Curr Opin Immunol.* (2013) 25:389–95. doi: 10.1016/j.coi.2013.03.001
43. Wang C, Ye Y, Hu Q, Bellotti A, Gu Z. Tailoring biomaterials for cancer immunotherapy: emerging trends and future outlook. *Adv Mater*. (2017) 29:1606036. doi: 10.1002/adma.201606036
44. Hassan HAFM, Smyth L, Wang JTW, Costa PM, Ratnasothy K, Diebold SS, et al. Dual stimulation of antigen presenting cells using carbon nanotube-based vaccine delivery system for cancer immunotherapy. *Biomaterials* (2016) 104:310–22. doi: 10.1016/j.biomaterials.2016.07.005
45. Zhang P, Chiu Y-C, Tostanoski LH, Jewell CM. Polyelectrolyte multilayers assembled entirely from immune signals on gold nanoparticle templates promote antigen-specific T cell response. *ACS Nano* (2015) 9:6465–77. doi: 10.1021/acsnano.5b02153
46. Cruz LJ, Rueda F, Simón L, Cordobilla B, Albericio F, Domingo JC. Liposomes containing NY-ESO-1/tetanus toxoid and adjuvant peptides targeted to human dendritic cells via the Fc receptor for cancer vaccines. *Nanomedicine* (2014) 9:435–49. doi: 10.2217/NNM.13.66
47. Van Broekhoven CL, Parish CR, Demangel C, Britton WJ, Altin JG. Targeting dendritic cells with antigen-containing liposomes: a highly effective procedure for induction of antitumor immunity and for tumor immunotherapy. *Cancer Res.* (2004) 64:4357–65. doi: 10.1158/0008-5472.CAN-04-0138
48. Yoshizaki Y, Yuba E, Sakaguchi N, Koiwai K, Harada A, Kono K. Potentiation of pH-sensitive polymer-modified liposomes with cationic lipid inclusion as antigen delivery carriers for cancer immunotherapy. *Biomaterials* (2014) 35:8186–96. doi: 10.1016/j.biomaterials.2014.05.077
49. Jahan ST, Sadat SM, Haddadi A. Design and immunological evaluation of anti-CD205-tailored PLGA-based nanoparticulate cancer vaccine. *Int J Nanomed*. (2018) 13:367. doi: 10.2147/IJN.S144266
50. Cruz LJ, Tacken PJ, Fokkink R, Joosten B, Stuart MC, Albericio F, et al. Targeted PLGA nano-but not microparticles specifically deliver antigen to human dendritic cells via DC-SIGN *in vitro*. *J Control Release* (2010) 144:118–26. doi: 10.1016/j.jconrel.2010.02.013
51. Yoshikawa T, Okada N, Oda A, Matsuo K, Matsuo K, Mukai Y, et al. Development of amphiphilic γ-PGA-nanoparticle based tumor vaccine: potential of the nanoparticulate cytosolic protein delivery carrier. *Biochem Biophys Res Commun* (2008) 366:408–13. doi: 10.1016/j.bbrc.2007.11.153
52. Hirosue S, Kourtis IC, van der Vlies AJ, Hubbell JA, Swartz MA. Antigen delivery to dendritic cells by poly (propylene sulfide) nanoparticles with disulfide conjugated peptides: cross-presentation and T cell activation. *Vaccine* (2010) 28:7897–906. doi: 10.1016/j.vaccine.2010.09.077
53. Hangalapura BN, Oosterhoff D, de Groot J, Boon L, Tuting T, van den Eertwegh AJ, et al. Potent anti-tumor immunity generated by a CD40-targeted adenoviral vaccine. *Cancer Res.* (2011) 71:5827–37. doi: 10.1158/0008-5472.CAN-11-0804
54. Le Guével X, Perez Perrino M, Fernández TD, Palomares F, Torres M-J, Blanca M, et al. Multivalent glycosylation of fluorescent gold nanoclusters promotes increased human dendritic cell targeting via multiple endocytic pathways. *ACS Appl Mater Interfaces* (2015) 7:20945–56. doi: 10.1021/acsami.5b06541
55. Zhang LW, Bäumer W, Monteiro-Riviere NA. Cellular uptake mechanisms and toxicity of quantum dots in dendritic cells. *Nanomedicine* (2011) 6:777–91. doi: 10.2217/nnm.11.73
56. Silva JM, Vandermeulen G, Oliveira VG, Pinto SN, Rodrigues C, Salgado A, et al. Development of functionalized nanoparticles for vaccine delivery to dendritic cells: a mechanistic approach. *Nanomedicine* (2014) 9:2639–56. doi: 10.2217/nnm.14.135
57. Verma A, Uzun O, Hu Y, Hu Y, Han H-S, Watson N, et al. Surface-structure-regulated cell-membrane penetration by monolayer-protected nanoparticles. *Nat Mater* (2008) 7:588–95. doi: 10.1038/nmat2202
58. Fernández TD, Pearson JR, Leal MP, Torres MJ, Blanca M, Mayorga C, et al. Intracellular accumulation and immunological properties of fluorescent gold nanoclusters in human dendritic cells. *Biomaterials* (2015) 43:1–12. doi: 10.1016/j.biomaterials.2014.11.045
59. Migdal C, Rahal R, Rubod A, Callejon S, Colomb E, Atrux-Tallau N, et al. Internalisation of hybrid titanium dioxide/para-amino benzoic acid nanoparticles in human dendritic cells did not induce toxicity and changes in their functions. *Toxicol Lett.* (2010) 199:34–42. doi: 10.1016/j.toxlet.2010.07.017
60. Coester C, Nayyar P, Samuel J. *In vitro* uptake of gelatin nanoparticles by murine dendritic cells and their intracellular localisation. *Eur J Pharm Biopharm.* (2006) 62:306–14. doi: 10.1016/j.ejpb.2005.09.009
61. Elamanchili P, Diwan M, Cao M, Samuel J. Characterization of poly(d,l-lactic-co-glycolic acid) based nanoparticulate system for enhanced delivery of antigens to dendritic cells. *Vaccine* (2004) 22:2406–12. doi: 10.1016/j.vaccine.2003.12.032
62. Lutsiak MEC, Robinson D, Coester C, Kwon G, Samuel J. Analysis of poly(D,L-Lactic-Co-Glycolic Acid) nanosphere uptake by human dendritic cells and macrophages *in vitro*. *Pharm Res.* (2002) 19:1480–7. doi: 10.1023/a:1020452531828
63. Pelkmans L. Secrets of caveolae- and lipid raft-mediated endocytosis revealed by mammalian viruses. *Biochim Biophys Acta Mol Cell Res.* (2005) 1746:295–304. doi: 10.1016/j.bbamcr.2005.06.009
64. Xiang SD, Scholzen A, Minigo G, David C, Apostolopoulos V, Mottram PL, et al. Pathogen recognition and development of particulate vaccines: does size matter? *Methods* (2006) 40:1–9. doi: 10.1016/j.ymeth.2006.05.016
65. Oyewumi MO, Kumar A, Cui Z. Nano-microparticles as immune adjuvants: correlating particle sizes and the resultant immune responses. *Expert Rev Vaccines* (2010) 9:1095–107. doi: 10.1586/erv.10.89
66. Joshi VB, Geary SM, Salem AK. Biodegradable particles as vaccine delivery systems: size matters. *AAPS J.* (2013) 15:85–94. doi: 10.1208/s12248-012-9418-6
67. Reddy ST, van der Vlies AJ, Simeoni E, Angeli V, Randolph GJ, O'Neil CP, et al. Exploiting lymphatic transport and complement activation in nanoparticle vaccines. *Nat Biotechnol.* (2007) 25:1159–64. doi: 10.1038/nbt1332
68. Yan S, Gu W, Xu ZP. Re-considering how particle size and other properties of antigen–adjuvant complexes impact on the immune responses. *J Colloid Interface Sci.* (2013) 395:1–10. doi: 10.1016/j.jcis.2012.11.061
69. Fytianos K, Rodriguez-Lorenzo L, Clift MJ, Blank F, Vanhecke D, Von Garnier C, et al. Uptake efficiency of surface modified gold nanoparticles does not correlate with functional changes and cytokine secretion in human dendritic cells *in vitro*. *Nanomed Nanotechnol Biol Med.* (2015) 11:633–44. doi: 10.1016/j.nano.2014.11.004
70. Moyano DF, Goldsmith M, Solfiell DJ, Landesman-Milo D, Miranda OR, Peer D, et al. Nanoparticle hydrophobicity dictates immune response. *J Am Chem Soc.* (2012) 134:3965–7. doi: 10.1021/ja2108905
71. Seong SY, Matzinger P. Hydrophobicity: an ancient damage-associated molecular pattern that initiates innate immune responses. *Nat Rev Immunol.* (2004) 4:469–78. doi: 10.1038/nri1372
72. Shima F, Akagi T, Akashi M. Effect of hydrophobic side chains in the induction of immune responses by nanoparticle adjuvants consisting of amphiphilic poly (γ-glutamic acid). *Bioconj Chem.* (2015) 26:890–8. doi: 10.1021/acs.bioconjchem.5b00106
73. Shima F, Akagi T, Uto T, Akashi M. Manipulating the antigen-specific immune response by the hydrophobicity of amphiphilic poly (γ-glutamic acid) nanoparticles. *Biomaterials* (2013) 34:9709–16. doi: 10.1016/j.biomaterials.2013.08.064
74. Cruz LJ, Tacken PJ, Fokkink R, Figdor CG. The influence of PEG chain length and targeting moiety on antibody-mediated delivery of nanoparticle vaccines to human dendritic cells. *Biomaterials* (2011) 32:6791–803. doi: 10.1016/j.biomaterials.2011.04.082
75. Konduru NV, Tyurina YY, Feng W, Basova LV, Belikova NA, Bayir H, et al. Phosphatidylserine targets single-walled carbon nanotubes to professional phagocytes *in vitro* and *in vivo*. *PLoS ONE* (2009) 4:e4398. doi: 10.1371/journal.pone.0004398
76. Yang H, Zhou Y, Fung S-Y, Wu L, Tsai K, Tan R, et al. Amino acid structure determines the immune responses generated by peptide-gold nanoparticle hybrids. *Part Part Syst Charact.* (2013) 30:1039–43. doi: 10.1002/ppsc.201300213

77. Mammadov R, Cinar G, Gunduz N, Goktas M, Kayhan H, Tohumeken S, et al. Virus-like nanostructures for tuning immune response. *Sci Rep.* (2015) 5:16728. doi: 10.1038/srep16728
78. Agarwal R, Singh V, Jurney P, Shi L, Sreenivasan S, Roy K. Mammalian cells preferentially internalize hydrogel nanodiscs over nanorods and use shape-specific uptake mechanisms. *Proc Natl Acad Sci USA.* (2013) 110:17247-52. doi: 10.1073/pnas.1305000110
79. Fromen CA, Rahhal TB, Robbins GR, Kai MP, Shen TW, Luft JC, et al. Nanoparticle surface charge impacts distribution, uptake and lymph node trafficking by pulmonary antigen-presenting cells. *Nanomed Nanotechnol Biol Med.* (2016) 12:677–87. doi: 10.1016/j.nano.2015.11.002
80. Reddy ST, Rehor A, Schmoekel HG, Hubbell JA, Swartz MA. *In vivo* targeting of dendritic cells in lymph nodes with poly (propylene sulfide) nanoparticles. *J Control Release* (2006) 112:26–34. doi: 10.1016/j.jconrel.2006.01.006
81. Mahe B, Vogt A, Liard C, Duffy D, Abadie V, Bonduelle O, et al. Nanoparticle-based targeting of vaccine compounds to skin antigen-presenting cells by hair follicles and their transport in mice. *J Invest Dermatol.* (2009) 129:1156–64. doi: 10.1038/jid.2008.356
82. Rancan F, Gao Q, Graf C, Troppens S, Hadam S, Hackbarth S, et al. Skin penetration and cellular uptake of amorphous silica nanoparticles with variable size, surface functionalization, and colloidal stability. *ACS Nano* (2012) 6:6829–42. doi: 10.1021/nn301622h
83. Combadière B, Mahé B. Particle-based vaccines for transcutaneous vaccination. *Comp Immunol Microbiol Infect Dis.* (2008) 31:293–315. doi: 10.1016/j.cimid.2007.07.015
84. Kenney RT, Frech SA, Muenz LR, Villar CP, Glenn GM. Dose sparing with intradermal injection of influenza vaccine. *N Engl J Med.* (2004) 351:2295–301. doi: 10.1056/NEJMoa043540
85. Manolova V, Flace A, Bauer M, Schwarz K, Saudan P, Bachmann MF. Nanoparticles target distinct dendritic cell populations according to their size. *Eur J Immunol.* (2008) 38:1404–13. doi: 10.1002/eji.200737984
86. Shima F, Uto T, Akagi T, Baba M, Akashi M. Size effect of amphiphilic poly (γ-glutamic acid) nanoparticles on cellular uptake and maturation of dendritic cells *in vivo*. *Acta Biomater.* (2013) 9:8894–901. doi: 10.1016/j.actbio.2013.06.010
87. Kim H, Uto T, Akagi T, Baba M, Akashi M. Amphiphilic poly (amino acid) nanoparticles induce size-dependent dendritic cell maturation. *Adv Funct Mater* (2010) 20:3925–31. doi: 10.1002/adfm.201000021
88. Kourtis IC, Hirosue S, De Titta A, Kontos S, Stegmann T, Hubbell JA, et al. Peripherally administered nanoparticles target monocytic myeloid cells, secondary lymphoid organs and tumors in mice. *PLoS ONE* (2013) 8:e61646. doi: 10.1371/journal.pone.0061646
89. e Sousa CR. Dendritic cells in a mature age. *Nat Rev Immunol.* (2006) 6:476–83. doi: 10.1038/nri1845
90. Lambrecht BN, Hammad H. The role of dendritic and epithelial cells as master regulators of allergic airway inflammation. *Lancet* (2010) 376:835–43. doi: 10.1016/S0140-673661226-3
91. Kieng Bao V, Safina I, Darrigues E, Nedosekin D, Nima ZA, Majeed W, et al. Modifying dendritic cell activation with plasmonic nano vectors. *Sci Rep.* (2017) 7:5513. doi: 10.1038/s41598-017-04459-1
92. Babensee JE, Paranjpe A. Differential levels of dendritic cell maturation on different biomaterials used in combination products. *J Biomed Mater Res Part A* (2005) 74:503–10. doi: 10.1002/jbm.a.30429
93. Gong H, Xiang J, Xu L, Song X, Dong Z, Peng R, et al. Stimulation of immune systems by conjugated polymers and their potential as an alternative vaccine adjuvant. *Nanoscale* (2015) 7:19282–92. doi: 10.1039/c5nr06081h
94. Heng BC, Zhao X, Tan EC, Khamis N, Assodani A, Xiong S, et al. Evaluation of the cytotoxic and inflammatory potential of differentially shaped zinc oxide nanoparticles. *Arch Toxicol.* (2011) 85:1517–28. doi: 10.1007/s00204-011-0722-1
95. Andersson-Willman B, Gehrmann U, Cansu Z, Buerki-Thurnherr T, Krug HF, Gabrielsson S, et al. Effects of subtoxic concentrations of TiO2 and ZnO nanoparticles on human lymphocytes, dendritic cells and exosome production. *Toxicol Appl Pharmacol.* (2012) 264:94–103. doi: 10.1016/j.taap.2012.07.021
96. Tkach AV, Yanamala N, Stanley S, Shurin MR, Shurin GV, Kisin ER, et al. Graphene oxide, but not fullerenes, targets immunoproteasomes and suppresses antigen presentation by dendritic cells. *Small* (2013) 9:1686–90. doi: 10.1002/smll.201201546
97. Porter M, Karp M, Killedar S, Bauer SM, Guo J, Williams DA, et al. Diesel-enriched particulate matter functionally activates human dendritic cells. *Am J Respir Cell Mol Biol.* (2007) 37:706–19. doi: 10.1165/rcmb.2007-0199OC
98. Koike E, Takano H, Inoue KI, Yanagisawa R, Kobayashi T. Carbon black nanoparticles promote the maturation and function of mouse bone marrow-derived dendritic cells. *Chemosphere* (2008) 73:371–6. doi: 10.1016/j.chemosphere.2008.05.054
99. Yang D, Zhao Y, Guo H, Li Y, Tewary P, Xing G, et al. [Gd@ C82 $(OH)_{22}$] n nanoparticles induce dendritic cell maturation and activate Th1 immune responses. *ACS Nano* (2010) 4:1178–86. doi: 10.1021/nn901478z
100. Liu Y, Jiao F, Qiu Y, Li W, Lao F, Zhou GQ, et al. The effect of Gd@C-82(OH) nanoparticles on the release of Th1/Th2 cytokines and induction of TNF-alpha mediated cellular immunity. *Biomaterials* (2009) 30:3934–45. doi: 10.1016/j.biomaterials.2009.04.001
101. Li A, Qin LL, Zhu D, Zhu RR, Sun J, Wang SL. Signalling pathways involved in the activation of dendritic cells by layered double hydroxide nanoparticles. *Biomaterials* (2010) 31:748–56. doi: 10.1016/j.biomaterials.2009.09.095
102. Petersen LK, Xue L, Wannemuehler MJ, Rajan K, Narasimhan B. The simultaneous effect of polymer chemistry and device geometry on the *in vitro* activation of murine dendritic cells. *Biomaterials* (2009) 30:5131–42. doi: 10.1016/j.biomaterials.2009.05.069
103. Tomić S, Dokić J, Vasilijić S, Ogrinc N, Rudolf R, Pelicon P, et al. Size-dependent effects of gold nanoparticles uptake on maturation and antitumor functions of human dendritic cells *in vitro*. *PLoS ONE* (2014) 9:e96584. doi: 10.1371/journal.pone.0096584
104. Okada N, Mori N, Koretomo R, Okada Y, Nakayama T, Yoshie O, et al. Augmentation of the migratory ability of DC-based vaccine into regional lymph nodes by efficient CCR7 gene transduction. *Gene Ther.* (2005) 12:129–39. doi: 10.1038/sj.gt.3302358
105. Xu H, Cao X. Dendritic cell vaccines in cancer immunotherapy: from biology to translational medicine. *Front Med.* (2011) 5:323–32. doi: 10.1007/s11684-011-0172-4
106. Verdijk P, Aarntzen E, Punt CJA, de Vries IJM, Figdor CG. Maximizing dendritic cell migration in cancer immunotherapy. *Expert Opin Biol Ther.* (2008) 8:865–74. doi: 10.1517/14712590802102740
107. Jin HL, Qian Y, Dai YF, Qiao S, Huang C, Lu LS, et al. Magnetic enrichment of dendritic cell vaccine in lymph node with fluorescent-magnetic nanoparticles enhanced cancer immunotherapy. *Theranostics* (2016) 6:2000–14. doi: 10.7150/thno.15102
108. de Vries IJM, Krooshoop D, Scharenborg NM, Lesterhuis WJ, Diepstra JHS, van Muijen GNP, et al. Effective migration of antigen-pulsed dendritic cells to lymph nodes in melanoma patients is determined by their maturation state. *Cancer Res.* (2003) 63:12–7.
109. Blum JS, Wearsch PA, Cresswell P. Pathways of Antigen Processing. *Annu Rev Immunol.* (2013) 31:443–73. doi: 10.1146/annurev-immunol-032712-095910
110. Munz C. Autophagy Beyond Intracellular MHC Class II Antigen Presentation. *Trends Immunol.* (2016) 37:755–63. doi: 10.1016/j.it.2016.08.017
111. Mak T, Saunders M, Jett B. *Chapter 7 - Antigen Processing and Presentation. Primer to the Immune Response.* 2nd ed. Boston: Academic Cell (2014). p. 161–79
112. Tkach AV, Shurin GV, Shurin MR, Kisin ER, Murray AR, Young S-H, et al. Direct effects of carbon nanotubes on dendritic cells induce immune suppression upon pulmonary exposure. *ACS Nano* (2011) 5:5755–62. doi: 10.1021/nn2014479
113. Blank F, Gerber P, Rothen-Rutishauser B, Sakulkhu U, Salaklang J, De Peyer K, et al. Biomedical nanoparticles modulate specific CD4+ T cell stimulation by inhibition of antigen processing in dendritic cells. *Nanotoxicology* (2011) 5:606–21. doi: 10.3109/17435390.2010.541293
114. Mukai Y, Yoshinaga T, Yoshikawa M, Matsuo K, Yoshikawa T, Matsuo K, et al. Induction of endoplasmic reticulum–endosome fusion for antigen cross-presentation induced by poly (γ-Glutamic Acid) nanoparticles. *J Immunol.* (2011):1001093. doi: 10.4049/jimmunol.1001093
115. Yoshikawa T, Okada N, Oda A, Matsuo K, Matsuo K, Kayamuro H, et al. Nanoparticles built by self-assembly of amphiphilic γ-PGA can deliver

antigens to antigen-presenting cells with high efficiency: a new tumor-vaccine carrier for eliciting effector T cells. *Vaccine* (2008) 26:1303–13. doi: 10.1016/j.vaccine.2007.12.037
116. Song C, Noh YW, Lim YT. Polymer nanoparticles for cross-presentation of exogenous antigens and enhanced cytotoxic T-lymphocyte immune response. *Int J Nanomed.* (2016) 11:3753. doi: 10.2147/IJN.S110796
117. Chen J, Li Z, Huang H, Yang Y, Ding Q, Mai J, et al. Improved antigen cross-presentation by polyethyleneimine-based nanoparticles. *Int J Nanomed.* (2011) 6:77–84. doi: 10.2147/IJN.S15457
118. Han R, Zhu J, Yang X, Xu H. Surface modification of poly (d, l-lactic-co-glycolic acid) nanoparticles with protamine enhanced cross-presentation of encapsulated ovalbumin by bone marrow-derived dendritic cells. *J Biomed Mater Res Part A* (2011) 96:142–9. doi: 10.1002/jbm.a.32860
119. Yang YW, Hsu PYJ. The effect of poly (D, L-lactide-co-glycolide) microparticles with polyelectrolyte self-assembled multilayer surfaces on the cross-presentation of exogenous antigens. *Biomaterials* (2008) 29:2516–26. doi: 10.1016/j.biomaterials.2008.02.015
120. Dong H, Wen Z-F, Chen L, Zhou N, Liu H, Dong S, et al. Polyethyleneimine modification of aluminum hydroxide nanoparticle enhances antigen transportation and cross-presentation of dendritic cells. *Int J Nanomed.* (2018) 13:3353. doi: 10.2147/IJN.S164097
121. Mou Y, Xing Y, Ren H, Cui Z, Zhang Y, Yu G, et al. The effect of superparamagnetic iron oxide nanoparticle surface charge on antigen cross-presentation. *Nanoscale Res Lett.* (2017) 12:52. doi: 10.1186/s11671-017-1828-z
122. Shahbazi M-A, Fernández TD, Mäkilä EM, Le Guével X, Mayorga C, Kaasalainen MH, et al. Surface chemistry dependent immunostimulative potential of porous silicon nanoplatforms. *Biomaterials* (2014) 35:9224–35. doi: 10.1016/j.biomaterials.2014.07.050
123. Wang X, Li X, Ito A, Watanabe Y, Sogo Y, Hirose M, et al. Rod-shaped and substituted hydroxyapatite nanoparticles stimulating type 1 and 2 cytokine secretion. *Colloids Surf B Biointerfaces* (2016) 139:10–6. doi: 10.1016/j.colsurfb.2015.12.004
124. Inoue K-i, Yanagisawa R, Koike E, Nishikawa M, Takano H. Repeated pulmonary exposure to single-walled carbon nanotubes exacerbates allergic inflammation of the airway: possible role of oxidative stress. *Free Radic Biol Med.* (2010) 48:924–34. doi: 10.1016/j.freeradbiomed.2010.01.013
125. Zhu M, Tian X, Song X, Li Y, Tian Y, Zhao Y, et al. Nanoparticle-induced exosomes target antigen-presenting cells to initiate Th1-type immune activation. *Small* (2012) 8:2841–8. doi: 10.1002/smll.201200381
126. Holmstrom KM, Finkel T. Cellular mechanisms and physiological consequences of redox-dependent signalling. *Nat Rev Mol Cell Biol.* (2014) 15:411–21. doi: 10.1038/nrm3801
127. Lutsiak MEC, Kwon GS, Samuel J. Biodegradable nanoparticle delivery of a Th2-biased peptide for induction of Th1 immune responses. *J Pharm Pharmacol.* (2006) 58:739–47. doi: 10.1211/jpp.58.6.0004
128. Schanen BC, Das S, Reilly CM, Warren WL, Self WT, Seal S, et al. Immunomodulation and T helper TH1/TH2 response polarization by CeO_2 and TiO_2 nanoparticles. *PLoS ONE* (2013) 8:e62816. doi: 10.1371/journal.pone.0062816
129. Hardy CL, LeMasurier JS, Belz GT, Scalzo-Inguanti K, Yao J, Xiang SD, et al. Inert 50-nm polystyrene nanoparticles that modify pulmonary dendritic cell function and inhibit allergic airway inflammation. *J Immunol.* (2012) 188:1431–41. doi: 10.4049/jimmunol.1100156
130. You R, Lu W, Shan M, Berlin JM, Samuel EL, Marcano DC, et al. Nanoparticulate carbon black in cigarette smoke induces DNA cleavage and Th17-mediated emphysema. *eLife* (2015) 4:e09623. doi: 10.7554/eLife.09623
131. Keijzer C, Spiering R, Silva AL, van Eden W, Jiskoot W, Vervelde L, et al. PLGA nanoparticles enhance the expression of retinaldehyde dehydrogenase enzymes in dendritic cells and induce FoxP3+ T-cells *in vitro*. *J Control Release* (2013) 168:35–40. doi: 10.1016/j.jconrel.2013.02.027
132. Zhang Y, Bai Y, Jia J, Gao N, Li Y, Zhang R, et al. Perturbation of physiological systems by nanoparticles. *Chem Soc Rev.* (2014) 43:3762–809. doi: 10.1039/C3CS60338E
133. Broos S, Lundberg K, Akagi T, Kadowaki K, Akashi M, Greiff L, et al. Immunomodulatory nanoparticles as adjuvants and allergen-delivery system to human dendritic cells: implications for specific immunotherapy. *Vaccine* (2010) 28:5075–85. doi: 10.1016/j.vaccine.2010.05.004
134. Hamasaki T, Uto T, Akagi T, Akashi M, Baba M. Modulation of gene expression related to toll-like receptor signaling in dendritic cells by poly(gamma-glutamic acid) nanoparticles. *Clin Vaccine Immunol.* (2010) 17:748–56. doi: 10.1128/cvi.00505-09
135. Uto T, Akagi T, Hamasaki T, Akashi M, Baba M. Modulation of innate and adaptive immunity by biodegradable nanoparticles. *Immunol Lett.* (2009) 125:46–52. doi: 10.1016/j.imlet.2009.05.008
136. Zhu M, Li Y, Shi J, Feng W, Nie G, Zhao Y. Exosomes as extrapulmonary signaling conveyors for nanoparticle-induced systemic immune activation. *Small* (2012) 8:404–12. doi: 10.1002/smll.201101708
137. Mizuashi M, Ohtani T, Nakagawa S, Aiba S. Redox imbalance induced by contact sensitizers triggers the maturation of dendritic cells. *J Invest Dermatol* (2005) 124:579–86. doi: 10.1111/j.0022-202X.2005.23624.x
138. Koike E, Takano H, Inoue KI, Yanagisawa R, Sakurai M, Aoyagi H, et al. Pulmonary exposure to carbon black nanoparticles increases the number of antigen-presenting cells in murine lung. *Int J Immunopathol Pharmacol.* (2008) 21:35–42. doi: 10.1177/039463200802100105

Conflict of Interest Statement: The authors declare that the research was conducted in the absence of any commercial or financial relationships that could be construed as a potential conflict of interest.

frontiers in Pharmacology

SYSTEMATIC REVIEW
published: 31 October 2018
doi: 10.3389/fphar.2018.01230

Tumor Microenvironment Targeted Nanotherapy

Clara Fernandes[†], *Divya Suares*[†] *and Mayur Yergeri C*[*]

Shobhaben Pratapbhai Patel School of Pharmacy and Technology Management, SVKM's Narsee Monjee Institute of Management Studies - NMIMS, Mumbai, India

Recent developments in nanotechnology have brought new approaches to cancer diagnosis and therapy. While enhanced permeability and retention effect promotes nano-chemotherapeutics extravasation, the abnormal tumor vasculature, high interstitial pressure and dense stroma structure limit homogeneous intratumoral distribution of nano-chemotherapeutics and compromise their imaging and therapeutic effect. Moreover, heterogeneous distribution of nano-chemotherapeutics in non-tumor-stroma cells damages the non-tumor cells, and interferes with tumor-stroma crosstalk. This can lead not only to inhibition of tumor progression, but can also paradoxically induce acquired resistance and facilitate tumor cell proliferation and metastasis. Overall, the tumor microenvironment plays a vital role in regulating nano-chemotherapeutics distribution and their biological effects. In this review, the barriers in tumor microenvironment, its consequential effects on nano-chemotherapeutics, considerations to improve nano-chemotherapeutics delivery and combinatory strategies to overcome acquired resistance induced by tumor microenvironment have been summarized. The various strategies viz., nanotechnology based approach as well as ligand-mediated, redox-responsive, and enzyme-mediated based combinatorial nanoapproaches have been discussed in this review.

Keywords: tumor microenviroment, cancer, nano therapy, nano carrier, resistance

OPEN ACCESS

Edited by:
Bing Yan,
Shandong University, China

Reviewed by:
Nelson Shu-Sang Yee,
Penn State Milton S. Hershey Medical Center, United States
Fabrizio Martelli,
Istituto Superiore di Sanità (ISS), Italy

***Correspondence:**
Mayur Yergeri C
mayuryc@rediffmail.com

[†]*These authors have contributed equally to this work*

Specialty section:
This article was submitted to Cancer Molecular Targets and Therapeutics, a section of the journal Frontiers in Pharmacology

Received: *30 June 2018*
Accepted: *08 October 2018*
Published: *31 October 2018*

Citation:
Fernandes C, Suares D and Yergeri MC (2018) Tumor Microenvironment Targeted Nanotherapy. Front. Pharmacol. 9:1230. doi: 10.3389/fphar.2018.01230

INTRODUCTION

Worldwide, tackling cancer still remains a daunting task for clinicians and researchers. Ferlay et al. (2015) have reported that among the different types of cancers, lung cancer is prominently associated with highest mortality rate followed by liver and stomach cancer. In recent times, there has been increased incidences of patients afflicted with breast and colorectal cancers. By the year 2025, it is estimated that, globally, there will be a surge in the number of cancer cases (>20 million annually) (Zugazagoitia et al., 2016). This alarming statistics has compelled the researchers across the globe to expedite the research for newer and potent molecules to overcome the acquired resistance and eradicate the cancerous cells from the biological milieu. However, the complexity of the disease, demands exhaustive efforts to design chemotherapeutics for curbing tumor growth (Raavé et al., 2018).

Nonetheless, these efforts have been translated into cancer molecules capable of combating the cancer progression, albeit in preclinical setting. Their implementation in the clinical setting is yet fraught with non-specificity resulting in undesirable side effects (Dai et al., 2016). Another

debilitating issue plaguing the chemotherapeutic arena is the development of acquired resistance which is often a distressing fact after the initial responsive period for both individual and combinational cancer therapy (Cree and Charlton, 2017). Compelling clinical findings incriminate the presence of malignant and metastatic components in tumor microenvironment to be an underlying mechanism of tumor resistance to chemotherapy (Cheng et al., 2016).

Due to complexity of tumor microenvironment (**Figure 1**), the conventional drug delivery system fails to deliver the chemotherapeutics in effective concentration for cancer cell kill and is associated with debilitating side effects. This has prompted to exploit the alternative nanoparticulate strategy to achieve tumor specificity, if possible, improve therapeutic index and the pharmacokinetic profile of chemotherapeutic agents (Danhier, 2016). By virtue of enhanced permeability and retention (EPR effect), passive diffusion has been found to enable tumor localization of nano-chemotherapeutics. With the limited understanding of tumor microenvironment and initial success accrued exploiting EPR effect; the earlier research was primarily focused on designing stable long-circulating nanocarriers to enable superior drug localization with minimal loss of drugs in systemic circulation. To-date, these efforts have translated into commercialization of first generation FDA-approved nano-chemotherapeutics; liposomal formulation of doxorubicin (DOX) (Doxil® or Caelex®), daunorubicin (DaunoXome®) and albumin-bound paclitaxel (PTX) (Abraxane®) (Overchuk and Zheng, 2017). However, clinically these formulations have been found to be moderately successful due to inadequate tumoral delivery of the nano-chemotherapeutics (Primeau et al., 2005; Kyle et al., 2007). The probable reasons for this discrepancy can be ascribed to the confinement of nano-chemotherapeutics to highly perfused regions, often depriving the low perfused or avascular tumor regions. This inhomogeneity in tumoral distribution has shown to contribute to sub-optimal therapeutic efficacy, acquired resistance, tumor recurrences and hence, necessitates the need for high drug dosing. Consequently, leading to undesirable adverse or toxic effects (Waite and Roth, 2012; Stapleton et al., 2015).

For tumoral uptake, the nano-chemotherapeutics rely on the tumor vasculature wherein they are extravasted into the tumor interstitium. However, within the tumor microenvironment, the localization of nano-chemotherapeutics may also be obstructed by the high interstitial fluid pressure, altered extracellular matrix (ECM) structure, increased cell division and impaired lympathic drainage (Wong et al., 2011; Ozcelikkale et al., 2013). Thus, there is a dearth in understanding of the complex parameters governing these transport processes and localization in tumor are posing huge bottlenecks for designing an effective nano-strategy for eradicating tumor. In this perspective, this review focuses on understanding the barriers and opportunities proffered by tumor microenvironment and summarizes the diverse strategies to modulate tumor microenvironment for enhanced delivery of nano-chemotherapeutics to overcome acquired resistance.

UNDERSTANDING THE CHALLENGES AND OPPORTUNITIES PRESENTED BY TUMOR MICROENVIRONMENT TO NANO-CHEMOTHERAPEUTICS

Mounting evidences give an insight about the crucial role of tumor microenvironment in controlling the abnormal tissue growth, tumor progression, development of localized resistance to chemotherapeutics and metastasis. Overall, tumor microenvironment plays a pivotal role in the therapeutic outcome of the chemotherapeutics in clinical oncology. Thus, it is imperative to have an understanding of the tumor biology for designing effective therapeutic interventions to overcome acquired drug resistance, abrogate tumor progression, and prevent metastasis (Chen et al., 2015). In this section, we recapitulate the hallmarks of the malignant tumor microenvironment which have been targeted for effective anticancer therapy and the challenges for nanoparticulate drug delivery. Broadly, the targeting strategies employed focus on; (i) Priming of tumor microenvironment to facilitate better uptake of nano-chemotherapeutics (**Figure 2**) and (ii) Tumor targeting of nanocarriers by using suitable approaches designed on the specific expression of receptors, enzymes or modulation of tumor microenvironment.

Considering these stratagems, the section Understanding the Challenges and Opportunities Presented by Tumor Microenvironment to Nano-Chemotherapeutics will provide insight about the tumor priming strategies and section Types of Nanocarriers will discuss the widely known approaches to target nano-chemotherapeutics.

Tumor-Associated Vasculature

Generally, tumor-associated vasculature is a key target exploited to achieve localization of the anti-angiogenic chemotherapeutics for suppression of tumor growth. The underlying rationale for anti-angiogenesis, is that an unhindered tumor growth essentially requires independent and unperturbed blood supply. In general, it is assumed that for solid tumors to grow beyond a size of 1–2 mm, a steady supply of oxygen and nutrients is a pre-requisite. Hence, by obstructing the blood supply, tumor regression can be induced *in vivo*. Several mechanisms have been reported (Chen and Cai, 2014) to contribute to tumor-associated vasculature, namely;

i. Sprouting angiogenesis, a dynamic and complex process characterized by formation of new blood vessels arising due to proliferation of endothelial cells of pre-existing capillaries.
ii. Vasculogenesis, a type of "back-up" pathway predominant on inhibition of angiogenesis, wherein, *de novo* capillaries are formed from circulating endothelial progenitor cells (Brown, 2014).
iii. Intussusceptive microvascular growth, another variant of angiogenesis, wherein interstitial tissue pillars (invagination of capillary walls) are inserted into pre-existing capillary resulting in splitting of initial new capillary into two new capillaries. It is considered to be a faster process compared to sprouting angiogenesis and characterized by non-leaky

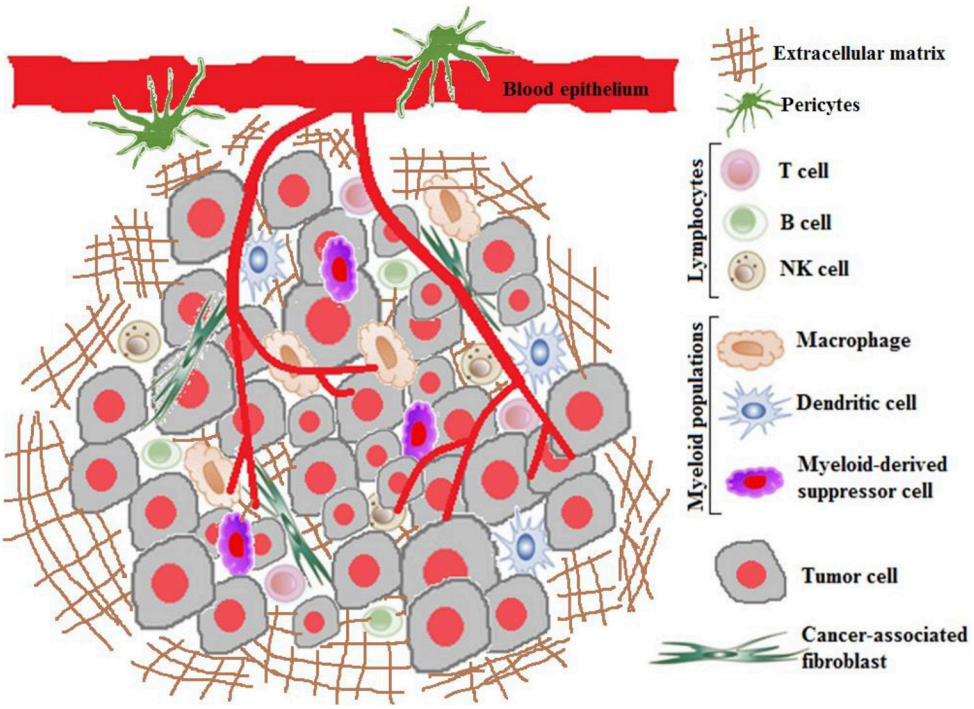

FIGURE 1 | Tumor microenvironment.

capillaries (De Spiegelaere et al., 2012; Ribatti and Djonov, 2012).

iv. Vessel co-option, a characteristic of aggressive and non-angiogenic tumors, exploits the pre-existing capillaries of the surrounding host tissue. Hence, is a major contributor to resistance to anti-angiogenic therapy and metastasis (Donnem et al., 2013; Bridgeman et al., 2017).

v. Vasculogenic mimicry, an alternate pseudo-vascular channel comprising of predominantly differentiated tumor cells for ensuring blood supply. These channels were discovered initially in highly aggressive melanoma cells. However, in recent times, they have also been reported in other malignant tumors, to name a few, lung cancer, ovarian cancer, breast cancer (Angara et al., 2017; Shen et al., 2017).

The onset of angiogenesis widely known as angiogenic switch is induced by plethora of pro- and anti-angiogenic factors. Most widely known and exploited factors comprise of vascular endothelial growth factor (VEGF), fibroblast growth factor (FGF), platelet-derived growth factor (PDGF), angiopoietin, hypoxia-inducible factor-1 (HIF-1), and transforming growth factor (TGF) which have shown to interact with receptors expressed in the endothelial cells (Carmeliet, 2003; Gacche and Meshram, 2013).

Unlike normal blood vessels which are governed by co-ordinated dynamics of pro- and anti-angiogenic factors, the rapid growing tumor microvasculature are found to be abnormally fragile, irregularly shaped, dilated, tortuous, highly permeable with increased geometric resistance (Geevarghese and Herman, 2014). This abnormality renders the tumor vascular network disorganized and tortuous with a tendency of exclusion of downstream vessels from blood supply. Thus, resulting in discrete hypo-perfused areas or necrotic areas within tumor tissue (Stylianopoulos et al., 2018). Further, the heterogeneous nature of the vascular network, non-laminar blood flow and leaky nature, often result in variability in blood distribution across tumor tissues i.e., showing regions of turbulent or static blood flow. An outcome of this is; (i) Poor accessibility of chemotherapeutics or immune cells present in the bloodstream to poorly perfused tumor regions, (ii) Exacerbation of hypoxic conditions and extracellular acidic pH in tumor, and (iii) Increased interstitial fluid pressure (Jain, 2013; Belli et al., 2018).

Tumor Pericytes

Although associated with tumor vasculature, in recent times, pericytes, a subtype of mural cells (other types include vascular smooth muscle cells) have garnered attention for their role in tumor microenvironment. In normal tissues, pericytes have shown to act as "angioregulators" i.e., they stabilize as well as promote angiogenesis; however, their role in tumor microenvironment is yet unclear (Kelly-Goss et al., 2014). Literature cites that they strengthen the blood vessel barrier in co-ordination with endothelial cells or other blood components, thereby preventing vascular leakage. Besides this, they are also known as metastatic stimulators and contribute in accumulation of cancer stem cells within tumor

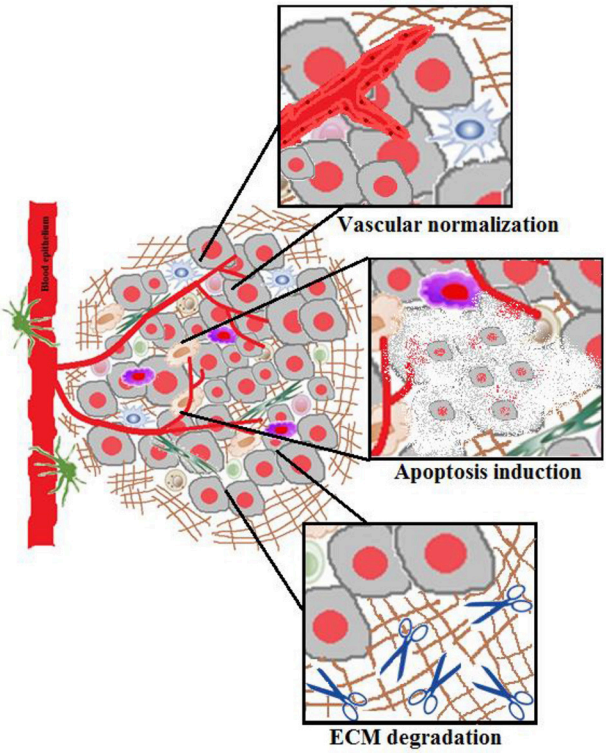

FIGURE 2 | Tumor microenvironment priming.

microenvironment (Gerhardt and Betsholtz, 2003; Kang and Shin, 2016; Ferland-McCollough et al., 2017).

Structurally, pericytes are highly elongated, slender, branched cells, with cytoplasmic projections encircling the vessel wall (Diaz-Flores et al., 2009; Sena et al., 2018). They are situated in the basement membrane of tumor blood vessel either as solitary cells or as single-cell layer (Armulik et al., 2011). It is assumed that, in tumor, pericytes are differentiated either from progenitors in the host tissue or from bone-marrow-derived cells (Liu and Ouyang, 2013). In normal angiogenesis, pericytes control the VEGF-mediated endothelial cell proliferation via the direct cell-to-cell contact and paracrine signaling pathways. Through both these mechanisms, pericytes have shown to exert control on proliferation of endothelial cells. Subsequently, they facilitate migration of endothelial cells by degrading the basement membrane and liberate matrix-bound growth factors (Franco et al., 2011; Stapor et al., 2014; Ribeiro and Okamoto, 2015). It has been documented that the endothelial cells on the tip of newly sprouted vascular channel recruit pericytes via secretion of PDGF-BB. This factor activates the pericytes by binding with PDGFR-β receptors expressed on the pericyte surface and induce its migration across the sprouted vascular channel, thereby modulating the pericyte coverage on tumor vessels (Armulik et al., 2011; Minami et al., 2013).

Besides PDGF-BB, other factors such as Angiopoietin-1/Tyrosine Kinase-2 (Ang-1/Tie2), TGF-β, and matrix metalloproteinases (MMP) play a vital role in pericyte-endothelial cell interactions (Chen Z. et al., 2016). Ang-1, reported to be produced by pericyte, binds to Tie2 receptor expressed on endothelium and plays a pivotal role in maturation as well as stabilization of newly formed blood vessels. Similarly, TGF-β, another important factor secreted by endothelial cells for vessel development, facilitate the recruitment of pericytes toward endothelium. Ang-1 primarily induces stabilization of blood vessel by increasing the pericyte coverage over the blood vessels (Fuxe et al., 2011). Similar to Ang-1, Ang-2 is also secreted by endothelial cells activated by cancer-derived modulators, however, it has shown to exert antagonizing effect (Augustin et al., 2009). It is reported that Ang-2 promotes detachment of pericytes from endothelial cells thereby destabilizing the newly formed blood vessels by initiating uncontrolled sprouting of endothelial cells. In case of MMPs, they indirectly promote pericyte recruitment, proliferation and activation by modifying or degrading the basement membrane and enhancing the release of basement membrane bound growth factors (such as VEGF) (Chantrain et al., 2006).

Studies have revealed that pericyte coverage does vary with different malignant tumors (Eberhard et al., 2000). Morikawa et al. (2002) reported that in tumor tissue, pericytes were found to be loosely associated with endothelial cells in both, basement membrane and on tumor micro vessel. Further, their cytoplasmic processes were found to be deeply penetrated into the tumor parenchyma, a distinct feature of tumor vasculature. Yao et al. (2007) demonstrated that in clear cell renal cell carcinoma tumor tissue, pericyte coverage was visibly absent in undifferentiated vessels while for differentiated vessels, loose association, partial or total absence of pericyte coverage was noted. Zhang et al. (2012) have demonstrated that pericyte coverage was found to be more in aggressive cancers such as pancreatic cancer as compared to relatively lesser threatening cancers such as ovarian or colon cancer. Studies by Welén et al. (2008) on prostate cancer cell line LNCaP demonstrated that high pericyte coverage was associated with decrease in tumor metastasis ascribed to reduction in endothelial cell migration. Similarly, Cooke et al. (2012) reported that low pericyte coverage was associated with reduced tumor growth. However, there was increased metastasis in colorectal, prostate, pancreatic and invasive breast cancers. This influential role of pericyte coverage in tumor growth could be due to the overexpression of PDGF-BB by tumors which governs extent of pericyte coverage and inhibit endothelial cell proliferation resulting in reduction of vessel density and overall tumor growth (McCarty et al., 2007; Raza et al., 2010).

Evidently, the researchers have concluded that, both, the aberrant pericyte-endothelial cell interaction and abnormalities in pericyte structure, do contribute to the leakiness of tumor vasculature (Xian et al., 2006). Recent advances in understanding of tumor microenvironment has led to speculation that pericytes may contribute to the acquired resistance to anti-angiogenic therapy (Bergers and Hanahan, 2008). This is believed to be arising either by enhancing endothelial cell survival via crosstalk or by upregulation of the endothelial survival factor Ang-1 or by producing VEGF (Reddy et al., 2008; Welti et al., 2013). Besides this, pericytes owing to the inherent progenitor

properties on detachment from tumor vasculature have also shown to differentiate into stromal fibroblasts, a contributor to tumor invasion and metastasis (Hosaka et al., 2016; Paiva et al., 2018).

Challenges and Opportunities for Nano-Chemotherapeutics in Targeting Tumor Vasculature

For efficient interaction of nano-chemotherapeutics with the cancerous cells in tumor milieu, it is essential that nano-chemotherapeutics are accumulated in the tumor through normal vascular network. Subsequently, their interaction with target cells should be facilitated via selective extravasation from tumor microvasculature and their passage through the ECM (Miao and Huang, 2015). Matsumura and Maeda (1986) were the first to demonstrate the phenomenon of EPR effect of macromolecules in tumor, ascribed to leaky tumor vasculature (**Figure 3**). Preclinically, ten times higher localization was reported for nanoparticles in the particle size range of 10–100 nm in diameter (Miao and Huang, 2015; Muntimadugu et al., 2017). However, in clinical setting, owing to the complex and heterogenous nature of human tumors, intra-/inter- variability in both tumor characteristics and tumor microenvironment in patient populations, EPR based paradigm approach failed to replicate the success of preclinical studies (Bjrnmalm et al., 2017). Hence, for enhancing the extravasation of nanoparticles, tumor pre-conditioning or priming is being explored. Herein, remodeling of tumor vasculature can be done either by Zhang et al. (2017b) **(i)** Reducing the pericyte coverage, **(ii)** Increasing permeability of tumor microvessels, **(iii)** Tumor vessel dilation or **(iv)** Vascular normalization wherein anti-angiogenic drugs repair the anomalous structure and function of the tumor vasculature network thereby contributing to enhanced tumor perfusion and oxygenation.

The seminal work done by Kano et al. (2007) demonstrated TβR-I (crucial for TGF-β signaling) inhibitor mediated enhanced extravasation of Doxil® (108 nm diameter) as well as micellar adriamycin (65 nm diameter) induced by decreased pericyte coverage of tumor endothelial cells in pre-treated xenografted BxPC3 human pancreatic adenocarcinoma cell line in nude mice. Chaudhuri et al. (2016) showed that at low dose of smoothened inhibitors of hedgehog signaling (erismodegib) pre-treated patient-derived PaCA xenografts promoted extravasation of DOX-loaded sterically-stabilized liposomes (80–100 nm) by promoting formation of immature blood vessels lacking in pericyte coverage with endothelium-poor basement membrane structures. Chauhan et al. (2012) reported that vascular normalization in orthotopic E0771 mammary tumors with anti-VEGF-receptor-2 antibody DC101 showed size-dependent enhancement in tumor reduction, it was superior at lower particle size of ∼10 nm (Abraxane) while at higher particle size ∼100 nm (Doxil®) it remained unaffected. The reasons ascribed were increase in steric and hydrodynamic barrier with the reduction in pore-size of normalized tumor vessels which benefitted predominantly tumor penetration of smaller particle size. Jiang et al. (2015) suggested controlled dosing of anti-VEGF-receptor-2 antibody DC101 in orthotopically implanted breast adenocarcinoma MCaP0008 cells restored vascular normalization. This ensured enhanced deep tumoral accessibility and penetration of pegylated quantum dots (both 20 and 40 nm) within the tumor stromal matrix. Nevertheless, smaller sized nanoparticles i.e., around 10 nm had superior penetrability across the tumor matrix owing to less diffusional restrictions. Wang et al. (2017) showed that BQ123, a vasodilator which alters an ET-1/ETA transduction pathway as well as blocks the ETA receptor triggered a tumor-specific delivery of photothermal nanomedicine (100 nm) for effective photothermal mediated therapy of tumors.

Tumor Stroma

Broadly, tumor stroma comprises of the following components (Bremnes et al., 2011; Hanahan and Weinberg, 2011; Valkenburg et al., 2018);

i. Cellular components such as non-malignant cells widely known as cancer-associated fibroblasts (CAF), host tissue specific specialized mesenchymal stromal cells, osteoblasts, chondrocytes, innate and adaptive immune cells, endothelial cells, and pericytes (Hughes, 2008).

ii. Extracellular matrix (ECM) comprises of distinct components having different physical and biochemical properties such as structural proteins (collagen and elastin), specialized proteins (fibrilin, fibronectin, and elastin), proteoglycans, and polysaccharides (hyaluronan) (Özbek et al., 2010). They are further classified into the interstitial matrix and the basement membrane (Xiong and Xu, 2016). The components for interstitial matrix are produced by stromal cells and basement membrane; collectively by epithelial, endothelial, and stromal cells (Lu et al., 2012). Basement membrane is a specialized compact, less porous, thin layers of tumor ECM acting as a supporting scaffold for blood vessels and capillaries. It is situated at the basal surface of epithelial and endothelial cells wherein it plays a crucial role in tissue polarity. It is primarily composed of non fibrillar type IV collagen, laminins, entactins, and proteoglycans (Egeblad et al., 2010; Liotta, 2016).

Tumor Extracellular Matrix

Transformation from normal tissue to tumor tissue is accompanied with profound changes in the tumor microenvironment arising due to enhancement in tumor cell contractility, uncontrolled expansion of the growing tumor tissue, and modifications of the attributes of ECM (Northcott et al., 2018). Generally, tumor ECM (∼400 Pa) is found to be stiffer in comparison to normal ECM (150 Pa), and the stiffness is thought to contribute to tumor metastasis, activation of adjoining stromal fibroblast to CAF and can be correlated with the number of tumor associated macrophages (TAM) (Cox and Erler, 2011; Reid et al., 2017). The stiffness of tumor ECM is often associated with relatively high levels of crosslinked collagen (Type I), occurring due to the excessive activity of lysyl oxidase (LOX), as well as increased integrin signaling in the tumor microenvironment mediated by collagen modifying enzymes such as P4HA1, P4HA2, PLOD2, and LOX (Holback

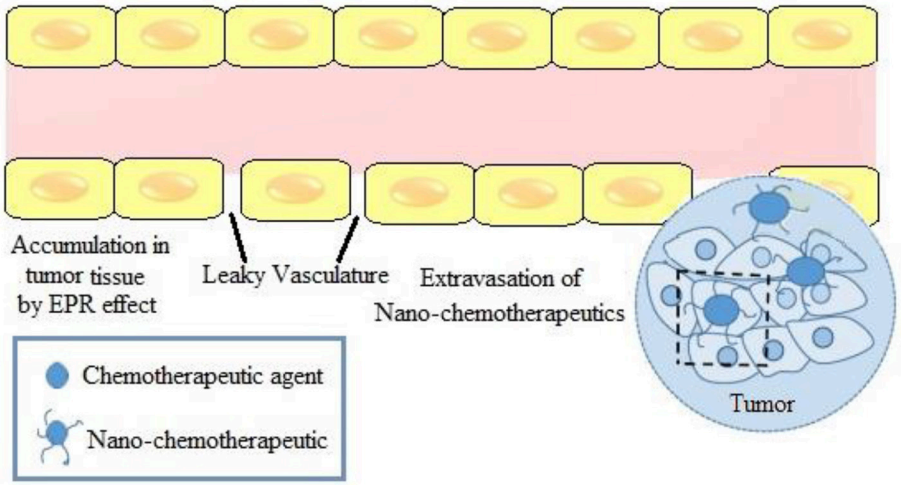

FIGURE 3 | EPR effect in a tumor microenvironment.

and Yeo, 2011). Han et al. (2016) demonstrated that abnormal orientation of collagen I fiber in tumor ECM defined the direction of cell migration and promoted cell breakage into the basement membrane before metastasis. For this, tumor cells via contact guidance, used contractile force to align the ECM fibers perpendicularly to the tumor, thereby induced remodeling of the fibers in the vicinity of tumor (Kraning-Rush and Reinhart-King, 2012). Balcioglu et al. (2016) showed that when 4T1 breast cancer spheroids were kept in contact with collagen based ECM, resulted in re-orientation of surrounding collagen-based ECM network upto five times their radius which further acted as a mechanical cue to guide the movement of microvascular endothelial cells, thereby influencing angiogenesis. Besides this, the increased deposition of ECM in tumor microenvironment governed by various angiogenic growth factors, VEGF, stromal cell derived factor 1, Ang-2, PDGF-B, placental growth factor, and connective tissue growth factors are all associated with solid stress (Danhier et al., 2010; Muntimadugu et al., 2017).

The solid stress constitutes two opposing stress, **(i)** Compressive growth-induced (or residual) stress arising inside the tumor due to both, the expansion of collagen fibers and resistance of proliferating cancer cells as well as activated CAF on compression and **(ii)** Externally applied tensile stress occurring at the interface of tumor-normal tissue exerted by normal host tissue to resist tumor expansion (Kalli and Stylianopoulos, 2018). In ECM, it is reported that owing to its stiffness, cross-linked collagen resists tensile stress, whereas hyaluronan resists compressive stress, attributed to its negatively charged hydrophilic chains which induce electrostatic repulsion and retains water, thereby resulting in a poorly-compressible matrix (Stylianopoulos et al., 2012; Kharaishvili et al., 2014; Pirentis et al., 2015). The stiffness of ECM has shown to promote tumorigenesis by; favoring cell proliferation, triggering epithelial-mesenchymal transition via epithelial cell-ECM interaction, increasing adherence junctions motility, inhibiting apoptosis in a TGF-β1-dependent process and so on. However, there are exceptions such as neuroblastoma cells, colon, prostate cancerous cells, and human tongue squamous carcinoma cells which require low stiffness (Broders-Bondon et al., 2018). Similar observations have been noted for solid stress, Fernández-Sánchez et al. (2015) examined that solid stress via the mechanical activation of β-cat pathway provided mechanical cues in the *in vivo* malignant phenotype of murine colon tissue, for inducing the transformation of surrounding normal epithelial cells into cancer cells. Nguyen et al. (2014) demonstrated that the stiffness due to dense network of collagen-rich fibers also hampered the anticancer activity and conferred resistance against Raf kinase inhibitor, sorafenib.

Tumor Associated Macrophages

TAM are one of the important tumor stromal cells (accounting to ∼30% of immune cells) implicated in tumor survival, growth, and metastasis. They are either transformed from the existing macrophages of host tissue or localized to the tumor site from the bone marrow and spleen under the influence of monocyte chemo attractant protein-1 (Binnemars-Postma et al., 2017; Quail and Joyce, 2017). Due to their plastic nature, depending on the type of cytokine exposure, they have been known to exhibit either pro- or anti-inflammatory activities (Quail and Joyce, 2017). Widely investigated TAM include tumor resolving classical M1 macrophage and pro-tumorigenic alternative M2 tumor associated macrophage, together they play pivotal role in tumor vessel abnormalization/normalization in tumor microenvironment (Ngambenjawong et al., 2017). Typically, M1 macrophage normalize tumor vascular network and induce immune response thereby causing the phagocytosis or destruction of tumor cells i.e. tumor regression. In contrast, M2 TAM have anti-inflammatory properties thereby stimulating immunosuppression and formation of abnormal tumor vasculature, indirectly contributing to tumor progression (Jarosz-Biej et al., 2018). It is reported that in an invasive cancer, polarization of M1 to M2 macrophages takes place, making M2

macrophage constitute 50% of the tumor stroma. Functionally, they are known to regulate tumorigenesis, metastasis as well as abnormal angiogenesis, in association with tumor related growth factors, inflammatory components such as cytokines and ECM remodeling molecules such as C-C motif chemokine ligand 2, C-X-C motif chemokine 12, CXCR4, TGF-β, VEGF, PDGF, COX-2, and MMP (Zheng X. et al., 2017). Based on these observations, anti-tumor macrophage therapy is primarily focused either on depletion or re-programming M2 macrophage or regulation of polarization of macrophage (Goswami et al., 2017; Hoves et al., 2018).

Cancer-Associated Fibroblasts

Morphologically and functionally, CAF are a type of mesenchymal cells which are endowed with migratory and contractile properties of myofibroblasts, secreting various factors such as; collagen, cytokines, and chemokines into tumor stroma (Pankova et al., 2016). They play a crucial role in remodeling the tumor stroma by co-ordinating the enzymes responsible for secretion as well as crosslinking of the collagen network of ECM thereby increasing the stiffness of ECM (Clark and Vignjevic, 2015). Further, in presence of tumorigenic hypoxia, they generate collagen reticulation which enhances cancer cell invasiveness, contractility and motility (Pankova et al., 2016). Residing within or across the marginal surface of tumor, the resident fibroblasts on activation via growth factors, direct cell-cell communication, interaction with adhesion molecules, interaction with leukocytes, presence of reactive oxygen species (ROS), and microRNA, transform into CAF (Tao L. et al., 2017). These fibroblasts originate either by alteration of smooth muscle cells or bone marrow-derived stem cells by tumor cells, or transdifferentiation of epithelial cells-to-myofibroblasts, or through endothelial-to-mesenchymal transition (Gascard and Tlsty, 2016). Zhuang et al. (2015) documented CAF induced epithelial-to-mesenchymal transition via growth factor such as TGF-β1. Zhang A. et al. (2017) showed that CAF polarized M2 macrophages mediated through increased production of soluble cytokine macrophage colony-stimulating factor thereby promoting cancer proliferation, invasion, and metastasis in pancreatic ductal adenocarcinoma. Based on the role of CAF in modulating tumor microenvironment, anti-cancer associated fibroblast therapies are being designed to overcome the acquired resistance with anti-cancer therapies.

Challenges and Opportunities for Nano-Chemotherapeutics to Target Tumor Stroma

After extravasation, the stiff ECM presents itself as a barrier to the diffusional movement of nano-chemotherapeutics in the interstitial space. The diffusional movement is inversely related to the size of nanoparticles i.e., particles exceeding matrix mesh size ranges 20–40 nm are restricted from diffusing across the ECM in solid tumors. While the nanoparticles nearing the aforementioned mesh size range are hindered to lesser extent and particles less than mesh size range are found to penetrate relatively easily. Besides this, the tortuosity of the interstitial space further lengthens the diffusional path-length of the nanoparticles from normal vessels to tumor cells (Zhang et al., 2017a). It is also believed that the high amount of collagen reduces the hydraulic conductivity thereby decreasing the convective flow in the interstitium (Nichols and Bae, 2014). Hence, tumor matrix degrading enzymes i.e., collagenase and hyaluronidase contribute to improved intratumoral dispersion of nanoparticles by disruption of ECM. This holds true, especially, for collagenase which is found to be more effective in case of nanoparticles, in comparison whereas hyaluronidase is known to facilitate distribution of smaller molecules such as DOX (Au et al., 2016). However, disruption of ECM helps relieve the solid stress by reopening the collapsed tumor vessels but has little or null effect on their leakiness. Similarly, vascular normalization is ineffective for distribution of nano-chemotherapeutics, moreover, it is unable to reduce the solid stress and decompress the tumor vessels compressed by rigid ECM or proliferating cells (Stylianopoulos and Jain, 2013).

Zhang et al. (2017a) demonstrated the use of a selective COX-2 inhibitor, celecoxib in improving the tumor localization of PTX-loaded micelles in a human-derived A549 tumor xenograft nude mice model. Celecoxib was found to modulate tumor microenvironment, by varied mechanisms, viz. reduction of the expression of CAF, distortion of ECM by fibronectin bundle disruption and normalization of tumor vasculature, resulting in improved tumor perfusion. This enabled and improved *in vivo* delivery as well as therapeutic benefits of PTX-loaded micelles. Interestingly, Chen B. et al. (2016) have demonstrated the effect of Tenascin C, a tumor-specific ECM targeted FHKHKSPALSPVGGG peptide-coated liposomal delivery of Navitoclax (NAV), a targeted high-affinity small molecule for priming tumor microenvironment. Tenascin C facilitated tumor localization of liposomal formulation by specifically inducing CAF apoptosis (at a very low dose 5 mg/kg), by reducing interstitial fluid pressure and vascular normalization. The liposomal NAV when used in conjunction or separately with liposomal delivery of DOX was found to improve the tumor localization of DOX. The proposed mechanisms for the enhanced anti-tumor effect included; synergistic anti-cancer activity between DOX and NAV, eradication of CAFs, and deeper penetration of liposomal DOX into tumor tissue. Similarly, Geretti et al. (2015) revealed that the appropriate dose sequencing of cyclophosphamide, enhanced tumoral uptake of HER2-targeted pegylated liposomal DOX in MDA-MB-361 cells, by induction of tumor cell apoptosis, decrease of tumor cell density, reduction of interstitial fluid pressure, with enhanced vascular perfusion.

Tumor Interstitial Fluid Pressure

In normal tissues, under the influence of capillary hydrostatic pressure there is an extravasation of fluid from the capillaries leading to increased interstitial pressures. However, the pressure is controlled by systemic re-absorption of accumulated interstitial fluid through the post-capillary veins and drainage via lymphatic flow (Scallan et al., 2010). In general, the components of the tumor interstitium can be broadly categorized into the colloid-rich gel domain; comprising predominantly of hydrophilic hyaluronate and proteoglycans, and the colloid-poor fluid-free domain (Omidi and Barar, 2014). Structurally, in

cancerous conditions, owing to the irregular geometry, abnormal vasculature, increased ease of transcapillary fluid flow (i.e., vessel leakage), dysfunctional lymphatic drainage system and rapidly proliferating cell burden in the ECM (solid stress), there is constant build-up of interstitial fluid (Lunt et al., 2008; Wiig and Swartz, 2012). The outcome of these solid and fluid pressures in the tumor is the tumor interstitial fluid pressure (Ariffin et al., 2014; Stylianopoulos, 2017). Literature states that for normal tissues interstitial fluid pressure is in the range of −3 to +3 mmHg, whereas for solid malignant tumors, it increases within a range of 5 to 40 mmHg (Baronzio et al., 2012; Simonsen et al., 2012; Yu T. et al., 2013; Wagner and Wiig, 2015). It is experimentally found that the interstitial fluid pressure is greater in the interiors of tumor and precipitously drops across the tumor boundary and surrounding host tissues, possibly in the periphery connected to the normal tissue blood vessels (Siemann and Horsman, 2015). Conversely, the interstitial fluid flow is relatively lower in the tumor interior and is found to be directed toward the tumor boundary and the surrounding tissue (Wu et al., 2013). Increase in interstitial fluid pressure stimulates stretching of tumor cortex, as a consequence, the cell proliferation in the tumor tissue is triggered (Hofmann et al., 2006). Yu T. et al. (2013) demonstrated that high tumor interstitial fluid pressure markedly altered the expression of $\sim$ >1,800 genes associated with invasion and metastasis in SCC-4 and SCC-9 human tongue squamous cell carcinoma cell lines, as a result, there was enhancement in *in vitro* cancer cell proliferation and invasion.

Challenges and Opportunities for Nano-Chemotherapeutics to Target Tumor Interstitial Fluid Pressure

Due to transient high local interstitial fluid pressure, chemotherapeutics are often expelled into systemic circulation from the tumor periphery into adjoining tissues, thereby reducing the efficacy as well as tumor specificity of cancer therapy. Moreover, due to the absence of fluid pressure gradients across the vessel wall and within the tumor, there is a decrease in both, transcapillary flow and convective transport of chemotherapeutics, making diffusion the primary mechanism for transvascular and interstitial transport of drug in tumor (Cairns et al., 2006; Chauhan et al., 2011; Stylianopoulos et al., 2018).

With regards to nano-chemotherapeutics, both diffusion process and outward direction of the interstitial fluid pressure from the core of tumor compromises the distribution as well as localization of nano-chemotherapeutics into tumor tissue (Nakamura et al., 2016). Torosean et al. (2013) demonstrated that uptake of 40 nm fluorescent beads was found to be drastically reduced in tumor having higher interstital pressure arising due to increased collagen content. Hylander et al. (2015) showcased the tumor priming potential of cytotoxic biological therapy Apo2L/TRAIL in lowering interstitial fluid pressure in three different human tumor xenograft models (Colo205, MiaPaca-2 and a patient gastrointestinal adenocarcinoma tumor xenograft). The study revealed that via apoptosis, a single dose of Apo2L/TRAIL drastically lowered the interstitial fluid pressure in treated tumors with broadening of the stromal areas at 48 h. Post treatment, there was significant improvement in tumoral uptake and anti-tumor efficacy of both gemcitabine and liposomal gemcitabine. Interestingly, another study carried out using single dose of tumor priming agent, liposomal imatinib (50 mg/kg) showed reduction in the interstitial pressure in B16 melanoma achieved by inhibition of tumor fibroblasts via blocking PDGF and vascular normalization for almost 50 h. Further, the liposomal tumor priming agent at 20 mg/kg significantly improved the intra-tumoral delivery, accumulation and anti-tumor efficacy of liposomal DOX (Fan et al., 2013).

Tumor Chemical Microenvironment

An outcome of aberrant tumor vaculogenesis is inadequate diffusion and perfusion within and across the uncontrollably proliferating tumor tissue leading to generation of two potentially debilitating metabolic crisis i.e., hypoxia and extracellular acidosis (Mistry et al., 2017).

Tumor Hypoxia

Tumor hypoxia is a consequence of overconsumption of accessible oxygen by rapidly proliferating cells present at the periphery of tumor and also possibly due to inconsistent erythrocyte flux in the abnormal tumor vasculature (Michiels et al., 2016). This variability of oxygen supply arises due to the hindered diffusion of oxygen at a depth beyond 70–150 μm from the peripheral tumor vasculature thereby contributing to an oxygen tension of <0.1 mmHg (anoxia) to 15 mmHg (Bennewith and Dedhar, 2011; Chitneni et al., 2011; Michiels et al., 2016). Typically, the oxygen concentration in normal tissue and hypoxic solid tumors is found to be in the range of 3–6 and 1–2%, respectively (Ivanovic, 2009; Tian and Bae, 2012). Broadly, tumor hypoxia is classified as chronic hypoxia/diffusion-limited hypoxia and acute cyclic hypoxia/perfusion-limited hypoxia (Dewhirst et al., 1999; Yasui et al., 2010; Patel and Sant, 2016). Chronic hypoxia is a condition characterized by deficit in oxygen level for a prolonged duration (atleast several hours). This is ascribed to longitudinal oxygen gradient i.e., oxygen concentration in the blood remains low, which drastically shortens the length of radial oxygen diffusion in tumor blood vessels causing chronic hypoxia (Matsumoto et al., 2011). In contrast, acute cycling hypoxia affects cancer, endothelial cells and stromal cells adjacent to poorly perfused blood vessels. Herein, the tumor cellular components are exposed to fluctuating periods of re-oxygenation and deep/moderate hypoxia, attributed to cycle of angiogenesis and vascular remodeling activity (occurring over days) and varying erythrocyte flux owing to the redundant tumor vascular network (normally 1–3 fluctuations/h) (Dewhirst, 2007). Pathologically, hypoxia is associated with angiogenesis, metastasis and responsible for acquired resistance to cancer therapy (Muz et al., 2015). In tumor tissues, hypoxia has also shown to induce production of PDGF-BB and other angiogenic factors via HIF-1 (Rankin and Giaccia, 2016). Similarly, hypoxia results in phenotype re-programming of macrophages rendering M1 macrophages unable to present antigens or release pro-angiogenic and immunosuppressive factors, transforming them into anti-inflammatory M2 phenotype (Chanmee et al., 2014).

Tumor Acidic Environment

In normal cells, energy is obtained via oxidative phosphorylation. In contrast, owing to abnormal tumor vasculature and hypoxia, tumor cells derive the energy from the oxygen-independent glycolysis also known as the Warburg effect. The tumor acidic milieu is characterized by increased glucose uptake and fermentation of glucose to lactate. This leads to increase in H^+ ions production and excretion, however, due to poor tumor vascular perfusion, an acidic extracellular pH (pH_e) is generated in malignant tumors, pH_e of 6.5–6.9 in comparison to physiological pH_e of 7.2–7.4. This acidic environment causes efflux of H^+ ions along the concentration gradient from tumor into adjoining normal non-cancerous tissue, leading to cellular death (Estrella et al., 2013). Besides this, carbonic anhydrase (CA) also contributes to the production of H^+ ions by catalyzing hydration of excess CO_2, a by-product of pentose phosphate pathway in tumor (Kato et al., 2013). Thus, a hostile environment encompassing; acidic microenvironment, poor vasculature, proliferating cells, and acidic pH-mediated degradation of ECM by proteinases and subsequent remodeling proves to be detrimental to normal cells. Interestingly, cancerous cells are shown to exhibit better tolerance to the acidic pH by virtue of upregulation of the sodium-hydrogen exchanger or CA (Iessi et al., 2018). Generally, the loss of normal cells and breakdown of ECM has shown to propel the proliferation and invasion of cancerous cells in the vacant space i.e., acidosis contributes to tumor progression via invasion and metastasis (Damaghi et al., 2015). Contrastingly, Warburg phenomenon has also shown to upregulate the expression of crucial transporters for glucose uptake byproducts arising due to glucose metabolism. This enables cancer cells to maintain intracellular pH at 7.4 despite the acidic extracellular pH (Barar and Omidi, 2013; Liberti and Locasale, 2016).

Challenges and Opportunities for Nano-Chemotherapeutics to Target Tumor Chemical Environment

In general, abnormality of tumor chemical environment is an outcome of aberrant tumor vasculture. Hence, normalizing of tumor vasculature to an extent has shown to counteract tumor hypoxia and tumor acidity, thereby improving the tumoral uptake of nano-chemotherapeutics (Xiao et al., 2017). Herein, the strategies widely explored exploit the tumor microenvironment to deliver environment responsive nano-chemotherapeutics (section Types of Nanocarriers).

TYPES OF NANOCARRIERS

Conventional Nanocarriers

Taking into consideration the various attributes for facilitating cell-nanoparticle interaction (Fernandes et al., 2018), several nanocarriers have been designed and explored for the treatment as well as management of cancer. Nano-chemotherapeutics provide several advantages over the conventional cancer therapies, such as superior drug efficiency with minimum toxicity, specificity to tumor site, improved drug solubility and stability, greater circulatory half-life of drug, sustained/controlled release, stimuli-activated drug release, nano-chemotherapeutics with imaging modalities and so on. Since the discovery of EPR effect, several formulation scientists have successfully explored nanocarriers which are stable in the blood during their transit to the tumor cells, penetrate deeper into the layers of tumor tissue and accumulate at the tumor site.

Conventionally, nanocarriers may be broadly classified as follows (**Figure 4**): (a) lipid-based nanosystems viz. liposomes (Zhang X. et al., 2017), solid lipid nanoparticles (Delgado et al., 2012), nanostructured lipid nanocarriers (Shete et al., 2014), nanoemulsions (Izadiyan et al., 2017), lipoplexes (Hattori et al., 2013); phospholipid based microemulsions (Jain et al., 2010) (b) metal-based nanosystems viz. iron oxide, gold, silver, platinum nanoparticles (Bishop et al., 2015); (c) carbon- (Wan et al., 2016) and silica-based (Yu M. et al., 2013) nanosystems; (d) polymer-based nanosystems viz. polymeric nanoparticles (Shen et al., 2013), polymeric micelles (Hao et al., 2015), dendrimers, nanocapsules, polymerosomes, polymer conjugates; (e) surfactant-based nanosystems (Wu et al., 2017); (f) virus-based nanosystems (Ling et al., 2011); (g) biological membrane-based nanosystems and (h) hybrid nanosystems with combination of any above mentioned systems (Shi et al., 2017).

In the last few decades, research has shown that the shape of nano-chemotherapeutics does influence the nanoparticle intravascular, transvascular, and/or interstitial transport as well as their subsequent cellular interaction. This insight about the role of shape of nanocarriers has led to diverse shapes based nano-chemotherapeutics viz., nanospheres, nanoprisms, nanoplates, nanocages, nanorings, nanoboxes, nanostars, nanoflowers, nanodiamonds, nanoshells, nanorods, nanocrystals, nanosheets, nanotubes, nanosnowflakes, and so on (Grazu et al., 2012; Toy et al., 2014). Xie et al. (2017) demonstrated the influence of diverse nanocarrier shapes i.e., nanostar, nanorod, and nanotriangle of methyl-pegylated-anisotropic gold nanoparticles on cellular internalization in RAW264.7 cells (mouse leukaemic monocyte macrophage). The study revealed that the cellular uptake of gold nanoparticles was in the ascending order of nanostar < nanorod < nanotriangle. The dissimilar uptake behavior was ascribed to the endocytotic process. The nanostars were preferrentially internalized via clathrin-mediated endocytotic process. While nanorods were taken up by both via clathrin- and caveolae/lipid raft-mediated endocytosis and were also shown to undergo exocytosis. For nanotriangles, both, clathrin-mediated and cytoskeletal rearrangement enabled dynamin-dependent pathways were found to contribute to superior uptake of nanocarriers.

Pioneering research on nano-chemotherapeutics have reported that the non-spherical nano-chemotherapeutics such as filamentous micelles, nanoneedles, nanorod, or nanodisks displayed greater tumor targeting potential. However spherical nano-chemotherapeutics have shown greater benefits with respect to ease of synthesis, development and evaluation (Truong et al., 2015). The study by Champion and Mitragotri (2006) elucidated the mechanism of uptake of diverse shapes of nano-chemotherapeutics using nonopsonized and IgG-opsonized anisotropic polystyrene particles in continuous alveolar rat macrophage cells NR8383. The researchers designed

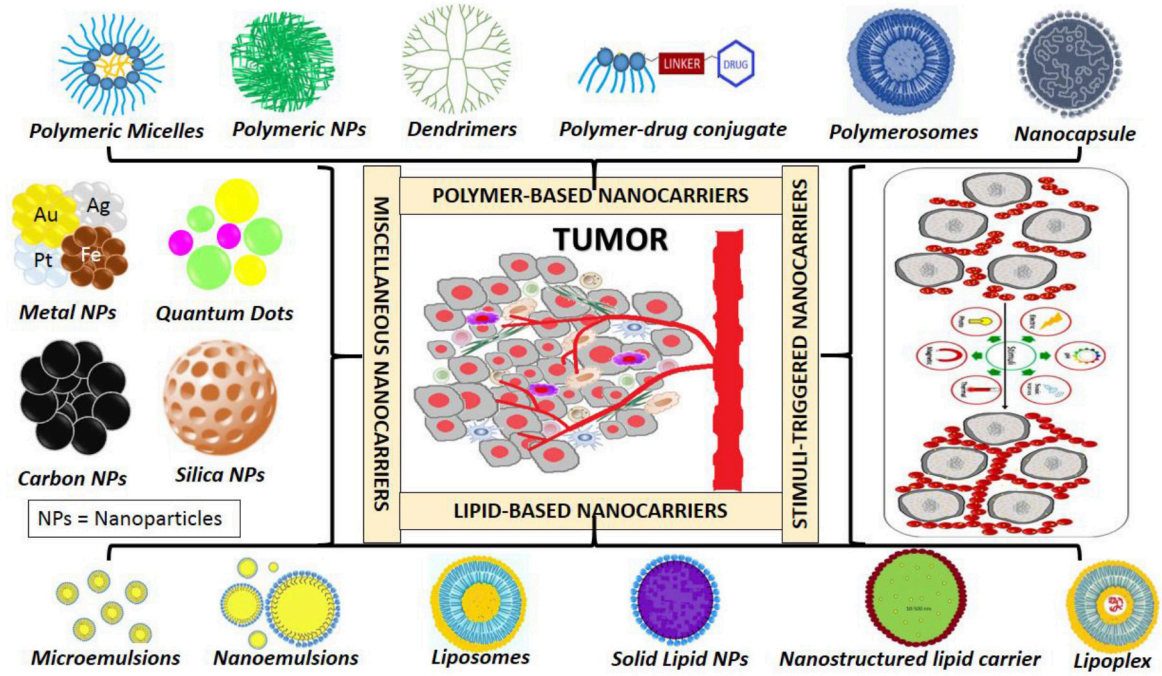

FIGURE 4 | Types of nanocarriers.

six different geometric shaped nanocarriers viz., spheres (radius 1.0-12.5 μm), oblate ellipsoids (major axis 4 μm, aspect ratio 4), prolate ellipsoids (major axis 2-6 μm, aspect ratio 1.3–3.0), elliptical disks (major axis 3–14 μm, aspect ratio 2–4, thickness 400–1,000 nm), rectangular disks (major axis 4–8 μm, aspect ratio 1.5–4.5), and UFOs (sphere radius 1.5 μm, ring radius 4 μm). The study documented that for cellular uptake of nano-chemotherapeutics, the angle of contact between the cellular membrane and nanocarriers is the important governing factor. It was stated that the tangent angles of nanocarriers during initial contact either led to orientation-dependent phagocytosis or simple spreading of macrophages without internalization. Study carried by Geng et al. (2007) also demonstrated ten times longer circulation time of PTX-loaded filomicelles of amphiphilic block copolymers of PEG-polyethylethylene or PEG-polycaprolactone than their spherical counterpart in rodents, post intravenous administration. *In vitro* phagocytosis assays were conducted using blood-drawn human neutrophils and human macrophage cell line, THP1. Spherical nanoparticles and short filomicelles (<4 μm) were taken up by cells more readily than long filomicelles (∼18 μm) as the longer filaments were shown to be extended into long chains in the presence of fluid flow. Similarly, Zhou et al. (2013) studied the effect of shape of amphiphilic PEG-*block*-dendritic polylysine-camptothecin conjugates on the cellular uptake, *in vivo* blood clearance, biodistribution and tumor targeting. DOX was used as a tracer to evaluate the cell internalization of nanorod-shaped and nanosphere-shaped conjugates in non-drug resistant cells (MCF-7) and multidrug-resistant cells (MCF-7/ADR). Nanorod-shaped conjugates showed efficient cellular uptake than nanosphere-shaped conjugates owing to their elongated shape. Additionally, long nanorods (>500 nm) exhibited lower blood circulation than medium size nanorods (∼1,000 nm) owing to rapid RES clearance and lung accumulation.

Tumor Microenvironment Targeted Nano-Chemotherapeutics

Although, in the last decades, EPR targeting was an underlying paradigm to target nano-chemotherapeutics, there were some limitations involving nano-chemotherapeutics having low molecular weight. In such cases, it was observed that the nano-chemotherapeutics had the tendency to re-enter the systemic circulation via diffusion. Thus, this led to reduced tumor residence time, making it essential to improve the nanotargeting of such chemotherapeutics by considering the overall changing pathophysiological characteristics of the tumoral tissues (Din et al., 2017). Considering this shortcoming, nano-chemotherapeutics targeting to tumor microenvironment has shown to be a promising approach to mitigate drug resistance.

Generally, delivery of effective nano-chemotherapeutics to the tumor microenvironment takes into consideration various endogenous factors such as acidosis, enzyme activity, redox potential, hypoxia, hyperthermia, oxidative stress, high interstitial fluid pressure, and ATP. Additionally, it takes into account, explicit pathophysiological conditions in the tumor microenvironment, such as varying levels of amino acids, functional proteins, DNA fragments and inflammatory cells, such as macrophages, mast cells, lymphocytes, and neutrophils (Chen Y. et al., 2017).

Preclinically, strategies involving pegylated nanocarriers, stimuli-responsive nanocarriers, dual-functional nanocarriers, have demonstrated successful outcomes in abrogating tumor growth by targeting tumor microenvironment. Mostly, these strategies, involve site-specific detachment of PEG linkage (Ding et al., 2015), reversing surface-charge, reduction in particle size, hyperthermia-induced CO_2 generation (Han et al., 2015), responsiveness to stimuli such as pH (Jiang et al., 2015; Yoshizaki et al., 2016), temperature (Needham et al., 2013; Kokuryo et al., 2017), or responsiveness to external-trigger such as magnetic field (Clares et al., 2013), light (Li et al., 2015), ultrasonic waves, laser (Li et al., 2017), and so on. Broadly, tumor microenvironment targeted nano-chemotherapeutics may be categorized as polymeric-, surfactant-, lipid-, carbon-, silica-, metal-, or metal oxide- based nano-chemotherapeutics.

Targeting the acidic microenvironment of tumor, nano-chemotherapeutics designed using acid-sensitive polymers such as polyethylenimine-Schiff base (Zhao et al., 2017), poly(styrene-co-maleic anhydride) (Dalela et al., 2015), poly(beta-amino ester) (Min et al., 2010), poly-(2-(diisopropylamino)-ethylmethacrylate) (Xu X. et al., 2016), and so on, have been explored. Lee et al. (2008) developed DOX-loaded polymeric micelles comprising of two block copolymers of poly(L-lactic acid)-b-poly(ethylene glycol)-b-poly(L-histidine)-TAT (transactivator of transcription) and poly(L-histidine)-b-poly(ethylene glycol), wherein the micelles were found to protect the TAT and DOX during circulation. Thereafter, in slightly acidic tumor extracellular pH, the micelles were shown to expose TAT to enable the internalization process. Subequently, the internalized copolymers were shown to ionize and disrupt the endosomal membrane facilitating tumor specific DOX release in the xenografted tumors of human ovarian tumor drug-resistant A2780/AD in nude mice. Similarly, Min et al. (2010) designed camptothecin encapsulated pH-responsive micelles comprising of methyl ether PEG-poly(β-amino ester) block copolymer. Within the acidic tumor microenvironment, the micelle disintegrated to release the chemotherapeutic within the MDA-MB231 human breast tumor-bearing mice. Further, the authors explored the tumor microenvironment responsive nature of micelles for noninvasive *in vivo* fluorescence imaging of MDA-MB231 human breast tumor-bearing mice by encapsulating optical imaging fluorescent dye, tetramethylrhodamine isothiocyanate within the micelles. Another approach involved the use of amphiphilic polymer-based self-assembled nanocarriers. These systems have a tendency to undergo protonation-induced hydrophobic-hydrophilic switch in presence of acidic tumor microenvironment. Since such switch destabilizes the assembled nanocarriers, it leads to the release of chemotherapeutics within the tumor microenvironment. Besides this, there are studies which illustrate the role of tumor hypoxia in triggering hydrophobic 2-nitroimidazole-to-hydrophilic 2-aminoimidazole switch leading to destabilization of the nano-chemotherapeutics and subsequent release of chemotherapeutics at the desired site (Chen B. et al., 2017). Zhu et al. (2014) designed tumor reductive environment responsive surface functionalized cationic polylysine endowed with cleavable pegylation and lipophilic histidylation (mPEG-SS-Lysn-r-Hism) for intracellular delivery of siRNA. Cleavable pegylation ensured long circulation of nano-chemotherapeutics in the systemic circulation with selective PEG detachment in response to intracellular tumor reductive microenvironment, facilitating tumoral localization of nano-chemotherapeutics. In this system, histidine conferred lipophilic histidylation for proton sponge effect of imidazole ring and lipophilic benzyl group which led to osmotic swelling of the endosome, disruption of the membrane and promoted release of siRNA intracellularly. In general, PEG-based amphiphilic nano-chemotherapeutics have known to exhibit several advantages such as ability to; overcome multi-drug resistance, co-deliver hydrophobic and hydrophilic drugs, provide longer circulation time of nano-chemotherapeutics, avoid rapid RES clearance and enhance EPR effect (Chen S. et al., 2016). For instance, Mu et al. (2010) developed mixed mPEG-PLA-Pluronic copolymer nano-micelles for better drug bioavailability and to overcome multidrug resistance of docetaxel (DTX).

Modified-liposomes also have been one of the most extensively explored modalities for targeting tumor microenvironment. Liposomes as drug delivery nanocarriers possess advantages of biocompatibility, nonimmunogenicity and delivery of array of chemotherapeutic agents, however they lack tumor specificity which may lead to increased adverse off-target effects. Nevertheless, surface modification of liposomes have enabled multiple functionalities, such as enhanced blood circulation, higher accumulation at tumor site, greater cell internalization and so on (Deshpande et al., 2013). Most prominently, pegylation of liposomes has been done which ensure prolonged systemic circulation of nano-chemotherapeutics. However, there are instances the PEG brush may impede generalized cellular uptake by inhibiting the endosomal escape of liposomes causing degradation of the encapsulated content. Hence, acid-sensitive linkages between PEG chain and hydrophobic moiety such as diortho esters, vinyl esters, cysteine-cleavable lipopolymers, double esters, and hydrazones (stable at pH 7.5, but rapidly hydrolyze at pH <6) are often incorporated to impart pH-sensitive attribute to liposomes for the specific delivery of cargo in acidic milieu of endocytic vacuole or tumor microenvironment (Deshpande et al., 2013). Liu Y. et al. (2014) have designed DOX- and verapamil-loaded liposomes containing pH-responsive molecule, malachite green carbinol base. This base, on exposure to acidic milieu converted to carbocationic form leading to disorientation of the liposome and target site-specific release of DOX. The anti-cancer activity was further augemented by incorporation of a P-gp inhibitor Verapamil, which aided reversal of multi-drug resistance effect in resistant *in vitro* and *in vivo* breast cancer model. Yan et al. (2015) designed pH-responsive DOX-loaded liposomes coated with glycol chitosan which showed the conversion of anionic nature on the liposomes at physiological pH to cationic nature in acidic extracellular tumor microenvironment. This change in charge facilitated cellular uptake of liposomes in T6-17 tumor-bearing mice thereby enhancing the overall anti-cancer activity. Koren et al. (2012) developed a multifunctional pH-sensitive pegylated long-circulating liposomes of Doxil®, modified with cell-penetrating TAT peptide and cancer-specific mAb 2C5.

The immunoliposome contained a pH-sensitive hydrazone bond between long PEG chains and phosphatidylethanolamine component (PE) which degraded specifically at the acidic tumor microenvironment, causing removal of long PEG chains and deshielding the TAT peptide. This multifunctional liposomal system minimized the destruction of non-target cells for much improved anti-cancer therapy.

Apart from pH-sensitivity, hyperthermia-responsive liposomes containing thermosensitive-lipids or polymers have also been studied. Hyperthermia at tumor site has shown to increase tumor permeability and drug uptake by increasing the microvasculature pore size and blood circulation. Prominent advantage of thermosensitive liposomes is its ability to release the contents at phase transition temperature due to melting of liposomes causing open nature and pore-like structures for content release. Park et al. (2014) developed DOX-loaded thermosensitive liposomes of 1,2-dipalmitoyl-sn-glycero-3-phosphocholine, 1,2-distearoyl-sn-glycero-3-phosphoethanolamine-N-[methoxy(polyethyleneglycol)-2000], cholesterol, and a fatty acid conjugated elastin-like polypeptide in the molar ratio, 55:2:15:0.41, respectively. The research protocol contained induction of local heating (42°C) of 30 min prior to i.v. injection, at the tumor site of tumor-bearing BALB/c nude mice for enhanced EPR effect. The study outcomes suggested better accumulation of DOX-loaded liposomes when compared to free DOX-treated group, both, in presence and absence of preheating. DOX-loaded liposomes under preheated conditions exhibited 5-fold, 11-fold, and 31-fold increase in drug accumulation at 6 h after i.v. injection when compared to DOX-loaded liposomes without preheating, free DOX-treated group without preheating, and free-DOX treated group with preheating, respectively. Similarly, Achim et al. (2009) developed DOX-loaded liposomes composed of thermosensitive lipids; dipalmitoylphosphatidylcholine (DPPC) and distearoylphosphatidylcholine (DSPC) alongwith cholesterol in the molar ratio, 26:4:6, respectively; DOX-loaded lyso-thermosensitive liposomes composed of 1-palmitoyl-2-hydroxy-3-glicerophosphatidylcholine, DPPC, DSPC and cholesterol in the molar ratio of 2:24:4:6, respectively and DOX-loaded non-thermosensitive liposomes composed of L-α-phosphatidylcholine and cholesterol in the molar ratio of 30:6, respectively. Though, DPPC showed gel-to-liquid phase transition temperature (Tc) at a clinically attainable local hyperthermia, 41.5°C, it was associated with poor rate and reduced amount of drug release. Hence, it is used in combination with other lipids such as DSPC having higher Tc at 54.9°C.

Mesoporous silica nanochemotherapeutics as drug delivery carriers have also been explored for its ability to have higher drug loading (about 60%). However, they have limitations, due to the porous structure of the silica nanoparticles there is often leakage of drugs and undesirable burst release. To address this issue, tumor microenvironment-responsive mesoporous silica nano-chemotherapeutics have been designed, wherein stimuli-triggered caps may be provided for protecting the drug-loaded pores in the mesoporous silica nano-chemotherapeutics and promoting drug release only in the tumor microenvironment (Schlossbauer et al., 2009; Liu et al., 2015). Various molecules which behave as gatekeepers include ferric oxide, avidin, peptides, human serum albumin, β-cyclodextrin, gelatin etc., may be incorporated during the designing of silica-based nano-chemotherapeutics. Removal of these gatekeepers, triggered by tumor microenvironment-related factors such as acidic pH, redox potential, over-expressed enzymes have shown advantages over non-triggered systems (Chen B. et al., 2017).

Metal or metal oxide nano-chemotherapeutics have also shown potential in the tumor microenvironment. For instance, Crayton and Tsourkas (2011) explored the pH-titratable superparamagnetic iron oxide for accumulation of nanoparticles in the tumor microenvironment. The metal oxide nanoparticles were conjugated with glycol chitosan, a water-soluble polymer with pH-titratable charge, demonstrating *in vitro* pH-dependent cellular association. Zhong et al. (2013) developed hybrid micelles using PEG-PLA (organic-inorganic) copolymers, which were further coated with gold nanorod in order to improve the stability of nanocarriers during systemic circulation. In addition to this, these systems were designed to release the anti-tumor agent on exposure to NIR radiation due to the phase transition of PLA induced by the photothermal effect.

Few examples of tumor microenvironment governed conventional nano-chemotherapeutics are shown in **Table 1**.

Recently, multistage nano-chemotherapeutic approach has evolved which has helped in reducing the shortcomings of conventional nanotherapy such as drug resistance, circulatory half-life of the actives, heterogeneity of cancer cells, and suppression of immunity by the tumor microenvironment (Conniot et al., 2014). As mentioned earlier, tumor microenvironment over-expresses various receptors, possesses higher redox potential and increases levels of certain enzymes. Thus, the approaches further discussed in this review are focused on ligand-mediated, redox-responsive, and enzyme-mediated nano-chemotherapeutics.

Ligand-Mediated Nano-Chemotherapeutics

Ligand-mediated nano-chemotherapeutics have shown promising outcomes due to their passive as well as predominant active targeting. However, they lack clinical outcome due to diverse expression of membrane receptors between patients, type- and stage- of tumor and prevention of penetration of extravasated nano-chemotherapeutics due to peripheral receptor-ligand interactions with the tumor cells (Chen B. et al., 2017). For successful active targeting, it is desirable that the ligand functionalized on the surface of the nano-chemotherapeutics have selectivity toward the receptors over-expressed homogenously and specifically by tumor cells at all tumor sites. In addition to this, the selected ligand should either bind or modify the tumor core vasculature (Lammers et al., 2008) or facilitate cellular internalization of nano-chemotherapeutics (Cho et al., 2008). For effective internalization of ligand-mediated nano-chemotherapeutics (**Figure 5**), various over-expressed internalization-prone receptors on tumor cell surface have been explored, which include, transferrin receptor, folate receptor, epidermal growth factor receptor (EGFR) and fibroblast growth factor receptor (FGFR). Besides this, internalization-prone receptors are also

TABLE 1 | Few examples of tumor microenvironment governed conventional nano-chemotherapeutics targeted for tumor therapy.

Tumor microenvironment	Type of Nano carriers	Reference(s)
Acidic pH	Iron oxide nanoparticles	Crayton and Tsourkas, 2011
	Liposomes	Yan et al., 2015
	Silica nanoparticles	Deng et al., 2011
	Polymeric nanoparticles	Dalela et al., 2015; Sun et al., 2015; Hung et al., 2016; Xu C. F. et al., 2016
	Polymeric micelles	Hu et al., 2013; Ouahab et al., 2014
Hypoxia	Polymeric nanoparticles	Perche et al., 2014; Thambi et al., 2014
Oxidative stress	Polymeric nanoparticles	Kwon et al., 2013
Hyperthermia	Quantum dots	Tao W. et al., 2017
	Iron oxide nanocubes	Guardia et al., 2012
	Liposomes	Peng et al., 2014
	Magnetic nanoparticles	Yu et al., 2014
ATP	Micelles	Naito et al., 2012
	Polymeric Nanogel	Mo et al., 2014
	Microcapsules	Liao et al., 2015
PEG detachment	Polymeric nanocarriers	Dong et al., 2015
	Liposomes	Yan et al., 2015
	Silica nanoparticles	He et al., 2016
	Polymeric nanoparticles	Dreaden et al., 2014
	Layer-by-layer films on nanoparticles	Deng et al., 2013
Particle-size shrinkage	Nanoparticles	Ruan et al., 2015
	Polymeric nanoparticles with Dendrimers	Li et al., 2016
	Nanogel	Ju et al., 2014; Zan et al., 2014
	Gold nanoparticles	Huang et al., 2012; Huo et al., 2013
	Lipid-dendrimer nanoassembly	Sun et al., 2014

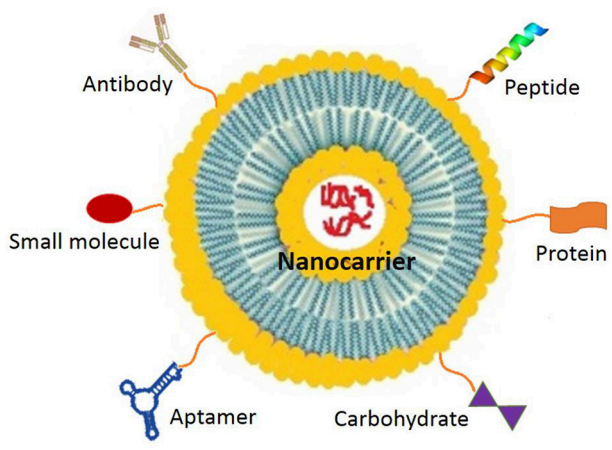

FIGURE 5 | Different types of ligands for targeting nano-chemotherapeutics.

over-expressed in the cytoplasm and nucleus of the tumor cell namely, peroxisome proliferator-activated receptor γ (PPAR-γ). Similarly, in tumor microenvironments or tumor vasculature or endothelium of tumor neovasculature, overexpressed receptors include; VEGF receptor, $\alpha_v\beta_3$ integrin receptor, vascular cell adhesion molecule-1 (VCAM-1) glycoprotein and MMPs (Danhier et al., 2010).

Literature cites that targeting ligands could also include monoclonal antibodies or antibodies, such as trastuzumab, bevacizumab, etaracizumab, Ibritumomab tiuxetan, denosumab, or antibody fragments such as fragment antigen-binding (Fab') or single-chain fragment variable (scFv). Surface functionalization using antibody and their fragments have paved way for immunotherapy in oncology. It is proposed that during functionalization use of fragments instead of whole antibody is more advisable to preclude the risk of antibody inactivation. Further, reduced size of the ligand has shown to minimize untoward immune response and promote effective targeted delivery. Besides this, non-antibody ligands, peptides such as endostatin, aptamers, small molecules such as folates, carbohydrates, affibody, and so on have also been explored. Widely known techniques of functionalization of nano-chemotherapeutics employ chemical interaction through covalent or non-covalent bonding between nanocarrier and functional group. For instance, in case of liposomes, functionalization may involve formation of amide bonds; disulfide bonds; thioether bonds or PEG-linkages (Riaz et al., 2018).

Using this strategy, endothelial cell receptor (such as integrin $\alpha_v\beta_3$) targeted ligand-nano-chemotherapeutics has been developed having the ability to perturb angiogenic vessels and tumoric cells. This approach has shown to enable bypass of biological tumor barriers, mitigation of drug resistance

due to endothelial cells genetic stability, and generation of verstaile nano-chemotherapeutics having widespread application in several tumor types (Ji et al., 2013). Kibria et al. (2013) investigated the effect of size of arginine-glycine-aspartic acid peptide (RGD) pegylated liposome on the target specific delivery of DOX to integrin $\alpha_v\beta_3$-expressing tumor endothelial cells. The study was carried out for two size populations; average diameter ∼100 nm (small size) and ∼300 nm (large size) and marketed product Doxil® (∼100 nm in diameter) in DOX resistant OSRC-2 (Renal cell carcinoma) tumor xenografts. The study results verified that the size of liposomes strongly influenced ligand-receptor interaction, internalization of liposomes into the cell and distribution in the tumor microenvironment. Despite the accumulation of Doxil® in the tumor cells, the marketed formulation failed to suppress tumor growth. Similarly, owing to extravasation of small-sized ligand-mediated and pegylated liposomes to tumor cells, there was lack of appreciable anti-tumor activity. Interestingly, large-sized ligand mediated and pegylated liposomes having minimized EPR effect demonstrated superior targeting to tumor endothelial cells via integrin $\alpha_v\beta_3$. Consequently, it exhibited anti-angiogenic activity on tumor vasculature and thereby reduced tumor growth. Babu et al. (2017) fabricated RGD-modified polylactic acid-co-glycolic acid-chitosan nanoparticles for integrin $\alpha_v\beta_3$ receptor targeted PTX delivery in lung cancer cells. The approach resulted in superior uptake via integrin receptor-mediated endocytosis, cell-specific delivery, elicited improved apoptosis, and induced G2/M cell cycle arrest.

Another approach involves inhibition of VEGF or VEGFR binding to regulate tumor angiogenesis and neovascularization (Ji et al., 2013). Feng et al. (2014) developed VEGF-targeted siRNA- (siVEGF) and PTX-loaded vapreotide-modified core-shell type nanoparticles for improved intracellular siRNA accumulation and VEGF down-regulation in human breast cancer MCF-7 cells as compared to non-ligand nano-chemotherapeutics. *In vivo* study results of ligand-based nano-chemotherapeutics demonstrated enhanced tumor tissue localization and efficient inhibition of tumor growth via siVEGF silencing induced neovascularization inhibition. In another study, siRNA- and DTX-loaded two receptor-specific peptides-modified liposomes [i.e., LDL receptor-related protein receptor (Angiopep-2) and neuropilin-1 receptor (tLyP-1)] were found to be having superior brain tumor targeting and tumor penetration (Yang et al., 2014). Shein et al. (2016) focused on studying the effect of VEGF- and VEGFR2-targeted liposomes for delivery of cisplatin to C6 and U-87 MG glioma cells. The drug and antibody-conjugated liposomes exhibited prolonged release *in vivo*, superior affinity to antigens and enhanced uptake by the glioma cell lines. Li et al. (2015) developed a human epidermal growth factor receptor-2 antibody-conjugated drug delivery system, using near-infrared (NIR) light-sensitive DOX-loaded liposomes and hollow gold nanospheres. These systems showed superior and specific binding and selective toxicity to human epidermal growth factor receptor-2-positive tumor cells. Combination of liposomes with NIR laser irradiation led to 92.7% tumor inhibition due to enhanced accumulation in tumors, which was further attributed to photo-thermal-chemotherapy. Furthermore, vascular cell adhesion molecule-1 (VCAM-1), an angiogenic factor and MT1-MMP, an enzyme, both expressed on the tumor endothelial cells in several tumor types are also considered as potential broad-spectrum targets for ligand-mediated nano-chemotherapeutics.

Hypoxia, a tumor condition characterized by overexpressing CA (e.g., their transmembrane isoforms which include CA IX and CA XII) in the tumor microenvironment (Mahon et al., 2015). Thus, the widely known approach to counteract this condition involves inhibition of CA activity. Stiti et al. (2008) developed CA inhibitor coated gold nanoparticles for combating hypoxic tumors by selectively inhibiting tumor-associated CA isoform IX over cytosolic isozymes I and II. For *in vivo* inhibition of transmembrane vs. cystolic isozymes, the researchers investigated the penetrability of sulphonamide inhibitors and CA inhibitors using red blood cells (RBC) as experimental model. Study results revealed higher diffusibility of sulfonamide inhibitors through the RBC membranes, while CA inhibitor coated gold nanoparticles showed membrane impermeability. This impermeable nature was found to be contributing factor for selective inhibition of CA IX expressing tumors. Similarly, Krall et al. (2014) developed a small molecule-disulfide-linked-drug conjugate for inhibiting CA IX expressed in renal cell carcinoma SKRC52. Herein, maytansinoid DM1 a chemotherapeutic conjugated to CA IX specific ligand, a derivative of acetazolamide showed enhanced internalization of chemotherapeutic agent and exhibited a potent antitumor effect. Lin et al. (2017) also surface functionalized triptolide-loaded liposomes with anti-CA IX antibody to target CA IX-positive human non-small cell lung cancer cells (A549) and A549 tumor spheroids, resulting in the efficient cell apoptosis as compared to free drug and non-targeted liposomes. In a study by Takacova et al. (2016), instead of surface functionalization, the scientists encapsulated the monoclonal antibody M75 into alginate microbeads and sodium alginate-cellulose sulfate-poly(methylene-co-guanidine) based microcapsules to knock down the CA IX expressed by tumor cells.

Cell-penetrating peptides (CPPs) mediated drug delivery has emerged as a promising strategy to deliver nano-chemotherapeutics through tissue and cell membranes either using an energy-dependent or -independent process. Generally, they are conjugated to nano-chemotherapeutics either via stable, non-covalent complexes or via covalent bond. However, they have limitations, some peptides lack stability as they are scavenged (especially, cationic peptides) by reticulo-endothelial system (RES) and also specificity deficient for cancerous cell targeting, leading to toxicity. To circumvent this issue, new generation multistage ligand-mediated nano-chemotherapeutics that are responsive to tumor microenvironment are designed, which are classified as follows: (a) activatable CPPs (ACPPs), (b) de-shielding systems, (c) "pop-up" systems, and (d) trojan-horse targeting systems (for detailed review, refer, Chen B. et al., 2017; Kebebe et al., 2018). In ACPPs, tumor microenvironment responsive materials are exploited to display CPPs either at lower pH or in presence of overexpression of ECM development-remodeling proteases, or in response to external stimuli of heat or light to a disease site (MacEwan and Chilkoti, 2013). Lee

et al. (2017) synthesized poly-l-lysine-based pH-controllable CPPs which undergo pH-dependent conformational transition and display CPPs at the target site. It was reported that at physiological pH, the electrostatic attractions existing between carboxylate and protonated amine groups in side chain of CPPs contributed to its low helical tendency, thereby preventing unselective cellular internalization. However, in tumor acidic microenvironment, the helical conformation was attained enabling cell-penetrating properties at specific cancer sites (Lee et al., 2017). Zhang Y. et al. (2017) developed DOX- and vincristine-loaded liposomes, which were modified with 2 ligands, i.e., T7, seven-peptide ligand of transferrin receptors (TfR) and ^{D}A7R, d-peptide ligand of VEGFR 2 for efficient targeting to glioma. The dual peptide conjugated liposomes were capable of circumventing blood brain barrier and possess glioma-homing property due to the presence of the dual peptides. Singh et al. (2016) designed RGD-conjugated d-alpha-tocopheryl PEG 1000 succinate (TPGS) theranostic liposomes comprising of DTX and quantum dots, showing potential for brain tumor treatment and imaging. On similar lines, Chen Y. et al. (2017) developed PTX-loaded mixed micelles of vitamin E succinate-grafted-chitosan oligosaccharide/RGD-conjugated TPGS for human glioma U87MG tumor targeting. In addition to the earlier conventional nano-chemotherapeutics developed by Zhong et al. (2013), they developed multistage nano-chemotherapeutics by functionalizing the gold nanorod coated micelles with a cRGD ligand. This advancement overcome MDR effect by improving the tumor penetration of the active moiety (Zhong et al., 2014). Zhao et al. (2016) also developed tumor-specific DOX-loaded pH-responsive liposomes with peptide H7K(R2)2 as a targeting ligand.

Combining the benefits of ligand-mediated nano-chemotherapeutics with stimuli responsiveness, Zang et al. (2016) successfully developed a pH-sensitive cholesterol-Schiff base-PEG-modified cationic liposome-siRNA complex conjugated with recombinant humanized anti-EphA10 antibody. The study results revealed that the complex was able to escape from the endo-lysosomal organelle and release the active drug into cytoplasm, which was evident by *in vivo* studies, wherein the complex was able to target the tumor site. Similarly, Al-Ahmady et al. (2014) designed an approach combining the benefits of ligand-mediated response with tumor induced-hyperthermia. In the study, DOX-loaded thermo-sensitive liposomes were designed and conjugated with hCTMO1 monoclonal antibody (anti-MUC-1). Receptor-mediated cellular uptake and cytotoxic effects of antibody-targeted thermo-sensitive liposomes was observed in MUC-1 over-expressed breast cancer cells (MDA-MB-435), post-heating for 1 h at 42°C.

Other agents such as hyaluronic acid (HA), transferrin and aptamers have also been reported as ligands to confer nano-chemotherapeutics with tumor targeting ability. Zheng T. et al. (2017) developed negatively charged HA-coated silica nanoparticles loaded with two chemotherapeutic agents, candesartan, and trastuzumab. The ligand-mediated delivery system facilitated cell internalization of nano-chemotherapeutics within tumor cells of an ovarian cancer. In a study carried out by Han et al. (2014), they successfully developed surface-modified, co-encapsulated solid lipid nanoparticles containing green fluorescence protein plasmid and DOX for multifunctional delivery to lung cancer cells (human alveolar adenocarcinoma cell line-A549 cells). Transferrin-containing ligands were surface-coated on the vectors and the study results demonstrated superior lung cancer gene therapy. Qin et al. (2014) designed dual cyclic RGD peptide- and transferrin-conjugated PTX-loaded liposomes for targeting the blood-brain-barrier and targeting to brain glioma cell. Wang et al. (2015) successfully encapsulated MicroRNA-34a into a S6 aptamer-conjugated dendrimer to create lung cancer-targeted gene delivery nanoparticles. Aptamer-conjugated nano-chemotherapeutics improved cellular uptake and gene transfection efficiency of the dendrimeric nano-chemotherapeutics in cultured non-small cell lung cancer cells. The nano-chemotherapeutics also inhibited cell growth, migration, and invasion and induced apoptosis when compared to non-targeted nanoparticles, thus proving better systems for tumor targeting.

Redox-Responsive Nano-Chemotherapeutics

Redox potential, an intracellular stimulus, is the outcome of reduced glutathione concentration in extracellular space as compared to intracellular space, whose amplification causes cleavage of disulfide bond by glutathione leading to disassembly and degradation of nano-chemotherapeutics, followed by release of the chemotherapeutics (**Figure 6**) (Chen B. et al., 2017). Several researchers have designed nano-chemotherapeutics having disulphide bonds rendering them redox-responsive within tumor microenvironment. Sun et al. (2010) developed amphiphilic polyamide amine-g-PEG graft copolymer containing disulfide linkages which degraded in presence of reducing agent, dithiothreitol, leading to disassembly of micelles and complete release of chemotherapeutics within 10 h as compared to 25% release in 24 h. Wu L. et al. (2016) developed DOX-loaded zwitterionic nanoparticles comprising of dextran using succinic acid and crosslinked with cystamine which showed rapid internalization of Hela cells, making it suitable alternative to target tumor reductive environment. Similarly, Hou et al. (2016) fabricated HA-modified single-walled carbon nanotubes wherein the HA was further conjugated to DOX by disulphide bonds making the nano-chemotherapeutics sensitive to redox potential. Whereas, Lin et al. (2016) developed bioreducible DOX-loaded chitosan-based nano-chemotherapeutics with HA for production of intracellular glutathione-triggered reactive oxygen species and simultaneous release of chemotherapeutics. Shi et al. (2014) developed DOX-loaded star-shaped micellar system made up of amphiphilic co-polymer crosslinked with phenylboronic acid-functionalized reduction-sensitive amphiphilic co-polymer having tumor targeting ability. Yin et al. (2018) designed redox-responsive, estrogen-functionalized liposomes covalently tethered to biocompatible chotooligosaccharides, via disulphide links, for intracellular delivery to osteosarcoma MG63 cells. The liposomes demonstrated high drug loading with average diameter of ∼110 nm which were capable of exploiting the EPR effect. These multifunctional liposomes showed immediate cellular uptake via estrogen-receptors followed by rapid drug release due to

the reduction of disulphide bond by intracellular glutathione concentration. Maggini et al. (2016) explored the redox-mediated drug release by designing redox-responsive mesoporous organosilica nanoparticles containing disulphide bridges inside glioma C6 cancer cells. Similarly, Wu M. et al. (2016) developed redox-sensitive huge pore-sized hollow mesoporous organosilica nanoparticles for concurrent delivery of P-gp modulator siRNA and chemotherapeutics for reversal of MDR effect of tumor cells. Koo et al. (2012) fabricated a multi-unit nano-chemotherapeutics i.e., core-shell-corona micelle comprising of redox-responsive shell-specific cross-links. The DTX-loaded core shell composed of poly(L-phenylalanine), while the mid-shell was made up of poly(L-lysine), providing the disulphide bonds for reductive cleavage by the intracellular glutathione and finally the PEG-based outer corona for enhanced systemic circulation of the nano-chemotherapeutics. Exemplifying the potentials of multi-unit nano-chemotherapeutics, Li et al. (2016) fabricated a pH-sensitive cluster nanoparticles combined with platinum prodrug-conjugated poly(amidoamine) dendrimers possessing multiple-trigger induced drug release in the tumor microenvironment. Herein, the various tumoral barriers were disrupted sequentially; the strategy involved tumor localization by promoting size-dependent extravastion of ∼100 nm polymer-based cluster nanoparticles. Following which, the nanocarriers shrunk in size to ∼5 nm platinum-linked dendrimer in response to acidic tumor microenvironment. This facilitated tumor penetration and cell internalization followed by rapid reduction of dendrimer-prodrug by the intracellular glutathione in the cytosol to release the chemotherapeutic agent. Similarly, Chi et al. (2017) designed PEG stabilized drug-loaded liposomes conjugated with cholesterol using reducible disulfide linkages wherein the cationic liposomes were coated with a CD44 sensitive ligand i.e., HA. The redox-sensitive liposomes showed 60% release of actives in presence of glutathione, when compared to the redox-insensitive liposomes. This multi-triggered concept provided CD44-mediated tumoral delivery with improved systemic circulation and cancer cell specific glutathione-triggered cytoplasmic release of chemotherapeutics.

Yang et al. (2016) also developed a dual-stimulus system, exploiting two-triggers, i.e. hyperthermia and reductive tumor microenvironment. The researchers fabricated thermosensitive liposome conjugated with Asparagine-Glycine-Arginine (NGR) peptide as ligand and reducible siRNA-CPPs for tumor-specific siRNA transfection in order to prevent CPP degradation and reduction of disulphide linkages, *in vivo*. In comparison to conventional siRNA-CPPs, the dual-stimulus nano-chemotherapeutics under hyperthermic condition showed 2-fold gene silencing efficiency and 3-fold higher antitumor activity in HT-1080 xenograft murine model. This dual responsive nature is well understood by a study carried out by Ghosh et al. (2009), wherein the researchers developed a supramolecular complex of cationic surfactant and anionic disulfide containing polyelectrolyte formed micelles having redox- and acidic pH-responsive attributes. The study ascribed the responsive nature to the micellar changes arising due to reductive disulfide bond cleavage-mediated conversion of polyvalent-to-monovalent interaction and acidic pH-mediated reduced electrostatic interactions between polymer and surfactant.

Enzyme-Mediated Nano-Chemotherapeutics

Over-expression of enzymes such as peptidases (e.g., aminopeptidase), proteases (e.g., MMP and cathepsin B), and lipases (e.g., phospholipase A2) by the stromal cells or tumor cells for their growth, angiogenesis, invasion and metastasis have paved way for developing enzyme-mediated nano-chemotherapeutics (Gullotti and Yeo, 2009; Chen B. et al., 2017). Roy et al. (2010) reviewed the use of different enzyme-responsive polymers in designing the nano-chemotherapeutics which are susceptible to enzymes overexpressed by tumor cells. Yamada et al. (2010) used the protease activity of MMP2 to selectively deliver PTX to tumor site. Two different prodrugs of PTX (i.e., PTX-2'AcG and PTX-7AcG wherein the 2'- and 7-hydroxyl groups were conjugated to C-terminus of glutamine of octapeptide) were found to be vulnerable to cleavage by the MMP2 at tumor site, to release PTX. In addition to this, the presence of octapeptide minimized the affinity of the drug to MDR1, thus abrogating MDR effect. Hatakeyama et al. (2007) developed an enzymatically cleavable PEG-peptide-lipid ternary conjugate based carrier of a gene for cancer therapy. The *in vitro* study showed that the MMP-sensitive liposomes exhibited superior gene transfection efficiency in overexpressed MMPs in comparison to MMP-insensitive liposomes. Similarly, Chau et al. (2006a,b), designed a dextran-peptide-methotrexate conjugate for tumor site specific release of chemotherapeutics in response to tumor-associated enzymes i.e., MMP-2 and MMP-9 via cleavage of peptide linkage. However, their study revealed a reduction in tumor growth by nano-chemotherapeutics containing MMP-sensitive and MMP-insensitive linkers as compared to chemotherapeutic alone. The probable reason cited for this anomalous behavior was the endocytic uptake of the conjugate prior to cleavage by the enzymes. Harnoy et al. (2014) synthesized enzyme-responsive amphiphilic hybrids containing linear PEG and a stimuli-responsive dendron with enzyme-cleavable hydrophobic end groups, with a potential to self-assemble in water as smart micellar nano-chemotherapeutics for encapsulation of hydrophobic chemotherapeutics. The hybrids accommodated phenyl acetamide as hydrophobic end groups cleavable by the enzyme penicilin G amidase, which on enzyme-induced degradation, resulted in the destabilization of micelles and formation of monomeric hydrophilic hybrids, with subsequesnt release of chemotherapeutics.

Another protease enzyme that is over-expressed in the extracellular tumor microenvironment by stromal, TAM and endothelial cells in tumors is Legumain, making it potential stimulus in targeting the tumor stroma. Ruan et al. (2016) successfully developed enzyme-responsive nanoplatforms that activated the accumulation of gold nanoparticles using legumain for improved localization of chemotherapeutics in brain tumors. Researchers designed a mixed surface decorated gold nanoparticles (i.e., AuNPs-A&C) comprised of Ala-Ala-Asn-Cys-Lys modified nanoparticles (termed as

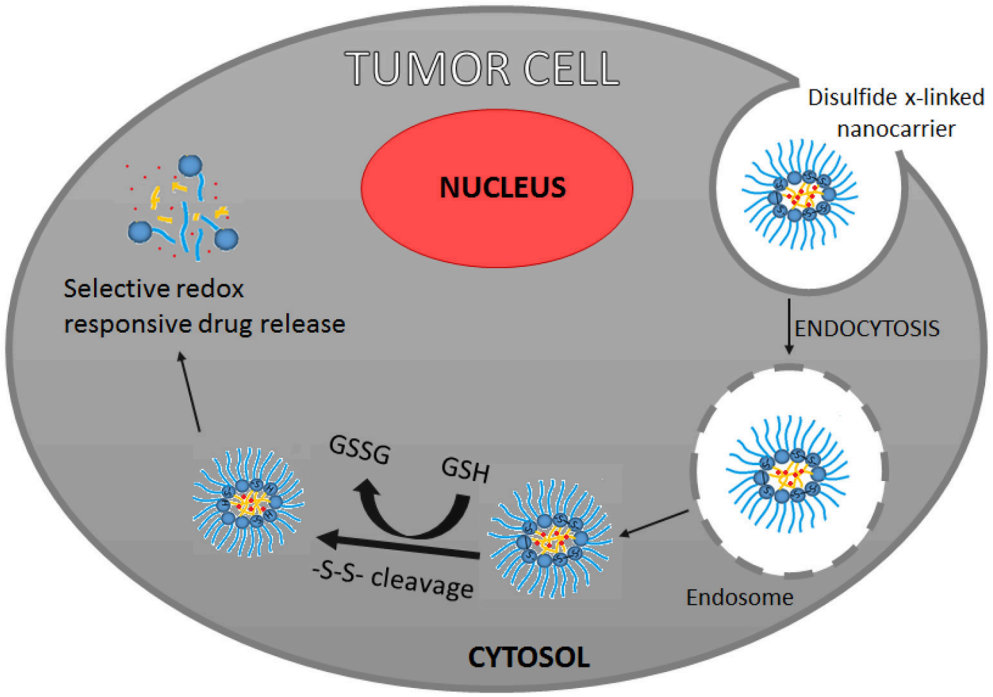

FIGURE 6 | Redox responsive nanocarriers.

AuNPs-AK) and 2-cyano-6-aminobenzothiazole modified nanoparticles (termed as AuNPs-CABT). In presence of enzyme legumain, AuNPs-AK hydrolysed to expose 1,2-thiolamino groups, which further underwent click cycloaddition with contiguous cyano group on AuNPs-CABT, forming gold nanoparticle aggregates. These systems possessed enhanced retention capability in the tumor cell due to the inhibition of nanoparticle exocytosis and prevention of backflow into the systemic circulation. Using the similar concept, Xiao et al. (2017) developed an enzyme-induced size-changeable gold nanoparticles loaded with cediranib, a tumor vessel normalizing agent for breast cancer tumor imaging and therapy. Ruan et al. (2017) further explored dual-functional gold nanoparticles with enzyme-responsiveness and integrin $\alpha_v\beta_3$-ligand-mediated targeting. Liu Z. et al. (2014) fabricated a legumain protease-activated TAT-liposome, wherein the substrate for endoprotease legumain, alanine-alanineasparagine, was linked to the 4th lysine of TAT. The substrate was susceptible to breakage by legumain enzyme overexpressed in tumor microenvironment, leading to tumor targeting of liposomes to the desired site.

Hyaluronidase is another enzyme expressed 20–1000 times higher by the tumor cells having capability of degrading HA-coated nano-chemotherapeutics (Li and Xie, 2017). Yim et al. (2013) designed a PTX-loaded degradable cationic nanogel comprising of acetylated pullulan and low molecular weight polyethyleneimine. The cationic charge on the nanogel was restored by coating with HA, making it susceptible to degradation by the hyaluronidase in the tumor microenvironment. The HA-coated nano-chemotherapeutics showed enhanced tumoral permeation with a 2-fold increase in the amount of nanogel localized within the deep tissue regions when compared to non-HA systems. Zhang and Xu (2018) fabricated a bienzyme-responsive multifunctional envelope-type mesoporous silica nanoparticles in which the nanoparticles were first functionalized with HA for successful targeting to breast cancer cells and then exposing the system to hyaluronidase-induced intracellular release of chemotherapeutic. The outer layer of the nanoparticles contained a capping layer of gelatin, grafted via glutaraldehyde-mediated cross-linking. Further, in order to protect and prolong the systemic circulation of nanoparticles, they were pegylated. Post-administration, on exposure to the MMP-2 enzymes over-expressed by the cells, the gelatin was hydrolysed, de-shielding the PEG coating. This exposed the HA and led to hyaluronidase-mediated degradation of HA within the tumor microenvironment for successful drug delivery. In-order to explore the dual benefits of redox- and enzyme-responsiveness, Xu et al. (2015) developed DTX-loaded shrapnel nano delivery system. The nanocarrier system comprised of methoxy PEG-peptide-vitamin E succinate, a MMP-sensitive co-polymer, synthesized by conjugating PEG and vitamin E succinate using an enzyme-sensitive peptide. Further, drug-loaded PEG-disulfide-vitamin E succinate micelles were incorporated into PEG-peptide-vitamin E-based liposomes. This unique nanocarrier exhibited shrapnel structure with average particle size 113.3 $\pm$ 2.7 nm. These dual-responsive nano-chemotherapeutics were capable of inhibiting the metastasis and growth of breast cancer simultaneously.

CONCLUSIONS

Tumor microenvironment has been implicated in cancer growth and metastasis. With growing understanding of tumor, it is established that tumors grow in highly heterogeneous and complex microenvironment consisting of the ECM components, immune cells, vasculature, TAMs, and CAFs. Recent advancements pinpoints that the alteration of tumor microenvironment and its abnormal composition is an important strategy in curtailing cancer progression, invasion, and metastasis. With the advent of nanotechnology in drug delivery arena, newer approaches to tackle growing menace of cancer have evolved. However, the complexity of tumor microenvironment has shown to play a crucial, yet controversial role in regulating deeper tumoral penetration of nano-chemotherapeutics and subsequently, their biological effects. Tackling this obstacle, strategies have been designed using nanotechnology to overcome acquired resistance induced by tumor milieu either by targeting tumor vasculature or by altering the stromal properties or by exploiting the tumor chemical microenvironment.

Hence, nano-chemotherapeutics can alter the tumoral drug delivery by inducing pertubations in the tumor microenvironment. Thus, nanotechnology offers a versatile tool by enabling delivery of either single or combination of chemotherapeutics alongwith multiple targeting ligands to specifically target overexpressed receptors or enzymes or reductive environment, a common feature of tumor microenvironment. This approach confers target specificity thereby providing efficacious therapy with minimal adverse off-target effects. Besides this, the growing understanding of targeting tumor microenvironment using nanotools is paving way for designing combined strategy of therapeutics and diagnostics viz. nanotheranostics. With growing number of clinical trials on nanotherapy, different strategies combining nano-chemotherapeutics with radiotherapy and other allied therapies will translate into successful strategy for overcoming drug resistance.

Overall, it can be stated that nano-chemotherapeutics does hold promise in the early stages of cancer, as these highly multifunctionalized nanocarriers ensure delivery of chemotherapeutics either by exploiting EPR effect or tumor microenvironment. However, there still lies a challenge in translating this success from bench to bedside. As from a commercialization perspective, there is still a need for an in-depth stability and nanotoxicology studies to ensure regulatory compliance.

AUTHOR CONTRIBUTIONS

CF and DS devised the outline, drafted as well as revised the manuscript. MY reviewed the manuscript, contributed to the **Figure 3**, summarized the review abstract and conclusion. All authors have seen and agreed on the final version of the manuscript.

ACKNOWLEDGMENTS

Authors would like to thank Ms. Kushi Mayur for illustration (**Figure 3**) in this manuscript.

REFERENCES

Achim, M., Precup, C., Gonganaunitu, D., Barbu-Tudoran, L., Porfire, A. S., Scurtu, R., et al. (2009). Thermosensitive liposomes containing doxorubicin. Preparation and *in vitro* evaluation. *Farmacia* 57, 703–710.

Al-Ahmady, Z. S., Chaloin, O., and Kostarelos, K. (2014). Monoclonal antibody-targeted, temperature-sensitive liposomes: *in vivo* tumor chemotherapeutics in combination with mild hyperthermia. *J. Control. Rel.* 196, 332–343. doi: 10.1016/j.jconrel.2014.10.013

Angara, K., Borin, T. F., and Arbab, A. S. (2017). Vascular mimicry: a novel neovascularization mechanism driving anti-angiogenic therapy (AAT) resistance in glioblastoma. *Transl. Oncol.* 10, 650–660. doi: 10.1016/j.tranon.2017.04.007

Ariffin, A. B., Forde, P. F., Jahangeer, S., Soden, D. M., and Hinchion, J. (2014). Releasing pressure in tumors: what do we know so far and where do we go from here? A review. *Cancer Res.* 74, 2655–2662. doi: 10.1158/0008-5472.CAN-13-3696

Armulik, A., Genové, G., and Betsholtz, C. (2011). Pericytes: developmental, physiological, and pathological perspectives, problems, and promises. *Dev. Cell* 21, 193–215. doi: 10.1016/j.devcel.2011.07.001

Au, J. L. S., Yeung, B. Z., Wientjes, M. G., Lu, Z., and Wientjes, M. G. (2016). Delivery of cancer therapeutics to extracellular and intracellular targets: determinants, barriers, challenges and opportunities. *Adv. Drug Del. Rev.* 97, 280–301. doi: 10.1016/j.addr.2015.12.002

Augustin, H. G., Koh, G. Y., Thurston, G., and Alitalo, K. (2009). Control of vascular morphogenesis and homeostasis through the angiopoietin–Tie system. *Nat. Rev. Mol. Cell Biol.* 10, 165–177. doi: 10.1038/nrm2639

Babu, A., Amreddy, N., Muralidharan, R., Pathuri, G., Gali, H., Chen, A., et al. (2017). Chemodrug delivery using integrin-targeted PLGA-Chitosan nanoparticle for lung cancer therapy. *Sci. Rep.* 7:14674. doi: 10.1038/s41598-017-15012-5

Balcioglu, H. E., Van De Water, B., and Danen, E. H. (2016). Tumor-induced remote ECM network orientation steers angiogenesis. *Sci. Rep.* 6:22580. doi: 10.1038/srep22580

Barar, J., and Omidi, Y. (2013). Dysregulated pH in tumor microenvironment checkmates cancer therapy. *BioImpacts* 3, 149–162. doi: 10.5681/bi.2013.036

Baronzio, G., Schwartz, L., Kiselevsky, M., Guais, A., Sanders, E., Milanesi, G., et al. (2012). Tumor interstitial fluid as modulator of cancer inflammation, thrombosis, immunity and angiogenesis. *Anticancer Res.* 32, 405–414.

Belli, C., Trapani, D., Viale, G., D'Amico, P., Duso, B. A., Della Vigna, P., et al. (2018). Targeting the microenvironment in solid tumors. *Cancer Treat. Rev.* 65, 22–32. doi: 10.1016/j.ctrv.2018.02.004

Bennewith, K. L., and Dedhar, S. (2011). Targeting hypoxic tumour cells to overcome metastasis. *BMC Cancer.* 11:504. doi: 10.1186/1471-2407-11-504

Bergers, G., and Hanahan, D. (2008). Modes of resistance to anti-angiogenic therapy. *Nat. Rev. Cancer.* 8, 592–603. doi: 10.1038/nrc2442

Binnemars-Postma, K., Storm, G., and Prakash, J. (2017). Nanomedicine strategies to target tumor-associated macrophages. *Int. J. Mol. Sci.* 18, 979. doi: 10.3390/ijms18050979

Bishop, C. J., Tzeng, S. Y., and Green, J. J. (2015). Degradable polymer-coated gold nanoparticles for co-delivery of DNA and siRNA. *ActaBiomater* 11, 393–403. doi: 10.1016/j.actbio.2014.09.020

Bjrnmalm, M., Thurecht, K. J., Michael, M., Scott, A. M., and Caruso, F. (2017). Bridging bio–nano science and cancer nanomedicine. *ACS Nano* 11, 9594–9613. doi: 10.1021/acsnano.7b04855

Bremnes, R. M., Dønnem, T., Al-Saad, S., Al-Shibli, K., Andersen, S., Sirera, R., et al. (2011). The role of tumor stroma in cancer progression and prognosis: emphasis on carcinoma-associated fibroblasts and non-small cell lung cancer. *J. Thorac. Oncol.* 6, 209–217. doi: 10.1097/JTO.0b013e3181f8a1bd

Bridgeman, V. L., Vermeulen, P. B., Foo, S., Bilecz, A., Daley, F., Kostaras, E., et al. (2017). Vessel co-option is common in human lung metastases and mediates resistance to anti-angiogenic therapy in preclinical lung metastasis models. *J. Pathol.* 241, 362–374. doi: 10.1002/path.4845

Broders-Bondon, F., Ho-Bouldoires, T. H. N., Fernandez-Sanchez, M. E., and Farge, E. (2018). Mechanotransduction in tumor progression: the dark side of the force. *J. Cell Biol.* 217, 1571–1587. doi: 10.1083/jcb.201701039

Brown, J. M. (2014). Vasculogenesis: a crucial player in the resistance of solid tumours to radiotherapy. *Br. J. Radiol.* 87:20130686. doi: 10.1259/bjr.20130686

Cairns, R., Papandreou, I., and Denko, N. (2006). Overcoming physiologic barriers to cancer treatment by molecularly targeting the tumor microenvironment. *Mol. Cancer Res.* 4, 61–70. doi: 10.1158/1541-7786.MCR-06-0002

Carmeliet, P. (2003). Angiogenesis in health and disease. *Nat. Med.* 9, 653–660. doi: 10.1038/nm0603-653

Champion, J. A., and Mitragotri, S. (2006). Role of target geometry in phagocytosis. *Proc. Natl. Acad. Sci. USA.* 103, 4930–4934. doi: 10.1073/pnas.0600997103

Chanmee, T., Ontong, P., Konno, K., and Itano, N. (2014). Tumor-associated macrophages as major players in the tumor microenvironment. *Cancers* 6, 1670–1690. doi: 10.3390/cancers6031670

Chantrain, C. F., Henriet, P., Jodele, S., Emonard, H., Feron, O., Courtoy, P. J., et al. (2006). Mechanisms of pericyte recruitment in tumour angiogenesis: a new role for metalloproteinases. *Eur. J. Can.* 42, 310–318. doi: 10.1016/j.ejca.2005.11.010

Chau, Y., Dang, N. M., Tan, F. E., and Langer, R. (2006b). Investigation of targeting mechanism of new dextran-peptide-methotrexate conjugates using biodistribution study in matrix-metalloproteinase-overexpressing tumor xenograft model. *J. Pharm. Sci.* 95, 542–551. doi: 10.1002/jps.20548

Chau, Y., Padera, R. F., Dang, N. M., and Langer, R. (2006a). Antitumor efficacy of a novel polymer–peptide–drug conjugate in human tumor xenograft models. *Int. J. Cancer* 118, 1519–1526. doi: 10.1002/ijc.21495

Chaudhuri, T. R., Straubinger, N. L., Pitoniak, R. F., Hylander, B. L., Repasky, E. A., Ma, W. W., et al. (2016). Tumor-priming Smoothened inhibitor enhances deposition and efficacy of cytotoxic nanoparticles in a pancreatic cancer model. *Mol. Cancer Ther.* 15, 84–93. doi: 10.1158/1535-7163.MCT-15-0602

Chauhan, V. P., Stylianopoulos, T., Boucher, Y., and Jain, R. K. (2011). Delivery of molecular and nanoscale medicine to tumors: transport barriers and strategies. *Annu. Rev. Chem. Biomol. Eng.* 2, 281–298. doi: 10.1146/annurev-chembioeng-061010-114300

Chauhan, V. P., Stylianopoulos, T., Martin, J. D., Popovi,ć, Z., Chen, O., Kamoun, W. S., et al. (2012). Normalization of tumour blood vessels improves the delivery of nanomedicines in a size-dependent manner. *Nat. Nanotechnol.* 7, 383–388. doi: 10.1038/nnano.2012.45

Chen, B., Dai, W., He, B., Zhang, H., Wang, X., Wang, Y., et al. (2017). Current multistage drug delivery systems based on the tumor microenvironment. *Theranostics* 7, 538. doi: 10.7150/thno.16684

Chen, B., Dai, W., Mei, D., Liu, T., Li, S., He, B., et al. (2016). Comprehensively priming the tumor microenvironment by cancer-associated fibroblast-targeted liposomes for combined therapy with cancer cell-targeted chemotherapeutic drug delivery system. *J. Control. Rel.* 241, 68–80. doi: 10.1016/j.jconrel.2016.09.014

Chen, F., and Cai, W. (2014). Tumor vasculature targeting: a generally applicable approach for functionalized nanomaterials. *Small* 10, 1887–1893. doi: 10.1002/smll.201303627

Chen, F., Zhuang, X., Lin, L., Yu, P., Wang, Y., Shi, Y., et al. (2015). New horizons in tumor microenvironment biology: challenges and opportunities. *BMC Med.* 13:45. doi: 10.1186/s12916-015-0278-7

Chen, S., Yang, K., Tuguntaev, R. G., Mozhi, A., Zhang, J., Wang, P. C., et al. (2016). Targeting tumor microenvironment with PEG-based amphiphilic nanoparticles to overcome chemoresistance. *Nanomedicine* 12, 269–286. doi: 10.1016/j.nano.2015.10.020

Chen, Y., Feng, S., Liu, W., Yuan, Z., Yin, P., and Gao, F. (2017). Vitamin E succinate-grafted-chitosan oligosaccharide/RGD-conjugated TPGS mixed micelles loaded with paclitaxel for U87MG tumor therapy. *Mol. Pharm.* 14, 1190–1203. doi: 10.1021/acs.molpharmaceut.6b01068

Chen, Z., Xu, X. H., and Hu, J. (2016). Role of pericytes in angiogenesis: focus on cancer angiogenesis and anti-angiogenic therapy. *Neoplasma* 63, 173–182. doi: 10.4149/201_150704N369

Cheng, Y. T., Yang, C. C., and Shyur, L. F. (2016). Phytomedicine—Modulating oxidative stress and the tumor microenvironment for cancer therapy. *Pharmacol. Res.* 114, 128–143. doi: 10.1016/j.phrs.2016.10.022

Chi, Y., Yin, X., Sun, K., Feng, S., Liu, J., Chen, D., et al. (2017). Redox-sensitive and hyaluronic acid functionalized liposomes for cytoplasmic drug delivery to osteosarcoma in animal models. *J. Control. Rel.* 261, 113–125. doi: 10.1016/j.jconrel.2017.06.027

Chitneni, S. K., Palmer, G. M., Zalutsky, M. R., and Dewhirst, M. W. (2011). Molecular imaging of hypoxia. *J. Nucl. Med.* 52, 165–168. doi: 10.2967/jnumed.110.075663

Cho, K., Wang, X. U., Nie, S., and Shin, D. M. (2008). Therapeutic nanoparticles for drug delivery in cancer. *Clin. Cancer Res.* 14, 1310–1316. doi: 10.1158/1078-0432.CCR-07-1441

Clares, B., Biedma-Ortiz, R. A., Sáez-Fernández, E., Prados, J. C., Melguizo, C., Cabeza, L., et al. (2013). Nano-engineering of 5-fluorouracil-loaded magnetoliposomes for combined hyperthermia and chemotherapy against colon cancer. *Eur. J. Pharm. Biopharm.* 85, 329–338. doi: 10.1016/j.ejpb.2013.01.028

Clark, A. G., and Vignjevic, D. M. (2015). Modes of cancer cell invasion and the role of the microenvironment. *Curr. Opin. Cell Biol.* 36, 13–22. doi: 10.1016/j.ceb.2015.06.004

Conniot, J., Silva, J. M., Fernandes, J. G., Silva, L. C., Gaspar, R., Brocchini, S., et al. (2014). Cancer immunotherapy: nanodelivery approaches for immune cell targeting and tracking. *Front. Chem.* 2:105. doi: 10.3389/fchem.2014.00105

Cooke, V. G., LeBleu, V. S., Keskin, D., Khan, Z., O'Connell, J. T., Teng, Y., et al. (2012). Pericyte depletion results in hypoxia-associated epithelial-to-mesenchymal transition and metastasis mediated by met signaling pathway. *Cancer Cell* 21, 66–81. doi: 10.1016/j.ccr.2011.11.024

Cox, T. R., and Erler, J. T. (2011). Remodeling and homeostasis of the extracellular matrix: implications for fibrotic diseases and cancer. *Dis. Models Mech.* 4, 165–178. doi: 10.1242/dmm.004077

Crayton, S. H., and Tsourkas, A. (2011). pH-titratable superparamagnetic iron oxide for improved nanoparticle accumulation in acidic tumor microenvironments. *ACS Nano* 5, 9592–9601. doi: 10.1021/nn202863x

Cree, I. A., and Charlton, P. (2017). Molecular chess? *Hallmarks of anti-cancer drug resistance. BMC Cancer* 17:10. doi: 10.1186/s12885-016-2999-1

Dai, L., Liu, J., Luo, Z., Li, M., and Cai, K. (2016). Tumor therapy: targeted drug delivery systems. *J. Mater. Chem. B.* 4, 6758–6772. doi: 10.1039/c6tb01743f

Dalela, M., Shrivastav, T. G., Kharbanda, S., and Singh, H. (2015). pH-sensitive biocompatible nanoparticles of paclitaxel-conjugated poly (styrene-co-maleic acid) for anticancer drug delivery in solid tumors of syngeneic mice. *ACS Appl. Mater. Interfaces.* 7, 26530–26548. doi: 10.1021/acsami.5b07764

Damaghi, M., Tafreshi, N. K., Lloyd, M. C., Sprung, R., Estrella, V., Wojtkowiak, J. W., et al. (2015). Chronic acidosis in the tumour microenvironment selects for overexpression of LAMP2 in the plasma membrane. *Nature Commun.* 6:8752. doi: 10.1038/ncomms9752

Danhier, F. (2016). To exploit the tumor microenvironment: since the EPR effect fails in the clinic, what is the future of nanomedicine? *J. Control. Rel.* 244, 108–121. doi: 10.1016/j.jconrel.2016.11.015

Danhier, F., Feron, O., and Préat, V. (2010). To exploit the tumor microenvironment: passive and active tumor targeting of nanocarriers for anti-cancer drug delivery. *J. Control. Rel.* 148, 135–146. doi: 10.1016/j.jconrel.2010.08.027

De Spiegelaere, W., Casteleyn, C., Van den Broeck, W., Plendl, J., Bahramsoltani, M., Simoens, P., et al. (2012). Intussusceptive angiogenesis: a biologically relevant form of angiogenesis. *J. Vasc. Res.* 49, 390–404. doi: 10.1159/000338278

Delgado, D., Gascón, A. R., del Pozo-Rodríguez, A., Echevarría, E., de Garibay, A. P. R., Rodríguez, J. M., et al. (2012). Dextran–protamine–solid lipid nanoparticles as a non-viral vector for gene therapy: *in vitro* characterization and *in vivo* transfection after intravenous administration to mice. *Int. J. Pharm.* 425, 35–43. doi: 10.1016/j.ijpharm.2011.12.052

Deng, Z., Zhen, Z., Hu, X., Wu, S., Xu, Z., and Chu, P. K. (2011). Hollow chitosan–silica nanospheres as pH-sensitive targeted delivery carriers in breast cancer therapy. *Biomaterials.* 32, 4976–4986. doi: 10.1016/j.biomaterials.2011.03.050

Deng, Z. J., Morton, S. W., Ben-Akiva, E., Dreaden, E. C., Shopsowitz, K. E., and Hammond, P. T. (2013). Layer-by-layer nanoparticles for systemic codelivery of an anticancer drug and siRNA for potential triple-negative breast cancer treatment. *ACS Nano*. 7, 9571–9584. doi: 10.1021/nn4047925

Deshpande, P. P., Biswas, S., and Torchilin, V. P. (2013). Current trends in the use of liposomes for tumor targeting. *Nanomedicine*. 8, 1509–1528. doi: 10.2217/nnm.13.118

Dewhirst, M. W. (2007). Intermittent hypoxia furthers the rationale for hypoxia-inducible factor-1 targeting. *Cancer Res.* 67, 854–855. doi: 10.1158/0008-5472.CAN-06-4744

Dewhirst, M. W., Ong, E. T., Braun, R. D., Smith, B., Klitzman, B., Evans, S. M., et al. (1999). Quantification of longitudinal tissue pO_2 gradients in window chamber tumours: impact on tumour hypoxia. *Br. J. Cancer* 79: 1717. doi: 10.1038/sj.bjc.6690273

Diaz-Flores, L., Gutierrez, R., Madrid, J. F., Varela, H., Valladares, F., Acosta, E., et al. (2009). Pericytes. Morphofunction, interactions and pathology in a quiescent and activated mesenchymal cell niche. *Histol. Histopathol.* 24, 909–969. doi: 10.14670/HH-24.909

Din, F., Aman, W., Ullah, I., Qureshi, O. S., Mustapha, O., Shafique, S., et al. (2017). Effective use of nanocarriers as drug delivery systems for the treatment of selected tumors. *Int. J. Nanomed.* 12, 7291–7309. doi: 10.2147/IJN.S146315

Ding, Y., Sun, D., Wang, G. L., Yang, H. G., Xu, H. F., Chen, J. H., et al. (2015). An efficient PEGylated liposomal nanocarrier containing cell-penetrating peptide and pH-sensitive hydrazone bond for enhancing tumor-targeted drug delivery. *Int. J. Nanomed.* 10, 6199–6214. doi: 10.2147/IJN.S92519

Dong, H., Tang, M., Li, Y., Li, Y., Qian, D., and Shi, D. (2015). Disulfide-bridged cleavable PEGylation in polymeric nanomedicine for controlled therapeutic delivery. *Nanomedicine* 10, 1941–1958. doi: 10.2217/nnm.15.38

Donnem, T., Hu, J., Ferguson, M., Adighibe, O., Snell, C., Harris, A. L., et al. (2013). Vessel co-option in primary human tumors and metastases: an obstacle to effective anti-angiogenic treatment? *Cancer Med.* 2, 427–436. doi: 10.1002/cam4.105

Dreaden, E. C., Morton, S. W., Shopsowitz, K. E., Choi, J. H., Deng, Z. J., Cho, N. J., et al. (2014). Bimodal tumor-targeting from microenvironment responsive hyaluronan layer-by-layer (LbL) nanoparticles. *ACS Nano* 8, 8374–8382. doi: 10.1021/nn502861t

Eberhard, A., Kahlert, S., Goede, V., Hemmerlein, B., Plate, K. H., and Augustin, H. G. (2000). Heterogeneity of angiogenesis and blood vessel maturation in human tumors: implications for antiangiogenic tumor therapies. *Cancer Res.* 60, 1388–1393.

Egeblad, M., Rasch, M. G., and Weaver, V. M. (2010). Dynamic interplay between the collagen scaffold and tumor evolution. *Curr. Opin. Cell Biol.* 22, 697–706. doi: 10.1016/j.ceb.2010.08.015

Estrella, V., Chen, T., Lloyd, M., Wojtkowiak, J., Cornnell, H. H., Ibrahim-Hashim, A., et al. (2013). Acidity generated by the tumor microenvironment drives local invasion. *Cancer Res.* 73, 1524–1535. doi: 10.1158/0008-5472.CAN-12-2796

Fan, Y., Du, W., He, B., Fu, F., Yuan, L., Wu, H., et al. (2013). The reduction of tumor interstitial fluid pressure by liposomal imatinib and its effect on combination therapy with liposomal doxorubicin. *Biomaterials* 34, 2277–2288. doi: 10.1016/j.biomaterials.2012.12.012

Feng, Q., Yu, M. Z., Wang, J. C., Hou, W. J., Gao, L. Y., Ma, X. F., et al. (2014). Synergistic inhibition of breast cancer by co-delivery of VEGF siRNA and paclitaxel via vapreotide-modified core–shell nanoparticles. *Biomaterials* 35, 5028–5038. doi: 10.1016/j.biomaterials.2014.03.012

Ferland-McCollough, D., Slater, S., Richard, J., Reni, C., and Mangialardi, G. (2017). Pericytes, an overlooked player in vascular pathobiology. *Pharmacol. Ther.* 171, 30–42. doi: 10.1016/j.pharmthera.2016.11.008

Ferlay, J., Soerjomataram, I., Dikshit, R., Eser, S., Mathers, C., Rebelo, M., et al. (2015). Cancer incidence and mortality worldwide: sources, methods and major patterns in GLOBOCAN 2012. *Int. J. Cancer* 136, E359–E386. doi: 10.1002/ijc.29210

Fernandes, C. B., Suares, D., and Dhawan, V. (2018). "Lipid nanocarriers for intracellular delivery." in *Multifunctional Nanocarriers for Contemporary Healthcare Applications*. M. A. Barkat, A. B. Harshita, S. Beg, and F. J. Ahmad, eds. Hershey, PA: IGI Global, 129–156.

Fernández-Sánchez, M. E., Barbier, S., Whitehead, J., Béalle, G., Michel, A., Latorre-Ossa, H., et al. (2015). Mechanical induction of the tumorigenic β-catenin pathway by tumour growth pressure. *Nature* 523, 92–95. doi: 10.1038/nature14329

Franco, M., Roswall, P., Cortez, E., Hanahan, D., and Pietras, K. (2011). Pericytes promote endothelial cell survival through induction of autocrine VEGF-A signaling and Bcl-w expression. *Blood* 118, 2906–2917. doi: 10.1182/blood-2011-01-331694

Fuxe, J., Tabruyn, S., Colton, K., Zaid, H., Adams, A., Baluk, P., et al. (2011). Pericyte requirement for anti-leak action of angiopoietin-1 and vascular remodeling in sustained inflammation. *Am. J. Pathol.* 178, 2897–2909. doi: 10.1016/j.ajpath.2011.02.008

Gacche, R. N., and Meshram, R. J. (2013). Targeting tumor micro-environment for design and development of novel anti-angiogenic agents arresting tumor growth. *Prog. Biophys. Mol. Biol.* 113, 333–354. doi: 10.1016/j.pbiomolbio.2013.10.001

Gascard, P., and Tlsty, T. D. (2016). Carcinoma-associated fibroblasts: orchestrating the composition of malignancy. *Genes Dev.* 30, 1002–1019. doi: 10.1101/gad.279737.116

Geevarghese, A., and Herman, I. M. (2014). Pericyte-endothelial crosstalk: implications and opportunities for advanced cellular therapies. *Transl. Res.* 163, 296–306. doi: 10.1016/j.trsl.2014.01.011

Geng, Y. A. N., Dalhaimer, P., Cai, S., Tsai, R., Tewari, M., Minko, T., et al. (2007). Shape effects of filaments versus spherical particles in flow and drug delivery. *Nat. Nanotech.* 2, 249–255. doi: 10.1038/nnano.2007.70

Geretti, E., Leonard, S. C., Dumont, N., Lee, H., Zheng, J., De Souza, R., et al. (2015). Cyclophosphamide-mediated tumor priming for enhanced delivery and antitumor activity of HER2-targeted liposomal doxorubicin (MM-302). *Mol. Cancer Ther.* 14, 2060–2071. doi: 10.1158/1535-7163.MCT-15-0314

Gerhardt, H., and Betsholtz, C. (2003). Endothelial-pericyte interactions in angiogenesis. *Cell. Tissue. Res.* 314, 15–23. doi: 10.1007/s00441-003-0745-x

Ghosh, S., Yesilyurt, V., Savariar, E. N., Irvin, K., and Thayumanavan, S. (2009). Redox, ionic strength, and pH sensitive supramolecular polymer assemblies. *J. Polym. Sci. A Polym. Chem.* 47, 1052–1060. doi: 10.1002/pola.23204

Goswami, K. K., Ghosh, T., Ghosh, S., Sarkar, M., Bose, A., and Baral, R. (2017). Tumor promoting role of anti-tumor macrophages in tumor microenvironment. *Cell. Immunol.* 316, 1–10. doi: 10.1016/j.cellimm.2017.04.005

Grazu, V., Moros, M., and Sanchez-Espinel, C. (2012). *Nanobiotechnology: Inorganic Nanoparticles vs Organic Nanoparticles.* Oxford, UK: Elsevier.

Guardia, P., Di Corato, R., Lartigue, L., Wilhelm, C., Espinosa, A., Garcia-Hernandez, M., et al. (2012). Water-soluble iron oxide nanocubes with high values of specific absorption rate for cancer cell hyperthermia treatment. *ACS Nano*. 6, 3080–3091. doi: 10.1021/nn2048137

Gullotti, E., and Yeo, Y. (2009). Extracellularly activated nanocarriers: a new paradigm of tumor targeted drug delivery. *Mol. Pharm.* 6, 1041–1051. doi: 10.1021/mp900090z.

Han, H. D., Jeon, Y. W., Kwon, H. J., Jeon, H. N., Byeon, Y., Lee, C. O., et al. (2015). Therapeutic efficacy of doxorubicin delivery by a CO_2 generating liposomal platform in breast carcinoma. *ActaBiomater* 24, 279–285. doi: 10.1016/j.actbio.2015.06.019

Han, W., Chen, S., Yuan, W., Fan, Q., Tian, J., Wang, X., et al. (2016). Oriented collagen fibers direct tumor cell intravasation. *PNAS.* 113, 11208–11213. doi: 10.1073/pnas.1610347113

Han, Y., Zhang, P., Chen, Y., Sun, J., and Kong, F. (2014). Co-delivery of plasmid DNA and doxorubicin by solid lipid nanoparticles for lung cancer therapy. *Int. J. Mol. Med.* 34, 191–196. doi: 10.3892/ijmm.2014.177

Hanahan, D., and Weinberg, R. A. (2011). Hallmarks of cancer: the next generation. *Cell.* 144, 646–674. doi: 10.1016/j.cell.2011.02.013

Hao, S., Yan, Y., Ren, X., Xu, Y., Chen, L., and Zhang, H. (2015). Candesartan-graft-polyethyleneimine cationic micelles for effective co-delivery of drug and gene in anti-angiogenic lung cancer therapy. *Biotechnol. Bioprocess Eng.* 20, 550–560. doi: 10.1007/s12257-014-0858-y

Harnoy, A. J., Rosenbaum, I., Tirosh, E., Ebenstein, Y., Shaharabani, R., Beck, R., et al. (2014). Enzyme-responsive amphiphilic PEG-dendron hybrids and their assembly into smart micellar nanocarriers. *J. Am. Chem. Soc.* 136, 7531–7534. doi: 10.1021/ja413036q

Hatakeyama, H., Akita, H., Kogure, K., Oishi, M., Nagasaki, Y., Kihira, Y., et al. (2007). Development of a novel systemic gene delivery system for

cancer therapy with a tumor-specific cleavable PEG-lipid. *Gene Ther*. 14, 68. doi: 10.1038/sj.gt.3302843

Hattori, Y., Yamasaku, H., and Maitani, Y. (2013). Anionic polymer-coated lipoplex for safe gene delivery into tumor by systemic injection. *J. Drug Target*. 21, 639–647. doi: 10.3109/1061186X.2013.789035

He, Y., Su, Z., Xue, L., Xu, H., and Zhang, C. (2016). Co-delivery of erlotinib and doxorubicin by pH-sensitive charge conversion nanocarrier for synergistic therapy. *J. Control. Rel.* 229, 80–92. doi: 10.1016/j.jconrel.2016.03.001

Hofmann, M., Guschel, M., Bernd, A., Bereiter-Hahn, J., Kaufmann, R., Tandi, C., et al. (2006). Lowering of tumor interstitial fluid pressure reduces tumor cell proliferation in a xenograft tumor model. *Neoplasia* 8, 89–95. doi: 10.1593/neo.05469

Holback, H., and Yeo, Y. (2011). Intratumoral drug delivery with nanoparticulate carriers. *Pharm. Res.* 28, 1819–1830. doi: 10.1007/s11095-010-0360-y

Hosaka, K., Yang, Y., Seki, T., Fischer, C., Dubey, O., Fredlund, E., et al. (2016). Pericyte–fibroblast transition promotes tumor growth and metastasis. *PNAS.* 113, E5618–E5627. doi: 10.1073/pnas.1608384113

Hou, L., Yang, X., Ren, J., Wang, Y., Zhang, H., Feng, Q., et al. (2016). A novel redox-sensitive system based on single-walled carbon nanotubes for chemo-photothermal therapy and magnetic resonance imaging. *Int. J. Nanomedicine* 11:607. doi: 10.2147/IJN.S98476

Hoves, S., Ooi, C. H., Wolter, C., Sade, H., Bissinger, S., Schmittnaegel, M., et al. (2018). Rapid activation of tumor-associated macrophages boosts preexisting tumor immunity. *J. Exp. Med.* 215, 859–876. doi: 10.1111/j.0105-2896.2010.00889.x

Hu, J., Miura, S., Na, K., and Bae, Y. H. (2013). pH-responsive and charge shielded cationic micelle of poly (L-histidine)-block-short branched PEI for acidic cancer treatment. *J. Control. Release* 172, 69–76. doi: 10.1016/j.jconrel.2013.08.007

Huang, K., Ma, H., Liu, J., Huo, S., Kumar, A., Wei, T., et al. (2012). Size-dependent localization and penetration of ultrasmall gold nanoparticles in cancer cells, multicellular spheroids, and tumors *in vivo*. *ACS Nano*. 6, 4483–4493. doi: 10.1021/nn301282m

Hughes, C. C. (2008). Endothelial–stromal interactions in angiogenesis. *Curr. Opin. Hematol.* 15, 204–209. doi: 10.1097/MOH.0b013e3282f97dbc

Hung, C. C., Huang, W. C., Lin, Y. W., Yu, T. W., Chen, H. H., Lin, S. C., et al. (2016). Active tumor permeation and uptake of surface charge-switchable theranostic nanoparticles for imaging-guided photothermal/chemo combinatorial therapy. *Theranostics* 6:302. doi: 10.7150/thno.13686

Huo, S., Ma, H., Huang, K., Liu, J., Wei, T., Jin, S., et al. (2013). Superior penetration and retention behavior of 50 nm gold nanoparticles in tumors. *Cancer Res*. 73, 319–330. doi: 10.1158/0008-5472.CAN-12-2071

Hylander, B. L., Sen, A., Beachy, S. H., Pitoniak, R., Ullas, S., Gibbs, J. F., et al. (2015). Tumor priming by Apo2L/TRAIL reduces interstitial fluid pressure and enhances efficacy of liposomal gemcitabine in a patient derived xenograft tumor model. *J. Control. Rel.* 217, 160–169. doi: 10.1016/j.jconrel.2015.08.047

Iessi, E., Logozzi, M., Mizzoni, D., Di Raimo, R., Supuran, C. T., and Fais, S. (2018). Rethinking the combination of proton exchanger inhibitors in cancer therapy. *Metabolites* 8:2. doi: 10.3390/metabo8010002

Ivanovic, Z. (2009). Hypoxia or *in situ* normoxia: the stem cell paradigm. *J. Cell. Physiol.* 219, 271–275. doi: 10.1002/jcp.21690

Izadiyan, Z., Basri, M., Masoumi, H. R. F., Karjiban, R. A., Salim, N., and Shameli, K. (2017). Modeling and optimization of nanoemulsion containing Sorafenib for cancer treatment by response surface methodology. *Chem. Cent. J.* 11:21. doi: 10.1186/s13065-017-0248-6

Jain, J., Fernandes, C., and Patravale, V. (2010). Formulation development of parenteral phospholipid-based microemulsion of etoposide. *AAPS PharmSciTech*. 11, 826–831. doi: 10.1208/s12249-010-9440-x

Jain, R. K. (2013). Normalizing tumor microenvironment to treat cancer: bench to bedside to biomarkers. *J. Clin. Oncol.* 31, 2205–2218. doi: 10.1200/JCO.2012.46.3653

Jarosz-Biej, M., Kamińska, N., Matuszczak, S., Cicho,ń, T., Pamuła-Piłat, J., Czapla, J., et al. (2018). M1-like macrophages change tumor blood vessels and microenvironment in murine melanoma. *PLoS ONE* 13:e0191012. doi: 10.1371/journal.pone.0191012

Ji, T., Zhao, Y., Ding, Y., and Nie, G. (2013). Using functional nanomaterials to target and regulate the tumor microenvironment: diagnostic and therapeutic applications. *Adv. Mater*. 25, 3508–3525. doi: 10.1002/adma.201300299

Jiang, L., Li, L., He, X., Yi, Q., He, B., Cao, J., et al. (2015). Overcoming drug-resistant lung cancer by paclitaxel loaded dual-functional liposomes with mitochondria targeting and pH-response. *Biomaterials* 52, 126–139. doi: 10.1016/j.biomaterials.2015.02.004

Jiang, W., Huang, Y., An, Y., and Kim, B. Y. (2015). Remodeling tumor vasculature to enhance delivery of intermediate-sized nanoparticles. *ACS Nano*. 9, 8689–8696. doi: 10.1021/acsnano.5b02028

Ju, C., Mo, R., Xue, J., Zhang, L., Zhao, Z., Xue, L., et al. (2014). Sequential intra-intercellular nanoparticle delivery system for deep tumor penetration. *Angew. Chem. Int. Ed.* 53, 6253–6258. doi: 10.1002/anie.201311227

Kalli, M., and Stylianopoulos, T. (2018). Defining the role of solid stress and matrix stiffness in cancer cell proliferation and metastasis. *Front. Oncol.* 8:55. doi: 10.3389/fonc.2018.00055

Kang, E., and Shin, J. W. (2016). Pericyte-targeting drug delivery and tissue engineering. *Int. J. Nanomed.* 11, 2397–2406. doi: 10.2147/IJN.S105274

Kano, M. R., Bae, Y., Iwata, C., Morishita, Y., Yashiro, M., Oka, M., et al. (2007). Improvement of cancer-targeting therapy, using nanocarriers for intractable solid tumors by inhibition of TGF-β signaling. *PNAS.* 104, 3460–3465. doi: 10.1073/pnas.0611660104

Kato, Y., Ozawa, S., Miyamoto, C., Maehata, Y., Suzuki, A., Maeda, T., et al. (2013). Acidic extracellular microenvironment and cancer. *Cancer Cell Int.* 13:89. doi: 10.1186/1475-2867-13-8

Kebebe, D., Liu, Y., Wu, Y., Vilakhamxay, M., Liu, Z., and Li, J. (2018). Tumor-targeting delivery of herb-based drugs with cell-penetrating/tumor-targeting peptide-modified nanocarriers. *Int. J. Nanomed.* 13, 1425–1442. doi: 10.2147/IJN.S156616

Kelly-Goss, M. R., Sweat, R. S., Stapor, P. C., Peirce, S. M., and Murfee, W. L. (2014). Targeting perciytes for angiogenic therapies. *Microcirculation* 21, 345–357. doi: 10.1111/micc.12107

Kharaishvili, G., Simkova, D., Bouchalova, K., Gachechiladze, M., Narsia, N., and Bouchal, J. (2014). The role of cancer-associated fibroblasts, solid stress and other microenvironmental factors in tumor progression and therapy resistance. *Cancer Cell Int.* 14, 41. doi: 10.1186/1475-2867-14-41

Kibria, G., Hatakeyama, H., Ohga, N., Hida, K., and Harashima, H. (2013). The effect of liposomal size on the targeted delivery of doxorubicin to Integrin αvβ3-expressing tumor endothelial cells. *Biomaterials* 34, 5617–5627. doi: 10.1016/j.biomaterials.2013.03.094

Kokuryo, D., Aoki, I., Yuba, E., Kono, K., Aoshima, S., Kershaw, J., et al. (2017). Evaluation of a combination tumor treatment using thermo-triggered liposomal drug delivery and carbon ion irradiation. *Transl. Res.* 185, 24–33. doi: 10.1016/j.trsl.2017.04.001

Koo, A. N., Min, K. H., Lee, H. J., Lee, S. U., Kim, K., Kwon, I. C., et al. (2012). Tumor accumulation and antitumor efficacy of docetaxel-loaded core-shell-corona micelles with shell-specific redox-responsive cross-links. *Biomaterials* 33, 1489–1499. doi: 10.1016/j.biomaterials.2011.11.013

Koren, E., Apte, A., Jani, A., and Torchilin, V. P. (2012). Multifunctional PEGylated 2C5-immunoliposomes containing pH-sensitive bonds and TAT peptide for enhanced tumor cell internalization and cytotoxicity. *J. Control. Release* 160, 264–273. doi: 10.1016/j.jconrel.2011.12.002

Krall, N., Pretto, F., Decurtins, W., Bernardes, G. J., Supuran, C. T., and Neri, D. (2014). A small-molecule drug conjugate for the treatment of carbonic anhydrase IX expressing tumors. *Angew. Chem. Int. Ed.* 53, 4231–4235. doi: 10.1002/anie.201310709

Kraning-Rush, C. M., and Reinhart-King, C. A. (2012). Controlling matrix stiffness and topography for the study of tumor cell migration. *Cell Adh. Migr.* 6, 274–279. doi: 10.4161/cam.21076

Kwon, J., Kim, J., Park, S., Khang, G., Kang, P. M., and Lee, D. (2013). Inflammation-responsive antioxidant nanoparticles based on a polymeric prodrug of vanillin. *Biomacromolecules* 14, 1618–1626. doi: 10.1021/bm400256h

Kyle, A. H., Huxham, L. A., Yeoman, D. M., and Minchinton, A. I. (2007). Limited tissue penetration of taxanes: a mechanism for resistance in solid tumors. *Clin. Can. Res.* 13, 2804–2810. doi: 10.1158/1078-0432.CCR-06-1941

Lammers, T. G. G. M., Hennink, W. E., and Storm, G. (2008). Tumour-targeted nanomedicines: principles and practice. *Br. J. Cancer*. 99:392. doi: 10.1038/sj.bjc.6604483

Lee, D., Noh, I., Yoo, J., Rejinold, N. S., and Kim, Y. C. (2017). pH-controllable cell-penetrating polypeptide that exhibits cancer targeting. *Acta Biomater*. 57, 187–196. doi: 10.1016/j.actbio.2017.05.040

Lee, E. S., Gao, Z., Kim, D., Park, K., Kwon, I. C., and Bae, Y. H. (2008). Super pH-sensitive multifunctional polymeric micelle for tumorpHe specific TAT exposure and multidrug resistance. *J. Control. Rel*. 129, 228–236.doi: 10.1016/j.jconrel.2008.04.024

Li, H., Yang, X., Zhou, Z., Wang, K., Li, C., Qiao, H., et al. (2017). Near-infrared light-triggered drug release from a multiple lipid carrier complex using an all-in-one strategy. *J. Control. Rel*. 261, 126–137. doi: 10.1016/j.jconrel.2017.06.029

Li, H. J., Du, J. Z., Du, X. J., Xu, C. F., Sun, C. Y., Wang, H. X., et al. (2016). Stimuli-responsive clustered nanoparticles for improved tumor penetration and therapeutic efficacy. *PNAS*. 113, 4164–4169. doi: 10.1073/pnas.1522080113

Li, Q., Tang, Q., Zhang, P., Wang, Z., Zhao, T., Zhou, J., et al. (2015). Human epidermal growth factor receptor-2 antibodies enhance the specificity and anticancer activity of light-sensitive doxorubicin-labeled liposomes. *Biomaterials* 57, 1–11.doi: 10.1016/j.biomaterials.2015.04.009

Li, R., and Xie, Y. (2017). Nanodrugdelivery systems for targeting the endogenous tumor microenvironment and simultaneously overcoming multidrug resistance properties. *J. Control. Rel*. 251, 49–67. doi: 10.1016/j.jconrel.2017.02.020

Liao, W. C., Lu, C. H., Hartmann, R., Wang, F., Sohn, Y. S., Parak, W. J., et al. (2015). Adenosine triphosphate-triggered release of macromolecular and nanoparticle loads from aptamer/DNA-cross-linked microcapsules. *ACS Nano*. 9, 9078–9086. doi: 10.1021/acsnano.5b03223

Liberti, M. V., and Locasale, J. W. (2016). The Warburg effect: how does it benefit cancer cells? *Trends Biochem. Sci.* 41, 211–218. doi: 10.1016/j.tibs.2015.12.001

Lin, C., Wong, B. C. K., Chen, H., Bian, Z., Zhang, G., Zhang, X., et al. (2017). Pulmonary delivery of triptolide-loaded liposomes decorated with anti-carbonic anhydrase IX antibody for lung cancer therapy. *Sci. Rep*. 7:1097. doi: 10.1038/s41598-017-00957-4

Lin, C. W., Lu, K. Y., Wang, S. Y., Sung, H. W., and Mi, F. L. (2016). CD44-specific nanoparticles for redox-triggered reactive oxygen species production and doxorubicin release. *ActaBiomater* 35, 280–292. doi: 10.1016/j.actbio.2016.02.005

Ling, C., Lu, Y., Cheng, B., McGoogan, K. E., Gee, S. W., Ma, W., et al. (2011). High-efficiency transduction of liver cancer cells by recombinant adeno-associated virus serotype 3 vectors. *J. Vis. Exp*. 49:2538. doi: 10.3791/2538

Liotta, L. A. (2016). Adhere, degrade, and move: the three-step model of invasion. *Cancer Res*. 76, 3115–3117. doi: 10.1158/0008-5472.CAN-16-1297

Liu, A. Y., and Ouyang, G. (2013). Tumor angiogenesis: a new source of pericytes. *Curr. Biol.* 23, R565–R568. doi: 10.1016/j.cub.2013.05.023

Liu, J., Zhang, B., Luo, Z., Ding, X., Li, J., Dai, L., et al. (2015). Enzyme responsive mesoporous silica nanoparticles for targeted tumor therapy *in vitro* and *in vivo*. *Nanoscale* 7, 3614–3626. doi: 10.1039/C5NR00072F

Liu, Y., Li, L. L., Qi, G. B., Chen, X. G., and Wang, H. (2014). Dynamic disordering of liposomal cocktails and the spatio-temporal favorable release of cargoes to circumvent drug resistance. *Biomaterials* 35, 3406–3415. doi: 10.1016/j.biomaterials.2013.12.089

Liu, Z., Xiong, M., Gong, J., Zhang, Y., Bai, N., Luo, Y., et al. (2014). Legumain protease-activated TAT-liposome cargo for targeting tumours and their microenvironment. *Nat. Commun*. 5:4280. doi: 10.1038/ncomms5280

Lu, P., Weaver, V. M., and Werb, Z. (2012). The extracellular matrix: a dynamic niche in cancer progression. *J. Cell Biol.* 196, 395–406. doi: 10.1083/jcb.201102147

Lunt, S. J., Fyles, A., Hill, R. P., and Milosevic, M. (2008). Interstitial fluid pressure in tumors: therapeutic barrier and biomarker of angiogenesis. *Future Oncol.* 4, 793–802. doi: 10.2217/14796694.4.6.793

MacEwan, S. R., and Chilkoti, A. (2013). Harnessing the power of cell-penetrating peptides: activatable carriers for targeting systemic delivery of cancer therapeutics and imaging agents. *Wiley Interdiscip. Rev. Nanomed. Nanobiotechnol.* 5, 31–48. doi: 10.1002/wnan.1197

Maggini, L., Cabrera, I., Ruiz-Carretero, A., Prasetyanto, E. A., Robinet, E., and De Cola, L. (2016). Breakable mesoporous silica nanoparticles for targeted drug delivery. *Nanoscale* 8, 7240–7247. doi: 10.1039/C5NR09112H

Mahon, B. P., Pinard, M. A., and McKenna, R. (2015). Targeting carbonic anhydrase IX activity and expression. *Molecules* 20, 2323–2348. doi: 10.3390/molecules20022323

Matsumoto, S., Batra, S., Saito, K., Yasui, H., Choudhuri, R., Gadisetti, C., et al. (2011). Anti-angiogenic agent sunitinib transiently increases tumor oxygenation and suppresses cycling hypoxia. *Cancer Res.* 71, 6350–6359. doi: 10.1158/0008-5472.CAN-11-2025

Matsumura, Y., and Maeda, H. (1986). A new concept for macromolecular therapeutics in cancer chemotherapy: mechanism of tumoritropic accumulation of proteins and the antitumor agent smancs. *Cancer Res.* 46, 6387–6392.

McCarty, M. F., Somcio, R. J., Stoeltzing, O., Wey, J., Fan, F., Liu, W., et al. (2007). Overexpression of PDGF-BB decreases colorectal and pancreatic cancer growth by increasing tumor pericyte content. *J. Clin. Invest.* 117, 2114–2122. doi: 10.1172/JCI31334

Miao, L., and Huang, L. (2015). Exploring the tumor microenvironment with nanoparticles. *Cancer Treat Res.* 166, 193–226. doi: 10.1007/978-3-319-16555-4_9

Michiels, C., Tellier, C., and Feron, O. (2016). Cycling hypoxia: a key feature of the tumor microenvironment. *Biochim. Biophys. Acta* 1866, 76–86. doi: 10.1016/j.bbcan.2016.06.004

Min, K. H., Kim, J. H., Bae, S. M., Shin, H., Kim, M. S., Park, S., et al. (2010). Tumoral acidic pH-responsive MPEG-poly (β-amino ester) polymeric micelles for cancer targeting therapy. *J. Control. Release* 144, 259–266. doi: 10.1016/j.jconrel.2010.02.024

Minami, Y., Sasaki, T., Kawabe, J. I., and Ohsaki, Y. (2013). "Accessory cells in tumor angiogenesis—tumor-associated pericytes," in *Research Directions in Tumor Angiogenesis* (London: InTechOpen Limited), 73–88.

Mistry, I. N., Thomas, M., Calder, E. D., Conway, S. J., and Hammond, E. M. (2017). Clinical advances of hypoxia-activated prodrugs in combination with radiation therapy. *Int. J. Radiat. Oncol. Biol. Phys.* 98, 1183–1196. doi: 10.1016/j.ijrobp.2017.03.024

Mo, R., Jiang, T., DiSanto, R., Tai, W., and Gu, Z. (2014). ATP-triggered anticancer drug delivery. *Nat.Commun*. 5:3364. doi: 10.1038/ncomms4364

Morikawa, S., Baluk, P., Kaidoh, T., Haskell, A., Jain, R. K., and McDonald, D. M. (2002). Abnormalities in pericytes on blood vessels and endothelial sprouts in tumors. *Am. J. Pathol.* 160, 985–1000. doi: 10.1016/S0002-9440(10)64920-6

Mu, C. F., Balakrishnan, P., Cui, F. D., Yin, Y. M., Lee, Y. B., Choi, H. G., et al. (2010). The effects of mixed MPEG–PLA/Pluronic® copolymer micelles on the bioavailability and multidrug resistance of docetaxel. *Biomaterials* 31, 2371–2379. doi: 10.1016/j.biomaterials.2009.11.102

Muntimadugu, E., Kommineni, N., and Khan, W. (2017). Exploring the potential of nanotherapeutics in targeting tumor microenvironment for cancer therapy. *Pharmacol. Res.* 126, 109–122. doi: 10.1016/j.phrs.2017.05.010

Muz, B., de la Puente, P., Azab, F., and Azab, A. K. (2015). The role of hypoxia in cancer progression, angiogenesis, metastasis, and resistance to therapy. *Hypoxia* 3, 83–92. doi: 10.2147/HP.S93413

Naito, M., Ishii, T., Matsumoto, A., Miyata, K., Miyahara, Y., and Kataoka, K. (2012). A phenylboronate-functionalized polyion complex micelle for ATP-triggered release of siRNA. *Angew. Chem. Int. Ed*. 51, 10751–10755.doi: 10.1002/anie.201203360

Nakamura, Y., Mochida, A., Choyke, P. L., and Kobayashi, H. (2016). Nanodrug delivery: is the enhanced permeability and retention effect sufficient for curing cancer? *Bioconjugate Chem.* 27, 2225–2238. doi: 10.1021/acs.bioconjchem.6b00437

Needham, D., Park, J. Y., Wright, A. M., and Tong, J. (2013). Materials characterization of the low temperature sensitive liposome (LTSL): effects of the lipid composition (lysolipid and DSPE–PEG2000) on the thermal transition and release of doxorubicin. *Faraday Discuss*. 161, 515–534. doi: 10.1039/C2FD20111A

Ngambenjawong, C., Gustafson, H. H., and Pun, S. H. (2017). Progress in tumor-associated macrophage (TAM)-targeted therapeutics. *Adv. Drug Deliv. Rev*. 114, 206–221. doi: 10.1016/j.addr.2017.04.010

Nguyen, T. V., Sleiman, M., Moriarty, T., Herrick, W. G., and Peyton, S. R. (2014). "Extracellular matrix stiffness protects carcinoma cells from sorafenib via JNK signaling," in *Bioengineering Conference (NEBEC), 2014 40th Annual Northeast.* IEEE, 1-2.

Nichols, J. W., and Bae, Y. H. (2014). EPR: Evidence and fallacy. *J. Control. Release* 190, 451–464. doi: 10.1016/j.jconrel.2014.03.057

Northcott, J. M., Dean, I. S., Mouw, J. K., and Weaver, V. M. (2018). Feeling stress: the mechanics of cancer progression and aggression. *Front. Cell Dev. Biol.* 6:17. doi: 10.3389/fcell.2018.00017

Omidi, Y., and Barar, J. (2014). Targeting tumor microenvironment: crossing tumor interstitial fluid by multifunctional nanomedicines. *BioImpacts* 4, 55–67. doi: 10.5681/bi.2014.021

Ouahab, A., Cheraga, N., Onoja, V., Shen, Y., and Tu, J. (2014). Novel pH-sensitive charge-reversal cell penetrating peptide conjugated PEG-PLA micelles for docetaxel delivery: *in vitro* study. *Int. J. Pharm.* 466, 233–245. doi: 10.1016/j.ijpharm.2014.03.009

Overchuk, M., and Zheng, G. (2017). Overcoming obstacles in the tumor microenvironment: recent advancements in nanoparticle delivery for cancer theranostics. *Biomaterials* 156, 217–237. doi: 10.1016/j.biomaterials.2017.10.024

Özbek, S., Balasubramanian, P. G., Chiquet-Ehrismann, R., Tucker, R. P., and Adams, J. C. (2010). The evolution of extracellular matrix. *Mol. Biol. Cell.* 21, 4300–4305. doi: 10.1091/mbc.E10-03-0251

Ozcelikkale, A., Ghosh, S., and Han, B. (2013). Multifaceted transport characteristics of nanomedicine: needs for characterization in dynamic environment. *Mol. Pharm.* 10, 2111–2126. doi: 10.1021/mp3005947

Paiva, A. E., Lousado, L., Guerra, D. A., Azevedo, P. O., Sena, I. F., Andreotti, J. P., et al. (2018). Pericytes in the premetastatic niche. *Cancer Res.* 78, 1–8. doi: 10.1158/0008-5472.CAN-17-3883

Pankova, D., Chen, Y., Terajima, M., Schliekelman, M. J., Baird, B. N., Fahrenholtz, M., et al. (2016). Cancer-associated fibroblasts induce a collagen cross-link switch in tumor stroma. *Mol. Cancer Res.* 14, 287–295. doi: 10.1158/1541-7786.MCR-15-0307

Park, S. M., Cha, J. M., Nam, J., Kim, M. S., Park, S. J., Park, E. S., et al. (2014). Formulation optimization and in vivo proof-of-concept study of thermosensitive liposomes balanced by phospholipid, elastin-like polypeptide, and cholesterol. *PLoS ONE* 9:103116. doi: 10.1371/journal.pone.0103116

Patel, A., and Sant, S. (2016). Hypoxic tumor microenvironment: Opportunities to develop targeted therapies. *Biotechnol. Adv.* 34, 803–812. doi: 10.1016/j.biotechadv.2016.04.005

Peng, Z., Wang, C., Fang, E., Lu, X., Wang, G., and Tong, Q. (2014). Co-delivery of doxorubicin and SATB1 shRNA by thermosensitive magnetic cationic liposomes for gastric cancer therapy. *PLoS ONE* 9:e92924.doi: 10.1371/journal.pone.0092924

Perche, F., Biswas, S., Wang, T., Zhu, L., and Torchilin, V. P. (2014). Hypoxia-Targeted siRNA Delivery. *Angew. Chem. Int. Ed. Engl.* 126, 3430–3434. doi: 10.1002/anie.201308368

Pirentis, A. P., Polydorou, C., Papageorgis, P., Voutouri, C., Mpekris, F., and Stylianopoulos, T. (2015). Remodeling of extracellular matrix due to solid stress accumulation during tumor growth. *Connect. Tissue Res.* 56, 345–354. doi: 10.3109/03008207.2015.1047929

Primeau, A. J., Rendon, A., Hedley, D., Lilge, L., and Tannock, I. F. (2005). The distribution of the anticancer drug Doxorubicin in relation to blood vessels in solid tumors. *Clin. Can. Res.* 11, 8782–8788. doi: 10.1158/1078-0432.CCR-05-1664

Qin, L., Wang, C. Z., Fan, H. J., Zhang, C. J., Zhang, H. W., Lv, M. H., et al. (2014). A dual-targeting liposome conjugated with transferrin and arginine-glycine-aspartic acid peptide for glioma-targeting therapy. *Oncol. Lett.* 8, 2000–2006. doi: 10.3892/ol.2014.2449

Quail, D. F., and Joyce, J. A. (2017). Molecular pathways: deciphering mechanisms of resistance to macrophage-targeted therapies. *Clin. Cancer Res.* 23, 876–884. doi: 10.1158/1078-0432.CCR-16-0133

Raavé, R., van Kuppevelt, T. H., and Daamen, W. F. (2018). Chemotherapeutic drug delivery by tumoral extracellular matrix targeting. *J. Control. Release* 274, 1–8. doi: 10.1016/j.jconrel.2018.01.029

Rankin, E. B., and Giaccia, A. J. (2016). Hypoxic control of metastasis. *Science* 352, 175–180. doi: 10.1126/science.aaf4405

Raza, A., Franklin, M. J., and Dudek, A. Z. (2010). Pericytes and vessel maturation during tumor angiogenesis and metastasis. *Am. J. Hematol.* 85, 593–598. doi: 10.1002/ajh.21745

Reddy, K., Zhou, Z., Jia, S. F., Lee, T. H., Morales-Arias, J., Cao, Y., et al. (2008). SDF-1 stimulates vasculogenesis and enhances Ewing's sarcoma tumor growth in the absence of VEGF. *Int. J. Cancer* 123, 831–837. doi: 10.1002/ijc.23582

Reid, S. E., Kay, E. J., Neilson, L. J., Henze, A., Serneels, J., McGhee, E. J., et al. (2017). Tumor matrix stiffness promotes metastatic cancer cell interaction with the endothelium. *The EMBO J.* 36, 2373–2389. doi: 10.15252/embj.201694912

Riaz, M. K., Riaz, M. A., Zhang, X., Lin, C., Wong, K. H., Chen, X., et al. (2018). Surface functionalization and targeting strategies of liposomes in solid tumor therapy: a review. *Int. J. Mol. Sci.* 19:195. doi: 10.3390/ijms19010195

Ribatti, D., and Djonov, V. (2012). Intussusceptive microvascular growth in tumors. *Cancer Lett.* 316, 126–131. doi: 10.1016/j.canlet.2011.10.040

Ribeiro, A. L., and Okamoto, O. K. (2015). Combined effects of pericytes in the tumor microenvironment. *Stem Cells. Int.* 2015:868475. doi: 10.1155/2015/868475

Roy, D., Cambre, J. N., and Sumerlin, B. S. (2010). Future perspectives and recent advances in stimuli-responsive materials. *Prog. Polym. Sci.* 35, 278–301. doi: 10.1016/j.progpolymsci.2009.10.008

Ruan, S., Cao, X., Cun, X., Hu, G., Zhou, Y., Zhang, Y., et al. (2015). Matrix metalloproteinase-sensitive size-shrinkable nanoparticles for deep tumor penetration and pH triggered doxorubicin release. *Biomaterials* 60, 100–110. doi: 10.1016/j.biomaterials.2015.05.006

Ruan, S., Hu, C., Tang, X., Cun, X., Xiao, W., Shi, K., et al. (2016). Increased gold nanoparticle retention in brain tumors by *in situ* enzyme-induced aggregation. *ACS Nano* 10, 10086–10098. doi: 10.1021/acsnano.6b05070

Ruan, S., Xiao, W., Hu, C., Zhang, H., Rao, J., Wang, S., et al. (2017). Ligand-mediated and enzyme-directed precise targeting and retention for the enhanced treatment of glioblastoma. *ACS Appl. Mat. Interfaces* 9, 20348–20360. doi: 10.1021/acsami.7b02303

Scallan, J., Huxley, V. H., and Korthuis, R. J. (2010). "Capillary fluid exchange: regulation, functions, and pathology," in *Colloquium Lectures on Integrated Systems Physiology-\nl\hspace* 18pt From Molecules to Function Vol. 2* (San Rafael, CA: Morgan and Claypool Publishers), 1–94.

Schlossbauer, A., Kecht, J., and Bein, T. (2009). Biotin-avidin as a protease responsive cap system for colloidal mesoporous silica. *Angew. Chem. Int. Ed. Engl.* 121, 3138–3141. doi: 10.1002/anie.200805818

Sena, I. F., Paiva, A. E., Prazeres, P. H., Azevedo, P. O., Lousado, L., Bhutia, S. K., et al. (2018). Glioblastoma-activated pericytes support tumor growth via immunosuppression. *Cancer. Med.* 7, 1232–1239. doi: 10.1002/cam4.1375

Shein, S. A., Kuznetsov, I. I., Abakumova, T. O., Chelushkin, P. S., Melnikov, P. A., Korchagina, A. A., et al. (2016). VEGF-and VEGFR2-targeted liposomes for cisplatin delivery to glioma cells. *Mol. Pharm.* 13, 3712–3723. doi: 10.1021/acs.molpharmaceut.6b00519

Shen, J., Sun, H., Xu, P., Yin, Q., Zhang, Z., Wang, S., et al. (2013). Simultaneous inhibition of metastasis and growth of breast cancer by co-delivery of twist shRNA and paclitaxel using pluronic P85-PEI/TPGS complex nanoparticles. *Biomaterials* 34, 1581–1590. doi: 10.1016/j.biomaterials.2012.10.057

Shen, Y., Quan, J., Wang, M., Li, S., Yang, J., Lv, M., et al. (2017). Tumor vasculogenic mimicry formation as an unfavorable prognostic indicator in patients with breast cancer. *Oncotarget* 8, 56408–56416. doi: 10.18632/oncotarget.16919

Shete, H. K., Selkar, N., Vanage, G. R., and Patravale, V. B. (2014). Tamoxifen nanostructured lipid carriers: enhanced *in vivo* antitumor efficacy with reduced adverse drug effects. *Int. J. Pharm.* 468, 1–14. doi: 10.1016/j.ijpharm.2014.03.056

Shi, C., Guo, X., Qu, Q., Tang, Z., Wang, Y., and Zhou, S. (2014). Actively targeted delivery of anticancer drug to tumor cells by redox-responsive star-shaped micelles. *Biomaterials*. 35, 8711–8722. doi: 10.1016/j.biomaterials.2014.06.036

Shi, J., Kantoff, P. W., Wooster, R., and Farokhzad, O. C. (2017). Cancer nanomedicine: progress, challenges and opportunities. *Nat. Rev. Cancer* 17:20. doi: 10.1038/nrc.2016.108

Siemann, D. W., and Horsman, M. R. (2015). Modulation of the tumor vasculature and oxygenation to improve therapy. *Pharmacol. Ther.* 153, 107–124. doi: 10.1016/j.pharmthera.2015.06.006

Simonsen, T. G., Gaustad, J. V., Leinaas, M. N., and Rofstad, E. K. (2012). High interstitial fluid pressure is associated with tumor-line specific vascular abnormalities in human melanoma Xenografts. *PLoS ONE* 7:e40006. doi: 10.1371/journal.pone.0040006

Singh, R. P., Sharma, G., Kumari, L., Koch, B., Singh, S., Bharti, S., et al. (2016). RGD-TPGS decorated theranostic liposomes for brain targeted delivery. *Colloids Surf. B Biointerfaces*. 147, 129–141. doi: 10.1016/j.colsurfb.2016.07.058

Stapleton, S., Milosevic, M., Tannock, I. F., Allen, C., and Jaffray, D. A. (2015). The intra-tumoral relationship between microcirculation, interstitial fluid pressure and liposome accumulation. *J. Control. Rel.* 211, 163–170. doi: 10.1016/j.jconrel.2015.06.008

Stapor, P. C., Sweat, R. S., Dashti, D. C., Betancourt, A. M., and Murfee, W. L. (2014). Pericyte dynamics during angiogenesis: new insights from new identities. *J. Vasc. Res.* 51, 163–174. doi: 10.1159/000362276

Stiti, M., Cecchi, A., Rami, M., Abdaoui, M., Barragan-Montero, V., Scozzafava, A., et al. (2008). Carbonic anhydrase inhibitor coated gold nanoparticles selectively inhibit the tumor-associated isoform IX over the cytosolic isozymes I and II. *J. Am. Chem. Soc.* 130, 16130–16131. doi: 10.1021/ja805558k

Stylianopoulos, T. (2017). The solid mechanics of cancer and strategies for improved therapy. *J. Biomech. Eng.* 139:021004. doi: 10.1115/1.4034991

Stylianopoulos, T., and Jain, R. K. (2013). Combining two strategies to improve perfusion and drug delivery in solid tumors. *PNAS.* 110, 18632–18637. doi: 10.1073/pnas.1318415110

Stylianopoulos, T., Martin, J. D., Chauhan, V. P., Jain, S. R., Diop-Frimpong, B., Bardeesy, N., et al. (2012). Causes, consequences, and remedies for growth-induced solid stress in murine and human tumors. *PNAS.* 109, 15101–15108. doi: 10.1073/pnas.1213353109

Stylianopoulos, T., Munn, L. L., and Jain, R. K. (2018). Reengineering the physical microenvironment of tumors to improve drug delivery and efficacy: from mathematical modeling to bench to bedside. *Trends Cancer* 4, 292–319. doi: 10.1016/j.trecan.2018.02.005

Sun, C. Y., Shen, S., Xu, C. F., Li, H. J., Liu, Y., Cao, Z. T., et al. (2015). Tumor acidity-sensitive polymeric vector for active targeted siRNA delivery. *J. Am. Chem. Soc.* 137, 15217–15224.doi: 10.1021/jacs.5b09602

Sun, Q., Sun, X., Ma, X., Zhou, Z., Jin, E., Zhang, B., et al. (2014). Integration of nanoassembly functions for an effective delivery cascade for cancer drugs. *Adv. Mater.* 26, 7615–7621. doi: 10.1002/adma.201401554

Sun, Y., Yan, X., Yuan, T., Liang, J., Fan, Y., Gu, Z., et al. (2010). Disassemblable micelles based on reduction-degradable amphiphilic graft copolymers for intracellular delivery of doxorubicin. *Biomaterials* 31, 7124–7131. doi: 10.1016/j.biomaterials.2010.06.011

Takacova, M., Hlouskova, G., Zatovicova, M., Benej, M., Sedlakova, O., Kopacek, J., et al. (2016). Encapsulation of anti-carbonic anhydrase IX antibody in hydrogel microspheres for tumor targeting. *J. Enzyme Inhib. Med. Chem.* 31, 110–118. doi: 10.1080/14756366.2016.1177523

Tao, L., Huang, G., Song, H., Chen, Y., and Chen, L. (2017). Cancer associated fibroblasts: An essential role in the tumor microenvironment. *Oncol. Lett.* 14, 2611–2620. doi: 10.3892/ol.2017.6497

Tao, W., Ji, X., Xu, X., Ariful Islam, M., Li, Z., Chen, S., et al. (2017). Antimony Quantum Dots: Synthesis and Application as Near-Infrared Photothermal Agents for Effective Cancer Therapy. *Angew. Chem. Int. Ed. Engl.* 56, 11896–11900. doi: 10.1002/anie.201703657

Thambi, T., Deepagan, V. G., Yoon, H. Y., Han, H. S., Kim, S. H., Son, S., et al. (2014). Hypoxia-responsive polymeric nanoparticles for tumor-targeted drug delivery. *Biomaterials* 35, 1735–1743. doi: 10.1016/j.biomaterials.2013.11.022

Tian, L., and Bae, Y. H. (2012). Cancer nanomedicines targeting tumor extracellular pH. *Colloids. Surf. B Biointerfaces* 99, 116–126. doi: 10.1016/j.colsurfb.2011.10.039

Torosean, S., Flynn, B., Axelsson, J., Gunn, J., Samkoe, K. S., Hasan, T., et al. (2013). Nanoparticle uptake in tumors is mediated by the interplay of vascular and collagendensity with interstitial pressure. *Nanomedicine* 9, 151–158. doi: 10.1016/j.nano.2012.07.002

Toy, R., Peiris, P. M., Ghaghada, K. B., and Karathanasis, E. (2014). Shaping cancer nanomedicine: the effect of particle shape on the *in vivo* journey of nanoparticles. *Nanomedicine* 9, 121–134. doi: 10.2217/nnm.13.191

Truong, N. P., Whittaker, M. R., Mak, C. W., and Davis, T. P. (2015). The importance of nanoparticle shape in cancer drug delivery. *Expert Opin. Drug Deliv.* 12, 129–142. doi: 10.1517/17425247.2014.950564

Valkenburg, K. C., de Groot, A. E., and Pienta, K. J. (2018). Targeting the tumour stroma to improve cancer therapy. *Nat. Rev. Clin. Oncol.* 15, 366–381. doi: 10.1038/s41571-018-0007-1

Wagner, M., and Wiig, H. (2015). Tumor interstitial fluid formation, characterization, and clinical implications. *Front. Oncol.* 5:115. doi: 10.3389/fonc.2015.00115

Waite, C. L., and Roth, C. M. (2012). Nanoscale drug delivery systems for enhanced drug penetration into solid tumors: current progress and opportunities. *Crit. Rev. Biomed. Eng.* 40, 21–41.

Wan, L., Jiao, J., Cui, Y., Guo, J., Han, N., Di, D., et al. (2016). Hyaluronic acid modified mesoporous carbon nanoparticles for targeted drug delivery to CD44-overexpressing cancer cells. *Nanotechnology* 27:135102. doi: 10.1088/0957-4484/27/13/135102

Wang, H., Zhao, X., Guo, C., Ren, D., Zhao, Y., Xiao, W., et al. (2015). Aptamer-dendrimer bioconjugates for targeted delivery of miR-34a expressing plasmid and antitumor effects in non-small cell lung cancer cells. *PLoS ONE* 10:e0139136. doi: 10.1371/journal.pone.0139136

Wang, X., Li, H., Liu, X., Tian, Y., Guo, H., Jiang, T., et al. (2017). Enhanced photothermal therapy of biomimetic polypyrrole nanoparticles through improving blood flow perfusion. *Biomaterials* 143, 130–141. doi: 10.1016/j.biomaterials.2017.08.004

Welén, K., Jennbacken, K., Tesan, T., and Damber, J. E. (2008). Pericyte coverage decreases invasion of tumour cells into blood vessels in prostate cancer xenografts. *Prostate. Cancer. Prostatic. Dis.* 12, 41–46. doi: 10.1038/pcan.2008.33

Welti, J., Loges, S., Dimmeler, S., and Carmeliet, P. (2013). Recent molecular discoveries in angiogenesis and antiangiogenic therapies in cancer. *J. Clin. Invest.* 123, 3190–3200. doi: 10.1172/JCI70212

Wiig, H., and Swartz, M. A. (2012). Interstitial fluid and lymph formation and transport: physiological regulation and roles in inflammation and cancer. *Physiol. Rev.* 92, 1005–1060. doi: 10.1152/physrev.00037.2011

Wong, C., Stylianopoulos, T., Cui, J., Martin, J., Chauhan, V. P., Jiang, W., et al. (2011). Multistage nanoparticle delivery system for deep penetration into tumor tissue. *Proc. Natl. Acad. Sci. U.S.A.* 108, 2426–2431. doi: 10.1073/pnas.1018382108

Wu, J., Zhang, J., Deng, C., Meng, F., Cheng, R., and Zhong, Z. (2017). Robust, Responsive, and targeted PLGA anticancer nanomedicines by combination of reductively cleavable surfactant and covalent hyaluronic acid coating. *ACS Appl. Mater. Interfaces.* 9, 3985–3994. doi: 10.1021/acsami.6b15105

Wu, L., Zhang, L., Shi, G., and Ni, C. (2016). Zwitterionic pH/redox nanoparticles based on dextran as drug carriers for enhancing tumor intercellular uptake of doxorubicin. *Mater. Sci. Eng. Biol. Appl. C.* 61, 278–285. doi: 10.1016/j.msec.2015.12.025.

Wu, M., Frieboes, H. B., McDougall, S. R., Chaplain, M. A. J., Cristini, V., and Lowengrub, J. (2013). The effect of interstitial pressure on tumor growth: coupling with the blood and lymphatic vascular systems. *J. Theor. Biol.* 320, 131–151. doi: 10.1016/j.jtbi.2012.11.031

Wu, M., Meng, Q., Chen, Y., Zhang, L., Li, M., Cai, X., et al. (2016). Large pore-sized hollow mesoporous organosilica for redox-responsive gene delivery and synergistic cancer chemotherapy. *Adv. Mater.* 28, 1963–1969. doi: 10.1002/adma.201505524

Xian, X., Håkansson, J., Ståhlberg, A., Lindblom, P., Betsholtz, C., Gerhardt, H., et al. (2006). Pericytes limit tumor cell metastasis. *J. Clin. Invest.* 116, 642–651. doi: 10.1172/JCI25705

Xiao, W., Ruan, S., Yu, W., Wang, R., Hu, C., Liu, R., et al. (2017). Normalizing tumor vessels to increase the enzyme-induced retention and targeting of gold nanoparticle for breast cancer imaging and treatment. *Mol. Pharm.* 14, 3489–3498. doi: 10.1021/acs.molpharmaceut.7b00475

Xie, X., Liao, J., Shao, X., Li, Q., and Lin, Y. (2017). The effect of shape on cellular uptake of gold nanoparticles in the forms of stars, rods, and triangles. *Sci. Rep.* 7:3827. doi: 10.1038/s41598-017-04229-z

Xiong, G. F., and Xu, R. (2016). Function of cancer cell-derived extracellular matrix in tumor progression. *J. Cancer Metastasis Treat.* 2, 357–364. doi: 10.20517/2394-4722.2016.08

Xu, C. F., Zhang, H. B., Sun, C. Y., Liu, Y., Shen, S., Yang, X. Z., et al. (2016). Tumor acidity-sensitive linkage-bridged block copolymer for therapeutic siRNA delivery. *Biomaterials* 88, 48–59. doi: 10.1016/j.biomaterials.2016.02.031

Xu, P., Meng, Q., Sun, H., Yin, Q., Yu, H., Zhang, Z., et al. (2015). Shrapnel nanoparticles loading docetaxel inhibit metastasis and growth of breast cancer. *Biomaterials* 64, 10–20. doi: 10.1016/j.biomaterials.2015.06.017

Xu, X., Wu, J., Liu, Y., Yu, M., Zhao, L., Zhu, X., et al. (2016). Ultra-pH-responsive and tumor-penetrating nanoplatform for targeted siRNA delivery with robust anti-cancer efficacy. *Angew. Chem. Int. Ed. Engl.* 55, 7091–7094. doi: 10.1002/anie.201601273

Yamada, R., Kostova, M. B., Anchoori, R. K., Xu, S., Neamati, N., and Khan, S. (2010). Biological evaluation of paclitaxel-peptide conjugates as a model for MMP2-targeted drug delivery. *Cancer Biol. Ther*. 9, 192–203. doi: 10.4161/cbt.9.3.10656

Yan, L., Crayton, S. H., Thawani, J. P., Amirshaghaghi, A., Tsourkas, A., and Cheng, Z. (2015). A pH-responsive drug-delivery platform based on glycol chitosan–coated liposomes. *Small* 11, 4870–4874. doi: 10.1002/smll.201501412

Yang, Y., Yang, Y., Xie, X., Xu, X., Xia, X., Wang, H., et al. (2016). Dual stimulus of hyperthermia and intracellular redox environment triggered release of siRNA for tumor-specific therapy. *Int. J. Pharm*. 506, 158–173. doi: 10.1016/j.ijpharm.2016.04.035

Yang, Z. Z., Li, J. Q., Wang, Z. Z., Dong, D. W., and Qi, X. R. (2014). Tumor-targeting dual peptides-modified cationic liposomes for delivery of siRNA and docetaxel to gliomas. *Biomaterials* 35, 5226–5239. doi: 10.1016/j.biomaterials.2014.03.017

Yao, X., Qian, C. N., Zhang, Z. F., Tan, M. H., Kort, E. J., Yang, X. J., et al. (2007). Two distinct types of blood vessels in clear cell renal cell carcinoma have contrasting prognostic implications. *Clin. Cancer Res.* 13, 161–169. doi: 10.1158/1078-0432.CCR-06-0774

Yasui, H., Matsumoto, S., Devasahayam, N., Munasinghe, J. P., Choudhuri, R., Saito, K., et al. (2010). Low field magnetic resonance imaging to visualize chronic and cycling hypoxia in tumor-bearing mice. *Cancer Res.* 70, 6427–6436. doi: 10.1158/0008-5472.CAN-10-1350

Yim, H., Park, S. J., Bae, Y. H., and Na, K. (2013). Biodegradable cationic nanoparticles loaded with an anticancer drug for deep penetration of heterogeneous tumours. *Biomaterials* 34, 7674–7682. doi: 10.1016/j.biomaterials.2013.06.058

Yin, X., Feng, S., Chi, Y., Liu, J., Sun, K., Guo, C., et al. (2018). Estrogen-functionalized liposomes grafted with glutathione-responsive sheddablechotooligosaccharides for the therapy of osteosarcoma. *Drug Deliv*. 25, 900–908. doi: 10.1080/10717544.2018.1458920

Yoshizaki, Y., Yuba, E., Komatsu, T., Udaka, K., Harada, A., and Kono, K. (2016). Improvement of peptide-based tumor immunotherapy using pH-sensitive fusogenic polymer-modified liposomes. *Molecules* 21: 1284. doi: 10.3390/molecules21101284

Yu, L., Liu, J., Wu, K., Klein, T., Jiang, Y., and Wang, J. P. (2014). Evaluation of hyperthermia of magnetic nanoparticles by dehydrating DNA. *Sci. Rep*. 4:7216. doi: 10.1038/srep07216

Yu, M., Jambhrunkar, S., Thorn, P., Chen, J., Gu, W., and Yu, C. (2013). Hyaluronic acid modified mesoporous silica nanoparticles for targeted drug delivery to CD44-overexpressing cancer cells. *Nanoscale* 5, 178–183. doi: 10.1039/c2nr32145a

Yu, T., Liu, K., Wu, Y., Fan, J., Chen, J., Li, C., et al. (2013). High interstitial fluid pressure promotes tumor cell proliferation and invasion in oral squamous cell carcinoma. *Int. J. Mol. Med.* 32, 1093–1100. doi: 10.3892/ijmm.2013.1496

Zan, M., Li, J., Luo, S., and Ge, Z. (2014). Dual pH-triggered multistage drug delivery systems based on host–guest interaction-associated polymeric nanogels. *Chem. Commun*. 50, 7824–7827. doi: 10.1039/c4cc03120b

Zang, X., Ding, H., Zhao, X., Li, X., Du, Z., Hu, H., et al. (2016). Anti-EphA10 antibody-conjugated pH-sensitive liposomes for specific intracellular delivery of siRNA. *Int. J. Nanomedicine* 11:3951. doi: 10.2147/IJN.S107952

Zhang, A., Qian, Y., Ye, Z., Chen, H., Xie, H., Zhou, L., et al. (2017). Cancer-associated fibroblasts promote M2 polarization of macrophages in pancreatic ductal adenocarcinoma. *Cancer Med.* 6, 463–470. doi: 10.1002/cam4.993

Zhang, B., Hu, Y., and Pang, Z. (2017a). Modulating the tumor microenvironment to enhance tumor nanomedicine delivery. *Front. Pharmacol.* 8:952. doi: 10.3389/fphar.2017.00952

Zhang, B., Jin, K., Jiang, T., Wang, L., Shen, S., Luo, Z., et al. (2017b). Celecoxib normalizes the tumor microenvironment and enhances small nanotherapeutics delivery to A549 tumors in nude mice. *Sci. Rep.* 7:10071. doi: 10.1038/s41598-017-09520-7

Zhang, L., Nishihara, H., and Kano, M. R. (2012). Pericyte-coverage of human tumor vasculature and nanoparticle permeability. *Biol. Pharm. Bull.* 35, 761–766. doi: 10.1248/bpb.35.761

Zhang, X., Liu, Y., Kim, Y. J., Mac, J., Zhuang, R., and Wang, P. (2017). Co-delivery of carboplatin and paclitaxel via cross-linked multilamellar liposomes for ovarian cancer treatment. *RSC Adv*. 7, 19685–19693. doi: 10.1039/c7ra01100h

Zhang, Y., and Xu, J. (2018). Mesoporous silica nanoparticle-based intelligent drug delivery system for bienzyme-responsive tumour targeting and controlled release. *R. Soc. Open Sci*. 5:70986. doi: 10.1098/rsos.170986

Zhang, Y., Zhai, M., Chen, Z., Han, X., Yu, F., Li, Z., et al. (2017). Dual-modified liposome codelivery of doxorubicin and vincristine improve targeting and therapeutic efficacy of glioma. *Drug Deliv*. 24, 1045–1055. doi: 10.1080/10717544.2017.1344334

Zhao, G., Long, L., Zhang, L., Peng, M., Cui, T., Wen, X., et al. (2017). Smart pH-sensitive nanoassemblies with cleavable PEGylation for tumor targeted drug delivery. *Sci. Rep*. 7:3383. doi: 10.1038/s41598-017-03111-2

Zhao, Y., Ren, W., Zhong, T., Zhang, S., Huang, D., Guo, Y., et al. (2016). Tumor-specific pH-responsive peptide-modified pH-sensitive liposomes containing doxorubicin for enhancing glioma targeting and anti-tumor activity. *J. Control. Release*. 222, 56–66. doi: 10.1016/j.jconrel.2015.12.006

Zheng, T., Wang, A., Hu, D., and Wang, Y. (2017). Tumor-targeting templated silica nanoparticles as a dual-drug delivery system for anti-angiogenic ovarian cancer therapy. *Exp. Ther. Med*. 14, 2162–2170. doi: 10.3892/etm.2017.4777

Zheng, X., Turkowski, K., Mora, J., Brüne, B., Seeger, W., Weigert, A., et al. (2017). Redirecting tumor-associated macrophages to become tumoricidal effectors as a novel strategy for cancer therapy. *Oncotarget* 8, 48436–48452. doi: 10.18632/oncotarget.17061

Zhong, Y., Wang, C., Cheng, L., Meng, F., Zhong, Z., and Liu, Z. (2013). Gold nanorod-cored biodegradable micelles as a robust and remotely controllable doxorubicin release system for potent inhibition of drug-sensitive and-resistant cancer cells. *Biomacromolecules* 14, 2411–2419. doi: 10.1021/bm400530d

Zhong, Y., Wang, C., Cheng, R., Cheng, L., Meng, F., Liu, Z., et al. (2014). cRGD-directed, NIR-responsive and robust AuNR/PEG–PCL hybrid nanoparticles for targeted chemotherapy of glioblastoma *in vivo*. *J. Control. Release* 195, 63–71. doi: 10.1016/j.jconrel.2014.07.054

Zhou, Z., Ma, X., Jin, E., Tang, J., Sui, M., Shen, Y., et al. (2013). Linear-dendritic drug conjugates forming long-circulating nanorods for cancer-drug delivery. *Biomaterials* 34, 5722–5735. doi: 10.1016/j.biomaterials.2013.04.012

Zhu, H., Dong, C., Dong, H., Ren, T., Wen, X., Su, J., et al. (2014). Cleavable PEGylation and hydrophobic histidylation of polylysine for siRNA delivery and tumor gene therapy. *ACS Appl. Mater. Interfaces* 6, 10393–10407. doi: 10.1021/am501928p

Zhuang, J., Lu, Q., Shen, B., Huang, X., Shen, L., Zheng, X., et al. (2015). TGFβ1 secreted by cancer-associated fibroblasts induces epithelial-mesenchymal transition of bladder cancer cells through lncRNA-ZEB2NAT. *Sci. Rep.* 5:11924. doi: 10.1038/srep11924

Zugazagoitia, J., Guedes, C., Ponce, S., Ferrer, I., Molina-Pinelo, S., and Paz-Ares, L. (2016). Current challenges in cancer treatment. *Clin. Ther.* 38, 1551–1566. doi: 10.1016/j.clinthera.2016.03.026

Conflict of Interest Statement: The authors declare that the research was conducted in the absence of any commercial or financial relationships that could be construed as a potential conflict of interest.

frontiers in Pharmacology

REVIEW
published: 09 July 2018
doi: 10.3389/fphar.2018.00745

Potential Applications of Nanotechnology in Urological Cancer

Ming-Hui He[1], Li Chen[1], Ting Zheng[1], Yu Tu[1], Qian He[1], Hua-Lin Fu[1], Ju-Chun Lin[1], Wei Zhang[1], Gang Shu[1], Lili He[2] and Zhi-Xiang Yuan[1]**

[1] Department of Pharmacy, College of Veterinary Medicine, Sichuan Agricultural University, Chengdu, China, [2] College of Pharmacy, Southwest Minzu University, Chengdu, China

Nowadays, the potential scope of nanotechnology in uro-oncology (cancers of the prostate, bladder, and kidney) is broad, ranging from drug delivery, prevention, and diagnosis to treatment. Novel drug delivery methods using magnetic nanoparticles, gold nanoparticles, and polymeric nanoparticles have been investigated in prostate cancer. Additionally, renal cancer treatment may be profoundly influenced by applications of nanotechnology principles. Various nanoparticle-based strategies for kidney cancer therapy have been proposed. Partly due to the dilution of drug concentrations by urine production, causing inadequate drug delivery to tumor cells in the treatment of bladder cancer, various multifunctional bladder-targeted nanoparticles have been developed to enhance therapeutic efficiency. In each of these cancer research fields, nanotechnology has shown several advantages over widely used traditional methods. Different types of nanoparticles improve the solubility of poorly soluble drugs, and multifunctional nanoparticles have good specificity toward prostate, renal, and bladder cancer. Moreover, nanotechnology can also combine with other novel technologies to further enhance effectivity. As our understanding of nanotechnologies grows, additional opportunities to improve the diagnosis and treatment of urological cancer are excepted to arise. In this review, we focus on nanotechnologies with potential applications in urological cancer therapy and highlight clinical areas that would benefit from nanoparticle therapy.

Keywords: nanotechnology, urological cancer, nanoparticles, diagnosis, therapy

OPEN ACCESS

Edited by:
Qingxin Mu,
University of Washington,
United States

Reviewed by:
Gaoxing Su,
Nantong University, China
Weikuan Gu,
University of Tennessee Health Science Center, United States

****Correspondence:***
Lili He
lilihes@163.com
Zhi-Xiang Yuan
zhixiang-yuan@hotmail.com

Specialty section:
This article was submitted to Cancer Molecular Targets and Therapeutics, a section of the journal Frontiers in Pharmacology

Received: *28 April 2018*
Accepted: *19 June 2018*
Published: *09 July 2018*

Citation:
He M-H, Chen L, Zheng T, Tu Y, He Q, Fu H-L, Lin J-C, Zhang W, Shu G, He L and Yuan Z-X (2018) Potential Applications of Nanotechnology in Urological Cancer. Front. Pharmacol. 9:745. doi: 10.3389/fphar.2018.00745

INTRODUCTION

Urological cancers, which include cancers of the prostate, kidneys, and bladder, are an international public health problem. Minimally invasive surgical approaches are now the most common treatments for urological malignancies, although open radical nephrectomy was the most common treatment for non-metastasized lesions in the 1980s. Most prostate cancers, regardless of tumor size, are treated by laparoscopic nephrectomy (Rassweiler et al., 2013). In contrast, bladder cancer (BCa) is treated with different approaches depending on the stage of the cancer. Transurethral resection of bladder tumors (TUR-BT) is the first strategy for curing non-invasive bladder tumors, and Bacillus Cal-mette-Guérin (BCG) and chemotherapeutic agents are also widely used (Chen et al., 2015a). Many novel techniques for use in urological cancer have been developed in the past decade. For example, focal ablation using cryotherapy or radiofrequency (RF) is becoming more popular for small renal masses (Park et al., 2006; Lusch et al., 2013), and new methods,

such as real-time peripheral temperature monitoring, are involved in establishing the efficacy of RF ablation (Leveillee et al., 2013). Similarly, in the treatment of prostate tumors, high-intensity focused ultrasound, a minimally invasive therapy, can be accurately targeted to a portion of the prostate gland and has been widely used for the treatment of prostate cancer (Crouzet et al., 2014). However, these traditional surgical therapies sometimes lack accuracy and have a high risk of complications, including tumor relapse (Kondylis et al., 2000). Moreover, the use of chemical agents may cause negative side effects in normal cells and could be associated with relapse.

Imaging of tumors can facilitate early diagnosis and influence patients' treatment decisions. Computed tomography (CT), Positron emission tomography (PET), and magnetic resonance imaging (MRI) are traditionally used for detection of non-invasive malignancies. However, these traditional approaches have limited sensitivity and ability to provide specific and functional information on the disease (Wang et al., 2008).

Nanoparticles (NPs, size in nanometer range) are novel materials used that were initially used for invention of the scanning probe microscopy and the discovery of molecular structures (Menter et al., 2014). Different manufacturing methods and materials have enabled the production of NPs with various shapes and sizes. One nanometer (10^{-9} m) is the scale at which most biological molecules operate inside living cells; thus, NPs may have many applications in the field of medicine. NPs can accumulate in tumor tissues via the enhanced permeability and retention (EPR) effect; under certain circumstances, typically for tumors, the endothelial lining of the blood vessel wall becomes more permeable than in the normal state, allowing NPs to enter tumors (Ojha et al., 2017). NPs can be used for encapsulation of poorly soluble drugs, protection of therapeutic molecules, modification of their blood circulation and tissue distribution profiles, and facilitation of combination regimens commonly used in cancer therapy (Bertrand et al., 2014). Many types of NPs, including liposomes and other lipid-based carriers (such as lipid emulsions and lipid-drug complexes), polymer-drug conjugates, polymer microspheres, micelles, and various ligand-targeted products (such as immunoconjugates), are under various stages of development as drug delivery systems (Wang et al., 2008). Additionally, NPs play an important role in cancer diagnosis, and may have applications in the treatment of tumors (**Figure 1**). Contemporary cancer therapy, particularly with respect to drug delivery, has evolved from traditional methodology to new technology. Thus, nanotechnology-based

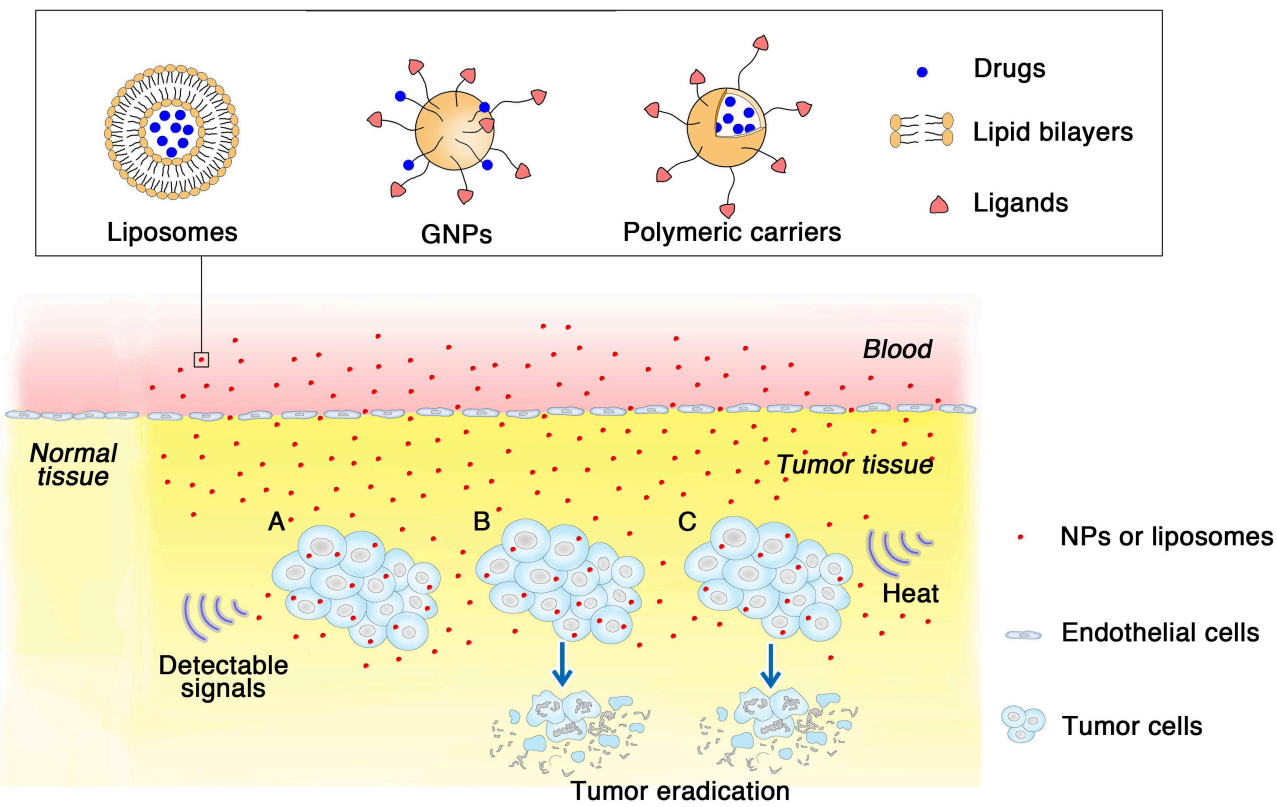

FIGURE 1 | How different kinds of NPs applied in urological cancer diagnosis and therapeutics. Three types of NPs are listed for examples, liposomes, GNPs and polymeric NPs. With specific ligands modified on the surface, NPs show specifia targeting to the tumor cells via EPR effect. **(A)** NPs as imaging agents gather around tumor tissues then send and amplify detectable signals which are received subsequently. **(B)** NPs loaded with cytotoxic drugs arrive at tumor tissue, and then lead to tumor eradication. **(C)** In hyperthermia therapy, NPs absorbing heat energy induce a high temperature, causing focal cell death and preserve the circumambient normal tissue.

combination drug delivery to tumor tissues has emerged as a potential effective strategy for cancer therapy.

Nanotechnology has shown several advantages over widely used traditional methods. Different types of NPs improve the solubility of poorly soluble drugs and multifunctional NPs have good specificity toward prostate, renal and bladder cancers. Moreover, nanotechnology can also combine with other upcoming technologies and enhance the effectivity. As our understanding of nanotechnologies grows, opportunities to improve the diagnosis and treatment methods for urological cancer have also increased. In this review, we focus on nanotechnologies with potential applications in prostate, renal, bladder, and other urologic cancer. In each of these fields, we discuss various NP-based strategies for diagnosis as well as treatment. In addition, we provide future perspectives to highlight the requirement for further studies.

NANOTECHNOLOGY IN PROSTATE CANCER

Prostate cancer is one of the leading causes of cancer-related deaths among men (Siegel et al., 2018). Chemotherapeutic agents, such as docetaxel and paclitaxel, which are widely used for the treatment of prostate cancer, are not selective to cancerous tissues and can cause injury to normal tissues, leading to a low therapeutic index and even increasing drug resistance. Consequently, novel approaches are urgently needed for the development of improved therapeutic options for the management of prostate cancer, particularly with regard to inhibition of the proliferation of precancerous and malignant lesions and/or to improvement of the effectiveness of conventional chemotherapeutic agents. NP technology is being widely used in prostate cancer, both in diagnostic and therapeutic fields, providing a promising strategy for drug delivery; such approaches with NP technology can make up for the lack of specificity of traditional therapy. Emerging NP technologies use for imaging and therapy in prostate cancer will be discussed in this section, with the aim of highlighting novel advances in NP technology for applications in prostate cancer.

Imaging in Prostate Cancer

Magnetic resonance imaging and CT are two of the most critical and widely used methods for disease staging and diagnosis. In both methods, magnetic NPs (MNPs) can provide an encouraging solution as precursors for targeted contrast agents. MNPs in the form of superparamagnetic iron oxides (SPIOs) and ultrasmall SPIOs (USPIOs) have already been applied in clinical trials, with several advantages, including long blood-retention time, biocompatibility, and minimal biotoxicity (Feldman et al., 2008; Sun et al., 2008). Huang colleagues formulated new cationic lipid NPs containing SPIOs (L-SPIOs) to solve the problem of low efficiency of direct loading into cells and the cytotoxicity of SPIOs. The study used PC3 prostate cancer cells to test the efficiency of cellular uptake of these L-SPIOs, and the results showed that these L-SPIOs, which exhibited high loading efficiency, low cytotoxicity, and long-term imaging signals, are versatile image probes for cell tracking (Huang et al., 2009). Other metallic materials are also being developed. For example, Ghasemian et al. (2015) recently showed the potential applications of cobalt zinc ferrite NPs (CZF-MNPs) as a T2 contrast agent. *In vitro*, dimercaptosuccinic acid (DMSA)-coated or uncoated CZF-MNPs were incubated with PC3 or DU145 prostate cancer cells for 2 h at room temperature. Using a T2-weighted MRI system, researchers found that both uncoated and coated NPs were imported in PC3 and DU145 cells, resulting in a dramatic signal intensity reduction. In addition, the enhanced intensity observed using CZF-MNPs was similar to that of an equal amount of DMSA-coated CZF-MNPs, indicating that these particles were both suitable for T2 contrast enhancement (Ghasemian et al., 2015).

Photoacoustic imaging (PAI) is an emerging non-invasive imaging modality that combines the spectral selectivity of molecular excitation by laser light with the high resolution of ultrasound imaging. Some types of NPs, particularly gold NPs (GNPs), are designed for high photoacoustic contrast based on surface plasmon resonance (SPR) to enhance absorption (Agarwal et al., 2007; Yang et al., 2009). In addition to its apparent clinical safety and tolerability due to its physical inertness, gold can be used to synthesize NPs with very precise sizes, shapes, and surface chemistries at the nanoscale using simple techniques and relatively inexpensive reagents (Daniel and Astruc, 2004). A study demonstrated that PAI based on a targeted gold nanorod contrast agent could provide a clear anatomical view with targeted tissue highlighted in a contrasting color in LNCaP prostate cancer cells (Agarwal et al., 2007). The gold nanorods could be also used for detection of other lesions. Currently, GNPs are being used in several clinical trials as radiopaque markers that can be implanted into patients with prostate cancer for image-guided therapy (Kliton et al., 2014; Jorgo et al., 2017). The results showed that implantation had no apparent side effects, such as fever or infection, and none of the patients required analgesics after implantation, suggesting that GNPs could be potential imaging agents for use in clinic applications.

Molecular targets of prostate cancer, including prostate-specific antigen (PSA), prostate-specific membrane antigen (PSMA), and prostate cancer lipid antigen, are products of prostate cells and are used as potential NP targets (Cheng et al., 2012; Sanna and Sechi, 2012). Normal PSA immunoassays are often not able to detect PSA in the serum after radical prostatectomy due to the low sensitivity of the assays. However, using an extremely sensitive nanotechnology-based tool known as the "bio-barcode" system, the sensitivity of immunoassays has increased by 300-fold compared with that of commercial immunoassays, and the results of clinical studies have also confirmed these findings. This ultrasensitive technology is based on GNP probes decorated with DNA and antibodies that can recognize and bind to PSA when presenting at extremely low levels in blood samples (Thaxton et al., 2009). GNPs have also shown great efficiency and robustness as probes for sensing ultralow levels of PSA in patient serum samples. The limit of detection of the probe for PSA reached 32 fg/mL, which is more than two orders of magnitude lower than that of the conventional fluorescence probe and even lower than that of the

GNP bio-barcode assay (330 fg/mL) (Liu et al., 2013). Many other nanomaterials, such as carbon nanotubes (Patra et al., 2015) and quantum dots (Brazhnik et al., 2015), which can detect PSA at low levels and do not harm the body or normal cells, are also being applied as sensors for detection of PSA.

Therapeutics in Prostate Cancer

In the clinical setting, prostate cancer can roughly be classified as localized, expansively localized, or metastatic. Localized cancer is thought to be curable, whereas metastatic cancer leads to androgen-independent progression and death within a few years (Salvador-Morales et al., 2009). Traditional methods include chemotherapy using chemopreventive agents and radical prostatectomy, and new methods, such as cryosurgery, radiation with conformal external beam radiation, and brachytherapy, have also recently emerged. However, current treatments for prostate cancer are not sufficiently reliable for targeting of neoplastic cells without damaging normal cells. Finding new ways to overcome the disadvantages of conventional therapy methods is necessary, and nanotechnology may provide one such relevant approach. **Table 1** provides an overview of NPs that are promising for prostate cancer treatment.

Many studies have shown that natural products are potent chemopreventive agents in prostate cancer due to their considerable efficacy against tumor cells and low toxicity (Jeong et al., 2011; Sanna et al., 2013; Kumar et al., 2015). For example, a recent study on chrysophanol, a natural compound extracted from plants of the genus *Rheum*, using GNPs as carriers to improve its bioavailability and water solubility successfully showed that chrysophanol suppresses human prostate cancer progression at the molecular level (Lu et al., 2017). Molecular targeted cancer therapy mediated by NPs is a promising strategy to overcome the non-specific biodistribution and therapeutic index of conventional chemotherapeutic drugs. Importantly, PSMA-modified NPs have been developed as a powerful treatment for prostate cancer. By conjugating PSMA to NPs, the functional particles can have good selectivity and target drugs, such as natural products or other chemotherapeutic drugs, to diseased tissue. For example, a natural product isolated from green tea, (−)-epigallocatechin 3-gallate (EGCG) shows potent chemopreventive effects in *in vitro* and *in vivo* models of prostate cancer, and several clinical trials have been conducted to determine the ability of green tea extracts to prevent the development and progression of prostate cancer (Stuart et al., 2006). A recent study showed that EGCG may be beneficial in the early stages of prostate cancer. Sanna colleagues designed biocompatible polymeric EGCG-encapsulated NPs modified with PSMA to selectively deliver EGCG to prostate cancer cells. Experiments *in vitro* demonstrated that these novel NPs could lead to increased antiproliferative activity toward PSMA-positive prostate cancer cells, without affecting normal cell viability (Sanna et al., 2011). Similarly, by conjugating GNPs with an ONT-hybridized, PSMA-specific aptamer, a GC-rich duplex acting as a loading site for doxorubicin was formed. Kim et al. (2010) established multifunctional NPs for both prostate imaging and treatment. This novel NP bioconjugate not only enabled

TABLE 1 | Overview of NPs designed for urological cancer treatments.

Cancer types	Treatment strategies	Applied NPs	Reference
Prostate cancer	Chemotherapy	GNPs loaded with chrysophanol	Lu et al., 2017
		EGCG-encapsulated polymeric NPs modified with PSMA	Sanna et al., 2011
	Gene therapy	Polymeric NPs loaded with GS25	Voruganti et al., 2015
		GNPs loaded with miRNA	Ekin et al., 2014
	Thermal therapy	MNPs and GNPs	Johannsen et al., 2007a, 2010
Renal cancer	Targeted therapy	Sorafenib-loaded PLGA NPs, DPPC liposomes and HMC-coated DPPC liposomes	Liu et al., 2015a,b
	Gene therapy	FA-PEAs:VHL complexes	Sudimack and Lee, 2000
	Thermal therapy	PEGylated gold nanoshells	Pannerec-Varna et al., 2013
		MWCNTs	Burke et al., 2009
	PDT	GNPs with radiofrequency radiation	Nikzad et al., 2017
	Targeted therapy	Cuprous oxide nanoparticles	Yang et al., 2017
		Superparamagnetic-like particles	Leulmi et al., 2015
Bladder cancer	Immunotherapy	Liposomes encapsulating BCG's CWS	Nakamura et al., 2014
	Gene therapy	PEGylated cationic liposome carriers (PCat, PPCat) and modified PLGA NPs delivering siSurvivin	Martin et al., 2014; Cui et al., 2015
	Targeted therapy	PLGA NPs loaded with belinostat	Martin et al., 2013
	Chemotherapy	Paclitaxel-loaded protein NPs	Lu et al., 2011; McKiernan et al., 2011
	PTT	GNPs	Chen et al., 2015b
		Silica-Au nanoshells, Au/Ag nanospheres, and Au nanorods modified with tumor targeting antibodies	Juarranz et al., 2008; Cheng et al., 2009
		NP-AAG	Long et al., 2018

visualization of target-specific binding by silver staining and clinical CT scanning but also efficiently induced cell death in prostate cancer cells (Kim et al., 2010).

Gene therapy is an extensive method used for the treatment of prostate cancer. Generally, there are four main strategies for gene therapy: tumor-suppressor therapy, suicide gene therapy, immunomodulatory gene therapy, and anti-oncogene therapy. However, none of these approaches can be applied alone as therapeutic treatment due to the low specificity of cell targeting and inefficient gene transfer and expression (Djavan and Nasu, 2001). NPs are widely used in anti-oncogene therapy to overcome these problems, and many studies have used nanodelivery systems to enhance the activities of oncogene inhibitors. For example, 25-OCH_3-PPD (GS25) is a natural inhibitor of the *MDM2* oncogene, which can be amplified and/or overexpressed in prostate cancer. When loaded with polyethylene glycol-poly(lactic-co-glycolic acid) NPs, GS25 showed enhanced anticancer efficacy *in vitro* and *in vivo* without inducing toxicity and exhibited improved uptake in cancer cells (Voruganti et al., 2015). MicroRNAs are commonly used as tools in gene cloning to induce post-transcriptional gene silencing. Some studies have shown that GNP-based nanocarriers (Ekin et al., 2014) and prostate cancer-targeted polyarginine-disulfide linked polyetherimide (PEI) nanocarriers (Zhang et al., 2015) can promote *miR-145* delivery into prostate tumors.

Magnetic fluid hyperthermia (MFH) is another promising method of prostate cancer treatment using biocompatible MNPs injected directly into superficial or deep-seated tumors and consecutively heated in an alternating magnetic field (Johannsen et al., 2010). Because tumor cells have a lower heat tolerance than normal cells, increasing the temperature to 40–43°C by hyperthermia (HT) can lead to tumor cell necrosis and apoptosis. MNPs play an important role in this novel therapy due to the excellent power absorption capabilities of magnetic fluids in a magnetic field (Jordan et al., 1993). A prospective clinical study investigated MFH as a monotherapy used in patients with locally recurrent prostate cancer and showed that this approach was feasible and well-tolerated; additionally, deposition of NPs in the prostate was highly durable (Johannsen et al., 2005a, 2007a,b). Recent studies have shown that HT combined with radiotherapy (RT) may be effective for the treatment of prostate cancer (Hurwitz et al., 2011; Datta et al., 2015), and MFH can effectively enhance RT, leading to significant growth inhibition in mouse models of human prostate cancer (Johannsen et al., 2005b; Attaluri et al., 2015).

In addition to MNPs, GNPs have also shown several advantages in HT therapy, including good biocompatibility. In a study of the influence of different physical characteristics (shape, size, surface properties, and concentration) of GNPs on cellular uptake, adsorption of proteins, and toxicity in PC3 human prostate cancer cells, size-dependent uptake and negligible toxicity were observed (Arnida et al., 2010). Similar to HT therapy, thermal ablative energy causes necrosis of target tissues by inducing a high temperature, leading to focal cell death and preserving the circumambient normal tissue (Sanna et al., 2011). Studies using systemically administered non-targeted NIR-activatable gold nanoshells for thermal ablation of tumors date back to the early 21st century; however, very few reports have documented its utility in the treatment of prostate cancer (Krishnan et al., 2010). Stern et al. (2007) studied gold nanoshell-mediated photothermal ablation of prostate cancer cells and found complete loss of cell viability while maintaining intact cellular morphology. A subsequent study evaluated the efficacy of laser-activated gold nanoshell thermal ablation for eradicating prostate cancer *in vivo* and compared the therapeutic efficacies of two doses of gold nanoshells (7 and 8.5 μL/g body weight). The results demonstrated that the low concentration of gold nanoshells arrested cell growth, whereas the high concentration of gold nanoshells dramatically decreased tumor volume (93% tumor necrosis and regression) within just 1 week (Stern et al., 2008). Other applications of GNPs are also being investigated. For example, genetically modified phages (with both gold-binding peptide and PC3-binding peptide) were induced to attract GNPs to form a cluster, enabling stable maintenance of cell-targeting functionality and killing of the targeted prostate cancer cells within a short time. The prostate cancer cells were killed more efficiently and selectively than non-GNP-treated cells (Oh et al., 2015).

NANOTECHNOLOGY IN RENAL CANCER

Renal cell carcinoma (RCC) is not a single entity, but includes a group of tumors with a highly heterogeneous epithelium originating from the renal tubules. There are three dominant histopathological types of RCC: clear cell (65%), papillary (15–20%), and chromophobe (5%) (Bouchelouche, 2016; Yuan et al., 2016). RCC is the third most common urinary system cancer, with an incidence rate of about 5–10 cases per 100,000 people, and accounts for 2–3% of all malignant tumors (Xu et al., 2010). Although chemotherapy is one of the main modes of cancer treatment, its effectiveness is limited by drug resistance. For example, sunitinib is currently the standard first-line treatment for advanced RCC, and patient inevitably become resistant to sunitinib treatment (Yang et al., 2017). In addition, the clinical outcomes in patients with RCC remain poor. Therefore, rapid development of nanotechnologies may improve therapeutic strategies for the diagnosis and treatment of RCC (Yang et al., 2017).

Imaging in Renal Cancer

Pinpoint imaging of RCC is one of the main issues for the diagnosis, staging, and clinical treatment of patients (Bouchelouche, 2016). In current oncology, a series of NPs for diagnostic assays have been developed, and these NPs are commonly used as contrast agents for MRI and CT imaging (Sanna et al., 2011; Williams et al., 2016).

Lu et al. (2014) conjugated the monoclonal antibody G250 and SPIO into molecular MRI probes for the *in vitro* detection of clear cell RCC (ccRCC) using a 3.0-Tesla MRI. An *in vitro* MRI study of ccRCC and control cells confirmed that the fabricated mAb G250-SPIO nanoprobe could be used as a specific marker for ccRCC cells (Lu et al., 2014). Moreover, the nanoprobe could be easily conjugated with other antitumor drugs and

imaging materials to achieve multimodal imaging and diagnostic treatment integration. For example, the combination of Cy5-labeled glycosylated bleomycin (Yu et al., 2013; Bhattacharya et al., 2014) and the nanoprobe may provide a new direction for the design of novel tumor imaging and therapeutic agents. Besides, GNPs or quantum dots as imaging materials (Mieszawska et al., 2013; Zrazhevskiy and Gao, 2013) could also be developed with the mAb G250 nanoprobe to promote highly multiplexed parallel staining, resulting preferable imaging.

Many studies have demonstrated that the diagnosis of RCC can be performed by multifarious NP imaging. However, urologists are often faced with imaging dilemmas, including lack of definitive answers in clinical practice during the diagnosis of RCC histology (Farber et al., 2015). In addition, whether contrast-enhanced imaging of RCC has any side effects in patients is worth considering. We expect to see a growing number of nanotechnologies to fill technological gaps in the diagnosis and treatments of RCC.

Therapeutics in Renal Cancer

Nanomedicine strategies may be more effective than other strategies for controlling drug delivery and release. Due to the high porosity of the tumor vasculature, impaired lymphatic drainage, known as the enhanced permeability and retention effect, or the high affinity of the NPs for markers specifically expressed on cancer cells can result in easy accumulation at the tumor site. Therapeutic nanotechnology focuses on the utilization of photothermal-based ablative energy, which is sent to the targeted lesion by activating various types of NPs (Sanna et al., 2011). Typical nanomedicine delivery vehicles include liposomes, polymeric NPs, nanoshells, and MNPs (**Table 1**).

Many preclinical studies have examined liposomal strategies for drug delivery in RCC; however, only a few clinical studies have been conducted (Williams et al., 2016). Polyethylene glycol (PEG)-ylated-liposomal doxorubicin (Doxil) was used for the treatment of patients with intractable RCC in a phase II clinical trial. The results showed that Doxil was ineffective in patients with RCC, although slightly toxic side effects were observed (Skubitz, 2002). Liu et al. (2015a,b) systemically estimated the *in vitro* applicabilities of several drugs as delivery systems for the treatment of RCC, including sorafenib-loaded poly(lactic-co-glycolic acid) (PLGA) NPs, 1, 2-dipalmitoyl-sn-glycero-3-phosphocholine (DPPC) liposomes, and hydrophobically modified chitosan (HMC)-coated DPPC liposomes. The results showed that sorafenib-loaded PLGA NPs and HMC-coated DPPC liposomes could apparently kill more RCC cells than sorafenib alone at lower concentrations. Moreover, XL184 liposomes counteracted tumor activity by inhibiting the phosphorylation of Met, AKT, and mitogen-activated protein kinase pathways in RCC cells (Kulkarni et al., 2016). The above studies indicated that liposomes may have applications in multikinase pathway inhibition as a prospective treatment for RCC.

Folic acid-modified poly(ε-caprolactone)-pluronic-poly (ε-caprolactone) grafted isophorone diidocyanate-PEI (FA-PEAs) was developed as a low-toxicity carrier to transfer Von Hippel-Lindau (VHL) plasmids to treat mice in an RCC model. Johnson et al. (2010) found that the mean tumor volume in FA-PEAs:VHL-treated mice was decreased about 30% compared with that in the control group. Due to the limited expression of folate receptors on healthy cells and overexpression in RCC, FA-PEAs:pVHL complexes could specifically bind to the cell surface via a ligand–receptor incorporating mechanism (Sudimack and Lee, 2000). Thus, the FA-PEAs:VHL complexes could be released into the cytosol through endocytosis to exert therapeutic effects.

Currently, sunitinib is the standard first-line drug for RCC; however, patients inevitably develop resistance to this drug, leading to therapy failure and poor prognosis (Joosten et al., 2015; Stone, 2016). Therefore, new therapies are needed to improve treatment outcomes in patients with RCC. The rapid development of nanotechnology has provided emerging techniques for the treatment of drug-resistant RCC. Yang colleagues demonstrated that cuprous oxide NPs can markedly inhibit RCC tumor growth with minimum renal toxicity *in vitro* and *in vivo*, thereby reversing sunitinib resistance. The mechanism may involve the downregulation of copper chaperone proteins antioxidant 1 copper chaperone and copper chaperone for superoxide dismutase in RCC cells, influencing copper trafficking to the endoplasmic reticulum and mitochondria and thereby initiating endoplasmic reticulum stress and mitochondrion-mediated apoptosis by activating caspase-3, caspase-9, and caspase-12 (Yang et al., 2017). In addition, cell cycle and apoptosis regulator 1 functional mimetic compounds (CFMs) inhibit cell growth by inducing apoptosis in various cancer types, even drug-resistant cancer (Muthu et al., 2015). Cheriyan et al. (2017) found that CFM-4.16 had strong inhibitory effects on parental and everolimus-resistant RCC cells. Because of the poor aqueous solubility of CFM-4.16, it was encapsulated in PEGylated vitamin E-based nanomicelles generating water-soluble formulations with higher drug loading (30% w/w). The findings of this study suggested that CFM-4.16 nanomicelles inhibited the viability of parental and everolimus-resistant RCC cells *in vitro* and suppressed the growth of RCC cell-derived xenografts (Cheriyan et al., 2017).

The use of PEG-conjugated antibodies attached to nanoshells guarantees biocompatibility for drug delivery to tumor cells. Pannerec-Varna et al. (2013) developed large PEGylated gold nanoshells with distribution in the different cellular components of human renal cancer. The distribution kinetics progressed from intravascular flow at 30 min to intratumoral cells 24 h later, and no toxicity was detected in mice with PEGylated gold nanoshells at 6 months. This novel research provided important insights into the use of large PEGylated gold nanoshells by optimizing the time of targeted hyperthermia or topical drug delivery to carcinoma cells (Pannerec-Varna et al., 2013). Additionally, new studies have shown that diverse tumor types can be evaluated preclinically and clinically using CRLX101, an NP-drug conjugate containing camptothecin conjugated to a biocompatible cyclodextrin/PEG copolymer (Gaur et al., 2014; Lin C.J. et al., 2016). CRLX101 in combination with bevacizumab has been assessed in a phase I trial of mRCC treatment (NCT01625936[1]), and the initial data indicated that

[1]https://clinicaltrials.gov/

CRLX101 combined with bevacizumab was an adequate therapy in mRCC. The strategy of using biodegradable polymer NPs to control the delivery of medicines for multiple types of cancers has become feasible, although the therapeutic effects of these biodegradable polymer NPs in RCC are unknown (Schroeder et al., 2012; Devulapally and Paulmurugan, 2014). Nevertheless, Abraxane (albumin NPs conjugated to paclitaxel) was well-tolerated for the treatment of metastatic urothelial carcinoma and showed tumor responses in 27.7% of patients, revealing that this strategy may be a valid second-line treatment (Ko et al., 2013).

Gold NPs can be used in cancer treatment due to their remarkable compatibility, tunable stability, and low toxicity. Moreover, GNPs are often used in photodynamic therapy (PDT) by generating heat to kill tumor cells (Cabuzu et al., 2015). Nikzad et al. (2017) assessed the effects of treatment of RCC with RF radiation in the presence of GNPs. Human embryonic kidney cells were subjected to various tests in the presence of RF and GNPs. *In vitro* MTT assays showed that cell viability was dramatically reduced in the RF-treated groups in the presence of GNPs compared with that in the control group. Thus, this method may be suitable for the treatment of RCC, providing a new method for alternative nephrectomy (Nikzad et al., 2017).

Sreekanth et al. (2016) used sulforhodamine B assays and two-color flow cytometry analysis to test the toxic effects of CdO nanostructures on Madin-Darby canine kidney epithelial cells (MDCK cells) and Caki-2 human renal cancer cells. Compared with normal cells, CdO had significant cytotoxic effects on MDCK and Caki-2 cells. Thus, CdO could inhibit the growth of tumor cells and may be an effective drug for the treatment of RCC (Sreekanth et al., 2016).

Burke et al. (2009) confirmed the heating effects of treatment with multiwalled carbon nanotubes (MWCNTs) through magnetic resonance temperature-mapping and heat shock protein-reactive immunohistochemistry. The results showed that the use of MWCNTs could ablate tumors with low laser power and reduce treatment times, with minimal local toxicity and no significant systemic toxicity (**Figure 2**). MWCNTs are thermal ablation agents that can lead to long-term survival in tumor-bearing mice, which indicates that the combination of MWCNTs and laser may be a promising method for the treatment of RCC (Burke et al., 2009).

Recently, because of the low frequency of mechanical effects on cancer cell membranes, some original approaches have been developed to eradicate cancer cells. A study on human renal cancer cells with superparamagnetic-like particles was conducted by Leulmi et al. (2015), who confirmed that apoptosis could be

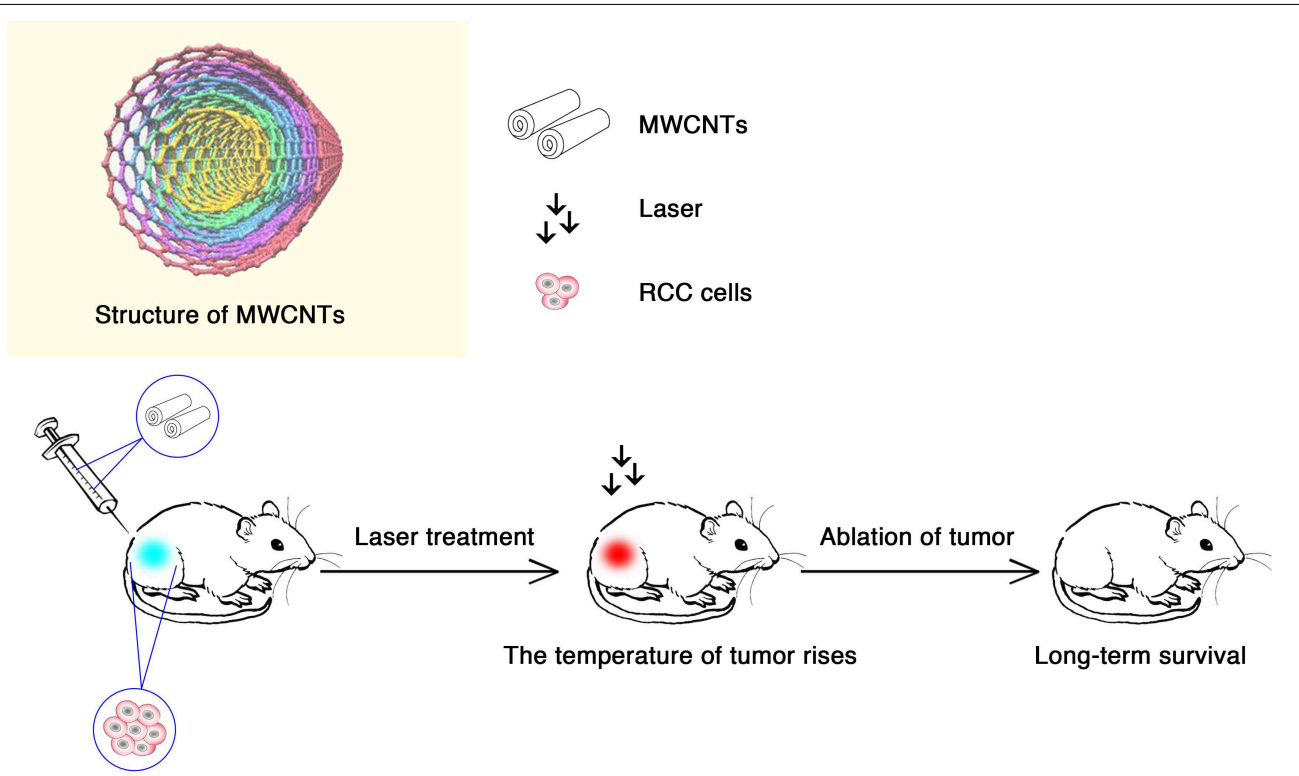

FIGURE 2 | Multiwalled carbon nanotubes (MWCNTs) ablate tumors. Tumor-bearing mice were injected intratumorally with 50 μL of treatment solution containing 100, 50, or 10 μg of MWCNTs (Burke et al., 2009). Tweety-four hours after the injection, they were irradiated with a 1,064-nm NIR laser for 30 s (3 W/cm^2; spot size, 5 mm). In the presence of the laser, MWCNTs increased intratumoral temperatures to a level sufficient to induce tumor ablation, resulting the long-term survival in tumor-bearing mice.

achieved by the vibration of MNPs attached to cancer cells. With regard to the invasiveness of the treatment, magneto-mechanical stimulation is superior to magnetic hyperthermia and is easy to put into practice (Drexler, 1986).

NANOTECHNOLOGY IN BLADDER CANCER

Bladder cancer is the seventh most commonly diagnosed cancer in the male population worldwide (Babjuk et al., 2017), and can be divided into non-muscle-invasive bladder cancer (NMIBC) and muscle-invasive bladder cancer (MIBC) according to the pathologic stage (Jiang et al., 2015). At diagnosis, approximately 75% of patients with BCa present with NMIBC (Babjuk et al., 2017). The most common method for detection of NMIBC is standard white light cystoscopy; however, it is difficult to detect flat lesions and differentiate benign from malignant lesions. TUR-BT, as the gold standard for primary treatment for NMIBC, frequently leads to tumor relapse. To prevent recurrence, various medicines, including BCG and mitomycin C, have been used extensively through intravesical instillation as adjuvant therapy after TUR-BT. However, these treatments can cause septicemia, disseminated intravascular coagulation, and multiple organ failure because of severe toxicity (Lodde et al., 2014). Therefore, more advanced diagnosis and therapies are needed (**Table 1**).

Imaging in Bladder Cancer

For the detection of NMIBC, fluorescent or photodynamic diagnosis has been developed as an improvement for contemporary white light microscopy. Photosensitizers, such as hexaminolevulinate, are used in fluorescence cystoscopy and are preferentially absorbed by cancer cells, resulting in a red appearance in comparison with surrounding tissues. Although these compounds exhibit high sensitivity, they may show low specificity, particularly after BCG therapy (Ray et al., 2010). Previous studies have shown that nanotechnology can enhance the specificity of photosensitizers to tumor cells and improve the identification of cancer by increasing the uptake of NPs within tumor cells (Olivo et al., 2012; Yan et al., 2013). Recently, Lin T.Y. et al. (2016) developed a multifunctional nanoporphyrin called PLZ4-nanoporphyrin (PNP) due to its coating with the BCa-specific ligand PLZ4. PNP displays the ability to preferably emit fluorescence/heat/reactive oxygen species upon illumination with near infrared light, allowing the fluorescence signal of PNPs to efficiently and selectively increase in BCa cells.

As metal NPs, GNPs can be modified with functional groups by being combined with ligands, antibodies, and other medicines (Cheng et al., 2014). Due to its characteristic SPR signal according to the distance of NPs, GNPs can modify protein molecules and particular nucleic acids to show different colors (Larguinho and Baptista, 2012). Because of SPR, colloidal GNPs are red in color and can be 4–5 orders of magnitude larger than the traditional dye in absorption and scattering cross-sections (Azzazy et al., 2006). These properties can be used to develop easier and faster methods for diagnosing diseases. When GNPs aggregate, their color changes from red to blue due to a second phenomenon known as plasmon-plasmon transfer (Huang and El-Sayed, 2010). The rationale is that GNPs are stabilized by the adsorption of single-stranded DNA through their nitrogenous bases, preventing the salt-induced aggregation of GNPs and keeping the solution red in color. In contrast, the repulsion between the GNP surface and double-stranded DNA (dsDNA) prevents dsDNA from adsorbing to the NP surface (Li and Rothberg, 2004, 2005); because of this, GNPs are not protected from salt-induced aggregation, and the color of the solution turns blue.

Based on these phenomena, Eissa et al. (2014) have developed colorimetric GNP assays to detect unamplified hepatoma upregulated protein RNA (HURP RNA) in urine directly for BCa diagnosis. The principle is shown in **Figure 3A**. Briefly, the purified HURP RNA was mixed with hybridization buffer containing NaCl and a specific oligotargeter. After denaturation and annealing, hybridization between the oligotargeter and the HURP RNA occurred, and the added GNPs were aggregated without the protection of the oligotargeter. The solution color then shifted from red to blue. If there was no HURP RNA in the samples, the GNP surface was fully adsorbed with the oligotargeter, and the solution color remained red. Using this sensitive and non-invasive assay, BCa could be detected at an early stage, making it possible to begin treatment earlier and achieve better therapeutic effects. In another study, GNPs were also developed for rapid and sensitive detection of urinary hyaluronidase (HAase) activity (Nossier et al., 2014). The charge interaction between polyanionic hyaluronic acid (HA) and cationic GNPs stabilized with cetyl trimethyl ammonium bromide can lead to the formation of gold aggregates and a red to blue color shift. After the enzymatic reaction of HAase, the polymeric HA is degraded into small fragments that cannot aggregate GNPs (**Figure 3B**). Similarly, the developed cationic GNP assay was used for qualitative detection of urinary HAase activity (a urinary marker of BCa) in patients with bladder carcinoma by detecting the absorption ratio (A_{530}/A_{620}) of the reacted GNP solution, which showed a better sensitivity (82.5%) than that of zymography (Nossier et al., 2014).

Nuclear matrix protein 22 (NMP22) is a monitoring tool for predicting the recurrence/clearance of BCa and for screening undiagnosed individuals who have symptoms or are at risk for the disease. Lee colleagues demonstrated a novel strategy to sense NMP22 in urine samples by using a sensing element comprised of molecularly imprinted polymers (MIPs) to specifically recognize NMP22 molecules. In this study, zinc oxide nanorods were hydrothermally grown on the sensing electrodes to increase the surface area to be coated with MIPs and therefore enhance the electrochemical response (Lee et al., 2016).

Therapeutics in Bladder Cancer

Liposomes as carriers of molecules, such as small-molecule cytotoxic agents (Guhasarkar et al., 2017), nucleotides (Cuomo et al., 2013), and proteins (Vila-Caballer et al., 2016), have also been developed for BCa therapy. To improve the poor solubility and enhance the efficiency of the cell wall skeleton (CWS) of BCG, Nakamura's group encapsulated the CWS of BCG within

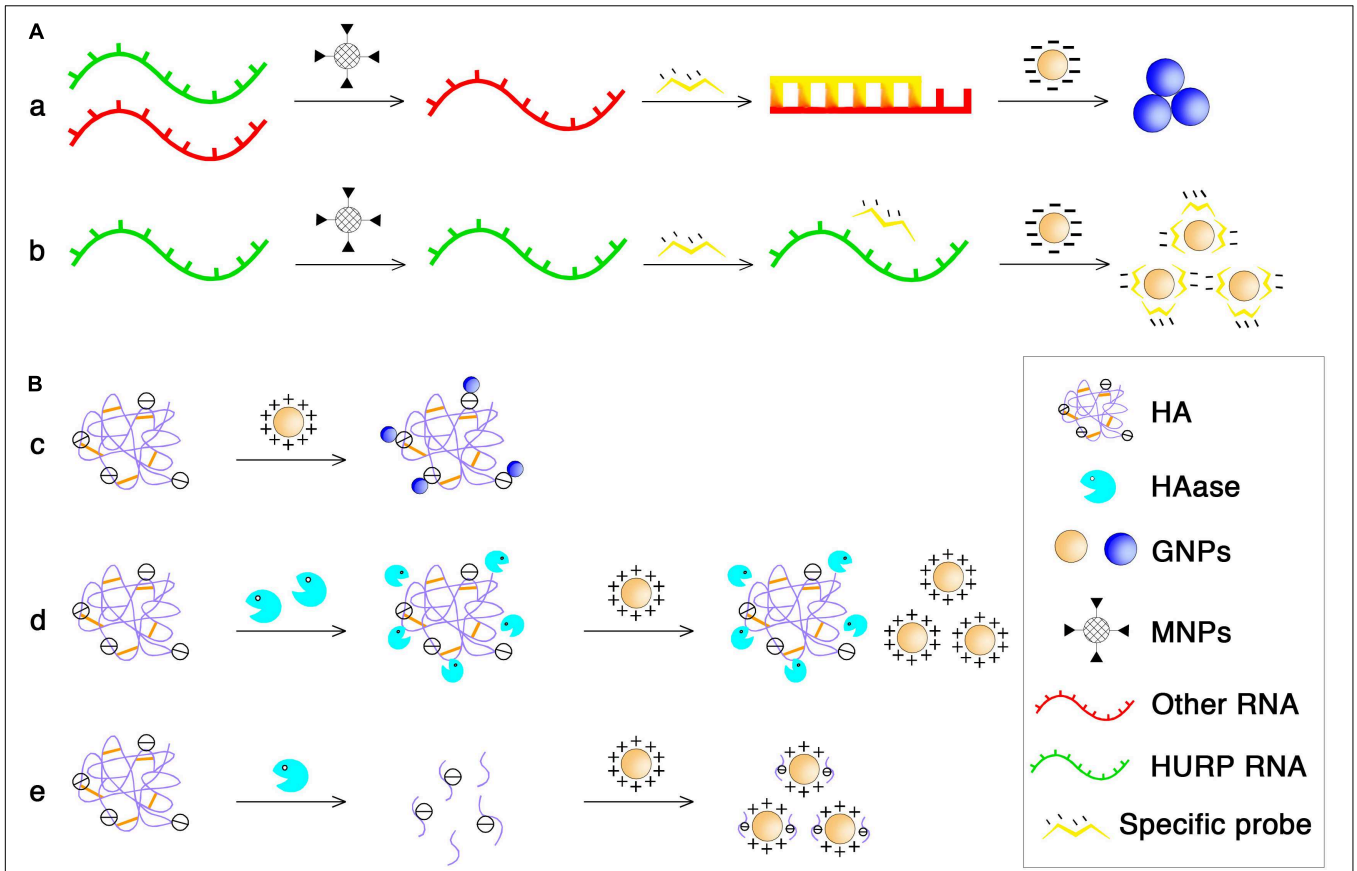

FIGURE 3 | The principle of NP-based diagnosis of BCa. **(A)** MNPs and GNPs used in purifying total RNA to obtain HURP RNA. **(a)** MNPs functionalized with oligonucleotide sequences specific for HURP RNA were added followed by mixing with hybridization buffer which contained NaCl, and HURP specific oligonucleotide with purified HURP RNA. After denaturation and annealing, the negatively charged GNPs were added and in the presence of HURP RNA, hybridization occured between the oligotargeter and the HURP RNA, and the solution color shifted from red to blue due to salt-induced aggregation of GNPs. **(b)** Without HURP RNA, GNPs would not aggregate and the solution color remained red because the oligotargeter remained adsorbed onto the surface of the GNPs. **(B)** Cationic GNPs directly detected HAase activity. **(c)** The charge interaction between polyanionic HA and cationic GNPs can lead to the formation of gold aggregates and at the same time a red to blue color shifted. **(d)** Under conditions of high HAase concentration, the enzyme and HA binds electrostatically even at a 0-min incubation time at 37°C, no aggregation occurs when the GNP solution is added, and the solution remains red in color. **(e)** At low concentration conditions, enzymatical reaction at 37°C for a period of time could lead to the enzyme molecule digest HA into small fragments, resulting in the failure of GNPs aggregation.

liposomes (Nakamura et al., 2014). Recently, they modified cationic liposomal surfaces with cholesteryl-PEG to overcome urine aggregation and promote cellular uptake into cancerous urothelial tissues (Nakamura et al., 2017). Liposomes can be also used to envelop small interfering RNA (siRNA) silencing oncogenes or other tumor-related genes for the prevention or treatment of BCa. Cui et al. (2015) adopted two newly developed PEGylated cationic liposome carriers (PCat, PPCat) for delivering survivin siRNA (siSurvivin) and enhancing the activity of mitomycin C in human BCa cells. A fusogenic lipid was used in both carriers to destabilize the endosomal membrane, and PPCat further contained paclitaxel to enhance the *in vivo* delivery and transfection of siSurvivin.

Several studies have shown that polymeric NPs as drug carriers have great promise in the treatment of BCa (Huang et al., 2012; Yan et al., 2013). To utilize polymeric NPs as carriers, the polymers must have a biodegradable structure and show changes in composition to carry a specific drug to a specified location to achieve targeted drug delivery. The improved polymeric NPs also need to be less expensive, easier to synthesize, and non-immunogenic. One of the most widely used polymeric NPs is PLGA NPs, which show outstanding biocompatibility, biodegradability, ability to be modified with polymers and peptides (Cu et al., 2011), and ability to facilitate controlled release of loaded drugs (Hua et al., 2014). Martin et al. (2013) designed PLGA NPs loaded with belinostat, a histone deacetylase inhibitor, for BCa treatment. PLGA NPs were surface modified with a novel cell penetrating polymer, poly(guanidinium oxanorbornene). The results showed that intracellular uptake was also enhanced significantly and tissue penetration ability was improved by 10-fold in intravesically treated mouse bladders and *ex vivo* human ureters. In a subsequent study, researchers used a low-molecular-weight (2.5 or 20 kDa) positively charged mucoadhesive polysaccharide, chitosan, to modify the surface of PLGA NPs in order to deliver siSurvivin to

the BCa cells (Martin et al., 2014). These surface-modified PLGA NPs could not only cross the urothelium and target the exact tumor site but also load a large number of siRNAs.

Protein NPs have been used as drug carriers in the treatment of many cancers (Lee et al., 2017; Palchetti et al., 2017). Using proteins as carrier materials *in vivo* may solve enzyme-induced degradation problems, reduce the effects of drug toxicity, and offer good biocompatibility compared with other types of materials, such as metals. The production of urine during treatment leads to dilution of the drug concentration used for intravesical instillation, resulting in the failure of intravesical treatment of NMIBC. However, studies have found that the use of paclitaxel-gelatin NPs can solve the problem of drug dilution by newly produced urine through constant drug release and that achieving a constant drug concentration can reduce the frequency of treatment. For example, paclitaxel-loaded gelatin protein NPs have been developed to improve the delivery and retention properties of paclitaxel in intravesical therapy against BCa (Lu et al., 2011). Compared with docetaxel, NP albumin-bound paclitaxel (Nab-paclitaxel) has been shown to have increased solubility and lower toxicity in systemic treatment, and minimal toxicity and systemic absorption were demonstrated in the first human intravesical phase I trial (McKiernan et al., 2011). Phase II trials have shown that Nab-paclitaxel is well-tolerated in patients with pretreated advanced urothelial cancer and has a good tumor response (Ko et al., 2013). These results have highlighted the potential applications of Nab-paclitaxel in cancer treatment.

Recently, novel MNPs coated with three broad-spectrum lectins, namely concanavalin A (ConA; MNP@ConA), wheat germ agglutinin (WGA; MNP@WGA), and Sambucus nigra (SNA; MNP@SNA), have been developed to selectively capture glycoproteins from the urine of patients with different types of BCa (Azevedo et al., 2018). In this case, lectins were used for targeting glycan moieties in cancer-associated glycoproteins, indicating the possibility of targeting local release of drugs.

The optical properties of SPR are used to assist laser-induced thermotherapy in plasmonic photothermal therapy (PTT) with GNPs to enhance the effects of target therapy (Nergiz et al., 2014), avoiding damage to neighboring normal tissues because of the hyperthermic state induced by the relatively low laser power. Chen et al. (2015b) showed that GNPs require only half the laser power of regular laser treatment, and Cheng et al. (2009) demonstrated that silica-Au nanoshells, Au/Ag nanospheres, and Au nanorods modified with tumor targeting antibodies, such as anti-epidermal growth factor receptor and anti-epidermal growth factor receptor 2 antibodies, were internalized by tumor cells, resulting in photothermal-induced death of BCa cells *in vitro*. Among the three types of nanomaterials, silica@Au nanoshells require a minimum number of particles to produce effective photodestruction. In contrast, PDT is also a promising strategy for BCa therapy, involving the use of photosensitizers, which are usually large cyclic compounds, such as porphyrins, chlorins, and phthalocyanines. These substances will produce free radicals when exposed to near infrared or visible light. However, the products currently on the market have quite a few limitations, including specific differences in the ability to act on the tumor alone (Juarranz et al., 2008). In a recent study, Long et al. (2018) designed a novel multifunctional nanoporphyrin platform loaded with the heat-shock protein 90 inhibitor 17AAG (NP-AAG) and found that bladder tumors could be synergistically eradicated with a single intravenous injection of NP-AAG followed by multiple light treatments within 7 days.

NANOTECHNOLOGY IN OTHER UROLOGICAL CANCER

Other urological carcinomas have received limited attention with regard to nanotechnology applications. Feldman et al. (2008) conducted a preliminary study of the potential of USPIOs for accurate detection of lymph node metastases of penile and testicular cancers through lymphotropic NP-enhanced MRI. Patients with penile carcinoma underwent a pelvic MRI after using USPIOs. The results showed that better sensitivity, specificity, and accuracy could be obtained by comparing conventional imaging techniques, suggesting that the pathological status of local lymph nodes could be accurately predicted by MRI in patients with penile cancer (Tabatabaei et al., 2005; Mueller-Lisse et al., 2008; Hughes et al., 2009). Similarly, a prospective pilot study examined the use of lymphotropic NP-enhanced MRI to detect lymph node metastasis in patients with testicular cancer after injection of USPIOs. The data suggested that USPIOs greatly improved the specificity and sensitivity of accurate lymph node metastasis diagnosis (Harisinghani et al., 2005).

FUTURE PERSPECTIVES

Despite the use of nanotechnologies with tremendous potential for the detection, diagnosis, and treatment of urological cancers, more studies are still required. First, safety profiles must be studied in detail because of insufficient knowledge regarding the biocompatibility of nanocarriers. The safety of GNPs and gold nanoshells has been widely evaluated in preclinical trials, and full clinical trials are still underway for many of these materials. USPIOs have been under continued scrutiny, and ferumoxtran-10 is currently entering phase III clinical trials in Europe (Daldrup-Link, 2017). Additionally, iron-oxide NPs have been approved as an MRI contrast agent by the US Food and Drug Administration (Wang et al., 2014). A database on health risks linked to different types of NPs should also be established according to different pharmacokinetic behaviors. Second, additional research into the design and development of NPs with multiple functions (single or dual imaging, targeted therapy, and combination therapy) is needed. Moreover, the development of multifunctional NPs loaded with targeted agents may eventually be permitted for both PTT and targeted therapy to achieve simultaneous detection and treatment of urological cancer. Third, a widely used and well-accepted dosimetry model is needed to estimate the NP concentration in tumors of interest. Dosimetry formulations have been used to guide radiation

therapy, but not for PTT because of the uneven distribution of particles and the effects of tissue physiology. Thus, further studies are required to establish such formulas. Lastly, in the future, more studies are needed to examine the environmental influence of manufactured NPs, which are deliberately produced with specific properties; these NPs have been shown to enter air, water, and soil from a range of routes (Kumar et al., 2012). Thus, there is an urgent need for the development of safety guidelines for NPs.

CONCLUSION

During recent decades, many efforts have been made to combine novel technologies and conventional methods to combat cancer. The potential applications of nanotechnology were reviewed in this article. Nanotechnologies are promising tools to enhance the specificity and sensitivity of both the diagnosis and treatment of cancer and have been shown to have several feasible applications in urological cancer. Many studies and clinical trials have demonstrated that NPs can overcome the limitations of current medical approaches. Various metallic nanomaterials are used as contrast agents for MRI and CT imaging, providing a higher probability of detecting early urological cancer. The excellent photothermal properties of GNPs have led to their extensive application in imaging. Moreover, by application in HT therapy and thermal therapy, GNPs have shown potential to generate heat more efficiently. In contrast, many researchers have clearly demonstrated that NPs are ideal candidates for drug delivery systems because of their special size and are able to combine the benefits of drug delivery systems with improved safety and efficacy. Polymeric NPs have the capacity to be used for various applications from imaging to drug delivery systems. Several different types of polymeric materials can be used, and well-developed fabrication techniques have enabled them to be mass produced. Multifunctional NPs have many advantages because they are uniquely designed to target specific cancer cells. However, there are still some issues that need to be clarified, such as the safety of these NPs when used in the human body. Additional studies are still needed to clarify the details of nanotechnology-based methods and to establish these NPs as tools for the treatment of cancers.

AUTHOR CONTRIBUTIONS

M-HH, LC, TZ, and YT summarized the literatures and wrote the manuscript. QH and H-LF revised and edited the manuscript. J-CL, WZ, and GS provided critical comments and revised the manuscript. LH and Z-XY revised the manuscript and supervised all the works.

FUNDING

This work was supported by the project (2016M602706) funded by China Postdoctoral Science Foundation and the International Exchange and Collaboration Project (2018HH0057) funded by Science and Technology Department of Sichuan Province.

REFERENCES

Agarwal, A., Huang, S. W., Odonnell, M., and Day, K. C. (2007). Targeted gold nanorod contrast agent for prostate cancer detection by photoacoustic imaging. *J. Appl. Phys.* 102:064701. doi: 10.1063/1.2777127

Arnida, Malugin, A., and Ghandehari, H. (2010). Cellular uptake and toxicity of gold nanoparticles in prostate cancer cells: a comparative study of rods and spheres. *J. Appl. Toxicol.* 30, 212–217. doi: 10.1002/jat.1486

Attaluri, A., Kandala, S. K., Wabler, M., Zhou, H., Cornejo, C., Armour, M., et al. (2015). Magnetic nanoparticle hyperthermia enhances radiation therapy: a study in mouse models of human prostate cancer. *Int. J. Hyperthermia* 31, 359–374. doi: 10.3109/02656736.2015.1005178

Azevedo, R., Soares, J., Gaiteiro, C., Peixoto, A., Lima, L., Ferreira, D., et al. (2018). Glycan affinity magnetic nanoplatforms for urinary glycobiomarkers discovery in bladder cancer. *Talanta* 184, 347–355. doi: 10.1016/j.talanta.2018.03.028

Azzazy, H. M., Mansour, M. M., and Kazmierczak, S. C. (2006). Nanodiagnostics: a new frontier for clinical laboratory medicine. *Clin. Chem.* 52, 1238–1246. doi: 10.1373/clinchem.2006.066654

Babjuk, M., Bohle, A., Burger, M., Capoun, O., Cohen, D., Comperat, E. M., et al. (2017). EAU guidelines on non-muscle-invasive urothelial carcinoma of the bladder: update 2016. *Eur. Urol.* 71, 447–461. doi: 10.1016/j.eururo.2016.05.041

Bertrand, N., Wu, J., Xu, X., Kamaly, N., and Farokhzad, O. C. (2014). Cancer nanotechnology: the impact of passive and active targeting in the era of modern cancer biology. *Adv. Drug Deliv. Rev.* 66, 2–25. doi: 10.1016/j.addr.2013.11.009

Bhattacharya, C., Yu, Z., Rishel, M. J., and Hecht, S. M. (2014). The carbamoylmannose moiety of bleomycin mediates selective tumor cell targeting. *Biochemistry* 53, 3264–3266. doi: 10.1021/bi500482q

Bouchelouche, K. (2016). "Diagnostic applications of nuclear medicine: kidney and bladder cancer," in *Nuclear Oncology: From Pathophysiology to Clinical Applications*, eds H. W. Strauss, G. Mariani, D. Volterrani, and S. M. Larson (Cham: Springer International Publishing), 1–43.

Brazhnik, K., Sokolova, Z., Baryshnikova, M., Bilan, R., Efimov, A., Nabiev, I., et al. (2015). Quantum dot-based lab-on-a-bead system for multiplexed detection of free and total prostate-specific antigens in clinical human serum samples. *Nanomedicine* 11, 1065–1075. doi: 10.1016/j.nano.2015.03.003

Burke, A., Ding, X., Singh, R., Kraft, R. A., Levi-Polyachenko, N., Rylander, M. N., et al. (2009). Long-term survival following a single treatment of kidney tumors with multiwalled carbon nanotubes and near-infrared radiation. *Proc. Natl. Acad. Sci. U.S.A.* 106, 12897–12902. doi: 10.1073/pnas.0905195106

Cabuzu, D., Cirja, A., Puiu, R., and Grumezescu, A. M. (2015). Biomedical applications of gold nanoparticles. *Curr. Top. Med. Chem.* 15, 1605–1613. doi: 10.2174/1568026615666150414144750

Chen, C. H., Chan, T. M., Wu, Y. J., and Chen, J. J. (2015a). Review: application of nanoparticles in urothelial cancer of the urinary bladder. *J. Med. Biol. Eng.* 35, 419–427.

Chen, C. H., Wu, Y. J., and Chen, J. J. (2015b). Gold nanotheranostics: photothermal therapy and imaging of Mucin 7 conjugated antibody nanoparticles for urothelial cancer. *Biomed Res. Int.* 2015:813632. doi: 10.1155/2015/813632

Cheng, D., Han, W., Yang, K., Song, Y., Jiang, M., and Song, E. (2014). One-step facile synthesis of hyaluronic acid functionalized fluorescent gold nanoprobes sensitive to hyaluronidase in urine specimen from bladder cancer patients. *Talanta* 130, 408–414. doi: 10.1016/j.talanta.2014.07.005

Cheng, F. Y., Chen, C. T., and Yeh, C. S. (2009). Comparative efficiencies of photothermal destruction of malignant cells using antibody-coated silica@Au nanoshells, hollow Au/Ag nanospheres and Au nanorods. *Nanotechnology* 20:425104. doi: 10.1088/0957-4484/20/42/425104

Cheng, Z., Al Zaki, A., Hui, J. Z., Muzykantov, V. R., and Tsourkas, A. (2012). Multifunctional nanoparticles: cost versus benefit of adding targeting and imaging capabilities. *Science* 338, 903–910. doi: 10.1126/science.1226338

Cheriyan, V. T., Alsaab, H. O., Sekhar, S., Stieber, C., Kesharwani, P., Sau, S., et al. (2017). A CARP-1 functional mimetic loaded vitamin E-TPGS micellar

nano-formulation for inhibition of renal cell carcinoma. *Oncotarget* 8, 104928–104945. doi: 10.18632/oncotarget.20650

Crouzet, S., Rouviere, O., Martin, X., and Gelet, A. (2014). High-intensity focused ultrasound as focal therapy of prostate cancer. *Curr. Opin. Urol.* 24, 225–230. doi: 10.1097/MOU.0000000000000053

Cu, Y., Booth, C. J., and Saltzman, W. M. (2011). In vivo distribution of surface-modified PLGA nanoparticles following intravaginal delivery. *J. Control. Release* 156, 258–264. doi: 10.1016/j.jconrel.2011.06.036

Cui, M. J., Au, J. L. S., Wientjes, M. G., O'Donnell, M. A., Loughlin, K. R., and Lu, Z. (2015). Intravenous siRNA silencing of survivin enhances activity of mitomycin C in human bladder RT4 xenografts. *J. Urol.* 194, 230–237. doi: 10.1016/j.juro.2015.02.036

Cuomo, F., Mosca, M., Murgia, S., Avino, P., Ceglie, A., and Lopez, F. (2013). Evidence for the role of hydrophobic forces on the interactions of nucleotide-monophosphates with cationic liposomes. *J. Colloid Interface Sci.* 410, 146–151. doi: 10.1016/j.jcis.2013.08.013

Daldrup-Link, H. E. (2017). Ten things you might not know about iron oxide nanoparticles. *Radiology* 284, 616–629. doi: 10.1148/radiol.2017162759

Daniel, M. C., and Astruc, D. (2004). Gold nanoparticles: assembly, supramolecular chemistry, quantum-size-related properties, and applications toward biology, catalysis, and nanotechnology. *Chem. Rev.* 104, 293–346. doi: 10.1021/cr030698+

Datta, N. R., Ordonez, S. G., Gaipl, U. S., Paulides, M. M., Crezee, H., Gellermann, J., et al. (2015). Local hyperthermia combined with radiotherapy and-/or chemotherapy: recent advances and promises for the future. *Cancer Treat. Rev.* 41, 742–753. doi: 10.1016/j.ctrv.2015.05.009

Devulapally, R., and Paulmurugan, R. (2014). Polymer nanoparticles for drug and small silencing RNA delivery to treat cancers of different phenotypes. *Wiley Interdiscip Rev Nanomed Nanobiotechnol* 6, 40–60. doi: 10.1002/wnan.1242

Djavan, B., and Nasu, Y. (2001). Prostate cancer gene therapy-what have we learned and where are we going? *Rev. Urol.* 3, 179–186.

Drexler, K. E. (1986). *Engines of Creation*. New York, NY: Anchor Press.

Eissa, S., Shawky, S. M., Matboli, M., Mohamed, S., and Azzazy, H. M. (2014). Direct detection of unamplified hepatoma upregulated protein RNA in urine using gold nanoparticles for bladder cancer diagnosis. *Clin. Biochem.* 47, 104–110. doi: 10.1016/j.clinbiochem.2013.10.022

Ekin, A., Karatas, O. F., Culha, M., and Ozen, M. (2014). Designing a gold nanoparticle-based nanocarrier for microRNA transfection into the prostate and breast cancer cells. *J. Gene Med.* 16, 331–335. doi: 10.1002/jgm.2810

Farber, N. J., Wu, Y., Zou, L., Belani, P., and Singer, E. A. (2015). Challenges in RCC imaging: renal insufficiency, post-operative surveillance, and the role of radiomics. *Kidney Cancer J.* 13, 84–90.

Feldman, A. S., McDougal, W. S., and Harisinghani, M. G. (2008). The potential of nanoparticle-enhanced imaging. *Urol. Oncol.* 26, 65–73. doi: 10.1016/j.urolonc.2007.03.016

Gaur, S., Wang, Y. F., Kretzner, L., Chen, L. L., Yen, T., Wu, X. W., et al. (2014). Pharmacodynamic and pharmacogenomic study of the nanoparticle conjugate of camptothecin CRLX101 for the treatment of cancer. *Nanomedicine* 10, 1477–1486. doi: 10.1016/j.nano.2014.04.003

Ghasemian, Z., Shahbazi-Gahrouei, D., and Manouchehri, S. (2015). Cobalt zinc ferrite nanoparticles as a potential magnetic resonance imaging agent: an in vitro study. *Avicenna J. Med. Biotechnol.* 7, 64–68.

Guhasarkar, S., More, P., and Banerjee, R. (2017). Urothelium-adherent, ion-triggered liposome-in-gel system as a platform for intravesical drug delivery. *J. Control. Release* 245, 147–156. doi: 10.1016/j.jconrel.2016.11.031

Harisinghani, M. G., Saksena, M., Ross, R. W., Tabatabaei, S., Dahl, D., Mcdougal, S., et al. (2005). A pilot study of lymphotrophic nanoparticle-enhanced magnetic resonance imaging technique in early stage testicular cancer: a new method for noninvasive lymph node evaluation. *Urology* 66, 1066–1071. doi: 10.1016/j.urology.2005.05.049

Hua, X., Tan, S., Bandara, H. M., Fu, Y., Liu, S., and Smyth, H. D. (2014). Externally controlled triggered-release of drug from PLGA micro and nanoparticles. *PLoS One* 9:e114271. doi: 10.1371/journal.pone.0114271

Huang, C., Neoh, K. G., Xu, L., Kang, E. T., and Chiong, E. (2012). Polymeric nanoparticles with encapsulated superparamagnetic iron oxide and conjugated cisplatin for potential bladder cancer therapy. *Biomacromolecules* 13, 2513–2520. doi: 10.1021/bm300739w

Huang, H. C., Chang, P. Y., Chang, K., Chen, C. Y., Lin, C. W., Chen, J. H., et al. (2009). Formulation of novel lipid-coated magnetic nanoparticles as the probe for in vivo imaging. *J. Biomed. Sci.* 16:86. doi: 10.1186/1423-0127-16-86

Huang, X., and El-Sayed, M. A. (2010). Gold nanoparticles: optical properties and implementations in cancer diagnosis and photothermal therapy. *J. Adv. Res.* 1, 13–28. doi: 10.1016/j.jare.2010.02.002

Hughes, B., Leijte, J., Shabbir, M., Watkin, N., and Horenblas, S. (2009). Non-invasive and minimally invasive staging of regional lymph nodes in penile cancer. *World J. Urol.* 27, 197–203. doi: 10.1007/s00345-008-0288-6

Hurwitz, M. D., Hansen, J. L., Prokopios-Davos, S., Manola, J., Wang, Q., Bornstein, B. A., et al. (2011). Hyperthermia combined with radiation for the treatment of locally advanced prostate cancer: long-term results from Dana-Farber Cancer Institute study 94-153. *Cancer* 117, 510–516. doi: 10.1002/cncr.25619

Jeong, N. Y., Yoon, Y. G., Rho, J. H., Lee, J. S., Lee, S. Y., Yoo, K. S., et al. (2011). The novel resveratrol analog HS-1793-induced polyploid LNCaP prostate cancer cells are vulnerable to downregulation of Bcl-xL. *Int. J. Oncol.* 38, 1597–1604. doi: 10.3892/ijo.2011.979

Jiang, X., Du, L., Wang, L., Li, J., Liu, Y., Zheng, G., et al. (2015). Serum microRNA expression signatures identified from genome-wide microRNA profiling serve as novel noninvasive biomarkers for diagnosis and recurrence of bladder cancer. *Int. J. Cancer* 136, 854–862. doi: 10.1002/ijc.29041

Johannsen, M., Gneueckow, U., Thiesen, B., Taymoorian, K., Cho, C. H., Waldofner, N., et al. (2007a). Thermotherapy of prostate cancer using magnetic nanoparticles: feasibility, imaging, and three-dimensional temperature distribution. *Eur. Urol.* 52, 1653–1662. doi: 10.1016/j.eururo.2006.11.023

Johannsen, M., Gneveckow, U., Eckelt, L., Feussner, A., Waldofner, N., Scholz, R., et al. (2005a). Clinical hyperthermia of prostate cancer using magnetic nanoparticles: presentation of a new interstitial technique. *Int. J. Hyperthermia* 21, 637–647.

Johannsen, M., Gneveckow, U., Taymoorian, K., Thiesen, B., Waldofner, N., Scholz, R., et al. (2007b). Morbidity and quality of life during thermotherapy using magnetic nanoparticles in locally recurrent prostate cancer: results of a prospective phase I trial. *Int. J. Hyperthermia* 23, 315–323.

Johannsen, M., Thiesen, B., Jordan, A., Taymoorian, K., Gneveckow, U., Waldofner, N., et al. (2005b). Magnetic fluid hyperthermia (MFH)reduces prostate cancer growth in the orthotopic Dunning R3327 rat model. *Prostate* 64, 283–292.

Johannsen, M., Thiesen, B., Wust, P., and Jordan, A. (2010). Magnetic nanoparticle hyperthermia for prostate cancer. *Int. J. Hyperthermia* 26, 790–795. doi: 10.3109/02656731003745740

Johnson, J. J., Bailey, H. H., and Mukhtar, H. (2010). Green tea polyphenols for prostate cancer chemoprevention: a translational perspective. *Phytomedicine* 17, 3–13. doi: 10.1016/j.phymed.2009.09.011

Joosten, S. C., Hamming, L., Soetekouw, P. M., Aarts, M. J., Veeck, J., van Engeland, M., et al. (2015). Resistance to sunitinib in renal cell carcinoma: from molecular mechanisms to predictive markers and future perspectives. *Biochim. Biophys. Acta* 1855, 1–16. doi: 10.1016/j.bbcan.2014.11.002

Jordan, A., Wust, P., Fahling, H., John, W., Hinz, A., and Felix, R. (1993). Inductive heating of ferrimagnetic particles and magnetic fluids: physical evaluation of their potential for hyperthermia. *Int. J. Hyperthermia* 9, 51–68. doi: 10.3109/02656739309061478

Jorgo, K., Agoston, P., Major, T., Takacsi-Nagy, Z., and Polgar, C. (2017). Transperineal gold marker implantation for image-guided external beam radiotherapy of prostate cancer : a single institution, prospective study. *Strahlenther. Onkol.* 193, 452–458. doi: 10.1007/s00066-017-1104-2

Juarranz, A., Jaen, P., Sanz-Rodriguez, F., Cuevas, J., and Gonzalez, S. (2008). Photodynamic therapy of cancer. Basic principles and applications. *Clin. Transl. Oncol.* 10, 148–154. doi: 10.1007/s12094-008-0172-2

Kim, D., Jeong, Y. Y., and Jon, S. (2010). A drug-loaded aptamer-gold nanoparticle bioconjugate for combined CT imaging and therapy of prostate cancer. *ACS Nano* 4, 3689–3696. doi: 10.1021/nn901877h

Kliton, J., Agoston, P., Szabo, Z., Major, T., and Polgar, C. (2014). [Use of gold radionuclide markers implanted into the prostate for image-guided radiotherapy in prostate cancer: side effects caused by the marker implantation]. *Magy. Onkol.* 58, 182–187.

Ko, Y. J., Canil, C. M., Mukherjee, S. D., Winquist, E., Elser, C., Eisen, A., et al. (2013). Nanoparticle albumin-bound paclitaxel for second-line treatment of

metastatic urothelial carcinoma: a single group, multicentre, phase 2 study. *Lancet Oncol.* 14, 769–776. doi: 10.1016/S1470-2045(13)70162-1

Kondylis, F. I., Demirci, S., Ladaga, L., Kolm, P., and Schellhammer, P. F. (2000). Outcomes after intravesical bacillus Calmette-Guerin are not affected by substaging of high grade T1 transitional cell carcinoma. *J. Urol.* 163, 1120–1123. doi: 10.1016/S0022-5347(05)67706-3

Krishnan, S., Diagaradjane, P., and Cho, S. H. (2010). Nanoparticle-mediated thermal therapy: evolving strategies for prostate cancer therapy. *Int. J. Hyperthermia* 26, 775–789. doi: 10.3109/02656736.2010.485593

Kulkarni, A. A., Vijaykumar, V. E., Natarajan, S. K., Sengupta, S., and Sabbisetti, V. S. (2016). Sustained inhibition of cMET-VEGFR2 signaling using liposome-mediated delivery increases efficacy and reduces toxicity in kidney cancer. *Nanomedicine* 12, 1853–1861. doi: 10.1016/j.nano.2016.04.002

Kumar, N. B., Pow-Sang, J., Egan, K. M., Spiess, P. E., Dickinson, S., Salup, R., et al. (2015). Randomized, placebo-controlled trial of green tea catechins for prostate cancer prevention. *Cancer Prev. Re.s* 8, 879–887. doi: 10.1158/1940-6207.CAPR-14-0324

Kumar, P., Kumar, A., and Lead, J. R. (2012). Nanoparticles in the Indian environment: known, unknowns and awareness. *Environ. Sci. Technol.* 46, 7071–7072. doi: 10.1021/es302308h

Larguinho, M., and Baptista, P. V. (2012). Gold and silver nanoparticles for clinical diagnostics - From genomics to proteomics. *J. Proteomics* 75, 2811–2823. doi: 10.1016/j.jprot.2011.11.007

Lee, J. J., Kang, J. A., Ryu, Y., Han, S. S., Nam, Y. R., Rho, J. K., et al. (2017). Genetically engineered and self-assembled oncolytic protein nanoparticles for targeted cancer therapy. *Biomaterials* 120, 22–31. doi: 10.1016/j.biomaterials.2016.12.014

Lee, M. H., Thomas, J. L., Chang, Y. C., Tsai, Y. S., Liu, B. D., and Lin, H. Y. (2016). Electrochemical sensing of nuclear matrix protein 22 in urine with molecularly imprinted poly(ethylene-co-vinyl alcohol) coated zinc oxide nanorod arrays for clinical studies of bladder cancer diagnosis. *Biosens. Bioelectron.* 79, 789–795. doi: 10.1016/j.bios.2016.01.005

Leulmi, S., Chauchet, X., Morcrette, M., Ortiz, G., Joisten, H., Sabon, P., et al. (2015). Triggering the apoptosis of targeted human renal cancer cells by the vibration of anisotropic magnetic particles attached to the cell membrane. *Nanoscale* 7, 15904–15914. doi: 10.1039/c5nr03518j

Leveillee, R. J., Castle, S. M., Gorbatiy, V., Salas, N., Narayanan, G., Morillo-Burgos, G., et al. (2013). Oncologic outcomes using real-time peripheral thermometry-guided radiofrequency ablation of small renal masses. *J. Endourol.* 27, 480–489. doi: 10.1089/end.2012.0305

Li, H., and Rothberg, L. (2005). Detection of specific sequences in RNA using differential adsorption of single-stranded oligonucleotides on gold nanoparticles. *Anal. Chem.* 77, 6229–6233. doi: 10.1021/ac050921y

Li, H., and Rothberg, L. J. (2004). Label-free colorimetric detection of specific sequences in genomic DNA amplified by the polymerase chain reaction. *J. Am. Chem. Soc.* 126, 10958–10961. doi: 10.1021/ja048749n

Lin, C. J., Lin, Y. L., Luh, F., Yen, Y., and Chen, R. M. (2016). Preclinical effects of CRLX101, an investigational camptothecin-containing nanoparticle drug conjugate, on treating glioblastoma multiforme via apoptosis and antiangiogenesis. *Oncotarget* 7, 42408–42421. doi: 10.18632/oncotarget.9878

Lin, T. Y., Li, Y., Liu, Q., Chen, J. L., Zhang, H., Lac, D., et al. (2016). Novel theranostic nanoporphyrins for photodynamic diagnosis and trimodal therapy for bladder cancer. *Biomaterials* 104, 339–351. doi: 10.1016/j.biomaterials.2016.07.026

Liu, D., Huang, X., Wang, Z., Jin, A., Sun, X., Zhu, L., et al. (2013). Gold nanoparticle-based activatable probe for sensing ultralow levels of prostate-specific antigen. *ACS Nano* 7, 5568–5576. doi: 10.1021/nn401837q

Liu, J., Boonkaew, B., Arora, J., Mandava, S. H., Maddox, M. M., Chava, S., et al. (2015a). Comparison of sorafenib-loaded poly (lactic/glycolic) acid and DPPC liposome nanoparticles in the in vitro treatment of renal cell carcinoma. *J. Pharm. Sci.* 104, 1187–1196. doi: 10.1002/jps.24318

Liu, J., Boonkaew, B., Mandava, S. H., Arora, J., Maddox, M., Chava, S., et al. (2015b). In vitro performance of sorafenib-loaded plga and liposome nanoparticles as a delivery system in the treatment of renal cell carcinoma. *J. Urol.* 193, E454–E455. doi: 10.1016/j.juro.2015.02.751

Lodde, M., Mian, C., Mayr, R., Comploj, E., Trenti, E., Melotti, R., et al. (2014). Recurrence and progression in patients with non-muscle invasive bladder cancer: prognostic models including multicolor fluorescence in situ hybridization molecular grading. *Int. J. Urol.* 21, 968–972. doi: 10.1111/iju.12509

Long, Q., Lin, T.-Y., Huang, Y., Li, X., Ma, A.-H., Zhang, H., et al. (2018). Image-guided photo-therapeutic nanoporphyrin synergized HSP90 inhibitor in patient-derived xenograft bladder cancer model. *Nanomedicine* 14, 789–799. doi: 10.1016/j.nano.2017.12.014

Lu, C., Li, J., Xu, K., Yang, C., Wang, J., Han, C., et al. (2014). Fabrication of mAb G250-SPIO molecular magnetic resonance imaging nanoprobe for the specific detection of renal cell carcinoma in vitro. *PLoS One* 9:e101898. doi: 10.1371/journal.pone.0101898

Lu, L., Li, K., Mao, Y. H., Qu, H., Yao, B., Zhong, W. W., et al. (2017). Gold-chrysophanol nanoparticles suppress human prostate cancer progression through inactivating AKT expression and inducing apoptosis and ROS generation in vitro and in vivo. *Int. J. Oncol.* 51, 1089–1103. doi: 10.3892/ijo.2017.4095

Lu, Z., Yeh, T. K., Wang, J., Chen, L., Lyness, G., Xin, Y., et al. (2011). Paclitaxel gelatin nanoparticles for intravesical bladder cancer therapy. *J. Urol.* 185, 1478–1483. doi: 10.1016/j.juro.2010.11.091

Lusch, A., Graversen, J. A., Liss, M. A., and Landman, J. (2013). Ablative techniques: radiofrequency and cryotherapy, which is the best? *Arch. Esp. Urol.* 66, 71–78.

Martin, D. T., Hoimes, C. J., Kaimakliotis, H. Z., Cheng, C. J., Zhang, K., Liu, J., et al. (2013). Nanoparticles for urothelium penetration and delivery of the histone deacetylase inhibitor belinostat for treatment of bladder cancer. *Nanomedicine* 9, 1124–1134. doi: 10.1016/j.nano.2013.05.017

Martin, D. T., Steinbach, J. M., Liu, J., Shimizu, S., Kaimakliotis, H. Z., Wheeler, M. A., et al. (2014). Surface-modified nanoparticles enhance transurothelial penetration and delivery of survivin siRNA in treating bladder cancer. *Mol. Cancer Ther.* 13, 71–81. doi: 10.1158/1535-7163.MCT-13-0502

McKiernan, J. M., Barlow, L. J., Laudano, M. A., Mann, M. J., Petrylak, D. P., and Benson, M. C. (2011). A phase I trial of intravesical nanoparticle albumin-bound paclitaxel in the treatment of bacillus Calmette-Guerin refractory nonmuscle invasive bladder cancer. *J. Urol.* 186, 448–451. doi: 10.1016/j.juro.2011.03.129

Menter, D. G., Patterson, S. L., Logsdon, C. D., Kopetz, S., Sood, A. K., and Hawk, E. T. (2014). Convergence of nanotechnology and cancer prevention: are we there yet? *Cancer Prev. Res.* 7, 973–992. doi: 10.1158/1940-6207.CAPR-14-0079

Mieszawska, A. J., Mulder, W. J., Fayad, Z. A., and Cormode, D. P. (2013). Multifunctional gold nanoparticles for diagnosis and therapy of disease. *Mol. Pharm.* 10, 831–847. doi: 10.1021/mp3005885

Mueller-Lisse, U. G., Scher, B., Scherr, M. K., and Seitz, M. (2008). Functional imaging in penile cancer: PET/computed tomography, MRI, and sentinel lymph node biopsy. *Curr. Opin. Urol.* 18, 105–110. doi: 10.1097/MOU.0b013e3282f151fd

Muthu, M., Cheriyan, V. T., and Rishi, A. K. (2015). CARP-1/CCAR1: a biphasic regulator of cancer cell growth and apoptosis. *Oncotarget* 6, 6499–6510. doi: 10.18632/oncotarget.3376

Nakamura, T., Fukiage, M., Higuchi, M., Nakaya, A., Yano, I., Miyazaki, J., et al. (2014). Nanoparticulation of BCG-CWS for application to bladder cancer therapy. *J. Control. Release* 176, 44–53. doi: 10.1016/j.jconrel.2013.12.027

Nakamura, T., Noma, Y., Sakurai, Y., and Harashima, H. (2017). Modifying cationic liposomes with cholesteryl-PEG prevents their aggregation in human urine and enhances cellular uptake by bladder cancer cells. *Biol. Pharm. Bull.* 40, 234–237. doi: 10.1248/bpb.b16-00770

Nergiz, S. Z., Gandra, N., Tadepalli, S., and Singamaneni, S. (2014). Multifunctional hybrid nanopatches of graphene oxide and gold nanostars for ultraefficient photothermal cancer therapy. *ACS Appl. Mater. Interfaces* 6, 16395–16402. doi: 10.1021/am504795d

Nikzad, S., Mahmoudi, G., Amini, P., Baradaran-Ghahfarokhi, M., Vahdat-Moaddab, A., Sharafi, S. M., et al. (2017). Effects of radiofrequency radiation in the presence of gold nanoparticles for the treatment of renal cell carcinoma. *J. Renal Inj. Prev.* 6, 103–108. doi: 10.15171/jrip.2017.20

Nossier, A. I., Eissa, S., Ismail, M. F., Hamdy, M. A., and Azzazy, H. M. (2014). Direct detection of hyaluronidase in urine using cationic gold nanoparticles: a potential diagnostic test for bladder cancer. *Biosens. Bioelectron.* 54, 7–14. doi: 10.1016/j.bios.2013.10.024

Oh, M. H., Yu, J. H., Kim, I., and Nam, Y. S. (2015). Genetically programmed clusters of gold nanoparticles for cancer cell-targeted photothermal therapy. *ACS Appl. Mater. Interfaces* 7, 22578–22586. doi: 10.1021/acsami.5b07029

Ojha, T., Pathak, V., Shi, Y., Hennink, W. E., Moonen, C. T. W., Storm, G., et al. (2017). Pharmacological and physical vessel modulation strategies to improve EPR-mediated drug targeting to tumors. *Adv. Drug Deliv. Rev.* 119, 44–60. doi: 10.1016/j.addr.2017.07.007

Olivo, M., Fu, C. Y., Raghavan, V., and Lau, W. K. (2012). New frontier in hypericin-mediated diagnosis of cancer with current optical technologies. *Ann. Biomed. Eng.* 40, 460–473. doi: 10.1007/s10439-011-0462-7

Palchetti, S., Pozzi, D., Capriottic, A. L., La Barbera, G., Chiozzi, R. Z., Digiacomo, L., et al. (2017). Influence of dynamic flow environment on nanoparticle-protein corona: From protein patterns to uptake in cancer cells. *Colloid Surface B* 153, 263–271. doi: 10.1016/j.colsurfb.2017.02.037

Pannerec-Varna, M., Ratajczak, P., Bousquet, G., Ferreira, I., Leboeuf, C., Boisgard, R., et al. (2013). In vivo uptake and cellular distribution of gold nanoshells in a preclinical model of xenografted human renal cancer. *Gold Bull.* 46, 257–265. doi: 10.1007/s13404-013-0115-8

Park, S., Anderson, J. K., Matsumoto, E. D., Lotan, Y., Josephs, S., and Cadeddu, J. A. (2006). Radiofrequency ablation of renal tumors: intermediate-term results. *J. Endourol.* 20, 569–573. doi: 10.1089/end.2006.20.569

Patra, S., Roy, E., Madhuri, R., and Sharma, P. K. (2015). Nano-iniferter based imprinted sensor for ultra trace level detection of prostate-specific antigen in both men and women. *Biosens. Bioelectron.* 66, 1–10. doi: 10.1016/j.bios.2014.10.076

Rassweiler, J., Rassweiler, M. C., Kenngott, H., Frede, T., Michel, M. S., Alken, P., et al. (2013). The past, present and future of minimally invasive therapy in urology: a review and speculative outlook. *Minim. Invasive Ther. Allied Technol.* 22, 200–209. doi: 10.3109/13645706.2013.816323

Ray, E. R., Chatterton, K., Khan, M. S., Chandra, A., Thomas, K., Dasgupta, P., et al. (2010). Hexylaminolaevulinate fluorescence cystoscopy in patients previously treated with intravesical bacille Calmette-Guerin. *BJU Int.* 105, 789–794. doi: 10.1111/j.1464-410X.2009.08839.x

Salvador-Morales, C., Gao, W., Ghatalia, P., Murshed, F., Aizu, W., Langer, R., et al. (2009). Multifunctional nanoparticles for prostate cancer therapy. *Expert Rev. Anticancer Ther.* 9, 211–221. doi: 10.1586/14737140.9.2.211

Sanna, V., Pintus, G., Roggio, A. M., Punzoni, S., Posadino, A. M., Arca, A., et al. (2011). Targeted biocompatible nanoparticles for the delivery of (-)-epigallocatechin 3-gallate to prostate cancer cells. *J. Med. Chem.* 54, 1321–1332. doi: 10.1021/jm1013715

Sanna, V., and Sechi, M. (2012). Nanoparticle therapeutics for prostate cancer treatment. *Nanomedicine* 8(Suppl. 1), S31–S36. doi: 10.1016/j.nano.2012.05.009

Sanna, V., Siddiqui, I. A., Sechi, M., and Mukhtar, H. (2013). Nanoformulation of natural products for prevention and therapy of prostate cancer. *Cancer Lett.* 334, 142–151. doi: 10.1016/j.canlet.2012.11.037

Schroeder, A., Heller, D. A., Winslow, M. M., Dahlman, J. E., Pratt, G. W., Langer, R., et al. (2012). Treating metastatic cancer with nanotechnology. *Nat. Rev. Cancer* 12, 39–50. doi: 10.1038/nrc3180

Siegel, R. L., Miller, K. D., and Jemal, A. (2018). Cancer statistics, 2018. *CA Cancer J. Clin.* 68, 7–30. doi: 10.3322/caac.21442

Skubitz, K. M. (2002). Phase II trial of pegylated-liposomal doxorubicin (Doxil) in renal cell cancer. *Invest. New Drugs* 20, 101–104. doi: 10.1023/A:1014428720551

Sreekanth, T. V., Pandurangan, M., Dillip, G. R., Kim, D. H., and Lee, Y. R. (2016). Toxicity and efficacy of CdO nanostructures on the MDCK and Caki-2 cells. *J. Photochem. Photobiol. B* 164, 174–181. doi: 10.1016/j.jphotobiol.2016.09.028

Stern, J. M., Stanfield, J., Kabbani, W., Hsieh, J. T., and Cadeddu, J. A. (2008). Selective prostate cancer thermal ablation with laser activated gold nanoshells. *J. Urol.* 179, 748–753. doi: 10.1016/j.juro.2007.09.018

Stern, J. M., Stanfield, J., Lotan, Y., Park, S., Hsieh, J. T., and Cadeddu, J. A. (2007). Efficacy of laser-activated gold nanoshells in ablating prostate cancer cells in vitro. *J. Endourol.* 21, 939–943. doi: 10.1089/end.2007.0437

Stone, L. (2016). Kidney cancer: exosome transmission of sunitinib resistance. *Nat. Rev. Urol.* 13:297. doi: 10.1038/nrurol.2016.88

Stuart, E. C., Scandlyn, M. J., and Rosengren, R. J. (2006). Role of epigallocatechin gallate (EGCG) in the treatment of breast and prostate cancer. *Life Sci.* 79, 2329–2336. doi: 10.1016/j.lfs.2006.07.036

Sudimack, J., and Lee, R. J. (2000). Targeted drug delivery via the folate receptor. *Adv. Drug Deliv. Rev.* 41, 147–162. doi: 10.1016/S0169-409X(99)00062-9

Sun, C., Lee, J. S., and Zhang, M. (2008). Magnetic nanoparticles in MR imaging and drug delivery. *Adv. Drug Deliv. Rev.* 60, 1252–1265. doi: 10.1016/j.addr.2008.03.018

Tabatabaei, S., Harisinghani, M., and Mcdougal, W. S. (2005). Regional lymph node staging using lymphotropic nanoparticle enhanced magnetic resonance imaging with ferumoxtran-10 in patients with penile cancer. *J. Urol.* 174, 923–927. doi: 10.1097/01.ju.0000170234.14519.19

Thaxton, C. S., Elghanian, R., Thomas, A. D., Stoeva, S. I., Lee, J. S., Smith, N. D., et al. (2009). Nanoparticle-based bio-barcode assay redefines "undetectable" PSA and biochemical recurrence after radical prostatectomy. . *Proc. Natl. Acad. Sci. U.S.A.* 106, 18437–18442. doi: 10.1073/pnas.0904719106

Vila-Caballer, M., Codolo, G., Munari, F., Malfanti, A., Fassan, M., Rugge, M., et al. (2016). A pH-sensitive stearoyl-PEG-poly(methacryloyl sulfadimethoxine)-decorated liposome system for protein delivery: an application for bladder cancer treatment. *J. Control. Release* 238, 31–42. doi: 10.1016/j.jconrel.2016.07.024

Voruganti, S., Qin, J. J., Sarkar, S., Nag, S., Walbi, I. A., Wang, S., et al. (2015). Oral nano-delivery of anticancer ginsenoside 25-OCH3-PPD, a natural inhibitor of the MDM2 oncogene: nanoparticle preparation, characterization, in vitro and in vivo anti-prostate cancer activity, and mechanisms of action. *Oncotarget* 6, 21379–21394. doi: 10.18632/oncotarget.4091

Wang, D., Fei, B., Halig, L. V., Qin, X., Hu, Z., Xu, H., et al. (2014). Targeted iron-oxide nanoparticle for photodynamic therapy and imaging of head and neck cancer. *ACS Nano* 8, 6620–6632. doi: 10.1021/nn501652j

Wang, X., Yang, L., Chen, Z. G., and Shin, D. M. (2008). Application of nanotechnology in cancer therapy and imaging. *CA Cancer J. Clin.* 58, 97–110. doi: 10.3322/CA.2007.0003

Williams, R. M., Jaimes, E. A., and Heller, D. A. (2016). Nanomedicines for kidney diseases. *Kidney Int.* 90, 740–745. doi: 10.1016/j.kint.2016.03.041

Xu, K., Ding, Q., Fang, Z., Zheng, J., Gao, P., Lu, Y., et al. (2010). Silencing of HIF-1alpha suppresses tumorigenicity of renal cell carcinoma through induction of apoptosis. *Cancer Gene Ther.* 17, 212–222. doi: 10.1038/cgt.2009.66

Yan, X., Al-Hayek, S., Huang, H., Zhu, Z., Zhu, W., and Guo, H. (2013). Photodynamic effect of 5-aminolevulinic acid-loaded nanoparticles on bladder cancer cells: a preliminary investigation. *Scand. J. Urol.* 47, 145–151. doi: 10.3109/00365599.2012.713000

Yang, Q., Wang, Y., Yang, Q., Gao, Y., Duan, X., Fu, Q., et al. (2017). Cuprous oxide nanoparticles trigger ER stress-induced apoptosis by regulating copper trafficking and overcoming resistance to sunitinib therapy in renal cancer. *Biomaterials* 146, 72–85. doi: 10.1016/j.biomaterials.2017.09.008

Yang, X., Stein, E. W., Ashkenazi, S., and Wang, L. V. (2009). Nanoparticles for photoacoustic imaging. *Wiley Interdiscip. Rev. Nanomed. Nanobiotechnol.* 1, 360–368. doi: 10.1002/wnan.42

Yu, Z., Schmaltz, R. M., Bozeman, T. C., Paul, R., Rishel, M. J., Tsosie, K. S., et al. (2013). Selective tumor cell targeting by the disaccharide moiety of bleomycin. *J. Am. Chem. Soc.* 135, 2883–2886. doi: 10.1021/ja311090e

Yuan, Z. X., Mo, J., Zhao, G., Shu, G., Fu, H. L., and Zhao, W. (2016). Targeting strategies for renal cell carcinoma: from renal cancer cells to renal cancer stem cells. *Front. Pharmacol.* 7:423. doi: 10.3389/fphar.2016.00423

Zhang, T., Xue, X., He, D., and Hsieh, J. T. (2015). A prostate cancer-targeted polyarginine-disulfide linked PEI nanocarrier for delivery of microRNA. *Cancer Lett.* 365, 156–165. doi: 10.1016/j.canlet.2015.05.003

Zrazhevskiy, P., and Gao, X. (2013). Quantum dot imaging platform for single-cell molecular profiling. *Nat. Commun.* 4:1619. doi: 10.1038/ncomms2635

Conflict of Interest Statement: The authors declare that the research was conducted in the absence of any commercial or financial relationships that could be construed as a potential conflict of interest.

frontiers in Pharmacology

ORIGINAL RESEARCH
published: 13 July 2018
doi: 10.3389/fphar.2018.00763

Cytotoxicity of InP/ZnS Quantum Dots With Different Surface Functional Groups Toward Two Lung-Derived Cell Lines

*Ting Chen[1,2], Li Li[1,2], Gaixia Xu[2], Xiaomei Wang[1], Jie Wang[1], Yajing Chen[1], Wenxiao Jiang[1], Zhiwen Yang[1] and Guimiao Lin[1]**

[1] Department of Physiology, School of Basic Medical Sciences, Shenzhen University Health Sciences Center, Shenzhen, China, [2] Key Laboratory of Optoelectronics Devices and Systems of Ministry of Education, College of Optoelectronic Engineering, Shenzhen University, Shenzhen, China

Although InP/ZnS quantum dots (QDs) have emerged as a presumably less hazardous alternative to cadmium-based QDs, their toxicity has not been fully understood. In this work, we report the cytotoxicity of InP/ZnS QDs with different surface groups (NH_2, COOH, OH) toward two lung-derived cell lines. The diameter and the spectra of InP/ZnS QDs were characterized and the hydrodynamic size of QDs in aqueous solution was compared. The confocal laser scanning microscopy was applied to visualize the labeling of QDs for human lung cancer cell HCC-15 and Alveolar type II epithelial cell RLE-6TN. The flow cytometry was used to confirm qualitatively the uptake efficiency of QDs, the cell apoptosis and ROS generation, respectively. The results showed that in deionized water, InP/ZnS-OH QDs were easier to aggregate, and the hydrodynamic size was much greater than the other InP/ZnS QDs. All these InP/ZnS QDs were able to enter the cells, with higher uptake efficiency for InP/ZnS-COOH and InP/ZnS-NH_2 at low concentration. High doses of InP/ZnS QDs caused the cell viability to decrease, and InP/ZnS-COOH QDs and InP/ZnS-NH_2 QDs appeared to be more toxic than InP/ZnS-OH QDs. In addition, all these InP/ZnS QDs promoted cell apoptosis and intracellular ROS generation after co-cultured with cells. These results suggested that appropriate concentration and surface functional groups should be optimized when InP/ZnS QDs are utilized for biological imaging and therapeutic purpose in the future.

Keywords: InP/ZnS quantum dots, cytotoxicity, cellular uptake, cell apoptosis, ROS generation

OPEN ACCESS

Edited by:
Qingxin Mu,
University of Washington,
United States

Reviewed by:
Nanasaheb D. Thorat,
University of Limerick, Ireland
Hongyu Zhou,
Jinan University, China
Debasis Nayak,
Government of Odisha, India

***Correspondence:**
Guimiao Lin
gmlin@szu.edu.cn

Specialty section:
This article was submitted to Cancer Molecular Targets and Therapeutics, a section of the journal Frontiers in Pharmacology

Received: *28 April 2018*
Accepted: *22 June 2018*
Published: *13 July 2018*

Citation:
Chen T, Li L, Xu G, Wang X, Wang J, Chen Y, Jiang W, Yang Z and Lin G (2018) Cytotoxicity of InP/ZnS Quantum Dots With Different Surface Functional Groups Toward Two Lung-Derived Cell Lines. Front. Pharmacol. 9:763. doi: 10.3389/fphar.2018.00763

INTRODUCTION

QuantumDot (QD), also known as semiconductor nanometer microcrystal, is currently one of the most popular nano materials (Pohanka, 2017) owing to its unique optical features, such as wide absorption spectrum, narrow emission spectrum, long fluorescence lifetime, high intensity and strong resistance to photobleaching, etc. (Bruchez et al., 1998). QDs has been developed rapidly and widely used in biomedical research such as biological sensing, imaging, food quality control and biochip technology (Lin et al., 2015b; Peng et al., 2018; Zhou et al., 2018). However, more QDs nanoparticles are entering into the environment with the increasing development of QDs, more QD exposure hazards from product industries and research institutions resulting in toxicity *in vitro*

and *in vivo* are increased. Thus, serious concerns have been raised about the biosafety of QDs due to limited understanding of the toxicological behavior of quantum dots (QDs).

The impacts of QDs on the environment and human being have been put forward recently by many scientists and organizations (Manshian et al., 2016, 2017; Liu et al., 2017). The toxicity of QDs has been evaluated using multiple *in vitro* cell models including human bronchial epithelial cells (Zheng et al., 2018), HepG2 cell line (Paesano et al., 2016), macrophages and lymphocytes (Wang X. et al., 2016) and *in vivo* animal models such as mice (Liu et al., 2017), rat (Ma-Hock et al., 2012), and non-human primate (Ye et al., 2012). So far, the collected data is still inconclusive because many factors are responsible for the toxicity of QDs. QD-induced toxicity is closely related to their surface properties (including shell, ligand and surface modifications), size, biological model, and exposure route and time (Oh et al., 2016).

Although some progress has been made in the toxicity study on QDs, most of the research still focused on cadmium-containing QDs, such as CdTe, CdS, and CdSe. Studies have shown that the release of cadmium ion from cadmium-containing QDs caused damage to cells (Li et al., 2009) or organs (Wang M. et al., 2016). The risk of cadmium exposure and the toxicity of cadmium-containing QDs (Mo et al., 2017) have initiated a heated debate over whether or not to keep on pursuing the translation of QDs into clinical research and applications.

In order to overcome this problem, several strategies have been proposed, such as the generation of cadmium-free QD dots. InP/ZnS (indium phosphide/zinc sulfide) nanocrystals are the most commonly used core/shell cadmium-free QDs. InP/ZnS QDs have appeared to be a less hazardous nanocrystal in comparison with cadmium-containing nanoparticles (Brunetti et al., 2013) since they are free of cadmium and also have greater degree of covalent bonding, comparing to those made up of group II–VI elements. Chibli et al found a small amount of hydroxyl radical formed under visible illumination of biocompatible InP/ZnS QDs, comparable to what is seen with CdTe, indicating that InP/ZnS QDs are a useful alternative to cadmium-containing QDs (Chibli et al., 2011). Previously, we have systematically studied the *in vivo* biodistribution and long term toxicity of InP/ZnS QDs in BALB/c mice (Lin et al., 2015a). We found that accumulation of indium element from injected InP/ZnS QDs still remained at major organs even after 84 days of injection. But hematology, blood biochemistry, and histological analysis indicated that there are no acute toxic effects.

Although InP/ZnS QDs have emerged as a presumably less hazardous alternative to cadmium-based particles, their toxicity has not been fully observed. In comparison to cadmium-containing QDs, the understanding of InP QD toxicity is still in its infancy stage, and little is known about their toxicological effects (Soenen et al., 2014). Lung is the first exposed target for inhaled nanoparticles, and it also receives the entire cardiac output, which makes the risk of lung injury high. Previously, Ho et al reported that pulmonary exposure to cadmium-based QDs will result in persistent inflammation and granuloma formation in the mouse lung (Ho et al., 2013). Furthermore, surface coating to influence the disposition and toxicity of QDs in animal lungs (Roberts et al., 2013). Injures of lung will seriously damage the respiratory function and cause serious lung disease. Study of cytotoxicity toward these two lung-derived cell lines help to understand the impact of InP/ZnS QDs on respiratory function.

In this study, we investigated the *in vitro* toxicity of InP/ZnS terminated with different surface groups (COOH, NH_2 and OH respectively) on two lung-derived cell lines, human lung cancer cell HCC-15 and Alveolar epithelial type II (AEII) cell RLE-6TN, which are common cell models for studying respiratory toxicity of nanoparticles (Zienolddiny et al., 2000; Schwotzer et al., 2018). AEII cells are an important component of the respiratory defense system against foreign material, including nanoparticles. They are responsible for production and recycling of lung surfactant, play a role in turnover of the alveolar epithelia, and bear the ability to transform into alveolar epithelial type I (AEI) cells (e.g., for replacement of damaged cells) (Schwotzer et al., 2018). HCC-15 cells is immortalized cell lines derived from squamous cell lung cancer, which is the second most common type of lung cancer, usually originating in the large airways in the central part of the lungs (Wu et al., 2013). We found that all the QDs could enter the cells at similar percentage when the dose reached 20 μg/mL. While at the dose of 2 μg/mL, the uptake efficiency of QDs with hydroxyl was relatively lower than the others. All these QDs caused the cell proliferation inhibition, cell apoptosis and ROS generation. These results suggested that we should optimize the concentration of quantum dot within a safe range while using InP/ZnS QDs as optical probes for cell imaging or other clinical applications.

MATERIALS AND METHODS

Preparation and Characterization of QDs

InP/ZnS QDs were purchased from Najingtech Company. The morphology images of InP/ZnS QDs dispersed in toluene were obtained with a transmission electron microscope (TEM) (Tecnai G2 F20 S-TWIN, FEI, United States) operating at an accelerating voltage of 200 kV at room temperature. When inversed from oil phase to aqueous phase, InP/ZnS QDs was coated with a polymer layer and terminated with carboxyl, hydroxyl and amino surface groups respectively. Before experiment, the content of indium element in the three QDs solutions was measured by ICP-MS (7500C1, Agilent, United States) analysis and the result was normalized to equalize the concentrations of the three QDs. The absorption spectra of InP/ZnS QDs were measured by a UV-Vis spectrophotometer (Cary 5000, Agilent, United States). The photoluminescence emission spectra were determined by a Fluorescence spectrophotometer (F-4600, Hitachi, Japan) with an excitation wavelength of 400 nm. The hydrodynamic size distribution of InP/ZnS QDs was obtained using a dynamic light scattering (DLS) machine (Zetasizer Nano ZS, Malvern, United Kingdom).

Cell Culture

The human lung cancer cell HCC-15 and Alveolar type II epithelial cell RLE-6TN were obtained from American Type Culture Collection (ATCC) and cultured in Dulbecco's Modified

Eagle's Medium (DMEM, Gibco, United States) supplemented with 10% fetal bovine serum (FBS, Gibco, United States) and 100 U penicillin/streptomycin (Gibco, United States). All cells were cultured at 37°C in humidified atmosphere with 5% CO_2.

Confocal Laser Scanning Microscopy

The day before imaging, cells were planted onto 35 mm confocal dishes (Thermo Scientific™ Nunc™, United States) to give 30–50% density. Cells were left untreated or co-incubated with 2 μg/mL InP/ZnS QDs. After 4–6 h of incubation, the culture medium was removed and cells were washed with phosphate-buffered saline (PBS) twice, fixed with 4% paraformaldehyde for 15 min. Then the paraformaldehyde solution was abandoned and the cell nucleuses were stained with DAPI for 5 min. The confocal images were obtained using a laser scanning confocal microscope (LSCM, TCS SP5, Leica, DEU).

Uptake Efficiency Detected by Flow Cytometry

The day before experiment, cells were seeded into 6-well plates in medium to give 30–50% density. Cells were left untreated or co-incubated with InP/ZnS QDs (2 and 20 μg/mL, respectively). After 4–6 h of incubation, the culture medium was removed and cells were washed with PBS, harvested by trypsin (Gibco). After centrifugation, cells were resuspended in 300 μL PBS solutions and analyzed immediately by a flow cytometer (FACS Aria II, BD, United States).

Cell Viability Detected by MTT Assay

The cell viability of HCC-15 and RLE-6TN cells were evaluated by MTT (Sigma-Aldrich, United States) assay. Cells were seeded in 96-well plates (5×10^3 cells/well) and incubated with different concentrations of InP/ZnS QDs for 24 or 48 h. The MTT solution (5 mg/mL) was added into cells for 10 μL/well. After 4 h incubation, the culture medium was removed carefully and DMSO (150 μL/well) was added to sufficiently dissolve the blue crystals. The plates were gently shaken for 5 min and absorbance was measured with a microplate reader (Multiskan FC, Thermo Fisher, Finland) at a wavelength of 570 nm. The cell viability was calculated by normalizing the absorbance of the sample well against that of the control well and expressed as a percentage, assigning the cell viability of non-treated cells as 100%.

Cell Apoptosis Detected by Flow Cytometry

The cell apoptosis was measured by Annexin V-FITC Apoptosis Detection Kit (BD Pharmingen®, United States). The day before assay, cells were planted onto 6-well plates. For apoptosis detection, cells were left untreated or exposed to InP/ZnS QDs for 24 or 48 h. All cells were dissociated with trypsin solution (Gibco, United States) without EDTA and collected by centrifugation at 1,500 rpm for 5 min. After washed with pre-cooling PBS, cells were resuspended in 300 μL 1 × binding buffer. Five microliter Annexin V-FITC solution was added into cells and cells were incubated for 15 min at room temperature and protected from light. The signals of FITC fluorescence were detected by a flow cytometer (FACSAria II, BD, United States).

Detection of Reactive Oxygen Species (ROS)

The production of cellular ROS was detected by the carboxy-dichlorofluorescein diacetate (carboxy-DCFH-DA) assay kit (Sigma-Aldrich, United States). Cells were planted onto 6-well plates and left untreated or treated with InP/ZnS QDs. After 4–6 h of stimulation, the culture medium was removed and 10 μM DCFH-DA solutions was added into cells to load the probe. Cells were incubated for 20 min at 37°C with 5% CO_2 and washed with serum-free medium twice to remove the extra DCFH-DA. Cells were collected and analyzed immediately by a flow cytometer (FACS Calibur, BD, United States).

Statistical Analysis

All experimental data were expressed as mean ± standard deviation (SD). Multigroup comparisons of the means were carried out by one-way analysis of variance (ANOVA) test. Dunnett's test was used to compare the differences between the experimental groups and the control group. All statistical calculations were performed with the SPSS 11.0 software package. The statistical significance for all tests was set at $p < 0.05$.

RESULTS

Characterization of InP/ZnS QDs

The TEM image of InP/ZnS QDs before surface modifications was shown in **Figure 1A**. It demonstrated a relatively monodispersed size distribution with averaged size of ∼5 ± 0.5 nm. After coating with a polymer layer and terminated with carboxyl, hydroxyl or amino surface groups, we performed the FT-IR spectra analysis of the QDs which indicating successful functionalization of the three surface groups (Supplementary Figure S1). The InP/ZnS QDs modified with carboxyl, hydroxyl and amino groups, respectively, exhibited consistent absorption spectra with the same absorption peak around 580 nm (**Figure 1B**). Under excited by 400 nm light source, the three QDs all exhibited relatively symmetrical photoluminescence spectra with the emission peak around 625 nm (**Figure 1C**). The average hydrodynamic diameters of the aqueous QDs characterized by DLS technique were 9.267 ± 2.769 nm, 11.70 ± 3.031 nm and 97.79 ± 31.74 nm for InP/ZnS-COOH QDs, InP/ZnS-NH_2 QDs and InP/ZnS-OH QDs, respectively (**Figures 1D–F**). Accordingly, the zeta potentials of these QDs were −43.1 ± 8.13 mV, −54.6 ± 7.06 mV, −40.5 ± 8.33 mV, respectively.

Uptake of Quantum Dots by Lung-Derived Cells

The confocal images of HCC-15 and RLE-6TN cells treated with the 2 μg/mL QDs for 4 h were shown in **Figure 2**. Compared with the control group, obvious red signals from QDs were observed around the cell nucleuses in the QDs treated groups,

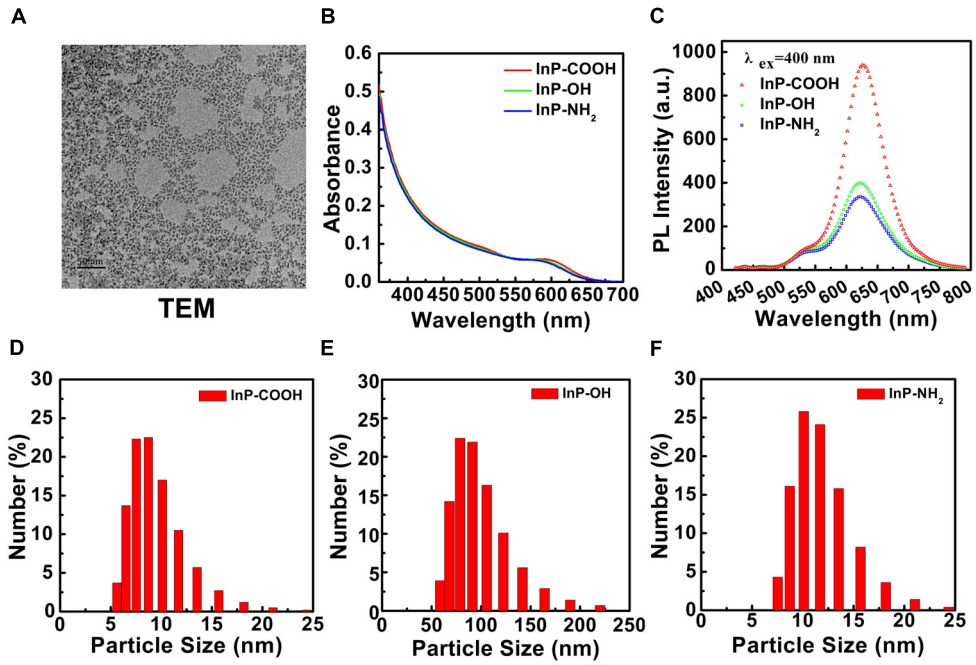

FIGURE 1 | Characterization of InP/ZnS QDs with various surface functional groups. **(A)** TEM image of InP/ZnS QDs dispersed in toluene. Scale bar: 50 nm. **(B)** Absorption spectra and **(C)** photoluminescence (PL) spectra of InP/ZnS-COOH QDs, InP/ZnS-OH QDs, and InP/ZnS-NH_2 QDs, respectively. Hydrodynamic size distributions of **(D)** InP/ZnS-COOH QDs, **(E)** InP/ZnS-OH QDs, and **(F)** InP/ZnS-NH_2 QDs dispersed in deionized water.

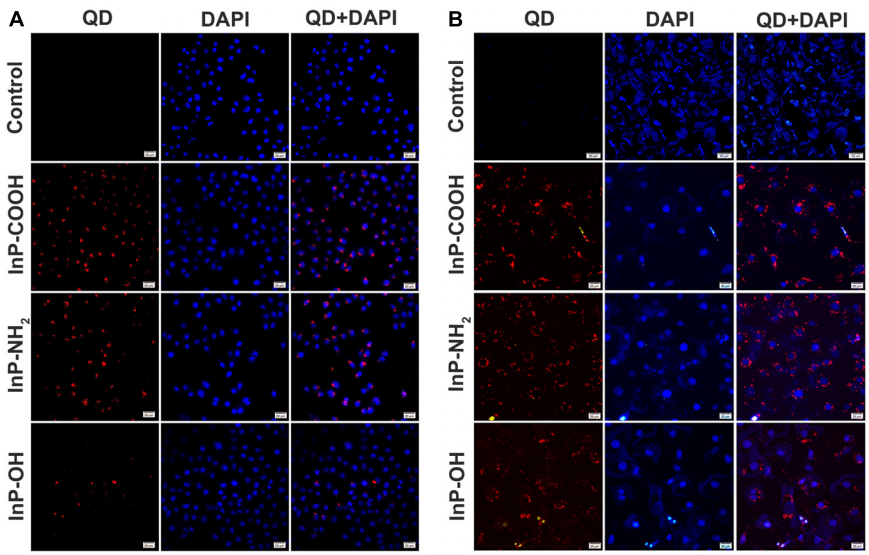

FIGURE 2 | Fluorescence images of **(A)** HCC-15 and **(B)** RLE-6TN cells treated with (i) Blank, (ii) InP/ZnS-COOH, (iii) InP/ZnS-NH_2, and (iv) InP/ZnS-OH QDs for 4 h. The cell nucleuses are stained with DAPI (in blue), and the signals from QDs are in red. Scale bar: 20 μm.

which indicated that the QDs could be taken up by human lung cancer cell HCC-15 and Alveolar type II epithelial cell RLE-6TN. It can also be clearly seen that the intake of InP/ZnS-OH QDs is relatively lower than InP/ZnS-COOH QDs and InP/ZnS-NH_2 QDs.

To further quantitatively evaluate the uptake efficiency of QDs by HCC-15 and RLE-6TN cells, flow cytometry analysis was performed (**Figure 3**). For HCC-15 cells treated with 2 μg/mL QDs, the uptake efficiency of InP/ZnS-COOH, InP/ZnS-NH_2 and InP/ZnS-OH are 87.4 ± 2.67%, 89.0 ± 2.15%, and

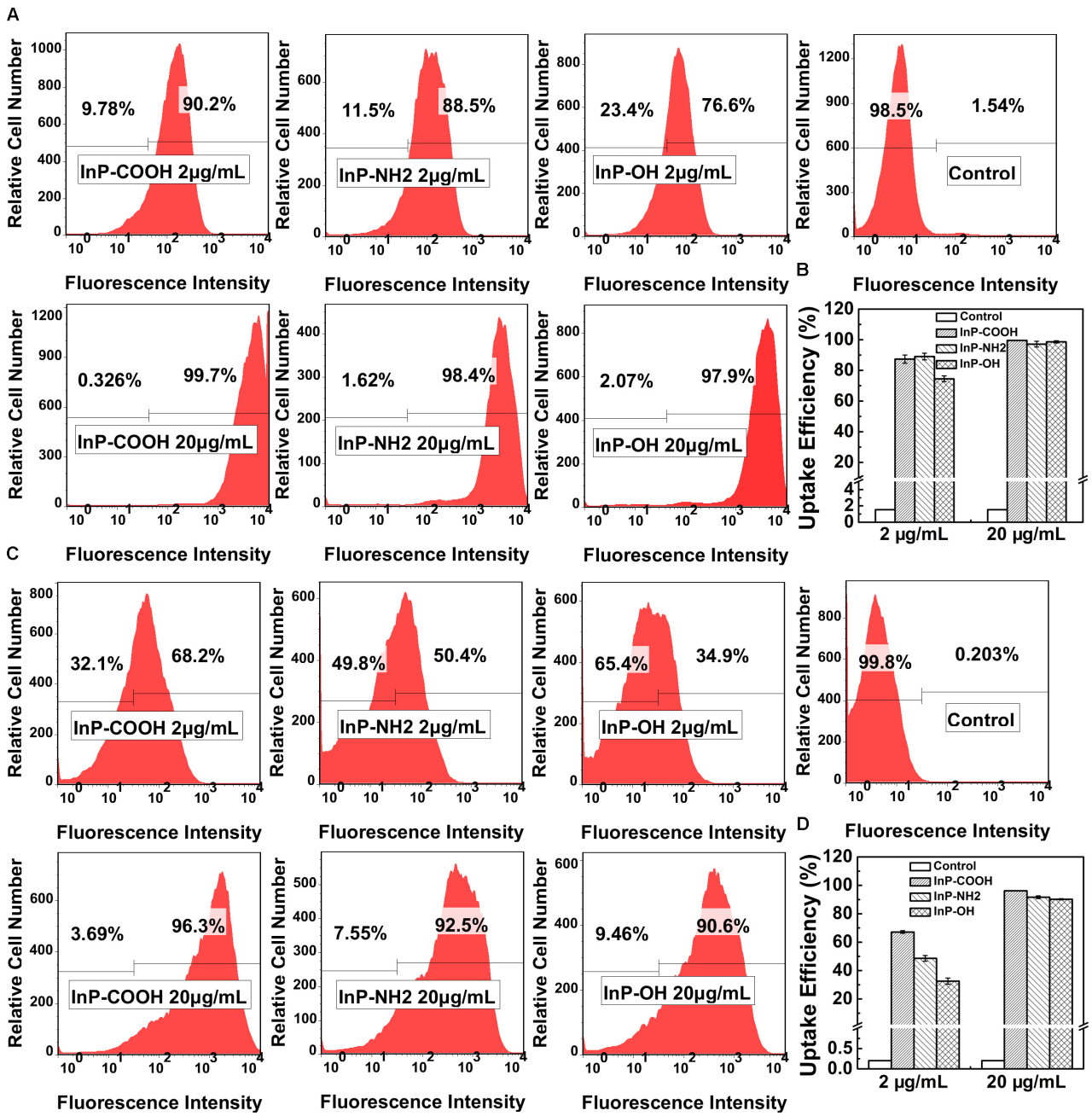

FIGURE 3 | The uptake efficiency of InP/ZnS-COOH, InP/ZnS-NH_2, and InP/ZnS-OH QDs by cells treated for 4 h. Representative plots of the fluorescence intensity in **(A)** HCC-15 and **(C)** RLE-6TN cells treated with 2 and 20 μg/mL QDs. The uptake efficiency of **(B)** HCC-15 and **(D)** RLE-6TN cells, evaluated from experiments shown in **(A,C)**. Values are means ± SD, $n = 3$.

74.5 ± 1.89%, respectively. And for RLE-6TN cells treated with 2 μg/mL QDs, the uptake efficiency of the three QDs are 67.1 ± 0.95%, 48.6 ± 2.03%, and 32.6 ± 2.14%, respectively. From the data we can see that for both cells, the uptake efficiency of QDs terminated with hydroxyl is relatively lower than the QDs modified with carboxyl or amino, which is consistent with fluorescence imaging results. Nevertheless, for 20 μg/mL QDs treated cells, the uptake efficiency of the three QDs are comparable (all above 97% for HCC-15 and all above 90% for RLE-6TN). These results indicate that the *in vitro* uptake of the InP/ZnS QDs is concentration dependent.

Effect of InP/ZnS QDs on Cell Viabilities

In order to evaluate the cytotoxicity of the QDs terminated with carboxyl, hydroxyl or amino groups on lung tissue cells,

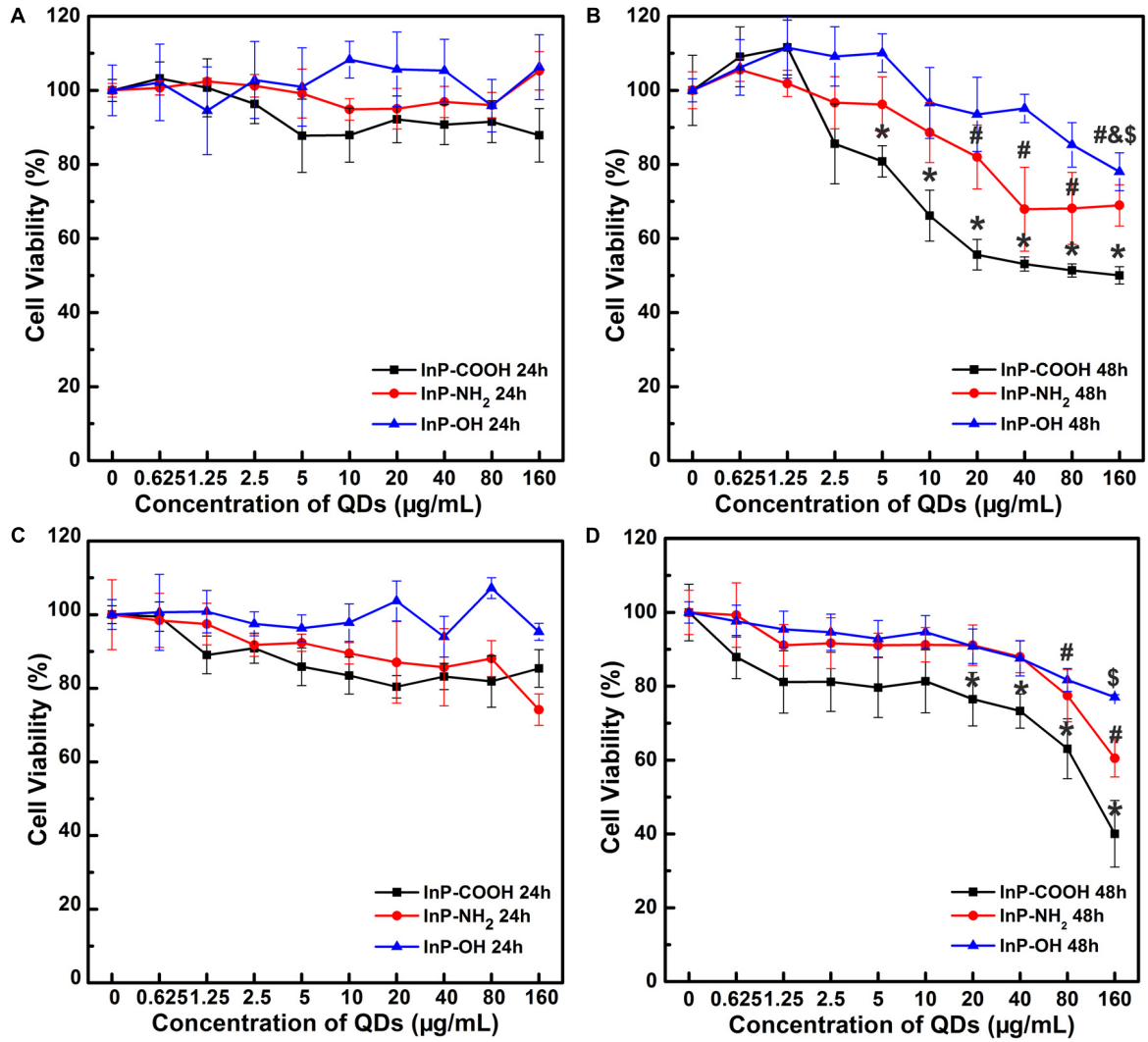

FIGURE 4 | Relative cell viability of HCC-15 **(A,B)** and RLE-6TN cells **(C,D)** treated with (i) InP/ZnS-COOH, (ii) InP/ZnS-NH_2, and (iii) InP/ZnS-OH QDs, respectively. The cells are incubated with different concentrations of QDs for 24 **(A,C)** and 48 h **(B,D)**. Values are means ± SD, $n = 6$. (*$p < 0.05$ vs. control of InP/ZnS-COOH; #$p < 0.05$ vs. control of InP/ZnS-NH_2; \$$p < 0.05$ vs. control of InP/ZnS-OH).

MTT assays were conducted on HCC-15 and RLE-6TN cells with QDs for 24 and 48 h. For the case of HCC-15 cells treated for 24 h, the cell viability of the three groups remained above 90% when the applied QD concentrations range from 0.625 to 160 μg/mL (**Figure 4A**). Similar pattern of cell viability trends are shared for RLE-6TN cells treated for 24 h (**Figure 4C**), the cell viability remained above 90% for InP-NH_2 and InP/ZnS-OH groups and above 80% for InP/ZnS-COOH groups. The results here show that InP/ZnS QDs terminated with carboxyl, hydroxyl or amino groups have no considerable cytotoxicity within 24 h. However, a different trend was observed when we extend the incubation time to 48 h. The cell viability of 48 h post-treatment decreased evidently as QD concentration increased (**Figures 4B,D**), which indicated that the InP/ZnS QDs showed a concentration dependent cytotoxicity pattern in the cell viability.

InP/ZnS QDs Promote Cell Apoptosis

To systematically assess the toxicity of InP/ZnS QDs on cells, the fraction of apoptotic cells caused by QDs were determined by flow cytometry analysis. **Figures 5A,B** are the representative plots of flow cytometry analysis in HCC-15 and RLE-6TN cells, respectively. For the case of HCC-15 cells treated with 20 μg/mL QDs for 24 h, the cell apoptosis rates of the three QDs groups presented comparable to the control group (**Figure 5C**). However, when the exposure time extend to 48 h, the cell apoptosis rates increased dramatically to 30.0 ± 3.26%, 27.9 ± 1.42%, and 38.0 ± 5.06%, respectively (**Figure 5C**), which presented significant difference compared with the control group ($P < 0.01$). The same set of experiments was performed using the RLE-6TN cell line (**Figures 5B,D**). When compared to the untreated cells, the apoptosis rates of the three QDs treated cells all exhibited remarkable increase ($P < 0.01$) (**Figure 5D**). These

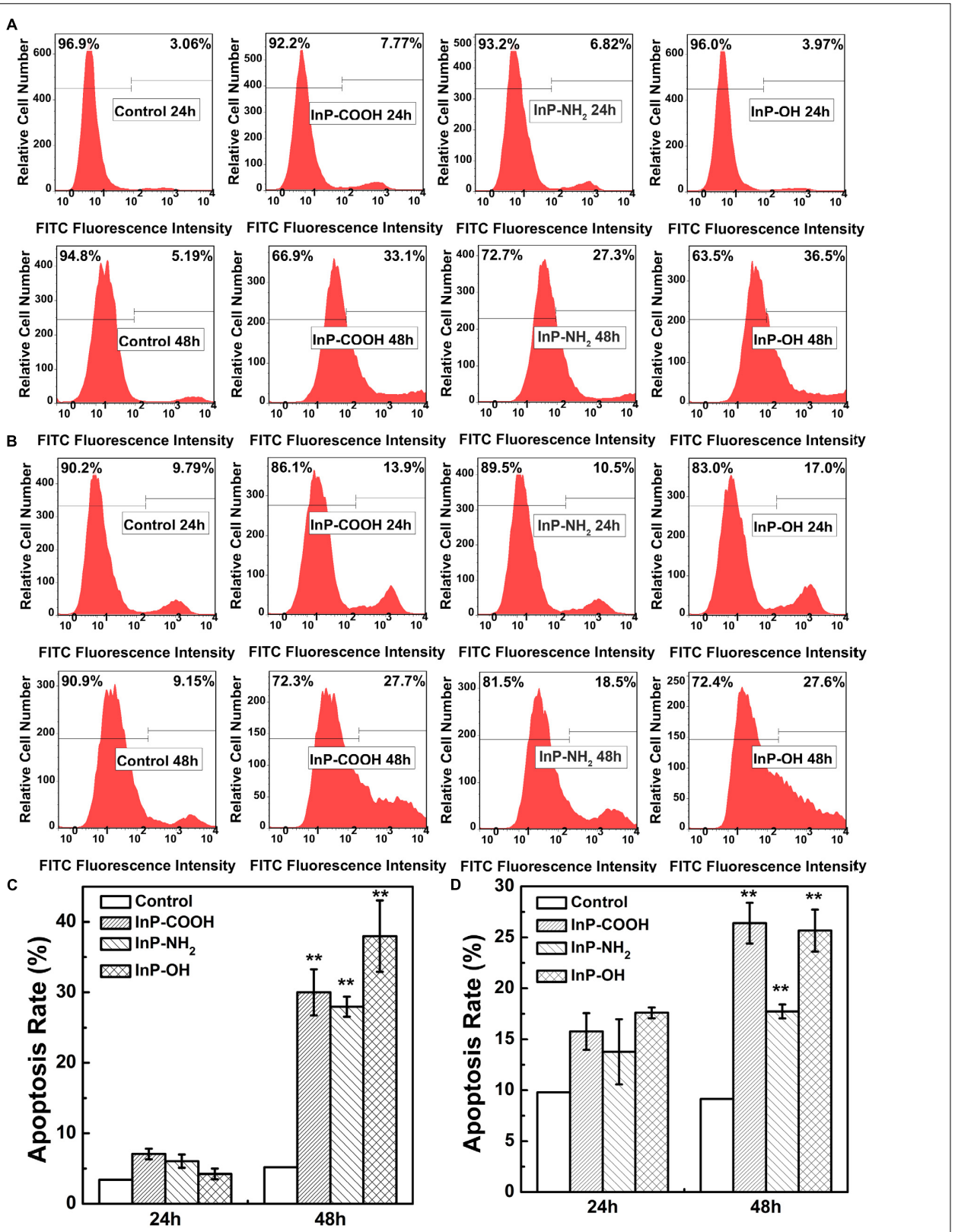

FIGURE 5 | Apoptosis rate of HCC-15 cells **(A,B)** and RLE-6TN cells **(C,D)** treated with (i) Blank, (ii) InP/ZnS-COOH QDs, (iii) InP/ZnS-NH_2 QDs, and (iv) InP/ZnS-OH QDs respectively. Representative plots of FITC fluorescence intensity in HCC-15 **(A)** and RLE-6TN cells **(C)** treated for 24 and 48 h. The apoptosis rate of HCC-15 cells **(B)** and RLE-6TN cells **(D)**, evaluated from experiments shown in **(A,C)**. Values are means ± SD, $n = 3$. (*$p < 0.05$ vs. control; **$p < 0.01$ vs. control).

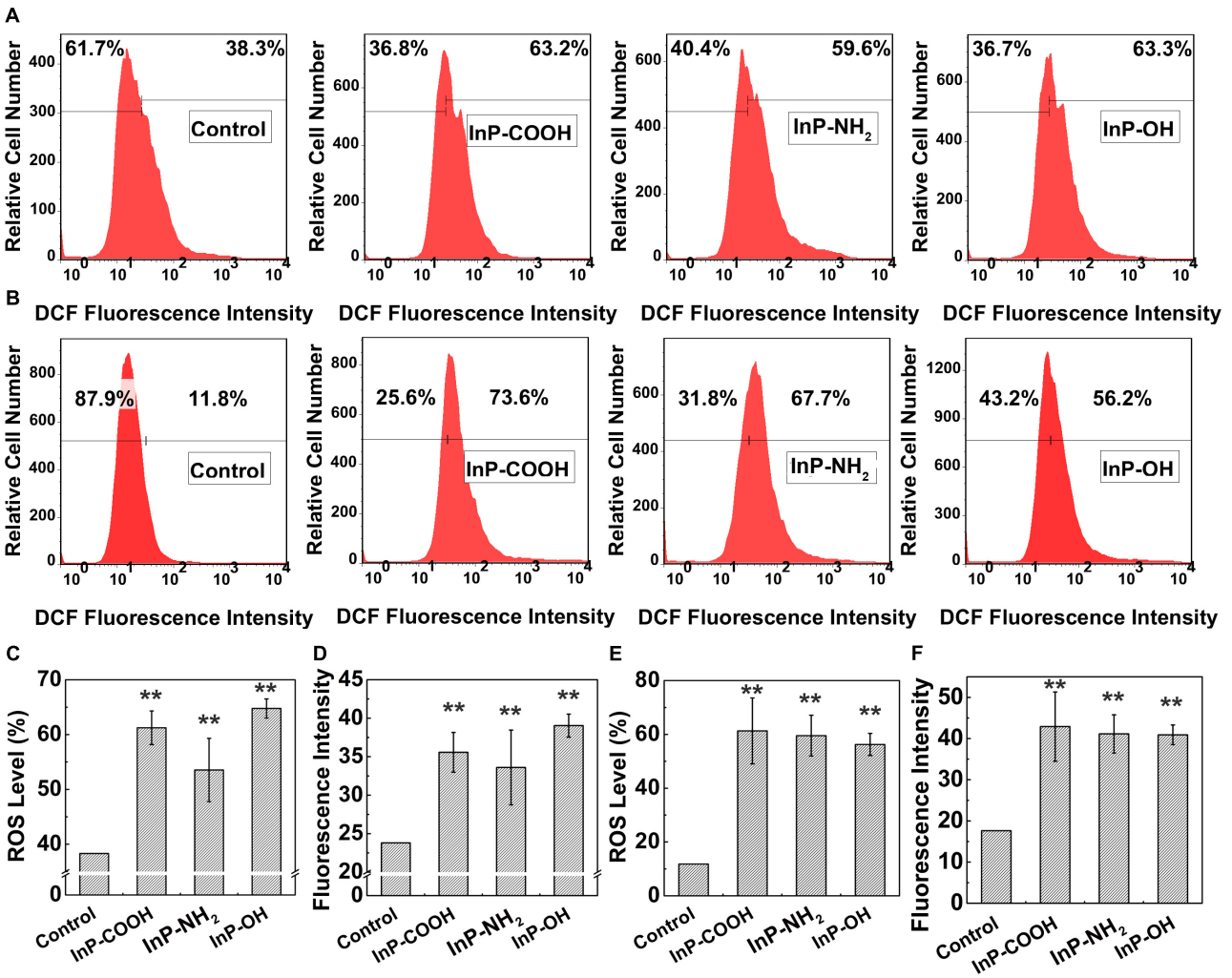

FIGURE 6 | The ROS level in HCC-15 **(A,C,D)** and RLE-6TN cells **(B,E,F)** treated with (i) Blank, (ii) InP/ZnS-COOH QDs, (iii) InP/ZnS-NH_2 QDs, and (iv) InP/ZnS-OH QDs for 4 h. Representative plots of the DCF fluorescence intensity in HCC-15 **(A)** and RLE-6TN cells **(B)**. The ROS level in HCC-15 **(C)** and RLE-6TN cells **(E)**. The average fluorescence intensity of HCC-15 **(D)** and RLE-6TN cells **(F)**. **(C–F)** are evaluated from experiments shown in **(A,B)**. Values are means ± SD, $n = 3$. (*$p < 0.05$ vs. control; **$p < 0.01$ vs. control).

results demonstrated that InP/ZnS QDs increased the occurrence of apoptotic events in cells after 48 h treatment.

InP/ZnS QDs Induce ROS Generation in Lung-Derived Cells

To further probe the mechanism of cytotoxicity, cellular reactive oxygen species (ROS) levels were measured by flow cytometry analysis. **Figures 6A,B** are the representative plots of flow cytometry analysis in HCC-15 and RLE-6TN cells, respectively. For the case of HCC-15 cells, the fraction of cells generated reactive oxygen were 61.2 ± 3.07%, 53.5 ± 5.78%, and 64.8 ± 1.75%, respectively (**Figure 6C**), which showed significantly difference compared with the control ($P < 0.01$). The average DCF fluorescence intensity was correlated with the amount of ROS generated in the cell. The average fluorescence intensity of the QDs treated cells (35.56 ± 2.58, 33.6 ± 4.86, and 39.0 ± 1.50) were significantly stronger than the untreated cells ($P < 0.01$), which implied plentiful ROS generation in the treated cells (**Figure 6D**). The same set of experiments was performed using the RLE-6TN cell line (**Figures 6E,F**) and the data also presented increased intracellular ROS levels of the experiment groups compared to the control ($P < 0.01$). These results suggested that InP/ZnS QDs had the potential to induce the intracellular ROS generation after being uptake by the cells.

DISCUSSION

In recent years, people have developed many non-cadmium QDs because of their concerns on the risk of cadmium exposure from cadmium-containing QDs. InP/ZnS QDs as frequently used non-cadmium QDs have emerged as a presumably less hazardous alternative to cadmium-based QDs (Kuo et al., 2017).

However, toxicity studies on InP/ZnS QDs have just begun, and little has been known about their toxicological effects. Thus, the present study investigated the cytotoxicity of InP/ZnS QDs toward two lung-derived cell lines, HCC-15 and RLE-6TN cells.

It is well known that surface modification and stabilization of QDs appears to be the most key steps to make them hydrophilic and functionalized. The functional groups on the surface make it feasible to cross-link with desired small molecules or ligand of biomolecules (e.g., peptide, antigen or antibody) by means of conjugating. Among these surface coating groups, carboxyl, hydroxyl and amino groups are most frequently used for such biological functionalization (Mashinchian et al., 2014). In this study, QDs with different surface functional groups (carboxyl, hydroxyl or amino groups) were used for the cytotoxicity evaluation.

The different surface functional group of QDs makes them different in water stability and hydrodynamic size distributions. Bantz et al investigated the agglomeration behavior of two SiO_2-based nanoparticles with different surface functional groups. They found that the negatively charged silica particles are easier to agglomerate than the positively charged ones (Bantz et al., 2014). Here, our data showed that InP/ZnS coated with hydroxyl group were more likely to aggregate, and the particle size in the water was far greater than the other QDs coated with carboxyl or amino group. It is mainly because that the hydroxyl groups around the particles couldn't provide sufficient steric hindrance to counterbalance the attractive Van der Waal forces between particles (Wiogo et al., 2011). Apart from the stability and hydrodynamic size distribution, the surface properties also influence the fluorescence intensity of the QDs. Nguyen et al reported that the intense photoluminescence in carbon nanodots is originated from abundant surface functional groups (Vanthan et al., 2016). According to the study of Lu et al. (2000) Mn^{2+}-doped ZnS nanoparticles exhibit a 30-fold increase in PL intensity after surface passivation by carboxylic functional groups. In our study, InP/ZnS QDs terminated with carboxyl groups exhibits evidently enhanced fluorescence intensity than QDs terminated with hydroxyl or amino groups. It is because the exchange process of carboxyl groups and other ligands caused damage to the surface of the QDs to a certain degree (Xiao et al., 2015).

Different physiochemical properties of these three QDs influenced how they interact with cells and, which induced different toxicological patterns. In the last decade, confocal fluorescence microscopy has emerged as an ultra-sensitive tool to probe the interaction between NPs and cells. For example, in order to identify the effect of the PEG-capped LSMO MNPs on MCF7 cells, Thorat and colleagues carried out confocal microscopy aided with multiple staining to observe the morphology of the cells as well as the induced apoptosis and necrosis (Thorat et al., 2016a). In our study, confocal microscopy is performed to determine the uptake of InP/ZnS QDs by HCC-15 and RLE-6TN cells and suggest the distribution of QDs in cytoplasm. Similar results were obtained from the confocal imaging of mPEG capped IONPs in MCF7 cells (Thorat et al., 2016b). Here we showed that InP/ZnS-COOH and InP/ZnS-NH_2 were able to enter the cells more easily than InP/ZnS-OH which was possibly owing to different hydrodynamic size and functional groups on the surface. It is known that the nanoparticle size is one important factor in determining the ability of nanoparticles to enter cells. For example, Huo and his colleagues demonstrated that gold nanoparticles (<6 nm) were able to enter the cell nucleus effectively, whereas larger nanoparticles (10 or 16 nm) only penetrate through the cell membrane, and were found only in the cytoplasm (Huo et al., 2014). Saw et al reported the effect of four sizes of cystine/citric acid-coated confeito-like gold nanoparticles (30, 60, 80, and 100nm) on cellular uptake. They showed that cellular uptake was size dependent with the smallest size of gold nanoparticles (30nm) having the highest cellular internalization in MDA-MB231 breast cancer cells (Saw et al., 2018). Besides nanoparticle size, the cellular uptake of nanoparticles is still influenced by many other factors, including shape, zeta potential, specific surface area, surface charge, catalytic activity, the presence or absence of a shell, and functional groups on the surface (Jayagopal et al., 2007; Ma et al., 2013; Nam et al., 2013; Rivera-Gil et al., 2013). For instance, Zheng et al. studied the uptake of CdSe/ZnS QDs with two commonly reported positive charged (polyethylenimine, cysteamine) and two negative charged (dihydrolipoic acid, glutathione) ligands in human keratinocytes, and they found the selective accumulation of CdSe/ZnS QDs with glutathione in vesicles in the mitochondria matrix (Zheng et al., 2017). Manshian et al showed that intracellular uptake levels of NH_2-QDs and COOH-QDs were very similar after 24 h exposure, NH_2-QDs mainly remained in the lysosomes, while COOH-QDs appeared to be continuously internalized and transported by both endosomes and lysosomes (Manshian et al., 2017).

Consequently, the cellular trafficking by QDs influenced their toxicity profiles. The nanoparticles that are more easily to penetrate the cells will possibly result in higher cytotoxicity. In this study, InP/ZnS-COOH and InP/ZnS-NH_2 showed higher cytotoxicity on two lung-derived cell lines than InP/ZnS-OH. Consistently, Pan et al. have investigated the dependence of the toxicity of gold Nanoparticles on their size in the range from 0.8 to 15 nm. The nanoparticles with 15 nm in size have been found to be 60 times less toxic than 1.4 nm nanoparticles for fibroblasts, epithelial cells, macrophages, and melanoma cells (Pan et al., 2007). The researcher proved that differences in the extent of their cellular uptake resulted in differences in consequent toxicological effects. The continuous flux of CdSe/ZnS QDs terminated with carboxylic acid showed their higher toxicity compared to the NH_2-QDs, resulting in mitochondrial ROS generation and cytoskeletal remodeling (Manshian et al., 2017). It is worth mentioning that, in this study, the toxicity effect of QDs on the two lung-derived cell lines was different. MTT assay showed that RLE-6TN cell line appeared to be more sensitive to QDs treatment. The cytotoxicity of QDs varies by cell type, which is in line with the previous report (Kim et al., 2015). For example, Mortensen et al manifested that ROS responses induced by QD exposure was correlated with the level of QD

uptake and was cell type dependent. Keratinocytes appeared to be at greater risk for QD induced ROS generation than melanocytes after pre-exposing cells to UVB (Mortensen et al., 2015).

One of the common cytotoxicity when living organisms are treated with QDs is apoptosis, where many attempts have been made to explain the mechanisms of apoptosis caused by QDs' use. Excess generation of ROS will result in oxidative stress that would mediate apoptosis. For example, CdTe QDs have been proposed to induce oxidative stress, which plays a crucial role in CdTe QDs-mediated mitochondrial-dependent apoptosis in HUVECs cells (Yan et al., 2016). Luo et al. (2013) reported that QDs in RAG cells increased intracellular ROS levels and induced autophagy, leading to subsequent apoptosis, which suggest that oxidative stress-induced autophagy is a defense/survival mechanism against the cytotoxicity of QD. Furthermore, the activation of cell death receptors and mitochondria-dependent way could onset apoptosis. Singh et al. (2012) demonstrated that CdS QDs induce apoptotic cell death in LNCaP cells via p53, survivin, Bax/Bcl-2 and caspase pathways by alleviating ROS-mediated oxidative stress. Signal transduction also plays an important role in the regulation of apoptosis. Motohashi and Yamamoto (2004) once reported that Nrf2 controlled the transcription of target genes by binding to the antioxidant response element (ARE) located at the enhancer regions of the genes, giving rise to regulations against xenobiotic and oxidative stresses that could induce cell apoptosis.

There are several physicochemical and molecular mechanisms enabling nanoparticles to cause toxicity toward cells. These include ROS generation, DNA damage and membrane perturbation etc. Oxidative stress is considered to be responsible for toxicity triggered by QDs, as it can induce the intracellular production of ROS. According to existing studies, the majority of nanoparticles have been reported to cause excessive ROS generation in affected cells or organs. Our data showed an increase of intracellular ROS level in HCC-15 and RLE-6TN cells after exposure to InP/ZnS QDs, which aligned to some extent with the previous study retaining cadmium-based QDs in other cell types (Wang X. et al., 2016). Lee et al examined the toxicity effect of carboxylic acid-coated QDs (QD 565 and QD 655) on human keratinocytes. The cell viability of keratinocytes was obviously inhibited by these two types of QDs in a concentration-dependent manner. QD-induced intracellular ROS levels resulted in cell apoptosis via blockade of AKT phosphorylation (Lee et al., 2017). Peynshaert and his colleagues showed that PEGylated QDs were significantly more toxic than MPA-coated QDs due to increased ROS production and lysosomal impairment, which next resulted in autophagy dysfunction and cytotoxicity (Peynshaert et al., 2017).

Reactive oxygen species are chemically reactive species containing oxygen. Oxygen atom has two unpaired electrons in separate orbits in its outer electron shell. This electron structure makes oxygen susceptible to radical formation. The sequential reduction of oxygen through the addition of electrons leads to the formation of a number of ROS including $O_2^{\cdot-}$, H_2O_2, $^{\cdot}OH$, HOCl, $ONOO^-$, and NO. DCFH-DA probe used in our study was considered to be used for detecting intracellular H_2O_2 and oxidative stress. It is cell-permeable and is enzymatically hydrolyzed by intracellular esterase to DCFH which is retained in the cell (Halliwell and Whiteman, 2004). Oxidation of DCFH by H_2O_2 results in DCF, a fluorescent product which can be monitored by fluorescence-based techniques. However, it is reported that DCFH does not directly react with H_2O_2 to form DCF, it can also be oxidized by other ROS, such as $^{\cdot}OH$, $ROO^{\cdot}$, $O_2^{\cdot-}$ (Crow, 1997). Due to the existence of several substances that interfere with the formation of DCF, the probe DCFH-DA, when used in cellular systems, cannot be seen as a specific indicator for H_2O_2.

Taken together, our results on cell uptake, cell viability, apoptosis and ROS generation indicated that InP/ZnS QDs can enter these two lung-derived cells with exerting obvious cytotoxicity. InP/ZnS-COOH and InP/ZnS-NH_2 were able to enter the cells more easily than InP/ZnS-OH, in turn caused more toxic to cells. Although InP/ZnS have regarded as a presumably less hazardous alternative to cadmium-based QDs, appropriate concentration and surface functional groups are needed to be optimized for biological and therapeutic applications in the future.

CONCLUSION

In summary, we reported the cytotoxicity of InP/ZnS QDs with different surface groups (NH_2, COOH, OH) toward two lung-derived cell lines, HCC-15 and RLE-6TN cells. The results showed that InP/ZnS-OH was more likely to aggregate, and the particle size in the water was far greater than the other InP/ZnS-COOH and InP/ZnS-NH_2. InP/ZnS-COOH and InP/ZnS-NH_2 were able to enter the cells more easily than InP/ZnS-OH. High doses of all these QDs caused the cell viability to decrease, and InP/ZnS-COOH and InP/ZnS-NH_2 appeared to be more toxic than InP/ZnS-OH. In addition, InP/ZnS QDs treatment presented increased cell apoptosis and enhanced intracellular ROS levels. These results suggested that appropriate concentration and surface functional groups should be optimized when InP/ZnS QDs are utilized for biological and therapeutic purpose in the future.

AUTHOR CONTRIBUTIONS

GL designed the experiments. TC carried out the experiments and wrote the manuscript. LL, JW, YC, and ZY assisted with sample collection. GX, XW, and WJ helped with experiment results analysis.

FUNDING

The authors would like to acknowledge the funding support from National Natural Science Foundation of China (NSFC) (Nos. 21677102 and 31671491), Natural Science Foundation of

SZU (No. 827-000100, Starting Project of Shenzhen high-level overseas talents), the Chinese Ministry of Science and Technology (No. 2016YFC0904600), and Shenzhen Science and Technology Project (Nos. JCYJ20160331114230843, JCYJ20170817093725277, and GJHZ20170313111237888).

SUPPLEMENTARY MATERIAL

The Supplementary Material for this article can be found online at: https://www.frontiersin.org/articles/10.3389/fphar.2018.00763/full#supplementary-material

REFERENCES

Bantz, C., Koshkina, O., Lang, T., Galla, H., Kirkpatrick, C. J., and Stauber, R. H., et al. (2014). The surface properties of nanoparticles determine the agglomeration state and the size of the particles under physiological conditions. *Beilstein J. Nanotechnol.* 5, 1774–1786. doi: 10.3762/bjnano.5.188

Bruchez, M., Moronne, M., Gin, P., Weiss, S., and Alivisatos, A. P. (1998). Semiconductor nanocrystals as fluorescent biological labels. *Science* 281, 2013–2016. doi: 10.1126/science.281.5385.2013

Brunetti, V., Chibli, H., Fiammengo, R., Galeone, A., Malvindi, M. A., and Vecchio, G., et al. (2013). InP/ZnS as a safer alternative to CdSe/ZnS core/shell quantum dots: in vitro and in vivo toxicity assessment. *Nanoscale* 5, 307–317. doi: 10.1039/c2nr33024e

Chibli, H., Carlini, L., Park, S., Dimitrijevic, N. M., and Nadeau, J. L. (2011). Cytotoxicity of InP/ZnS quantum dots related to reactive oxygen species generation. *Nanoscale* 3, 2552–2559. doi: 10.1039/c1nr10131e

Crow, J. P. (1997). Dichlorodihydrofluorescein and dihydrorhodamine 123 are sensitive indicators of peroxynitrite in vitro: implications for intracellular measurement of reactive nitrogen and oxygen species. *Nitric Oxide* 1, 145–157. doi: 10.1006/niox.1996.0113

Halliwell, B., and Whiteman, M. (2004). Measuring reactive species and oxidative damage in vivo and in cell culture: how should you do it and what do the results mean? *Br. J. Pharmacol.* 142, 231–255. doi: 10.1038/sj.bjp.0705776

Ho, C., Chang, H., Tsai, H., Tsai, M., Yang, C., Ling, Y., et al. (2013). Quantum dot 705, a cadmium-based nanoparticle, induces persistent inflammation and granuloma formation in the mouse lung. *Nanotoxicology* 7, 105–115. doi: 10.3109/17435390.2011.635814

Huo, S., Jin, S., Ma, X., Xue, X., Yang, K., Kumar, A., et al. (2014). Ultrasmall gold nanoparticles as carriers for nucleus-based gene therapy due to size-dependent nuclear entry. *ACS Nano* 8, 5852–5862. doi: 10.1021/nn5008572

Jayagopal, A., Russ, P. K., and Haselton, F. R. (2007). Surface engineering of quantum dots for in vivo vascular imaging. *Bioconjug. Chem.* 18, 1424–33. doi: 10.1021/bc070020r

Kim, I. Y., Joachim, E., Choi, H., and Kim, K. (2015). Toxicity of silica nanoparticles depends on size, dose, and cell type. *Nanomedicine* 11, 1407–1416. doi: 10.1016/j.nano.2015.03.004

Kuo, T. R., Hung, S. T., Lin, Y. T., Chou, T. L., Kuo, M. C., Kuo, Y. P., et al. (2017). Green synthesis of InP/ZnS core/shell quantum dots for application in heavy-metal-free light-emitting diodes. *Nanoscale Res. Lett.* 12:537. doi: 10.1186/s11671-017-2307-2302

Lee, E. Y., Bae, H. C., Lee, H., Jang, Y., Park, Y. H., Kim, J. H., et al. (2017). Intracellular ROS levels determine the apoptotic potential of keratinocyte by quantum dot via blockade of AKT Phosphorylation. *Exp. Dermatol.* 26, 1046–1052. doi: 10.1111/exd.13365

Li, K. G., Chen, J. T., Bai, S. S., Wen, X., Song, S. Y., Yu, Q., et al. (2009). Intracellular oxidative stress and cadmium ions release induce cytotoxicity of unmodified cadmium sulfide quantum dots. *Toxicol. In Vitro* 23, 1007–1013. doi: 10.1016/j.tiv.2009.06.020

Lin, G., Ouyang, Q., Hu, R., Ding, Z., Tian, J., Yin, F., et al. (2015a). In vivo toxicity assessment of non-cadmium quantum dots in BALB/c mice. *Nanomedicine* 11, 341–350. doi: 10.1016/j.nano.2014.10.002

Lin, G., Wang, X., Yin, F., and Yong, K. (2015b). Passive tumor targeting and imaging by using mercaptosuccinic acid-coated near-infrared quantum dots. *Int. J. Nanomed.* 10, 335–345. doi: 10.2147/IJN.S74805

Liu, J., Yang, C., Liu, J., Hu, R., Hu, Y., Chen, H., et al. (2017). Effects of Cd-based quantum dot exposure on the reproduction and offspring of Kunming mice over multiple generations. *Nanotheranostics* 1, 23–37. doi: 10.7150/ntno.17753

Lu, S. W., Lee, B. I., Wang, Z. L., Tong, W. S., Wagner, B. K., Park, W., et al. (2000). Synthesis and photoluminescence enhancement of Mn2 + -doped ZnS nanocrystals. *J. Lumin.* 92, 73–78. doi: 10.1016/S0022-2313(00)00238-236

Luo, Y., Wu, S., Wei, Y., Chen, Y., Tsai, M., Ho, C., et al. (2013). Cadmium-based quantum dot induced autophagy formation for cell survival via oxidative stress. *Chem. Res. Toxicol.* 26, 662–673. doi: 10.1021/tx300455k

Ma, N., Ma, C., Li, C., Wang, T., Tang, Y., Wang, H., et al. (2013). Influence of nanoparticle shape, size, and surface functionalization on cellular uptake. *J. Nanosci. Nanotechnol.* 13, 6485–6498.

Ma-Hock, L., Brill, S., Wohlleben, W., Farias, P. M. A., Chaves, C. R., Tenorio, D. P., et al. (2012). Short term inhalation toxicity of a liquid aerosol of CdS/Cd(OH)(2) core shell quantum dots in male wistar rats. *Toxicol. Lett.* 208, 115–124. doi: 10.1016/j.toxlet.2011.10.011

Manshian, B. B., Abdelmonem, A. M., Kantner, K., Pelaz, B., Klapper, M., Nardi Tironi, C., et al. (2016). Evaluation of quantum dot cytotoxicity: interpretation of nanoparticle concentrations versus intracellular nanoparticle numbers. *Nanotoxicology* 10, 1318–1328. doi: 10.1080/17435390.2016.1210691

Manshian, B. B., Martens, T. F., Kantner, K., Braeckmans, K., De Smedt, S. C., Demeester, J., et al. (2017). The role of intracellular trafficking of CdSe/ZnS QDs on their consequent toxicity profile. *J. Nanobiotechnol.* 15, 1–14. doi: 10.1186/s12951-017-0279-270

Mashinchian, O., Johari-Ahar, M., Ghaemi, B., Rashidi, M., Barar, J., and Omidi, Y. (2014). Impacts of quantum dots in molecular detection and bioimaging of cancer. *Bioimpacts* 4, 149–66. doi: 10.15171/bi.2014.008

Mo, D., Hu, L., Zeng, G., Chen, G., Wan, J., Yu, Z., et al. (2017). Cadmium-containing quantum dots: properties, applications, and toxicity. *Appl. Microbiol. Biotechnol.* 101, 2713–2733. doi: 10.1007/s00253-017-8140-8149

Mortensen, L. J., Faulknor, R., Ravichandran, S., Zheng, H., and DeLouise, L. A. (2015). UVB dependence of quantum dot reactive oxygen species generation in common skin cell models. *J. Biomed. Nanotechnol.* 11, 1644–1652.

Motohashi, H., and Yamamoto, M. (2004). Nrf2-Keap1 defines a physiologically important stress response mechanism. *Trends Mol. Med.* 10, 549–557. doi: 10.1016/j.molmed.2004.09.003

Nam, J., Won, N., Bang, J., Jin, H., Park, J., Jung, S., et al. (2013). Surface engineering of inorganic nanoparticles for imaging and therapy. *Adv. Drug Deliv. Rev.* 65, 622–648. doi: 10.1016/j.addr.2012.08.015

Oh, E., Liu, R., Nel, A., Gemill, K. B., Bilal, M., Cohen, Y., et al. (2016). Meta-analysis of cellular toxicity for cadmium-containing quantum dots. *Nat. Nanotechnol.* 11, 479–486. doi: 10.1038/NNANO.2015.338

Paesano, L., Perotti, A., Buschini, A., Carubbi, C., Marmiroli, M., Maestri, E., et al. (2016). Markers for toxicity to HepG2 exposed to cadmium sulphide quantum dots; damage to mitochondria. *Toxicology* 374, 18–28. doi: 10.1016/j.tox.2016.11.012

Pan, Y., Neuss, S., Leifert, A., Fischler, M., Wen, F., Simon, U., et al. (2007). Size-dependent cytotoxicity of gold nanoparticles. *Small* 3, 1941–1949. doi: 10.1002/smll.200700378

Peng, C., Liu, J., Yang, G., and Li, Y. (2018). Lysyl oxidase activates cancer stromal cells and promotes gastric cancer progression: quantum dot-based identification of biomarkers in cancer stromal cells. *Int. J. Nanomed.* 13, 161–174. doi: 10.2147/IJN.S143871

Peynshaert, K., Soenen, S. J., Manshian, B. B., Doak, S. H., Braeckmans, K., De Smedt, S. C., et al. (2017). Coating of quantum dots strongly defines their effect on lysosomal health and autophagy. *Acta Biomater.* 48, 195–205. doi: 10.1016/j.actbio.2016.10.022

Pohanka, M. (2017). Quantum dots in the therapy: current trends and perspectives. *Mini Rev. Med. Chem.* 17, 650–656. doi: 10.2174/1389557517666170120153342

Rivera-Gil, P., Jimenez, D. A. D., Wulf, V., Pelaz, B., Del, P. P., Zhao, Y., et al. (2013). The challenge to relate the physicochemical properties of colloidal nanoparticles to their cytotoxicity. *Acc. Chem. Res.* 46, 743–749. doi: 10.1021/ar300039j

Roberts, J. R., Antonini, J. M., Porter, D. W., Chapman, R. S., Scabilloni, J. F., Young, S., et al. (2013). Lung toxicity and biodistribution of Cd/Se-ZnS quantum dots with different surface functional groups after pulmonary exposure in rats. *Part. Fibre Toxicol.* 10:5. doi: 10.1186/1743-8977-10-15

Saw, W. S., Ujihara, M., Chong, W. Y., Voon, S. H., Imae, T., Kiew, L. V., et al. (2018). Size-dependent effect of cystine/citric acid-capped confeito-like gold nanoparticles on cellular uptake and photothermal cancer therapy. *Colloids Surf. B Biointerfaces* 161, 365–374. doi: 10.1016/j.colsurfb.2017.10.064

Schwotzer, D., Niehof, M., Schaudien, D., Kock, H., Hansen, T., Dasenbrock, C., et al. (2018). Cerium oxide and barium sulfate nanoparticle inhalation affects gene expression in alveolar epithelial cells type II. *J. Nanobiotechnol.* 16:16. doi: 10.1186/s12951-018-0343-344

Singh, B. R., Singh, B. N., Khan, W., Singh, H. B., and Naqvi, A. H. (2012). ROS-mediated apoptotic cell death in prostate cancer LNCaP cells induced by biosurfactant stabilized CdS quantum dots. *Biomaterials* 33, 5753–5767. doi: 10.1016/j.biomaterials.2012.04.045

Soenen, S. J., Manshian, B. B., Aubert, T., Himmelreich, U., Demeester, J., De Smedt, S. C., et al. (2014). Cytotoxicity of cadmium-free quantum dots and their use in cell bioimaging. *Chem. Res. Toxicol.* 27, 1050–1059. doi: 10.1021/tx5000975

Thorat, N. D., Bohara, R. A., Malgras, V., Tofail, S. A. M., Ahamad, T., Alshehri, S. M., et al. (2016a). Multimodal superparamagnetic nanoparticles with unusually enhanced specific absorption rate for synergetic cancer therapeutics and magnetic resonance imaging. *ACS Appl. Mater. Interfaces* 8, 14656–14664. doi: 10.1021/acsami.6b02616

Thorat, N. D., Lemine, O. M., Bohara, R. A., Omri, K., El Mir, L., and Tofail, S. A. M. (2016b). Superparamagnetic iron oxide nanocargoes for combined cancer thermotherapy and MRI applications. *Phys. Chem. Chem. Phys.* 18, 21331–21339. doi: 10.1039/c6cp03430f

Vanthan, N., Si, J., Yan, L., and Hou, X. (2016). Direct demonstration of photoluminescence originated from surface functional groups in carbon nanodots. *Carbon* 108, 268–273. doi: 10.1016/j.carbon.2016.07.019

Wang, M., Wang, J., Sun, H., Han, S., Feng, S., Shi, L., et al. (2016). Time-dependent toxicity of cadmium telluride quantum dots on liver and kidneys in mice: histopathological changes with elevated free cadmium ions and hydroxyl radicals. *Int. J. Nanomedicine* 11, 2319–2328. doi: 10.2147/IJN.S103489

Wang, X., Tian, J., Yong, K. T., Zhu, X., Lin, M. C., Jiang, W., et al. (2016). Immunotoxicity assessment of CdSe/ZnS quantum dots in macrophages, lymphocytes and BALB/c mice. *J. Nanobiotechnol.* 14:10. doi: 10.1186/s12951-016-0162-164

Wiogo, H. T. R., Lim, M., Bulmus, V., and Amal, R. (2011). "Effects of surface functional groups on the aggregation stability of magnetite nanoparticles in biological media containing serum," in *Proceedings of the 11th IEEE International Conference on Nanotechnology*, Portland, OR, 841–844.

Wu, D., Pang, Y., Wilkerson, M. D., Wang, D., Hammerman, P. S., and Liu, J. S. (2013). Gene-expression data integration to squamous cell lung cancer subtypes reveals drug sensitivity. *Br. J. Cancer* 109, 1599–1608. doi: 10.1038/bjc.2013.452

Xiao, J., Liu, P., Li, L., and Yang, G. (2015). Fluorescence origin of nanodiamonds. *J. Phys. Chem. C* 119, 2239–2248. doi: 10.1021/jp512188x

Yan, M., Zhang, Y., Qin, H., Liu, K., Guo, M., Ge, Y., et al. (2016). Cytotoxicity of CdTe quantum dots in human umbilical vein endothelial cells: the involvement of cellular uptake and induction of pro-apoptotic endoplasmic reticulum stress. *Int. J. Nanomed.* 11, 529–542. doi: 10.2147/IJN.S93591

Ye, L., Yong, K., Liu, L., Roy, I., Hu, R., Zhu, J., et al. (2012). A pilot study in non-human primates shows no adverse response to intravenous injection of quantum dots. *Nat. Nanotechnol.* 7, 453–458. doi: 10.1038/NNANO.2012.74

Zheng, H., Mortensen, L. J., Ravichandran, S., Bentley, K., and DeLouise, L. A. (2017). Effect of nanoparticle surface coating on cell toxicity and mitochondria uptake. *J. Biomed. Nanotechnol.* 13, 155–66.

Zheng, W., Xu, Y., Wu, D., Yao, Y., Liang, Z., Tan, H. W., et al. (2018). Acute and chronic cadmium telluride quantum dots-exposed human bronchial epithelial cells: the effects of particle sizes on their cytotoxicity and carcinogenicity. *Biochem. Biophys. Res. Commun.* 495, 899–903. doi: 10.1016/j.bbrc.2017.11.074

Zhou, J., Zou, X., Song, S., and Chen, G. (2018). Quantum dots applied to methodology on detection of pesticide and veterinary drug residues. *J. Agric. Food Chem.* 66, 1307–1319. doi: 10.1021/acs.jafc.7b05119

Zienolddiny, S., Svendsrud, D. H., Ryberg, D., Mikalsen, A. B., and Haugen, A. (2000). Nickel(II) induces microsatellite mutations in human lung cancer cell lines. *Mutat. Res.* 452, 91–100. doi: 10.1016/S0027-5107(00)00060-69

Conflict of Interest Statement: The authors declare that the research was conducted in the absence of any commercial or financial relationships that could be construed as a potential conflict of interest.

Advantages of publishing in Frontiers

OPEN ACCESS
Articles are free to read for greatest visibility and readership

FAST PUBLICATION
Around 90 days from submission to decision

HIGH QUALITY PEER-REVIEW
Rigorous, collaborative, and constructive peer-review

TRANSPARENT PEER-REVIEW
Editors and reviewers acknowledged by name on published articles

Frontiers
Avenue du Tribunal-Fédéral 34
1005 Lausanne | Switzerland

Visit us: www.frontiersin.org
Contact us: info@frontiersin.org | +41 21 510 17 00

REPRODUCIBILITY OF RESEARCH
Support open data and methods to enhance research reproducibility

DIGITAL PUBLISHING
Articles designed for optimal readership across devices

FOLLOW US
@frontiersin

IMPACT METRICS
Advanced article metrics track visibility across digital media

EXTENSIVE PROMOTION
Marketing and promotion of impactful research

LOOP RESEARCH NETWORK
Our network increases your article's readership